Study of Electro-Optics of Anisotropic Molecules for Photonics Applications

Thesis

Submitted for the Award of the Degree

of

Doctor of Philosophy

In

Applied Physics

Submitted By

Pawan Singh

Enrollment No. 067/14

Under the supervision of

Dr. Khem Bahadur Thapa

BABASAHEB BHIMRAO AMBEDKAR UNIVERSITY
LUCKNOW
प्रज्ञा शील करुणा
ESTABLISHED 1996

Department of Applied Physics
School for Physical Sciences
Babasaheb Bhimrao Ambedkar University
(A Central University)
Lucknow -226025, U.P. (India)

October, 2020

Dedicated to Guruji

And

My Parents

DECLARATION

I declare that the thesis entitled "***Study of Electro-Optics of Anisotropic Molecules for Photonics Applications***" has been prepared by me under the supervision of **Dr. Khem Bahadur Thapa**, Department of Applied Physics, School for Physical Sciences, Babasaheb Bhimrao Ambedkar University, Lucknow. No part of this thesis has formed the basis for the award of any degree, diploma or fellowship previously. Further, I declare that the material embodied in the present work is based on original research work and the indebtedness to others has been duly acknowledged at relevant places. This is also declared that the thesis is essentially free from all kinds of plagiarism.

पवन सिंह

(Pawan Singh)

Date: 19|10|2020

Place: Lucknow

Department of Applied Physics,
School for Physical Sciences,
Babasaheb Bhimrao Ambedkar University,
Vidya Vihar, Raebareli Road,
Lucknow-226025, U.P., India

CERTIFICATE

This is to certify that the thesis titled **"*Study of Electro-Optics of Anisotropic Molecules for Photonics Applications*"** submitted by **Mr. Pawan Singh** is an original research work and has not been previously submitted in part or full for the award of any other degree or diploma to this or any other university.

The thesis submitted to the Babasaheb Bhimrao Ambedkar University, Lucknow satisfies all the requirements as stipulated in the *Doctor of Philosophy (Ph.D.) regulations -1999 as amended in 2013* and it is fit for submission and evaluation for the award of the degree of Doctor of Philosophy of the University.

(Supervisor)

Dr. Rhem B. Thapa
Assistant Professor
Department of Applied Physics
Babasaheb Bhimrao Ambedkar University
(A Central University) Lucknow-226025

Date: 19/10/2020

(Head of the Department)

विभागाध्यक्ष
Head
भौतिकी विभाग
Deptt. of Physics
बाबा साहेब भीमराव अम्बेडकर विश्वविद्यालय
Baba Saheb Bhimrao Ambedkar University
लखनऊ - 226025 उ० प्र०, भारत
Lucknow - 226025, U.P., India

ACKNOWLEDGEMENT

It is my firm belief that any major research work to result in a positive outcome including a worthy thesis requires the culmination of several factors such as a meaningful subject which can motivate a determined researcher to take up the challenge, a learned and sincere guide in the form of friend, relative and colleague who selflessly encourage and help the researcher throughout the research. I have the honour and privilege to **Dr. Khem Bahadur Thapa** as an excellent guide. I take this opportunity to place on record my heart felt and sincere gratitude and deep indebtedness to him without whose guidance this work could not have been meaningfully concluded. I also owe my sincere thanks and sense of deep gratitude to **Prof. Bal Chandra Yadav**, Head, Department of Physics, School of Physical & Decision Sciences, Babasaheb Bhimrao Ambedkar University, for providing necessary facilities in the department in a very kind behavior.

I am extremely thankful to my teachers **Prof. Devesh Kumar, Dr. Ramesh Chandra**, **Dr. Anil K. Yadav**, **Dr. Devendra Singh** for their valuable suggestions and encouragements which have been a great asset to me during the entire course of study. I owe my deep gratitude towards them for their constant motivation and moral support. I feel myself blessed to have such teachers. Also, I am thankful to staff members at Babasaheb Bhimrao Ambedkar University especially **Department of Physics (DOP).**

I am highly thankful to **Dr. Dharmendra Kumar Singh,** faculty at Department of Mathematics, UIET, CSJM University, and **Dr. Sudesh Kumar Singh**, faculty at Department of Physics, T. D. P. G. College, Jaunpur for his valuable suggestions and encouragements. Also, I am highly grateful to **Mr. Narinder Kumar, Dr. Ravi Kant Tripathi, Dr. Pranav Upadhyay** and **Dr. Vivek Kumar Nautiyal**, Department of Physics, BBAU Lucknow for his constant support and providing help at the hour of need. Without his support, the thesis cannot be in its present form.

I am also thankful to my seniors **Dr. Samiksha Sikarwar, Ms. Priyanka Chaudhary, Mr. Shakti Singh, Dr. Yashkaur Singh, Dr. Ratindra Gautam, Mr. Sudhir Kumar** for his valuable suggestions and encouragement.

I am also thankful to our research group members **Mr. Krishan Pal, Ms. Abhisikta Bhaduri, and Asish Kumar** for his supporting every moment of my journey.

I would like to acknowledge the contribution of my friends and colleagues, **Mr. Manjeet Kumar, Mr. Pushpesh Pathak, Mr. Anwesh Pandey, Mr. Shyam Sundar, Mr. Kuldeep Kumar, Ms. Shivani Chaudhary, Ms. Bhavna Pal, Mr. Arpit Verma, Mr. Sumit Tiwari** for a joyful and healthy environment around me to work.

Finally, I would like to pay my highest regard to my grandparents **Late Kamla** and **Late Bhoop Ram**. I owe my indebtedness towards my parents **Shri Jandail Singh** and **Smt. Hemlata Singh** for their love, support and sacrifice from the very first day of my journey of life. I am highly thankful to my family for moral support and encouragement.

Last but not the least, my final words of thanks will be for Almighty God, for his countless blessings, mercy and companionship through all turmoil of my life.

Pawan Singh

(Ph.D. Scholar)

LIST OF PUBLICATIONS

Part of the thesis published and communicated in the refereed journals:

1. **Pawan Singh,** Narinder Kumar, Khem B. Thapa*, Devesh Kumar, Tunable transmission of a nematic liquid crystal defect in 1D periodic structure of dielectric materials due to orientation/re-orientation of nematic molecules, *in European Journal of Physics E (EPJ E)*, 41, 100, 2018.
2. **Pawan Singh,** Khem B Thapa, Narinder Kumar, Krishan Pal and Devesh Kumar, Graphene layers on semi-finite 1D asymmetric periodic structure of Si/Glass materials with defect of nematic liquid crystal for a sensor device, *Mater. Res. Express*, 6, 066209, 2019.
3. **Pawan Singh,** Khem B. Thapa, Narinder Kumar, Devendra Singh, Devesh Kumar, Study of transmission property of periodic layer consisting of SiO_2 and TiO_2 layers with anisotropic liquid crystal (LC) and $LiNbO_3$ as defect layers for optical switching, *Results in Physics*, 13, 102346, 2019.
4. **Pawan Singh,** Khem B. Thapa, Narinder Kumar, Devendra Singh, Devesh Kumar, Effective optical properties of one-dimensional periodic structure of TiO_2 and SiO_2 layers with a defect layer of nano-composite consisting of silver nanoparticle and E7 liquid crystal, *Pramana- Journal of Physics*, 93, 50, 2019.
5. **Pawan Singh,** Vivek K. Nautiyal, Ram Janma, Khem B. Thapa, Theoretical investigation of one-dimensional periodic structure of TiO_2/SiO_2 layers containing a defect layer of the nanocomposite with different radii of silver nanoparticles in the host liquid crystal, *Physica Scripta*, 95(6), 065507, 2020.

Work not included in thesis:

6. **Pawan Singh**, Khem B. Thapa, Narinder Kumar, Anil K. Yadav, Devesh Kumar, Tunable optical filter based on one-dimensional periodic structure composed of SiO_2 and anisotropic meta-material with a liquid crystal defect layer sandwiched by SiO_2, *International Journal of Modern Physics B*, 33, 950194, 2019.
7. **Pawan Singh,** Khem B. Thapa, And Girijesh N. Pandey, Temperature sensor and monochromatic filter based on one-dimensional photonic crystal

containing Si and SiO_2 with a defect layer of liquid crystal, *Optoelectronics and Advanced Materials – Rapid Communications*, 13, 401, 2019.

8. **Pawan Singh,** Khem. B. Thapa, Narinder Kumar, and Devesh Kumar, Omnidirectional reflection band of one dimensional periodic structure (1DPS) of Si/SiO_2 with defect mode of nematic liquid crystal (5CB), *Journal of Physical Science*, 30(3), 117, 2019.
9. **Pawan Singh,** Krishan Pal, Khem B. Thapa, Narinder Kumar, Devesh Kumar, Embedded Liquid Crystal Defect with Graphene Layers in Asymmetric One-Dimensional Photonic Crystal as Sensor Application, Book Chapter in CRC Press, *Advances in Photonic Crystals and Devices*, 2019.
10. **Pawan Singh,** Krishan Pal, Narinder Kumar, Sudesh K. Singh, Khem B. Thapa, Devesh Kumar, Tunable Sensing Property of 1D Periodic Structure with Defect of Liquid Crystal Sandwiched by Metallic Layers, *Sensor Letters*, 17(10), 800, 2019.
11. **Pawan Singh,** Khem B. Thapa, & Sudesh K. Singh & Alok K. Gupta, Study of design tunable optical sensor and monochromatic filter of the one-dimensional periodic structure of TiO_2/MgF_2 with defect layer of liquid crystal (LC) sandwiched with two silver layers, *Plasmonics*, 2020.
12. Krishan Pal, **Pawan Singh,** Abhishikta Bhaduri, Khem B. Thapa, Current challenges and future prospects for a highly efficient (>20%) kesterite CZTS solar cell: A review, *Solar Energy Materials and Solar Cells*, 196, 138-156, 2019.
13. Narinder Kumar, **Pawan Singh,** Pranav Upadhyay, Shivani Chaudhary, Khem B Thapa, AK Dwivedi, Devesh Kumar, Odd–even effect of 7O. m liquid crystal compound series studied under the effect of the electric field by density functional theory (DFT) methods, *The European Physical Journal Plus (EPJ P),* 135(5), 388, 2020.
14. Roshni Maurya, **Pawan Singh,** Prabal P. Singh, Krishan Pal, Girijesh N Pandey, Khem B. Thapa, Absorption and bandwidth properties of graphene based 1D-photonic crystal for THz devices, *AIP Conference Proceedings*, 2220(1), 020084, 2020.
15. Asish Kumar, **Pawan Singh,** Krishan Pal, Narendra Kumar, and Khem B. Thapa, Broadband reflector of 1D photonic crystal containing

TiO_2/SiO_2 material at visible region, *AIP Conference Proceedings*, 2220, 020068 (2020).

16. Narinder Kumar, **Pawan Singh,** Khem B. Thapa, Devesh Kumar, Molecular spectroscopy and adverse optical properties of N-(p-hexyloxy-benzylidene)–p-toluidine (HBT) liquid crystal molecule studied by DFT methodology, *IOP SciNotes*, 1(1), 015202, 2020.
17. Narinder Kumar, **Pawan Singh,** Shivani Chaudhary, Khem B. Thapa, Pranav Upadhyay, Devesh Kumar, Spectroscopy Exiting behind the Electro-Optical Properties with an Even-Odd Effect of nCB Liquid Crystal Molecules: A Theoretical Approach, Acta Physica Polonica A, 137, 1135, 2020.
18. Asish Kumar, **Pawan Singh**, Khem B. Thapa, Study of super absorption properties of 1D graphene and dielectric photonic crystal for novel applications, *Opt. Quan. Electronics*, 52, 1, 2020.
19. Narinder Kumar, Shivani Chaudhary, **Pawan Singh,** Khem B. Thapa, Devesh Kumar, Electro-optical odd-even effect of APAPA liquid crystal molecules studied under the influence of an extraneous electric field (THz): A theoretical approach, *J. Mol. Liq.,* 318, 114254, 2020.
20. Narinder Kumar, **Pawan Singh**, Khem B. Thapa, and Devesh Kumar, Electro-optical effect of the nCOOCB liquid crystal molecules under the terahertz (THz) frequency range: A theoretical approach, *Journal of Physical Science (Accepted),* 2020.
21. Narinder Kumar, **Pawan Singh**, Khem B. Thapa, and Devesh Kumar Odd-Even effect observed in the electro-optical properties of the homologous series of HnCBP liquid crystal studied under the impact of the electric field: A theoretical approach, *Iranian Journal of Mathematical Chemistry (Accepted),* 2020.

Papers presented in International Conferences/Proceedings

1. Poster Presentation in **"International Conference on Structure and Dynamics of Biomolecules (SDBM-2017)"** during 27th Jan. -2017 to 28th Jan.- 2017, held at Department of Physics, DDU Gorakhpur University, Gorakhpur, Uttar Pradesh.

2. Poster Presentation in **"24th National Conference on Liquid Crystals"** during 11-13 October, 2017 held at Department of Chemical Sciences, IISER Mohali, Punjab **(First Best Poster Presentation Award)**.
3. Poster presentation in the National Seminar held on **"Nano Science and Nano Biotechnology**" during February 25-26, 2017, organized by D. A. V College Kanpur, U. P. **(First Best Poster Presentation Award)**.
4. Poster presentation, in **"4th Lucknow Science Congress (LUSCON-2017)"** during March 03-04, 2017 held at BBA University, Lucknow, (UP) INDIA.
5. Poster presentation, in **"International Conference on Nanoscience and Nanotechnology (ICNN-2017)"** during September 22-24, BBAU, Lucknow, Uttar Pradesh.
6. Poster presentation in the National Symposium held on **"Multidimensional Aspect of Spectroscopy"** during November 17-18, 2017, in D. D. U Gorakhpur (UP).
7. Attended the National Seminar held on **"CSIR-National botanical research institute, Lucknow"** during November 20, 2017, organized by S. J. N. P. G. College Lucknow (UP).
8. Oral presentation in the International Conference held on **"Science and Tech. for sustainable future (NISC-2018)"** during January 10-11, 2018, organized by B. B. A. U. Lucknow (U.P).
9. Oral presentation in the National Conference held on **"Smart Materials, Devices, and sustainable tech. (SMDST-2019)"** organized by M. M. M. University of tech. during March 15-16, 2018 (UP).
10. Poster Presentation in "**National Conference on Soft matter (NCSM-2018)"** during 27th March 2018 to 28th March 2018 held at Department of Physics DDU University, Gorakhpur, Uttar Pradesh.
11. Poster Presentation in **"International Conference on Chemical Sciences: National and Global Prospective"** during 29th October 2018 to 31th October 2018 held at Department of Chemistry, Lucknow Christian College, Lucknow, Uttar Pradesh.

12. Oral Presentation in **"National Symposium on Advanced Material Science"** during 7-8 December, 2018 held at Department of Physics, DDU Gorakhpur University, Gorakhpur, Uttar Pradesh.
13. Oral Presentation in **"25th National Conference on Liquid Crystals"** during 19-21 December, 2018 held at Centre of Material Sciences, University of Allahabad, Prayagraj, Uttar Pradesh.
14. Poster Presentation in **"ANVESHAN"** during 16th to 17th January 2019 held at NIFTEM, Sonipat, Haryana.
15. Poster Presentation in **"National Conference on Advances in Materials Science"** during 21-22 February, 2019 held at Department of Physics, Marwar Business School, Gorakhpur, Uttar Pradesh.
16. Oral Presentation in **"National Conference on Smart Materials, Devices and Sustainable Technologies"** during 15-16 March, 2019 held at MMM University of Technology, Gorakhpur.
17. Participated in **"Workshop on Advances in Optics and Photonics"** held at School of Physics, University of Hyderabad, during 17-23th March 2019.
18. Poster Presentation in **"National Conference on Innovations in Applied Science and Engineering"** held at Dr B R Ambedkar National Jalandhar, during 27-28th April 2019.
19. Paper Presentation in **"Workshop on Computational Physics in Applied Research"**, held at Department of Applied Physics, Gautam Buddha University, Noida, during 25-27th July, 2019.
20. Poster Presentation in **"International Conference on Condensed Matter and Applied Physics"** during 14th to 15th October 2019 held at Govt. Engineering College, Bikaner, India.
21. Poster Presentation in "**Student Conference on Optics and Photonics (SCOP-2019)"** during 24-26 September, 2019 held PRL Ahmedabad.
22. Poster Presentation in **"International Conference on Ultrasonics and Material Science for Advanced Technology (ICUMSAT-2019)"** during 16th to 18th November 2019 held at VBSP University, Jaunpur, 222003.

23. Participated in "**Two Dimensional Materials for Diverse Applications"** on 23 May, held at Cambridge Institute of Technology, Bengaluru, 560036.

24. Participated in **"Lecture Series on Recent Advances in Fundamental and Applied Physics"** during 10^{th} to 14^{th} June 2020 held at Department of Physics, University of Science and Technology, Meghalaya, 793101.

25. Paper Presentation in **"International e-Conference on Recent Advances in Physics & Materials Science"** 2020 during 9^{th} to 10^{th} July 2020 held at Kurseong College, Darjeeling, West Bengal, 734203.

ABSTRACT

Isotropic material is an special class of anisotropic materials which show same dielectric indices in all directions. The anisotropic molecules of the materials have different dielectric indices in different directions and hence such materials possess dielectric permittivity in tensor form like liquid crystals (LCs). LCs has molecular orientation dependent dielectric tensor which tunes with external fields. The field dependent dielectric tensor of anisotropic molecules regulates the optical transmission; correspondingly the transmission properties of 1-D periodic structure with anisotropic molecules or materials which tunable optical characteristics with applied external field. The tunable properties are very useful in electro-optical and photonic devices. Besides LCs, various materials also have anisotropic molecules which could be used in various photonic devices and to study the optical properties of such materials various theoretical methods are available.

Chapter 1 presents the basic introduction of electro-optics and a brief history of LCs. This chapter also describes the types of LCs and their coupling with electric fields. By the study the total free energy of any type of LCs and coupling with the applied electric field, the electro-optical characteristics can be determined. The literature survey of the liquid crystals is the main part of this chapter that presents the brief history of the electro-optical properties of LCs and the photonic crystals with LCs, and the various types of liquid crystals in the photonic applications are discussed. Besides this, the brief studies of the photonic crystals are also included in this chapter, which suggests the basic motivation to work in this field.

Chapter 2 deals with the theory and possible mathematical formulation to investigate the optical properties of photonic crystals using materials such as liquid crystals, $LiNbO_3$, graphene, etc. The given possible mathematical formulations are based on Maxwell's equations and Bloch's theorem; the solutions of such wave equations describe the interaction of the electromagnetic wave with the material. The mathematical methods, plane wave expansion (PWE) method, finite element method (FEM), finite difference time domain method (FDTD), and transfer matrix method (TMM) are briefly described. In the whole thesis, we have adopted TMM for the

study of transmission, reflection, and absorption characteristics of the 1-DPC containing the anisotropic material as a defect because one-dimensional periodic structures are easy to fabricate using modern advanced thin-film technology.

Chapter 3 introduces the interaction of electromagnetic waves with nematic liquid crystals (PAA) and this interaction has obtained a relation between liquid crystals director for increasing and decreasing the intensity of the incident wave. After a certain value of intensity, Freedericksz transition, the molecules show orientation/reorientation for both intensities, this leads to hysteresis in the process. Further, we have used NLC as a defect layer in the 1-DPS of glass/Si materials and calculated the transmission properties at different orientation angles of the NLC layer. The hysteresis of the LCs for the different wavelengths has been also calculated. Again, we have used a defect layer liquid crystal embedded with graphene layers in the 1-DPS and calculated the transmission and absorption properties of the defect peaks by using TMM. The effect of the periodicity of photonic crystals on the transmissions is also included in the chapter.

Chapter 4 gives the study of tunable transmission properties of 1-DPS of SiO_2/TiO_2 dielectric materials with a defect layer $LiNbO_3$ embedded with LC layers with at different parameters using the 4x4 Barreman matrix method. The optical properties have been calculated at different temperatures, incident angles, voltages, and orientation angles for the TE and TM modes. The transmissions of terminal wavelengths through the considered structure have been also calculated in this chapter. Such periodic structures show switching behavior at certain suitable parameters of considered anisotropic materials, which may be used, in many electro-optical devices.

Chapter 5 illustrates the dielectric property of LC-based nanocomposite (NC) of E7 with silver nanoparticles (Ag-NPs) of different sizes at different filling fractions. The chapter includes the transmission properties of 1-DPS of TiO_2/SiO_2 materials with the defect of NC at different sizes and filling fractions of Ag-NPs with different orientations of the molecules. Surface plasmon supported optical devices show novel applications. The optical properties have been calculated using TMM for the 0^o and 90^o orientations of the molecules and different temperatures. The considered periodic

structure with surface plasmon property may be used to study the optical properties of various materials for electro-optical applications.

Chapter 6 gives brief conclusions and future prospects of the thesis. This chapter discusses the basic idea of the applications of anisotropic molecules of various LCs, with LNO and graphene materials in the field of photonics, spintronics, and quantum computers

LIST OF FIGURES

LIST OF TABLES

LIST OF ABBREVIATIONS AND SYMBOLS

EMWs	Electromagnetic waves
η_{ij}	Impermeability tensor
ε	Dielectric permittivity
μ	Magnetic permeability
LC	Liquid crystal
NLC	Nematic liquid crystal
CLC	Cholesteric liquid crystal
χ	Electric susceptibility
χ^m	Magnetic susceptibility
K_1, K_2, K_3	Frank elastic constants
ϕ	Director tilt angle
E_F	Threshold electric field
ξ	Azimuthal angle
FLC	Ferroelectric liquid crystal
Q_B	internal wavenumbers for bend transitions
Q_T	internal wavenumbers for twist transitions
PC	Photonic crystal
PBG	Photonic band gap
1-DPC	One-dimensional photonic crystal
2-DPC	Two-dimensional photonic crystal
3-DPC	Three-dimensional photonic crystal
TMM	Transfer matrix method
FDTD	Finite difference time domain
FEM	Finite element method
PWE	Plane wave expansion
BPM	Beam propagation method
EBG	Electronic band gap
q_o	Pitch wave vector
p_0	Initial pitch of cholesteric liquid crystal

κ_{el}	Elastic constant of Smectic-C phase
n_e	Extraordinary refractive index
n_o	Ordinary refractive index
θ	Incident angle of electromagnetic wave
TE	Transverse electric
TM	Transverse magnetic
ψ	Column vector of tangential component of electric and magnetic fields
r	Reflection coefficient
t	Transmission coefficient
T	Total transmission
R	Total reflection
$\tilde{\varepsilon}$	Dielectric tensor
$\tilde{\mu}$	Permeability tensor
PAA	Para-azoxy-anisole
ε_a	Dielectric anisotropy,
$\varepsilon_\perp$	Perpendicular component of dielectric permittivity
$\varepsilon_{\|\|}$	Parallel component of dielectric permittivity
σ	Conductivity
ε_{eff}	Effective dielectric permittivity
I	Intensity of electromagnetic wave
I_{fr}	Threshold intensity of electromagnetic wave
1-DPS	One-dimensional periodic structure
NC	Nanocomposite
NP	Nanoparticle
SPR	Surface plasmon resonance
Ag-NPs	Silver nanoparticles

TABLE OF CONTENTS

CHAPTER 1

Introduction

CHAPTER 1

Introduction

1.1 Electro-optics

Electro-optics is a branch of optics in which the optical properties of the materials under the electric field are studied. Certain types of materials possess the variations in orientation and dimension of their ellipsoid index on the application of the electric field. Such material known as electro-optical materials and the process of modification of the ellipsoid index is termed as electro-optic effect. Through the electro-optic effects, the phase and intensity of the electromagnetic waves (EMWs) can be manipulated. The modulations in the phase and intensity of the propagating optical radiation can be used to design the various electro-optical devices.

1.1.1 Electro-optic effect

The transmission of electromagnetic waves (EMWs) in any crystal or material can be defined in the expression of impermeability tensor η_{ij} . The refractive indices and polarizations states can be deliberated by the ellipsoid index reliant on the principal co-ordinates of the crystals as;

$$\frac{x^2}{n_x^2}+\frac{y^2}{n_y^2}+\frac{z^2}{n_z^2}=1 \qquad (1.1)$$

where n_x= refractive index along the principal x-axis, n_y= refractive index along the y-axis, and n_z= refractive index along the principal z-axis in the crystal.

When an electric field operates on the crystal, the impermeability tensor changes and governs the electro-optic coefficients through the electro-optical effect and the modifications in the impermeability tensor can be termed as equation 1.2.

$$\Delta\eta_{ij} = r_{ijk}E_k + s_{ijkl}E_kE_l = f_{ijk}P_k + g_{ijkl}P_kP_l \qquad (1.2)$$

where E, P = electric field, polarization vector in the crystal, r_{ijk}, f_{ijk} = linear electro-optic coefficients, and s_{ijkl}, g_{ikjl}, = quadratic electro-optic coefficients of the crystals. The linear and nonlinear coefficients are related to each other as;

$$f_{ijk} = \frac{r_{ijk}}{\varepsilon_k - \varepsilon_0} \tag{1.3}$$

$$g_{ijkl} = \frac{s_{ijkl}}{(\varepsilon_k - \varepsilon_0)(\varepsilon_l - \varepsilon_0)} \tag{1.4}$$

where ε_l , ε_k = principal dielectric constants of the crystal and the s_{ijkl} is given by;

$$s_{ijkl} = \frac{1}{2}\left(\frac{\partial^2 \eta_{ij}}{\partial E_k \partial E_l}\right)_{E=0} \tag{1.5}$$

The electro-optical coefficients show symmetrical permutations that are related to the crystal symmetry.

$$\begin{aligned} r_{ijk} &= r_{jik} \\ s_{ijkl} &= s_{ijlk} \\ s_{ijkl} &= s_{jikl} \end{aligned} \tag{1.6}$$

1.1.1.1 Linear electro-optic effect

The electro-optic effects are dependent on the strength of the operative electric fields and the intra-atomic field presented within the atoms. When the applied field is smaller in comparison to the field confined within the atom, the quadratic effects are significantly small to neglect and such linear electro-optical effect is known as the Pockels effect [1-3].

In the existence of an external electric field, the ellipsoid index of the crystal is described as equation 1.7.

$$\left(\frac{1}{n_x^2} + r_{1k}E_k\right)x^2 + \left(\frac{1}{n_y^2} + r_{2k}E_k\right)y^2 + \left(\frac{1}{n_z^2} + r_{3k}E_k\right)z^2 + 2yzr_{4k}E_k + 2zxr_{5k}E_k + 2xyr_{6k}E_k = 0 \tag{1.7}$$

where E_k is the factor of the applied electric field along the z-axis. For linear effect, the modification in the impermeability tensor or refractive index of crystal leads to the following equation 1.8 as;

$$\Delta\left(\frac{1}{n^2}\right)_{1,2,3,4,5,6} = \begin{pmatrix} r_{11} & r_{22} & r_{13} \\ r_{21} & r_{22} & r_{23} \\ r_{31} & r_{32} & r_{33} \\ r_{41} & r_{42} & r_{43} \\ r_{51} & r_{52} & r_{53} \\ r_{61} & r_{62} & r_{63} \end{pmatrix} \begin{pmatrix} E_x \\ E_y \\ E_z \end{pmatrix} \tag{1.8}$$

An example of a linear electro-optic effect in the crystal is $LiNbO_3$ (LNO) with an applied electric field and the LNO crystal has 3m symmetry. The electro-optic coefficients for such crystals can be written in matrix form as;

$$\begin{pmatrix} 0 & -r_{22} & r_{13} \\ 0 & r_{22} & r_{13} \\ 0 & 0 & r_{33} \\ 0 & r_{51} & 0 \\ r_{51} & 0 & 0 \\ -r_{22} & 0 & 0 \end{pmatrix} \tag{1.9}$$

With the application of the electric field, the ellipsoid index equation can be presented as equation 1.10, and the refractive indices in x, y, z cartesian system have the linear relation with the applied field as;

$$\left(\frac{1}{n_0^2} + r_{13}E\right)x^2 + \left(\frac{1}{n_0^2} + r_{13}E\right)y^2 + \left(\frac{1}{n_e^2} + r_{33}E\right)z^2 = 1 \tag{1.10}$$

$$n_x = n_0 - \frac{1}{2}n_0^2 r_{13}E \tag{1.11}$$

$$n_y = n_0 - \frac{1}{2}n_0^2 r_{13}E \tag{1.12}$$

$$n_z = n_0 - \frac{1}{2}n_0^2 r_{33}E \tag{1.13}$$

The z-component of the refractive index is equivalent to the extra-ordinary refractive index, however, other refractive indices along x, y components are equivalent to the ordinary index of the crystals. The n_e is extraordinary and n_o is ordinary refractive indices of the electro-optic material. The ordinary refractive index remains constant and independent of the incident angle of EMW, while the extraordinary index is influenced by the propagation angle of the wave, which is given as;

$$n_e(\theta) = \frac{n_e n_o}{\sqrt{n_e^2 \cos^2\theta + n_o^2 \sin^2\theta}} \tag{1.14}$$

Like lithium niobate ($LiNbO_3$), the potassium dihydrate phosphate (KH_2PO_4) also shows the linear electro-optic effect.

1.1.1.2 Quadratic electro-optic effect

The quadratic electro-optic (QEO) effect consists of the higher-order terms of the electric field in comparison to the linear electro-optic (LEO) effect, and this effect can be exhibited by crystals having any symmetry. The Kerr effect is an example of a quadratic electro-optic effect [1-3]. The index equation of the crystals under the electric field for quadratic electro-optic effect in a crystal is given as;

$$\begin{aligned}
&\left(\frac{1}{n_x^2} + s_{11}E_x^2 + s_{12}E_y^2 + s_{13}E_z^2 + 2s_{14}E_yE_z + 2s_{15}E_zE_x + 2s_{16}E_xE_y\right)x^2 \\
&+\left(\frac{1}{n_y^2} + s_{21}E_x^2 + s_{22}E_y^2 + s_{23}E_z^2 + 2s_{24}E_yE_z + 2s_{25}E_zE_x + 2s_{26}E_xE_y\right)y^2 \\
&+\left(\frac{1}{n_z^2} + s_{31}E_x^2 + s_{32}E_y^2 + s_{33}E_z^2 + 2s_{34}E_yE_z + 2s_{35}E_zE_x + 2s_{36}E_xE_y\right)z^2 \\
&+2yz\left(s_{41}E_x^2 + s_{42}E_y^2 + s_{43}E_z^2 + 2s_{44}E_yE_z + 2s_{45}E_zE_x + 2s_{46}E_xE_y\right) \\
&+2zx\left(s_{51}E_x^2 + s_{52}E_y^2 + s_{53}E_z^2 + 2s_{54}E_yE_z + 2s_{55}E_zE_x + 2s_{56}E_xE_y\right) \\
&+2xy\left(s_{61}E_x^2 + s_{62}E_y^2 + s_{63}E_z^2 + 2s_{64}E_yE_z + 2s_{65}E_zE_x + 2s_{66}E_xE_y\right) = 1
\end{aligned} \tag{1.15}$$

where s_{ij} = electro-optic coefficients of the crystal. The obtained index equation is reduced to an unperturbed state without an electric field. A simple example of such an effect is barium titanate ($BaTiO_3$) under the electric field. The $BaTiO_3$ is a ferroelectric crystal, which shows the phase transition at 120^{o}C temperature. The $BaTiO_3$ has acentric nature for the temperature below than the transition temperature (120^{o}C) having a 4mm point group but the crystal is converted into cubic conformation having a m3m point group at below 120^{o}C. The ellipsoid index of the crystal under the electric field is given below;

$$\left(\frac{1}{n^2} + s_{11}E^2 + s_{12}E^2\right)x^2 + \left(\frac{1}{n^2} + s_{11}E^2 + s_{12}E^2\right)y^2 + \left(\frac{1}{n^2} + s_{12}E^2\right)z^2 + 2xys_{44}E^2 = 1 \tag{1.16}$$

With 45^o rotation of the x-y plane, the index ellipsoid is transformed as;

$$\frac{x'^2}{n_{x'}^2}+\frac{y'^2}{n_{y'}^2}+\frac{z'^2}{n_{z'}^2}=1 \tag{1.17}$$

With the condition $(1/n^2) >> sE^2$, the index of ellipsoid reduces into the following equations;

$$n_{x'}=n-\frac{1}{2}n^3s_{44}E^2-\frac{1}{4}n^3(s_{11}+s_{12})E^2 \tag{1.18}$$

$$n_{y'}=n+\frac{1}{2}n^3s_{44}E^2-\frac{1}{4}n^3(s_{11}+s_{12})E^2 \tag{1.19}$$

$$n_{z'}=n-\frac{1}{2}n^3s_{12}E^2 \tag{1.20}$$

Another illustration of the QEO effect is the effect of the electric field on the isotropic media and isotropic materials also show some birefringent characteristics under the applied electric fields. Both linear and quadratic electro-optic (EO) effects are used in various applications in electro-optical devices and also used to study the intermolecular behavior of the crystals under the applied field. The electro-optic coefficients occur in the both electro-optic effect depend on the wavelength of the wave, modulation process, and operating temperature of the material. By determining the phase change of electromagnetic waves and the intensity of the bands, the electro-optic coefficients can be determined.

1.2 Maxwell's equations

Four fundamental Maxwell's equations consisting of electric (E) and magnetic (H) field vectors describe the property of the material through transmission and reflection of EMW. The EMW in the vacuum/space or materials shows interaction with any materials that can be characterized by introducing the terms of magnetic induction and electric displacement vectors of the material. The four fundamental Maxwell's equations are following that is given as;

$$\nabla . D = \rho \tag{1.21}$$

$$\nabla . B = 0 \tag{1.22}$$

$$\nabla \times E = -\frac{\partial B}{\partial t} \tag{1.23}$$

$$\nabla \times H = J + \frac{\partial D}{\partial t} \tag{1.24}$$

where, ρ and J = electric charge density and the electric current density in the material. The above presented Maxwell's equations associate the electricity and magnetism in differential forms. The first differential equation is Coulomb's law which links the electric field distribution with charge distribution. The second differential equation informs the nonexistence of the magnetic monopoles. The third differential equation is Faraday's law which points out that the time-variant magnetic field induces the electric field, and the fourth differential equation is modified Ampere's law by Maxwell, which specifies the formation of the induced magnetic field due to the movement of charges in the material.

To study the electric and magnetic field vectors in any materials, the consecutive equations are given as:

$$D = \varepsilon E = \varepsilon_0 E + P \tag{1.25}$$

$$B = \mu H = \mu_0 H + M \tag{1.26}$$

where ε = dielectric permittivity and μ = magnetic permeability of the material and both are 2-rank tensor; ε_0 = permittivity and μ_0= permeability of the free space or vacuum; P = electric polarization and M= magnetic polarization/magnetization.

1.3 Interaction of electromagnetic wave with anisotropic medium

When an electromagnetic wave interacts with anisotropic media, the phase velocity relies on the propagation direction and polarization states of the waves in the medium. For certain propagation direction, two eigen waves are having eigen phase velocities and polarizations. The electromagnetic wave, which has polarizations in analogous to certain directions, is transmitted through the anisotropic medium [1-4]. An electromagnetic wave of frequency ω interacts with anisotropic medium with electric and magnetic fields, and the waves of the fields are in plane wave forms which are given as;

$$E \exp(i\omega t - ik \cdot r) \tag{1.27}$$

$$H\exp(i\omega t - ik\cdot r) \tag{1.28}$$

where $k = n\omega\hat{s}/c$, k is the wave vector and $\hat{s}$ is a unit vector in the direction of wave propagation; n is the refractive index and c is speed of light. Using the equations 1.27 and 1.28, the Maxwell's equations 1.23 and 1.24 can be re-written as;

$$k\times E = \omega\mu H \tag{1.29}$$

$$k\times H = -\omega\varepsilon E \tag{1.30}$$

On solving above equations, we found equation 1.31 as;

$$k\times(k\times E)+\omega^2\mu\varepsilon E = 0 \tag{1.31}$$

The uniaxial material has dielectric permittivity as;

$$\varepsilon = \begin{bmatrix} \varepsilon_x & 0 & 0 \\ 0 & \varepsilon_y & 0 \\ 0 & 0 & \varepsilon_z \end{bmatrix} \tag{1.32}$$

Using the above equation 1.32, the equation 1.31 can be written for the uniaxial material as;

$$\begin{pmatrix} \omega^2\mu\varepsilon_x - k_y^2 - k_z^2 & k_xk_y & k_xk_z \\ k_xk_y & \omega^2\mu\varepsilon_y - k_x^2 - k_y^2 & k_yk_z \\ k_xk_z & k_yk_z & \omega^2\mu\varepsilon_z - k_x^2 - k_y^2 \end{pmatrix}\begin{pmatrix} E_x \\ E_y \\ E_z \end{pmatrix} = 0 \tag{1.33}$$

For the non-trival solution of the equation 1.33, the determinant must be zero.

$$\begin{vmatrix} \omega^2\mu\varepsilon_x - k_y^2 - k_z^2 & k_xk_y & k_xk_z \\ k_xk_y & \omega^2\mu\varepsilon_y - k_x^2 - k_y^2 & k_yk_z \\ k_xk_z & k_yk_z & \omega^2\mu\varepsilon_z - k_x^2 - k_y^2 \end{vmatrix} = 0 \tag{1.34}$$

The solution of the equation 1.34 leads to two equations as;

$$\underbrace{\left(\frac{k_x^2+k_y^2}{n_e^2}+\frac{k_z^2}{n_0^2}-\frac{\omega^2}{c^2}\right)}_{i}\underbrace{\left(\frac{k^2}{n_0^2}+\frac{\omega^2}{c^2}\right)}_{ii} = 0 \tag{1.35}$$

The normal surface considering equation 1.35 consists of two surfaces of revolution: (i) sphere and (ii) ellipsoid. The two planes cross each other at two points on the z-axis for uniaxial crystal is shown in figure 1.1.

If the z-axis is only the optic axis, then the materials belong to the uniaxial e.g. ice, quartz, BeO, ZnS, rutile, $LiNbO_3$, $BaTiO_3$. If all three principal indices are the same and two planes are reduced to a single sphere, then the material belongs to the isotropic e.g. NaCl, CdTe, Diamond, GaAs. If the normal surfaces have two optical axes and all the three principal indices are different, then the material is termed as biaxial e.g. Mica, Topaz, $NaNO_2$, SbSI, etc. as shown in figure 1.1(a).

If $n_e > n_o$ for the uniaxial crystals, then the crystals have positive anisotropy; and if $n_e < n_o$ for uniaxial crystals, then the crystals have negative anisotropy. Besides these described examples of the uniaxial and biaxial crystals, the liquid crystals (LCs) are also found in the uniaxial and biaxial conformations and have various novel and interesting electro-optical application with the nonlinear properties, which can be used to design the nonlinear electro-optical devices.

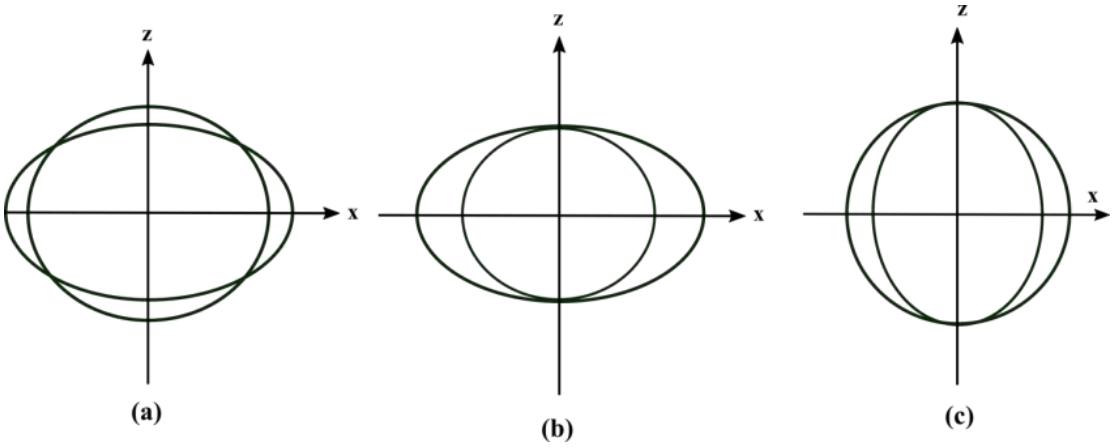

Figure 1.1: Crossing of two normal surfaces with the x-z plane; (a) biaxial, (b) positive uniaxial, and (c) negative uniaxial crystal.

1.4 Liquid crystal

In 1888, German botanist Reinitzer [5] discovered the liquid crystal (LC) by observing a phenomenon processing in the melting of cholesteryl benzoate and cholesteryl acetate. He noted the compounds transforming the state which was depending on the temperature; and crystals show a cloudy state at 145.5^{o}C and then changed into the clarified state at 178.5^{o}C temperature. Hence, the double melting point behavior in the cholesteryl systems was reported and the appearance of different colors depending on the varying temperature of the compound was illustrated which shows the selective reflections of the circularly polarized light by crystals. Reinitzer

also observed that the crystals show colors at low temperatures while the blue phase of the compound is shown at high temperatures. Although, Renitzer discovered the liquid crystals, Lehmann introduced the term “liquid crystal” first time [6].

Generally, liquid crystals (LCs) are organic materials, and exhibit different mesophases, so, the liquid crystals are also termed as mesogens. LC is an intermediate state between the pure liquid phase and the perfect crystalline phase, as shown in figure 1.2. LCs exhibit both types of characteristics as they flow like liquid phase and crystal phase that depends on the temperature. Such organic LCs are found in different types: thermotropic, polymerics, and lyotropic. Depending on the temperature, component, concentration, and so on, the thermotropic liquid crystals show nematic, cholesteric, smectic, and ferroelectric phases [7-10].

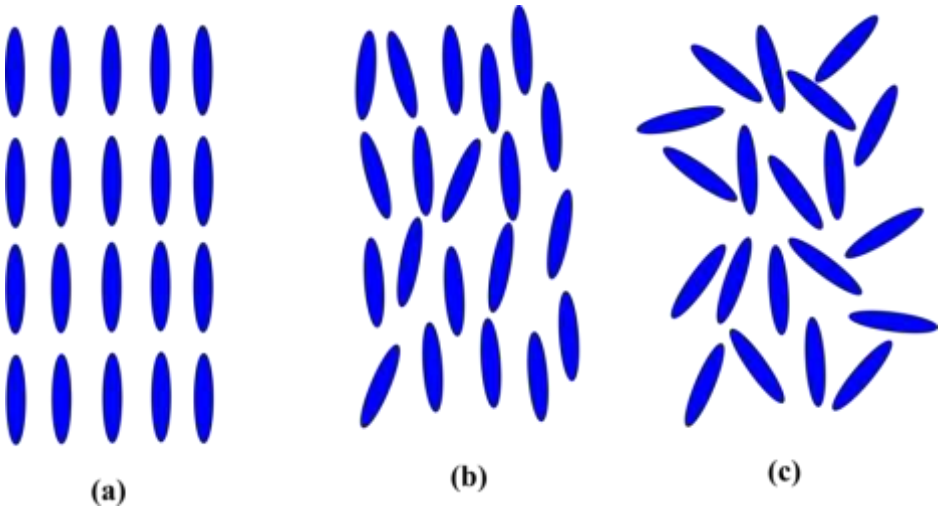

Figure 1.2: The phase of crystal: (a) pure crystalline phase, (b) liquid crystal phase, (c) pure liquid phase.

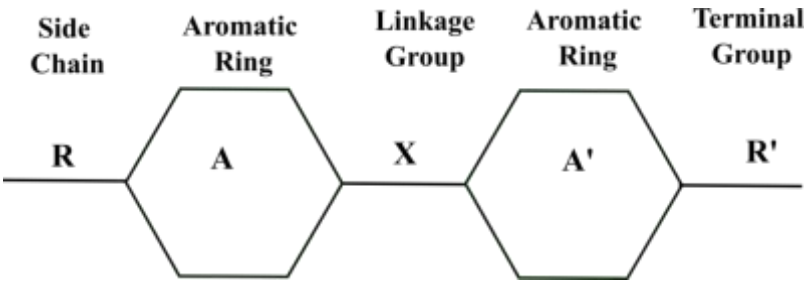

Figure 1.3: Basic structure of liquid crystal consisting of the side chain, linkage, terminal group, and aromatic rings.

Basically, LCs are aromatic materials and benzene derivatives, which contain the benzene rings in their chemical structure as an important signature. The general structure of LC is shown in figure 1.3, and it contains a side chain R, aromatic rings A or A', a linkage group X, and a terminal group R'. A simple example of the liquid crystal is 5CB liquid crystal, which is shown in figure 1.4.

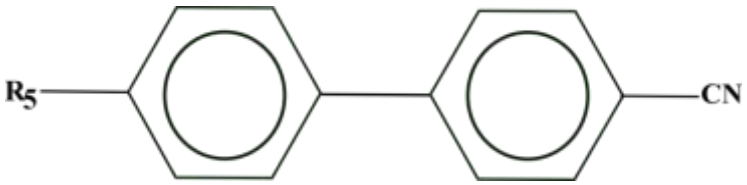

Figure 1.4: Structure of 5CB (pentylcyanobiphenyl) liquid crystal.

It has an alkyl chain (R_5) and cyano group (-CN) as terminal in the molecular structure. The example of a side chain and a terminal group can be alkyl or alkoxy or any other groups like alkyl carbonate or nitro or cyano group etc. The linkage group can be bonds or groups like azoxy, ester, and tolane, etc. Alongside the benzene-derivative liquid crystals, LCs are also found in other forms e.g. organometallics, heterocyclics, sterols, fatty acids. Heterocyclic liquid crystals contain pyrimidine, or pyridine, or other similar groups instead of the aromatic benzene ring in the structure [7, 11].

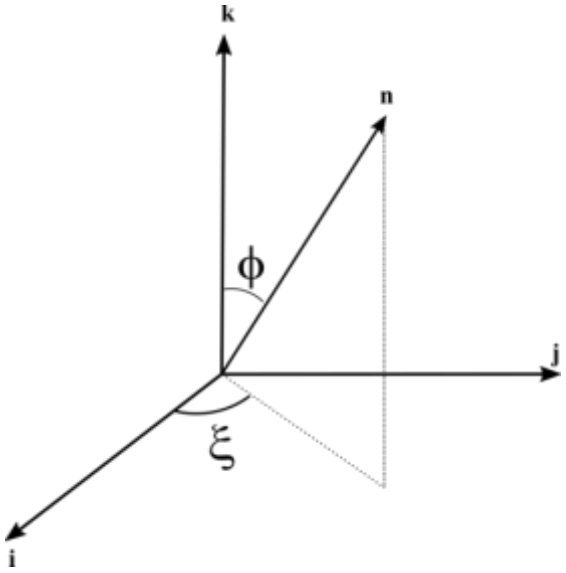

Figure 1.5: Representation of liquid crystal director in i, j, k axes.

The material parameters and optical properties of LCs like dielectric constant, viscosity, anisotropy, absorption spectrum, optical nonlinearity, and so on depend on

the synthesis and engineering process of LCs. The stability in the crystal structure depends on the linkage groups, and the azo, azoxy, ester-based liquid crystals are stable while Schiff based liquid crystals are unstable [7, 10, 11].

1.4.1 Types of liquid crystals

Liquid crystals are found in the three types depending on the physical and chemical properties as well as the temperature. The lyotropic, polymeric, and thermotropic are three types of liquid crystals and a brief introduction has been given in the following sections.

1.4.1.1 Lyotropic Liquid crystal

Lyotropic liquid crystals (LLCs) are created by the solution of suitable concentration dissolved in a solvent. The most common example of lyotropic systems is a mixture of water with soaps, or detergents, lipids, etc. The effecting parameter of such a system is the concentration of the solvent. The physical properties of such systems vary with the temperature and the composition of the materials. So, the system can show one, two, or three-dimensional positional orders. An example of such a system is shown in figure 1.6. The lyotropic liquid crystals are mostly used in biological applications [7,10,11].

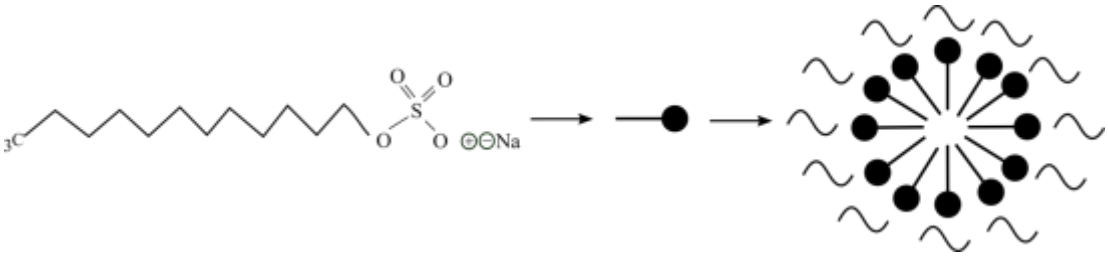

Figure 1.6: Formation of sodium dodecyl sulfate in micelles arrangement.

1.4.1.2 Polymeric liquid crystal

Polymeric liquid crystals are generally polymers and found in different categories depending on the flexibility. The most common examples of the polymer are vinyl type polymer, polypeptide chains, and Kevlar polymers. These polymers are dependent on the flexibility limit; vinyl type shows the most flexibility, polypeptide chain type shows the most rigid nature while Kevlar type (figure 1.7) shows semi-rigid behavior. In point of view of optical storage device applications, polymer liquid crystals can be branched into the diverse types depending upon the viscosity of the

polymers. Such polymer liquid crystals also can be classified that depend upon the arrangement of the monomers in the polymer structures.

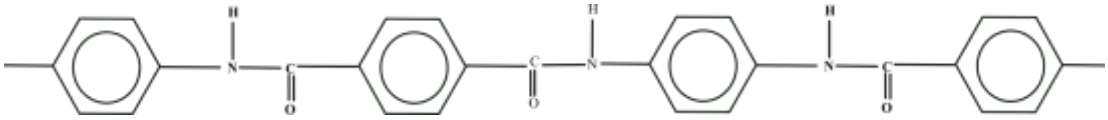

Figure 1.7: Molecular structure of Kevlar type polymer.

The important chain of the polymer structures can be made of rigid polymers or groups by attaching side-by-side and joint by a flexible chain or group in the final structure [7,10,11].

1.4.1.3 Thermotropic liquid crystal

As the termed thermotropic suggests the optical properties, and its nature depends on the applied thermal effects. They are the most used liquid crystals in different optical devices of the linear as well as nonlinear applications. The thermotropic liquid crystals are mostly rigid rod-shaped molecules interacting with each other, which forms unique ordered patterns, and the phase of such liquid crystals changes with the applied temperature. Depending upon the physical parameter like molecular distribution function, short or long-range interaction, etc., such thermotropic liquid crystals show different phases: nematic, cholesteric, smectic.

By observing the arrangement of the molecules, the phase of the liquid crystals can be identified as nematic or cholesteric. In the nematic phase, the position of the molecules can be random but arranged and aligned in the proper direction marked by a unit vector $\hat{n}$, which is called as the director axis. All the physical and optical properties of nematic LCs are identical in both the positive and negative direction of the directors and these liquid crystals show centrosymmetric nature. On the interaction of X-rays, no diffraction peaks are observed for the nematic type because such liquid crystal does not have any perfect crystalline nature but it has the partially patterned structures, which is affected by the temperature and the molecular parameter [7, 10-12].

Cholesteric liquid crystals (CLCs) show the arrangement of its molecules in helical or chiral patterns and CLCs have all physical properties like the nematic phase as shown in figure 1.8. Due to chiral nature, such liquid crystals are also known as chiral liquid

crystals. A simple example of chiral material is cholesterol ester, which forms a cholesteric liquid crystal when the cholesterol ester is mixed with nematic liquid crystal [7,10,11].

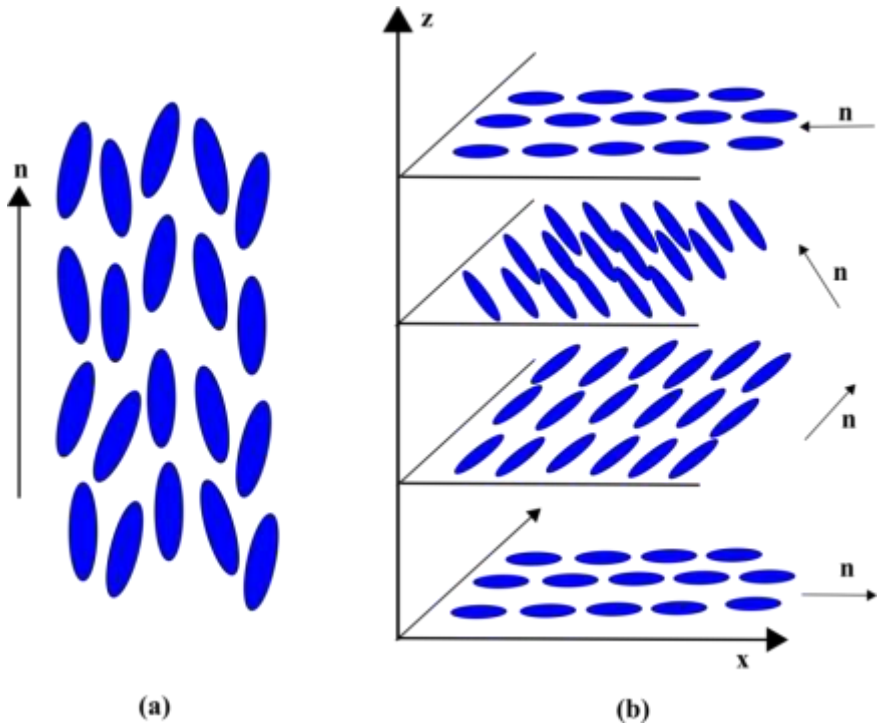

Figure 1.8: Phase of the liquid crystals: (a) nematic, (b) cholesteric phase.

Another phase of the liquid crystal is smectic phase and has a complicated structure as shows the positional order of the molecules, which also has a certain ordered pattern in the whole structure. The smectic liquid crystals are also found in three types depending upon the order and arrangement of the molecules; smectic A, smectic C, and smectic C*.

The structure of smectic types can be studied by the layer-by-layer system. In the smectic-A type, the position of molecules in each layer can be random but they are well ordered in a certain direction with long axis normal to the plane of the layer. With rotational symmetry, the smectic-A has uniaxial behavior while the smectic-C phase has biaxial nature along with a normal tilted long axis. Smectic–C* liquid crystals have a tilted director axis and rotate around the z-axis (normal to layer). Besides all phases of liquid crystals, such liquid crystals possess spontaneous electric polarization in the molecules, which show a breakdown of the reflection symmetry due to chiral symmetry.

Besides the above-mentioned phases, the LCs have more phases like smectic G, H, I,… and blue phase. The major liquid crystals can be prepared by the mixture of different liquid crystals and the mixed liquid crystal has enhanced the optical properties (along with anisotropy, viscosity, dielectric constant) than their parent liquid crystals, e.g. E7 is the eutectic composition of the four different LCs and has enhanced optical characteristics. The mixing of liquid crystals also shows tremendous applications in optical device applications. All physical and electronic properties of the chemically interact with each other. Other types can be classified based on doping of dye in LCs and polymer containing LCs. By doping of the appropriate dye in the liquid crystals, the linear and nonlinear responses of the liquid crystals could be modified. The absorption properties of liquid crystals in a certain range of wavelength get enhanced due to dissolved dye in the liquid crystal and wavelength regions can be changed by the fluctuations in the orientations, and the physical changes in the dye molecules. Such liquid crystals also show the guest-host system that is widely used in the linear and nonlinear electro-optical and storage applications. In the dye-doped liquid crystal, the appropriate concentration is dissolved in the liquid crystal while some LC droplets of micro-size are dispersed in the polymer, and such arrangement is called polymer-dispersed LCs (PDLCs). The optical characteristics of such PDLCs are dependent on the interaction of the polymers with LCs, which induce the large scattering of light. Generally, the molecules of LCs are randomly orientated in the nonappearance of the electric field, but the droplet shows the isotropic nature in presence of an electric field. With changing the phase, the optical indices of the liquid crystals get affected and tune the optical characteristics of the system. The PDLCs can be used in optical devices e.g. one-dimensional photonic crystals, lasing devices, etc. [13, 14].

1.4.2 Order parameter and free energy

As we know that LCs are the intermediate state of the properties that lie between liquids and solids. Therefore, to define the physical properties and molecular arrangement in LC, a physical parameter known as order parameter (S) is used to study the phase of LCs. The phases of the LCs depend on the temperature. Therefore, the order and arrangement of the molecules also depend on the temperature. Besides this, the order parameter also depends on the position coordinates of the molecules. If

we consider the $\hat{k}$ longer axis of the molecule as the reference, then the macroscopic order parameter can be defined as;

$$S = \frac{1}{2}\left\langle 3(\hat{k}\cdot\hat{n})(\hat{k}\cdot\hat{n}) - 1 \right\rangle \tag{1.36}$$

$$S = \frac{1}{2}\left\langle 3\cos^2\phi - 1 \right\rangle \tag{1.37}$$

where ϕ is the angle between the director axis and molecular axis of the molecule. The average over the ensemble is considered, so, the order parameter is the microscopic quantity [11].

A more general form of the order parameter also can be represented as;

$$S_{ij} = \frac{1}{2}\left\langle 3(\hat{n}\cdot\hat{i})(\hat{n}\cdot\hat{j}) - 1 \right\rangle \tag{1.38}$$

With the reference of the figure 1.5, i, j, and k are the unit vectors along the molecular axes. The other diagonal components of order parameter are presented as;

$$S_{ii} = \frac{1}{2}\left\langle 3\sin^2\phi\cos^2\xi - 1 \right\rangle \tag{1.39}$$

$$S_{jj} = \frac{1}{2}\left\langle 3\sin^2\phi\sin^2\xi - 1 \right\rangle \tag{1.40}$$

$$S_{kk} = \frac{1}{2}\left\langle 3\cos^2\phi - 1 \right\rangle \tag{1.41}$$

The value of the tensor S is zero because the sum of the three diagonal elements is zero, i.e. $S_{ii}+S_{jj}+S_{kk}=0$.

The order parameter is the microscopic quantity as well as a directional dependent. So, it can be transformed into the macroscopic quantity by representing the order parameter in terms of the anisotropy of the LC's parameters like electric or magnetic susceptibilities. For example, the macroscopic order parameter can be expressed consisting of dielectric components and the dielectric anisotropy [7, 11, 15] as;

$$Q_{\alpha\beta} = \varepsilon_{\alpha\beta} - \frac{1}{3}\delta_{\alpha\beta}\sum_{\gamma}\varepsilon_{\gamma\gamma} \tag{1.42}$$

For the general case of the uniaxial material $\varepsilon_{\alpha\beta}$ can be represented as;

$$\varepsilon_{\alpha\beta} = \begin{pmatrix} \varepsilon_{\perp} & 0 & 0 \\ 0 & \varepsilon_{\perp} & 0 \\ 0 & 0 & \varepsilon_{\parallel} \end{pmatrix} \tag{1.43}$$

$$Q_{xx} = Q_{yy} = -\frac{\Delta\varepsilon}{3} \tag{1.44}$$

$$Q_{zz} = \frac{2\Delta\varepsilon}{3} \tag{1.45}$$

where $\varepsilon_{\alpha\beta}(\equiv \varepsilon_{\perp}\delta_{\alpha\beta} + \Delta\varepsilon n_{\alpha}n_{\beta})$ and $\Delta\varepsilon(= \varepsilon_{\parallel} - \varepsilon_{\perp})$ are the tensor dielectric permittivity and anisotropy of the liquid crystals, respectively and α, β are dummy indices for tensor representation. The dielectric constant ε is equal to $\varepsilon_{\parallel}$ or $\varepsilon_{\perp}$, it depends on the direction of the optical field, i.e. the parallel or normal (perpendicular) to the director axis $\hat{n}$ of LC. Similarly, the order parameter is also described with consisting of electric (χ) and magnetic (χ^{m}) susceptibilities as;

$$\chi_{\alpha\beta} \equiv \chi_{\perp}\delta_{\alpha\beta} + \Delta\chi n_{\alpha}n_{\beta} \tag{1.46}$$

$$\chi^{m}_{\alpha\beta} \equiv \chi^{m}_{\perp}\delta_{\alpha\beta} + \Delta\chi^{m} n_{\alpha}n_{\beta} \tag{1.47}$$

Now, the order parameter is also can be represented in terms of the magnetic or electric susceptibility.

$$Q_{\alpha\beta} = \chi^{m}_{\alpha\beta} - \frac{1}{3}\delta_{\alpha\beta}\sum_{\gamma}\chi^{m}_{\gamma\gamma} \tag{1.48}$$

As we know that the order parameter is also dependent on the type of interactions between the molecules, i.e. short-range or long order. The order parameter is one for the perfectly crystalline state and zero for the pure liquid state. The short-range order exists in the pure isotropic phase, i.e. the molecules show intermolecular interactions with one-another within short-range distances. So, the phase transition of liquid crystals depends on the temperature, which gives the isotropic phase at the clearing temperature with short-range correlation. In the long-range correlation, the molecules show minor disturbance in the orientation of the director axis. The average of the order parameter over the whole ensemble gives the existence of long-range order.

1.5 Free energy of the liquid crystal

The free energy of the liquid crystals is needed from the random order of molecules to uniformly crystalline order of molecules. This energy is also called free energy density. In this section, we will study the free energy density in nematic liquid crystals.

1.5.1 Nematic liquid crystal

In all existing phases of the LCs, the nematic liquid crystal (NLC) is mostly investigated liquid crystal in electro-optics. The optical properties of NLCs can be studied by the theoretical formulation of the hydrodynamics due to the dual nature of the NLCs. In such liquid crystals, all the molecules aligned in a proper direction are called as director axis $\hat{n}(r)$, which is varied with the applied external field on the liquid crystals. The temperature-dependent order parameter can be written as;

$$S_{\alpha\beta} = S(T)\left(n_\alpha n_\beta - \frac{\delta_{\alpha\beta}}{3} \right) \tag{1.49}$$

where S(T), n_α, n_β, $\delta_{\alpha\beta}$ are temperature-dependent order parameter, refractive index, depending on the dummy indices, respectively. With the external electric field, the NLC shows three possible deformations: twist, splay, and bend as shown in figure 1.9. In twist deformation, the center of gravity is fixed but the molecules only show orientation in the direction of induced torque. Therefore, the change in elastic energy is small. In the splay and bend deformations, the liquid crystals show the changes in the director axis and also slow flow coupling with the director axis. All the possible deformations depict the variation of the director, so the free energy involves spatial derivatives related to the director axis of the liquid crystals.

The free energy formulations were first established by Frank [15], and he gave the free energy terms depending on the deformations, i.e. splay: $f_1 = \frac{1}{2} K_1 (\nabla \cdot \hat{n})^2$, twist: $f_2 = \frac{1}{2} K_2 (\hat{n} \cdot \nabla \times \hat{n})^2$ and bend: $f_3 = \frac{1}{2} K_3 (\hat{n} \times \nabla \times \hat{n})^2$, where, K_1, K_2, K_3 are the elastic constants having an order of 10^{-6} dyes in the CGS units.

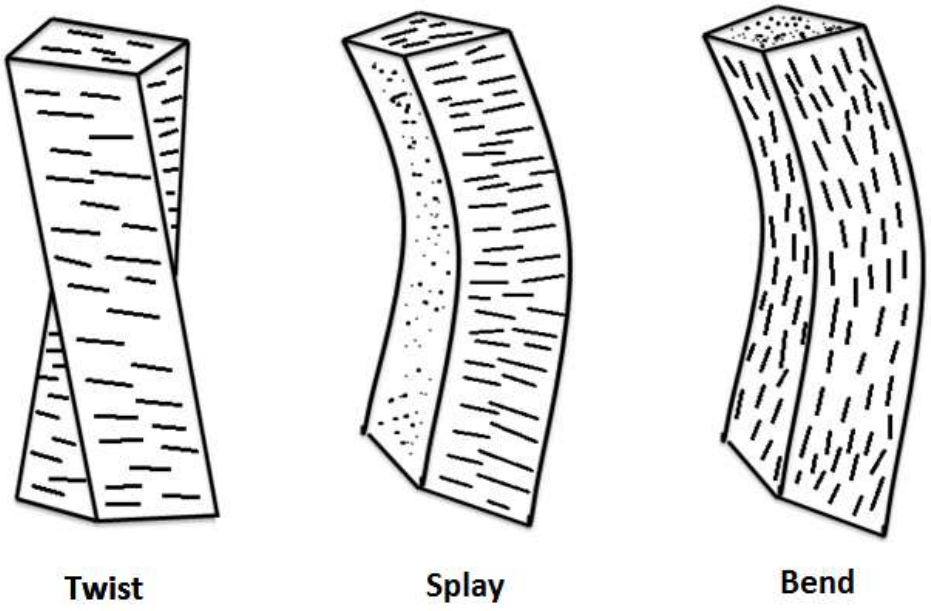

Figure 1.9: Representation of twist, splay, and bend deformations in the liquid crystals.

For MBBA (p-methoxybenzylidene-p'-butylaniline) LC, the values K_1, K_2, and K_3 are, 5.8x10^{-7}, 3.4 x10-7, and 7x10^{-7} dyne. If the all-possible deformations possess in the liquid crystals then the total deformation energy can be calculated as;

$$F_d = \frac{1}{2}K_1(\nabla \cdot \hat{n})^2 + \frac{1}{2}K_2(\hat{n} \cdot \nabla \times \hat{n})^2 + \frac{1}{2}K_3(\hat{n} \times \nabla \times \hat{n})^2 \qquad (1.50)$$

For the one-constant (K_1=K_2=K_3=K) approximation, the equation 1.50 reduced to the equation 1.51 as;

$$F_d = \frac{1}{2}K[(\nabla \cdot \hat{n})^2 + (\nabla \times \hat{n})^2] \qquad (1.51)$$

To investigate the observation of Freedericksz transition in LC, we must include the interaction of the boundary. So, surface interaction energies must be considered in the total distortion energy of LCs. So, the total free energy density can be written as;

$$F_d' = F_d + F_{surface} \qquad (1.52)$$

For the equilibrium conformation of the liquid crystals, the free energy must be minimized. The minimization of the total energy of liquid crystal also depends on the boundary interacting with liquid crystals. For the hard boundary condition, the surface

boundary contribution to the free total energy of the liquid crystals is small. But for the soft boundary condition, the orientation of molecules near the boundary is also affected by the externally applied field. Hence, the types of boundary interactions affect the total dynamics of the LC molecules.

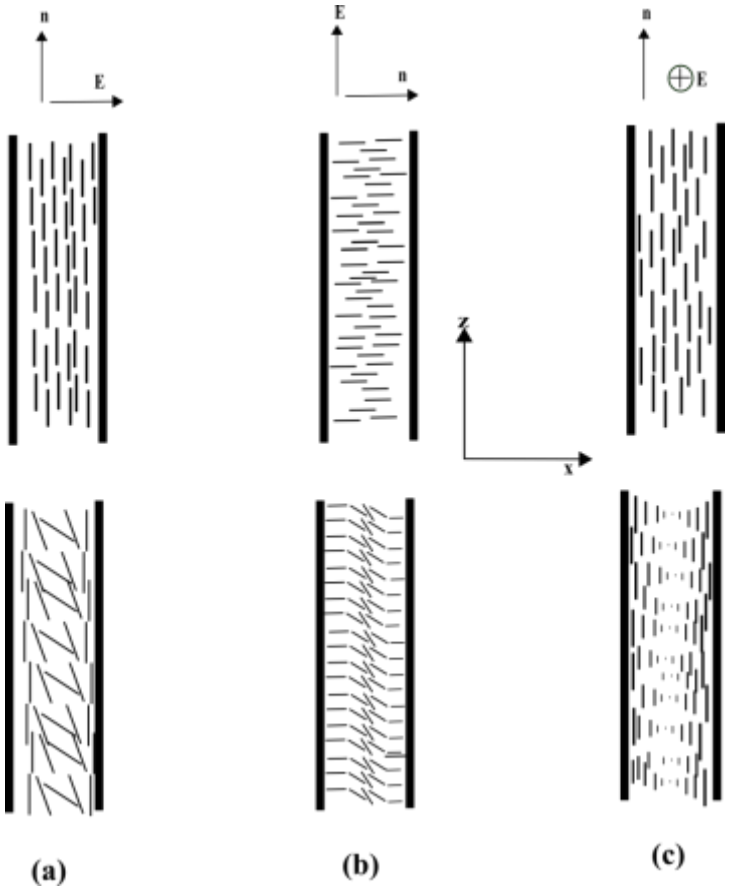

Figure 1.10: Orientations of liquid crystals having different conformations under electric field: (a) Splay (b) Bend, (c) Twist

When the external field is turned on the LC cell, the molecules interact with the external field and orient depending on the geometry of the LCs. The displacement in the cell varies with the electric field as;

$$D = \varepsilon_{\perp} E + (\varepsilon_{\parallel} - \varepsilon_{\perp})(\hat{n} \cdot E)\hat{n} \tag{1.53}$$

So, the interaction energy density is transcribed as;

$$\mu_E = -\int_0^E D \cdot dE = -\frac{\varepsilon_{\perp}(E \cdot E)}{2} - \frac{(\varepsilon_{\parallel} - \varepsilon_{\perp})(\hat{n} \cdot E)^2}{2} \tag{1.54}$$

The first term in equation 1.54 can be neglected due to the absence of orientation dependency. Therefore, the free energy term can be written as:

$$F_E = -\frac{(\varepsilon_{\parallel} - \varepsilon_{\perp})(\hat{n} \cdot E)^2}{2} \tag{1.55}$$

In terms of SI unit, the equation 1.55 can be re-written as;

$$F_E = -\frac{1}{4\pi}\frac{(\varepsilon_{\parallel} - \varepsilon_{\perp})(\hat{n} \cdot \vec{E})^2}{2} \tag{1.56}$$

The total torque produced by the field on the molecules is given as;

$$\Gamma_E = D \times E = (\varepsilon_{\parallel} - \varepsilon_{\perp})(\hat{n} \cdot E)(\hat{n} \times E) \tag{1.57}$$

Similarly, the magnetic torque can also be calculated as;

$$\Gamma_m = M \times H = (\chi_{\parallel}^m - \chi_{\perp}^m)(\hat{n} \cdot H)(\hat{n} \cdot H) \tag{1.58}$$

1.5.1.1 Orientation of the director axis with the flow in the cell

When a strong magnetic field has applied to the LC with a fixed director orientation, then three viscosity coefficients are involved in the orientation process of the director in the cell. These are:

a) When the director $\hat{n}$ is parallel to the velocity gradient along the x-axis (η_1).

b) When the director $\hat{n}$ is parallel to the flow velocity along the z-axis (η_2).

c) When the director $\hat{n}$ is perpendicular to the shared plane along the y-axis (η_3).

The theory of these coefficients was investigated by Miesowicz [16,17], Therefore, these coefficients are known as Miesowicz coefficients. Considering the shear plane of the LCs, the effective viscosity coefficient can be written as;

$$\eta_{eff} = \eta_1 + \eta_2 + \eta_2 \cos^2\theta \tag{1.59}$$

These coefficients can be also related to the Leslie coefficients α_i where i=1,2,3,…. as;

$$\eta_1 = \frac{(-\alpha_2 + \alpha_4 + \alpha_5)}{2} \tag{1.60}$$

$$\eta_2 = \frac{(\alpha_3 + \alpha_4 + \alpha_6)}{2} \tag{1.61}$$

$$\eta_3 = \frac{\alpha_4}{2} \tag{1.62}$$

1.5.1.2 Reorientation of the director axis with the flow of the liquid crystal

When the external field is turned on the LC, the external torque and viscous torque are generated in the system. Therefore, the equation for angular acceleration can be written in terms of the moment of inertia (I) and torque force $(\vec{\Gamma})$. The molecular field is written as;

$$\Gamma_{mol} = I\frac{d\Omega}{dt} = (\Gamma_{ext} + \hat{n} \times f) - \Gamma_{vis} \tag{1.63}$$

where $\Gamma_{vis} = \hat{n} \times [\gamma_1 N + \gamma_2 \hat{A}\hat{n}]$ with N =changing rate of director in fluid, f= molecular force, γ_1, γ_2 = viscosity coefficients. The first term in equation 1.63 gives the pure rotation effect and the second term in the equation arises due to the coupling with fluid motion.

Now, suppose the velocity gradient in the x-direction, and velocity in the z-direction, then the director has components with director angle (ϕ), A_{xz}, N_x, and N_z as,

$$\hat{n} = [\sin\phi, 0, \cos\phi] \tag{1.64}$$

$$v = [0, 0, v(x)] \tag{1.65}$$

$$A_{xz} = \frac{1}{2}\frac{dv}{dx} \tag{1.66}$$

$$N_x = -\omega_y n_z = A_{xz} n_z \tag{1.67}$$

$$N_z = \omega_y n_x = -A_{xz} n_x \tag{1.68}$$

By using above equation 1.64 to 1.68, the viscous torque can be simplified into the following equation as;

$$\Gamma_{vis} = -\gamma_1 (n_z N_x - n_x N_z) - \gamma_2 (n_z n_\mu A_{\mu x} - n_x n_\mu A_{\mu z}) \tag{1.69}$$

$$\Gamma_{vis} = -\frac{1}{2}\frac{dv}{dx}\left[\gamma_1 + \gamma_2 (\cos^2\phi - \sin^2\phi)\right] \tag{1.70}$$

The ϕ is the angle sustained between director axis orientation and flow of the liquid, where this angle is related as;

$$\cos 2\phi_{flow} = -\frac{\gamma_1}{\gamma_2} \tag{1.71}$$

1.5.1.3 Reorientation of director under the external field without coupling torque force with flow of the liquid crystals

Consider the twist configuration in LC is influenced by applied magnetic field (H) as shown in the figure 1.11. For the twist configuration, the director axis has profile with $\hat{n} = (\cos\phi, \sin\phi, 0)$ [7,11].

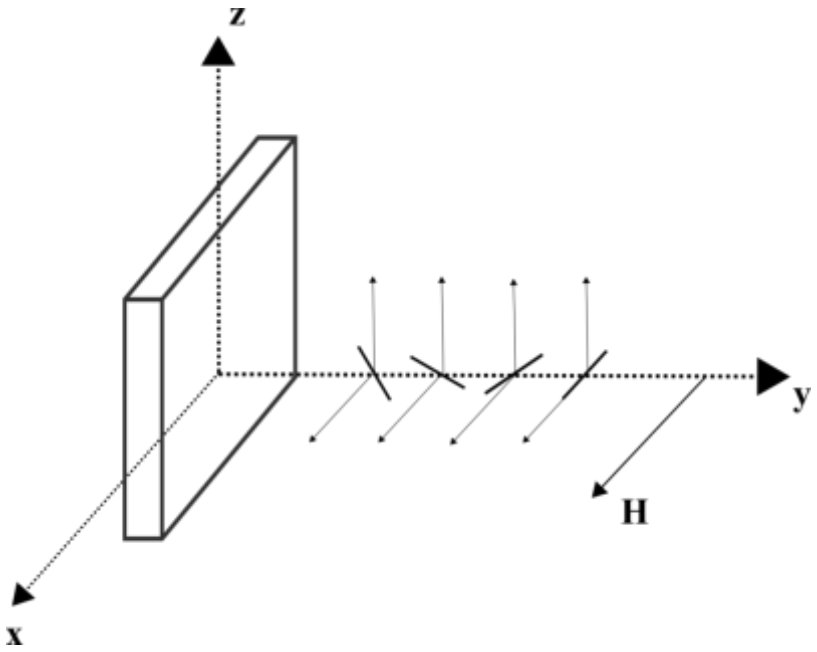

Figure 1.11: Twist deformations are influenced by the magnetic field (H) without the flow of molecules.

The corresponding free energy term is considered as;

$$F_2 = \frac{K_2}{2}\left(\frac{\partial\phi}{\partial z}\right)^2 \tag{1.72}$$

and

$$\Gamma = K_2 \frac{\partial^2\phi}{\partial z^2}\hat{z} \tag{1.73}$$

The viscous torque force is written as;

$$\Gamma_{vis} = -\gamma_1 \frac{d\phi}{dt} \tag{1.74}$$

The external torque is produced by the magnetic field, which can be written as;

$$\Gamma_{ext} = \Delta\chi^m H^2 \cos\phi \sin\phi \tag{1.75}$$

In the case of equilibrium state of toques in the cell, the final equation leads to the following equations:

$$\gamma_1 \frac{d\phi}{dt} = K_2 \frac{\partial^2 \phi}{\partial z^2} \hat{z} + \Delta\chi^m H^2 \cos\phi \sin\phi \tag{1.76}$$

$$K_2 \frac{\partial^2 \phi}{\partial z^2} \hat{z} + \Delta\chi^m H^2 \cos\phi \sin\phi = 0 \tag{1.77}$$

The solution of the above equation 1.77 gives the behavior of the director axis under the magnetic field. The molecules do not show any twist of the director of molecules for the applied field less than the critical value H_F, at ϕ=0. As the applied magnetic field exceeds up to the critical values, the director does not remain the fixed value and shows the twisting behavior for the higher magnetic fields with the hard boundary condition;

$$H_F = \frac{\pi}{d}\left(\frac{K}{\Delta\chi^m}\right)^{1/2} \tag{1.78}$$

The hard boundary condition means ϕ=0 at z=0 and d. The director profile of LC above the critical value is given by;

$$\phi = \phi_0 \sin\left(\frac{\pi z}{d}\right) \tag{1.79}$$

where, $\phi_0 \sim \frac{2\sqrt{(H - H_F)}}{H_F}$, when the value of the magnetic field is reduced from the H_F then the equation becomes;

$$A\gamma_1 \frac{d\phi}{dt} = K_2 \frac{\partial^2 \phi}{\partial z^2} \tag{1.80}$$

By putting the value of ϕ in equation 1.80 from equation 1.79, the equation 1.80 can be written as;

$$\frac{d\phi}{dt}\dot{\phi} = -K_2 \frac{\pi^2 \phi}{\gamma_1 d^2} \tag{1.81}$$

Thus, the solution of the equation 1.81 can be written as;

$$\phi_0(t) = \phi_0 \exp(-t/\tau) \tag{1.82}$$

where the relaxation time constant (τ) is given as;

$$\tau = \frac{\gamma_1 d^2}{K_2 \pi^2} \tag{1.83}$$

Under the electric field, such an effect can be easily studied by simply replacing H_F by E_F and $\Delta\chi^m$ with $\Delta\varepsilon$. The threshold values of the electric field and voltage are given as;

$$E_F = \frac{\pi}{d}\left(\frac{K}{\Delta\varepsilon}\right)^{1/2} \tag{1.84}$$

$$V_F = \pi\left(\frac{K}{\Delta\varepsilon}\right)^{1/2} \tag{1.85}$$

1.5.2 Cholesteric liquid crystal

Cholesteric liquid crystals (CLCs) have analogous properties like nematic liquid crystals (NLCs), but the director axis shows helical formation with a finite pitch p_o as discussed earlier. The general case in the cholesteric liquid crystals shows two types of director orientation: twist and fingerprint. Due to the helical formation of the molecules, the cholesteric liquid crystal shows unique optical properties, which can be applied in various novel optical devices.

1.5.2.1 Free energy of the cholesteric liquid crystal

The stable configuration of the cholesterics with pitch wave vector q_0 involves the contribution of q_o. In the cholesteric liquid crystal, the mirror symmetry is absent due to the helical pattern of the molecules. Basically, nematic liquid crystals can be treated as a special class of cholesteric liquid crystals having zero pitch wave vector. To calculate the free energy, the twist deformation contribution is modified with the pitch vector as;

$$K_2(\hat{n}\cdot\nabla\times\hat{n})^2 \rightarrow K_2(\hat{n}\cdot\nabla\times\hat{n}+q_0)^2 \tag{1.86}$$

For the CLCs, the director axis has a profile as;

$$\hat{n} = (\cos\phi, \sin\phi, 0) \tag{1.87}$$

The stable minimum free energy of the CLCs is written as;

$$F_d = \frac{1}{2}K_1(\nabla\cdot\hat{n})^2 + \frac{1}{2}K_2(\hat{n}\cdot\nabla\times\hat{n})^2 + \frac{1}{2}K_3(\hat{n}\times\nabla\times\hat{n})^2 \tag{1.88}$$

The cholesteric liquid crystals have similar properties to the uniaxial materials if the pitch of cholesteric liquid crystals does not change by the applied external field. In the cholesteric liquid crystals, the stable configuration is dependent on the external field directions, the sign of anisotropy, and orientation or configuration of the molecules.

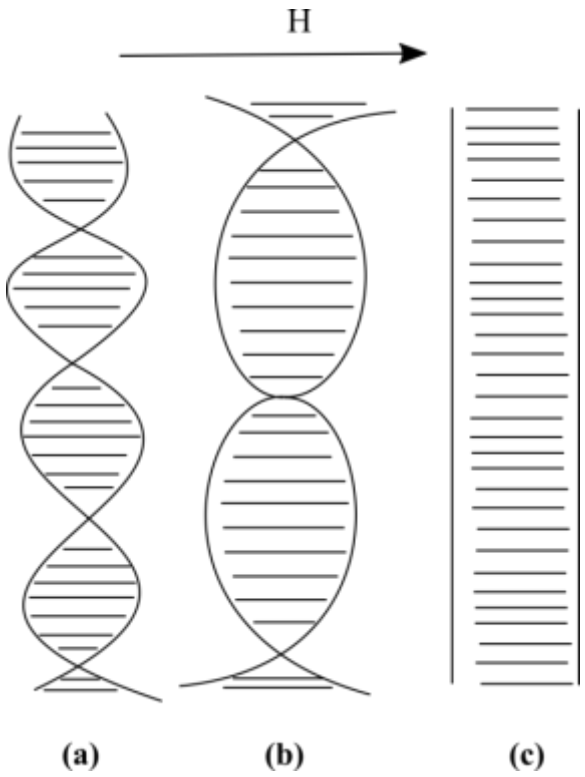

Figure 1.12: Deformation of helix under magnetic field: (a) absence of magnetic field, (b) incensement in pitch with the field, (c) perfect alignment of molecules with infinite pitch.

When the external field is applied to the CLCs, the molecules begin to orient in the field direction and the pitch of the CLC increases. If a sufficiently high field is applied to the liquid crystals, then the pitch of the cell approaches to infinity, and the

cholesteric liquid crystal converts into the nematic phase [18]. The free energy of the CLCs can be deliberated as;

$$F_{total} = \frac{1}{2}\int dz\left[K_2\left(\frac{\partial\xi}{\partial z} - q_0\right)^2 - \Delta\chi^m H^2 \sin^2\xi \right] \tag{1.89}$$

$$K_2 \frac{d^2\xi}{dz^2} + \Delta\chi^m H^2 \sin\xi\cos\xi = 0 \tag{1.90}$$

$$\vartheta_H \frac{d^2\xi}{dz^2} = \sin\xi\cos\xi, \tag{1.91}$$

where ϑ_H is the coherence length, which is given as;

$$\vartheta_H = \frac{K_2}{\Delta\chi^m H^2} \tag{1.92}$$

The equation may be simplified which gives as;

$$\vartheta_H\left(\frac{d\xi}{dz}\right)^2 = \sin^2\xi, \tag{1.93}$$

The solutions of the above-equation can be termed in elliptic functions. So that, we can take $\sin\xi(z) = S(u,\varsigma)$, here $u = z/\vartheta_H\varsigma$ =argument, ς = modulus of elliptic function. The free energy can be calculated by using minimizing conditions.

$$q_0\vartheta_H = 2\frac{E(\varsigma)}{\pi\varsigma} \tag{1.94}$$

The solution of the pitch can be given as;

$$p(H) = 4\vartheta\varsigma F(\varsigma) \tag{1.95}$$

When p tends to infinity, the $\varsigma = 1$ and $E(\varsigma) = 1$,

$$q_0\vartheta_H = \frac{2}{\pi} \tag{1.96}$$

$$q_0\frac{K_2}{\Delta\chi^m H} = \frac{2}{\pi}, \tag{1.97}$$

Hence, the critical field is given as;

$$H_C^2 = \frac{K_2 \pi^2}{\Delta\chi^m p_0} \tag{1.98}$$

where $p = p_0\left[1 + \frac{(\Delta\chi^m)^2 (Hp_0)^4}{32K_2^2(2\pi)^4} + \cdots\right]$ and p_0 = initial pitch without any disturbance.

Similarly, the effect of the electric field on the CLCs can be studied by replacing E with H and $\Delta\chi^m$ with $\Delta\varepsilon$. For the bulk cholesteric liquid crystals, the effect near the boundary can be negligible. Depending on the motion of the fluid, two types of conformations appear for the molecules of CLCs when the functioning field is abruptly turned off. The first is twisted conformation related to the motion of the fluid, and the second is iconic or umbrella mode with the absence of fluid motion.

The twist conformation can be described by a differential equation which is given as;

$$\gamma_1 \frac{\partial\xi}{\partial t} - K_2 \frac{d^2\xi}{dz^2} - \Delta\chi^m H^2 \sin\xi\cos\xi = 0\,, \tag{1.99}$$

The dynamical equation for the conic mode is complicated and the relaxation time for both modes can be written as;

$$\tau_{twist} = \frac{\gamma_1}{K_2 q^2} \tag{1.100}$$

$$\tau_{conic} = \frac{\gamma_1}{K_3 q_0^2 + K_1 q^2}\,. \tag{1.101}$$

where q =wave vector for the LCs.

1.5.3 Smectic liquid crystal

Smectic liquid crystal shows both directional and positional ordering in the arrangement of its molecules, and positional order is found in the layered structures with different orientations of the director axis in the liquid crystal. Depending upon the molecular arrangement and order, the smectic has different phases, smectic-A, smectic-B, smectic-C, smectic-D, so on. Liquid crystals OCB (4,4'–n-octylcyanobiphenyl) and nCB with n=8 to 12 show the smectic-A phase while OOCBP (4-n-octyloxy-4'-cyanobiphenyl) shows smectic-A and smectic-C phase. Due to different phases, pattering orders, and dipole moments, these liquid crystals have

different optical properties than the nemetic liquid crystals [19]. Smectic liquid crystals also have various applications due to their molecular orientation with the applied fields. Now, we discuss the smectic-A and smectic-C liquid crystals one by one.

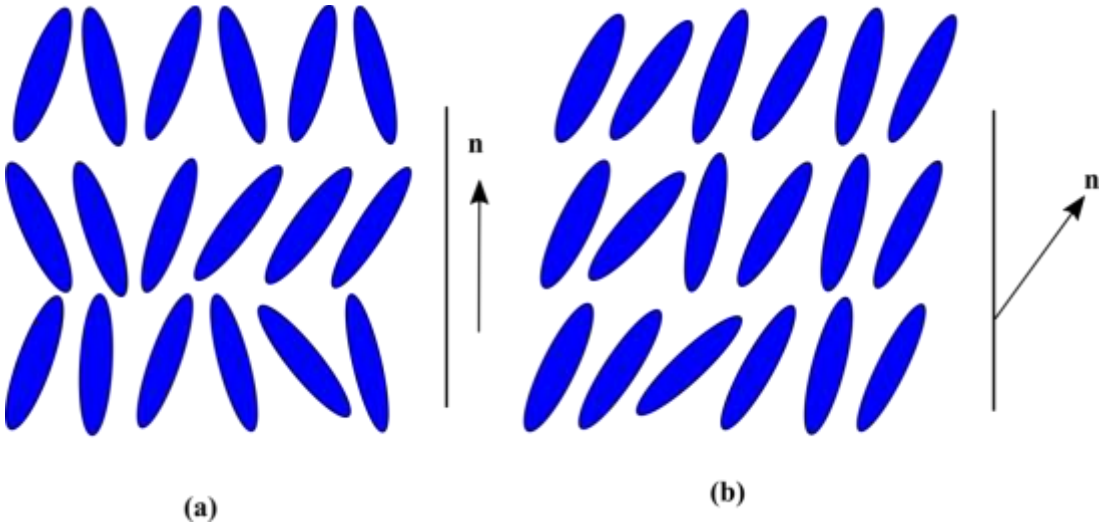

Figure 1.13: (a) Smectic-A (b) Smectic-C liquid crystals.

1.5.3.1 Smectic –A phase

The pattern structure of molecules in the smectic-A phase is shown in figure 1.13. In such liquid crystal molecules, small distortions and the distances between the parallel molecular layers are the same and the components of the director axis are also related to the displacement of the layers as;

$$n_x = -\frac{\partial u}{\partial x} \tag{1.102}$$

$$n_y = -\frac{\partial u}{\partial y} \tag{1.103}$$

The free energy of the molecular system can be described by an equation that is given as;

$$F_{total} = F_0 + \frac{1}{2}\vec{B}\left(\frac{\partial u}{\partial z}\right)^2 + \frac{1}{2}K_1\left(\frac{\partial^2 u}{\partial x^2} + \frac{\partial^2 u}{\partial y^2}\right) + \frac{1}{2}\Delta\chi^m H^2\left[\left(\frac{\partial u}{\partial x}\right)^2 + \left(\frac{\partial u}{\partial y}\right)^2\right] \tag{1.104}$$

where the first term F_0 is the unperturbed free energy part, the second is the distortion-free energy, the third is the splay deformation and the fourth term is the distortion energy term induced by field.

1.5.3.2 Smectic-C phase

In comparison to the smectic-A phase, the smectic-C phase has a revolution around the z-axis that remains the constant distance between the layers as shown in figure 1.14. The free energies in the smectic phase can be studied in the form of the layer spacing. The total free energy of the smectic C liquid crystals is the addition of rotation of director axis (F_c), distortion of the layers (F_d), and coupling between rotation with distortion, which can be described as;

$$F = F_c + F_c + F_{cd}; \tag{1.105}$$

$$F_c = \frac{1}{2}B_1\left(\frac{\partial\Omega_z}{\partial x}\right)^2 + \frac{1}{2}B_2\left(\frac{\partial\Omega_z}{\partial y}\right)^2 + \frac{1}{2}B_3\left(\frac{\partial\Omega_z}{\partial z}\right)^2 + \frac{1}{2}B_{13}\frac{\partial\Omega_z}{\partial x}\frac{\partial\Omega_z}{\partial z} \tag{1.106}$$

$$F_d = \frac{1}{2}A\left(\frac{\partial\Omega_x}{\partial x}\right)^2 + \frac{1}{2}A_{12}\left(\frac{\partial\Omega_y}{\partial x}\right)^2 + \frac{1}{2}A_{21}\left(\frac{\partial\Omega_x}{\partial y}\right)^2 + \frac{1}{2}\overline{B}\left(\frac{\partial u}{\partial z}\right) \tag{1.107}$$

$$F_{cd} = C_1\frac{\partial\Omega_x}{\partial x}\frac{\partial\Omega_z}{\partial x} + C_2\frac{\partial\Omega_x}{\partial y}\frac{\partial\Omega_z}{\partial y} \tag{1.108}$$

and

$$\Omega_x = \frac{\partial u}{\partial y}, \Omega_y = -\frac{\partial u}{\partial x}, \Omega_z \tag{1.109}$$

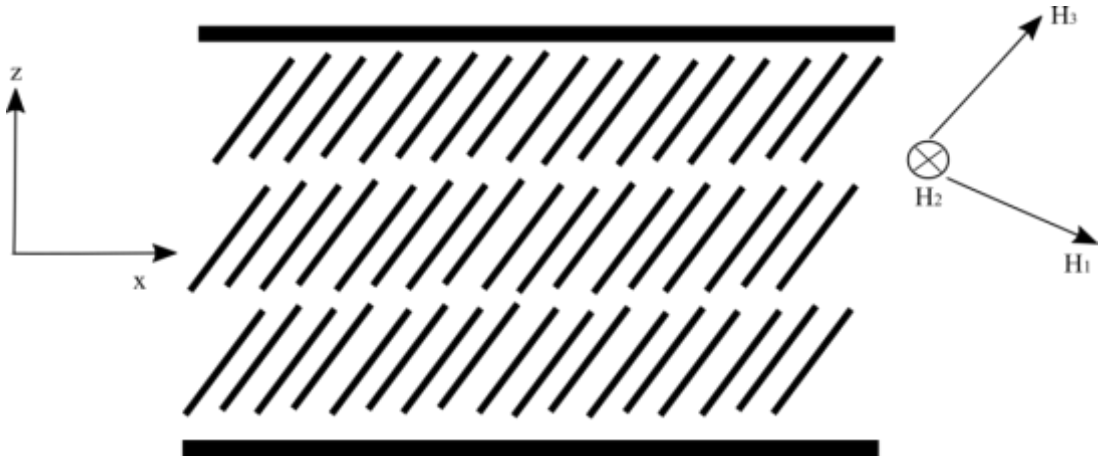

Figure 1.14: Smectic C liquid crystals under a magnetic field.

Smectic-C LC has the molecular arrangements in the different layers, So, when the external field is turned on the LCs, the field dissociates in three components and correspondingly three components of diamagnetic susceptibilities χ_1^m, χ_2^m, and χ_3^m.

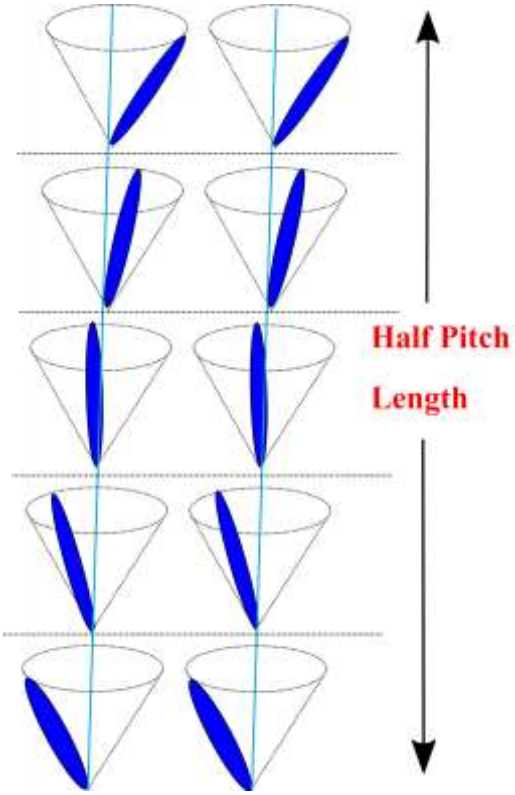

Figure 1.15: Orientation of molecules of Smectic-C phase liquid crystals under the magnetic field.

With the magnetic field, the projection of the director axis (c axis) must coincide with the y-axis and onto the molecule layers; then the threshold value, the Freedericksz transition field, can be written as;

$$H_{3c} = \frac{\pi \sin\phi}{d}\left(\frac{\kappa_{el}}{\chi_2^m - \chi_3^m}\right)^{1/2} \qquad (1.110)$$

where κ_{el} is the elastic constant. If the applied field along with the director of H_2 (y-axis), then the threshold value can be written as;

$$H_{3c} = \frac{\pi \sin\phi}{d}\left(\frac{\kappa_{el}}{\chi_1^m \cos^2\phi - \chi_3^m \sin^2\phi - \chi_2^m}\right)^{1/2} \qquad (1.111)$$

If the applied field along with the director of H_1, then the threshold value can be written as;

$$H_{1c} = \frac{\pi \sin\phi}{d\cos\phi}\left(\frac{\kappa_{el}}{\chi_2^m - \chi_1^m}\right)^{1/2} \qquad (1.112)$$

1.5.4 Smectic-C* phase (ferroelectric liquid crystal)

Ferroelectric liquid crystal (FLC) is another phase of the smectic liquid crystals (smectic C*) having a finite value of spontaneous polarization P. There are two kinds of the smectic liquid crystals, the first type is the direction of the P is fixed and the director axis is tilted at an angle ϕ, as shown in the figure 1.16. The second type is generally optically inhomogeneous and found as a twisted smectic-C* phase having a higher pitch than the thickness of the layer.

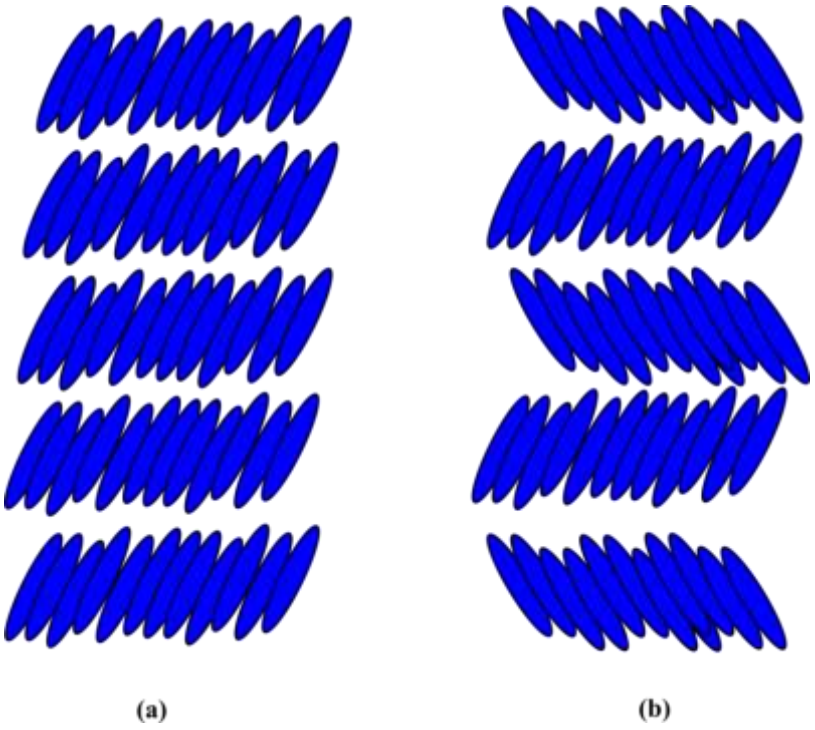

Figure 1.16: (a) Ferroelectric liquid crystals. (b) Antiferroelectric liquid crystals.

In the twisted phase, the director axis fluctuates in helical formation from layer to layer and the director axis revolves around the perpendicular direction to the layer. When the external field is applied in the parallel direction to the smectic layer, the layer shows unwinding of the helical form.

The free energy of the FLC is quite complicated and it depends on several parameters like elastic energy, surface energy, polarization density, dielectric interaction energy density [20].

Generally, the director axis of FLC has components as;

$$\hat{n} = (\sin\phi\cos\xi, \sin\phi\sin\xi, \cos\phi) \tag{1.113}$$

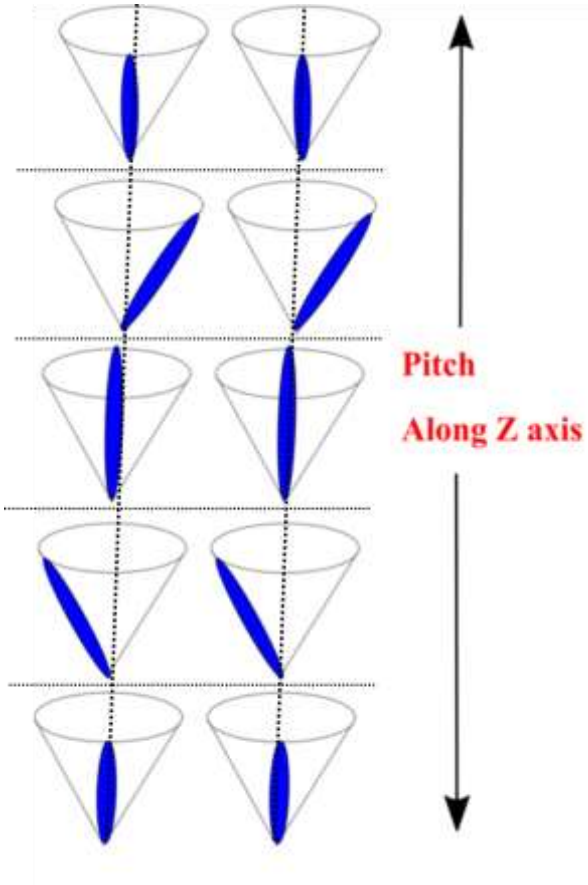

Figure 1.17: Orientation of ferroelectric liquid crystals under the magnetic field.

The total free energy of FLC is given by;

$$F_E = F_0 + \frac{1}{2}A(1+v\sin^2\xi)\left(\frac{\partial\xi}{\partial y}\right)^2 + A(1+v)\sin\xi Q_0\left(\frac{\partial\xi}{\partial y}\right) \tag{1.114}$$

The represented constant F_0, A, B, v, Q_0 in the above equations are given as;

$$F_0 = \frac{1}{2}\left[K_2 Q_T^2 + K_3 Q_B^2\right] \tag{1.115}$$

$$A = K_1 \sin^2\phi \tag{1.116}$$

$$B = (K_2 \cos^2\phi + K_3 \sin^2\phi)\sin^2\phi \tag{1.117}$$

$$v = (B - A)/A \tag{1.118}$$

$$Q_0 = \frac{K_2 Q_T \sin\phi\cos\phi + K_3 Q_B \sin^2\phi}{A(1+v)} \tag{1.119}$$

The constant K_1, K_2, K_3 are the frank elastic constants and Q_B, Q_T are the internal wavenumbers for bend and twist transitions. Now, the dielectric interaction energy is given by;

$$F_{diel} = -\frac{1}{2}\varepsilon_\perp(1 + \Delta\varepsilon'\sin^2\xi)E^2, \tag{1.120}$$

$$\Delta\varepsilon' = (\varepsilon'_\parallel - \varepsilon_\perp)/\varepsilon_\perp,\ \varepsilon'_\parallel = \varepsilon_\perp\cos^2\phi + \varepsilon_\parallel\sin^2\phi \tag{1.121}$$

The interaction of electric field density is given by;

$$F_P = -P_s E_y \cos\xi \tag{1.122}$$

The surface free energy term is given by [21];

$$F_s(\xi) = \sum_{1,2} h^{1,2}(\xi) \tag{1.123}$$

where $h^{1,2}(\xi) = -g^{1,2}C^{1,2}\exp\left[-\frac{\alpha'}{2}\sin^2(\xi - \xi^{1,2})\right] - g^{1,2}(1 - C^{1,2})\exp\left[-\frac{\alpha'}{2}\sin^2(\xi - \xi^{1,2})\right]$

and α is anchoring potential parameter, $C_{1,2}$ gives the relative stability between $\xi_{1,2}$ and π-$\xi_{1,2}$. The superscripts refer to the plates of the two cell boundaries.

The sufficient condition for such a process is $h^{1,2}(\pi - \xi) = h^{1,2}(\xi)$ with C_1=C_2=1/2.

With one constant approximation, the free energy terms gives;

$$K\sin^2\phi\frac{\partial^2\xi}{\partial y^2} + \frac{\Delta\varepsilon'}{2}\varepsilon_\perp E^2\sin 2\phi + P_s E\sin\xi = \gamma_1\frac{\partial\xi}{\partial t} \tag{1.124}$$

The first term is elastic torque, the second term is dielectric toque and the third term is polarization torque. The time constant which involves in the polarization process in the system is given by;

$$\tau = \frac{\gamma_1}{P_s E} \tag{1.125}$$

1.6 Photonic crystal

From the previous few years, photonic crystals (PCs) have attracted to the researchers in the field of advanced optics to examine their properties due to exhibiting photonic band gaps (PBGs) regions in which the transmission or flow of electromagnetic waves (EMWs) are forbidden. In 1887, Rayleigh [22] inspected that the propagation of an electromagnetic wave through the multilayered structure could be controlled in several aspects. In 1972, Baykov [23] proposed that spontaneous emission could be regulated by periodic structures. In 1987, Yablonovitch [24] and John [25] effectively explained that such a periodic structure could be used to execute the spontaneous emission and transmission of electromagnetic radiation. After these pioneer aspects for PCs, a huge number of research articles have been issued based on photonic crystals and their applications.

Generally, photonic crystals are the optical mediums having periodically arranged dielectric materials with periodic modulation or repetition of the dielectric constant in the possible directions. Such arranged multilayered structures of the dielectric constituents govern specific spectral characteristics and open an era in the advanced optics to use its properties in various scientific technologies; nanophotonics, optoelectronics, and nanotechnology, etc.

Depending on the dimensionality of dielectric constants, photonic crystals are categories in three configurations; one-dimensional photonic crystals (1-DPCs), two-dimensional photonic crystals (2-DPCs), and three-dimensional photonic crystals (3-DPCs) as shown in figure 1.18. One-dimensional photonic crystals (1-DPCs) are one-dimensionally arranged multilayered structure of dielectrics, and the fabrication of 1-DPC is easy due to the advanced development of the thin-film technology. The optical characteristics of 1-DPCs can be inspected using the transfer matrix method (TMM) and this method gives satisfying results with the experimental observations. Two-dimensional photonic crystals (2-DPCs) have periodic modulation of dielectric constants in two directions in the space and its optical transmission dispersions can be studied by using the plane wave expansions method (PWE), beam propagation method (BPM), finite difference time domain method (FDTD), finite element method (FEM), etc. 2-DPCs can be widely observed in nature e.g. butterfly wing. The wing of butterflies has a 2-D periodic lattice and this periodic structure in two directions

reflects the electromagnetic waves. In three-dimensional photonic crystals (3-DPCs), the dielectric permittivities of periodic layers diverge in three dimensions in the space that possesses larger probable conformations of 3-D photonic crystals than the 1-D and 2-D photonic crystals.

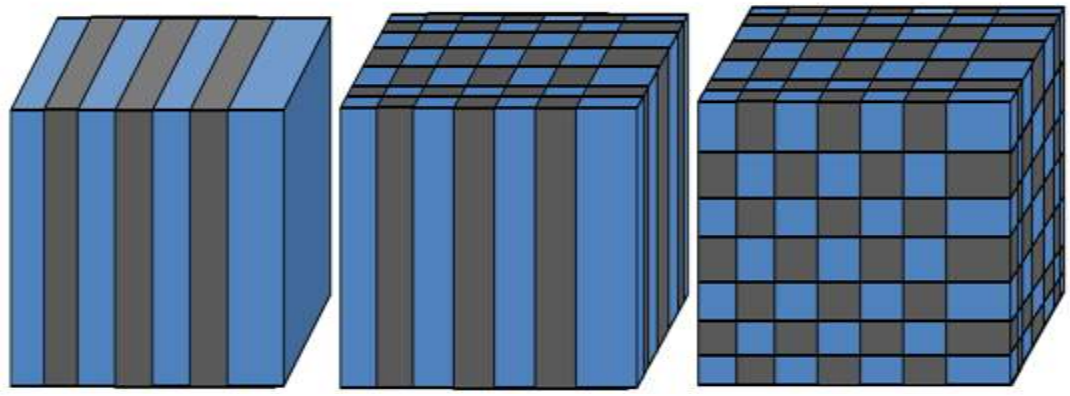

Figure 1.18: Schematic diagram of the Photonic Crystals (PCs): one-dimensional photonic crystal (1-DPC), two-dimensional photonic crystal (2-DPC), and three-dimensional photonic crystal (3-DPC).

In PCs, when the electromagnetic wave interacts with dielectric periodic layers, a certain range of wavelengths or frequencies exhibits is known as the photonic band gap (PBG) and such material is also called photonic band gap material. The band gap and dispersion of PBG materials as in figure 1.19 [26, 27] and such peculiar possessions of the PBG materials are used to manipulate and control the electromagnetic waves for applications in the optical devices. The photonic band gap materials, especially 1-DPCs, are used in the designing of omnidirectional reflectors, low-loss mirrors, optical fiber communications, antennas, precise emission devices, etc.

The PBG of periodic dielectric materials is analogous due to dielectric eigen states to the electronic band gap (EBG) of periodic potentials due to electronic eigen states in the crystal. We have learned that the localized states in the EBG region are strongly localized for the crystal with defect when an intrinsic crystal doped with certain impurities e.g. p-type and n-type semiconductors. Correspondingly, the localized states or defect modes in photonic band gaps can be achieved by inserting a dielectric

layer or LC in the periodic structures and such the defect in photonic crystals have strongly localized eigen functions. The obtained defect modes are strongly localized modes due to the interference of the waves in the defect layer. PCs with defect modes are useful in designing optical filters, multichannel filters, monochromatic wavelength transmitters, tunable electro-optical devices, omni-directional reflectors, etc.

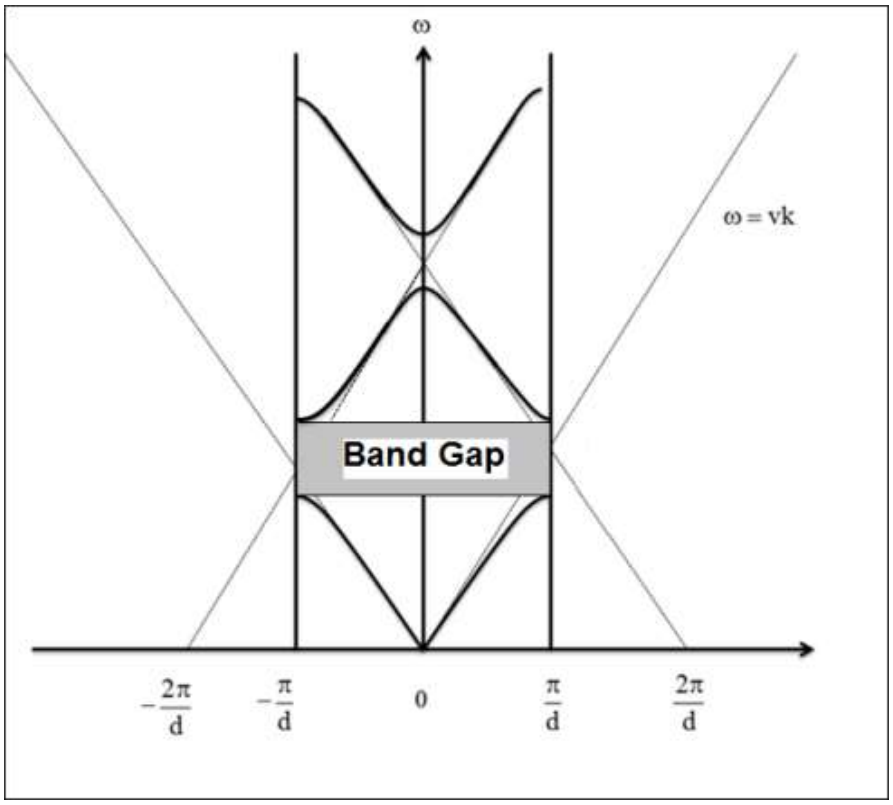

Figure 1.19: Band structure in the one-dimensional photonic crystal.

Artificial inverse opals, 3-DPCs, are to be made-up by using the simple and cost-effective self-colloidal method and the designed artificial opals have three-dimensional (3-D) periodicity of dielectric materials. Holographic lithography is also used to fabricate 2-D and 3-D photonic crystals. Electron beam lithography has also been used in the fabrications of photonic devices by patterning the different dielectrics materials. By using a systematic process of lithography with etching methods, 2-D low imperfection photonic crystals are fabricated [28-31]. The multistep methods with planer lithography techniques are used to fabricate 3-D photonic crystals. 1-D photonic crystals are designed with help of the thin-film technology where thin films are successively fabricated on the surface of each dielectric layer. Photonic crystals

have various applications depending upon the photonic band gap regions in the transmission spectra; e.g. tunable devices, optoelectronic devices, low-loss mirrors, optical filters, wave harmonic devices, beam-splitters, electro-optical switches, etc.

1.7 Literature Review

Liquid crystals are the electro-optical and organic materials and their optical properties are tuned with the orientation of liquid crystal director. Liquid crystals have a variety of applications depending on their types and optical parameters. The optical switching devices can be designed using tunable modes of photonic crystals containing liquid crystals. Various scientists and researchers have used liquid crystals to design the tunable photonic crystals.

In the cholesteric materials, the interaction of the electromagnetic field with materials leads to high transmission or low reflection of left-handed or right-hand polarized light fields. In 1968, Conners [32] derived the coupled time-independent equations for the propagation of the electromagnetic wave (EMW) in the cholesteric materials for the right and left-hand polarization of waves. The obtained results are good remarks for the interaction of the electromagnetic wave with cholesteric materials. The developed theory suggested the high reflection and the low transmission of left-hand and right-hand polarized electromagnetic waves, respectively when it is treated the interaction of the wave with right-handed material. By calculation, the intensities of both left and right-handed polarized waves, and the author calculated the circular dichroism (0.92) of the material. In 1971, Melamed and Rubin [33] investigated the optical characteristics of a mixture of different cholesteric liquid crystals; cholesteryl chloride, cholesteryl nonanoate, and cholesteryl oleyl carbonate. Along with optical properties, they also calculated optical activity, extinction ratio for the mixture. They reported that the asymptotic nature of the optical revolution which has positive and negative infinity at the wavelength (596 nm) with minimum transmittance and linear dependence of temperature for a certain range (20-35^{o}C). The wavelength corresponding to the maximum reflection showed shifting towards shorter wavelengths with the variation of the angles. The selective reflections waves were also observed in the narrow region for the small wavelengths [33].

In 1972, Berreman [34] developed a mathematical formulation to study the propagation of EMWs in the stratified anisotropic medium. The proposed theory was

established on the solutions of Maxwell's equations including optical activity and Faraday rotations. He generated a 4x4 matrix having 16 elements, which gave reflection, and transmission properties for coupled transverse electric and magnetic modes. Azzam and Bashara [35] also investigated the propagation of the polarized electromagnetic wave in the anisotropic medium including liquid crystals and found a solution of the differential equation, which was dealt with a complex quantity of elliptical polarization. They investigated the nature of this complex quantity in two different manners; along the random direction which satisfied with the conditions in Poincare sphere and along the helical optical axis of the chiral liquid crystal in which principal axes, birefringence, led to line up the axes of the elliptical surface in the molecular level. The solutions also suggested that the ellipticity has periodic variation having a smaller periodicity than the pitch of the used material.

Considering a complex plane helicity, the matrix based on left and right-hand polarization for inhomogeneous and homogeneous anisotropic media was developed. For the inhomogeneous case, the matrix depends on the distance along propagation direction and the solution for complex quantity shows the absence of analytical nature while the matrix did not depend on the distance and provided the existence of all laws in the Poincare-sphere illustrations with homogeneous case [35]. Helfrich [36] studied the effect of electric effects on the liquid crystals for different alignments. The homeotropic arrangement of liquid crystals shows the tunable birefringence but the molecules are showed the twisting behavior around the nematic axis that leads to polarization of incident light perpendicular parallel alignment of molecules. The liquid crystal has different values of threshold voltage for different alignment of the molecules. For the positive anisotropy, the molecules of the NLC orients along the electric field direction. The molecules show reorientation without any electric field or voltage application. LCs are used in phase-controlled optical devices due to having high sensitivity under the applied electric field. The materials parameters of liquid crystals are also studied by calculating time-dependent intensity patterns (phase delay and voltage) [37].

Elachi and Yeh [38] formulated the stopband properties for cholesteric liquid crystals (in half-space) considering the interaction of electromagnetic radiation with the LCs using Floquet theorem, and Brillouin illustrations while the other half-space is filled

with a uniform dielectric constant which leads to the subdivision of existing stop band depending on the incident angles. For the lower value of the incident angle, only one band exists but for the higher value of the incident angle, two or more stop bands exist. According to Brown [39], liquid crystals are found in two types, lyotropic and thermotropic; thermotropic LCs can be prepared by supplying heat to the organic materials while lyotropic LCs can be prepared by mixing of two or more compounds. The authors also suggested that the different classes of liquid crystals have different textures and structures and arrangement of the molecules. Kashnow and Stein [40] described that the transmission and reflection of liquid crystals, filled between two prisms, could be controlled by the incident angle of electromagnetic radiation. The total internal reflection conditions depend on the dielectric constant of the prisms and the refractive index of LCs suffers different values for s and p waves. The relative transmitted intensities have different maximum values with the incident angle for the field on and off conditions. The liquid crystals show very high switching of electromagnetic waves for a slightly higher incident angle than the total internal angle with on and off conditions of the applied field.

With the assumption of a twisting angle smaller than the maximum value of retardation, Grinberg, and Jacobson [41] investigated the transmission properties of twisted liquid crystal cell. The authors reported that the transmission properties of the cell are dependent on the wavelength of the incident wave as well as the specific thickness and birefringence of the used liquid crystal. Bigelow and Kashnow [42] used the Poincare-sphere representation for the investigating the propagation of polarized electromagnetic radiation in the twisted liquid crystal and suggested that normal modes in the undeformed state of liquid crystal have elliptical polarization in a very small manner. They also calculated the pitch near the boundaries of the twisted liquid crystal under the controlled orientation and alignments in the cell.

Riviere et al. [43] determined the refractive indices of the uniaxial 6CB liquid crystal by the transmitting plane wave into the cell containing 6CB with a semi-infinite transparent medium. They reported that the refractive indices are temperature and wavelength-dependent intensity transition behavior at critical values. Using Maxwell's equations, the authors also calculated the reflection properties, which were varied with incident angle, and the angle between the interface and optical axis of the

liquid crystals. For the incident angle higher than the critical angle, the total incident wave was reflected while for the angle below the critical value; the incident wave was partially transmitted. [44] Mclntyre also investigated the transmission properties of wave propagation through a layer of twisted liquid crystal. They suggested that the layer thickness is dependent on the twist angle without any transmission of waves [44]. Cox investigated the spectral properties of a mixture of liquid crystal with the dye that affected the material parameter such as order parameter, solubility, absorption, transmission, etc. The intensity of the transmitted wave was dependent on the solubility of the dye in the host liquid crystals. The optical properties were also affected by the nature of interaction presented between the guest and host in the system. Moreover, the order parameter depends on the structure of the dye and it has a higher value for the high ratio of length to breadth of the molecule. Due to dye molecules, the color switching properties do not change for the constant value of the thickness of the cell with the concentration of the dye [45].

Hajdo and Eringen [46] investigated the blue shifting in the reflection from the CLCs with shear and showed that the amplitude of the value of the applied field was dependent on the wave propagation vector and wave number. He concluded that there must have a finite number of pitches to reflect the light near the edge of the reflection band. The shift was found 6nm for the 23^{o} tilt angle of the liquid crystal due to rotation of molecules while the shift fluctuates for the angles higher than 23^{o}. The used perturbation theory did not give good results and the shifted has almost vanished. Due to the non-uniform rotation of the helix, the waves are linearly interacted with the inhomogeneous medium and generated the conversion of waves. The coupling of the critical field and the second-order phase transition are led to the threshold value of polarization cutoff of the wave due to the reorientation of liquid crystals director under external fields [47].

Chavel et al. [48] designed an optical transducer using liquid crystals due to the conversion ability of intensity to spatial frequency. With the help of such a transducer, the optically filtered intensities of the image could be manipulated by Fourier filters. They also demonstrated logic operation on the images using variable grating mode optical transducer based on liquid crystals. The proposed device has various advantages including flexibility, restoration of levels, parallel 2-D processing, etc.

Hinov [49] considered the attenuated total internal reflections for the interaction of the plane monochromatic wave with deformed liquid crystals under high-frequency fields but the surface anchoring was not controlled in the bulk layer of LCs. He also predicted that surface polarization, flexo-effect, formation, and vanishing of double layers and surface disclinations and various parameters could be traced.

Using LC chromatography, Ohgawara et al. [50] investigated the orientation of liquid crystal molecules on different surfaces. They found that the azoxy, Schiff, biphenyl, ester, based liquid crystals were aligned parallel to $In_2O_3Al_2O_3$ and other material surfaces while 5CB and MBBA liquid crystals aligned perpendicular manner due to the amphiphilic nature of impurities during hydrolysis. Gagnon [51] investigated the optical transmission through the twisted liquid crystals using a 4x4 matrix based on Maxwell's equations. The author used E7 liquid crystals with 45^o twisting of molecules and found that light reflects and leaves the cell by the same surface from which it is entered. The transmissions gained maximum value for intermediate voltages were showed broader declination in the high voltage. Wagner [52] reported the pair correlation function and order parameter of liquid crystals using the Bogoliubov-Born-Green-Kirkwood-Yvon theory. The order parameter is kept constant by varying temperature under short-range order correlations and some liquid crystals are showed the negative value of the order parameter at the clearing point. In this theory, the short-ranged repulsion is neglected due to angle-dependent terms while internal energies have low values due to interaction independent of orientations. He also suggested that the orientations pair correlation has vanished in the nematic clusters for the distances higher than the diameter of cluster size [52].

Durbin et al. [53] observed the optically induced Freederikcz transition and birefringence of liquid crystals. The authors reported that the maximum orientation of the molecules 30^o, for 100 W/cm^2 pump intensity with birefringence of 0.04 at 30^o incident angle. Moreover, the nonlinearity could be induced using the appropriate DC fields. The observed birefringence was found to be dependent on the pump intensity. The pump and probe intensities were suffered the shattering loss and transverse variations. In general, the Frredericksz transition was dependent on the temperature and directly proportional to the order parameter. Under a certain condition, the Freedericksz transition intensity was found to 155 W/cm^2. In 1981, Khoo [54] also

investigated optically induced effects in the NLCs and reported the four-wave mixing phenomena due to third-order nonlinear polarization in the NLCs. Using the intensity of $5W/cm^2$, the author observed the 0.1 conversion efficiency in wave mixing phenomena. The orientation relaxation was also reported and suggested that four-wave mixing could be used in holographic imaging as well as optical modulations. He also studied theoretically molecular reorientation and self-focusing effect of electromagnetic waves and found that an optical field lower than the threshold value could produce the molecular reorientation, self-focusing, and degenerate four-wave mixings depending on the geometrical parameters under small angle conditions [55].

Yang and Rosenblatt [56] determined the potential at the interface of NLC to the surface of the boundary. They also measured the birefringence of the liquid crystals, which was dependent on the magnetic field, and the cell alignment was related to the value of the Freedericksz transition. The maximum value of the orientation angle was found 90^o while the maximum value of the tilt at the boundary was found at the half value of the saturated value of the magnetic field (207kG). In 1983, Ong [57] studied the optically induced bistability and Freedericksz transitions in the nematic liquid crystals. The author used Maxwell's equations and Euler's equations to study the orientation in the nematic liquid crystals. He defined the criteria for first and second-order types of the Freedericksz transitions. Hence, PAA liquid crystals showed the first order Freedericksz transitions with hysteresis effects and the threshold intensity is the function of the thickness of the cell where it is inversely proportional to the square of the thickness of the cell. The study also agreed that the maximum value of the orientation angle was dependent on the intensity ratio of the incident wave to the Freedericksz transition. The hard boundaries did not affect the orientation of the molecules and threshold conditions. He concluded that when the intensity of incident EMW is lower than the Freedericksz transition value, the molecules did not show any variation but as the intensity of incident EMW is reached equal to the Freedericksz transitions molecules show switching behavior for increasing intensity. For the decreasing intensity (I) of EMW, the molecules acquire a different lower threshold value for the reorientation process discontinuously. If any noise is present in the nematic liquid crystal cell, then the threshold value is shifted to a lower value due to the nonlinear behavior of the noise. The response of the system is dependent on the noise intensity as well as the correlation time [58].

Ong and Meyer [59] generalized a formulation for the propagation of electromagnetic waves into inhomogeneous layers of liquid crystals using geometrical optics. They found that geometrical optics approximation is failed when the wavelength of the incident wave nearly approximates to the periodic of periodically bend liquid crystals. The expressions for electric fields was obtained through the geometrical optics has almost the same amplitude to the exact solutions for the all values of z, x, and y components of electric and magnetic fields, respectively and independent on the azimuthal angle but they are dependent on the tilt angle The z component of the electric field is dependent on the azimuthal angles and the amplitudes followed the reciprocal theorem. The distorted liquid crystals in a periodic manner worked as grating and produced fringes were calculated by Kosmopoulos and Zenginoglou [60] through geometrical optics approximations. The fringes were shown angular and spatial deviations of the propagating waves and were also shown the phase perturbation. For the weak distorted liquid crystal, the even-numbered fringes are important but for highly distorted liquid crystals, both even and odd fringes are important depending on the distortion angle. For the small deformation angle, the numbers of odd fringes are lower than even-numbered fringes. The grating factor of liquid crystals is dependent on the temporal phase difference and spatial path difference in the cell.

Using the interaction of low power lasers with liquid crystals, various parameters could be investigated e.g. orientation nonlinearity, high temporal resolution, and so on. The transverse inhomogeneity for the electric field with deformation energy led to weak interference with a weak response in the homeotropically arranged molecules within the cell. The director angle in the liquid crystals was varied according to applied magnetic fields. The ordinary wave could produce the reorientation of the molecules without threshold conditions [61]. When the laser incident on the liquid crystal, the molecules reoriented and the interface between 5CB liquid crystals and the air is acted as a hard boundary (rigid anchoring) for enhancing the backflow in the liquid crystals that lead to more relaxation of orientations. The interface of 5CB and air was found in homeotropic arrangements. The cell has high backflow due to the absence of positional anchoring which modified the relaxation process and decreased the orientational damping [62]. Lam et al. [63] studied the linear and nonlinear optical properties of anisotropic liquid crystals using the Ab-initio method and derived the

relation for the director fluctuations under electric dipole approximations, which is described the molecular reorientation on the propagation of the electromagnetic wave. Due to gradients of director fields, the induced dipoles in the molecules is supported by the flexoelectric effects and dielectric constant as the function of frequency. Both components of the dielectric constant have different resonant frequencies. Besides the electric field, the magnetic field has also produced the dipoles in the liquid crystals. Umeton et al. [64] suggested that liquid crystals could be used to tune the laser as well as an optical rotator and optical modulator. Using CLCs as active material in the laser cavity, the lasing action could be tuned. CLCs have huge rotatory power close to the wavelength of the peak reflection, which is regulated by the definite number of the pitch.

Frisken and Muhoray [65] studied the twist and bend transitions in the liquid crystals under electric fields and they proposed the induced transitions of first order with experimental illustrations. They also examined the effect of the magnetic field on the threshold values and transitions. The authors studied the exiting of hysteresis during the measurement of the dielectric constant. The transition in the cell was not uniform under the magnetic field and the obtained hysteresis was shown that the transition is first-order. The effect of the perpendicular electric field produces the stable conformation of LCs while the applied magnetic field produces the six possible transition deformations. If the applied electric field is parallel to the cell, then the Freedericksz transition is first order. For the 5CB liquid crystals, two deformations are first order and the other two exhibited the tricritical points. The order parameter has a high value for the first-order transition. The magnetic and electric field-induced the bend and splay transitions in the LCs which are second-order transitions [66]. Foresti [67] calculated the optical properties of LCs on the propagation of the plane wave. He obtained the solutions in form of the perturbative functions. Using the 4x4 matrix method, he obtained the Fresnel's coefficient of reflection and transmission through the liquid crystals. Sharp et al. [68] fabricated the tunable liquid crystals wave plate in the infrared region. They showed that the optical properties of the wave plate were dependent on the birefringence, thermal stability, and alignment of the liquid crystals. They also calculated the phase retardation at different voltages and reported the retardation was found 4^{o} at 25V and approached to 0^{o} for the higher voltages. If the director angles change, the azimuthal angle of the cell is affected. Wang et al. [69]

studied the frequency locking and quasi-periodic oscillations of the output intensity and chaos in the Fabry-Perot interferometer considering nematic liquid crystals. The used liquid crystals are acted as a nonlinear oscillator and the noise affected the frequency locking with winding numbers [69].

Lekner [70] calculated the electric field vectors for extraordinary and ordinary modes of the wave considering s and p polarizations for the uniaxial crystals in terms of direction cosines. Some specific conformations of the materials vanished the cross reflection terms. The ordinary and extraordinary electric field vectors were orthogonal to each other. Due to the Freedericksz transition in smectic-A, the liquid crystal showed a phase transition to smectic-C considering molecular tilt in the smectic layer. The transition temperature of smectic-A to smectic-C phase depends on the surface pre-tilt effect. The above the transition temperature threshold value increases having square values. The phase transition and threshold voltage were dependent on the temperature [71]. Busch and John [72] demonstrated that when the holes in the inverse opal infiltrated with liquid crystals, the materials exhibited tunable photonic band gap (PBG) regions; the PBG regions could be tuned by applying electric fields which orients the optical axis of the used liquid crystals. For the well order and aligned nematic liquid crystals, the material exhibited tunable wave-guide characteristics; the filled inverse opal supported with localization of the light and electro-optical modulation of the emitting light. Yang et al. [73] investigated the interaction of light with cholesteric liquid crystals and used as photonic band gap material due to exiting total reflection of the light with circular polarization but the orthogonal components were transmitted. The right circular polarization light is reflected but the left circular polarized light is transmitted. They also showed that defect modes in CLCs were dependent on the refractive index of the defect layer. When the refractive index of the defect layer is higher than the refractive index of liquid crystals than the wavelength of the transmitted peak shows blue shifting and two defect modes of transmission are obtained near the edges gaps and the long-wavelength mode of the transmission vanished while short wavelengths are shifted into forbidden gaps. At the center of the gap, the wavelength of defect modes transmission peaks was varied linearly with the refractive index of defect mode.

Swisher et al. [74] observed the nematic transition of cholesteric liquid crystals droplets when it is placed in the external electric field. Under the electric field, the surface of the droplets shows quasi-cylindrical twisting behavior. The cholesteric droplets were transformed in the nematic phase on further increasing the electric field. Having the confinement, the pitch calculation follows the same conventional theory. Etchegoin [75] studied the blues phases of dye-doped cholesteric liquid crystals and he found that the blue phase in the liquid crystals could be tuned with the temperature and the blue phase was modified the emission of fluorescence of the dye presented in the liquid crystal. Such dye-doped liquid crystals having low pitch could be used as weak or thermotropic photonic crystals. To study the anisotropy in the emission process, the single crystals with a blue phase could be used. Leonard et al. [76] investigated the optical properties of 2-DPCs filled with E7 LCs and they found that the photonic band gap was tuned with the temperature and refractive index of the liquid crystals. They synthesized the photonic crystals of silicon materials and the air holes filled with E7 liquid crystals. The filled liquid crystals were shown transition of nematic to isotropic nature at temperature 59^{o}C. The longer wavelength edge of the band gap remains fixed but the short-wavelength shifted by 70 nm. The band structure was also shown shifting by 113 nm by tuning the alignment of the liquid crystals. In conclusion, they investigated the first tunable 2D photonic crystals based on liquid crystals. Kang et al. [77] also synthesized the porous silica (closed packed) based photonic crystals filled (26%) with liquid crystals and showed shifting of the Bragg peaks of reflectance peaks. On the application of the electric field, the structure was shown the tuning of the reflection Bragg peaks with a hysteresis due to the parallel orientation of the molecules concerning the surface of the pre-synthesized structure. Kee and Lim [78] studied the optical properties of 2-D metallic photonic crystals with filled with 5CB liquid crystals. The authors suggested that infiltration of liquid crystals could be enlarged the wide of photonic band gaps and produces the other high ordered photonic band gaps in the transmission spectra. At the phase transition of liquid crystals, the temperature has affected the edges of the photonic band gaps. The shifting of the band gaps in case of s and p polarized light waves are in opposite directions. Using the metallic periodic structure instead of the dielectric periodic structures, the higher tunability could be achieved. Yoshino et al. [79] synthesized the 3-D periodic structure of SiO_2 infiltrated with liquid crystals and reported the tunable

stop band and band structures with the variation of temperature and refractive index of the liquid crystals. They illustrated that the periodic structure has had reflectance in comparison to the periodic structure filled with liquid crystals filled structure which shifted the stop band. The central frequency shifted to the longer wavelengths (low energy) at the L point, perpendicular direction of wave propagation. The theoretical calculations of the temperature-dependent central wavelengths were found between first and second bands that were matched with experimental values.

Shimoda et al. [80] also studied the stop band characteristics of the 3-D photonic crystals infiltrated with liquid crystals. They reported that the stop bands produced by periodic structure could be tuned by changing the parameters of the liquid crystals such as temperature. The refractive index of the filled organic material (liquid crystals) could also be calculated by analyzing the transmission spectra of the periodic structure. Moreover, the interactions between the liquid crystals and walls could be organized by considering the matrix of the optical replica. Due to anisotropy of liquid crystals, the uncoupled modes and mirror symmetries have vanished in the 2-D photonic crystals. The main reason for the breaking of mirror symmetry was the rotation of the director axis of the liquid crystals. The transmission has a high value for the director angle of 10^{o} to 88^{o} but the very low value at a low angle due to uncoupled modes. Hence, the higher tunability could be obtained by setting the range of director angles between 0^{o} to 10^{o}, and 88^{o} to 90^{o} [81]. Ruan et al. [82] studied that smectic-A liquid crystals (8CB) gave rise to two stable conformations of its directors, which supported the diffraction of electromagnetic waves, caused by disturbance and fixed amplitude of the density waves. The perpendicular layers of the smectic phase show the bend deformation in homogenous alignment by reducing the amplitude of the density waves of smectic layers. The parabolic line defects could be observed in the bulk of aligned smectic layers in a non-hybrid manner. The frustrated structure could be found in the non-chiral liquid crystal using hybrid alignment.

Based on the transfer matrix method (TMM), Ozaki et al. [83] discussed the tunability of the defect modes in the transmission of 1-DPS with the defect layer of ferroelectric and nematic LCs. The author also reported the fast electro-optical switching of the defect modes, which was agreed with experimental observations. Using the NLCs as defect layer, the wavelengths of the defect modes transmission were shifted but with

ferroelectric liquid crystals, intensities of the defect modes transmissions were modified by applying the voltage. The switching response time was found about of the order of ten microseconds for switching for defect mode transmission. At 0 V, the propagation of 632.8 nm was prohibited but at 12V, the propagation was allowed in the one-dimensional periodic structure. Again Ozaki et al. [84] described the optical properties of 1-DPCs with defect layer of NLC having in-plane switching or alignment. The authors found that two different modes were arisen in the photonic band gap depending on the ordinary and extraordinary refractive indices of the liquid crystals by considering the perpendicular orientation of the molecules. The intensities of the defect modes were varied according to the orientation of the LC director but the position of the defect modes has remained constant. By tuning the electric field, the polarization direction of the propagating EMW could be regulated with the in-plane alignment of nematic liquid crystals.

Matsui et al. [85] found that the deformation of the helical axis of the CLCs was tuned the defect modes in the periodic structures. The CLCs are allowed to pass the same circularly polarized light which has the same circular polarization to the cholesteric liquid crystals. The compression and elongation of the helical axis were tuned the position the defect modes in the opposite direction of shifting defect modes. The liquid crystals were also shown blue and red shifting in according to compression and elongation of the helical axis of the liquid crystals. Wang and He [86] proposed an effective method for the distribution of the twisted liquid crystals director with a hard boundary. They demonstrated the three-parameter model for the liquid crystal and also compared it with the two-parameter model. The used three-parameter model produced the stable results in comparison to the two-parameter model and these were used to study the electro-optical properties of the liquid crystals. The results suggested that identical liquid crystals with similar conformations could show different optical properties [86]. Chen and Chen [87] studied the optical transmission and defect modes in the periodic cholesteric liquid crystals layers having a variable pitch. Due to changes in the phase and pitch of the helical structure, the defect modes were obtained in the transmission. The different transmission peaks were arisen in the photonic band gap region because of similar handedness of the normally incident light and helical axis. An extra phase and enhanced twisting led to the blue shifting of the defect modes obtained in the transmitted spectra. The obtained transmissions were similar to

that from the Fabry-Perot interferometer. The intensity of defect mode was modified by introducing changes in the pitch for the critical value of layer thickness.

Graugnard et al. [88] have shown the tunable Bragg peak in the inverse opal coved with NLC. The structure was made of the high dielectric TiO_2 matrix with overlapped spherical holes of air. The reflection properties were dependent on the electric field and the layer structure. The layer showed a shifting of Bragg peak by 20 nm with a 50kV/cm electric field for the hydrophobic material. The width of Bragg peaks was also enhanced with the application of the electric field. To tune the Bragg peak, there was no threshold value and the hydrophobic sample showed hysteresis in corresponding to the surface effect of liquid crystals molecules. But for the hydrophilic sample, the LCs were reoriented due to high interaction with the TiO_2 surface without any electric fields. Ozaki et al. [89] studied the lasing action in the 1-DPCs of conducting polymer and liquid crystals layers under the applied electric field. The results suggested that the wavelength of the lasing defect mode was tuned by low voltage. The defect mode has also followed the shifting with a change of the refractive index of the LCs influenced by the reorientation process of molecules. Above the threshold value (01 V), the wavelength of lasing action was shifted to lower wavelength regions. The authors used 1-DPC with dye-doped NLC with a periodicity of 10 to design tunable lasers. Due to molecular orientation, the layer suffered to change in the optical length, and hence the defect mode was shifted in the transmission graph. The electric field distribution considering the defect model was dependent on the periodicity of the photonic crystals. The low threshold value for lasing action was found by optimizing the periodicity of the photonic crystal. Due to the existence of standing waves, the partial transmission of electromagnetic waves was possible. The electric field distribution in the LCs was dependent on the molecular orientation and operating wavelength [90].

Liu and Chen [91] numerically explained that PBG of the PCs with cylindrical square and triangular lattices filled with NLCs could be tuned under the external field for TE and TM modes. The molecules were tuned by the applied electric field higher than the Freedericksz transition. They found 0.669 V_{rms} of threshold value and response time in the order of 100 μs. Ozaki et al. [92] approached the tunable behavior of the 1-DPC with ferroelectric and nematic LCs as defect layers and observed that the angle

sustained between the molecular axis and polarization direction of propagating EMWs determined the intensity of the transmitting wavelengths. The periodic structure passed the wavelength depending on the directions of the ordinary and extra-ordinary optical axes in the defect layer. The polarization directing also regulated via applied field, which was induced the realignment of molecules in the plane. The cell has produced the stop band between 530nm to 740nm and three transmission defect peaks were originated inside the band gap region due to the localization of electromagnetic waves in the defect layer. But the six defect peaks appeared inside the band gap having half intensities for the 45^o orientation angle of the molecules. The transmitting wavelength of 609nm had maximum intensity for the director angle 0^o and 180^o, which indicated that the transmitting wave has parallel polarization to the long molecular axis. But for the 633nm, the transmitting intensity has a maximum value at 90^o orientation of the LC. By applying positive and negative voltages, the directions of the defect modes could be switched.

IIyina et al. [93] studied the Freederikcsz transition in the NLC at the different molecular orientations of molecules by using the relaxation method and Maxwell's equations for the FDTD quasi-statically method and found the first order Freedericksz transition in LC cell under one elastic constant approximation. A discontinuity was obtained in the transmission due to optical resonance for the large optical retardation of the e-wave. Besides the first order Freeriderikcsz transition, the bistability was also found along with quasi-stationary states. The phase shift was also found for the ordinary and the extraordinary waves during the jump between two bistable states. If the wavelength is short, then the large numbers of the quasi-states were observed. For the small ratio of thickness to wavelength, resonance was not observed due to the small phase shift. For the high ratio of thickness, the phase shift was sufficiently high to support the optical resonance. The variation of maximum orientations followed some discontinuity with intensity ratio for a high ratio of cell thickness to wavelength. The backflow and its coupling with the liquid crystal director affected the relaxation process in the cell.

Wang and He [94] designed optical attenuators based on the 90^o twisted parallel-aligned nematic liquid crystals. They also modeled the weak boundary conditions (BCs) for the parallel alignment of the LCs and suggested that high attenuation

independent of wavelength could be achieved using such conformations. Halevi and Avendaño [95] explained the behavior of cylindrical nematic liquid crystal under the electric field and found that the conformation of the molecules is escaped radial for the low electric field, which was higher than the critical field. At the critical value of the field, the molecules possessed second ordered phase transition and reached to axial conformation. By incorporating such evidence, photonic band gap effects and dielectric tensors reliant on structure were determined. The designed structure could be used as tunable and switching devices dependent on the polarization effects. Gottardo et al. [96] reported that the optical axes could be controlled by knowing the structural anisotropy of the colloidal periodic porous structures infilled with nematic liquid crystal and such structure also possessed self-alignments of molecules even when the distance is much larger than the size of the holes in the periodic structures. The porous structure also expressed the polarization-dependent optical properties, which was tuned by applying electric fields. The location of the stop band in the transmission spectra remained constant for the low electric field but higher value 5 V/μm, the central wavelength showed the blue shifting in the stop bands for both p and s polarizations. Such shifting reached an equal position for both polarizations at 50 volts per micrometer. Bechtold et al. [97] have studied the in-plane and out-plane orientational transitions for the patterned substrate having periodic dimensions below than 1 μm and the liquid crystals did not align along the surface of boundaries. The authors observed the reversible photoinduced effects and the photopolymer (azopolymer) made possible the manipulation of the surface energy. For the 3 μm and higher dimensions, the liquid crystals were aligned along the surface of the patterned structure and the elastic energy of the liquid crystal was minimized. The observed transitions were dependent on the texture, periodicity, elastic energy, and the distortions applied to the liquid crystals. Miroshnichenko et al. [98] suggested that the all-optical switching could be obtained by using liquid crystals as a defect layer in one-dimensional periodic structures. The authors used the nonlinearity of PAA liquid crystals to achieve the all-optical switching behavior of the periodic structures of the Si layer. They solved the coupled nonlinear equations for the liquid crystals director and found that the optically induced Freedericksz transitions have lower threshold value due to multiple reflections and such transitions were used in the fabrication of switching devices, diodes as well as bistable devices. The threshold value for the

optical Freedericksz transitions reduced for decreasing intensity, which was lower than that of increasing intensity, and hence a hysteresis existed in the transmission process.

Ozaki et al. [99] also investigated the transmission of 1-DPS with defect layer NLCs, where they obtained the dynamical responses of few μs and a sharp switching behavior considering distributions of the liquid crystal directors in the defect mode. By applying voltage, the molecules of the liquid crystals reoriented and followed the changes in the optical length; hence the defect mode wavelengths were shifted in the transmission spectra. The fast responses were found for both increasing and decreasing intensities of the waves. The optical thickness of the defect layer varied the line-width of the defect mode and manipulation of the light in the defect layer in the chiral photonic crystal. At a certain thickness of the defect layer, the polarization-dependent reflections vanished and such chiral photonic crystals also could be used as a source of tunable elliptical polarized light depending on the handedness of the material [100]. Reyes et al. [101] investigated the 2-D photonic crystals infiltrated with LCs under the external electric fields. The authors obtained a relation between the liquid crystals director and radial distance by minimizing the total free energy of the system. They suggested three possible deformations for the molecules, which were axial, escaped radial, and planer radial. The 5CB liquid crystals expressed the escaped radial configuration at 14 V per micrometer with the condition that the cylindrical radius was higher than 50nm. For the high field, the radial conformation changed to axial conformation in which all the liquid crystals directors were aligned along the axis of the cylinder. The dielectric tensor was dependent on the possessing conformation of the liquid crystals. The author explained the tunability of the photonic band gaps in the [100] direction of the crystal. The authors also found that quasi E and H bands tuned while the partial quasi bands were shifted upwards or downwards [101]. The transmission of defect mode wavelength was dependent on the matching condition of polarization and retardation in the cell. The location of the localized waves and optical retardation was regulated via applied voltage of the liquid crystal defect layer presented in the one-dimensional photonic crystals. The narrow bands of the photonic crystals showed switching behavior with the external field [102].

Using FEM, the deformation of liquid crystal director for hybrid and planer cells was studied. With the application of a high electric field, the molecules were suffered hydrodynamic backflow in the cell. For the low electric field, the backflow was decreased depending upon the magnetic coherence length torque that was induced on the director of the liquid crystal. The backflow reduced the molecular rotation in the middle of the cell due to weak elastic forces [103]. The interaction of electrically induced grating and LCs has produced the grating resonance in the photonic crystals, which was dependent on the ratio of layer thickness to modulation interval. The intensity of the diffraction grating and modulation was increased with applied voltage but the transmission selectivity was reduced [104]. The broadband electrical tunable band gap of the photonic crystal could be obtained using the doping of FLCs in the chiral LCs. Due to the in-plane orientation of FLCs, the pitch of the chiral LCs was reduced under the externally applied field. Due to the localization of helices in the structure, the two-band gaps appeared for the low field that disappears at high field [105]. The doping of nanoparticles in the liquid crystals showed various novel properties e.g. optical wave mixing, self-action, negative refraction, etc. The modulation of the optical index, all-optical tuning, nano, or microsecond response time was achieved by doping in the liquid crystals. Due to the doping of metallic nanoparticles, the liquid crystals showed Metamaterials characteristics and it had a tunable refractive index below than or equal to one, which turned with the index of liquid crystals and size of nanoparticles [106]. The interface of dielectric and anisotropic media also supported the Dyakonov surface wave that was regulated by the cutoff angle of wave propagations. Such waves were observed by using Otto-Kretschmann set up depending upon the index matching conditions and were detected by reflections (polarization conversion). The Dyakonov waves were observed in the surface of nanoparticle doped liquid crystal which could be tuned by the orientation of liquid crystals, filling fraction, and size of the nanoparticles [107]. The nanometer-sized particles in the nematic liquid crystal formed the stable entangled hyperbolic defect modes independent of the shape of nanoparticles. Such defects were transformed into a figure of eight structures for size between 100 nm to 1 μm. The generated were torque regulated with the length to breadth ratio of the sphere-cylindrical nanoparticles. The strong and anisotropic interactions were varied with the shape of the particles. Such interactions were forced to binding of particles and

aligned in ordered patterns [108]. The presence of ferroelectric nanoparticles in the nematic liquid crystals increased the transition temperature and sensitivity with externally applied fields. The nanoparticles also modified the interactions with the macroscopic order parameter and also enhanced the optical properties of liquid crystals. The Kerr effect also was explained the coupling of the electric field with order parameter and entropy of the nanoparticles based on Landau theory [109].

Cos et al. [110] theoretically studied the tunable optical properties of the Fabry-Perot filter based on liquid crystals. They found that the two different resonant wavelengths in the stop band in transmission due to the coupling of extraordinary and ordinary waves. The tunable properties were found by controlling the orientation of the defect layer of liquid crystals. The transmission properties were obtained using the 4x4 transfer matrix method (TMM) for TE and TM modes and concluded that the resonant wavelengths were related to the orientation of molecules in the cavity. When the optical axes are parallel then the two-channel arise which having different transmittance, where one channel has zero transmittance and the other has almost 100% transmission. Rezaei et al. [111] used the plane wave expansion method to study the tunable properties of the 2-D photonic crystals composed of tellurium and explained the tunability as a function of the orientation of liquid crystals. The triangular lattice has higher tunability than the square lattice in the photonic crystal. The magnetic field induced the rotation of the directors of the liquid crystal that tuned the transmission of light through the PC with the LC defect layer. The superposition of extraordinary and ordinary waves, location, and intensity of obtained defect modes, were controlled by applied fields [112].

Oliveira et al. [113] studied that the optical properties at two different orientations of liquid crystals in the 2-D photonic crystals for both negative and positive anisotropies under the external electric field. The different defect modes were obtained in the transmission spectra depending on the nature of anisotropy and the direction of the field. The electrical tunable properties of 1-DPC with the defect of twisted NLC were investigated by Lin et al. [114] and the defect modes in the transmitted graph showed both behaviors of shifting and switching with the angle of polarization of the incident wave. The defect wavelength of mixed twisted modes allowed the transmission for the centers while other intensities were prohibited. The mixed modes enhanced the

localization of defect modes. Such periodic arrangements with twisted liquid crystals could be used as monochromatic wave-selector. The cholesteric transition from the nematic phase was observed by immersing the chiral constituent in the nematic liquid crystals. The temperature and dopant concentration pitch was calculated by analyzing the transmission properties. The selectivity of the cholesteric phase was dependent on the chiral components of the mixture. At low temperature, the mixture also showed the smectic-A phase and the optical properties were reliant on the types of chiral components is mixed with NLCs. The CLC mixture (E7+S811) showed a blue shift to 2006nm to 860nm for temperature 12.2 to 39.7^{o}C with 16 % of chiral elements. The range of temperature was reduced by adding more chiral components in the mixture [115]. Beeckman et al. [116] studied that the liquid crystals could be used in the fabrication of various optical devices like optical switches, optical filters, light modulators, beam-starring devices, lasers, optical waveguides, and so on, due to exhibiting electro-optic effects of the LC [116].

He et al. [117] used 4x4 TMM to study the optical properties of 1-DPC containing CLC and found the dispersion relation for different chromaticity pictures. The obtained chromaticity was angle independent nature and the shifting was varied with layer thickness and dielectric permittivity of the dielectric layers in the one-dimensional photonic crystals. The proposed structure also showed common photonic band gaps for right and left-hand polarization. Avendao et al. [118] also used the 4x4 transfer matric method for the propagation of the electromagnetic wave in the twisted liquid crystals and obtained the different texture of the molecules for the different interactions. They reported that the transmission and reflection were the function of the applied field, the ratio of thickness to wavelength, and surface interactions for the parallel and perpendicular anchoring effect. The polar and azimuthal angles were set themselves to achieve a wide twist configuration of the liquid crystals. The edge of the band for lasing was switched by using negative dielectric anisotropy of chiral nematic liquid crystals under the electric field. Due to hydrodynamic stabilities, the scattering occurred in the liquid crystals and generated random lasing action for low frequencies but the band edge lasing possible for high frequencies. The line-width and feedback were regulated by appropriate electric fields and negative anisotropic cholesteric liquid crystals with dye doping [119]. The localization of the surface at the interface between the right hand and left-hand material was controlled by changing

the orientation of embedded liquid crystal layers at the appropriate incident angle and wavelength region. The tunability of the surface wave obtained at the zero and the nonzero average refractive index of the photonic crystals. For the zero index case, the zero-n gap was obtained in the photonic band gap and the high localization was also obtained for the high angle of the liquid crystals [120]. The distributed feedback lasing from the photonic crystal made of TiO_2 with dye-doped liquid crystals was described [121]. The lasing emission is organized and manipulated by applied electric fields on doped liquid crystals. The structure of inorganic and organic interface allowed the control of the selection pattern of lasing emission. The emission of the laser also was controlled via filling fraction, the lattice constant, and symmetry of the photonic crystals.

Borshch et al. [122] suggested an idea to achieve the fast nanosecond ordered response time for the field off and on conditions using NLCs. Such an idea was based on the modulation of the order parameter by electric fields. The observed phase retardation was directly proportional to the path of electromagnetic waves. Moreover, the electrically modulated order parameter modified busing bend core liquid crystals or chiral nematic liquid crystals. The change is the birefringence was found to be square of the magnitude of applied fields as in the Kerr- effect. They also found a unique formation of the NLC having helicoidally variation of director and molecules possessed the bend and the twist phase which has nanometer ordered pitch. The transmission electron micrographs showed that the liquid crystals have very low pitch 8nm-9nm with periodic modulation of liquid crystal director that was varied in a helical manner due to structural defects [123]. The temperature and orientation of the LC molecules in defective PCs changed the polarization and wavelength of defect mode in the transmission spectra. To exiting the threshold value, the bistability was obtained. Therefore, the photonic structure with liquid crystals is also used in the thermal switching devices. With the presence of the Kerr-effect, the defect modes were shifted and bistable conditions were produced. The maximum transmission was found 45^o angle of orientation, the transmission was decreased due to the absence of coupling for 0^o and 90^o orientation angle [124]. The negative dielectric anisotropic liquid crystal has suffered the modification of order parameter due to nanosecond formation of biaxial order, uniaxial modification in the order, and quenching of liquid crystal disturbance under the perpendicular electric field. The possible modification

has different characteristics times: up to 2ns for biaxial, up to 10ns for uniaxial, and 10ns to milliseconds for the quenching of LC director disturbances [125].

Ko et al. [126] measured the effective index of liquid crystal filled in the Fabry-Perot Etalon under the electric field and observed the value of Freedericksz transitions for different thicknesses of the liquid crystals layer. They found that the value of the Freedericksz transition remains constant. The refractive index was decreased with increasing intensity and above the threshold value; the refractive sharply decreases. Oraie et al. [127] studied the tunable wave-guiding properties of 1-DPC with LCs by using the 4x4 transfer matrix method and obtained two different defect modes in the transmission graph due to anisotropy of LC. The metamaterials were designed with liquid crystals and used to manipulate the phase and intensity of the radiation in the range of terahertz due to electrical in-plane switching. The applied electric field modified the dielectric constant of liquid crystal, and the effect of modification was found in the shifting of transmissions as well as absorption properties. Hence, the liquid crystal-based metamaterials could be used to fabricate waveguides, switches, modulation devices, etc. [128]. Mohamed et al. [129] studied the electric field distribution and transmission properties of 1-DPC with LC defect using the finite difference time domain method (FDTD) for transverse magnetic mode. They also reported an optical filter for 1300nm wavelength and the transmission properties were affected with structural parameters (thickness, temperature) and orientation angle of the molecules. They also proposed that the high tunability of the transmittance could be achieved due to nematic liquid crystals. Farrokhbin et al. [130] explained the effect of surface anchoring on the Freeedericksz transitions in nematic liquid crystals doped with ferroelectric nanoparticles. They used the finite difference and relaxation method to solve the total free energy of doped liquid crystals. Based on the Maxwell method, they gave three solutions for the director of the liquid crystal. The derived equation had only one solution for the interval of 0 to $\pi/2$. The other results suggested that the molecules had different orientations at the boundary for the higher values in comparison to the Freedericksz transitions. As the polarization of the nanoparticle decreased the saturation value of the Freederikcsz transition was achieved. The high concentration of nanoparticles produced the induced electric fields and the value of the threshold was reduced with affected coupling fields [130]. The transient domains in the liquid crystals were formed due to the coupling of optical and electric fields.

The pre-tilt angle was forced to reverse by the optical field but the tilt angle was amplified by applied voltages. This predicted that the orientation and reorientation depend on the coupling of the electric field with the optical field and the switching of the orientation also depends on the incident angle and pre-tilt angle of the liquid crystals [131]. The liquid crystals based photonic crystals were used to enhance the fluorescence property of the defect modes. Due to linear dispersion characteristics, the femtosecond laser was generated using such photonic crystals. The proposed structure showed the compression of pulses and expressed the 15 fold maximum gain. The designed structure is used in the fabrication of bio-sensing, bio-imaging, and tunable bio-photonic applications [132]. The multispectral narrowband tunable filters based on liquid crystals were used in various applications. The designed filter was composed of two-staged liquid crystal-based Lloyd filters and multiple band pass filters embedded with a retardation layer and the filter showed tunability between 450nm to 1000 nm having a bandwidth less than 10nm. By altering the orientation of the LCs, the effective index and birefringence could be tuned [133]. The doping of the carbon nanotubes and dyes in the polymer dispersed liquid crystals could regulate the orientation of the molecules, droplet size, and the dynamical properties. Due to doping, the threshold value was highly reduced and the doped liquid crystals showed fast response time in comparison to pure phase while the dye-doped cell showed high contrast in all conformations [134]. The dielectric and thermal properties of the mixture of nematic and twist-bend liquid crystals mixture were studied by Trbojevic et al. [135] and the range of the nematic phase increased and transition temperature decreased with the increase in the concentration of NLCs (5CB). The total free energies for the twist bend phase were found decreasing with a high concentration of 5CB liquid crystal. The dielectric constants were the function of frequencies for the homeotropic arrangements but it was decreased with temperature. The relaxation frequencies for all phases of the mixture and pure compound were shifted in the low energy rages with decreasing temperature.

The 1-D and 2-D diffraction gratings were prepared using twisted liquid crystal and photosensitive polymer. The efficiency of the grating was controlled by applying an electric field to the prepared structure. The structure was used as amplitude and phase grating in the low and high electric field, respectively. The obtained efficiency was independent of polarization in the wide spectral range. For the first-order diffraction,

the switching times were found in the range of milliseconds for the low electric fields [136]. The plasmonic structure based on the liquid crystals produced voltage-controlled tunability and metamaterial characteristics. The nano-scaled grating designed with aluminum and liquid crystals showed threshold independent electro-optical switching in the visible spectrum of electromagnetic waves and the switching was regulated by voltage. The switching times were found in the order of microseconds and alignments of liquid crystals could be determined by transmission obtained by the grating. Moreover, switching was also controlled by surface plasmon resonance, which was sensitive towards molecular alignment supported with metal gratings. Such metal grating could be used as a light modulator under low voltages [137]. The transmission of transducers was made of a mixture of nematic liquid crystals with quartz substrate which could be tuned by temperature. The transmission properties of such devices were also controlled by variation of the temperature [138]. The temperature-dependent dielectric constant of liquid crystals was used in the compression of chirped femtosecond pulses in photonic devices. By increasing the temperature, the duration of pulses was reduced up to 42fs. The transmission properties and dispersion graphs were obtained by the transfer matrix method and such structure was used as a tunable compressor in small dimensions [139].

Elmahdy et al. [140] studied that liquid crystal as a defect layer in one-dimensional periodic layers could be used as a thermal sensor. The author used the finite difference method to study the transmission characteristics with the variation of temperature for TE and TM modes. The defect modes and the sensitivity were dependent on the layer thickness and temperature of the LCs. LCs were used to design Tamm-Plasmon devices and with the appropriate thickness of the LC layer, the position of the resonance peaks in the photonic band gap of the PCs based on the metal layer and LCs could be determined. The change in the phase retardation, tilt angle, and birefringence of the liquid crystal shifted the resonance peaks by a few nanometers [141]. A waveguide based on the liquid crystal core and polymer substrate was designed by Asquini et al. [142] which confined the electromagnetic waves. The authors also used Monte Carlo simulation to study the orientation of LCs under electric fields. Such a designed structure was also used as a demultiplexer and optical switching devices. Meanwhile, the demultiplexer could function between the ranges of 980nm to 1550nm. The fluctuations in the director of the liquid crystal led to light

scattering phenomena, pre-tilt angle of liquid crystals was determined by using out of plane rotation method. When the pre-tilt angle was below 30^o, then transmitted intensity was easy to measure and satisfied with experimental results for both e and o modes but the measure of the extreme value of angular position was necessary for the higher angle. The incident angle and rotation angle were satisfied the Snell's law for transmission [143].

The transmission properties were tuned by changing the angle of twist and pitch of cholesteric liquid crystals with the applied electric field. The defect modes were coupled with localized states and formed the localized hybrid optical modes in the transmissions. The transmissions were different for different polarizations depending on the resonance conditions [144]. The cholesteric liquid crystals were supported the twist and bend conformations which were very sensitive towards induced torques by electromagnetic fields and hence the tunability of the pitch was achieved. The reflection and unwinding of the helical pitch were regulated by variation of intensity of the incident wave. The changes in the applied electric field produced extra torque on the molecules that affect the optical axes of the liquid crystals [145]. A tunable grating based on the Fibonacci sequence and liquid crystal was designed by Gupta et al. [146] using the photo-alignment method. The diffraction efficiency was tuned with the switching properties of liquid crystals by modulation of phase in the layer. The regions of the liquid crystal were obtained having different alignments; one region had plane alignment and the second had twisted alignment. With the 5.1 ms response time, the designed structure showed the enhanced diffraction efficiency but the diffraction pattern was contracted at 15V having fast response time (100 μs) with slower relaxation time due to the high viscosity of the liquid crystals. The variation of intensity transmitted by Fibonacci based gratings was used in super-resolution imaging and other optical applications [146].

The chirality of the cholesteric liquid crystals was used to enhance the self-focusing of electromagnetic waves using the nonlinear properties of birefringent organic materials. The reorientation of cholesteric molecules led to nonlinear properties by the minimization of free energy using the beam propagation method. The cholesteric liquid crystals and their nonlinear properties were used to study the optical topological solitons due to coupling with nonlinear effects [147]. The coupling of Dyakonov

surface waves at the interface between polycarbonate and 5CB was regulated by anisotropy with an external magnetic field. The equivalence of momentum led to a relation between the orientation angle and the angle of the incident wave. Therefore, the coupling with surface waves tuned the resulting controlled lossless circulation of Dyakonov waves by changing the incident angle [148]. The coupling with the externally applied field, the ferroelectric layers or platelets were reoriented in the layer. In the absence of an electric field, the dipole moments were very small and had very small hysteresis but it was coupled with the electric field and had a direction perpendicular to the applied field. By controlling the shape and size of the nanoscaled platelets, the ferroelectric nature of liquid crystals was observed. The dispersion of ferroelectric platelets created the mixture inhomogeneous due to clustering and asymmetrical profile and dimensions. A mixture of liquid crystals having negative and positive anisotropies was provided the resultant zero anisotropy and the coupling effect vanished for such liquid crystal mixture [149].

To exhibit the electronic and optical properties, the molecular structure was played an important role. A series of liquid crystal and the dimers showed different phases depending on the length of the molecular structure. The 1-7 member of the $MeOB_6O.m$ series showed the twist bend phase while 8-10 showed smectic phases, i.e. the molecular structure could control the phase of the liquid crystals. Due to inhomogeneity in the structure, the liquid crystals showed a smectic phase for higher members [150]. The ordering of the molecules in the liquid crystals affected the localization of light, the orientation of polarization through the magnetic and nematic periodic layers with defect layers. Such ordering of molecules was used to control the transmission properties of the magneto-photonic structure using the 4x4 Berreman matrix method. The periodic layers also showed the slow light effect for the resonant wavelengths, which could be tuned by external electric fields. The periodic structure with LC was also used in biosensing, solar cell, electro-optic modulator, and phase modulation [151, 152].

1.8 Objective of the thesis

The aim of the thesis is to investigate the study of electro-optics of anisotropic molecules for photonic applications. After the literature review, we aimed to study the electro-optical characteristics of 1-DPCs with LCs, graphene, $LiNbO_3$, and other

materials as defects. The 1-DPCs are the periodic arrangements of the dielectric materials and its properties are tuned with liquid crystals and various materials by varying their different parameters. On the interaction of optical radiation, the liquid crystals show the Freedericksz transition at a certain value of EMW intensity that is a very important phenomenon to study the electro-optical characteristics. To control the properties of 1-DPC with defect LCs, we have to solve the nonlinear differential equation for the director angle interacting with the incident electromagnetic wave and to achieve the tunability of transmittance of the 1-DPC. As we know, LCs show anisotropic behavior and it transforms into the isotropic phase at the transition temperature, and this transmission also tunes the optical properties.

1.9 Organization of the thesis

The presented thesis is divided into six chapters. The content of each chapter is given below:

Chapter 1 presents the basic introduction of electro-optics and a brief history of LCs. This chapter also describes the types of LCs and their coupling with electric fields. By the study the total free energy of any type of LCs and coupling with the applied electric field, the electro-optical characteristics can be determined. The literature survey of the liquid crystals is the main part of this chapter that presents the brief history of the electro-optical properties of LCs and the photonic crystals with LCs, and the various types of liquid crystals in the photonic applications are discussed. Besides this, the brief studies of the photonic crystals are also included in this chapter, which suggests the basic motivation to work in this field.

Chapter 2 deals with the theory and possible mathematical formulation to investigate the optical properties of photonic crystals using anisotropic molecules or materials such as liquid crystals, $LiNbO_3$, graphene, etc. The given possible mathematical formulations are based on Maxwell's equations and Bloch's theorem; the solutions of such wave equations describe the interaction of the electromagnetic wave with the material. The mathematical methods, plane wave expansion (PWE) method, finite element method (FEM), finite difference time domain method (FDTD), and transfer matrix method (TMM) are briefly described. In the whole thesis, we have adopted TMM for the study of transmission, reflection, and absorption characteristics of the 1-

DPC containing the anisotropic material as a defect because one-dimensional periodic structures are easy to fabricate using modern advanced thin-film technology.

Chapter 3 introduces the interaction of electromagnetic waves with nematic liquid crystals (PAA) and this interaction has obtained a relation between liquid crystals director for increasing and decreasing the intensity of the incident wave. After a certain value of intensity, Freedericksz transition, the molecules show orientation/reorientation for both intensities, this leads to hysteresis in the process. Further, we have used NLC as a defect layer in the 1-DPS of glass/Si materials and calculated the transmission properties at different orientation angles of the NLC layer. The hysteresis of the LCs for the different wavelengths has been also calculated. Again, we have used a defect layer liquid crystal embedded with graphene layers in the 1-DPS and calculated the transmission and absorption properties of the defect peaks by using TMM. The effect of the periodicity of photonic crystals on the transmissions is also included in the chapter.

Chapter 4 gives the study of tunable transmission properties of 1-DPS of SiO_2/TiO_2 dielectric materials with a defect layer $LiNbO_3$ embedded with LC layers with at different parameters using the 4x4 Barreman matrix method. The optical properties have been calculated at different temperatures, incident angles, voltages, and orientation angles for the TE and TM modes. The transmissions of terminal wavelengths through the considered structure have been also calculated in this chapter. Such periodic structures show switching behavior at certain suitable parameters of considered anisotropic materials, which may be used, in many electro-optical devices.

Chapter 5 illustrates the dielectric property of LC-based nanocomposite (NC) of E7 with silver nanoparticles (Ag-NPs) of different sizes at different filling fractions. The chapter includes the transmission properties of 1-DPS of TiO_2/SiO_2 materials with the defect of NC at different sizes and filling fractions of Ag-NPs with different orientations of the molecules. Surface plasmon supported optical devices show novel applications. The optical properties have been calculated using TMM for the 0^o and 90^o orientations of the molecules and different temperatures. The considered periodic structure with surface plasmon property may be used to study the optical properties of various materials for electro-optical applications.

Chapter 6 gives brief conclusions and future prospects of the thesis. This chapter discusses the basic idea of the applications of anisotropic molecules of various LCs, with LNO and graphene materials in the field of photonics, spintronics, and quantum computers.

References

[1] A. Yariv, P. Yeh, *Optical Waves in Crystals: Propagation and Control of Laser Radiation*, John Wiley and Sons, USA, 1984.

[2] P. Yeh, C. Gu, *Optics of Liquid Crystal Display*, John Wiley and Sons, USA, 1999.

[3] T. S. Narasimhamurty, *Photoelastic and Electro-Optic Properties of Crystals*, Springer, Boston, 1981.

[4] P. Yeh, *Optical Waves in Layered Media*, John Wiley and Sons, USA, 1988.

[5] H. Stegemeyer, Centenary of the discovery of liquid crystals, *Liquid Crystals*, 5, 5-6, 1989. DOI: 10.1080/02678298908026348

[6] D. Demus, J. Goodby, G. W. Gray, H.–W. Spiess, V. Vill, *Physical Properties of Liquid Crystals*, John Wiley and Sons, New York, 1999.

[7] P. G. de Gennes, *The Physics of Liquid Crystals*, Clarendon Press Oxford, 1974.

[8] S. Chandrasekhar, *Liquid Crystals*, Cambridge: Cambridge University Press, 1992.

[9] A. Ciferri, A., W. R. Krigbaum, and R. B. Meyer, *Polymer Liquid Crystals*, Academic Press., New York, 1982.

[10] L. M. Blinov, and V. G. Chigrinov, *Electrooptic Effects in Liquid Crystal Materials*, Springer-Verlag, New York 1994.

[11] I. C. Khoo, *Liquid Crystals*, John Wiley and Sons, New Jersey, 2007.

[12] G. W. Gray, M. Hird and K. J. Toyne, The Synthesis of Several Lateral Difluoro-substituted 4,4″-Dialkyl- and 4, 4″-Alkoxyalkyl-Terphenyls and a Rationalisation of the Effect of Such Substitution on Mesophase Type and Transition Temperatures, *Mol. Cryst. Liq. Cryst.*, 204, 43-64, 1991.

[13] R. Caputo, L. De Sio, A. V. Sukhov, A. Veltri, and C. Umeton, Development of a new kind of holographic grating made of liquid crystal films separated by slices of polymeric material, *Opt. Lett.*, 29, 1261, 2004.

[14] G. Strangi, V. Barna, R. Caputo, A. de Luca, C. Versace, N. Scaramuzza, C. Umeton, and R. Bartolino, Color tunable distributed feedback organic micro-cavity laser, *Phys. Rev. Lett*. 94, 63903, 2005.

[15] F. C. Frank, I. Liquid crystals: On the theory of liquid crystals, *Discuss. Faraday Soc.* 25, 19-28, 1958.

[16] M. Miesowicz, Influence of a Magnetic Field on the Viscosity of Para-Azoxyanisol, *Nature*, 136, 261, 1935.

[17] M. Miesowicz, The Three Coefficients of Viscosity of Anisotropic Liquids, *Nature*, 158, 27, 1946.

[18] R. B. Meyer, Distortion of a Cholesteric structure by a magnetic field, *App. Phys. Letts*., 14, 208-209, 1969.

[19] A. Jakli, A. Saupe, *One and two dimensional fluids: Properties of smectic, lamellar and columnar liquid crystals*, Taylor & Francis, New York, 2006.

[20] M. Nakagawa, M. Ishikawa, and I. Akhahane, Dynamic responses of Ferroelectric liquid crystals in the surface stabilized geometry I, *Jpn. J. Appl. Phys.*, 27, 456-463, 1988.

[21] M. A. Handschy and N. A. Clark, Structure and responses of Ferroelectric liquid crystals in the surface stabilized geometry, Ferroelectrics, 59, 69-116, 1984.

[22] L. Rayleigh, On the maintenance of vibrations by forces of double frequecy and on the propagation of waves through a medium endowed with a periodic structure, *Philosophical Magazine*, 24, 145-159, 1887.

[23] V. P. Bykov, Spontaneous emission in a periodic structure, *J. Exp. Theor. Phys.*, 62, 505-513, 1972.

[24] E. Yablonovitch, Inhibited spontaneous emission in solid –state physics and electronics, *Phys. Rev. Letts.*, 58, 2059-2062, 1987.

[25] S. John, Strong localization of photons in certain in disordered dielectric superlattices, *Phys. Rev. Letts*, 58, 2486-2489, 1987.

[26] R. Srivastava, K. B. Thapa, S. Pati, S. P. Ojha, Omni-direction reflection in one dimensional photonic crystal, *JPIER*, 7, 133-143, 2008.

[27] T. C. King, C. J. Wu, Properties of defect modes in one-dimensional symmetric defective photonic crystals, *Physica E*, 69, 39-46, 2015].

[28] J. D. Joannopoulos, R. D. Meade, and J. N. Winn, *Photonic Crystals: Molding the Flow of Electromagnetic wave*, Princeton, Princeton Univ. Press, 1995.

[29] M. Skorobogatiy, and J. Yang, *Fundamentals of Photonic Crystal Guiding*, New York, Cambridge University Press, 2009.

[30] I. A. Sukhoivanov, and I. V. Guryev, *Physics and Practical Modeling*, Berlin, Springer, 2009.

[31] K. Sakoda, *Optical Properties of Photonic Crystals*, New York, Springer, 2005.

[32] G. H. Conners, Electromagnetic Wave Propagation in Cholesteric Materials, *JOSA*, 58, 875-879, 1968.

[33] L. Melamed and D. Rubin, Selected Optical Properties of Mixtures of Cholesteric Liquid Crystals, *App. Opt.*, 10, 1103-1107, 1971.

[34] D. W. Berreman, Optics in Stratified and Anisotropic Media: 4x4-Matrix Formulation, *JOSA*, 62, 502-510, 1972.

[35] R. M. A. Azzam and *N.* M. Bashara, Simplified Approach to the Propagation of Polarized Light in Anisotropic Media-Application to Liquid Crystals*, *JOSA*, 62, 1252-1257, 1972.

[36] W. Helfrich, Electric Alignment of Liquid Crystal, *Molecular Crystals and Liquid Crystals*, 21, 187-209, 1973.

[37] P. D. Berezin, I. N. Kompanets, V. V. Nikitin, and S. A. Pikin, Orienting effect of an electric field on nematic liquid crystals, *Sov. Phys.-JETP*, 37, 305-308, 1973.

[38] Elachi and C. Yeh, Stop bands for optical wave propagation in cholesteric liquid crystals*, *JOSA*, 63, 840-842, 1973.

[39] G. H. Brown, Structure, properties, and some applications of liquid crystals*, *JOSA*, 63, 1505-1514, 1973.

[40] R. A. Kashnow and C. R. Stein, Total-Reflection Liquid-Crystal Electrooptic Device, *App. Opt.*, 12, 2309-2311, 1973.

[41] J. Grinberg and A. D. Jacobson, Transmission characteristics of a twisted nematic liquid-crystal layer*, *J. Opt. Soc. Am.*, 66, 1003-1009, 1976.

[42] J. E. Bigelow and R. A. Kashnow, Poincare sphere analysis of liquid crystal optics, *App. Opt.*, 16, 2090-2096, 1977.

[43] Riviere, Y. Levy And C. Imbert, Determination Of Liquid Crystal Refractive Indices From Critical Angle Measurements, *Opt. Commun.*, 25, 210, 1978.

[44] P. Mclntyre, Transmission of light through a twisted nematic liquid-crystal Layer, *J. Opt. Soc. Am.*, 68, 869-872,1978.

[45] R. J. Cox, Liquid Crystal Guest-Host Systems, *Mol. Cryst. Liq. Cryst*., 55, 1-32, 1979.

[46] L. E. Hajdo and A. C. Eringen, Theory of light reflection by cholesteric liquid crystals possessing a tilted structure, *J. Opt. Soc. Am.*, 69, 1509-1513, 1979.

[47] V. V. Zheleznyakov, V. V. Kocharovskil, and V. V. Kocharovskil, Linear interaction of waves in liquid-crystal optics, *Sov. Phys. JETP*, 52, 877-889, 1980.

[48] P. Chavel, A. A. Sawohuk, T. C. Strand, and A. R. Tanguay, Jr., B. H. Soffer, Optical logic with variable-grating-mode liquid-crystal devices, *Opt. Letts.*, 5, 398-400, 1980.

[49] H. P. Hinov, Total internal reflection from nematic liquid crystals, *Revue Phys. Appl.*, 15, 1307-1321, 1980.

[50] M. Ohgawara, T. Uchida & M. Wada, Liquid Crystal Orientation on Various Surfaces, *Molecular Crystals and Liquid Crystals*, 74, 227-242, 1981.

[51] R. J. Gagnon , Liquid-crystal twist-cell optics, *J. Opt. Soc. Am.*, 71, 348-353, 1981.

[52] W. Wagner, Molecular Correlations in a Nematic Liquid Crystal, *Molecular Crystals and Liquid Crystals*, 75, 169-177,1981.

[53] S. D. Durbin, S. M. Arakelian, and Y. H. Shen, Optical-Field-Induced Birefringence and Freedericksz Transition in a Nematic Liquid Crystal, *Phy. Rev, Letts*., 47, 1411-1414, 1981.

[54] I. C. Khoo, Optically induced molecular reorientation and third-order nonlinear optical processes in nematic liquid crystals, *Phys. Rev. A*, 23, 2077-2081, 1981.

[55] I. C. Khoo, Theory of optically induced molecular reorientations and quantitative experiments on wave mixing and the self-focusing of light, *Phys. Rev. A*, 25, 1636-1644, 1982.

[56] K. H. Yang and C. Rosenblatt, Determination of the anisotropic potential at the nematic liquid crystal to wall interface, *Appl. Phys. Letts*, 43, 62-64, 1983.

[57] H. L. Ong, Optically induced Freedericksz transition and bistability in a nematic liquid crystal, *Phys. Rev. A*, 28, 2393-2407, 1983.

[58] W. Horsthemke, C. R. Doering, R. Lefever and A. S. Chi, Effect of external-field fluctuations on instabilities in nematic liquid crystals, *Phys. Rev. A*, 31, 1123-1135, 1985.

[59] H. L. Ong and R. B. Meyer, Geometrical-optics approximation for the electromagnetic fields in layered-inhomogeneous liquid-crystalline structures, *J. Opt. Soc. Am. A*, 2, 198-201, 1985.

[60] J. A. Kosmopoulos and H. M. Zenginoglou, Geometrical optics approach to the nematic liquid crystal grating: numerical results, *App. Opt.*, 26, 1714, 1987.

[61] N. V. Tabiryan, A. V. Sukhov & B. YA. Zel'dovich, Orientational Optical Nonlinearity of Liquid Crystals, *Molecular Crystals and Liquid Crystals*, 136, 1-139, 1986.

[62] R.-P. Pan, H. Hsiung, and Y. R. Shen, Laser-induced Freedericksz transition in nematic-liquid-crystal films with an air interface: Study of orientation anchoring and damping, *Phys. Rev. A*, 36, 5505-5508, 1987].

[63] L. Lam, Z. C. Ou-Yang, M. Lax, Ab initio theory of linear and nonlinear optics of liquid crystals, *Phys. Rev. A*, 37, 3469-3474, 1988.

[64] C. Umeton, R. Bartolino, G. Cipparrone, and F. Simoni, Liquid crystal laser tuner, *App. Opt.*, 27, 210-211, 1988.

[65] B. J. Frisken and P. P. Muhoray, Electric-field-induced twist and bend Freedericksz transitions in nematic liquid crystals, *Phys. Rev. A*, 39, 1513-1518, 1989.

[66] B. J. Frisken and P. P. Muhoray, Freedericksz transitions in nematic liquid crystals: The effects of an in-plane electric field, *Phys. Rev. A*, 40, 6099-6102, 1989.

[67] M. Foresti, Plane-wave propagation in a plane-oriented nematic liquid-crystal multilayer: the case of a wave incident upon the plane containing the liquid-crystal directors, *J. Opt. Soc. Am. A*, 6, 1254-1259, 1989.

[68] R. C. Sharp, D. P. Resler, D. S. Hobbs, and T. A. Dorschner, Electrically tunable liquid-crystal wave plate in the infrared, *Opt. Letts.*, 15, 87-89, 1990.

[69] P.-Y. Wang, J.-H. Dai, and H.-J. Zhang, Optically induced frequency locking of a nematic liquid crystal in a Fabry-Perot interferometer, *Phys. Rev. A*, 41, 3250-3257, 1990.

[70] J. Lekner, Reflection, and refraction by uniaxial crystals, *J. Phys.: Condens. Matter*, 6121-6133, 1991.

[71] S. J. Elston, Smectic-*A* Freedericksz transition, *Phys. Rev. E*, 58, R1215-R1217, 1998.

[72] K. Busch and S. John, Liquid-Crystal Photonic-Band-Gap Materials: The Tunable Electromagnetic Vacuum, *Phys. Rev. Letts*., 83, 967-970, 1999.

[73] Y.- C.Yang, C.-S. Kee, J.-E. Kim, and H. Y. Park, J.-C. Lee, Y.-J. Jeon, Defect modes of cholesteric liquid crystals, *Phys. Rev. E*, 60, 6852-6854, 1999.

[74] R. R. Swisher, H. Huo, and P. P. Crooker, The cholesteric-nematic transition in droplets subjected to electric fields, *Liquid Crystals*, 26, 57-62, 1999.

[75] P. Etchegoin, Blue phases of cholesteric liquid crystals as thermotropic photonic crystals, *Phys. Rev. E*, 62, 1435-1437, 2000.

[76] S. W. Leonard, J. P. Mondia, H. M. van Driel, O. Toader, and S. John, K. Busch, A. Birner, and U. Gosele, V. Lehmann, Tunable two-dimensional photonic crystals using liquid-crystal infiltration, *Phys. Rev. B*, 61, R2389-R2392, 2000.

[77] D. Kang, J. E. Maclennan, N. A. Clark, A. A. Zakhidov, and R. H. Baughman, Electro-optic Behavior of Liquid-Crystal-Filled Silica Opal Photonic Crystals: Effect of Liquid-Crystal Alignment, *Phys. Rev. Letts.*, 86, 4052-4055, 2001.

[78] C.-S. Kee and H. Lim, Two-dimensional tunable metallic photonic crystals infiltrated with liquid crystals, *Phys. Rev. B*, 64, 085114(1-7), 2001.

[79] K. Yoshino, Y. Shimoda, K. Nakayama, T. Tamura, T. Matsui, H. Kajii and M. Ozaki, Novel Electrical and Optical Properties of Liquid Crystals Infiltrated in Opal as Photonic Crystal, Molecular Crystals and Liquid Crystals Science and Technology. Section A. *Molecular Crystals and Liquid Crystals*, 364, 501-509, 2001.

[80] Y. Shimoda, K. Nakayama, M. Ozaki, and K. Yoshino, Temperature Tuning of Optical Stop Band of Liquid-Crystal Infiltrated Synthetic Opal, *Mol. Cryst. Liq. Cryst.*, 68, 351-358, 2001.

[81] H. Takeda and K. Yoshino, Disappearances of uncoupled modes in two-dimensional photonic and crystals due to anisotropies of liquid crystals, *Phys. Rev. E*, 67, 056612(1-5), 2003.

[82] L. Z. Ruan, J. R. Sambles, I.W. Stewart, Self-Organized Periodic Photonic Structure in a Nonchiral Liquid Crystal, *Phys. Rev. Letts.*, 91, 033901(1-4), 2003.

[83] R. Ozaki, H. Miyoshi, M. Ozaki, and K. Yoshino, Fast Electrooptic Response Based on Defect Mode Switching in One-Dimensional Photonic Crystal Containing Nematic Liquid Crystal and Ferroelectric Liquid Crystal as a Defect Layer *Ferroelectrics*, 312, 63–69, 2004.

[84] R. Ozaki, M. Ozaki, and K. Yoshino, Defect Mode in One-Dimensional Photonic Crystal with In-Plane Switchable Nematic Liquid Crystal Defect Layer, *Jpn. J. Appl. Phys.*, 43, L1477-L1479, 2004.

[85] T. Matsui, M. Ozaki, and K.Yoshino, Tunable photonic defect modes in a cholesteric liquid crystal induced by optical deformation of helix, *Phys. Rev. E*, 69, 061715(1-4), 2004.

[86] Q. Wang and S. He, A new effective model for the director distribution of a twisted nematic liquid crystal cell, *J. Opt. A: Pure Appl. Opt.* 7, 438-444, 2005.

[87] J.-Y. Chen and L.-W. Chen, Defect modes in a stacked structure of chiral photonic crystals, *Phys. Rev. E*, 71, 061708(1-7), 2005.

[88] E. Graugnard, J. S. King, S. Jain, and C. J. Summers, Y. Zhang-Williams and I. C. Khoo, Electric-field tuning of the Bragg peak in large-pore TiO_2 inverse shell opals, *Phys. Rev. B*, 72, 233105(1-4), 2005.

[89] R. Ozaki, Y. Matsuhisa, M. Ozaki & K. Yoshino, Laser Action Based on Electrically Controllable Defect Mode in One-Dimensional Photonic Crystal Containing Conducting Polymer and Liquid Crystal Defect Layers, *Mol. Cryst. Liq. Cryst.*, 433, 237-245, 2005.

[90] R. Ozaki, Y. Matsuhisa, M. Ozaki and K. Yoshino (2005) Low Driving Voltage Tunable Laser Based on One-dimensional Photonic Crystal Containing Liquid Crystal Defect Layer, *Mol. Cryst. Liq. Cryst.*, 441, 87-95, 2005.

[91] C.-Y. Liu and L.-W. Chen, Tunable band gap in a photonic crystal modulated by a nematic liquid crystal, *Phys. Rev. B*, 72, 045133(1-5), 2005.

[92] R. Ozaki , H. Miyoshi , M. Ozaki and K. Yoshino, Tunable Defect Mode in One-Dimensional Photonic Crystal with Liquid Crystal Defect Layer, *Mol. Cryst. Liq. Cryst.*, 433, 247-257, 2005.

[93] V. Ilyina, S. J. Cox, T.J. Sluckin, A computational approach to the optical Freedericksz transition, *Opt. Commun.*, 260, 474-480, 2006.

[94] Q. Wang and S. He, Analysis and design of variable optical attenuators based on nematic liquid-crystal cells, *J. Mod. Opt.*, 53, 481-493, 2006.

[95] P. Halevi and J. A. R. Avendaño, J. A. R.-Cervantes, Electrically tuned phase transition and band structure in a liquid-crystal-infilled photonic crystal, *Phys. Rev. E*, 73, 040701(1-4), 2006.

[96] S. Gottardo, M. Burresi, F. Geobaldo, L. Pallavidino, F. Giorgis, and D. S. Wiersma, Self-alignment of liquid crystals in three-dimensional photonic crystals, *Phys. Rev. E*, 74, 040702(1-4), 2006.

[97] I. H. Bechtold, F. Batalioto, L. T. Thieghi, B. S. L. Honda, M. Pojar, J. Schoenmaker, A. D. Santos, V. Zucolotto, D. T. Balogh, O. N. Oliveira, Jr., and E. A. Oliveira, Transitions in the orientational order of liquid crystals induced by periodic patterned substrates, *Phys. Rev. E*, 74, 021714(1-6), 2006.

[98] A. E. Miroshnichenko, I. Pinkevych, and Y. S. Kivshar, Tunable all-optical switching in periodic structures with liquid-crystal defects, *Opt. Exp.*, 14, 2839-2844, 2006.

[99] R. Ozaki, H. Moritake, K. Yoshino, and M. Ozaki , Analysis of defect mode switching response in one-dimensional photonic crystal with a nematic liquid crystal defect layer, *J. Appl. Phys*., 101, 033503(1-6), 2007.

[100] A. H. Gevorgyan and M. Z. Harutyunyan, Chiral photonic crystals with an anisotropic defect layer, *Phys. Rev. E*, 76, 031701(1-9), 2007.

[101] J. A. Reyes, J.A. R.-Avendano, P. Halevi, Electrical tuning of photonic crystals infilled with liquid crystals, *Opt. Commun*., 281, 2535-2547, 2008.

[102] V. Ya. Zyryanov, V. A. Gunyakov, S. A. Myslivets , V. G. Arkhipkin, and V. F. Shabanov, Electrooptical Switching in a One-Dimensional Photonic Crystal, *Mol. Cryst. Liq. Cryst.*, 488, 118-126, 2008.

[103] S. Shoarinejad, M.A. Shahzamanian, On the numerical study of Frederick transition in nematic liquid crystals, *J. Mol. Liq.*, 138, 14-19, 2008.

[104] A. Denisov and J. L. de Bougrenet de la Tocnaye, Photonic Crystals based on Cholesteric Liquid Crystals, *Mol. Cryst. Liq. Cryst.*, 494, 179-186, 2008.

[105] S. S. Choi, S. M. Morris, W. T. S. Huck, and H. J. Coles, Electrically Tuneable Liquid Crystal Photonic Bandgaps, *Adv. Mater.*, 21, 3915–3918, 2009.

[106] I. C. Khoo, A. Diaz, J. Liou, D. Werner, J. H. Park, Y. Ma, and J. Huang, Liquid Crystal Nonlinear Optical Meta-Materials, *Mol. Cryst. Liq. Cryst.*, 502, 109-120, 2009.

[107] O. Takayama, L. Crasovan, D. Artigas, and L. Torner, Observation of Dyakonov Surface Waves, *Phys. Rev. Letts.*, 102, 043903(1-4), 2009.

[108] F. R. Hung, Quadrupolar particles in a nematic liquid crystal: Effects of particle size and shape, *Phys. Rev. E*, 79, 021705, 2009.

[109] L. M. Lopatina and J. V. Selinger, Theory of Ferroelectric Nanoparticles in Nematic Liquid Crystals, *Phys. Rev. Letts*., 102, 197802, 2009.

[110] J. Cos, J. Ferre-Borrull, J. Pallares, L.F. Marsal, Tunable Fabry–Pérot filter based on one-dimensional photonic crystals with liquid crystal components, *Opt. Commun*., 282, 1220-1225, 2009.

[111] B. Rezaei, M. Kalafi, Tunable full band gap in two-dimensional anisotropic photonic crystals infiltrated with liquid crystals, *Opt. Commun.*, 282, 1584–1588, 2009.

[112] V. Y. Zyryanov, S. A. Myslivets, V. A. Gunyakov, A. M. Parshin, V. G. Arkhipkin, V. F. Shabanov, and W. Lee, Magnetic-field tunable defect modes in a photonic-crystal/liquid-crystal cell, *Opt. Exp.*, 18, 1283, 2010.

[113] B. F. de Oliveira, P. P. Avelino, F. Moraes, and J. C. R. E. Oliveira, Nematic liquid crystal dynamics under applied electric fields, *Phys. Rev. E*, 82, 041707(1-6), 2010].

[114] Y.-T. Lin, W.-Y. Chang, C.-Y. Wu, V. Ya. Zyryanov, and W. Lee, Optical properties of one-dimensional photonic crystal with a twisted-nematic defect layer, *Opt. Exp.*, 18, 26959-26964, 2010.

[115] S.-Y. T. Tzeng , C.-N. Chen & Y. Tzeng, Thermal tuning band gap in cholesteric liquid crystals, *Liquid Crystals*, 37, 1221-1224, 2010.

[116] J. Beeckman, K. Neyts, P. J. M. Vanbrabant Liquid-crystal photonic applications, *Opt. Engineering*, 50, 081202(1-17), 2011.

[117] Z. He, Z. Ye, Q. Cui, J. Zhu, H. Gao, Y. Ling, H. Cui, J. Lu, X. Guo, Y. Su, Reflection chromaticity of cholesteric liquid crystals with sandwiched periodical isotropic defect layers, *Opt. Commun*., 284, 4022-4027, 2011.

[118] C. G. Avendao, I. Molina and J. A. Reyes, Anchoring effects on the electrically controlled optical band gap in twisted photonic liquid crystals, *Liquid Crystals*, 40, 172-184, 2013.

[119] S. M. Morris, D. J. Gardiner, P. J. W. Hands, M. M. Qasim, T. D. Wilkinson, I. H. White, and H. J. Coles, Electrically switchable random to photonic band-edge laser emission in chiral nematic liquid crystals, *Appl. Phys .Letts.,* 100, 071110(1-3), 2012.

[120] H. Hajian, B. Rezaei, A. S. Vala, and M. Kalafi, Tuned switching of surface waves by a liquid crystal cap layer in one-dimensional photonic crystals, *App. Opt.,* 51, 2909-2916, 2012.

[121] D.-H. Ko, S. M. Morris, A. Lorenz, F. Castles, H. Butt, D. J. Gardiner, M. M. Qasim, B. Wallikewitz, P. J. W. Hands, T. D. Wilkinson, G. A. J. Amaratunga, H. J. Coles, and R. H. Friend, A nano-patterned photonic crystal laser with a dye-doped liquid crystal, *Appl. Phys. Letts.*, 103, 051101-6, 2013.

[122] V. Borshch, S. V. Shiyanovskii, and O. D. Lavrentovich, Nanosecond Electro-Optic Switching of a Liquid Crystal, *Phys. Rev. Letts*., 111, 107802(1-5), 2013.

[123] V. Borshch, Y.-K. Kim, J. Xiang, M. Gao, A. Jakli, V. P. Panov, J.K. Vij, C.T. Imrie, M.G. Tamba, G.H. Mehl and O.D. Lavrentovich,Nematic twist-bend phase with nanoscale modulation of molecular orientation, *Nat. Commun.*, 4, 2635(1-8h), 2013.

[124] S. R. Entezar, A. Madani, M. K. Habil, A. Namdar and H. Tajalli, Temperature dependent transmission and optical bistability in a 1D photonic crystal with a liquid crystal defect layer, *J. Mod. Opt.*, 60, 1883-1891, 2013.

[125] V. Borshch, S. V. Shiyanovskii, B.-X. Li, and O. D. Lavrentovich, Nanosecond electro-optics of a nematic liquid crystal with negative dielectric anisotropy, *Phys. Rev. E*, 90, 062504(1-16), 2014.

[126] M. O. Ko, S.-J. Kim, J.-H. Kim, B. W. Lee and M. Y. Jeon, Measurement of Effective Refractive Index of Nematic Liquid Crystal in Fabry-Perot Etalon, *J. Opt. Soc. Korea*, 19, 348-350, 2015.

[127] M.R. Oraie, S.M. Hamidi, H. Latifi, One dimensional tunable Coupled Resonator Optical Waveguide based on Liquid- Crystal layers, *Optik - International Journal for Light and Electron Optics* (2015).

[128] R. Kowerdziej and L. Jaroszewicz, Active control of terahertz radiation using a metamaterial loaded with a nematic liquid crystal, *Liquid Crystals*, 2016. DOI: 10.1080/02678292.2016.1160297

[129] M. S. Mohamed, M. F. O. Hameed, M. M. El-Okr, S. S. A. Obayya, Characterization of One Dimensional Liquid Crystal Photonic Crystal Structure, *Optik*, 127, 8774-8781, 2016.

[130] M. Farrokhbin, E. Kadivar, Effects of surface anchoring on the electric Frederiks transition in ferronematic systems, *Physica A*, 462, 725–736, 2016.

[131] V. Nersesyan, T. Brans, F. Beunis, R. Drampyan, J. Beeckman & K. Neyts, Light-controlled reorientation of nematic liquid crystal driven by an electric field, *Liquid Crystals*, 2016. DOI: 10.1080/02678292.2016.1178350

[132] Y.-C. Hsiao, Liquid crystal-based tunable photonic crystals for pulse compression and signal enhancement in multiphoton fluorescence, *Opt. Mat. Exp.*, 6, 1929, 2016.

[133] M. Abuleil and I. Abdulhalim, Narrowband multispectral liquid crystal tunable filter, *Opt. Letts.*, 41, 1957-1960, 2016.

[134] P. Kumar, V. Sharma, C. Jaggi, P. Malik and K. K. Raina, Orientational control of liquid crystal molecules via carbon nanotubes and dichroic dye in polymer dispersed liquid crystal, *Liquid Crystals*, 2016. DOI: 10.1080/02678292.2016.1247476

[135] N. Trbojevic, D. J. Read, and M. Nagaraj, Dielectric properties of liquid crystalline dimer mixtures, *Phys. Rev. E*, 96, 052703(1-10), 2017.

[136] R. Węgłowski, A. K. -Szmigiel, W. Piecek, J. Konieczkowska, E. S.-Balcerzak, Electro-optically tunable diffraction grating with photoaligned liquid Crystals, *Opt. Commun.*, 400, 144-149, 2017.

[137] M. V. Gorkunov, V. Kasyanova, V. Artemov, M. I. Barnik, A. R. Geivandov, and S. P. Palto, Fast Surface-Plasmon-Mediated Electro-Optics of a Liquid Crystal on a Metal, *Phys. Rev. Appl.*, 8, 054051(1-10), 2017.

[138] R. Kowerdziej, K. Garbat and M. Walczakowski, Nematic liquid crystal mixtures dedicated to thermally tunable terahertz devices, *Liquid Crystals*, 2017. DOI:10.1080/02678292.2017.1404158

[139] R. Shiri, E. Safari and A. Bananej, Temperature control of the ultra-short laser pulse compression in a one-dimensional photonic band gap structure with nematic liquid crystal as a defect layer, *J. Mod. Opt.*, 2017. DOI:10.1080/09500340.2017.1401133

[140] N. A. Elmahdy, M. S. Esmail, M. M. El-OKr, Characterization of a Thermal Sensor Based on One-Dimensional Photonic Crystal with Central Liquid Crystal Defect, *Optik, 2018.* https://doi.org/10.1016/j.ijleo.2018.05.117

[141] H. -C. Cheng, C. -Y. Kuo, Y. -J. Hung, K. -P. Chen, and S. -C. Jeng, Liquid-Crystal Active Tamm-Plasmon Devices, *Phys. Rev. Appl.*, 9, 064034(1-8), 2018.

[142] R. Asquini, C. Chiccoli, P. Pasini, L. Civita and A. d'Alessandro, Low power photonic devices based on electrically controlled nematic liquid crystals embedded in poly (dimethylsiloxane), *Liquid Crystals*, 2018. DOI: 10.1080/02678292.2018.1494342

[143] C. -W. Chiang and K. -H. Yang, Optics of light scattering caused by liquid-crystal-director fluctuations, *Liquid Crystals*, 2018. DOI: 10.1080/02678292.2018.1473647

[144] M. V. Pyatnov, S. Y. Vetrov, and I. V. Timofeev, Tunable hybrid optical modes in a bounded cholesteric liquid crystal with a twist defect, *Phys. Rev. E,* 97, 032703(1-6), 2018.

[145] G. Nava, F. Ciciulla, O. S. Iadlovska, O. D. Lavrentovich, F. Simoni, and L. Lucchetti, Pitch tuning induced by optical torque in heliconical cholesteric liquid crystals, *Phys. Rev. Res*., 1, 033215(1-5), 2019.

[146] S. K. Gupta, Z. Sun, H. -S. Kwok and A. K. Srivastava, Low voltage tunable liquid crystal Fibonacci grating, *Liquid Crystals*, 2019. DOI:10.1080/02678292.2019.1706109

[147] G. Poy, A. J. Hess, I. I. Smalyukh, and S. Žumer , Chirality-Enhanced Periodic Self-Focusing of Light in Soft Birefringent Media, *Phys. Rev. Letts.,* 125, 077801(1-6), 2020.

[148] Y. Li, J. Sun, Y. Wen, and J. Zhou, Controllable Selective Coupling of Dyakonov Surface Waves at a Liquid-Crystal-Based Interface, *Phys. Rev. Appl.,* 13, 024024(1-7), 2020.

[149] M. Škarabot, M. M. Kržmanc, L. Rupnik, G. Lahajnar , D. Suvorov and I. Muševič, Electric-field-induced reorientation of ferroelectric micro- and nano-platelets in the nematic liquid crystal, *Liquid Crystals*, 2020. DOI: 10.1080/02678292.2020.1785026

[150] P. Abberley, R. Walker, J. M. D. Storey and C. T. Imrie, Molecular structure and the twist-bend nematic phase: the role of terminal chains, *Liquid Crystals*, 2020. DOI: 10.1080/02678292.2020.1770879

[151] E. J. Oliveira, P. B. de Melo, M. S. S. Pereira, F. M. Zanetti, and I. N. de Oliveira, Nematic reorientation effects on resonant modes, wavelength mismatch, and slow-light phenomena in one-dimensional magnetophotonic crystals with a dual anisotropic defect, *Phys. Rev. E,* 101, 052704(1-8), 2020.

[152] Y. Jin, S. J. Elston, J. A.J. Fells, M. J. Booth, C. Welch, G. H. Mehl, and S. M. Morris, Millisecond Optical Phase Modulation Using Multipass Configurations with Liquid-Crystal Devices. *Phys. Rev. Appl.,* 14, 024007, 2020.

CHAPTER 2

Theory and methodology

CHAPTER 2

Theory and methodology

The interaction of electromagnetic waves (EMWs) with any material or medium depends on the refractive index or dielectric function or optical density of the medium which gives the degree of propagation of EMW in materials. The interaction of the electromagnetic wave with the material or medium also depends on the surface and type of interacting material. The refractive index of the medium is related to the dielectric permittivity (ε) and the magnetic permeability (μ) of the material. The refractive index is the square root of the product of dielectric permittivity (ε) and magnetic permeability (μ) which is given as;

$$n = \pm\sqrt{\varepsilon\mu} \tag{2.1}$$

The directional propagation of EMWs through the material is given by its wave propagation vector as;

$$\vec{k} = \frac{n\omega}{c}\hat{k} \tag{2.2}$$

The interaction of EMW with any material exhibits reflection and refraction of the incident wave at the material interface, and these effects follow the Snell's law as;

$$n_1 \sin\theta_1 = n_2 \sin\theta_2 \tag{2.3}$$

where n_1, n_2 = refractive indices of the first, second medium, respectively, and θ_1, θ_2 = incident angle, refraction angle of EMW at the material interfaces, respectively. The refractive index is also can be defined as;

$$n = \frac{c}{v} \tag{2.4}$$

As we know that the propagation of EMW in the material also depends on the types of medium. In general, the materials are divided into two types: (i) isotropic medium (ii) anisotropic medium and thesis types of materials also depend on the crystal

symmetry. Therefore, the optical properties are varied with the types and symmetries of the materials.

2.1 Isotropic and anisotropic medium

As we know that the propagation of EMW inside any materials depends on the form of crystals and the optical responses of materials are also related to permittivity and permeability of the medium. Therefore, the permittivity and permeability are independent of direction and such materials are characterized as isotropic materials having equal values of principal indices, while the permittivity and permeability in the case of anisotropic material are tensor quantities and directionally dependent. Further, the anisotropic materials can also be divided depending on the principal dielectric constants. In the anisotropic materials, the electric and magnetic field vectors (E, H) are not parallel to displacement (D) and magnetic flux density (B) vectors. The material can be anisotropic in both electrically and magnetically depending on the dielectric permittivity and magnetic permeability values. When the cross-coupling between electric and magnetic field are found in any material, such material is termed as bianisotropic material and such material is electrically polarized and magnetized on the application of electric or magnetic field [1-3].

The interaction of EWM with the materials can be studied by solving Maxwell's equations which results in transmission and reflection coefficients of the material. The interaction of the wave with these materials generates various novel optical properties depending on the different arrangement of the material. The periodical arrangement of dielectric layers in different directions is known as photonic crystals (PCs) which exhibits the photonic bandgap region and such PCs are used in many optical applications; optical filters, mirrors, electro-optical devices, magneto-optical devices, optical switches, all-optical switching devices, etc. The optical properties of PCs crystals can be studied by Maxwell's equation but the calculation of transmission and reflection coefficients and dispersion relations for 3D photonic crystals are much more complicated in comparison to 1D or 2D photonic crystals.

Now, we discuss the EMW propagation in isotropic and anisotropic media using Maxwell's equations.

2.1.1 Propagation of electromagnetic wave in the isotropic medium

When the electromagnetic plane wave incident on the isotropic media, the electric field induces the polarization parallel to the electric field, and induced polarization is found proportional to the electric field as [1,4,5];

$$\vec{P} = \varepsilon_0 \chi \vec{E} \tag{2.5}$$

where P= Polarization, E = Electric field, χ = susceptibility of the medium, ε_0 = permittivity of vacuum. Maxwell gave the constitutive relations for electric displacement, electric field, magnetic field, and the magnetic inductions in the material as;

$$D = \varepsilon E = \varepsilon_0 E + P \tag{2.6}$$

$$B = \mu H = \mu_0 H + M \tag{2.7}$$

where P= Polarization (induced by an electric field), M= polarizations induced by the magnetic field in isotropic media.

On putting the value of P in the equation 2.6, it gives relative electric permittivity:

$$\varepsilon = 1 + \chi \tag{2.8}$$

Similarly, on putting the value of M in the equation 2.7, it gives the relative magnetic susceptibility that can be represented as;

$$\mu = 1 + \chi_m \tag{2.9}$$

The constitutive relations for the material are given as;

$$B = \mu_0 \mu H \tag{2.10}$$

$$D = \varepsilon_0 \varepsilon E \tag{2.11}$$

Now, Maxwell's equations for isotropic material are given as;

$$\nabla \cdot D = \frac{\rho}{\varepsilon_0} \tag{2.12}$$

$$\nabla \cdot B = 0 \tag{2.13}$$

$$\nabla \times E = -\frac{\partial B}{\partial t} \tag{2.14}$$

$$\nabla \times \mathrm{H} = \frac{\partial \mathrm{D}}{\partial \mathrm{t}} \tag{2.15}$$

On putting the values from equations 2.5 and 2.6 in equation 2.14 and divided by μ and taking the curl of both sides gives;

$$\nabla \times \left(\frac{1}{\mu} \nabla \times \mathrm{E} \right) + \frac{\partial}{\partial \mathrm{t}} \nabla \times \mathrm{H} = 0 \tag{2.16}$$

On differentiating equation 2.15 and combining with equation 2.16, it gives;

$$\nabla \times \left(\frac{1}{\mu} \nabla \times \mathrm{E} \right) + \varepsilon \frac{\partial^2 \mathrm{E}}{\partial \mathrm{t}^2} = 0 \tag{2.17}$$

The expansion of curl in equation 2.17 gives;

$$\nabla^2 \mathrm{E} - \varepsilon\mu \frac{\partial^2 \mathrm{E}}{\partial \mathrm{t}^2} - \nabla(\nabla \cdot \mathrm{E}) + (\nabla \log \mu) \times (\nabla \times \mathrm{E}) = 0 \tag{2.18}$$

For the isotropic media, the gradient and logarithm terms vanish and equation 2.18 is reduced to equation 2.19.

$$\nabla^2 \mathrm{E} - \varepsilon\mu \frac{\partial^2 \mathrm{E}}{\partial \mathrm{t}^2} = 0 \tag{2.19}$$

Similarly, we can obtain for the magnetic field as;

$$\nabla^2 \mathrm{H} - \varepsilon\mu \frac{\partial^2 \mathrm{H}}{\partial \mathrm{t}^2} = 0 \tag{2.20}$$

The equations 2.19 and 2.20 are electromagnetic wave equations and the solution of wave equations has exponential terms as exp[i(ωt-k.r)]. The magnitude of wave vector and velocity of wave written as;

$$\left| \vec{\mathrm{k}} \right| = \omega \sqrt{\varepsilon\mu} \tag{2.21}$$

$$\mathrm{v} = \omega / \mathrm{k} = 1 / \sqrt{\varepsilon\mu} \tag{2.22}$$

For the propagation of the electromagnetic wave in vacuum, the phase velocity is given by;

$$\mathrm{c} = \frac{1}{\sqrt{\varepsilon_0 \mu_0}} = 2.99793 \times 10^8 \mathrm{m/s} \tag{2.23}$$

The B and E vectors are orthogonal to each other and the magnitude of B can be given by;

$$|B| = \frac{n}{c}|E| \tag{2.24}$$

The energy density (u) and Poynting vector (S) of the electromagnetic wave is given by;

$$u = \frac{E \cdot D + H \cdot B}{2} \tag{2.25}$$

$$S = E \times H \tag{2.26}$$

2.1.2 The dielectric tensor of the anisotropic medium

In the case of an isotropic medium, the induced polarization is linearly related to susceptibility and persisted parallel to the direction of the applied field. But in anisotropic media, the direction and magnitude of the induced polarization depend on applied field direction. The polarization vector in the anisotropic medium is related to tensor electric susceptibility and the magnitude of such tensor quantity depends on the cartesian coordinate system, x, y, z axes in the crystal [1,6]. The polarization vectors along the x, y, and z-axis in the crystal are represented as;

$$P_x = \varepsilon_0\left(\chi_{11}E_x + \chi_{12}E_y + \chi_{13}E_z\right) \tag{2.27}$$

$$P_y = \varepsilon_0\left(\chi_{21}E_x + \chi_{22}E_y + \chi_{23}E_z\right) \tag{2.28}$$

$$P_z = \varepsilon_0\left(\chi_{31}E_x + \chi_{32}E_y + \chi_{33}E_z\right) \tag{2.29}$$

Consider a special arrangement of x, y, z axes in such a way that off elements of the dielectric tensor vanished, then the polarization along the principal axes can be written as;

$$P_x = \varepsilon_0\chi_{11}E_x \tag{2.30}$$

$$P_y = \varepsilon_0\chi_{22}E_y \tag{2.31}$$

$$P_z = \varepsilon_0\chi_{33}E_z \tag{2.32}$$

Similarly, the dielectric response is related to the tensor dielectric permittivity as;

$$D_x = \left(\varepsilon_{11}E_x + \varepsilon_{12}E_y + \varepsilon_{13}E_z\right) \tag{2.33}$$

$$D_y = \left(\varepsilon_{21}E_x + \varepsilon_{22}E_y + \varepsilon_{23}E_z\right) \tag{2.34}$$

$$D_y = \left(\varepsilon_{31}E_x + \varepsilon_{32}E_y + \varepsilon_{33}E_z\right) \tag{2.35}$$

The above equations 2.33, 2.34, and 2.35 can be representation in tensor form as;

$$D_i = \varepsilon_{ij}E_j \tag{2.36}$$

The dielectric permittivity is also associated with the susceptibility as;

$$\varepsilon_{ij} = \varepsilon_0(1+\chi_{ij}) \tag{2.37}$$

The dielectric tensor is the symmetric quantity and has only six independent elements. For the conservation of electromagnetic field energy, the dielectric tensor must be Hermitian.

2.1.3 Propagation of plane wave in anisotropic medium

When an electromagnetic plane wave propagates through the anisotropic medium, the velocity of the wave relies on the propagation directions and polarization states. For a certain propagation direction, two eigen waves with eigen phase velocities and polarizations exist [1,6,7]. The waves parallel to the polarization directions are transmitted through the medium while others are prohibited.

Consider an electromagnetic wave having frequency ω interacting with anisotropic medium, the electric and magnetic field are given as;

$$E\exp(i\omega t - ik\cdot r) \tag{2.38}$$

$$H\exp(i\omega t - ik\cdot r) \tag{2.39}$$

where $k = n\omega s/c$ = wave vector and $\hat{s}$ = unit vector in the propagation direction; n = refractive index.

From the Maxwell's equations 2.14 and 2.15, can be described as;

$$k\times E = \omega\mu H \tag{2.40}$$

$$k\times H = -\omega\varepsilon E \tag{2.41}$$

On solving the equations 2.40 and 2.41, we found equation 2.42 as;

$$k \times (k \times E) + \omega^2 \mu \varepsilon E = 0 \tag{2.42}$$

The uniaxial material has dielectric permittivity having only diagonal elements as;

$$\varepsilon = \begin{bmatrix} \varepsilon_x & 0 & 0 \\ 0 & \varepsilon_y & 0 \\ 0 & 0 & \varepsilon_z \end{bmatrix} \tag{2.43}$$

The equation 2.42, for the uniaxial crystal can be written as;

$$\begin{pmatrix} \omega^2 \mu \varepsilon_x - k_y^2 - k_z^2 & k_x k_y & k_x k_z \\ k_x k_y & \omega^2 \mu \varepsilon_y - k_x^2 - k_y^2 & k_y k_z \\ k_x k_z & k_y k_z & \omega^2 \mu \varepsilon_z - k_x^2 - k_y^2 \end{pmatrix} \begin{pmatrix} E_x \\ E_y \\ E_z \end{pmatrix} = 0 \tag{2.44}$$

For a non-trival solution of the equation 2.44, the determinant must be zero.

$$\begin{vmatrix} \omega^2 \mu \varepsilon_x - k_y^2 - k_z^2 & k_x k_y & k_x k_z \\ k_x k_y & \omega^2 \mu \varepsilon_y - k_x^2 - k_y^2 & k_y k_z \\ k_x k_z & k_y k_z & \omega^2 \mu \varepsilon_z - k_x^2 - k_y^2 \end{vmatrix} = 0 \tag{2.45}$$

The above equation 2.45 represents by 3D surface in k space; called a normal surface consists of two sheets having four mutual points. The two different lines that go from the origin are recognized as optic axes and the different k values resemble two different phase velocities. The direction of the electric field of propagating plane wave can be found by solving equation 2.44, which is given as;

$$\begin{pmatrix} \dfrac{k_x}{k^2 - \omega^2 \mu \varepsilon_x} \\ \dfrac{k_y}{k^2 - \omega^2 \mu \varepsilon_y} \\ \dfrac{k_z}{k^2 - \omega^2 \mu \varepsilon_z} \end{pmatrix} \tag{2.46}$$

The above two equations 2.42 and 2.44 can be written in the form of direction cosines as;

$$\frac{s_x^2}{n^2 - \varepsilon_x / \varepsilon_0} + \frac{s_y^2}{n^2 - \varepsilon_y / \varepsilon_0} + \frac{s_z^2}{n^2 - \varepsilon_z / \varepsilon_0} = \frac{1}{n^2} \tag{2.47}$$

$$\begin{pmatrix} \dfrac{s_x}{n^2 - \varepsilon_x / \varepsilon_0} \\ \dfrac{s_y}{n^2 - \varepsilon_y / \varepsilon_0} \\ \dfrac{s_z}{n^2 - \varepsilon_z / \varepsilon_0} \end{pmatrix} \tag{2.48}$$

The represented equation 2.47 is known as Fresnal's equation of wave normal which gives the refractive indices and equation 2.48 gives the polarization direction.

The index ellipsoid for the uniaxial crystals can be represented as;

$$\frac{x^2}{n_o^2} + \frac{y^2}{n_o^2} + \frac{z^2}{n_e^2} = 1 \tag{2.49}$$

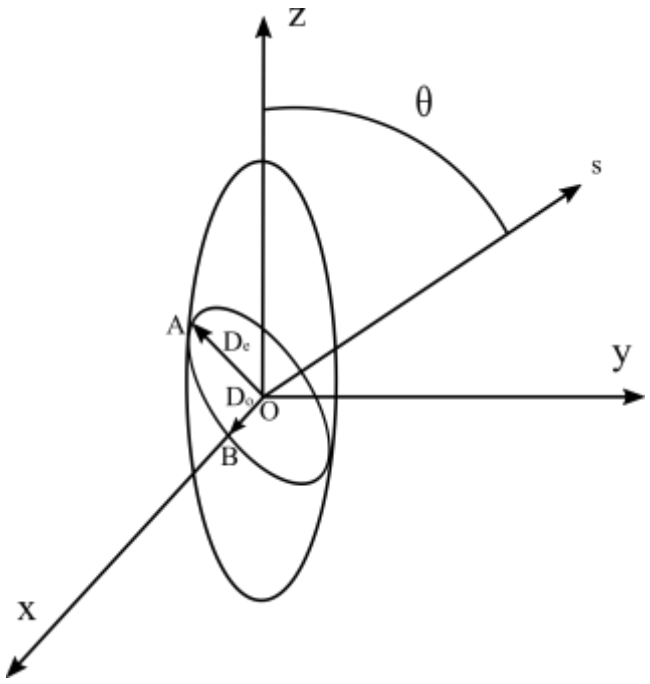

Figure 2.1: Construction of intersecting a plane with the origin for finding refractive indices for the uniaxial crystal.

The direction of the electromagnetic plane wave along the s direction for positive uniaxial crystals is shown in figure 2.1. The index ellipsoid of the crystals is invariant under the revolution about the z-axis and the projections of s vector on the x-y plane coincide with the y-axis. The intersection of the plane with the origin is an ellipse and the length of semi-major axis OA is equal to an extraordinary refractive index having electric displacement D_e (θ) parallel to OA as shown in figure 2.1.

The ordinary wave is along the OB direction having an ordinary refractive index and the polarization direction of the ordinary wave remains fixed having refractive index n_o; while the polarization direction of the extraordinary wave depends on the angle between the optic axis and s vector. The refractive index for the extraordinary waves varies from n_o up to n_e for angle 0^o and 90^o. The refractive index n_e follows the relation as;

$$\frac{1}{n_e^2(\theta)} = \frac{\cos^2\theta}{n_o^2} + \frac{\sin^2\theta}{n_e^2} \tag{2.50}$$

The extraordinary field has polarization direction in the crystal as;

$$\begin{pmatrix} 0 \\ \dfrac{\sin\theta}{n_e^2(\theta) - n_o^2} \\ \dfrac{\cos\theta}{n_e^2(\theta) - n_o^2} \end{pmatrix} \tag{2.51}$$

2.1.4 Double refraction at the boundary of the material

When an electromagnetic plane wave interacts with uniaxial crystals, the incident wave is reflected and refracted at material interfaces. The refracted waves are the combination of the ordinary and the extraordinary waves. For the continuity of refracted and reflected waves at the interface of uniaxial crystal, it requires the boundary conditions and the conditions are that all wave vectors must lie on the incident plane. The k_o is the wave vector of incident electromagnetic plane wave and the k_1,k_2 are wave vectors of refractive waves as shown in figure 2.2.

For the continuity of the wave propagation, the normal of components at the interfaces must be the same which leads to a condition for the refracted waves as;

$$k_0 \sin\theta_0 = k_1 \sin\theta_1 = k_2 \sin\theta_2 \tag{2.52}$$

The above condition is similar to Snell's law but the k_1, k_2 are not constant and varied with the directions. For the uniaxial crystals, one sheet of the normal surface is a sphere, therefore k is constant for all propagation directions and the ordinary wave of the uniaxial crystal follows the Snell's law as;

$$n_i \sin\theta_0 = n_o \sin\theta_1 \qquad (2.53)$$

The other sheet of the normal surface is an ellipsoid of revolution having direction-dependent k values. The refraction at interfaces in uniaxial crystals for the ellipsoid sheet can be shown in figure 2.3.

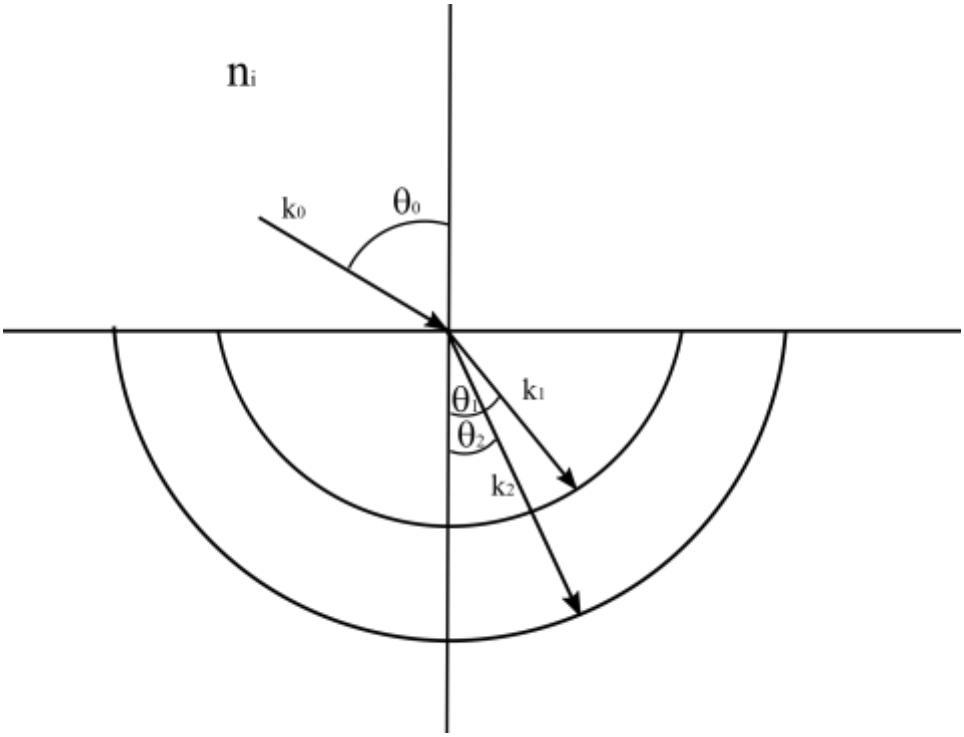

Figure 2.2: Graphical method to determine incident and refracted angles accompanying double refraction at the anisotropic medium boundary.

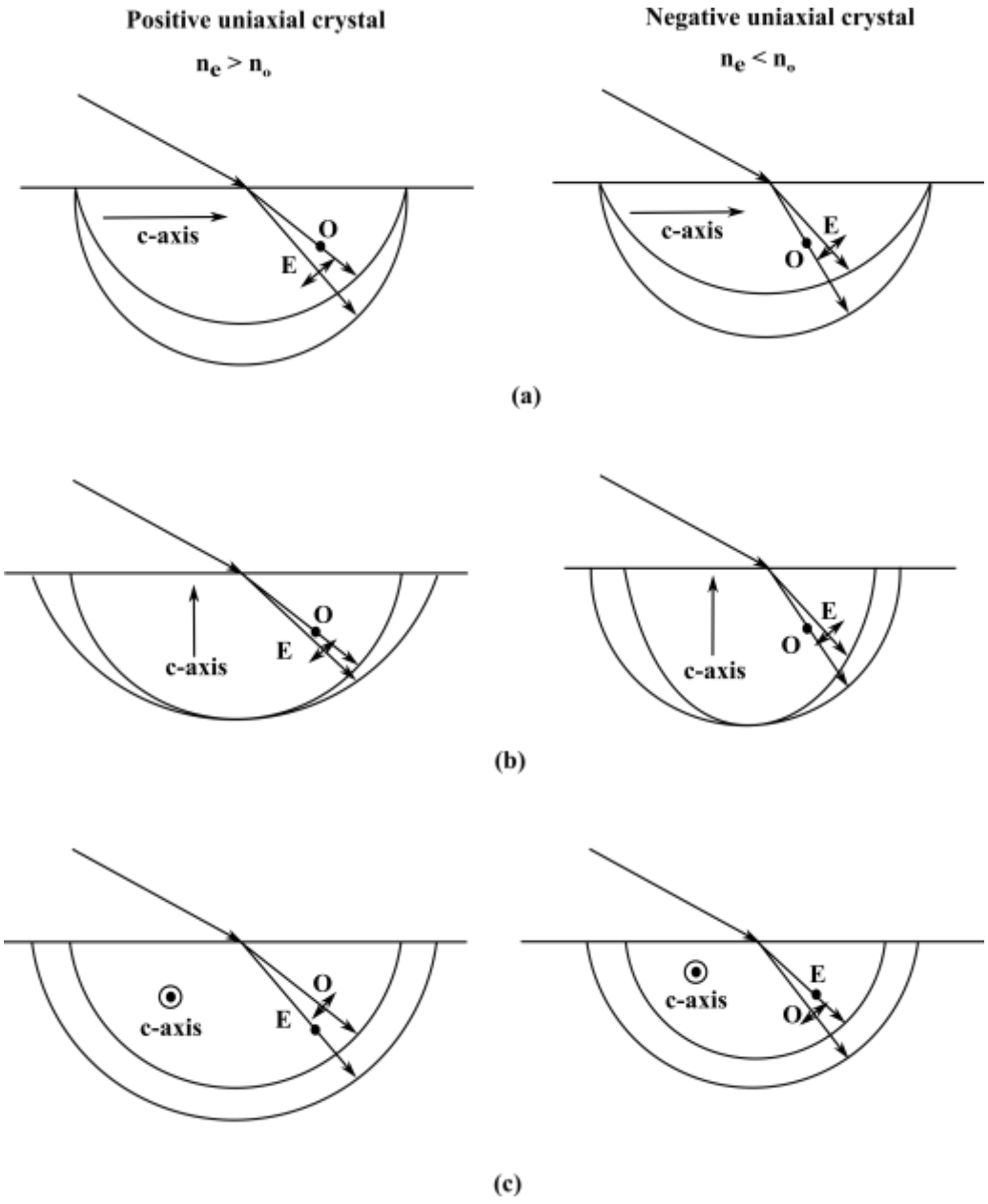

Figure 2.3: Double refraction in positive and negative uniaxial crystals (a) parallel to the incident plane and boundary, (b) perpendicular to the incident plane and boundary, (c) perpendicular to the incident plane and parallel to the boundary.

2.2 Theoretical method for PBG calculation

The propagation of electromagnetic waves in the isotropic and anisotropic medium has been studied by solving Maxwell's equations. On solving Maxwell's equation, we have obtained the dispersion relations, transmission, and reflection coefficients to study the optical properties of the materials. Similarly, we can apply for the periodic structure of the materials by considering Bloch's theorem. A lot of methods based on

the solutions of Maxwell's equations for periodic structures or photonic crystals (PCs) have been developed and among the all methods, the four methods are widely used to study the propagation of electromagnetic waves in the periodic materials; plane wave expansion (PWE), finite element method (FEM), finite difference time domain method (FDTD) and transfer matrix method (TMM) [8-11]. These methods give approximate results with high accuracy, generally, the PWE method used to study the band structure or dispersion behavior of 1D or 2D photonic crystals, whereas FEM gives the highly accurate results of 1-D, 2-D, or 3-D PCs, depending on the memory and storage of the computational system, FDTD is based on the solutions of Maxwell's equations expanding in time and space domain, where at each point of the time step, the values of the nodes for the field vectors are calculated, and TMM gives the details of band structure and optical properties (ATR) of the 1-D periodic structure/photonic crystals based on the solutions of Maxwell's equations. The TMM method can be generalized for both isotropic and anisotropic photonic crystals with Bloch's theorem which connect the field vectors of the electromagnetic wave at the interface between two mediums. In the following sections, we have given a brief study of the four mentioned methods.

2.2.1 Plane Wave Expansion (PWE) Method

The plane wave expansion (PWE) method is based on the expansion of periodic functions into the Fourier series considering the reciprocal lattice vectors and converting the differential equations into infinite matrix form. The PWE method is very easy to obtain the band structure of 1-D and 2-D photonic crystals and can be applied to linear, anisotropic, lossless, and inhomogeneous mediums. The PWE method affects the stability of numerical calculation due to the discontinuity of dielectric permittivity and electric field components. The band structure and dispersions of 1DPCs can be obtained by solving the Helmholtz equation as;

$$\frac{\partial}{\partial x}\frac{1}{\varepsilon(x)}\frac{\partial}{\partial x}H(x)+\frac{\omega^2}{c^2}H(x)=0 \qquad (2.54)$$

The eigen function follow the Bloch's theorem and hence the H(x) can be expanded in term of exponential as;

$$H(x)=h_{k,n}(x)e^{jkx} \qquad (2.55)$$

where $h_{k,n}(x)$ = periodicity dependent periodic function. Using the Fourier series and reciprocal lattice vectors G, the function H(x) expanded as;

$$H(x) = \sum_{G} h_{k,n}(G) e^{(j(k+G)x)} \tag{2.56}$$

The dielectric function can also be expanded using Fourier series due to having periodicity dependence and hence the dielectric function can be written as;

$$\frac{1}{\varepsilon(x)} = \sum_{G'' \in G} X(G'') e^{(j(k+G'')x)} \tag{2.57}$$

where $X(G'')$ = Fourier expansion coefficients of the inverse dielectric function. On solving equation 2.54, the Master equation for the 1D photonic crystals can be obtained as;

$$\sum_{G'} X(-GG')((k+G)(k+G'))h_{k,n}(G') + \frac{\omega^2}{c^2} h_{k,n}(G) = 0 \tag{2.58}$$

The given equation 2.58 is the Master equation for the 1-D photonic crystal which depends on the reciprocal vectors. The values of G and G' depends on the series expansion which follows the solutions of differential equations transforming in matrix form. By solving the eigen values problems with matrix, the band structure for the 1-DPC can be studied [12-16].

2.2.2 Finite Element Method (FEM)

The finite element method (FEM) is applied to obtain the solution of boundary value problems (BVPs), ordinary and partial differential equations (PDEs) and it gives the approximate solutions depending on the number of nodes. This method is extensively used in the different branches of engineering including aircraft designing. The boundary value problems can be solved by Ritz's method and Galenkin's method but such a method depends on the selection and accuracy of trial functions which are difficult sometimes. To overcome this difficulty, the entire domain is divided into small subdomains and then used the trial functions for each subdomain which gives the approximate solutions. Therefore, the size of the subdomain is important for the accuracy of the solutions. FEM converts the boundary value problem supporting the infinite quantity of degree of freedom into a problem having a finite amount of degree

of freedom with unknown coefficients. The FEM has some basic steps to follow to implement on the materials; subdivision or discretization of the domain, selection of trail function, formulation of system equations using Ritz's or Galenkin's method, and solutions of the equations. The discretization process affects memory storage depending on the choice of elements. The subdomain is generally called as element which can be one-dimensional, two-dimensional, and three-dimensional elements as linear line segment, triangular, tetrahedral structure. The different elements have various nodes that affect the discretization, and also the storage and processing of the system. The trail functions can be linear or higher-order polynomials. The higher-order polynomial gives accurate results but in a complicated manner; therefore, the linear polynomials are widely used in the FEM. Although FEM is complicated and expensive, it is a very useful tool to simulate electromagnetic devices and also in computational electrodynamics. The various commercial software like COMSOL, MAFIA, HFSS, and so on are based on the FEM and gives highly accurate simulated results of electromagnetic structure or optical devices [17-19].

2.2.3 Finite Difference Time Domain (FDTD) method

The finite difference time domain (FDTD) method is a more complex method but it provides higher numerical stability than the PWE method. FDTD is a very powerful tool to study the band structure of anisotropic medium such as liquid crystals, wave plates, etc. FDTD presents the explicit method to solve Maxwell's equations in time and space domain and provides the band structure of any arbitrary geometry, nonlinear responses, and inhomogeneous characteristics [19-21]. In 1966, Yeh [22] offered the basics of the FDTD method by simulating the linear and isotropic media. Further, the various researchers work to apply the FDTD to simulate the anisotropic media. In 1999, Zhou [23] designed the 3D algorithm to solve the general anisotropic media; and in 2002, Moss extends the PML method to solve anisotropic medium. In 2004, Akyurtlu, Werner, Mosallaei, and Sarabandi have used the FDTD method to analyze the magneto and biaxial anisotropic media [24-26]. To solve Maxwell's equations for the FDTD method, different finite differences methods can be employed. The derivative of any arbitrary function at any random point can be studied by forward finite difference, backward finite difference, and central difference.

The first derivative of a function f(x) at random point x_0 can be calculated using forward, backward, and central differences as;

$$f'(x_0) \cong \frac{[f(x_0 + \Delta x) - f(x_0)]}{\Delta x} \tag{2.59}$$

Using the backward finite difference;

$$f'(x_0) \cong \frac{[f(x_0) - f(x_0 - \Delta x)]}{\Delta x} \tag{2.60}$$

Using the central difference the

$$f'(x_0) \cong \frac{[f(x_0 + \Delta x) - f(x_0 - \Delta x)]}{2\Delta x} \tag{2.61}$$

Similarly, the second derivative using central difference can be calculated as;

$$f''(x_0) \cong \frac{[f(x_0 + \Delta x) - 2f(x_0) + f(x_0 - \Delta x)]}{(\Delta x)^2} \tag{2.62}$$

The central difference method is applied to explain Maxwell's equations with the electric and magnetic field at each time step (Δt). The harmonic solutions can be obtained by Fourier transformations. Although the FDTD method needs a large capacity memory and it is time taking process, the FDTD method gives more accurate results.

2.2.4 Transfer Matrix Method (TMM)

The transfer matrix method (TMM) is derived on the solutions of Maxwell's equations in the isotropic or anisotropic medium and such method connects the electric field or magnetic field on both sides of a layer. Depending on the type of material, the coupling of the electric field and magnetic field varied which forms the characteristics matrix having 2x2 or 4x4 matrix forms using boundary conditions [1,6]. The calculation of the optical properties of dielectric periodic materials is analogous to the calculation of the electronic properties of periodic atomic potentials in the materials. The eigen values of the wave function of periodic atomic potentials can be solved by the Schrödinger equation. Similarly, eigen values of dielectric function are also solved for the photonic crystals by Maxwell's equations and eigen

values can be obtained by solving the Helmholtz equation or Master equation $\vec{\nabla} \times (1/\varepsilon_r)\vec{\nabla} \times \vec{H} = (\omega^2/c^2)\vec{H}$.

The transfer matrix method (TMM) is used to calculate layer by layer interactions of electric field and magnetic field vectors at each interface of each dielectric medium. Generally, 2x2 TMM is used to study the dispersion behavior and optical properties (reflection and transmission) of 1-DPCs composed of the isotropic layer which is equivalent to the Fresnel's equations but 4x4 TMM can be used for the 1-DPC consisting of anisotropic layers and 4x4 TMM method coupled the transverse electric (TE) and transverse magnetic (TM) modes in a 4x4 matrix for the single anisotropic layer. In the following section, we have discussed the 2x2 and 4x4 matrix methods and focused on the TMM method in the whole thesis to study the optical properties of the periodic structure containing isotropic and anisotropic medium.

2.2.4.1 2x2 characteristic matrix for the single layer

Consider an electromagnetic plane wave incident on the isotropic homogeneous dielectric layer having relative dielectric permittivity and relative magnetic permeability (ε, μ) with finite thickness. The plane wave has two independent modes for propagations; transverse electric (TE) and transverse magnetic (TM) transmission modes. In the TE modes, the electric field component perpendicular to the incident plane while in the case of TM modes, the magnetic field is perpendicular to the incident plane [1,6,27]. If the wave propagates in the z-direction and x-y plane is the incident wave plane then the electric field is can be represented as, E=(0, Ey, 0) for TE mode and E=(Ex, 0, Ez) for TM mode. The magnetic field and electric displacement vector can be represented as;

$$B = \mu_0 \mu H \tag{2.63}$$

$$D = \varepsilon_0 \varepsilon E \tag{2.64}$$

On putting the values B and D in equations 2.14 and 2.15 gives;

$$\nabla \times E = i\omega \mu_0 \mu H \tag{2.65}$$

$$\nabla \times H = -i\omega \varepsilon_0 \varepsilon E \tag{2.66}$$

where ω = frequency of plane wave and the TE mode polarization, Ey = y-component of electric field, therefore, equation 2.65 gives

$$\frac{\partial E_y}{\partial z} = -i\omega\mu_0\mu H_x \tag{2.67}$$

$$0 = i\omega\mu_0\mu H_y \tag{2.68}$$

$$\frac{\partial E_y}{\partial x} = i\omega\mu_0\mu H_z \tag{2.69}$$

And the magnetic field has two H_x and H_z. equation 2.66 gives

$$\frac{\partial H_x}{\partial z} - \frac{\partial H_z}{\partial x} = -i\omega\varepsilon_0\varepsilon E_y \tag{2.70}$$

$$\frac{\partial H_x}{\partial y} = 0 \tag{2.71}$$

$$\frac{\partial H_z}{\partial y} = 0 \tag{2.72}$$

On solving the equations 2.67 to 2.72, we found the equation for electric field as;

$$\frac{\partial^2 E_y}{\partial x^2} + \frac{\partial^2 E_y}{\partial z^2} + k^2 E_y = 0 \tag{2.73}$$

where $k = n\omega/c$, $n = \sqrt{\varepsilon\mu}$ and the solution of the 2.73 can be written as;

$$E_y = E_{0y}\exp(ik_x x - i\omega t) \tag{2.74}$$

Similarly, we can obtain the solutions for the magnetic fields as;

$$H_x = H_{0x}\exp(ik_x x - i\omega t) \tag{2.75}$$

$$H_z = H_{0x}\exp(ik_x x - i\omega t) \tag{2.76}$$

Now, on putting the values of E_y, H_x and H_z in the equations 2.67, 2.69, 2.70 and further solving the equations gives;

$$\frac{d^2 E_{0y}}{dz^2} + k_z^2 E_{0y} = 0 \tag{2.77}$$

$$\frac{d^2 H_{0x}}{dz^2} + k_z^2 H_{0x} = 0 \tag{2.78}$$

The equations 2.77 and 2.78 have solutions as;

$$E_{0y} = A_1 \sin(k_z z) + A_2 \cos(k_z z) \tag{2.79}$$

$$H_{0x} = \frac{A_1 k_z}{i\omega\mu_0\mu}\cos(k_z z) - \frac{A_2 k_z}{i\omega\mu_0\mu}\sin(k_z z) \tag{2.80}$$

For TE mode, we can construct a column vector consisting tangential elements of field vectors as;

$$\psi(z) = \begin{bmatrix} E_{0y} \\ H_{0x} \end{bmatrix} \tag{2.81}$$

Similar, we can write for TM mode;

$$\psi(z) = \begin{bmatrix} H_{0y} \\ E_{0x} \end{bmatrix} \tag{2.82}$$

The incident electromagnetic wave can be coupled between two planes by a matrix based on solutions of Maxwell's equations as;

$$\psi(z) = M\psi(z_0) \tag{2.83}$$

where M is the characteristic matrix of the material which connects the field vectors at the interface of the materials from z_0 to z.

By applying the boundary conditions and further solving, we get the characteristics matrix M which can be written as;

$$M = \begin{bmatrix} \cos(k_z d) & i\sin(k_z d)/p \\ ip\cos(k_z d) & \cos(k_z d) \end{bmatrix} \tag{2.84}$$

where p=n cosθ for TE mode and p =cos θ/n for TE mode.

2.2.4.2 Total transfer matrix for 1-D photonic crystal

Consider 1-D photonic crystal of N layers of dielectric layers of thickness 'a' and 'b' with d periodicity of the periodic structure then d=a+b as figure 2.4.

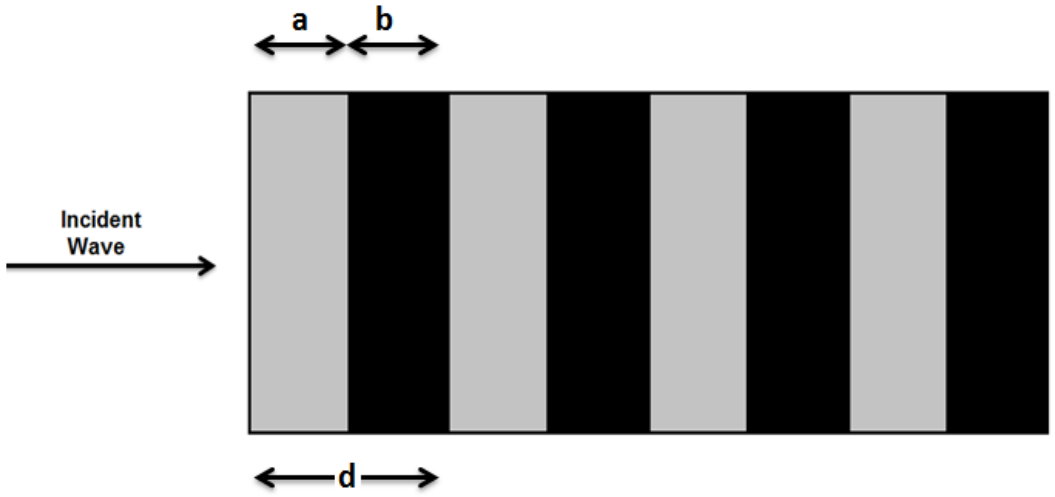

Figure 2.4: Schematic arrangement of 1-DPC of alternating layers of thicknesses 'a' and 'b' with periodicity d.

Consider the vector consisting of electric field and magnetic field elements at the interface of i^{th} layer can be related to the boundary of $(i-1)^{th}$ layer through a matrix M_{i-1} as;

$$\psi(z_i) = M(z_i - z_{i-1})\psi(z_{i-1}) \tag{2.85}$$

Thus for N dielectric layers, the final characteristic matrix is the product of all characteristics matrix of each layer in the structure as;

$$\psi(z_N) = M(z_N - z_0)\psi(z_0) \tag{2.86}$$

$$M(z_N - z_0) = M(z_N - z_{N-1}).....M(z_i - z_{i-1}).....M(z_1 - z_0) \tag{2.87}$$

The dispersion relation can be studied by Bloch's wave number; $K = (1/d)\cos^{-1}(\mathrm{Tr}(M(z_n - z_0))/2)$, where $M(d_j)$ is the characteristic matrix for the j^{th} layer in the periodic structure.

$$M(d_j) = \begin{bmatrix} \cos(k_{zj}d_j) & i\sin(k_{zj}d)/p_j \\ ip_j\cos(k_{zj}d_j) & \cos(k_{zj}d_j) \end{bmatrix} \tag{2.88}$$

Using equation 2.88, we can write the total transfer matrix for 1-DPC and the reflection and transmission coefficients of the 1-DPC can be found on solving as;

$$r = \frac{(M_{11} + M_{21}p_s)p_0 - (M_{21} + M_{22}p_s)}{(M_{11} + M_{21}p_s)p_0 + (M_{21} + M_{22}p_s)} \tag{2.89}$$

$$t = \frac{2p_0}{(M_{11} + M_{21}p_s)p_0 + (M_{21} + M_{22}p_s)} \tag{2.90}$$

These 'r', and 't' are also called Fresnel's coefficients. By considering conservation of energy, the total reflectance and transmittance of the 1-DPC can be obtained through the following equations;

$$R = |r|^2 \tag{2.91}$$

$$T = \frac{p_s}{p_0}|r|^2 \tag{2.92}$$

$$A=1-T-R. \tag{2.93}$$

2.2.4.3 4x4 Berreman matrix method

In 1972, Berreman developed a 4x4 differential matrix method for obtaining the reflectance and transmittance of the anisotropic materials. Berrreman transformed Maxwell's equations in 6x6 matrix form and obtained the 16 differential matrix elements which gave the complicated reflection and transmission of the anisotropic material. Consider the interaction of electromagnetic waves with the materials having dielectric permittivity $\tilde{\varepsilon}$ and magnetic permeability $\tilde{\mu}$ are studied by Maxwell's equations.

$$\nabla \times E = -\mu_0 \tilde{\mu} \frac{\partial H}{\partial t} \tag{2.94}$$

$$\nabla \times H = \varepsilon_0 \tilde{\varepsilon} \frac{\partial E}{\partial t} \tag{2.95}$$

Consider the interaction of electromagnetic wave having electric field and magnetic field vectors (equations 2.96 and 2.97) with materials have tensor dielectric permittivity $\tilde{\varepsilon}$ and magnetic permittivity $\tilde{\mu}$.

$$E(r,t) = E_0 \exp(i(\omega t - k \cdot r)) \tag{2.96}$$

$$H(r,t) = H_0 \exp(i(\omega t - k \cdot r)) \tag{2.97}$$

where r, k, ω are the position vector, vector, and frequency of the propagating wave.

For the tensor dielectric permittivity, the $\tilde{\varepsilon}$ is given as;

$$\tilde{\varepsilon} = \begin{pmatrix} \varepsilon_{xx} & \varepsilon_{xy} & \varepsilon_{xz} \\ \varepsilon_{yx} & \varepsilon_{yy} & \varepsilon_{yz} \\ \varepsilon_{zx} & \varepsilon_{zy} & \varepsilon_{zz} \end{pmatrix} \tag{2.98}$$

The Maxwell equations 2.94 and 2.95 can be written in 6x6 matric form consisting of dielectric tensor, electric and magnetic field components as [28-32];

$$\begin{pmatrix} 0 & 0 & 0 & 0 & -\frac{\partial}{\partial z} & \frac{\partial}{\partial y} \\ 0 & 0 & 0 & \frac{\partial}{\partial z} & 0 & -\frac{\partial}{\partial x} \\ 0 & 0 & 0 & -\frac{\partial}{\partial y} & \frac{\partial}{\partial x} & 0 \\ 0 & \frac{\partial}{\partial z} & -\frac{\partial}{\partial y} & 0 & 0 & 0 \\ -\frac{\partial}{\partial z} & 0 & \frac{\partial}{\partial x} & 0 & 0 & 0 \\ \frac{\partial}{\partial y} & -\frac{\partial}{\partial x} & 0 & 0 & 0 & 0 \end{pmatrix} \begin{pmatrix} E_x \\ E_y \\ E_z \\ H_x \\ H_y \\ H_z \end{pmatrix} = i\frac{\omega}{c} \begin{pmatrix} \varepsilon_{xx} & \varepsilon_{xy} & \varepsilon_{xz} & 0 & 0 & 0 \\ \varepsilon_{yx} & \varepsilon_{yy} & \varepsilon_{yz} & 0 & 0 & 0 \\ \varepsilon_{zx} & \varepsilon_{zy} & \varepsilon_{zz} & 0 & 0 & 0 \\ 0 & 0 & 0 & \mu & 0 & 0 \\ 0 & 0 & 0 & 0 & \mu & 0 \\ 0 & 0 & 0 & 0 & 0 & \mu \end{pmatrix} \begin{pmatrix} E_x \\ E_y \\ E_z \\ H_x \\ H_y \\ H_z \end{pmatrix} \tag{2.99}$$

Now, consider the x-z plane as the incident plane and the system is invariant with the y-axis; therefore, the derivative with respect to y must be zero.

$$\frac{\partial}{\partial y} = 0 \tag{2.100}$$

Hence, equation 2.99 is transformed into equation 2.101, as;

$$\begin{pmatrix} -\frac{\partial H_y}{\partial z} \\ \frac{\partial H_x}{\partial z} + i\varphi H_z \\ -i\varphi H_y \\ \frac{\partial E_y}{\partial z} \\ -\frac{\partial E_x}{\partial z} - i\varphi E_z \\ i\varphi E_y \end{pmatrix} = i\frac{\omega}{c} \begin{pmatrix} \varepsilon_{xx}E_x + \varepsilon_{xy}E_y + \varepsilon_{xz}E_z \\ \varepsilon_{yx}E_x + \varepsilon_{yy}E_y + \varepsilon_{yz}E_z \\ \varepsilon_{zx}E_x + \varepsilon_{zy}E_y + \varepsilon_{zz}E_z \\ \mu H_x \\ \mu H_y \\ \mu H_z \end{pmatrix} \tag{2.101}$$

where $\varphi=\omega n_0 \sin\theta_o/c$, c is the velocity of light in the vacuum.

On solving equation 2.101, we get the following equation as;

$$\frac{\partial}{\partial z}\begin{pmatrix} E_x \\ H_x \\ E_y \\ -H_x \end{pmatrix} = i\frac{\omega}{c}\begin{pmatrix} -\frac{\varepsilon_{zx}\varphi c}{\varepsilon_{zz}\omega} & \mu - \frac{\varphi^2 c^2}{\varepsilon_{zz}\omega^2} & -\frac{\varepsilon_{zy}\varphi c}{\varepsilon_{zz}\omega} & 0 \\ \varepsilon_{xx} - \frac{\varepsilon_{xz}\varepsilon_{zx}}{\varepsilon_{zz}} & -\frac{\varepsilon_{xz}c\varphi}{\varepsilon_{zz}\omega} & \varepsilon_{xy} - \frac{\varepsilon_{xz}\varepsilon_{zy}}{\varepsilon_{zz}} & 0 \\ 0 & 0 & 0 & \mu \\ \varepsilon_{yx} - \frac{\varepsilon_{yz}\varepsilon_{zx}}{\varepsilon_{zz}} & -\frac{\varepsilon_{yz}c\varphi}{\varepsilon_{zz}\omega} & \varepsilon_{yy} - \frac{\varepsilon_{yz}\varepsilon_{zy}}{\varepsilon_{zz}} - \frac{\varphi^2 c^2}{\mu\omega^2} & 0 \end{pmatrix}\begin{pmatrix} E_x \\ H_x \\ E_y \\ -H_x \end{pmatrix} \tag{2.102}$$

The differential equation 2.102 is also can be written as;

$$\frac{\partial}{\partial z}\psi = i\frac{\omega}{c}\Delta\psi \tag{2.103}$$

where Δ is known as differential propagation matrix and solution of the equation 2.103 can be obtained by using Taylor series expansion as:

$$\psi(z+h) = (I - i\Delta h\frac{\omega}{c} - \frac{\Delta^2 h^2}{2!}\frac{\omega^2}{c^2} + i\frac{\Delta^3 h^3}{3!}\frac{\omega^3}{c^3} + ...)\psi(z) \tag{2.104}$$

The solution connects the column vector of electric and magnetic field vectors at the boundary of the anisotropic layer with thickness 'h'.

Consider the stratified media of anisotropic layers, then the electric and magnetic field column vectors for the incident, reflected and transmitted wave can be written as;

$$\psi_i = \begin{pmatrix} E_{ip}\cos\theta_0 \\ n_0 E_{ip} \\ E_{is} \\ n_0 E_{is}\cos\theta_0 \end{pmatrix} \tag{2.105}$$

$$\psi_r = \begin{pmatrix} -E_{rp}\cos\theta_0 \\ n_0 E_{rp} \\ E_{rs} \\ -n_0 E_{rs}\cos\theta_0 \end{pmatrix} \tag{2.106}$$

$$\psi_t = \begin{pmatrix} E_{tp}\cos\theta_2 \\ n_2 E_{tp} \\ E_{ts} \\ n_2 E_{ts}\cos\theta_2 \end{pmatrix} \tag{2.107}$$

When the wave interacted with the medium, some fraction of the wave reflected and transmitted through the layer, therefore, the field vectors for the incident and reflected wave follows the addition rule and then operated on the layer matrix as;

$$\begin{pmatrix} E_{tp}\cos\theta_2 \\ n_2 E_{tp} \\ E_{ts} \\ n_2 E_{ts}\cos\theta_2 \end{pmatrix} = [M]_{4x4} \begin{pmatrix} (E_{ip} - E_{rp})\cos\theta_0 \\ n_0(E_{ip} + E_{rp}) \\ E_{is} + E_{rs} \\ n_0(E_{is} - E_{rs})\cos\theta_0 \end{pmatrix} \tag{2.108}$$

The solution of equations 2.103 has 4 unknown coefficients, and the reflection and transmission coefficients for the s and p polarization can be written as;

$$\begin{pmatrix} E_{rp} \\ E_{rs} \end{pmatrix} = \begin{pmatrix} R_{pp} & R_{ps} \\ R_{sp} & R_{ss} \end{pmatrix} \begin{pmatrix} E_{ip} \\ E_{is} \end{pmatrix} \tag{2.109}$$

$$\begin{pmatrix} E_{tp} \\ E_{ts} \end{pmatrix} = \begin{pmatrix} T_{pp} & T_{ps} \\ T_{sp} & T_{ss} \end{pmatrix} \begin{pmatrix} E_{ip} \\ E_{is} \end{pmatrix} \tag{2.110}$$

The solution of the equations 2.109 and 2.110 can be easily obtained which gives reflection and transmission coefficients for both s and p polarizations. The 4x4 Berreman matrix method is a very useful technique for obtaining the reflection and transmission of the stratified media of anisotropic layers which give the agreed results with experiments. This method is reduced to a 2x2 matrix for linear isotropic media as in the case of the *Jones matrix method*. For an example of calculation of transmission coefficients for TE and TM mode by using the 4x4 Berreman matrix method, consider a uniaxial anisotropic material lithium niobate ($LiNbO_3$) having voltage-dependent refractive indices as [31,32];

$$\tilde{\varepsilon} = \varepsilon_o \begin{bmatrix} n_o^{\,2} & 0 & 0 \\ 0 & n_o^{\,2} & 0 \\ 0 & 0 & n_e^{\,2} \end{bmatrix} \tag{2.111}$$

The extraordinary and ordinary refractive indices, n_e, n_o for the $LiNbO_3$ material are following as;

$$n_o(V) = n_o - \frac{1}{2} r_{13} n_o^{\,3} \left(\frac{V}{d_4} \right) \tag{2.112}$$

$$n_e(V) = n_e(\theta) - \frac{1}{2} r_{33} n_e(\theta)^3 \left(\frac{V}{d_4} \right) \tag{2.113}$$

where r_{13}, r_{33} = electro-optical coefficients, extraordinary refractive index of $LiNbO_3$ material. Extraordinary index is varies with voltage (V) and incident angle (θ) as;

$$n_e(\theta) = \frac{n_e n_o}{\sqrt{n_o^{\,2} \cos^2\theta + n_e^{\,2} \sin^2\theta}} \tag{2.114}$$

Now, the Maxwell's equations can be used for $LiNbO_3$ material as;

$$\vec{\nabla} \times \vec{E} = i\omega\mu_o \vec{H} \tag{2.115}$$

$$\vec{\nabla} \times \vec{H} = -i\omega\varepsilon_o \varepsilon \vec{E} \tag{2.116}$$

The tangential elements of fields are obtianed by solution of equations 2.115 & 2.116;

$$\frac{\partial \psi}{\partial z} = ik_o \Delta \psi \tag{2.117}$$

Where $k_o = \omega / c$, $\psi = \left(\sqrt{\varepsilon_o} E_x, \sqrt{\mu_o} H_y, \sqrt{\varepsilon_o} E_y, \sqrt{\mu_o} H_x \right)$, and Δ is differential propagation matrix containing dielectric tensor components which is similar to equation 2.103.

On solving equations 2.115 and 2.116, the differential propagation matrix Δ can be obtained as;

$$\Delta = \begin{bmatrix} 0 & 1 - n_0^{\,2} \sin^2\theta / \varepsilon_z & 0 & 0 \\ \varepsilon_x & 0 & 0 & 0 \\ 0 & 0 & 0 & 1 \\ 0 & 0 & \varepsilon_y - n_0^{\,2} \sin^2\theta & 0 \end{bmatrix} \tag{2.118}$$

where n_0 = refractive index of the incident medium, θ = incident angle of EMW.

The transfer matrix for uniaxial anisotropic material can be transcribed as;

$$M=\begin{bmatrix} \cos(\gamma_{1z}k_o d_4) & \frac{ik_{z1}\sin(\gamma_{1z}k_o d_4)}{\Delta_{12}} & 0 & 0 \\ \frac{i\Delta_{12}\sin(\gamma_{1z}k_o d_4)}{\gamma_{1z}} & \cos(\gamma_{1z}k_o d_4) & 0 & 0 \\ 0 & 0 & \cos(\gamma_{2z}k_o d_4) & \frac{i\sin(\gamma_{2z}k_o d_4)}{\gamma_{1z}} \\ 0 & 0 & ik_{z1}\sin(\gamma_{2z}k_o d_4) & \cos(\gamma_{2z}k_o d_4) \end{bmatrix} \tag{2.119}$$

where $\gamma_{1z}=\sqrt{\varepsilon_x(1-n_o{}^2\sin^2\theta/\varepsilon_z)}$ and $\gamma_{2z}=\sqrt{\varepsilon_y-n_o{}^2\sin^2\theta}$.

Similarly, the total transfer matrix for stratified media of different layers can be written as;

$$M=\begin{bmatrix} M_{11} & M_{12} & M_{13} & M_{14} \\ M_{21} & M_{22} & M_{23} & M_{24} \\ M_{31} & M_{32} & M_{33} & M_{34} \\ M_{41} & M_{42} & M_{43} & M_{44} \end{bmatrix} \tag{2.120}$$

The transmission coefficients of the considered stratified media for TE and TM polarizations as;

$$t_{TE}=\frac{M_{11}}{M_{11}M_{33}-M_{13}M_{31}} \tag{2.121}$$

$$t_{TM}=\frac{M_{33}}{M_{11}M_{33}-M_{13}M_{31}} \tag{2.122}$$

The total transmissions through the anisotropic media can be written as;

$$T_{TE}=|t_{TE}|^2,\ T_{TM}=|t_{TM}|^2 \tag{2.123}$$

2.2.4.4 4x4 transfer matrix method

In 1980, Yeh proposed a 4x4 matrix method in which a diagonal propagation matrix consisting of 4 partial plane waves can represent each layer of the periodic structure. In this method, each side of the layer can be characterized by a polarization direction-dependent dynamical matrix. For the interaction of EMWs with isotropic media, the interaction produced two uncoupled modes s and p modes, and hence only 2x2 matrix is needed for connecting the field vectors at the boundary of the media. In the case of anisotropic media, the s and p modes are coupled due to anisotropy of the media

which produces the different polarizations of incident waves, and hence the 4x4 matrices are required for the propagation or flow of EMWs through the media. The flow of EMWs in anisotropic media also can be studied by the 4x4 transfer matrix method [1,6,32]. Consider the flow of EMWs in the birefringent media having dielectric tensor as;

$$\tilde{\varepsilon} = A\begin{pmatrix} \varepsilon_1 & 0 & 0 \\ 0 & \varepsilon_2 & 0 \\ 0 & 0 & \varepsilon_3 \end{pmatrix} A^{-1}, \tag{2.124}$$

where ε_1, ε_2, ε_3, = diagonal dielectric permittivities, A = rotation matrix.

$$A = \begin{pmatrix} \cos\Psi\cos\Phi - \cos\Theta\sin\Psi\sin\Phi & -\sin\Psi\cos\Phi - \cos\Theta\sin\Psi\sin\Phi & \sin\Phi\sin\Theta \\ \cos\Psi\cos\Phi + \cos\Theta\sin\Psi\sin\Phi & -\sin\Psi\sin\Phi + \cos\Theta\cos\Psi\cos\Phi & -\cos\Phi\sin\Theta \\ \sin\Psi\sin\Theta & \sin\Psi\sin\Theta & \cos\Theta \end{pmatrix} \tag{2.125}$$

where Θ, Φ, Ψ are the Euler angles for the crystal axes orientation in the media. The z component of the vector can be found by solving the equation 2.126.

$$k \times (k \times E) + \omega^2 \mu \varepsilon E = 0 \tag{2.126}$$

Considering the generalized dielectric tensor equation 2.126 gives;

$$\begin{bmatrix} \omega^2\mu\varepsilon_{xx} - \beta^2 - \gamma^2 & \omega^2\mu\varepsilon_{xy} + \alpha\beta & \omega^2\mu\varepsilon_{xz} + \alpha\gamma \\ \omega^2\mu\varepsilon_{yx} + \alpha\beta & \omega^2\mu\varepsilon_{yy} - \alpha^2 - \gamma^2 & \omega^2\mu\varepsilon_{yz} + \beta\gamma \\ \omega^2\mu\varepsilon_{zx} + \alpha\gamma & \omega^2\mu\varepsilon_{zy} + \beta\gamma & \omega^2\mu\varepsilon_{zz} - \alpha^2 - \beta^2 \end{bmatrix} \begin{bmatrix} E_x \\ E_x \\ E_x \end{bmatrix} = 0 \tag{2.127}$$

For a non-trivial solution of the equation, the determinant must be zero, which gives the 4 solutions for γ which can be real or complex. Hence, the four partial waves with four wave vectors are also obtained. For the real values of the wave vector, the two of four values have group velocity with a positive z factor or component and the remaining two values have a negative z factor. While for the complex value of γ, the z factor of group velocity has vanished. The polarization of the waves can be represented by equation 2.128 as;

$$p = N_j \begin{bmatrix} (\omega^2\mu\varepsilon_{yy} - \alpha^2 - \gamma_j^2)(\omega^2\mu\varepsilon_{zz} - \alpha^2 - \beta^2) - (\omega^2\mu\varepsilon_{yz} + \beta\gamma_j)^2 \\ (\omega^2\mu\varepsilon_{yz} + \beta\gamma_j)(\omega^2\mu\varepsilon_{zx} + \alpha\gamma_j) - (\omega^2\mu\varepsilon_{xy} + \alpha\beta)(\omega^2\mu\varepsilon_{zz} - \alpha^2 - \beta^2) \\ (\omega^2\mu\varepsilon_{xy} + \alpha\beta)(\omega^2\mu\varepsilon_{yz} + \beta\gamma_j) - (\omega^2\mu\varepsilon_{xz} + \alpha\gamma_j)(\omega^2\mu\varepsilon_{yy} - \alpha^2 - \gamma_j^2) \end{bmatrix} \tag{2.128}$$

where N_j = normalization constant with condition $p \cdot p = 1$.

The distribution of electric field (E) of the propagating wave in n^{th} layer is given as;

$$E = \sum_{j=1}^{4} A_j(n) p_j(n) \exp[i(\omega t - \alpha x - \beta y - \gamma_j(n)(z - z_n)] \tag{2.129}$$

where n = number of layers. Due to continuity, the magnitude components of field vectors at the interface are related as;

$$\begin{pmatrix} A_1(n-1) \\ A_2(n-1) \\ A_3(n-1) \\ A_4(n-1) \end{pmatrix} = D^{-1}(n-1)D(n)P(n) \begin{pmatrix} A_1(n) \\ A_2(n) \\ A_3(n) \\ A_4(n) \end{pmatrix} \tag{2.130}$$

where

$$P = \begin{bmatrix} \exp[i\gamma_1(n)d_n] & 0 & 0 & 0 \\ 0 & \exp[i\gamma_2(n)d_n] & 0 & 0 \\ 0 & 0 & \exp[i\gamma_3(n)d_n] & 0 \\ 0 & 0 & 0 & \exp[i\gamma_4(n)d_n] \end{bmatrix} \tag{2.131}$$

and

$$D(n) = \begin{bmatrix} \hat{x} \cdot p_1(n) & \hat{x} \cdot p_2(n) & \hat{x} \cdot p_3(n) & \hat{x} \cdot p_4(n) \\ \hat{y} \cdot q_1(n) & \hat{y} \cdot q_2(n) & \hat{y} \cdot q_3(n) & \hat{y} \cdot q_4(n) \\ \hat{y} \cdot p_1(n) & \hat{y} \cdot p_2(n) & \hat{y} \cdot p_3(n) & \hat{y} \cdot p_4(n) \\ \hat{x} \cdot q_1(n) & \hat{x} \cdot q_2(n) & \hat{x} \cdot q_3(n) & \hat{x} \cdot q_4(n) \end{bmatrix} \tag{2.132}$$

where, D(n) = dynamical matrix having polarization, $q_j(n) = \frac{c}{\mu\omega} k_j(n) \times p_j(n)$, d_n=z_n-z_{n-1} direction dependent matrix elements, and P(n) = propagation matrix consisting matrix elements depending on the phase excursion of partial waves in the structure.

The transfer matrix for the interfaces of n^{th} and $(n-1)^{th}$ layers is represented as;

$$T_{n,n-1}=D^{-1}(n-1)D(n)P(n), \tag{2.133}$$

Thus, the final matrix is the multiplication of all transfer matrices of the periodic structure for the whole stratified media of N layers as;

$$T=T_{0,1}T_{1,2}\ldots.T_{N,s} \tag{2.134}$$

The transfer matrix T is the 4x4 matrix $[M]_{4x4}$ can be represented as;

$$\begin{bmatrix} A_s \\ B_s \\ A_p \\ B_p \end{bmatrix} = \begin{bmatrix} M_{11} & M_{12} & M_{13} & M_{13} \\ M_{21} & M_{22} & M_{23} & M_{24} \\ M_{31} & M_{32} & M_{33} & M_{34} \\ M_{41} & M_{42} & M_{43} & M_{44} \end{bmatrix} \begin{bmatrix} C_s \\ 0 \\ C_p \\ 0 \end{bmatrix}, \tag{2.135}$$

The transmission and reflection coefficients of the periodic structure of birefringent media for the s and p waves can be obtained as;

$$t_{ss} = \left(\frac{C_s}{A_s}\right)_{A_p=0} = \frac{M_{33}}{M_{11}M_{33} - M_{13}M_{31}} \tag{2.136}$$

$$t_{sp} = \left(\frac{C_p}{A_s}\right)_{A_p=0} = \frac{-M_{31}}{M_{11}M_{33} - M_{13}M_{31}} \tag{2.137}$$

$$t_{ps} = \left(\frac{C_s}{A_p}\right)_{A_s=0} = \frac{-M_{13}}{M_{11}M_{33} - M_{13}M_{31}} \tag{2.138}$$

$$t_{pp} = \left(\frac{C_p}{A_p}\right)_{A_s=0} = \frac{M_{11}}{M_{11}M_{33} - M_{13}M_{31}} \tag{2.139}$$

$$r_{ss} = \left(\frac{B_s}{A_s}\right)_{A_p=0} = \frac{M_{21}M_{33} - M_{23}M_{31}}{M_{11}M_{33} - M_{13}M_{31}} \tag{2.140}$$

$$r_{sp} = \left(\frac{B_p}{A_s}\right)_{A_p=0} = \frac{M_{41}M_{33} - M_{43}M_{31}}{M_{11}M_{33} - M_{13}M_{31}} \tag{2.141}$$

$$r_{ps} = \left(\frac{B_s}{A_p}\right)_{A_s=0} = \frac{M_{11}M_{23} - M_{21}M_{13}}{M_{11}M_{33} - M_{13}M_{31}} \tag{2.142}$$

$$r_{pp} = \left(\frac{B_p}{A_p} \right)_{A_s=0} = \frac{M_{11}M_{43} - M_{41}M_{13}}{M_{11}M_{33} - M_{13}M_{31}} \tag{2.143}$$

These elements are obtained by matrix multiplication of each 4x4 matrices of anisotropic layers for the s and p polarization of electromagnetic waves. In some cases, the derivations of reflection and transmission coefficients for anisotropic layers are highly complicated.

Besides the overhead four theoretical methods, various methods are also available to study the optical characteristics (ATR) of periodic structures. The finite difference frequency domain (FDFD) method also uses Maxwell's equations considering space and frequency domain. The FDFD method is based on the coupling of the transfer matrix method with Fourier transforms. In the rigorous coupled-wave analysis (RCWA) method, integration of coupled electromagnetic waves is also used and the various structures e.g. conical structures, nano-pillars, cones, core-shell structures, etc. which can be simulated with this method. RCWA method is useful in the reflectometry, transmission line method, and grating structure of periodic materials. RCWA method can also be used to simulate the optical properties of various antireflection coating materials. Due to the variation of dielectric function as in the FDTD method, finite integration technique (FIT) is also used in the expansion of dielectric function and vectorial solutions of Maxwell's equations through the Fourier transforms. In the FIT, the electromagnetic waves are discretized into space and frequency domains, and it is also used the transformation of integral Maxwell's equation into grid structures as the FDTD method. The FIT method is mostly applicable to study the transient fields in radio frequency applications; RF, CST, etc. Another method is the tight binding (TB) method which expands the magnetic fields into certain wave functions dependent on the orthogonal Wannier functions and the band structures can be studied by solving such functions. TB method is to detect the defect modes in the periodic structures just like the PWE method. All along with the discussed theoretical methods, discrete dipole approximation (DDA), and beam propagation method (BPM) are also very useful to study the optical properties of various photonic structures.

2.3 Conclusion

To study the propagation of electromagnetic waves in different periodic structures or materials, various scientists and researchers have developed lots of theoretical methods based on Maxwell's equations. The PWE method expands the dielectric function into the Fourier series and obtains the infinite matrix. By solving the obtained matrix, the dispersion relations can be studied considering reciprocal lattice vectors. The FEM method is very used to simulate the photonic structures using discretizing the boundary values problems or differential equations into subdomains with appropriate trial wave functions. The differential equations with trial functions can be solved by Ritz's or Gelenkin's method. The FEM gives accurate results but affects the memory and optical storage of the computational system. Based on discretization, the FDTD method also uses the transformation of Maxwell's equations into grids in space and time domains. FDTD method provides the values of electric and magnetic field vectors at each time step in the space-time domain and therefore the optical characteristics of 3-D periodic structures can be studied and this method gives highly accurate results depending on the number and size of time steps. TMM method is also a very useful and simple technique to study the optical properties of a 1-D periodic structure. TMM method correlates the electromagnetic field vectors at the interface of two media and the reflection and transmission coefficients can be studied. TMM is mostly applied in a 2x2 matrix form to study the optical properties of the periodic structure of isotropic layers, and a 4x4 matrix form in TMM is used for the anisotropic periodic layers. Basically, TMM is founded on the determination of Maxwell's equations; therefore, the accuracy of the results depends on the results of Maxwell's equations. The solutions for Maxwell's equations for certain anisotropic materials are complex, so a fast computational system is required for the simulation of anisotropic materials. All along with the overhead method, there are also so many theoretical methods that are also available like FDFD, RCWA, FIT, TB, DDA, BPM, PML, etc. The application of these methods depends on the desire results, types, and sizes of periodic structures.

References

[1] A. Yariv, P. Yeh, *Optical waves in crystals: Propagation and control of Laser radiation*, John Wiley & Sons, New York, 1984.

[2] J. A. Kong, *Electromagnetic Wave Theory*, John Wiley & Sons, New York, 1986, D. K. Yang, S. T. Wu, *Fundamentals of Liquid Crystals Devices*, John Wiley & Sons, New York, 2015.

[3] C. Davis, *Laser and Electro-Optics: Fundamentals and Engineering*, Cambridge University Press, United Kingdom, 1996.

[4] J. Griffiths, *Introduction of Electrodynamics*, Prentice Hall, New Jersey, 1999.

[5] P. Yeh, *Optics Waves in Layered Media*, John Wiley & Sons, New York, 1988.

[6] M. Born and E. Wolf, *Principle of Optics*, Pergmon Press, Oxford, 1999.

[7] J. B. Pendry, Calculating band structure, *J. Phys. Cond. Mat.*, 8, 1085-1108, 1996.

[8] G. Pelosi, R. Coccioli, and S. Selleri, *Quick Finite Elements for Electromagnetic Waves*, Artech Hosue, Boston, 2009.

[9] A. Taflove, *Computational electrodynamics: The Finite Difference Time Domain method*, Artech House, Boston, 2005.

[10] J. B. Pendry, and A. MacKinnon, Calculation of photon dispersion relations, *Phys. Rev. Letts.*, 69, 2772-2775, 1992.

[11] I. A. Sukhoivanov, I. V. Guryev, *Physics and Practical Modeling, Springer*, New York, 2009.

[12] S. G. Johnson, and J. D. Joannopoulos, Introduction to Photonic Crystals: Bloch's Theorem, Band Diagrams, and Gaps (But No Defects), MIT Tutorial, 2003.

[13] D. Hermann, M. Frank, K. Busch, and P. Wolfle, Photonic band structure computations, *Opt. Express*, **8**, 167–172, 2001.

[14] J. D. Shumpert, *Modeling of periodic dielectric structures (electromagnetic crystals)*, Ph.D. thesis. Michigan University, 2001.

[15] L. G. Zheng. and W.X. Zhang, Study on bandwidth of 2-D dielectric PBG material, *Prog. Electromagn. Res.*, **41**, 83–106, 2003.

[16] J. Jin, *The Finite Element Method in Electromagnetics*, John Wiley and Sons, New York, 2002.

[17] M. A. Bhatti, *Fundamental finite element analysis and applications: With Mathematica and MATLAB Computations*, John Wiley and Sons, New Jersey, 2005.

[18] S. Obayya, M. F. O. Hameed, N. F. F. Areed, *Computational Liquid Crystal Photonics: Fundamentals, Modelling, and Applications*, John Wiley and Sons, United Kingdom, 2016.

[19] A. Taflove, *Advances in Computational Electrodynamics: The Finite Difference Time Domain Method*, Artech House, Boston, 1998.

[20] A. Taflove, and C. Susan, *Hangness, Computational Electrodynamics: The Finite Difference Time Domain Method*, Artech House, Boston, 2002.

[21] K. S. Yee, Numerical solution of initial boundary value problem involving Maxwell's equations in isotropic media. *IEEE Trans. Antennas Propag.*, **AP-14**, 302–307, 1966.

[22] A. Zhao, An efficient FDTD algorithm for the analysis of microstrip patch antennas printed on a general anisotropic dielectric substrate. *IEEE Trans. Microw. Theory Tech.*, **47** (7), 1142–1146, 1999.

[23] C. D. Moss, and F. L. Teixeira, Analysis and compensation of numerical dispersion in the FDTD method for layered anisotropic media. *IEEE Trans. Antennas Propag.*, **50**, 1174–1184, 2002.

[24] A. Akyurtlu, and D. H. Werner, Modeling of transverse propagation through a uniaxial bianisotropic medium using the finite difference time domain technique. *IEEE Trans. Antennas Propag.*, **47** (7), 1142–1146, 1999.

[25] H. Mosallaei, and K. Sarabandi, Magneto-dielectrics in electromagnetics: concept and applications. *IEEE Trans. Antennas Propag.*, **52**, 1558–1567, 2004.

[26] M. Beggs, *Computational studies of one and two-dimensional photonic microstructures*, Ph. D. thesis, Durham University, 2006.

[27] D. W. Berreman, Optics in Stratified and Anisotropic media: 4x4-Matrix Formulation, *J. Opt. Soc. Am.*, 62, 502-510, 1972.

[28] P. Yeh, Electromagnetic Propagation in Birefringent layered Media, *J. Opt. Soc. Am.*, 69, 742-756, 1979.

[29] M. C. Bohley, *Polarization Optics of Periodic Media*, Ph. D. thesis, University of Neuchatel, 2004.

[30] K. J. Ghaleh, and B. Kazempour, Effect of incident angle and polarization on electrically-tunable defect mode in anisotropic photonic crystals, *App. Opt.*, 55, 4350-4356, 2016.

[31] R. Gnawali, P. Banerjee, J. W. Haus, V. Reshetnyak and D. R. Evans, Berreman approach to optical propagation through anisotropic Metamaterials: application to metallo-dielectric stacks, *Opt. Commun.*, 425, 71-79, 2018.

[32] P. Yeh, Optics of Anisotropic Layered Media, *Surface Science*, 96, 41-53, 1980.

CHAPTER 3

Tunable transmission of a nematic liquid crystal (NLC) without and with graphene layers as a defect in one-dimensional periodic structure (1-DPS) of dielectric materials by orientation/re-orientation of liquid crystal (LC)

CHAPTER 3

Tunable transmission of a nematic liquid crystal (NLC) without and with graphene layers as a defect in one-dimensional periodic structure (1-DPS) of dielectric materials by orientation/re-orientation of liquid crystal (LC) molecules

3.1 Introduction

The interaction of the electromagnetic wave with any material depends on the type of the material; isotropic or anisotropic. The isotropic materials have direction independent refractive index whilst anisotropic materials have a direction-dependent refractive index or tensor dielectric function. The interaction of wave anisotropic materials dissociates the incident wave in extraordinary and ordinary waves. The ordinary waves follow Snell's law of refraction but the extraordinary wave does not follow Snell's law and the direction of extraordinary waves can be found by geometrical construction of interaction plane with origin point considering normal surface. The anisotropic materials have two types; uniaxial and biaxial. In uniaxial crystals, two of the principal indices have the same values different from the third value but in the case of biaxial, all three principal indices have different values from each other. In the material science, the various anisotropic materials or molecules have been discovered; ice, rutile, zircon, ZnS, BeO, quartz, $NaNO_3$, $LiNbO_3$, $BaTiO_3$, $NaNO_2$, KH_2PO_4, SbSI, $YAlO_3$, mica, topaz, liquid crystals, graphene, etc. Due to having birefringence, anisotropic materials including liquid crystals (LCs) are used in various nonlinear and linear optical devices. Liquid crystals are the organic materials and intermediate phase between pure liquids and crystalline solids, i.e. LCs have flow property like liquid and ordered structure like crystals. LCs are widely used in optical devices due to having direction-dependent nonlinear properties and the molecules of the LCs are also affected with external and induced electric fields. The interaction of optical radiation with LCs induces electric field on the molecules and produces various optical effects including reflection, refraction, transmission, scattering, hysteresis, etc.

3.1.1 PAA (para-azoxy-anisole) liquid crystal

The PAA (para-azoxy-anisole) liquid crystal (LC) has melting point 119^{o}C and nematic to isotropic phase transition temperature 135^{o}C. Riste et al. [1] deliberated the consequence of the magnetic field and temperature on the nematic to isotropic phase transition in PAA liquid crystals. The authors determined the width 3.7x 10^{-4} m of thermally induced hysteresis for the weak magnetic fields. The transition temperature decreases with the field and the transition in the very weak fields found second-order transitions. As we know that the application of external fields on the LCs affects the optical properties of molecules and can be produced three types of configurations; splay, bend, and twist. These configurations have different elastic constants known as the Frank elastic constants and the values of theses constants can be determined by applying the threshold field on the LCs. Bradshaw et al. [2] reported the ratio of splay elastic to susceptibility and bend constants to susceptibility for different temperatures and found that these ratios increase for PAA LC as the difference between transition temperature and operating temperature increases. Chandrasekhar et al. [3] studied the orientation order of PAA liquid crystals and a mixture of PAA with other LCs. Based on Vuk's equations, the authors found that the graph between the order parameter and the temperature difference of transition temperature to operating temperature are the parallel lines. The order parameter was found high for the high phase transition temperatures for PAA LC. Sanyal et al. [4] suggested that the forces between the PAA molecules are weaker at high temperatures and the movement of the molecules was prohibited in the perpendicular direction but the molecules were free to move in the parallel direction to longer molecular axis under maximum 30^{o} orientation. The intensity of Raman lines was changed due to the softing mode in the PAA LC at the transition temperature. The obtained intensity of quasi-elastic scattering in the PAA was high and it is connected with Debye fluctuations (rotational fluctuations) about the loner molecular axis which is acted as soft modes in the transitions [5]. The elastic constants of the PAA LCs are $K_{11} = 4.5 \times 10^{-7}$ dyn, $K_{33} = 9.5 \times 10^{-7}$ dyn, $\varepsilon_a = 0.896$, $\varepsilon_{\perp} = 2.45$ $\varepsilon_{||} = 3.346$ ε_a =dielectric anisotropy, $\varepsilon_{\perp}, \varepsilon_{||}$ = perpendicular, parallel dielectric constants, respectively. The values of dielectric constant suggest that the PAA LC has negative anisotropy and it possesses the splay and bend configurations which can be used to design various nonlinear optical devices [6].

3.1.2 Graphene

The discovery of graphene has opened a new era in the field of nanotechnology [7]. Graphene is the first two-dimensional nanostructured material, which compacts the size of various electronic as well as optical devices and also enhances the optical properties of the photonic devices [8]. Graphene has a 2-D hexagonal lattice of sp^2 hybridized carbon atoms just like honeycomb structure as shown in figure 3.1. Graphene is the basic building block of all carbon allotropes including graphite, fullerene (C_{60}), carbon nanotube (CNT), etc. Graphene has versatile applications in various electronic devices due to having huge charge carrier mobility at room temperature.

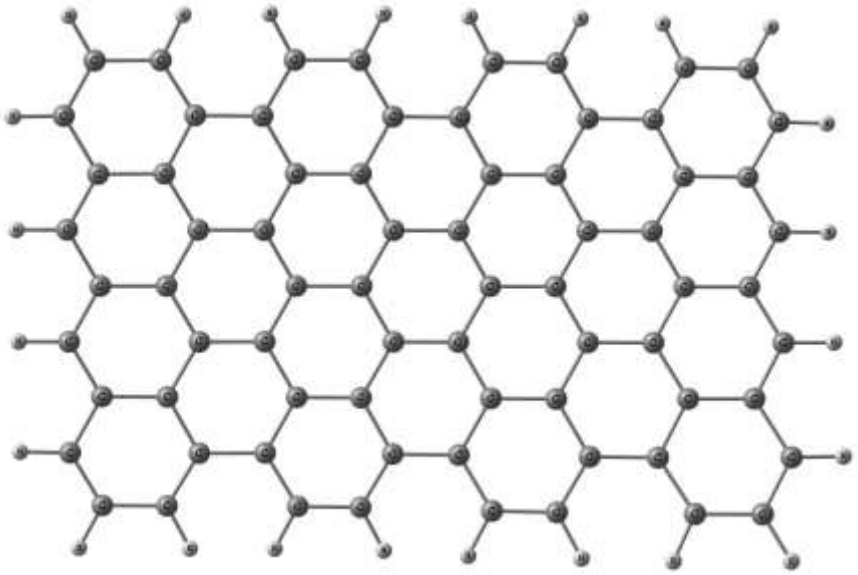

Figure 3.1: 2-D structure of graphene

The carbon lattice in graphene is hexagonal structure, so, the electronic wave functions overlap with other wave functions such as $p_z(\pi)$ with s or p_y and p_x is zero due to the presence of symmetry. The pi-bonds are formed in the hexagonal lattice due to p_z electrons which are independent of other valence electrons. Using the pi-band approximations and interaction of first nearest-neighbors, the Hamiltonian can be resolved in the electronic spectrum and the dispersion relations can be obtained as [9];

$$E^{\pm}(k_x, k_y) = \pm\gamma_0 \sqrt{1 + 4\cos\frac{\sqrt{3}k_x a}{2}\cos\frac{k_y a}{2} + 4\cos^2\frac{k_y a}{2}} \qquad (3.1)$$

where $a = \sqrt{3}a_{cc}$, γ_0 = transfer integral between first neighbor π-orbitals, and a_{cc}= distance between carbon-carbon atom.

Considering $1p_z$ electron/atom, the branch of negative energy is fully employed while the branch of positive energy is vacant according to n $\pi - \pi^*$ model. If the Fermi surface is described by the K and K'; the formation of π- and π^*- bands occur. The energy is given as;

$$E^{\pm}(\kappa) = \pm\hbar v_F|\kappa| \tag{3.2}$$

where $\kappa = k - K$ and v_F is the electronic group velocity has value 10^6 m s^{-1}.

The above equation 3.2 is the solution of the effective Hamiltonian at the point K (K'), $H = \pm\hbar v_F(\sigma \cdot \kappa)$, where $\kappa = -i\nabla$ and σ are the pseudo-spin Pauli matrices. The Pauli matrices operate on the amplitude of the electron in the sub-lattices of graphene. Due to the absence of bandgap, graphene has finite limits to operate in electronic devices. Graphene possesses a huge leakage current in numerous devices, which also limits the usage of graphene in electronic devices. Including fractional quantum Hall effect, graphene shows the properties of 2-D Dirac fermion. The graphene has a certain minimum value of conductivity ($4e^2/h$), even when the concentration of the charge carrier tends to zero. The complex dielectric constant of the Graphene depends upon the gate. The complex optical conductivity of graphene depends upon the intra-band and inter-band contributions. The total conductivity of the graphene is given by [10];

$$\sigma_{total} = \sigma_{intra} + \sigma'_{inter} + i\sigma''_{inter} \tag{3.3}$$

Where $\sigma_{intra} = \dfrac{\sigma_0 4\mu}{\pi\hbar(\tau_1 - i\omega)}$, and $\sigma'_{inter} = \sigma_0\left(1 + \dfrac{1}{\pi}\arctan\left(\dfrac{\hbar\omega - 2\mu}{\hbar\tau_2}\right) - \dfrac{1}{\pi}\arctan\left(\dfrac{\hbar\omega + 2\mu}{\hbar\tau_2}\right)\right)$

$\sigma''_{inter} = -\sigma_0 \dfrac{1}{2\pi}\ln\dfrac{(2\mu + \hbar\omega)^2 + (\hbar\tau_2)^2}{(2\mu - \hbar\omega)^2 + (\hbar\tau_2)^2}$ where $\sigma_0 = e^2/(4\hbar)$ is universal optical conductance having the value $60.8\mu S$. Using σ_{total} for graphene, the calculated dielectric function for the graphene sheet is given by equation 3.4 as;

$$\varepsilon(\omega) = 1 + \left(\frac{i\sigma(\omega)}{\omega\varepsilon_0 d_g}\right) \tag{3.4}$$

where d_g = thickness of graphene layer and ε_0 = vacuum permittivity.

The graphene sheets have the frequency-dependent dielectric function conductivity ($\sigma(\omega)$), chemical potential (μ_c), relaxation time (τ), and temperature (T) as represented in equation 3.4. The dielectric function of graphene has been described at μ_c=0.4eV, $\lambda = 1550\,\text{nm}$ temperature 296 K, and $\tau_1 = 1.2\text{ps}, \tau_2 = 10\text{fs}$ respectively [10].

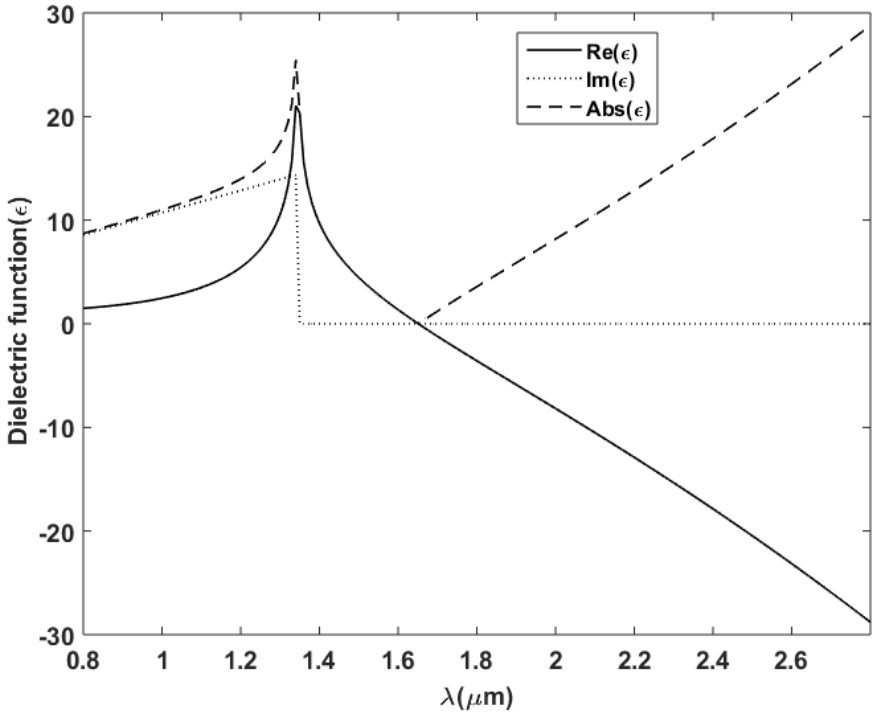

Figure 3.2: Variation of the real, imaginary, and absolute value of the dielectric function of graphene.

The real, imaginary, and absolute part of the dielectric function of graphene are shown in figure 3.2. The real values first increase and reach to its maximum value at 1.3μm wavelength (λ) and ant it reduces further with higher wavelength, while the imaginary part also increases first and becomes maximum at 1.3μm wavelength (λ) and it reduces abruptly to zero and turns out to be constant for further wavelengths up to 2.8μm wavelength.

In graphene, Shubnikov-de Haas oscillation also occurs with π shift considering Berry's phase [11,12]. Graphene acts as an effective material for high-frequency device applications due to exhibiting near ballistic transport at room temperature. Due to revealing linear dispersion of Dirac cones, graphene also has potential applications

in various nonlinear devices [13]. Although the graphene has no bandgap but the gate voltage-controlled tunable bandgap can be obtained through the applying electric field on the graphene layers or bilayers exiting in periodic structures [14,15]. Graphene plays a very crucial role to fabricate the optoelectronics and photonic devices. Along with the absence of bandgap, graphene also shows semi-metallic behavior. The theoretical description of graphene-based photonic modulators was investigated by Gosciniak et al. [16], and they suggested that 3dB modulation having energy/bit below than 1 fJ/bit could be obtained.

Graphene is a nonlinear material, so it can be applied in the microwave, terahertz, and optoelectronic applications, optical sensing applications, nonlinear photonic device applications, lasing action applications, transparent conducting windows, photoactive materials, channels for transport of charge and catalytic action, light-emitting devices, photo-detectors, smart windows, bi-stable displays, ultrafast lasers, optical limiters, terahertz devices, and optical frequency converters. Graphene is also used in the fabrication of dye-synthesized solar cells for the window electrodes applications [17-19]. Generally, graphene is synthesized by micromechanical exfoliation and liquid phase exfoliation methods in which graphene nanoribbons are produced with offering scalability and the width of nanoribbons is less than 10nm. Besides the mentioned method, chemical vapor deposition, carbon segregation, chemical methods are also used in the synthesis of graphene sheets [20, 21].

3.1.3 Liquid crystal and graphene-based 1-DPC

In 19^{th} century, LC was discovered by German botanist Reinitzer but the term introduced by Lehmann. LCs are interesting organic materials, which have a transitional phase between the pure liquids and the crystalline solids [22]. LCs have flow property like liquids and order structures like crystals. LCs are found in mainly three types; lyotropic, thermotropic, and metallotropic which have different optical characteristics due to the molecule orientations [23]. In the last few decades, photonic crystals (PCs) have been used in the study due to having novel optical responses in terms of the photonic band gap (PBG), which are helpful to design optical devices. PBGs obstruct the transmission of electromagnetic waves (EMWs) in certain frequency or wavelength regions and such material also called PBG materials [24]. Such PBG materials are capable to guide or mold the optical radiation in dielectric

mediums and hence they are widely used in the field of photonics. The guiding of EMW in optical media is analogous to regulate the motion of electrons in electronic materials [25]. The transmission or propagation of the EMW through the PCs relies on the dielectric function, topology, geometry, and other parameters of the dielectric material. By tuning of PBG regions, the dynamical regulation of the EMW in PCs can be obtained. [26]. Due to having dielectric function dependent propagation of EMW in periodic materials, PCs are classified into three forms considering the periodic variation of dielectric constant in the space: one-dimensional photonic crystal (1-DPC), two-dimensional photonic crystal (2-DPC), and three-dimensional (3-DPC). Moreover, the size and variation of PBG are dependent on the dielectric functions, thicknesses of layers, and structural constraints of PCs. [27]. PCs embedded with the defect layer possess various optical characteristics of the defect peaks and such defective periodic structures are used in the designing of photonic devices like switches, lasers, etc. [28, 29]. The transmission characteristics of PCs including PBG can be improved by altering the structural parameters of periodic layers. [30]. The existing nonlinear properties LCs are widely used in optoelectronics, electro-optical devices [6, 30]. The defective 1-DPC with a nematic liquid crystal (NLC) has exhibited all-optical switching properties of 1-DPC. [26]. To describe the switching of LCs, a nonlinear differential equation for LC director was solved which described the switching of molecules with incident EMW [31]. Considering the interaction of EMW with LC, the molecules show orientation in according to intensity ratio (I/I_{fr}), when the intensity (I) of EMW becomes equal to a threshold value, known as the Freedericksz transition (I_{fr}), and the transmission of 1-DPC is exhibited tunability with the orientation of molecules [32,33].

The PBG region also could be modulated by inverse opal with LC coating which was described by Busch et al. [34] and it was also established experimentally by Yoshino et al. [35]. The tunability of PBGs of the PCs with LC as a defect is dependent on the dielectric function, temperature, and applied external field on the LCs [36-41]. The tunability of PCs is also gained by the infiltration of individual holes or pores existing in the PCs with LCs, which tunes the optical characteristics of the whole photonic structure [42, 43]. LCs show huge nonlinear optical characteristics and are mostly used in nonlinear optical devices; all-optical switches and controlled EMW propagation in the photonic structures. Mohamed et al. [44] investigated the impact of

the orientation of molecules as well as temperature on the transmission responses of 1-DPC with NLC as a defect. Correspondingly, linear and non-linear effects of 1-DPC of dielectric layers containing LC as a defect layer were deliberated by Entezar et al. [45]. The authors established that the threshold intensity and bi-stable properties depend on the functioning temperatures. They also deliberated the consequence of the temperature on the transmission possessions of the 1-DPC. The obtained defect modes transmission in the PBG is dependent on the molecular orientation of LC. The extraordinary and ordinary refractive indices of LCs have also affected the propagation of EMWs in 1-DPC with LC as a defect layer [46]. As discussed earlier, LCs show electro-optic properties, and graphene (G) also shows unique electronic and optical characteristics property. The innovation of graphene opens new aspects to develop a novel nano-sized electronic and optical devices having high flexibility in nanotechnology [47]. Graphene has 2-D lattices of sp^2 hybridized carbon atoms arranged in a hexagonal structure, which is the fundamental planer construction for graphite. Graphene is mostly used as windows and transparent electrodes in solar cells [15,18,19]. With the absence of band gap, the graphene shows semiconducting behavior and massless carriers; electrons and holes are considered as Dirac-Fermions in the graphene. Due to having interband and intraband, graphene exhibits outstanding electronic and optical responses; the conductivity of graphene is also calculated by these-bands. The calculation of these bands leads to dielectric function depending on the chemical potential and collision time. [48, 49]. The absorption property of the graphene layer is found to vary with the incident angle of the EMWand position of the graphene layer in PCs [50]. Zhao et al. [51] described the absorption properties of graphene and amplified in the IR region considering the total reflection effect. The transmission properties of graphene layers are affected by strain in the material structure and polarization of incident EMW [52]. Using graphene with plasmonic structure and the Fabry-Perot cavity, the efficiency of photodetectors is enhanced [53, 54]. The polarization and coupling of incident EMW with graphene are also affected by the optical properties of graphene embedded periodic structures [55]. Under the total internal reflection, the absorption of nanodisk arrays of doped graphene could be attained the maximum value and such structures are used in various optical devices including solar cells. [56]. By varying the graphene parameters like chemical potential, the PBGs of the graphene-based PCs were tuned [57]. The transmission and

dispersion properties of graphene are modified with incident angle and such dispersion curves could be obtained through the effective medium theory. [58]. The obtained defect modes in the transmission of graphene embedded PCs are varied with incident angles and the chemical potentials, and such graphene-based PCs are used as tunable optical filters, optical sensors, etc. [59] PCs with graphene layer as defect are exhibited localization of certain wavelength and these localized wavelengths are tuned the PBG region of PCs [60]. Graphene-based PCs of various materials have a lot of novel applications in the field of photonics due to having operative parameters like chemical potential. Graphene-based 1-DPC has various applications in band gap engineering, polarization splitter, tunable optical device, stop band filter, potential device application, antenna, generator, terahertz band device, etc. The conductivity and dielectric function can be enhanced by varying chemical potentials of the graphene. Due to exhibiting absorption, graphene is a very significant material to examine the sensing phenomena produces by graphene embedded LC in photonic structures.

In this chapter, we have solved a nonlinear differential equation for the NLC director angle and discussed its variation with intensity ratio (I/I_{fr}), I is the intensity of incident EMW and I_{fr} is the threshold intensity or called the Freedericksz transition intensity in NLC. The LC molecules exhibit orientations whenever the intensity (I) of the incident EMW becomes equivalent to or greater to the threshold value, or the Freedericksz transition intensity (I_{fr}). We have also discussed the effect of orientation/reorientation of PAA molecules on the transmission characteristics of 1-DPS of glass and silica (Si) layers with the variation of intensities and incident angles of EMW. We have also calculated the transmission of the 1-DPS with NLC as a defect layer at dissimilar orientation angles of the NLC. The shifting property of the defect transmission modes in the PBG region is dependent on the incident angle as well as the director angle of the LC. To study the transmission properties of semi-finite 1-DPS of glass and Si layers with NLC as defect without/with graphene (G) layers, the well-known transfer matrix method (TMM) has been doped as discussed in chapter 2 [61]. The defect layer of NLC with graphene layers in 1-DPS of Si and glass materials denotes that an NLC is embedded with graphene layers and this defect layer of NLC with graphene layers is attached symmetry surface of 1-DPS of Si and glass materials. We have also discussed the absorption properties of asymmetric semifinite 1-DPS containing defect

of NLC with the variation of the periodicity of dielectric layers for TE and TM modes.

3.2 Theory and methodology

LCs are organic anisotropic materials and have tensor dielectric permittivity which can be expressed in matrix form as equation 3.6 [23].

$$\tilde{\varepsilon} = \begin{pmatrix} \varepsilon_{\perp} + \varepsilon_a \sin^2\phi & 0 & \varepsilon_a \sin\phi\cos\phi \\ 0 & \varepsilon_{\perp} & 0 \\ \varepsilon_a \sin\phi\cos\phi & 0 & \varepsilon_{\perp} + \varepsilon_a \cos^2\phi \end{pmatrix} \tag{3.6}$$

The dielectric tensor $(\tilde{\varepsilon})$ of LC consists of perpendicular $(\varepsilon_{\perp})$ and parallel (ε_{II}) constituents of the dielectric constants; and dielectric anisotropy $(\varepsilon_a = \varepsilon_{II} - \varepsilon_{\perp})$ and director angle (ϕ) of LC are constructed with z-axis as shown in figure 3.3 [26].

The dielectric tensor of LC in matrix form is reduced to diagonalized matrix form with considering the orientation angles: $\phi = 0^0$ and $\phi = 90^0$. To apply the transfer matrix method (TMM), we have diagonalized the dielectric tensor matrix for a certain orientation or director angles [45]. The dielectric tensor depends on the orientation angle of molecules including different parameters of LC and the variation in refractive index is equivalent to the effective dielectric function of the LC [23]. The effective dielectric function of the LC is described as;

$$\varepsilon_{eff} = \frac{\varepsilon^2 - \left(\frac{\varepsilon_a}{2}\right)^2}{\varepsilon - \left(\frac{\varepsilon_a \cos 2\phi}{2}\right)}, \varepsilon = \frac{\varepsilon_{\parallel} + \varepsilon_{\perp}}{2} \tag{3.7}$$

where ϕ = orientation angle or director tilt angle of the LC director constructed with the z-axis and considering the EMW propagation in the z-direction.

To inspect the variation of LC director orientation angle, an LC thickness L having homeotropic arrangement of LC molecules is considered as a defect layer in 1-DPS. The orientation of the LC director is given by $\phi(z)$. On the interaction of EMW with LC cell, the molecules orient sustaining an angle $\phi(z)$ with the normal axis (z-axis) of the cell as shown in figure 3.3. When the intensity of incident EMW is gained value

equal to the Freedericksz transition intensity, the molecules show orientation in the LC cell.

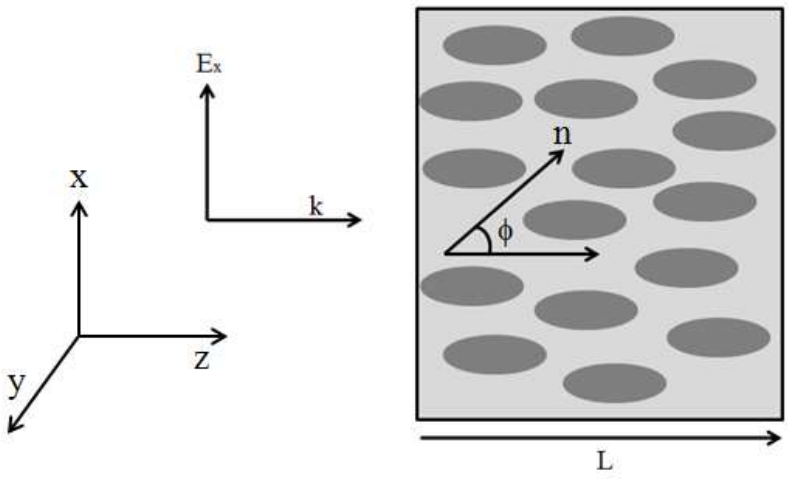

Figure 3.3: Diagram of molecular orientation (ϕ) of liquid crystal (LC) under the exterior electric field.

Considering the interaction between orientation angle and intensity ratio, the optical characteristics of LCs can be tuned. The orientation and reorientation of the LC molecules is due to the coupling with EMW, which can be investigated by solving nonlinear differential equation 3.8 as [31];

$$\phi_{zz} - \frac{K_r \sin(2\phi)}{2(1-K_r \sin^2\phi)}\phi_z^{\,2} + \frac{\pi^2 I \sin(2\phi)}{2L^2 I_{fr}(1-K_r \sin^2\phi)(1-\beta \sin^2\phi)^{3/2}} = 0 \quad (3.8)$$

The solution of equation 3.8 depends on the intensity ratio I/I_{fr} and the boundary conditions of the LC cell. Here, ϕ_{zz} and ϕ_z are the second and first-order partial derivatives of ϕ with respect to z, respectively. The constant K_r and β are given as;

$$K_r = \frac{K_{33} - K_{11}}{K_{33}}\ ,\ \beta = 1 - \left(\frac{n_o^{\,2}}{n_e^{\,2}}\right) \quad (3.9)$$

The constant parameters, K_{33} and K_{11} in the equation 3.9 are bend and splay elastic constants of LC, and β is also a constant depending upon the extraordinary (n_e) and the ordinary (n_o) refractive indices of the LC.

The Freedericksz or threshold intensity (I_{fr}) is given as:

$$I_{fr} = \frac{ck_{33}\pi^2}{n_o \beta L^2}, \tag{3.10}$$

where c = speed of light in the vacuum. To determine the orientation of LC director, Dirichlet boundary conditions (BCs) are used to solve the nonlinear equation of the NLC and the condition are given as;

$$\phi\ (z=0), \text{ and } \phi\ (z=L) \tag{3.11}$$

The conditions are considered for the strong anchoring of LCs; and to obtain the solution of nonlinear equation, we have multiplied the equation by $2\phi_z$ and integrated with respect to z, the integration constants can be obtained depending on the maximum value of director angle $\phi^0{}_{max}$ and the equation is reduced as;

$$(1 - K_r \sin^2\phi)\left(\frac{d\phi}{dz}\right)^2 = \frac{4A}{\beta}\left[\frac{1}{\left(1-\beta\sin^2\phi^0{}_{max}\right)^{1/2}} - \frac{1}{\left(1-\beta\sin^2\phi\right)^{1/2}}\right] \tag{3.12}$$

Using the one elastic constant approximation i.e. $K_{11}=K_{22}=K_{33}$, the equation is further reduced as;

$$\left(\frac{d\phi}{dz}\right)^2 = \frac{4A}{\beta}\left[\frac{1}{\left(1-\beta\sin^2\phi^0{}_{max}\right)^{1/2}} - \frac{1}{\left(1-\beta\sin^2\phi\right)^{1/2}}\right] \tag{3.13}$$

where $A = \frac{\pi^2 I}{2L^2 I_{fr}}$, and the orientation angle of NLC obtains the maximum value ($\phi^0{}_{max}$) that reaches the central position of the cell at z=L/2. For such condition, we have obtained;

$$\int_0^{\phi^0_{max}} \frac{d\phi}{\sin^2\phi^0_{max} - \sin^2\phi} = \frac{L}{2}(2A)^{1/2} \tag{3.14}$$

The simplification of the nonlinear differential equation produces a relation between the maximum orientation angle of the molecules and intensity ratio (I/I_{fr}) as;

$$\phi^0{}_{max} = \sin^{-1}\left[2\left(\frac{I}{I_{fr}} - 1\right)^{1/2}\right] \tag{3.15}$$

The obtained resultant equation 3.15 describes that the LC molecules show orientation according to intensity ratio (I/I_{fr}). The second-order term is used in calculations

considering the increasing intensity of EMW while high order degree terms, fourth-order is associated with the formulations of LC reorientations for decreasing intensity of EMW. The orientation/re-orientation of the LC molecules depends on the incident wave intensity, which may be lower or higher to the threshold value (I_{fr}) for the orientation/re-orientation of molecules inside the LC layer.

To understand the effect of the orientation/re-orientation of molecules inside the LC layer, we have considered the normal incident of EMW on the 1-DPS and the propagation of EMW in the positive z-direction as depicted in figure 3.4. The transmission characteristics of 1-DPS of glass/Si layers with NLC as defect are calculated using TMM.

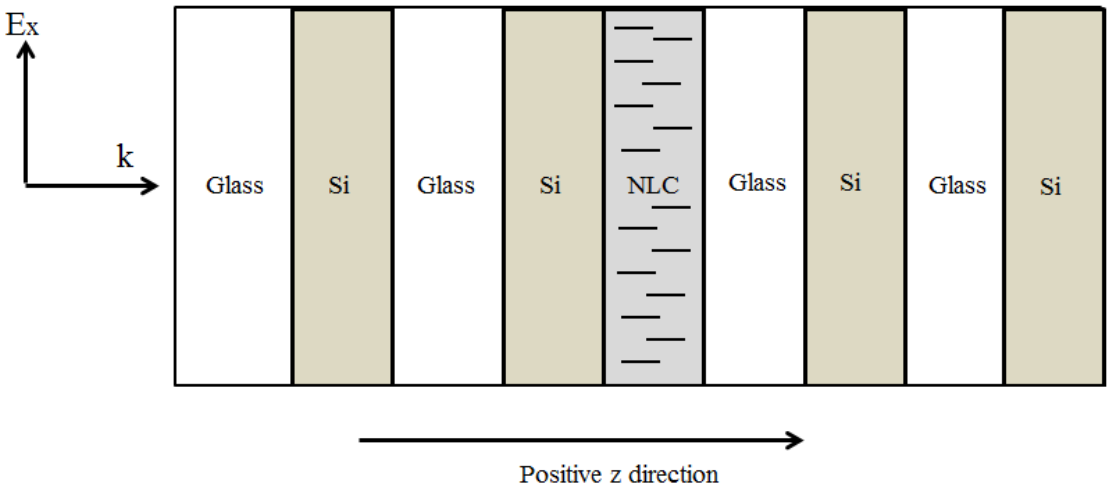

Figure 3.4: Schematic diagram of the 1-DPS of glass and Si layers with an NLC as a defect layer without graphene.

Before these calculations, the field of propagation of EMW in LC is described by equation 3.16, which depends on E_x and the dielectric constants ($\varepsilon_{\perp}, \varepsilon_{II}, \varepsilon_{33}$) of LC.

$$E_z = -\frac{\varepsilon_{13}}{\varepsilon_{33}} E_x = -\left[\frac{\varepsilon_a \sin\phi\cos\phi}{\left(\varepsilon_{\perp} + \varepsilon_a \cos^2\phi\right)}\right] E_x \qquad (3.16)$$

Using the master wave equation which was solved from Maxwell's equations, we can obtain the electric field equation as;

$$\frac{d^2 E_x}{dz^2} + k^2 E_x = 0 \qquad (3.17)$$

where $k^2 = k_0{}^2 \frac{\varepsilon_\perp \varepsilon_{II}}{\varepsilon_{33}}$, $k_0 = \frac{2\pi}{\lambda}$, λ = wavelength of incident EMW on the considered 1-DPS.

For the scattering of EMW in the layer, the z-component of the Poynting vector $I = S_z = (c/8\pi) E_x H_y^*$ is constant and this can be used to investigate the optical characteristics of the layer. The solution of equation 3.17 can be given as,

$$E_x = \begin{cases} A\exp(ikz) + B\exp(-ikz), z \le 0 \\ C\exp(ikz) + D\exp(-ikz), z \ge L \end{cases} \quad (3.18)$$

where A, B, C, D = incident, reflection, transmission coefficients of the EMW, which give the transmission and reflection of the considered material. The polarization of incident waves is considered in the x-z plane and parallel to the incident plane and EMW propagation in the z-direction. Further investigation of the graphene layer in 1-DPS, again, we have considered asymmetric 1-DPS of glass and Si layers containing NLC embedded with graphenes as defect layers; $(Si/glass)^m/G/NLC/G/(Si/glass)^n$, where m, n are periodicity of Si/glass, as represented in figure 3.5.

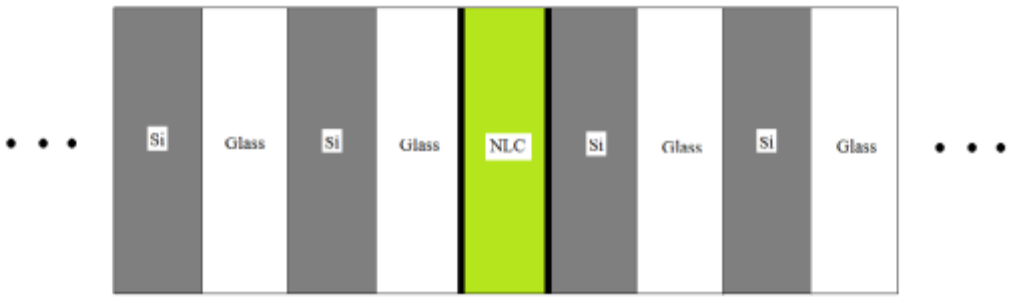

Figure 3.5: Schematic representation of 1-DPS containing Si and glass layers with NLC embedded with graphene layers as a defect material.

The optical characteristics of 1-DPS with a defect of NLC embedded graphene layers are studied with the variation of the periodicity of Si/glass materials and incident angle of EMW. The transmission and absorption characteristics of 1-DPS with a defect material of NLC without and with graphene layers are calculated by TMM [61].

3.3 Results and discussion

The results and discussion part is divided into two sections: the first section introduces the tunable optical properties of 1-DPS of dielectric materials with the

defect of NLC without graphene layers at different parameters, and the second section describes the transmission and absorption characteristics of 1-DPS consists of dielectric materials with the defect of NLC embedded graphene layers.

3.3.1 Tunable transmission of 1-DPS with a defect material NLC without graphene layers

3.3.1.1 Orientational behavior of the LC directors with a ratio of intensities (I/I_{fr})

In this part, we have described the orientation of the director angle of the NLC, PAA (p-Azoxyanisole), and the transmission of the NLC at a certain director angle with the variation of I/I_{fr}. The switching activities are inspected by solving the nonlinear differential of LC directors as equation 3.8 and the explanation is based on the Freedericksz transition effect in the LC layer. The derivative of the director angle ϕ with respect to z depends on the maximum magnitude of director angle ($\phi^0{}_{max}$) and the initial value of angle ϕ. As the solution, the maximum value of the director angle ($\phi^0{}_{max}$) is derived in terms of intensity ratio (I/I_{fr}) as equation 3.15. The orientation behavior of the LC director angle ($\phi^0{}_{max}$) with intensity ratio (I/I_{fr}) is described in figure 3.6, where I_{fr} is the threshold value of intensity or the Freedericksz transition. To calculate the optical characteristics, we have considered the splay and bend elastic constants of the PAA LC molecules with dielectric indices: $K_{11} = 4.5\times10^{-7}$ dyn, $K_{33} = 9.5\times10^{-7}$ dyn, $\varepsilon_{II} = 3.346$ $\varepsilon_{\perp} = 2.45$ and $\varepsilon_a = 0.896$, where $\varepsilon_{\parallel}, \varepsilon_{\perp}$ are the extraordinary and dielectric ordinary constants, ε_a is dielectric anisotropy, respectively [6]. The director angle ($\phi^0{}_{max}$) increases with the intensity of the EMWs and the different values of director angles is obtained i.e. 0^o, 28.71^o, 42.79^o, 56.3^o, 90^o. The obtained values of the director angle correspond to the intensity of incident EMW is equivalent or higher than threshold intensity. The director of LC found the different angles for decreasing intensity of EMW as 0^o, 21.26^o, 40.38^o, 57.29^o, and 90^o. Therefore, a hysteresis loop appears in the transmission through LC due to different threshold values of LCs. The analysis of the hysteresis loop suggests that the LC molecules follow the different paths for orientation and reorientation with increasing and decreasing intensities and this result in the existence of hysteresis loops in the transmission process. The hysteresis in transmission expresses the first order optically induced transition in LC cell and this type of transition, the director

angle shows discontinuity from the initial and final value (0^o, 90^o) at the threshold intensity (I_{fr}) of EMW. The free energy of LC system landscapes and obtains the minimum value near to the Freedericksz transition. This outcomes led to hysteresis and meta-stability in the LC cell. Based on the found consequences, we have accomplished that the LC molecules orients/re-orients in certain paths depending on the increasing/decreasing intensity of EMW.

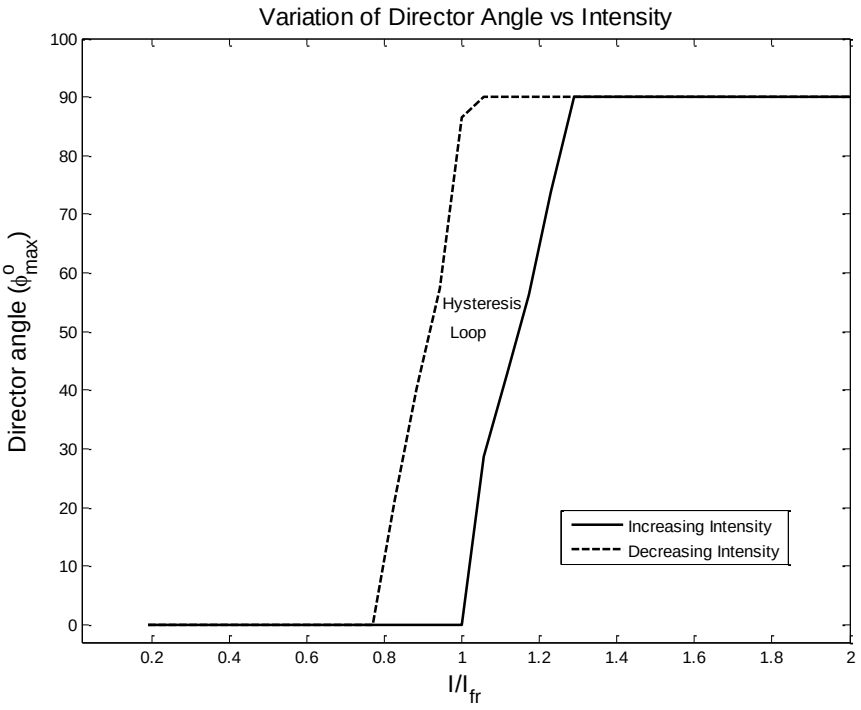

Figure 3.6: Maximum values of liquid crystal director (ϕ^0_{max}) versus intensity ratio (I/I_{fr}) for increasing and decreasing intensity.

3.3.1.2 Transmission properties with intensity ratio I/I_{fr}

The transmittance of EMW through the NLC layer as a defect in 1-DPS of glass and Si materials with intensity ratio (I/I_{fr}) for increasing/decreasing intensity at certain director angles are described as figure 3.7. The EMWs are transmitted through the LC with a finite value of transmission but as the intensity of EMW becomes identical or greater than the threshold value (I_{fr}), the LC molecule orients in certain directions. Hence, the transmission characteristics are affected and then shows lower values for intensity less than I_{fr}; $I<I_{fr}$. The transmissions of the 1-DPS with the NLC defect layer are 51%, 69%, 86% for 28.71^o, 42.79^o, and 56.31^o director angles of LC, respectively. As the LC molecules change the orientation, the transmissions are reduced up to 31%,

41%, and 54% for the similar director angles. The LC molecules orient/reorient in according to increasing/decreasing intensity of EMW, but the molecules cover a different path for the reorientation process with different director angles and suffer a different lesser threshold intensity I_{fr}'. The new director angles of LC are led to the uncommon transmission of 1-DPS as exposed in figure 3.7 (b).

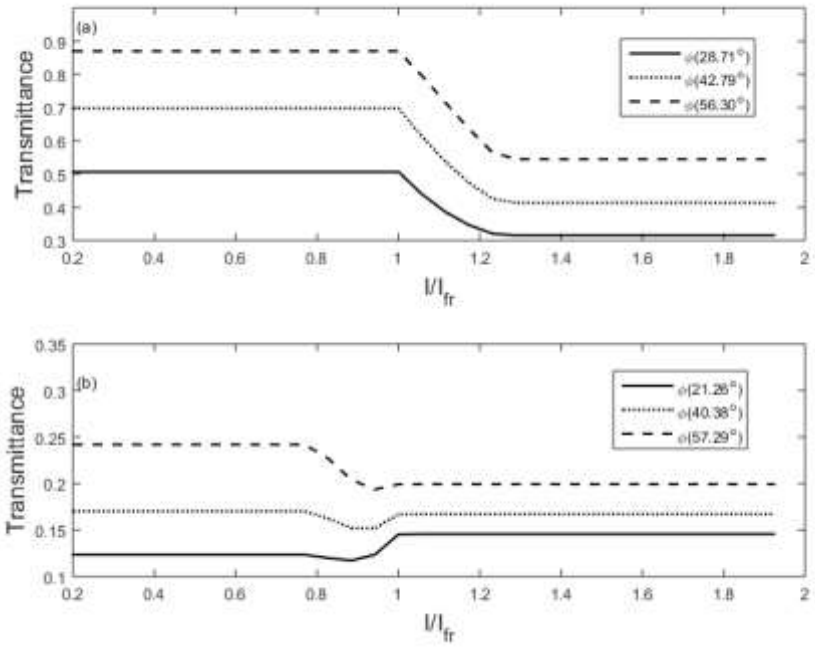

Figure 3.7: Comparative transmission versus intensity ratio (I/I_{fr}) at considered orientation angles of NLC for (a) increasing and, (b) decreasing intensity.

In decreasing intensity cases, the LC molecules have different paths for reorientation and resulted in the lower transmission of the 1-DPS with the NLC defect layer. The lower values of transmittance are 14%, 21%, 19% corresponding to 21.26^o, 40.38^o, and 57.29^o director angles, respectively. This transmittance associated with director angles 21.26^o, 40.38^o decreases but transmittance increases for the angle 57.29^o. This result suggests that the transmission of the LCs becomes unusual above the Freedericksz transition intensity (I_{fr}) due to the order parameter, polarization, and scattering in the LC layer. Likewise, a similar consequence is found for the decreasing intensity excluding the 57.29^o director angle.

3.3.1.3 Transmission of different wavelengths with intensity ratio I/I_{fr}

The orientation of LC molecules controls the transmission of EMW through the LC cell. Therefore, we have calculated the transmission of different wavelengths, 388nm,

1009nm, and 550nm with I/I_{fr} for the LC cell as revealed in figure 3.8. The considered values of wavelengths are taken from the band gap region of 1-DPS with the LC defect layer. The hysteresis loops corresponding to distinct wavelengths are obtained for increasing as well as decreasing intensity ratios (I/I_{fr}) as shown in figure 3.8. The transmissions of 388nm and 1009nm wavelength through the 1-DPS with the NLC defect layer are shortened 58%, 92% from 94%, respectively. The transmission for 550nm wavelength reduced to 2% from 10% at the Freedericksz transition intensity.

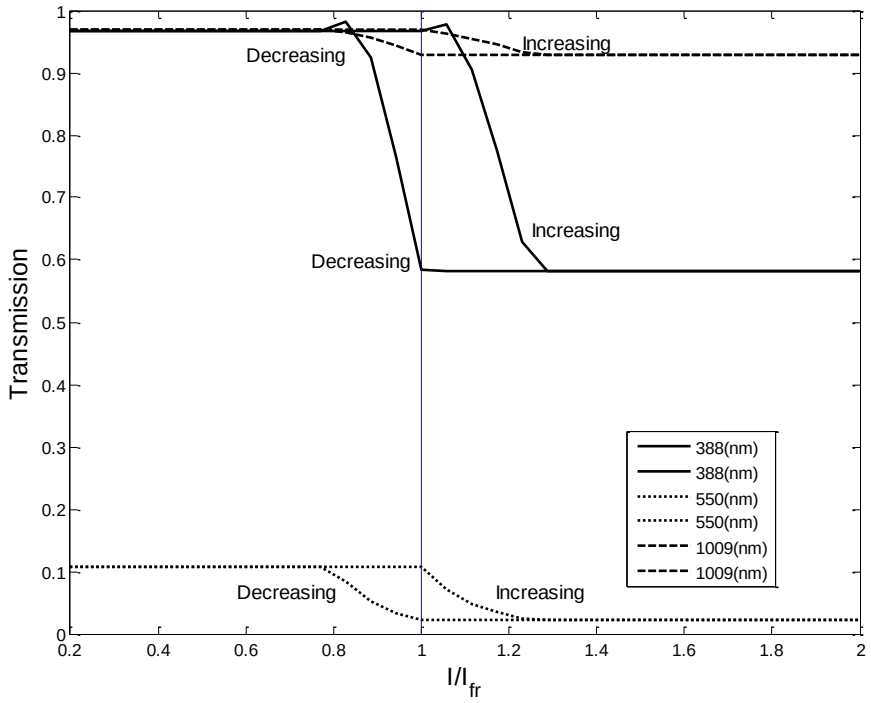

Figure 3.8: Comparative transmissions of different wavelengths versus intensity ratio (I/I_{fr}) for increasing and decreasing intensity of incident EMW.

3.3.1.4 Refractive index variation of LC

We know that the LCs are fascinating organic materials and its dielectric index depends on the various parameters like the external field, temperature, etc. The effective dielectric function or refractive index of LCs depends on the n_e, n_o, and ϕ with some finite values as equations 3.2. The director angle of LC diverges from 0^o to 90^o value and the calculated data matched with theoretical data which is given as figure 3.9. The dielectric constant of LC is lower director angle but the dielectric constant has high values with a higher director angle. The refractive index or dielectric constant of LC reaches the extreme value for the maximum director angle

(ϕ) in the middle of the LC cell. The obtained values of LC director angles are confirmed with the obtained values by *Gaussian 09 software package A02* [62]. Only three values of the director angle are considered for examining the influence of the orientation angle on the transmission of the 1-DPS with NLC as the defect layer.

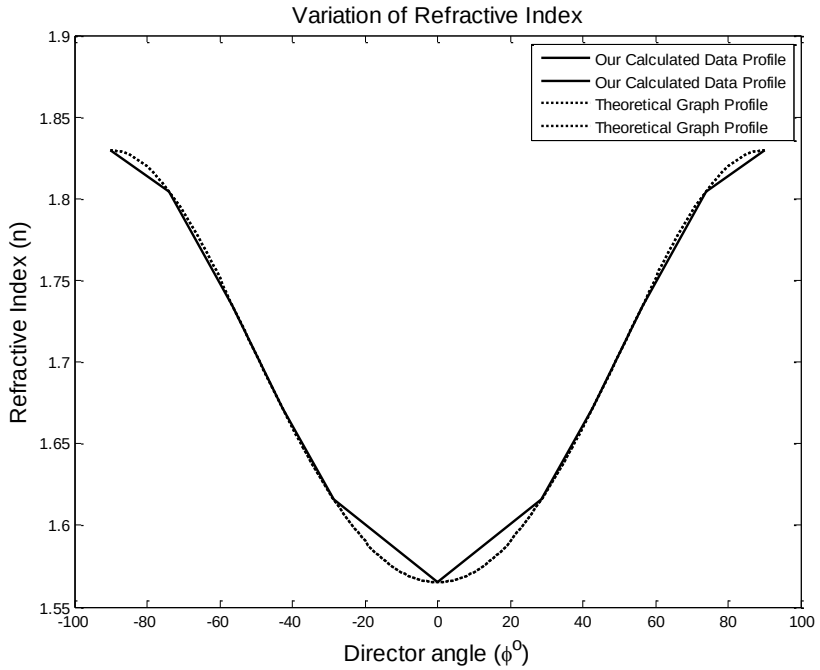

Figure 3.9: Comparative values of refractive index with director angles of the LC.

3.3.1.5 Transmission properties of periodic structure with NLC layer in the form of $(glass/Si)^2/NLC/(glass/Si)^2$

To study the transmission properties, we have considered 1-DPS of glass and Silica (Si) materials with the absence and presence of the PAA NLC defect layer. In absence of the defect layer, 1-DPS has a configuration in the form of $(glass/Si)^n$ with n=4; and in presence of PAA NLC defect layer, 1-DPS is considered in the form of $(glass/Si)^n/NLC/(glass/Si)^n$ with n=2. The considered defective 1-DPS with the PAA NLC layer is designed as figure 3.4. The refractive indices (n_1, n_2) of the glass and Si layers are 1.5 and 3.4 and corresponding thicknesses (d_1, d_2) are 91nm and 40nm, respectively for the central wavelength λ_0=550nm.

The transmissions of 1-DPS without and with the PAA NLC defect layer are obtained by the transfer matrix method (TMM) [61] as shown in figure 3.10. The obtained transmission of the 1-DPS $(glass/Si)^4$ exhibits the photonic band gap (PBG) in the range of 407nm to 848nm wavelength with a bandwidth ($\Delta\lambda$) of 441nm as shown in

figure 3.10(a). The transmissions of 1-DPS with the NLC defect layer are described at different orientation angle, 28.71^{o}, 42.79^{o,} and 56.30^{o} for increasing intensity ratio I/I_{fr}, and the values of the director angles are confirmed with *Gaussian 09 software package A02* [62].

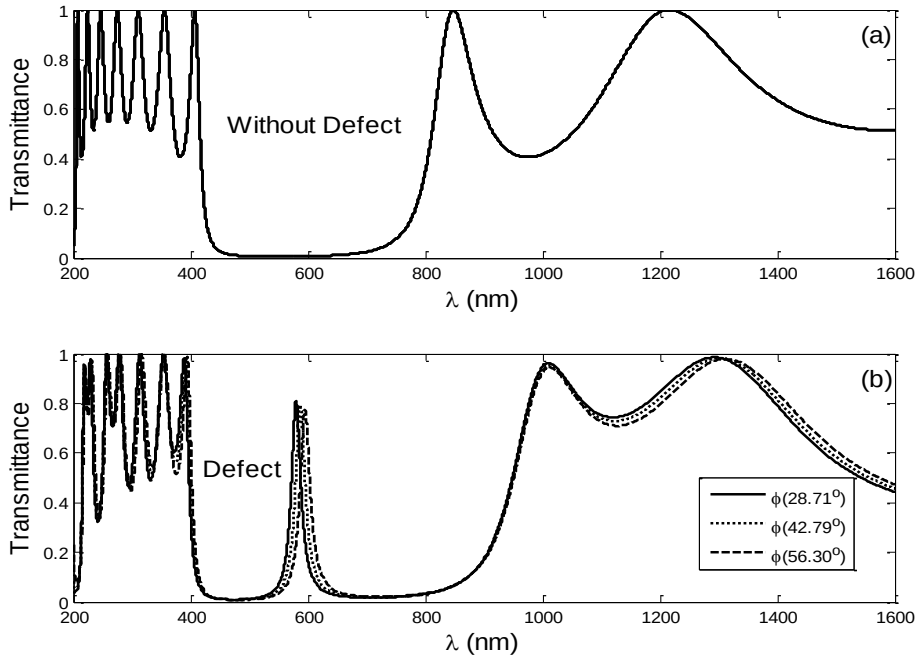

Figure 3.10: Comparative transmissions of 1-DPS without and with the NLC defect at different molecular orientation angles.

The sharp defect mode transmission in the PBG region of considered 1-DPS with the NLC defect layer tunes with orientation of the LC molecules in the defect layer [63]. Figure 3.10(b) expresses the transmission of the considered 1-DPS with NLC defect at 28.71^{o}, 42.79^{o,} and 56.10^{o} director angles. From the previous studies, we have confirmed that the propagation of EMW in NLC is led to switching characteristics due to the orientation of NLC molecules inside LC cell; and it is very fascinating to study the use of optical switching in photonic devices.

3.3.1.6 2-D and 3-D graphs of transmittance of periodic structure in the form (glass|Si)^2|NLC|(glass|Si)^2

To investigate the transmission of 1-DPS of glass and Si with the NLC defect layer with incident wavelength at different director angles of LC, 2-D, and 3-D diagrams are shown as figures 3.11 and 3.12. The 2-D and 3-D graphs demonstrate the defect

transmission mode shifting to a higher wavelength region at the director angles 28.71^{o}, $42.79^{o,}$ and 56.10^{o}.

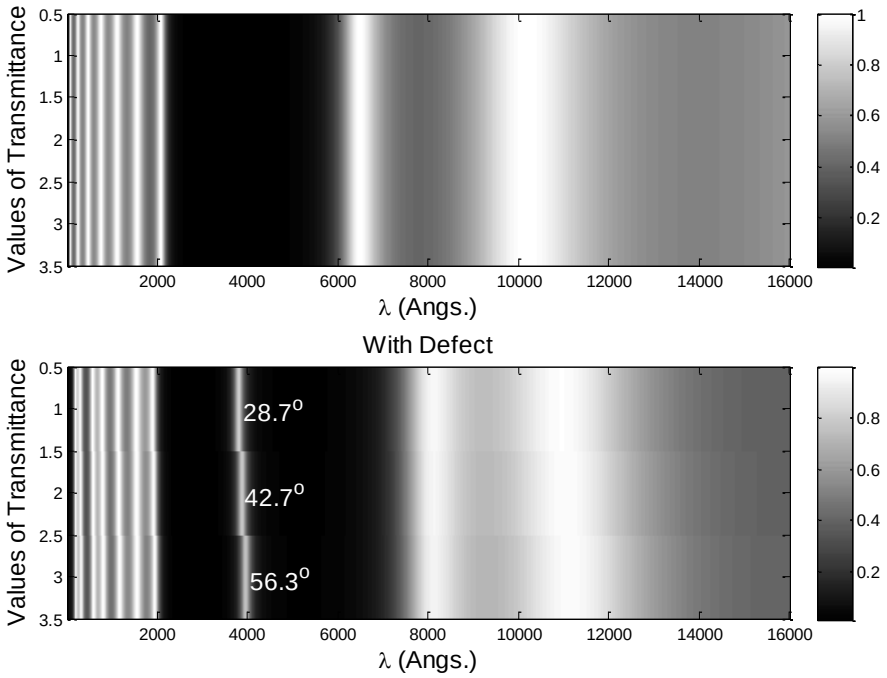

Figure 3.11: Comparative transmissions of 1-DPS without and with of NLC defect at considered orientation angles.

The director angles is able to LC tune the obtained defect mode transmission in the PBG region of 1-DPS and such sharp defect mode transmission could be helpful to use in optical switching and bi-stable photonic devices. The 2-D graph of transmission of the periodic structure without and with NLC defect against wavelength (λ) is exposed in figure 3.11. On comparing both 2-D and 3-D transmission graphs, we visibly explain the shifting nature of defect mode transmission with 28.71^{o}, 42.79^{o}, and 56.30^{o} director angles of LC. With the shifting of defect mode transmission, LC as defect layer in periodic structure is also enhanced width of the PBG region of 1-DPS due to change of director angles of LC.

The transmissions of the considered 1-DPS with NLC defect are also studied with the variation of incidence angle (θ) and director angle (ϕ) of NLC for transverse electric (TE) as well as transverse magnetic (TM) modes.

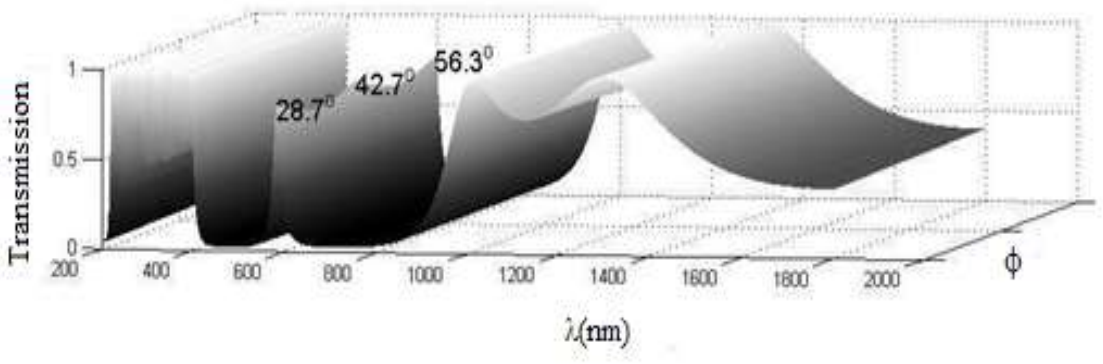

Figure 3.12: 3-D graph of transmission of 1-DPS with NLC defect for considered orientation angles.

The defect mode transmission in the PBG region is shifted towards shorter wavelengths for higher incident angles at considered director angles (ϕ) of NLC. Figure 3.13 displays the comparative defect mode transmission shifting with the incident angle at certain director angles considering TE and TM polarization modes. The study reveals that the transmission property of 1-DPS with the NLC relies on the incident angle of EMW. The obtained defect mode transmission in PBG is shifted to a shorter wavelength as the incident angle increases from 0^o up to 75^o. The transmittance of defect modes has a high value at the normal incident angle (0^o) but defect mode transmissions are moved towards lower values at a higher incident angle. By investigation of the shifting of defect mode transmissions, almost 8nm separation is found between the defect mode transmissions in PBG at different director angles of LC. The separation in the transmission is almost continuous for a lower incident angle but slightly increased for a higher incident angle. The complete comparative investigation reveals the shifting of defect transmission mode, where the transmission for TE mode is higher in comparison to the transmission for TM mode.

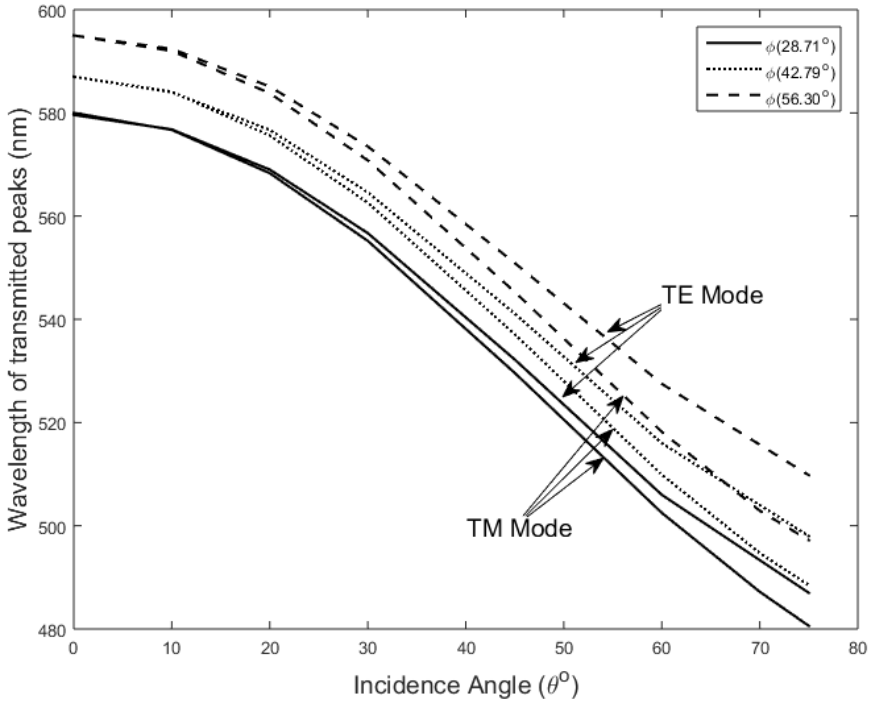

Figure 3.13: Comparative investigation of defect modes shifting with incidence angles at considered orientation angles for TE and TM polarizations.

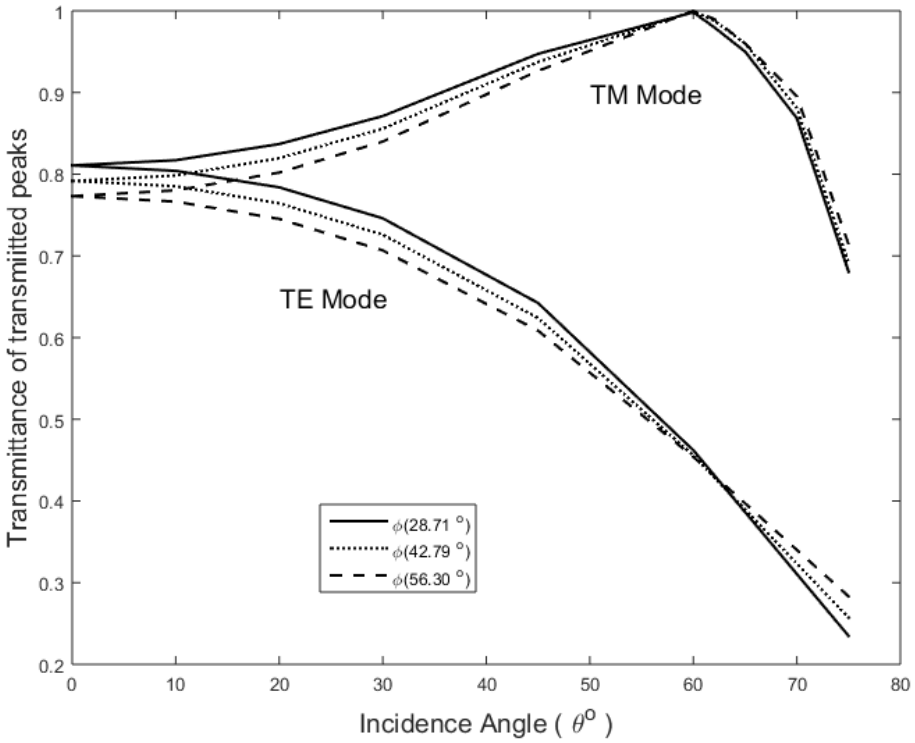

Figure 3.14: Comparative investigation of defect mode transmittances with incidence angle at considered orientation angle of LC for TE and TM polarization.

Further, we have comparatively investigated the transmittance of defect modes with incident angle considering TE and TM polarization modes with the variation of LC director angles as shown in figure 3.14. The transmittance of defect mode peaks for TE and TM modes is the same at normal incident angle, but it varies with higher incident angles for both modes. The transmittance continuously decreases with incident angle up to 63^o for TE mode while the transmittance is increased in the case of TM mode. The maximum transmittance is obtained at 63^o incident angle and then it is reduced with a higher incident angle. The effect of the director angle of the NLC on transmittance is comparatively higher in TM mode. The transmission for TM mode is followed by Brewster's angle at the boundaries of dielectric layers.

3.3.2 Tunable transmission of periodic structure with defect NLC embedded graphene layers

Graphene layers affect the optical characteristics of periodic structures. Therefore, to examine the impact of graphene layers on transmissions of periodic structures, we have considered a 1-DPS of glass and Si materials consisting of graphene and NLC defect layer as shown in figure 3.5. The thicknesses of glass, Si, graphene (G), NLC, layers are taken as 110nm, 250nm, 0.34nm, and 100nm respectively. The proposed 1-DPS with defect NLC without and with graphene layers have taken the configurations as $(Si/glass)^m/NLC/(Si/glass)^n$ and $(Si/glass)^m/G/NLC/G/(Si/glass)^n$ with m=n=3. The transmission and absorption characteristics of periodic structures; $(Si/glass)^3/NLC/(Si/glass)^3$ and $(Si/glass)^3/G/NLC/G/(Si/glass)^3$ at three different director angles are shown as figures 3.15 and 3.16, respectively. The transmission of both considered 1-DPS at 28.7^o, $42.7^{o,}$ and 56.3^o director angles are shown in figure 3.15. The transmittance of defect modes in the PBG region of periodic structure $(Si/glass)^3/NLC/(Si/glass)^3$ are found to be 90% 88% and 86%, respectively. In presence of graphene layers, the transmittance of defect modes for $(Si/glass)^3/G/NLC/G/(Si/glass)^3$ periodic structure is reduced to 48%, 46%, and 44% at considered director angles; 28.7^o, 42.7^o, and 56.3^o. The obtained defect mode transmission in the PBG region is also showed shifting with higher director angles of NLC. In the presence of graphene layers, the transmission of 1-DPS is tuned with the variation of optical parameters. Although, the defect mode transmission characteristics of 1-DPS are affected with the graphene layer, but the PBGs are not very much affected by the varying director angle.

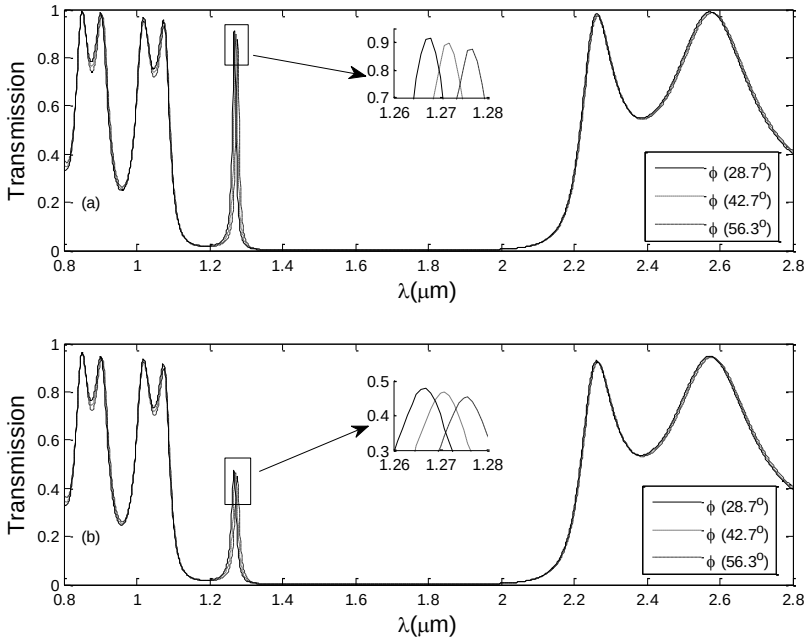

Figure 3.15: Transmission of 1-DPS at different orientation angle of LC with m=n=3; (a) $(Si/glass)^m/NLC/(Si/glass)^n$ (b) $(Si/glass)^m/G/NLC/G/(Si/glass)^n$.

The absorption characteristics of both periodic layers $(Si/glass)^3/NLC/(Si/glass)^3$ and $(Si/glass)^3/G/NLC/G/(Si/glass)^3$ are described as in figure 3.16. In the absence of graphene layers, the defect mode transmission of 1-DPS $(Si/glass)^3/NLC/(Si|glass)^3$ has no absorption at the different orientation of LC molecules as given in figure 3.16(a). But in presence of graphene layers, 1-DPS $(Si/glass)^3/G/NLC/G/(Si/glass)^3$ show absorption of defect mode peaks as shown in figure 3.16(b). The absorption value of defect mode peaks is increased from 0% to 28%, 27%, and 26% for 28.7^o, 42.7^o, and 56.3^o LC director angle, respectively. The periodic structure show absorption values of defect mode peaks due to the metallic nature of graphene layers. The absorption properties of periodic structure with defect material with NLC embedded graphene layeres are tuned with the varying gate voltage or chemical potential of the graphene layers and orientation of LC molecules.

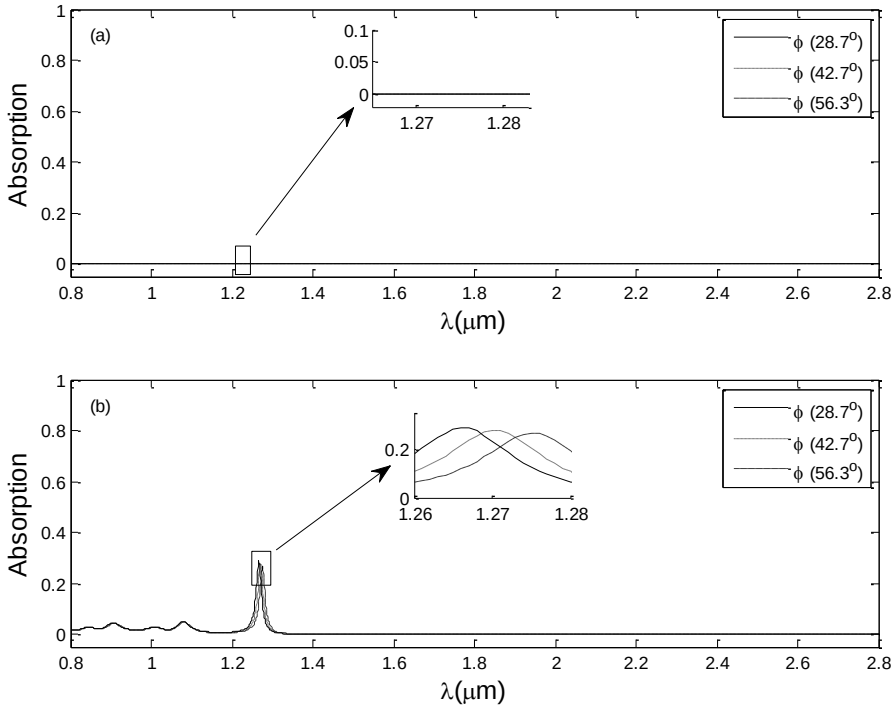

Figure 3.16: Absorption of 1-DPS at different orientation angle of LC with m=n=3; (a) $(Si/glass)^m/NLC/(Si/glass)^n$ (b) $(Si/glass)^m/G/NLC/G/(Si/glass)^n$.

The optical properties (transmission and absorption) of 1-DPS; $(Si/glass)^m/NLC/(Si/glass)^n$ and $(Si/glass)^mG/NLC/G/(Si/glass)^n$ with m=3, n=5 at considered orientation angles are presented in figures 3.17 and 3.18. The transmittance of defect mode peaks in the PBG attains the lower values; 48%, 50%, 52% from 90%, 88%, 86% for 28.7°, 42.7°, and 56.3° director angles, respectively as shown in figure 3.17(a). In presence of graphene layers, the transmission of periodic structure $(Si/glass)^3G/NLC/G/(Si/glass)^5$ has revealed in figure 3.17(b). The transmittances of defect modes peaks are found 13%, 12%, and 11% for LC director angles 28.7°, 42.7°, and 56.3°, respectively because the imaginary part of the dielectric constant of graphene is presented as discussed in the equation 3.4.

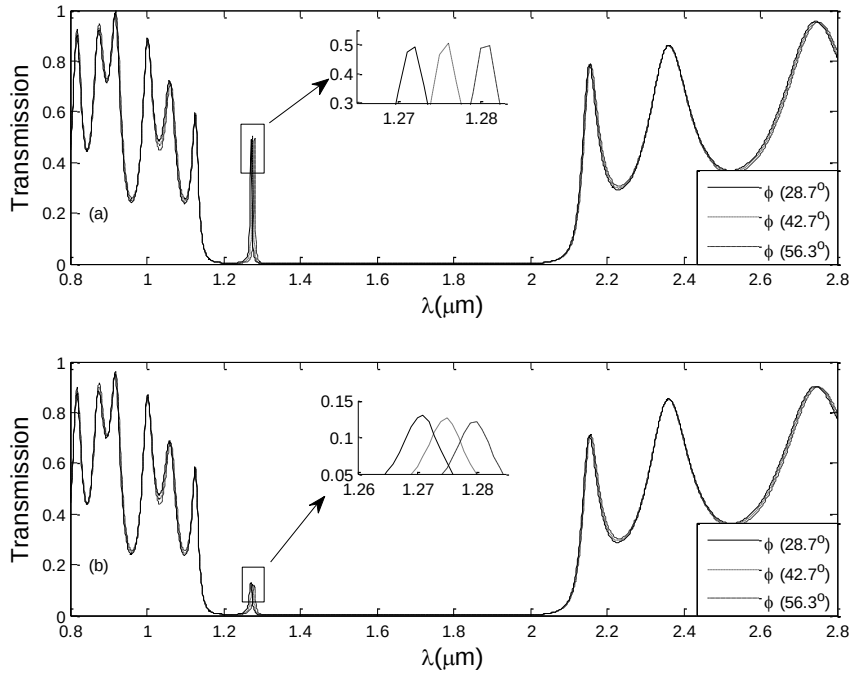

Figure 3.17: Transmission of 1-DPS at different orientation angle of LC with m=3, n=5; (a) $(Si/glass)^m/NLC/(Si/glass)^n$ (b) $(Si/glass)^m/G/NLC/G/(Si/glass)^n$.

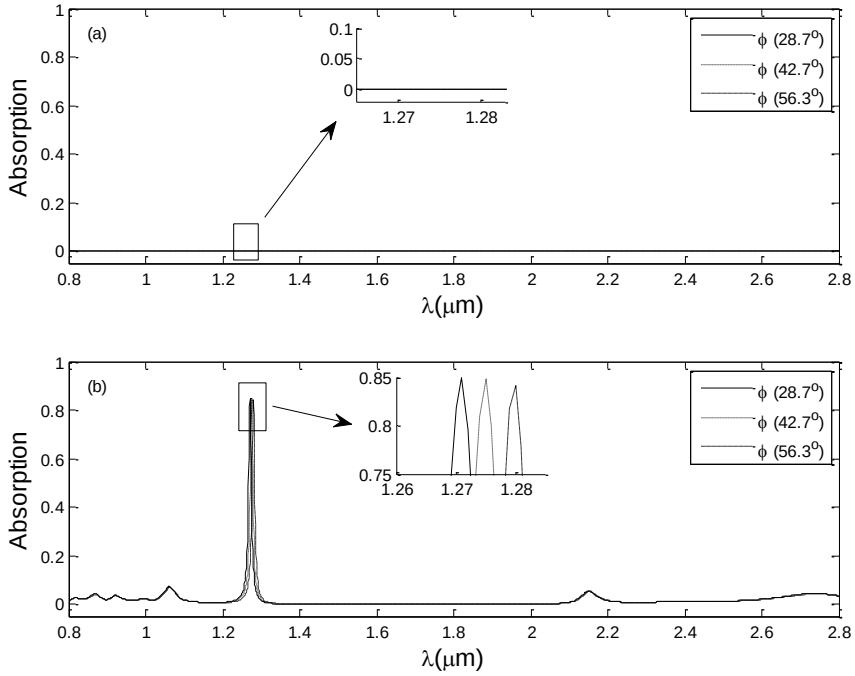

Figure 3.18: Absorption of 1-DPS at different orientation angle of LC with m=3, n=5; (a) $(Si/glass)^m/NLC/(Si/glass)^n$ (b) $(Si/glass)^m/G/NLC/G/(Si/glass)^n$.

Although the transmittances of defect modes peaks are reduced as shown in figure 3.17(a), but no absorption has occurred for any defect mode transmission in the PBG region as presented in figure 3.18(a). The absorption of defect mode is increased up to 85%, 84%, and 82% for 28.7^o, 42.7^o, and 56.3^o director angles, respectively as in figure 3.18(b). In comparison, the defect mode absorptions for 1-DPS $(Si/glass)^3/G/NLC/G/(Si/glass)^3$ are 28%, 27%, and 26% but the same 1-DPS with the different periodicity of binary layers as $(Si/glass)^3/G/NLC/G/(Si/glass)^5$ gives 85%, 84% and 82% absorption of defect modes peaks for 28.7^o,42.7^o, and 56.3^{o}orientation angles of LC, respectively. The maximum absorptions of defect modes wavelengths are obtained with 5 periodicity i.e. n=5 instead of 3 periodicity i.e. n=3 as defect NLC with graphene layers embedded 1-DPS.

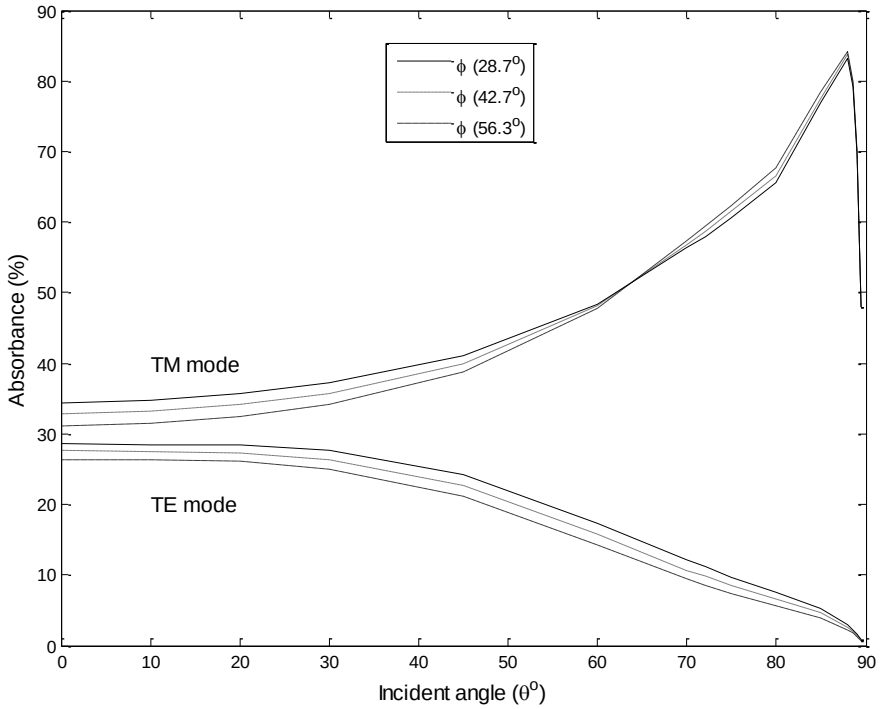

Figure 3.19: Variation of defect mode absorptions with the incident angle for $(Si/glass)^3/G/NLC/G/(Si/glass)^3$considering TE and TM polarization modes.

The absorption defect mode peak behavior in the transmission of 1-DPS $(Si/glass)^3/G/NLC/G/(Si/glass)^3$ with incident angle are also investigated at considered orientation angles for TE and TM polarizations as shown in figure 3.19. The absorption values of defect mode peaks for TE polarization are decreased for increasing the incident angle of EMW. But the absorption of defect mode peaks for

TM polarization first increases up to 88^o incident angle and then decreases sharply. A detailed comparative analysis suggests that the absorptions of defect mode peaks for TM polarization are more efficient than the absorptions of defect peaks TE polarization at chemical potential $(\mu) = 0.4\text{eV}$ as shown in figure 3.19.

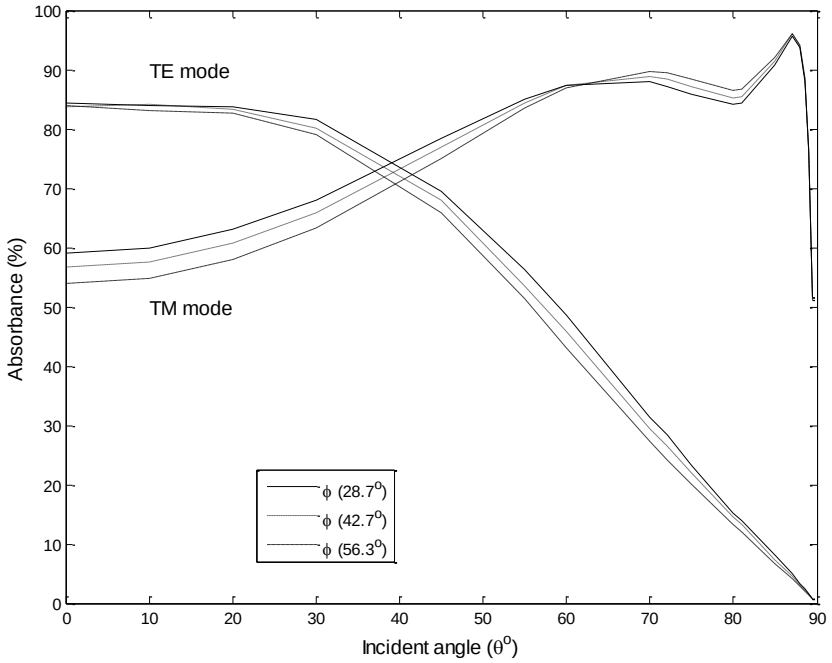

Figure 3.20: Variation of defect mode absorptions with the incident angle for $(Si/glass)^3/G/NLC/G/(Si/glass)^5$ considering TE and TM polarization modes.

Likewise, we have explained the absorption characteristics of defect mode peaks for $(Si/glass)^3/G/NLC/G/(Si/glass)^5$ multilayers for TE and TM polarizations at considered director angles as exposed in figure 3.20. The absorption defect mode peaks decreases with increasing incident angles for TE polarization, while the absorption defect peaks for TM polarization increase up to 63^o incident angle then decreases up to 80^o, and further increase up to 88^o and abruptly decrease for the higher incident angle. For the normal incident angle, the defect mode peaks have a high absorption value for TE polarization, but the absorption defect peaks for TM polarization fluctuate with increasing the incident angle.

3.4 Conclusion

In this chapter, a nonlinear differential equation defining the orientation behavior for of LC director with the EMW interaction was solved, and the optics of the LC layer

based on the molecular orientation was described. At the Freedericksz transition, threshold intensity of EMW, a sharp switching of NLC (PAA) molecules has occurred inside the LC layer. Due to optically induced transitions, a first-order transition of molecules has occurred and hence hysteresis loops are appeared in LC cell. Owing to molecular orientation/reorientation, the optical properties transmission of the 1-DPS of glass and Si materials with the defect layer of PAA NLC were studied and compared. The transmission of 1-DPS of the form $(glass/Si)^2/NLC/(glass/Si)^2$ shown sharp defect modes in the PBG region of transmission spectra. The transmissions of wavelengths in the PBG region were revealed that the molecular orientation of NLC controls the defect transmission peaks. The different orientations/reorientations of the molecules inside the LC layer are accountable for optical switching behavior. We have also explained the defect mode transmission and their shifting behavior with the incident angles for all three director angles. The orientation and re-orientation of LC molecules may be used to attain optical switching of 1-DPS with a defect of NLC and such periodic structures with the NLC layer may be used in various photonic and electronic devices, e.g. bi-stable devices, switches, optical filters, feedback lasers, and so on.

In the case of graphene-based structure in the form of $(Si/glass)^m/G/NLC/G/(Si/glass)^n$ multilayer structure with m, n periodicity of binary layers, the reduced transmission of defect modes shown at 28.7^o, 42.7^o, and 56.3^o director angles. The theoretically designed 1-DPS of the form $(Si/glass)^3/G/NLC/G/(Si/glass)^5$ has exhibited the high absorptions for 28.7^o, 42.7^o, 56.3^o director angles of NLC. The improved absorptions defect mode peaks for TE polarization were obtained for the periodic structure of form $(Si/glass)^3/G/NLC/G/(Si/glass)^5$ due to metallic nature of graphene layers. Such absorption of the periodic structure of form (Si/glass)3/G/NLC/G/(Si/glass)5 may be assisted to design sensors and detectors based optical devices for 1.26 μm, 1.273μm, and 1.278μm wavelengths corresponding to 28.7^o, 42.7^o, 56.3^o director angles. The absorption behavior of 1-DPS of the form $(Si/glass)^3/G/NLC/G/(Si/glass)^5$ was found to be more enhanced for TE polarization in contrast to TM polarization at a normal incident angle.

References

[1] T. Riste and L. Dobrzynski, Nematic-Isotropic Transition: Thermal Hysteresis and Magnetic Field Effects, *Phys. Rev. Letts.*, 74, 2737-2739, 1995.

[2] M. J. Bradshaw, E. P. Raynes, J. D. Bunning, T. E. Faber, The Frank constants of some nematic liquid crystals, *Journal de Physique*, 46, 513-1520, 1985.

[3] S. Chandrasekhar, N. Madhusudana, Orientational order in p-azoxyanisole, p-azoxyphenetole and their mixtures in the nematic phase. *Journal de Physique Colloques*, 30, C4-24-C4-27, 1969.

[4] N. K. Sanyal, S. N. Tiwari and M. R. Choudhury, Liquid Crystalline Behaviour of Paraazoxyanisole— A Theoretical Study of the Role of Intermolecular Interactions, *Mol. Cryst. Liq. Cryst.*, 140, 79-193, 1986.

[5] Z. Iqbal, F. J. Owens, C. W. Christoe, Light scattering study near the crystal to nematic transition in para-azoxyanisole (PAA), *Chem. Phys. Letts.*, 67, 157-159, 1979.

[6] M. J. Stephen, and J. P. Straley, Physics of liquid crystals, *Rev. Mod. Phys.*, 46, 617-704, 1974.

[7] K. Geim, K. S. Novoselov, The rise of graphene *Nat. Mat.*, 6, 183-191, 2007.

[8] O. L. Berman, R. Y. Kezerashvili, Graphene-based one-dimensional photonic crystal *J. Phys: Condens Matter*, 24 015305-7, 2012.

[9] F. Bonaccorso, Z. Sun, T. Hasan and A. C. Ferrari, Graphene photonics and optoelectronics, *Nat. Photonics*, 4, 611-15, 2010.

[10] Q. Bao, and K. P. Loh, Graphene Photonics, Plasmonics, and Broadband Optoelectronic Devices, *ACS Nano*, 6, 3677-3694, 2012.

[11] Y. Zhang, Y.-W. Tan, H. L. Stormer, and P. Kim, Experimental observation of quantum Hall effect and Berry's phase in graphene, *Nature,* 438, 201-204, 2005.

[12] X. Du, I. Skachko, F. Duerr, A. Luican, E. Andrei, Fractional quantum Hall effeect and insulatin of Dirac electrons in graphene, *Nature*, 462, 192-195, 2009.

[13] S. D. Sharma, E. H. Hwang, and W. K. Tse, Many-body interaction effects in doped and undoped graphene: Fermi liquid versus non-Fermi liquid, *Phys. Rev. B*, **75** 121406(R), 2007.

[14] J. Fu, W. Chen, B. Lv, Tunable defect mode realized by graphene-based photonic crystal, *Phys. Lett. A*, 380, 1793-1798, 2016.

[15] F. U. Y. Al-sheqefi, W. Belhadj, Photonic band characteristics of one-dimensional graphene-dielectric periodic structures, *Superlattice and Microstructures*, 88, 127-138, *2015.*

[16] J. Gosciniak, D. T. H. Tan, Theoretical investigation of graphene-based photonic modulators *Sci. Rep.* 3, 2013. doi:10.1038/srep01897

[17] Y. Zhang, J. P. Small, M. E. S. Amori and P. Kim, Electric field Modulation of Galvanomagnetic Properties of Mesoscopic Graphite *Phys. Rev. Lett.,* 94 176803, 2005.

[18] X. Wang, L. Zhi, K. Mullen, Transparent, Conductive graphene electrodes for Dye-sensitized solar cells *Nano Lett.,* 8 323-327, 2008.

[19] S. Bae, H. Kim, Y. Lee, X. Xu, J. Park, Y. Zheng, J. Balakrishnan, T. Lei, H. R. Kim, Y. I. Song, Y. J. Kim, K. S. Kim, B. Ozyilmaz, J. H. Ahn, B. H. Hong, S. Lijima, Roll-to-roll production of 30-inch graphene films for transparent electrodes *Nat. Nanotechnol.,* 5 574-578, 2010.

[20] F. Bonaccorso, A. Lombardo, T. Hasan, Z. Sun, L. Colombo, and A. C. Ferrari, A. C, Production and processing of graphene and 2d crystals, *Materails Today,* 25, 564-589, 2012.

[21] P. Avouris, C. Dimitrakopoulos, Graphene:synthesis and applications, *Materials Today*, 15, 86-97, 2012.

[22] S. Chandrasekhar, *Liquid Crystals*, Cambridge Univ. Press, New York, 1992.

[23] I. C. Khoo, *Liquid Crystals*, Wiley Interscience, New Jersey, 2007.

[24] J. D. Joannopoulos, R. D. Meade, and J.N. Winn, *Photonic Crystals: Molding the Flow of Electromagnetic wave*, Princeton Univ. Press, Princeton, 1995.

[25] E. Yablonovitch, Inhibited Spontaneous Emission in Solid-State Physics and Electronics, *Phys. Rev. Lett.,* 58**,** 2059-2062, 1987.

[26] A. E. Miroshnichenko, I. Pinkevych, and Y.S. Kivshar, Tunable all-optical switching in periodic structures with liquid crystal defects, *Opt. Express*, 14, 2839-2844, 2006.

[27] I. A. Sukhoivanov, I. V. Guryev, *Physics and Practical Modeling*, Springer, Berlin, 2009.

[28] P. Russell, Photonic crystal fibers, *Science*, 299, 358-362, 2003.

[29] Y. Akahane, T. Asano, B. Shik, S. Noda, High –Q photonic nanocavity in a two-dimensional crystal, *Nature*, 425, 944-947, 2003.

[30] L. M. Blinov, *Structure and Properties of Liquid Crystals*, Springer, New York, 2011.

[31] A. C. Polycarpou, M. A. Christou, and N. C. Papanicolaou, A Mode-Matching Approach to Electromagnetic Wave Propagation in Nematic Liquid Crystals *IEEE Trans on Micro. Theo. and Tech.*, 60, 2950-2958, 2012.

[32] B. Ya. Zel'dovich, N. V. Tabiryan, and Yu. S. Chilingaryan, Freedericksz transition induced by electromagnetic wave fields *Zh.Eksp.Teor.Fiz.* **81** 72-83, 1981.

[33] H. L. Ong, Optically induced Freedericksz transition and bistability in a nematic liquid crystal *Phys. Rev. A*, 28**,** 2393-2407, 1983.

[34] K. Busch and S. John, Liquid-Crystal Photonic-Band-Gap Materials: The Tunable Electromagnetic Vacuum, *Phys. Rev. Lett.*, 83, 967-970, 1999.

[35] K. Yoshino, Y. Shimoda, Y. Kawagishi, K. Nakayama, and M. Ozaki, Temperature tuning of the stop band in transmission spectra of liquid crystal infiltrated synthetic opal as tunable photonic crystal, *Appl. Phys. Lett.*,75, 932-934 (1999).

[36] S. W. Leonard, J. P. Mondia, H. M van Driel, O Toader, S. John, K. Busch, A. Birner, U. Gosele, and V. Lehmann, Tunable two-dimensional photonic crystals using liquid crystal infiltration, *Phys. Rev. B*, 61, R2389-R2392, 2003.

[37] Ch. Schuller, F. Klopf, J. P. Reithmaier, M.Kamp, and A. Forchel, Tunable photonic crystals fabricated in III-V semiconductor slab waveguides using infiltrated liquid crystals, *Appl. Phys. Lett.*, 82, 2767-2769, 2003.

[38] D. Kang, J.E. Maclennan, N. A. Clerk, A. A. Zakhidov, and R. H. Baughman, Electro-optic Behavior of Liquid-Crystal-Filled Silica Opal Photonic Crystals: Effect of Liquid-Crystal Alignment, *Phys. Rev. Lett.*, 86**,** 4052-4055, 2001.

[39] E. Graubard, J. S.King, S.Jain, C. J.Summers, Y.Zhang Williams, and I. C Khoo, Electric-field tuning of the Bragg peak in large-pore TiO2 inverse shell opals, *Phys. Rev. B*, 72 ,233105-4, 2005.

[40] V. G. Arkhipkin, V. A. Gunyakov, S. A. Myslivsts, V. Ya. Zyryanov, and V. F. Shabanov, Angular tuning of defect modes spectrum in the one-dimensional photonic crystal with liquid-crystal layer, *Eur. Phys. J. E*, 24, 297-302, 2007.

[41] Y. M. Strelniker, D. Stroud, and A. O. Voznesenkaya, Control of extraordinary light transmission through perforated metal films using liquid crystals, *Eur. Phys. J. B*, 52, 1-7, 2006.

[42] S. F. Mingaleev, M. Schillinger, D. Hermann, and K. Busch, Tunable photonic crystal circuits: concepts and designs based on single-pore infiltration, *Opt. Lett.*, 29, 2858-2860, 2004.

[43] E. P. Kosmidou, E. E Kriezis, and T. D Tsiboukis, Analysis of Tunable Photonic Crystal Devices Comprising Liquid Crystal Materials as Defects, *IEEE J. Quantum Electron*, 41 657-665, 2005.

[44] M.S. Mohamed, M. F. O.Hameed, M. M. El-Okr, Salah S. A. Obayya, Characterization of One Dimensional Liquid Crystal Photonic Crystal Structure, Optik**,** 127, 8774-8781, 2016.

[45] S. R. Entezar, A. Madani, M. K. Habil, A. Namdar, and H. Tajalli, Temperature dependent transmission and optical bistability in a 1D photonic crystal with a liquid crystal defect layer, *J. Mod .Opt*., 60, 1883-1891, 2013.

[46] R. Ozaki, H. Miyoshi, M. Ozaki, K. Yoshino, Tunable Defect Mode in One-Dimensional Photonic Crystal with Liquid Crystal Defect Layer, *Mol. Cryst. Liq. Cryst*., 433**,** 247-257, 2005.

[47] K. S. Novoselov, A. K. Geim, S. V. Morozov, D. Jiang, Y. Zhang, S. V. Dubonos, I. V. Grigorieva, and A. A. Firsov, Electric field effect in Atomically thin Carbon Films *Science* **306** 666-669, 2004.

[48] L. A. Falkovsky, Optical properties of graphene *J. Phys. Conf. Ser.***129** 012004-7 2008.

[49] A. Khaleque, H. T. Hattori, Absorption enhancement in graphene photonic crystal structures, *Appl. Opt.,* 55, 2936-2942, 2016.

[50] T. Liu, N. H. Liu, J. Li. X. J. Li, and J. H. Huang, Enhanced absorption of graphene with one-dimensional photonic crystal, *Appl. Phys. Lett.* **101** 052104, 2012.

[51] W. Zhao, K. Shi, and Z. Lu, Greatly enhanced ultrabroadband light absorption by monolayer graphene, *Opt. Lett.,* 38, 4352-4345, 2013.

[52] V. M. Pereira, R. M. Ribeiro, N. M. R. Peres, and A. C. Neto, Optical properties of strained graphene, *Europhys. Lett.,* 92, 67001, 2010.

[53] T. J. Echtermeyer, L. Britnell, P. K. Jasnos, A. Lombardo, R. V. Gorbachev, A. N. Grigorenko, A. K. Geim, A. C. Ferrari, and K. S. Novoselov, Strong plasmonic enhancement of photovoltage in graphene *Nat. Commun.,* 2, 458(1-5), 2011.

[54] A. Ferreira, N. M. R. Peres, R. M. Ribeiro, and T. Stauber, Graphene based photodetector with two cavities *Phys. Rev. B,* 85, 115438(1-9), 2012.

[55] Q. Ye, J. Wang, Z. Liu, Z. C. Deng, X. T. Kong, F. Xing, X. D. Chen, W. Y. Zhou, C. P. Zheng, and J. G. Tian, Polarization-dependent optical absorption of graphene under total internal reflection, *Appl. Phys. Lett.,* 102, 021912(1-4), 2013.

[56] S. Thongrattanasiri, F. H. Koppens and F. J. G. de Abajo, Complete optical absorption in periodically patterned graphene, *Phys. Rev. Lett.,* 108**,** 047401(1-5), 2012.

[57] G. P. Qiu, W. Qiu, Z. Lin, H. Chen, Y. Tang, J.-X. Wang, Q. Kan Q and J.-Q. Pan, Investigation of the Band Structure of Graphene-Based Plasmonic Photonic Crystals, *Nanomaterials,* 6, 166, (1-11), 2016.

[58] L. Qui and C. Liu, Complex band structures of 1D anisotropic graphene photonic crystal, *Photonics Research,* 5**,** 543-551, 2017.

[59] H. Mahmoodzadeh and B. Rezaei, Tunable Bragg defect mode in one-dimensional photonic crystal containing a graphene-embedded defect layer, *Appl. Opt.*, 57**,** 2172-2176, 2018.

[60] O. L. Berman, V. S. Boyko, R. Y. Kezerashvili, A. A. Kolesnikov, Y. E. Lozovik, On transmittance and localization of the electromagnetic wave in two-dimensional graphene-based photonic crystals *Phys. Lett. A,* 2018. https://doi.org/j.physleta.2018.05.023.

[61] P. Yeh, *Optical Waves in Layered Media*, John Wiley & Sons, New York, 1988.

[62] M. J. Frisch, G. W. Trucks, H. B. Schlegel, G. E. Scuseria, M. A. Robb, J. R. Cheeseman, G. Scalmani, V. Barone, G. A. Petersson, H. Nakatsuji, X. Li, M. Caricato, A. Marenich, J. Bloino, B. G. Janesko, R. Gomperts, B. Mennucci, H. P. Hratchian, J. V. Ortiz, A. F. Izmaylov, J. L. Sonnenberg, D. Williams-Young, F. Ding, F. Lipparini, F. Egidi, J. Goings, B. Peng, A. Petrone, T. Henderson, D. Ranasinghe, V. G. Zakrzewski, J. Gao, N. Rega, G. Zheng, W. Liang, M. Hada, M. Ehara, K. Toyota, R. Fukuda, J. Hasegawa, M. Ishida, T. Nakajima, Y. Honda, O. Kitao, H. Nakai, T. Vreven, K. Throssell, J. A. Montgomery, Jr., J. E. Peralta, F. Ogliaro, M. Bearpark, J. J. Heyd, E. Brothers, K. N. Kudin, V. N. Staroverov, T. Keith, R. Kobayashi, J. Normand, K. Raghavachari, A. Rendell, J. C. Burant, S. S. Iyengar, J. Tomasi, M. Cossi, J. M. Millam, M. Klene, C. Adamo, R. Cammi, J. W. Ochterski, R. L. Martin, K. Morokuma, O. Farkas, J. B. Foresman, and D. J. Fox, Gaussian, Inc., Wallingford CT, 2009.

[63] T. C. King, C. J. Wu, Properties of defect modes in one-dimensional symmetric defective photonic crystals, *Physica E,* 69, 39-46, 2015.

CHAPTER 4

Tunable transmission characteristics of periodic structure designed with SiO_2 and TiO_2 materials with anisotropic defect layers as liquid crystal (LC) and $LiNbO_3$ for optical switching application

CHAPTER 4

Tunable transmission characteristics of periodic structure designed with SiO_2 and TiO_2 materials with anisotropic defect layers as liquid crystal (LC) and $LiNbO_3$ for optical switching application

4.1 Introduction

Anisotropic materials have direction dependent properties and the optical characteristics tunes with temperature, electric field, voltage, and incident angle. In nature, various anisotropic materials exist but various anisotropic also can be prepared in the laboratories. In reference to control the optical responses of anisotropic materials through voltage and temperature, we have considered E7 LC and $LiNbO_3$ to investigate the tunable characteristics of one-dimensional periodic structures (1-DPS). In this chapter, the transmissions of 1-DPS consisting of SiO_2, TiO_2 materials with E7 LC, $LiNbO_3$ uniaxial materials as defects are investigated with changing internal and external parameters.

The theoretical transmission analysis of designed 1-DPS has been studied with the varying voltage across the crystal, temperature, and incident angle of EMW. The optical characteristics of the concerned 1-DPS are explained based on 4×4 matrix method. The designed 1-DPS with the defect E7 LC and $LiNbO_3$ give rise to tunable defect modes in the PBG region of resultant transmission spectra. The obtained defect modes show blue shifting with changing voltage, temperature, and incident angle considering TE and TM polarizations. Also, the transmissions of defect mode and terminal of considered wavelength range are examined with incident angle as well as temperature. The studied transmission of 1-DPS $(SiO_2/TiO_2)^5$/LC/LNO/LC/$(TiO_2/SiO_2)^5$ shows tunable nature due to anisotropic materials E7 LC, $LiNbO_3$ as defect layers, and such periodic structure with the defect of nonlinear materials may assist in designing of optical switching devices.

4.1.1 E7 liquid crystal (E7 LC)

The optical properties of liquid crystals (LCs) are changed with the orientation of molecules, applied field, and temperature, and hence the transmission through the PCs can be controlled with LC [1,2]. Besides the pure LCs, some LCs are also prepared by mixing two or more LCs; and such LC mixture have enhanced optical responses in comparison to parent LCs. The E7 LC is combination of 5CB ($C_{18}H_{19}N$), 8OCB ($C_{21}H_{25}NO$), 7CB ($C_{20}H_{23}N$), and 5CT ($C_{24}H_{23}N$) LCs [3]. The extraordinary and ordinary refractive indices (n_e, n_o) of the E7 LC depend on the temperature which is given as [4];

$$n_e(T) = A - BT + \frac{2(\Delta n)_o}{3}\left(1 - \frac{T}{T_C}\right)^{\beta} \tag{4.1}$$

$$n_o(T) = A - BT - \frac{(\Delta n)_o}{3}\left(1 - \frac{T}{T_C}\right)^{\beta} \tag{4.2}$$

where $A, B, (\Delta n)_0, \beta =$ temperature dependent LC parameter, T_C = clearing temperature or phase transition temperature of LCs. The extraordinary, ordinary and birefringence of E7 can be studied by using equations 4.1, 4.2.

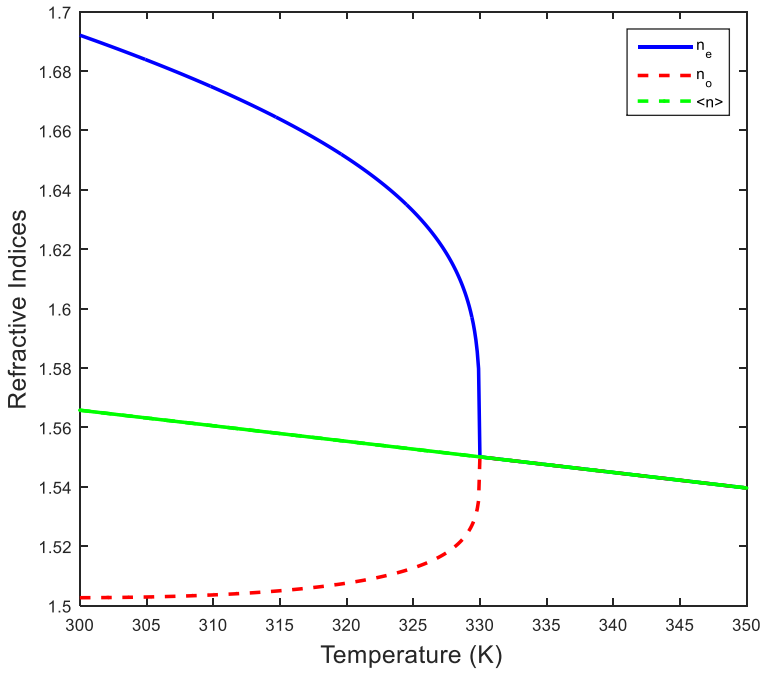

Figure 4.1: Variation of refractive indices (n_e, n_o, <n>) of E7 LC with temperature (K).

The constant parameters A, B, β, $(\Delta n)_o$, T_C for E7 LC are $1.7230, 5.24\times10^{-4}, 0.3485, 0.2542$ and 330K [4]. The average refractive index of such E7 LC is given as;

$$\langle n \rangle = \frac{2n_o + n_e}{3} \tag{4.3}$$

The deviations of refractive indices of E7 LC with the variation of temperature are shown in figure 4.1. The minimum and maximum magnitudes of ordinary, extraordinary refractive indices of E7 LC are1.55, 1.692 for 300K temperature and 1.50, 1.55 for 350K temperature, respectively. The both refractive indices of E7 LC mixture have same value 1.55 at the 330K temperature (i.e. phase transition). At the phase transition temperature, the E7 LC changes its phase and converts into the isotropic phase.

4.1.2 Lithium niobate ($LiNbO_3$)

The electro-optical materials tune their optical properties with the variation of applied voltage and incident angle of electromagnetic waves. As example, lithium niobate ($LiNbO_3$) change the optical properties with the variation in voltage and incident angle due to modification in index ellipsoid of the material. $LiNbO_3$ shows linear electro-optic effect and tunable refractive indices which are very useful to tune the optical characteristics of photonic crystals. The extraordinary (n_e) as well as ordinary (n_o) indices of the $LiNbO_3$ or LNO are formulated as [5];

$$n_o(V) = n_o - \frac{1}{2} r_{13} n_o^{\,3} \left(\frac{V}{d_4} \right) \tag{4.4}$$

$$n_e(V) = n_e(\theta) - \frac{1}{2} r_{33} n_e(\theta)^3 \left(\frac{V}{d_4} \right) \tag{4.5}$$

where r_{13}, r_{33} = electro-optical coefficients of $LiNbO_3$ crystals. The extraordinary index of LNO depends upon voltage (V) and incident angle (θ); while the ordinary refractive index of LNO depends upon the voltage only. The extraordinary refractive index can be studied by using equations 4.4, 4.5.

$$n_e(\theta) = \frac{n_e n_o}{\sqrt{n_o^{\,2} \cos^2\theta + n_e^{\,2} \sin^2\theta}} \tag{4.6}$$

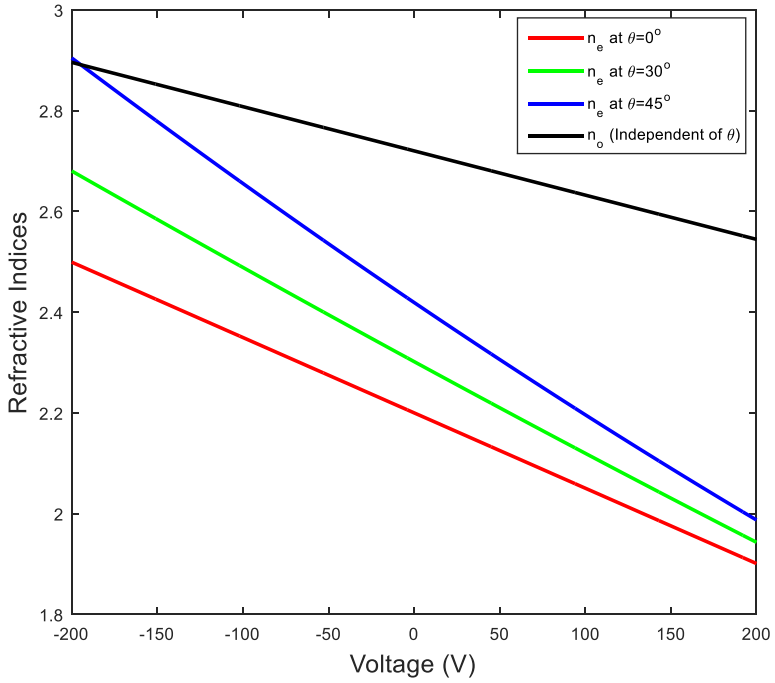

Figure 4.2: Deviation of refractive indices (n_e, n_o) of $LiNbO_3$ with voltage (-200V to 200V) at 0^o, 30^o, 45^o incident angles.

The dielectricor refractive indices (n_e, n_o) and electro-optical parameters (r_{13}, r_{33}) of $LiNbO_3$ in the absence of electric field are 2.20, and 2.70 and are $9.6pmV^{-1}$, $30.9pmV^{-1}$ respectively [6,7]. The behavior of refractive indices of electro-optical material $LiNbO_3$ with voltage range of -200V to +200V at 0^o, 30^o, 45^o incident angles are revealed in figure 4.2. This extraordinary index of $LiNbO_3$ increases with increases the incident angle, but it is linearly decreased with applied voltage. The extraordinary refractive index of $LiNbO_3$ is found 1.902 for -200V and 2.499 for +200V at 0^o incident angle. The minimum and maximum extraordinary index (n_e) values for -200V and +2000V are found 1.943 and 2.678 respectively at 30^o incident angle. Similarly, extraordinary index (n_e) values for -200V and +2000V are 1.987 and 2.904 at 45^o incidence angle. The ordinary refractive index for applied voltage is independent of the incidence angles and the minimum and maximum values of the ordinary refractive index for voltages from -200 V to +200 V are 2.544 and 2.896.

4.1.3 Photonic crystals (PCs) with anisotropic defect layer

Photonic crystal (PC) is a unique optical multilayered system which has periodicd ielectriclayers assisting periodic variation of dielectric functions in dissimilar

directions. The PCs have three types depending on the variation of refractive index: one-dimensional (1-D), two-dimensional (2-D), and three-dimensional (3-D) photonic crystal. The transmission characteristics of the multilayered media are dependent on the interaction of EMW with the materials and the periodicity of binary layers. PCs are able to regulate the transmission of EMWs due to periodicity of dielectric layers and also exhibited photonic band gap (PBG) in the transmission bands. The PBGs are distinctive range of definite frequencies, where it prohibits the transmission of EMWs in the PCs, and such unusual characteristics of the PCs are exploited in various photonic applications [8-18]. If a defect layer of dielectric materials is inserted in the PCs, then a sharp defect modes or localized state of transmissions in the PBG is exhibited [19-21]. The optical characteristic of PCs can be tunable with the variation of temperature, voltage, electric field, and so on; if the defect layer is a liquid crystal (LC). Therefore, such PCs are applicable as active material in photonic devices, optoelectronic and microwave applications [22-31]. A large quantity of research has been published on the tunability of PCs with exterior parameters e.g. electric field, magnetic field, temperature, and so on [32-34].The blue and red shifting of defect mode in transmission could be obtained by positive as well as negative voltages on the electro-optical defect material in PCs. The shifting of transmitted defect modes is dependent on the incident angle concerning TE and TM polarization states. As application, tunable filter based on 1-DPC with anisotropic defect layers is investigated by 4×4 matrix method [35,36].

The refractive indices of uniaxially crystalline material like $LiNbO_3$ has dependent on voltage and incident angle, and the tunability of the optical properties could be gained by embedding such anisotropic materials into PCs [5,7]. The LC and $LiNbO_3$ both are anisotropic materials and these can be used in the PCs to obtain the tunable transmittance. Generally, LC is intermediate phase between pure liquid and perfect solid, which have both characteristics of liquid and crystalline. The organic materials, LCs have three types: lyotropic, thermotropic and metallotropics. The dielectric properties of thermotropic LC have dependent of the temperature and external field; and normally such LC shows three phases: nematic, cholesteric, and smectic. A very common phase is nematic phase which is generally appeared in all LCs. The anisotropic nature of LC is changed into isotropic phase at phase transition, called clearing temperature (T_C), and thereby, LCs are useful in nonlinear optics applications

[1, 37]. The tunable transmission could be obtained by coating the inverse opal with LCs, which was proposed by Busch et al. [38] and letter it was confirmed experimentally by Yoshino et al. [39]. With the controlled optical properties of LCs through external fields, the transmission of PCs with LCs could be modulated by temperature and electric field. In the experimental point of view, the filling the pores in PCs with LCs is another technique to obtain tunable transmissions [40-44]. LCs are anisotropic organic materials have applications in tunable photonic devices due to having nonliner optical responses including all-optical switching to controlled transmission devices. The transmissions of 1-DPS with defect layer of LC were investigated with varying molecular orientation and temperature by Mohamed et al. [45]. By investigating the optical transmission of 1DPS with LC defect layer, Ozaki et al. [46] established that the tunability of PCs could be gained by controlling the LCs parameters [47-49] and also proposed that the bistability was dependent on temperature, and hence the optical transmission of the PCs are tunable with temperature. The organic material LC has anisotropic nature and the dielectric characteristics are dependent of the orientation angle of the molecules.

The hybrid Tamm-microcavity states in 1-DPS were investigated by Pankin et al. [60] and the authors suggested the tunable hybrid modes with variation of the electric field and temperature. The dielectric constant $(\varepsilon_{\parallel}, \varepsilon_{\perp})$ and anisotropy $(\varepsilon_a = \varepsilon_{\parallel} - \varepsilon_{\perp})$ dependent dielectric tensor $(\tilde{\varepsilon})$ has matrix form as [49, 51];

$$\tilde{\varepsilon} = \begin{pmatrix} \varepsilon_{\perp} + \varepsilon_a \sin^2\phi & 0 & \varepsilon_a \sin\phi\cos\phi \\ 0 & \varepsilon_{\perp} & 0 \\ \varepsilon_a \sin\phi\cos\phi & 0 & \varepsilon_{\perp} + \varepsilon_a \cos^2\phi \end{pmatrix} \qquad (4.7)$$

The dielectric tensor of LC has 3x3 matrix form including extraordinary and ordinary dielectric constant and anisotropy of LCs and such matrix can be diagonalized at 0^o and 90^o orientation angles and then the transfer matrix method (TMM) is applied to investigate the optical characteristics of the PCs [52].

In the chapter, the refractive indices of E7 LC and $LiNbO_3$ are studied firstly with the variation of temperatures, and voltages. The transmission of 1-DPS of dielectric layer with defect of the E7 LC and LNO material; $(SiO_2/TiO_2)^5$/LC/LNO/LC/$(TiO_2/SiO_2)^5$ are studied secondly with the variation of temperature, voltage and two orientation

angles of LC molecules for TE and TM modes by using 4×4 matrix method. We have also investigated the defect optical transmission of 1-DPC versus the terminal wavelength for TE and TM modes.

4.2 Theory and methodology

The 1-DPS of SiO_2 and TiO_2 materials with E7 LC and $LiNbO_3$ or LNO layers are considered to study the optical properties in this work. The defect layer of LNO material is sandwiched between two E7 LC layers as LC/LNO/LCin the periodic structure; $(SiO_2/TiO_2)^5$/LC/LNO/LC/$(TiO_2/SiO_2)^5$ as shown in figure 4.3. The propagation of EMW through 1-DPS is considered in z-direction and periodic structure is considered in x-y plane.

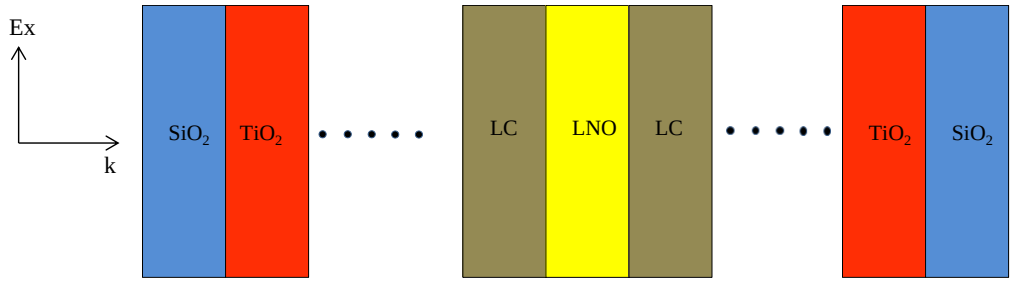

Figure 4.3: Schamatic design 1-DPS of SiO_2, TiO_2 materials with defect layers of LC and $LiNbO_3$; $(SiO_2/TiO_2)^5$/LC/LNO/LC/$(TiO_2/SiO_2)^5$.

The considered periodic structure with a defect LNO material embedded with LC has taken n_1, n_2 the refractive indices of SiO_2, TiO_2 materials with thicknesses d_1, d_2 respectively; and d_3, d_4 the thicknesses of $LiNbO_3$ and LC respectively while the refractive indices of LNO and E7 LC are discussed earlier in this chapter. The optical characteristic of periodic structure $(SiO_2|TiO_2)^5|LC|LNO|LC|(TiO_2|SiO_2)^5$ are calculated by 4×4 matrix method. In view of EMW interaction with periodic materials concerning electric and magnetic (E, H), fields, the optical transmissions of 1-DPS are obtained at incident angle of EMW. To study the optical properties, the 4x4 matrix for periodic structure are formulated using Maxwell's equations. In Maxwell's equations, we have;

$$\nabla \times E = i\omega\mu_o H \tag{4.8}$$

$$\nabla \times H = -i\omega\varepsilon_o \varepsilon E \tag{4.9}$$

The components of the electric and the magnetic fields are calculated by equations 4.8 and 4.9 which gives;

$$\frac{\partial \psi}{\partial z} = ik_o \Delta \psi \tag{4.10}$$

where $k_o = \omega / c$, $\psi = \left(\sqrt{\varepsilon_o} E_x, \sqrt{\mu_o} H_y, \sqrt{\varepsilon_o} E_y, \sqrt{\mu_o} H_x\right)$, and Δ is the coefficient matrix dependent on the optical parameters.

If the relative permittivity of uniaxial anisotropic material $LiNbO_3$ is given as;

$$\varepsilon = \varepsilon_o \begin{bmatrix} n_o^2 & 0 & 0 \\ 0 & n_o^2 & 0 \\ 0 & 0 & n_e^2 \end{bmatrix} \tag{4.11}$$

By solving equation 4.10 by using equation 4.11, differential Δ matrix is given as;

$$\Delta = \begin{bmatrix} 0 & 1 - n_0^2 \sin^2\theta / \varepsilon_z & 0 & 0 \\ \varepsilon_x & 0 & 0 & 0 \\ 0 & 0 & 0 & 1 \\ 0 & 0 & \varepsilon_y - n_0^2 \sin^2\theta & 0 \end{bmatrix} \tag{4.12}$$

where n_0 = refractive index of surrounding media, θ = incident angle of EMW. The 4x4 matrix for uniaxial $LiNbO_3$ material is calculated as;

$$M = \begin{bmatrix} \cos(\gamma_{1z} k_o d_4) & \frac{ik_{z1} \sin(\gamma_{1z} k_o d_4)}{\Delta_{12}} & 0 & 0 \\ \frac{i\Delta_{12} \sin(\gamma_{1z} k_o d_4)}{\gamma_{1z}} & \cos(\gamma_{1z} k_o d_4) & 0 & 0 \\ 0 & 0 & \cos(\gamma_{2z} k_o d_4) & \frac{i \sin(\gamma_{2z} k_o d_4)}{\gamma_{1z}} \\ 0 & 0 & ik_{z1} \sin(\gamma_{2z} k_o d_4) & \cos(\gamma_{2z} k_o d_4) \end{bmatrix} \tag{4.13}$$

where $\gamma_{1z} = \sqrt{\varepsilon_x (1 - n_o^2 \sin^2\theta / \varepsilon_z)}$ and $\gamma_{2z} = \sqrt{\varepsilon_y - n_o^2 \sin^2\theta}$. Likewise, we have obtained the 4x4matrices for E7 LC, SiO_2, and TiO_2 materials. The final 4x4 matrix for whole 1-DPS $(SiO_2/TiO_2)^5$/LC/LNO/LC/$(TiO_2/SiO_2)^5$ is formulated by multiplication of all 4x4 matrices of the layers one by one which is given as;

The final characteristics M matrix of the considered structure is the product of all characteristic matrices as;

$$M= (M_{SiO2}M_{TiO2})^5 M_{LC}M_{LNO}M_{LC} (M_{TiO2}M_{SiO2})^5 \quad (4.14)$$

$$M = \begin{bmatrix} M_{11} & M_{12} & M_{13} & M_{14} \\ M_{21} & M_{22} & M_{23} & M_{24} \\ M_{31} & M_{32} & M_{33} & M_{34} \\ M_{41} & M_{42} & M_{43} & M_{44} \end{bmatrix} \quad (4.15)$$

The transmission coefficients of the 1-DPS for TE and TM polarizations are given as;

$$t_{TE} = \frac{M_{11}}{M_{11}M_{33} - M_{13}M_{31}} \quad (4.16)$$

$$t_{TM} = \frac{M_{33}}{M_{11}M_{33} - M_{13}M_{31}} \quad (4.17)$$

The final normalized transmissions of the 1-DPS for TE and TM polarizations are obtained by;

$$T_{TE}=|t_{TE}|^2,\ T_{TM}=|t_{TM}|^2 \quad (4.18)$$

4.3 Results and discussion

In this segment, we have calculated the optical transmissions of 1-DPS with the changing refractive indices of the LNO and LC through the temperature, voltage and incident angle of EMW. The transmissions of 1-DPS are obtained the coupled waves with 4x4 matrix for TE and TM modes. The refractive indices (n_1, n_2) of used SiO_2, TiO_2 materials in 1-DPS are taken as 1.5, 2.49, respectively. The thicknesses of SiO_2, TiO_2, LNO and LC materials in the periodic structure are considered as 91.6nm, 55.2nm, 110nm, and 100nm, respectively.

4.3.1 Transmissions of 1-DPS with defect LNO embedded with LC layers at -200V, 0V, and 200V voltage

As discussed earlier, refractive indices of $LiNbO_3$ is dependent on the voltage. So the defect modes in the transmission of 1-DPS $(SiO_2/TiO_2)^5$/LC/LNO/LC/$(TiO_2/SiO_2)^5$ can be tuned by the applied voltage. Therefore, we have studied. the transmissions of 1-DPS at different voltages: -200V, 0V, and 200V for TE and TM polarizations.

The optical transmissions of 1-DPS at -200V, 0V, and 200V voltages for TE and TM modes are represented in figure 4.4. The defect mode transmissions in PBG region for +200V and -200V are shifted towards lower and longer wavelengths respectively due to dependency on the positive and negative biasing on the LNO material and such shifting of defect mode transmission for TE polarization is higher than defect mode transmission for TM polarization. The shifting of defect mode transmission is very useful in designing of optical switches with variation of voltages. The range of shifting in the defect mode transmission is reliant on the extent of voltage; i.e. the shifted defect mode transmissions are highly sensitive with voltages and such high shifting or tunability is more operative for TE polarization. The exhaustive analysis of defect mode shifting in the transmission of 1-DPS at different voltages is tabularized as table 4.1.

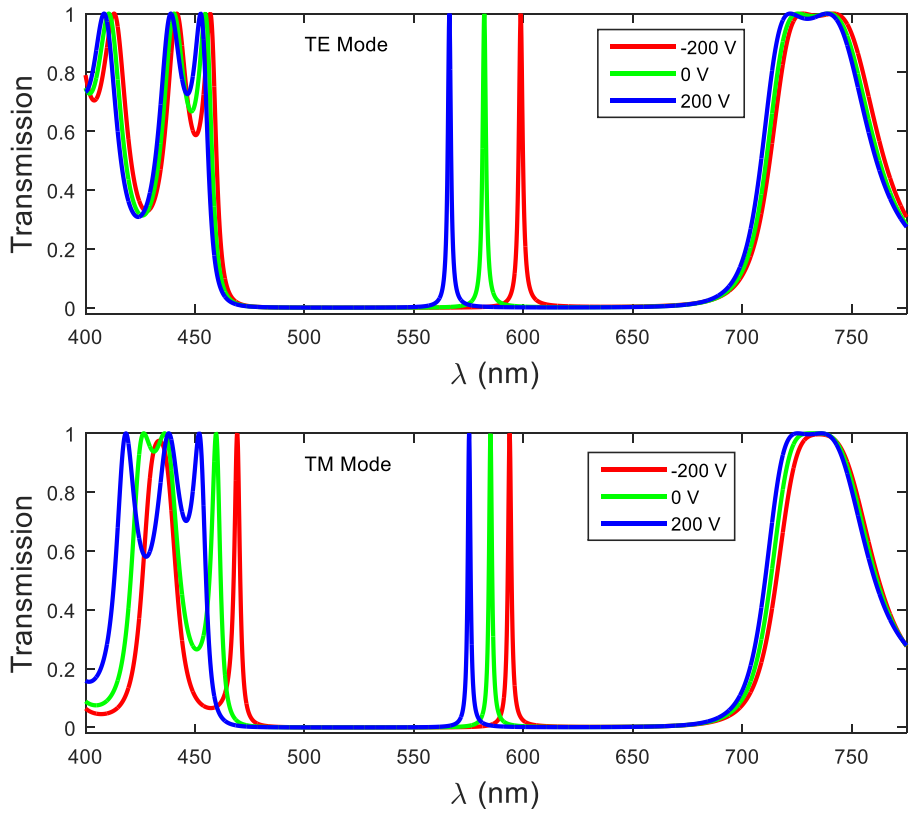

Figure 4.4: Transmission of 1-DPS with defect LNO embedded with LC layers $(SiO_2/TiO_2)^5$/LC/LNO/LC/$(TiO_2/SiO_2)^5$ at -200V, 0V, 200V voltages considering TE and TM polarizations.

Correspondingly, the optical transmissions of 1-DPS at -100V, 0V, 100V voltages are given as figure 4.5 and the study of defect mode transmissions is charted as table 4.1. The broadening effects for defect mode transmissions are compartively low in TM polarization.

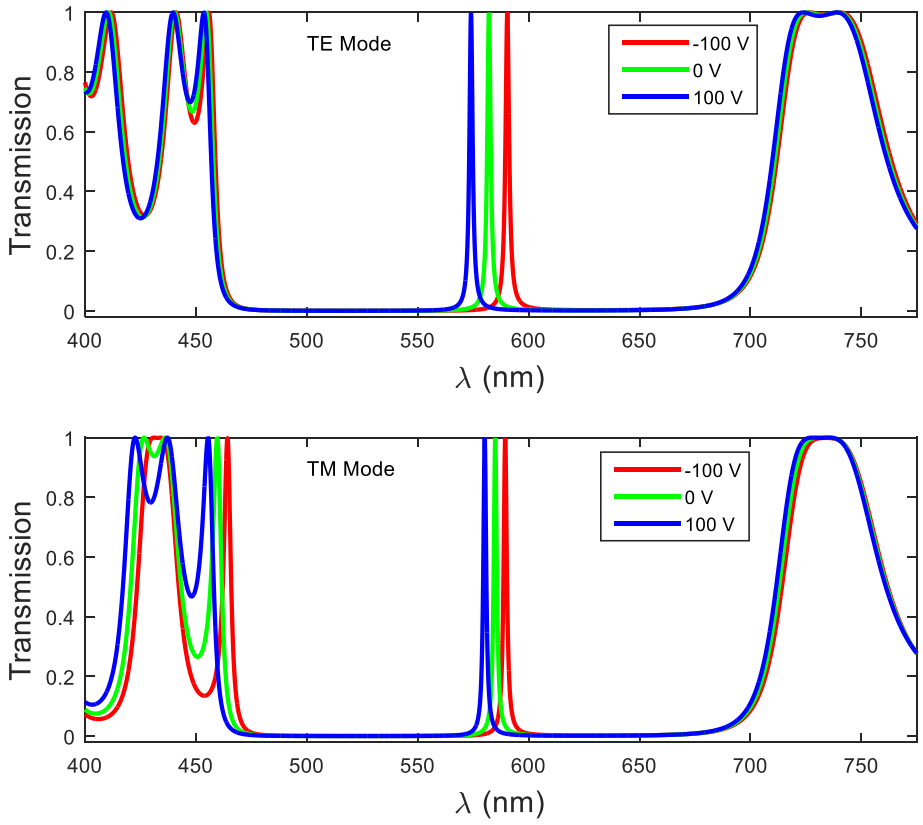

Figure 4.5: Transmissions of 1-DPS with defect LNO embedded with LC layers $(SiO_2/TiO_2)^5$/LC/LNO/LC/$(TiO_2/SiO_2)^5$ at -100V, 0V, 100V voltages considering TE and TM polarizations.

Table 4.1: Shifting wavelengths analysis of defect mode transmissions of 1-DPS at distinct voltages considering TE and TM polarizations.

Polari-zation	Voltage					
	-200V		0V		+200V	
	λ (nm)	Tr. (%)	λ (nm)	Tr. (%)	λ (nm)	Tr. (%)
TE	598.8	99.97	582.1	99.89	566.2	99.99
TM	593.7	99.94	585	99.86	575.2	99.95

	-100V		0V		+100V	
TE	590.4	100	582.2	99.43	574.1	99.57
TM	589.5	99.77	585	99.86	580.3	99.20

4.3.2 Transmission of 1-DPS with defect LNO embedded with LC layers at 300K, 330K, and 360K temperatures for distinct voltage

The optical transmissionsof 1-DPS with defect LNO embedded with LC layers at different temperature of E7 LC considering TE and TM polarization are given in figure 4.6. The refractive index of E7 LC is temperature dependent and LC transformed into isotropic phase from nematic at clearing temperature of LC. The phase transition of E7 LC affects the refractive indices of the material; therefore, the transmission of 1-DPS with defect LNO embedded with LC layers is also affected. The clearing temperature of E7 LC is 330K and hence the optical properties of 1DPS with defect LNO embedded with LC layers are also studied for 300K, 330K, and 360 K temperatures with 0V, -200V and +200V voltages. Figure 4.6 describes the transmission of 1-DPS with defect LNO embedded with LC layers at 300K, 330K, 360K temperature for 0V voltage considering the both polarization modes i. e. TE and TM. The study suggests that the defect mode transmission of 1DPS is effectively varied for TM polarization than the defect mode transmission for TE polarization. The wavelength of defect mode transmission for TE polarization are 582.1nm, 585.9nm 584.7nm for 300K, 330K, 360K temperatures, respectively.

Also, the wavelengths of defect mode transmission for TM polarization are 585nm, 593.7nm, and 590.8nm for 300 K, 330K and 330K temperatures, respectively. Along with such transmissions, we have also discussed the transmission characteristics of 1-DPS with defect LNO embedded with LC layers at -200V and +200V voltages as figures 4.7 and 4.8. The complete analysis of defect mode transmission at the different voltages is discussed as Table 4.2. On the basis of calculated results, we can fabricate temperature and voltage dependent optical switches. The temperature controls the dielectric constant of LCs and therefore, whole optical properties of 1-DPS also can be controlled by temperature and hence, temperature based sensors or switches of 1-DPS with defect LNO embedded with LC layers may be designed with the variation of voltages.

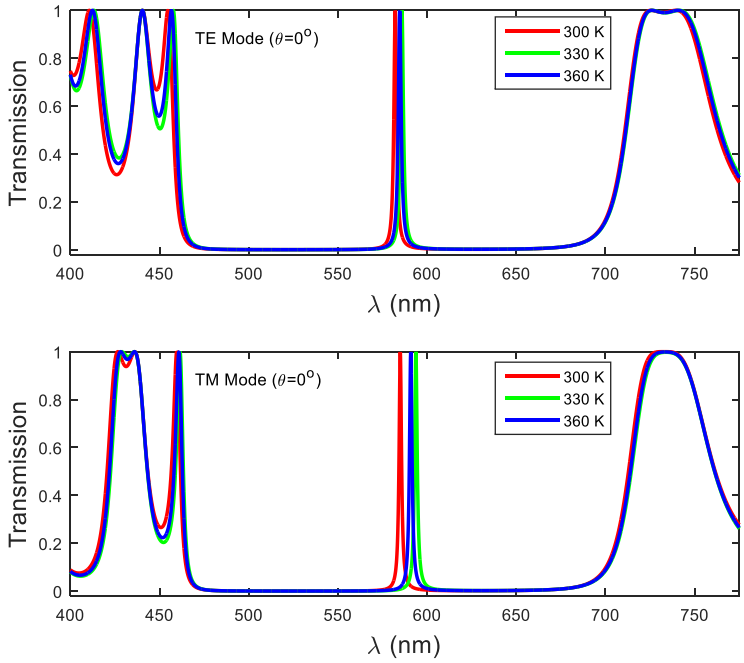

Figure 4.6: Transmissions of 1-DPS with defect LNO embedded with LC layers $(SiO_2|TiO_2)^5|LC|LNO|LC|(TiO_2|SiO_2)^5$ at 300K, 330K, 360K temperatures considering TE and TM polarizations with 0V.

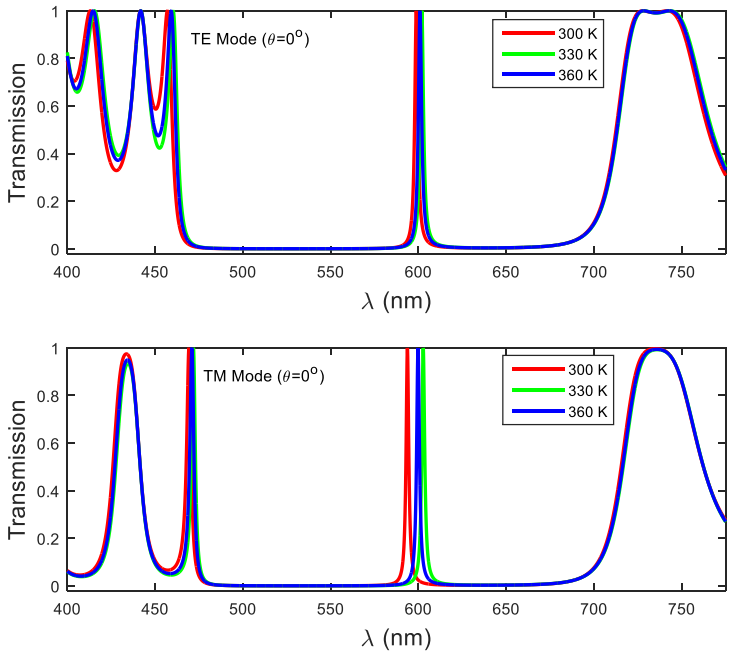

Figure 4.7: Transmissions of 1-DPS with defect LNO embedded with LC layers $(SiO_2/TiO_2)^5/LC/LNO/LC/(TiO_2/SiO_2)^5$ at 300K, 330K, 360K temperatures considering TE and TM polarizations with -200V.

Table 4.2: Shifting wavelengths analysis of defect mode transmissions at distinct voltages and temperatures considering TE and TM polarizations.

Polari-zation	Temperature					
	300K		330K		360K	
	λ(nm)	Tr. (%)	λ(nm)	Tr. (%)	λ(nm)	Tr. (%)
	Temperature (K) with 0 V					
TE	582.1	99.89	585.9	99.97	584.7	99.84
TM	585	99.86	593.7	99.94	590.8	99.84
	Temperature (K) with -200 V					
TE	599	99.97	601.9	99.85	600.9	100
TM	593.7	99.94	602.7	99.85	599.8	99.87
	Temperature (K) with 200 V					
TE	566.2	99.99	571	99.96	569	99.7
TM	575	99.95	583.6	99.93	580.8	99.66

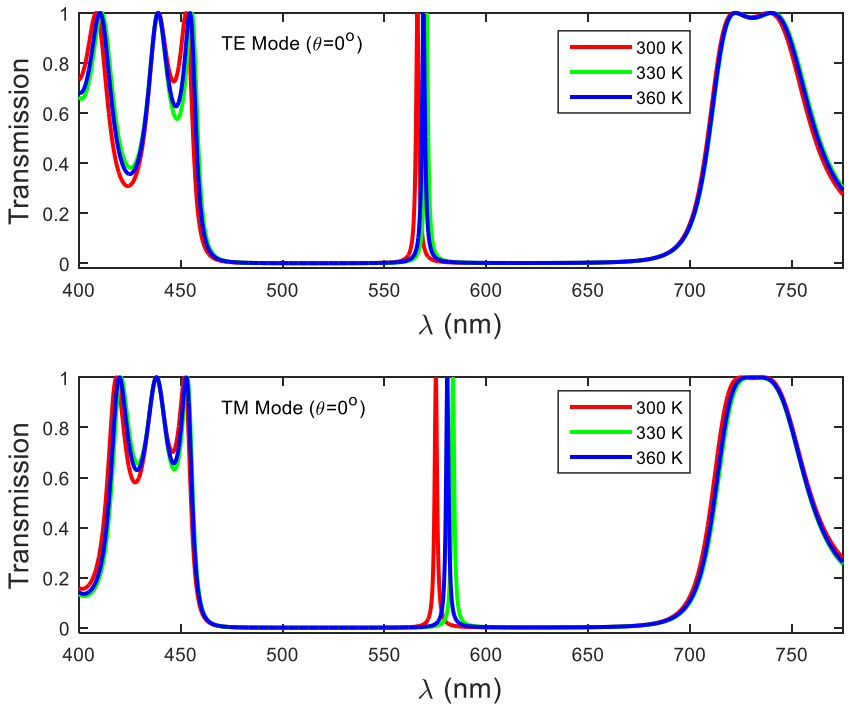

Figure 4.8: Transmissions of 1-DPS with defect LNO embedded with LC layers $(SiO_2/TiO_2)^5$/LC/LNO/LC/$(TiO_2/SiO_2)^5$ at 300K, 330K, 360K temperatures considering TE and TM polarizations with 200V.

4.3.3 Transmission of 1-DPS with defect LNO embedded with LC layers at 0^o, 30^o, and 45^o incident angles for 300K temperature

The extraordinary refractive index of LNO regulates with applied voltage and incident angle of EMW, thereby the transmissions of 1DPS can be controlled with incident angle and voltage of LNO material. So, the transmission characteristics of 1-DPS are calculated at 0^o, 30^o, and 45^o incident angle of EMW for 0V, -200V and +200V voltages. The transmission of 1-DPS at 0^o, 30^o and 45^o incident angle for 0V is shown in figure 4.9. The wavelengths of defect mode transmission in the PBG region for TE polarization are found 582.2nm, 568.8nm, and 554.7nm at 0^0, 30^0, and 45^0 incident angles, respectively. Similarly, the wavelengths of defect mode transmission for TM polarization are found 585nm, 564nm, and 543nm for same incident angles, respectively. The location of defect mode transmission varies with incident angle of EMW. A tunable omni-directional PBG also can be achieved with such 1-DPS at different voltages and may be used in various photonic applications.

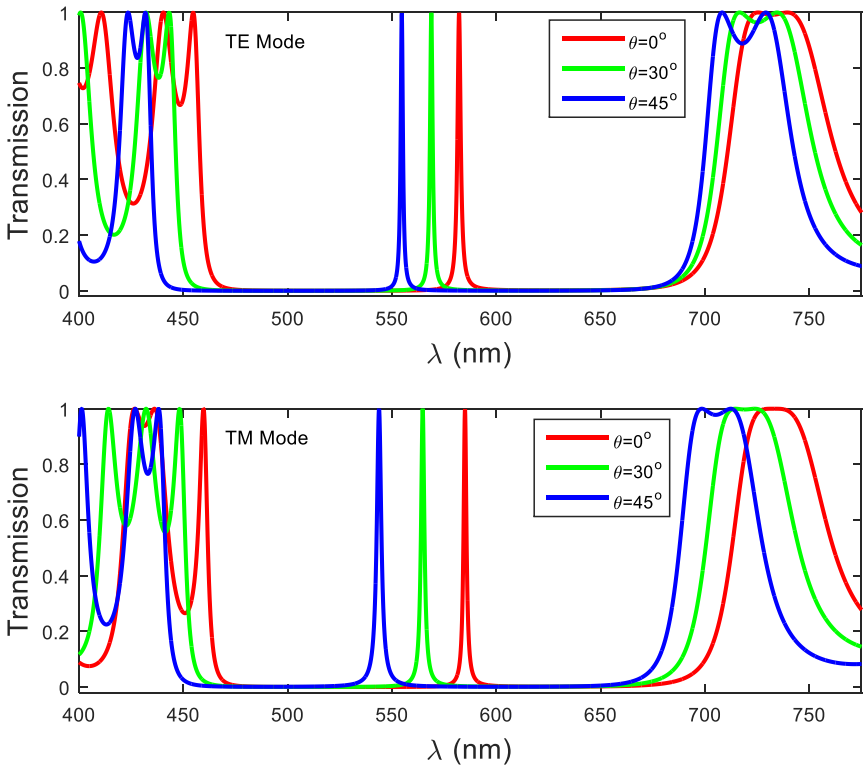

Figure 4.9: Transmissions of 1-DPS with defect LNO embedded with LC layers $(SiO_2/TiO_2)^5$/LC/LNO/LC/$(TiO_2/SiO_2)^5$ at incident 0^o, 30^o, and 45^o angles considering TE and TM polarizations with 0V.

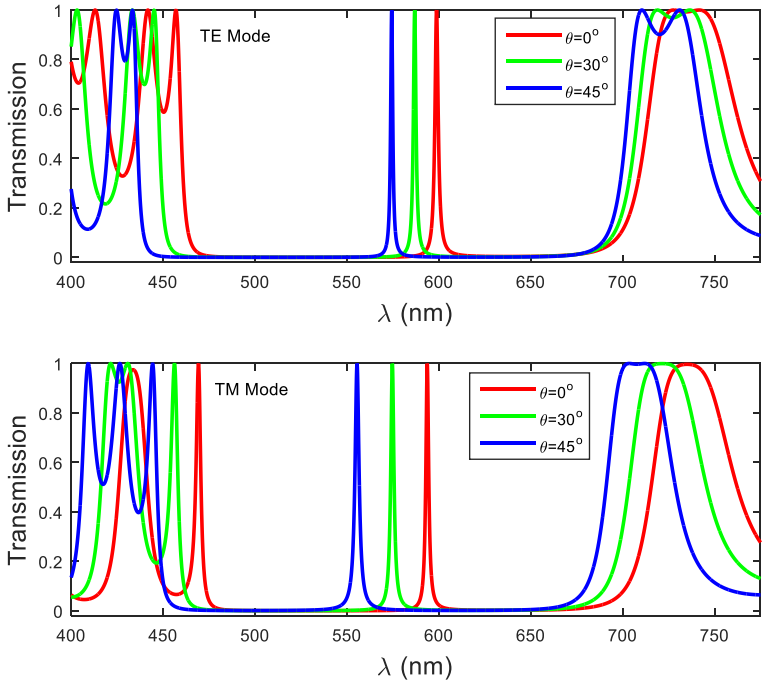

Figure 4.10: Transmissions of 1-DPS with defect LNO embedded with LC layers $(SiO_2/TiO_2)^5$/LC/LNO/LC/$(TiO_2/SiO_2)^5$ at incident 0^o, 30^o, and 45^o angles considering TE and TM polarizations with -200V.

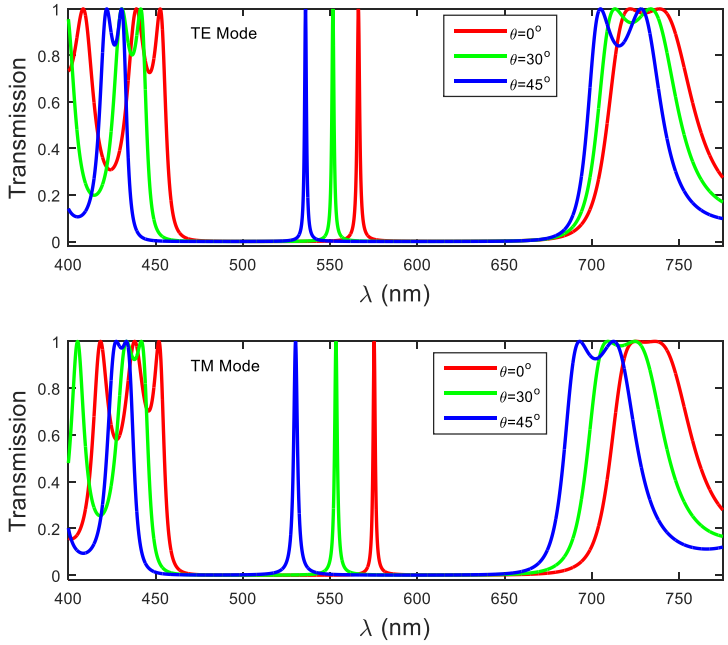

Figure 4.11: Transmissions of 1-DPS with defect LNO embedded with LC layers $(SiO_2/TiO_2)^5$/LC/LNO/LC/$(TiO_2/SiO_2)^5$ at 0^o, 30^o, and 45^o incident angles considering TE and TM polarizations with 200V.

The shifting of defect mode transmission in PBG region is comparatively high for TM polarization rather than TE polarization mode. We have observed that the effect mode transmission in PBG region is shifted lower wavelength region (blue shift) with higher incident angle of EMW. The transmission characteristics of 1-DPS at -200 V and 200V are given in table 3.

Table 4.3: Shifting wavelengths analysis of defect mode transmissions at distinct voltage and incident angle with constant 300K temperature.

Polarization	Incident angle (θ^o)					
	0^o		30^o		45^o	
	with 0 V					
	λ (nm)	Tr. (%)	λ (nm)	Tr. (%)	λ (nm)	Tr. (%)
TE	582.2	99.89	568.8	99.89	554.7	99.7
TM	585	99.86	564	100	543	99.96
	with -200 V					
TE	599	99.97	586.9	99.96	574	99.91
TM	593.7	99.94	574.4	98.46	555.6	99.65
	with 200 V					
TE	566.2	99.99	552.6	99.98	536	99.95
TM	575.2	99.95	553.3	99.93	530.2	99.97

4.3.4 Transmission of 1-DPS with defect LNO embedded with LC layers at 0^o, 30^o, and 45^o incident angles for 330K temperature

The optical transmission properties of 1-DPS with defect LNO embedded with LC layers at 0^o, 30^o, and 45^o incident angles are calculated for -200V, 0V, and +200V voltages and 330K temperature using 4x4 matrix method. The E7 LC changes its nematic phase to isotropic phase at 330K clearing temperature (T_C) and the average refractive index of the E7 LC constantly decreases with increases the temperature.

The defect mode transmission peaks in PBG for TE mode polarization are occurred at 586 nm, 573 nm, and 559 nm wavelengths corresponding to 0^o, 30^o, and 45^o incident angles with 0V. But in case of TM polarizations, these wavelengths of the transmission peaks are 593.8nm, 574.1nm, and 553.8nm for considered incident angle

of EMW with same applied voltage. The shifting of defect peak transmission in PBG region for TM polarization is higher in comparison to the shifting of defect peak transmission for TE polarization. Further, we have investigated the transmission characteristics of considered 1-DPS with defect LNO embedded with LC layers at -200V and +200V voltages as figures 4.12 and 4.13. The detailed study of defect mode transmission is tabulated in the table 4.4. An essential deduction is that the shifting of defect mode transmission in PBG for TM polarization mode is much more operative with the variation of incident angles while defect mode transmission for TE polarization is dominating than defect mode transmission for TM polarization mode with voltage variation. The incident angle of EMW also regulates the optical transmissions of 1-DPS with defect LNO embedded with LC layers and optical switches also may be designed with varying incident angles and voltages.

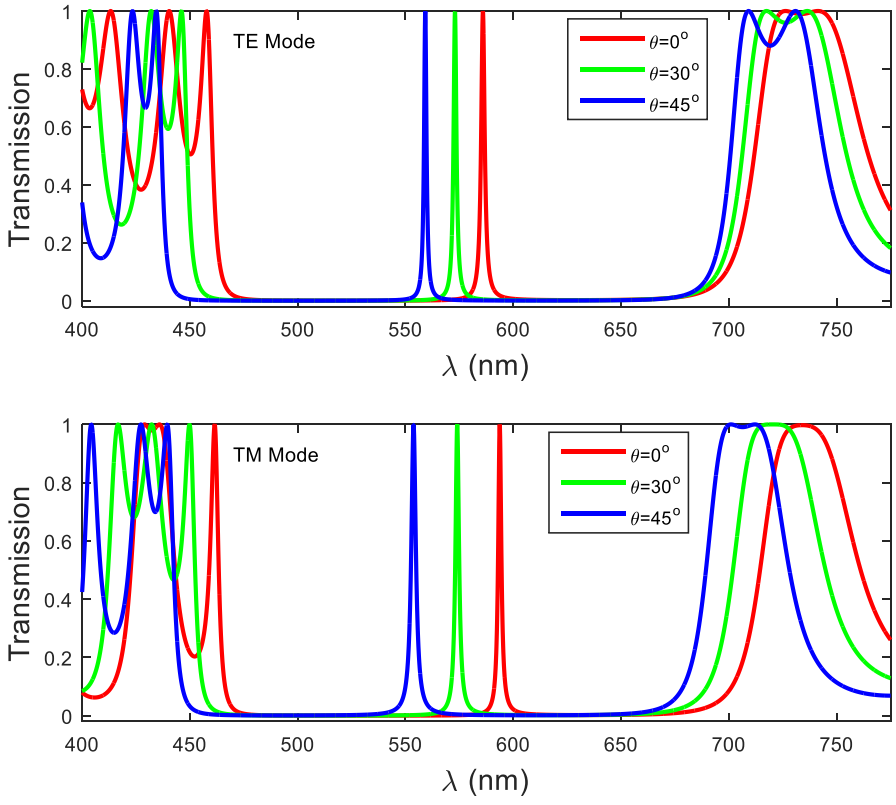

Figure 4.12: Transmissions of 1-DPS with defect LNO embedded with LC layers $(SiO_2/TiO_2)^5$/LC/LNO/LC/$(TiO_2/SiO_2)^5$ for TE and TM polarizations at 0^o, 30^o, and 45^oincident anglesand 330K temperature.

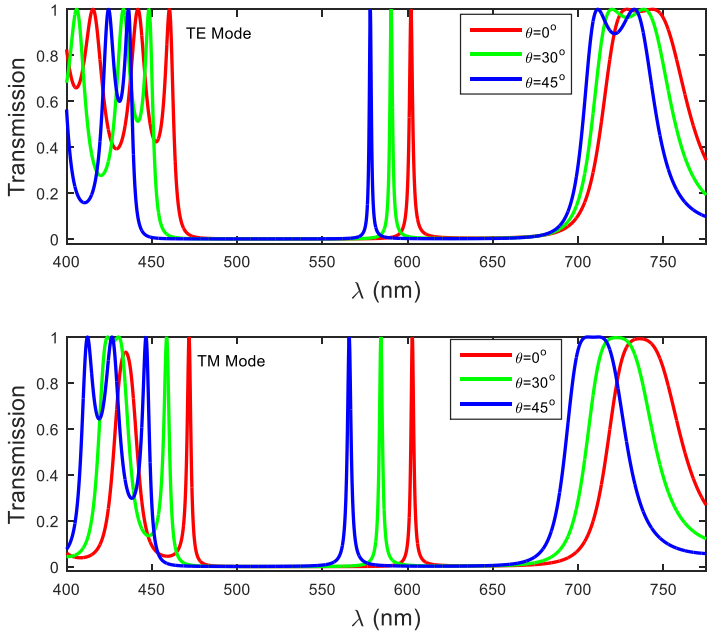

Figure 4.13: Transmission of 1-DPS with defect LNO embedded with LC layers $(SiO_2/TiO_2)^5$/LC/LNO/LC/$(TiO_2/SiO_2)^5$ for TE and TM polarizations at 0^o, 30^o, and 45^o incident angles and 330K temperature with -200V.

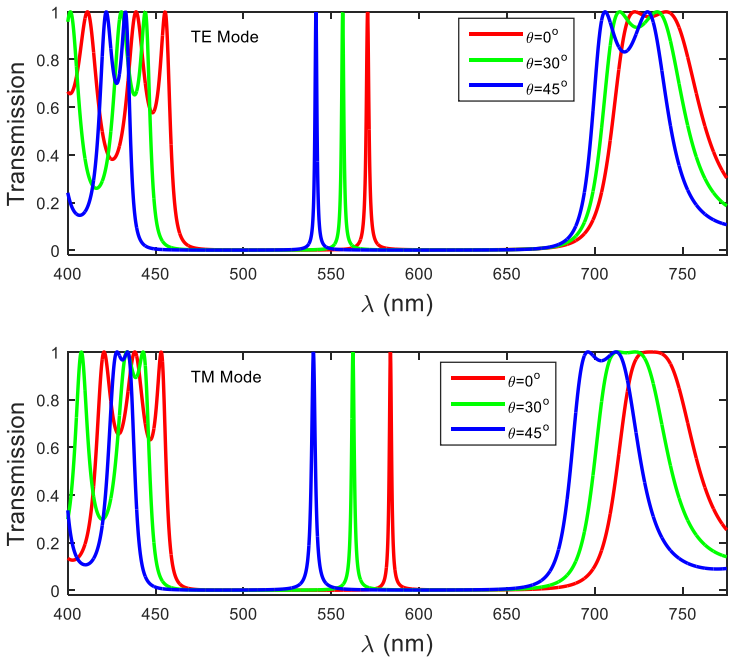

Figure 4.14: Transmissions of 1-DPS with defect LNO embedded with LC layers $(SiO_2/TiO_2)^5$/LC/LNO/LC/$(TiO_2/SiO_2)^5$for TE and TM polarizations at 0^o, 30^o, and 45^o incident angles and 330K temperature with +200V.

Table 4.4: Shifting wavelengths analysis of defect mode transmissions at distinct voltages and incident angles for 330K temperature.

Polari-zation	Incident angle (θ^o)					
	0^o		30^o		45^o	
	λ (nm)	Tr. (%)	λ (nm)	Tr. (%)	λ (nm)	Tr. (%)
TE	586	99.29	573	99.47	559	99.85
TM	593.8	99.20	574.1	98.96	553.8	99.84
	with -200 V					
TE	602	99.75	590	99.96	578	99.99
TM	602.8	99.61	584.9	98.99	565.7	99.95
	with 200 V					
TE	570.7	99.15	556.5	99.64	541.2	99.29
TM	584.6	99.93	562.3	99.84	539.9	99.23

4.3.5 Defect mode transmission characteristics variation with temperature at various voltages

The behavior of transmittance of defect mode for TE and TM polarization modes at wavelength 598.8 nm with the variation of temperature at -200V is show in figure 4.15. The defect mode transmission has maximum value at 310K temperature and then it is fall down with increase temperature and achieved the minimum value (~10%) at phase transition temperature 330K. After the transition state, the defect mode transmittance again increases with temperature. The defect mode transmittance for TM polarization at 593.7nm wavelength has maximum value for 305K temperature and then it is reduced up to minimum value (~0.9%). Again, the defect mode transmission for TM polarization increases with increase temperature as like the defect mode transmission for TE polarization.

Further, the defect mode transmittances for TE and TM polarizations are studied with the variation of temperature at 0V and +200V as depicted in figures 4.16 and 4.17. The nature of defect mode transmittance for 0V and +200V is almost similar to the defect mode transmittance behavior for -200V, but they have dissimilar in their minimum values for TE and TM polarizations. The defect mode transmission for TE

and TM polarizations at 582.1nm and 585nm are 5.4%, 0.8% at 0V and 330K temperature. The minimum defect mode transmission values for TE and TM polarizations at wavelengths 566.2nm, 575.2nm; are 3.37%, 7%, respectively at +200V. The minimum values of defect mode transmittance are found relatively lower values for -200V, 0V, and +200V voltages with phase transition temperature of LC.

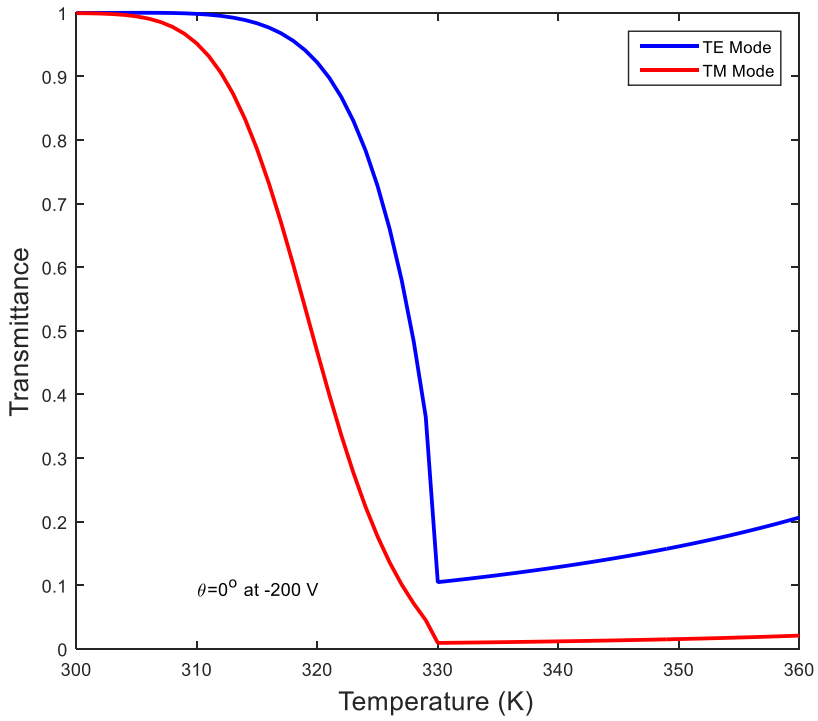

Figure 4.15: Defect mode transmittance variation with temperature at 0^o incident angle and -200V for TE and TM polarizations.

The acquired defect mode transmission of 1-DPS with defect LNO embedded with LC layers with the variation of temperature at distinct voltages may be useful to design optical switches due to fast reduction is obtained in defect mode transmission in the PBG of 1-DPS at transition temperature. The optical defect mode transmission for TE polarization is also supported the better optical switching property at different voltages. From the figures 4.15, 4.16 and 4.17, we have suggested that the defect mode transmission for TE and TM polarizations remains almost constant initially i.e. ON state and then reduces rapidly i.e. OFF state with varying the temperature. The optical switches based on variation of temperatures and voltages may be designed by using such periodic structures with defect LNO embedded with LC layers.

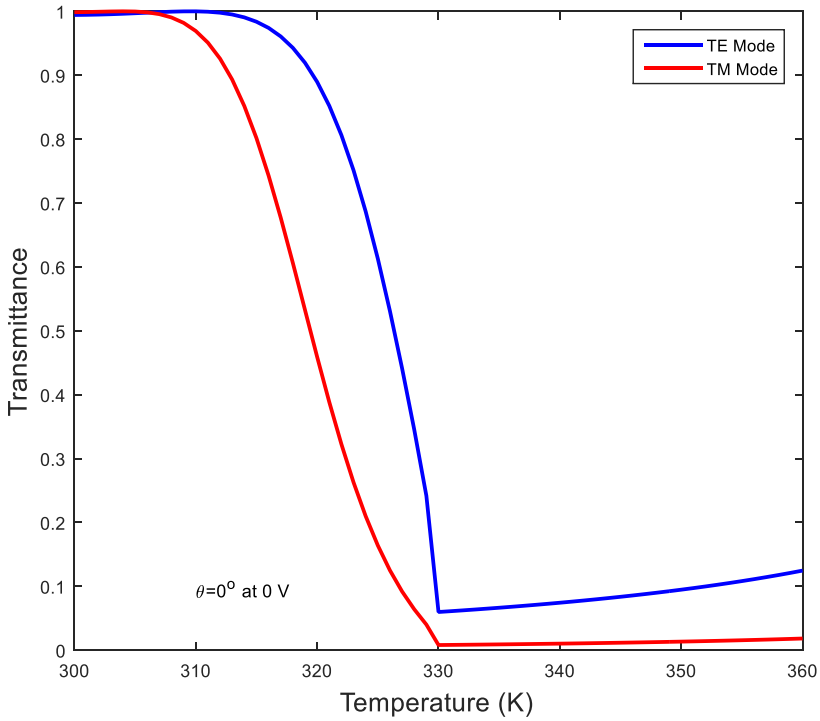

Figure 4.16: Defect mode transmittance with temperature at 0^{o} incident angle and 0V for TE and TM polarizations.

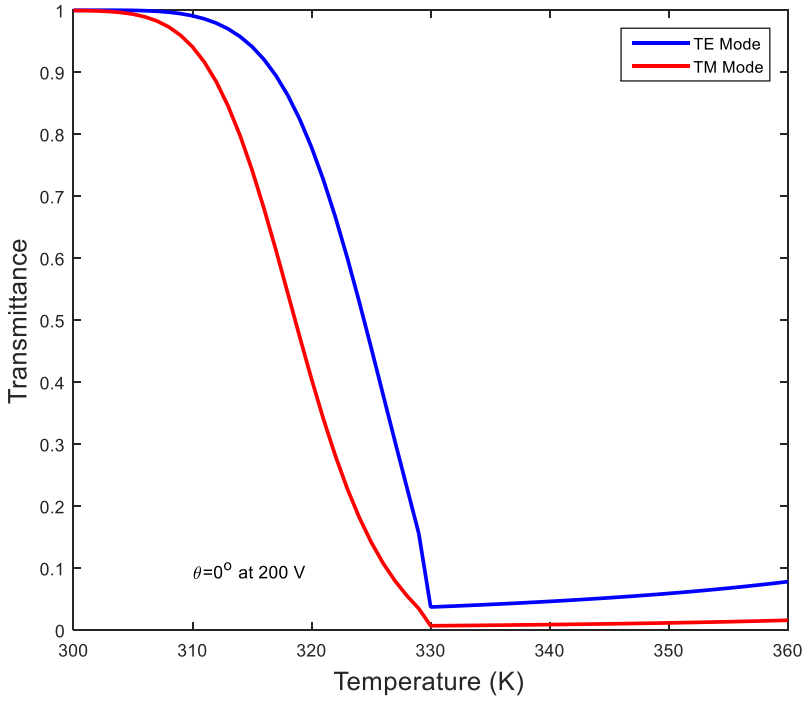

Figure 4.17: Defect mode transmittance with temperature at 0^{o} incident angle and +200V for TE and TM polarizations.

4.3.5 Transmission of wavelength wavelengths, 400nm and 800nm, variation with temperature at various incident angles

In this part, the transmission of terminal wavelengths (400nm, 800nm) through 1-DPS with defect LNO embedded with LC layers for TE and TM polarizations are discussed at different 0^o, 30^o, 45^o incident angles as represented in figure 4.18, 4.19, and 4.20. For TE polarization, 74% transmission almost remains constant below 330K temperature, and 72.92% transmission is also almost remains constant above 330 K temperature, but the 1.08% transmission is decreased at transition temperature for 0^o incidence angle, 0V and 400nm wavelength. Similarly for TM polarization, we have found decreased 1.10% transmission (9.0% and 7.9%) with same nature for 0^o incidence angle, 0V and 400nm wavelength. We have also done similar calculation for 800nm wavelength. For TE polarization, the 16% transmission almost remains constant below 330K temperature and the 17.39% transmission above 330 K temperature but the increased transmission is obtained 1.39% for 0^o incidence angle, 0V and 800nm wavelength. Similarly the transmissions for TM polarization are found 18% below 330K and 15.59% above 330K, it means 3.59% transmission is decreased at transition temperature at 0^o incidence angle, 0V and 800nm wavelength.

Considering the both polarization states, transmission for 400nm wavelength are helpful in designing of optical switching devices at high transmission (74% or 72.92%) for TE polarization mode, but the transmission for 800nm wavelengths may be used to design at low transmission (9% or 7.9%) for TM polarization at normal incident angle and 0V.

The transmission for 400nm, 800nm wavelengths are found as 82.16%, 8.54% for TE polarization mode respectively and 12.65 %, 12.05% for TM polarization mode respectively at 330K temperature and 30^o incident angle. But, the transmission of 400nm, 800nm wavelengths are acquired the lower values 42.45%, 33.93% respectively for TE and 8%, 10.5% for TM polarization respectively at 330K and 45^o incident angle. The result demonstrates that the transmissions for 400nm, 800nm wavelengths (terminal) are affected by variations of temperature as well as incident angle.

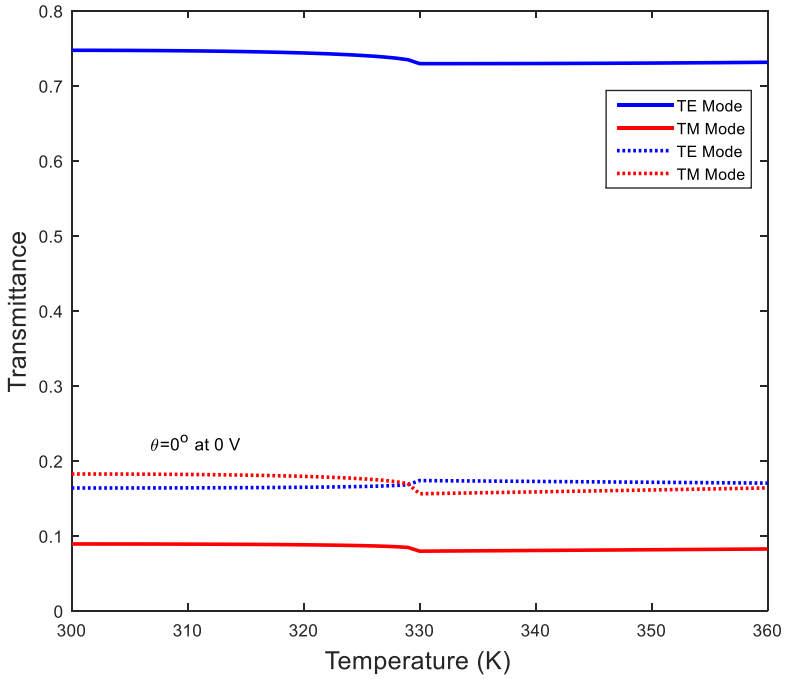

Figure 4.18: Transmittance variation of 400nm (-Solid lines), 800nm (Dotted lines) wavelengths with temperature at 0^o incident angle for 0V.

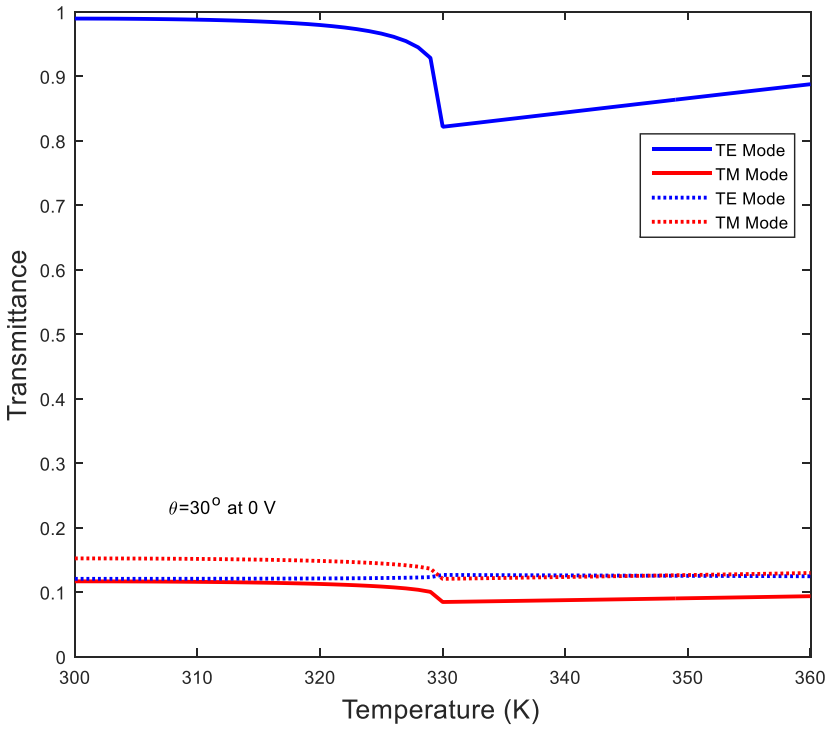

Figure 4.19: Transmittance variation of 400nm (solid lines), 800nm (dotted lines) wavelengths with temperature at 30^o incident angle for 0V.

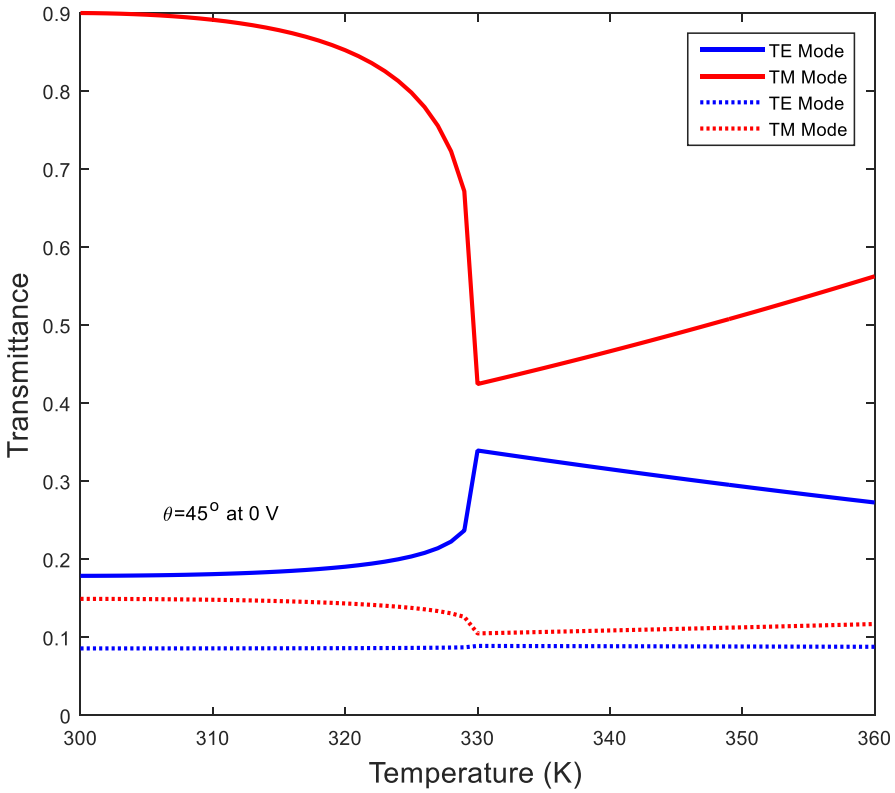

Figure 4.20: Transmittance variation of 400nm (solid lines), 800nm (dotted lines) wavelengths with temperature at 45^{o} incident angle for 0V.

On comparing the results, we have obtained that the transmission of both wavelengths are almost stable above and below the transition temperature for 0^{o} incident angle and considering TE and TM polarization states, but transmission of both wavelengths have very minor variation at 330K. In conclusion, the transmissions of the wavelengths are influenced by changing temperatures and refractive indices of E7 LC and $LiNbO_3$ materials as well as incident angle of EMW. The proposed 1-DPS with defect LNO embedded with LC layers shows the uncommon transmission and shifting properties of defect mode transmission at 45^{o} incident angle due to voltage dependent dielectric indices of $LiNbO_3$ material and orientation of LC.

4.4 Conclusion

The transmissions of 1-DPS consisting of SiO_2, TiO_2 materials with defect LNO embedded with LC layers are calculated by 4×4 matrix method. The detailed analysis reveals that the transmissions of defect mode in PBG region of 1-DPS with defect LNO embedded with LC layers $(SiO_2/TiO_2)^5$/LC/LNO/LC/$(TiO_2/SiO_2)^5$ are

sufficiently affected by variation of temperature and incident angle. The defect mode transmission in the PBG region shows blue shifting with the deviation in voltage, incident angle and temperature, due to changed refractive indices of $LiNbO_3$ layer. Further, E7 LC has obtained zero value of order parameter and converted into isotropic phase at the phase transition temperature. Therefore, the transmittances of corresponding wavelengths (terminal and defect modes) are influenced with the variation of temperature and incident angle. The shifting of defect mode transmission in PBG region with voltage variation is comparatively high for TE polarization state while such shifting of defect mode transmission with the varying incident angle is more effective for TM polarization state in contrast to shifting of defect mode transmission for TE polarization state. The studied 1-DPS based on anisotropic LNO embedded with LC layers as defect, $(SiO_2/TiO_2)^5$/LC/LNO/LC/$(TiO_2/SiO_2)^5$, may be used in tunable photonic and opto-electronic devices like optical switches, filters, modulators, wavelength selector, etc.

References

[1] I. C. Khoo, *Liquid Crystals*, Wiley Interscience, New Jersey, 2007.

[2] L. M. Blinov, *Structure and Properties of Liquid Crystals*, Springer, New York, 2011.

[3] J. Li, S. T. Wu, S. Brugioni, R. Meucci, and S. Faetti, Infrared refractive indices of liquid crystals, *J. Appl. Phys.*, 97, 073501(1-5), 2005.

[4] A. Mouquinho, M. Saavedra, A. Maiau, K. Petrova, M. T. Barros, J. L. Figueirinhas and J. Sotomayor, Films Based on New Methacrylate Monomers: Synthesis, Characterisation, and Electro-Optical Properties, *Mol. Cryst. Liq. Cryst.*, 542, 132-140, 2011.

[5] A. Yariv and P. Yeh, *Optical Waves in Crystals Propagation and Control of Laser Radiation*, John Wiley and Sons, 1983.

[6] K. J.-Ghaleh, B. Kazempour, Effect of incident angle and polarization on electrically-tunable defect mode in anisotropic photonic crystals, *App. Opt.*, 55, 4350-4356, 2016.

[7] J. Deng, S. Hussain, V. S. Kumar, W. Jia, C. E. Png, L. S. Thor, A. A. Bettiol, and A. J. Danner, Modeling and experimental investigations of Fano resonances in free-standing $LiNbO_3$ photonic crystal slabs, *Opt. Express*, 21, 3243-3252, 2013.

[8] E. Yablonovitch, Inhibited spontaneous emission in solid state physics and electronics, *Phys. Rev. Lett.*, 58, 2059-2062, 1987.

[9] S. John, Strong Localization of Photons in Certain Disordered Dielectric Superlattices, *Phys. Rev. Lett.*, 58, 2486-2489, 1987.

[10] J. D. Jonopoulos, P. Villeneuve, and S. Fan, Photonic crystals: Putting a new twist on light, *Nature*, 386, 143-149, 1997.

[11] Q. R. Zheng, Y. Q. Fu, and N. C. Yuan, Characteristics of planer PBG structures with a cover layer, *J. Electromag. Waves and Applications*, 20, 1439-1453, 2006.

[12] Y. Fink, J. N. Winn, S. Fan, C. Chen, J. Michel, J. D. Joannopoulos, and E. L. Thomas, A dielectric omnidirectional reflector, *Science*, 282, 1679-1682, 1998.

[13] J. A. M. Rojas, J. Alpuente, J. Pineiro, and R. Sanchez, Rigorous full vectorial analysis of electromagnetic wave propagation in 1D, *Progress In Electromagnetics Research*, 63, 89-105, 2006.

[14] J. D. Joannopoulos, R. D. Meade, and J. N. Winn, *Photonic Crystals: Molding the Flow of Light*, Princeton Univ. Press, Princeton, NJ, 1995.

[15] R. Srivastava, K. B. Thapa, S. Pati, S. P. Ojha, Omni-direction reflection in one dimensional photonic crystal, *Progress In Electromagnetics Research B*, 7, 133–143, 2008.

[16] K. B. Thapa, S. Srivastava, S. Tiwari, Enlarged photonic band gap in heterostructure of metallic photonic and superconducting photonic crystals, *J. Supercond. Novel Magn.*, 23, 517-525, 2010.

[17] K. B. Thapa, S. K. Singh and S. P. Ojha, Omnidirectional high reflector for infrared frequency, *Int J. Infrared Milli. Waves*, 27, 1257-1268, 2006.

[18] G. N. Pandey, K. B. Thapa, S.P. Ojha, Omni-directional reflection bands in one-dimensional plasma dielectric photonic crystals, *Optik*, 124, 3396– 3401, 2013.

[19] D. R. Smith, S. L. McCall, P. M. Platzman, R. Dalichaouch, N. Kroll, and S. Schultz, Photonic band structure and defects in one and two dimensions, *J. Opt. Soc. Am. B*, 10, 314–321, 1993.

[20] X. Y.-Jiang, D. X. Yu, and W. S. -Chun, Effects of negative index medium defect layers on the transmission properties of onedimensional photonic crystal, *Optoelectron. Lett*., 3, 144–147, 2007.

[21] H. Inouye, M. Arakawa, J. Y. Ye, T. Hattori, H. Nakatsuka, and K. Hirao, Optical properties of a total-reflection-type one dimensional photonic crystal, *IEEE J. Quantum Electron.*, 38, 867–871, 2002.

[22] C. Schuller, F. Klopf, J. P. Reithmaier, M. Kamp, and A. Forchel, Tunable photonic crystals fabricated in III-V semiconductor slab waveguides using infiltrated liquid crystals, *Appl. Phys. Lett*., 82, 2767–2769, 2003.

[23] S. W. Leonard, J. P. Mondia, H. M. van Driel, O. Toader, S. John, K. Busch, A. Birner, U. Gosele, and V. Lehmann, Tunable two dimensional photonic crystals using liquid crystal infiltration, *Phys. Rev. B*, 61. R2389–R2392, 2000.

[24] W. Jia, Y. Li, Y. Xi, P. Jiang, X. Xu, X. Liu, R. Fu, and J. Zi, Tunability of photonic crystals based on the Faraday effect, *J. Phys. Condens. Matter.*, 15, 6731–6737, 2003.

[25] C. C. Liu and C. J. Wu, Analysis of defect mode in a dielectric photonic crystal containing ITO defect, *Optik*, 125, 7140–7142, 2014.

[26] M.-R. Wu, C.-J. Wu, and S.-J. Chang, Investigation of defect modes in a defective photonic crystal with a semiconductor metamaterial defect, *Physica E*, 64, 146–151, 2014.

[27] Y.-K. Ha, Y.-C. Yang, J.-E. Kim, H. Y. Park, C.-S. Kee, H. Lim, and J.-C. Lee, Tunable omnidirectional reflection bands and defect modes of a one-dimensional photonic band gap structure with liquid crystals, *Appl. Phys. Lett.*, 79, 15–17, 2001.

[28] N. C. Panoiu, M. Bahl, and R. M. Osgood, All-optical tunability of a nonlinear photonic crystal channel drop filters, *Opt. Express*, 12, 1605–1610, 2004.

[29] N. N. Dadoenkova, A. E. Zabolotin, I. L. Lyubchanskii, Y. P. Lee, and T. Rasing, One-dimensional photonic crystal with a complex defect containing an ultrathin superconducting sublayer, *J. Appl. Phys*., 108, 093117, 2010.

[30] D. Park, S. Kim, I. Park, and H. Lim, Higher order optical resonant filters based on coupled defect resonators in photonic crystals, *J. Lightwave Technol*., 23, 1923–1928, 2005.

[31] P. T. Lin and B. W. Wessele, Ferroelectric thin film photonic crystal waveguide and its electro-optic properties, *J. Opt. A*, 11, 075005(1-7), 2009.

[32] Q. Zhu and Y. Zhang, Defect modes and wavelength tuning of one dimensional photonic crystal with lithium niobate, *Optik*, 120, 195–198, 2009.

[33] R. Ozaki, T. Matsui, M. Ozaki, and K. Yashino, Electrically color tunable defect mode lasing in one-dimensional photonic-band-gap system containing liquid crystal, *Appl. Phys. Lett.*, 82, 3593–3595, 2003.

[34] H. Nemec, P. Kuzel, L. Duvillaret, A. Pashkin, M.Dressel, and M. T. Sebastian, Highly tunable photonic crystal filter for the terahertz range, *Opt. Lett.*, 30, 549–551, 2005.

[35] I. Abdulhalim, Analytic propagation matrix method for linear optics of arbitrary biaxial layered media, *J. Opt. A*, 1, 646–653, 1999.

[36] P. Yeh, Electromagnetic propagation in birefringent layered media, J. *Opt. Soc. Am.*, 69, 742–756, 1979.

[37] S. Chandrasekhar, *Liquid Crystals*, Cambridge Univ. Press, New York, 1992.

[38] K. Busch, and S. John, Liquid-Crystal Photonic-Band-Gap Materials: The Tunable Electromagnetic Vacuum, *Phys. Rev. Lett.*, 83, 967-970, 1999.

[39] K. Yoshino, Y. Shimoda, Y. Kawagishi, K. Nakayama, and M. Ozaki, Temperature tuning of the stop band in transmission spectra of liquid-crystal infiltrated synthetic opal as tunable photonic crystal, *Appl. Phys. Lett.*, 75, 932-934, 1999.

[40] D. Kang, J. E. Maclennan, N. A. Clerk, A. A. Zakhidov, and R. H. Baughman, Electro-optic Behavior of Liquid-Crystal-Filled Silica Opal Photonic Crystals: Effect of Liquid-Crystal Alignment, *Phys. Rev. Lett.*, 86, 4052-4055, 2001.

[41] E. Graubard, J. S. King, S. Jain, C. J. Summers, Y. Z. Williams, and I. C Khoo, Electric-field tuning of the Bragg peak in large-pore TiO_2 inverse shell opals, *Phys. Rev. B*, 72, 233105-4, 2005.

[42] V. G. Arkhipkin, V. A. Gunyakov, S. A. Myslivsts, V. Ya. Zyryanov, and V. F. Shabanov, Angular tuning of defect modes spectrum in the one-dimensional photonic crystal with liquid-crystal layer, *Eur. Phys. J. E*, 24, 297-302, 2007.

[43] Y. M. Strelniker, D. Stroud, and A. O. Voznesenkaya, Control of extraordinary light transmission through perforated metal films using liquid crystals, *Eur. Phys. J. B*, 52, 1-7, 2006.

[44] S. F. Mingaleev, M. Schillinger, D. Hermann, and K. Bush, Tunable photonic crystal circuits: concepts and designs based on single-pore infiltration, *Opt. Lett.*, 29, 2858-2860, 2004.

[45] M. S. Mohamed, M. F. O. Hameed, M. M. El-Okr, Salah S. A. Obayya, Characterization of one dimensional liquid crystal photonic crystal structure, *Optik*, 127, 8774-8781, 2016.

[46] R. Ozaki, H. Miyoshi, M. Ozaki, K. Yoshino, Tunable Defect Mode in One-Dimensional Photonic Crystal with Liquid Crystal Defect Layer, *Mol. Cryst. Liq. Cryst.*, 433, 247-257, 2005.

[47] A. C. Polycarpou, M. A. Christou, and N. C. Papanicolaou, A mode-matching approach to electromagnetic wave propagation in nematic liquid crystals, *IEEE Trans. On Micro. Theo. and Tech.*, 60, 2950-2958, 2012.

[48] A. E. Miroshnichenko, I. Pinkevych, and Y. S. Kivshar, Tunable all-optical switching in periodic structures with liquid-crystal defects, *Opt. Express*, 14, 2839-2844, 2006.

[49] S. R. Entezar, A. Madani, M. K. Habil, A. Namdar, and H. Tajalli, Temperature dependent transmission and optical bistability in a 1D photonic crystal with a liquid crystal defect layer, *J. Mod. Opt.*, 60, 1883-1891, 2013.

[50] P. S. Pankin, S. Ya. Vetrov, and I. V. Timofeev, Tunable hybrid Tamm-microcavity states, *J. Opt. Soc. Am. B*, 34, 2633-2639, 2017.

[51] H. L. Ong, Optical-field-enhanced and static-field-induced first-order Fréedericksz transitions in a planar parallel nematic liquid crystal, *Phys. Rev. A*, 33, 3550-3553, 1986.

[52] P. Yeh, *Optical Waves in Layered Media*, John Wiley & Sons, New York, 1988.

CHAPTER 5

Theoretical investigation of effective optical characteristics of a one-dimensional periodic structure consisting of TiO_2 and SiO_2 materials with nanocomposite of silver nanoparticles (Ag-NPs) in the host E7 liquid crystal

CHAPTER 5

Theoretical investigation of effective optical characteristics of a one-dimensional periodic structure consisting of TiO_2 and SiO_2 materials with nanocomposite of silver nanoparticles (Ag-NPs) in the host E7 liquid crystal

5.1 Introduction

The birefringent materials show interesting optical properties depending on the refractive indices of the material and such materials also show variation in optical characteristics with exterior parameters like voltage, electric field, magnetic field, temperature, etc. The optical materials of birefringent materials can be investigated by the 4x4 matrix method. As an example, the 4x4 matrix method is used to calculate the optical transmission of electromagnetic waves (EMWs) in liquid crystals (LC). LCs show variation of orientation angle from 0^o to 90^o, therefore the 2x2 matrix method can be used to study the optical transmissions of LCs by considering 0^o and 90^o orientation of the molecules [1]. The dielectric properties and orientation angles of LC molecules are affected by doping materials in the LC, therefore, the optical features of LC embedded periodic structure also can be tuned with doping materials in the LC layer. The dielectric function of LC-based nanocomposite is also affected by the nature of doping elements; spherical, cubic, spheroid nanoparticles, etc. So, the dielectric characteristics of nanocomposite (NC) of E7 LC with spherical silver nanoparticles are studied at different radii, filling fractions of NPs and orientations, temperatures of LCs by using the Maxwell-Garnett model. The dielectric nature of LC nanocomposite is affected by the variation of filling fractions of NPs through surface plasmon resonance (SPR). The optical transmission and absorption characteristics of one-dimensional periodic structure (1-DPS) of TiO_2 and SiO_2 materials with NC defect layers; $(TiO_2|SiO_2)^m|NC|(TiO_2|SiO_2)^m$ with m=5, 3 at two orientation (0^o, 90^o) of LC molecules are investigated by TMM. The defect mode transmissions of 1-DPS are studied at two different orientations (0^o, 90^o) of LC with for different size of NPs.

The absorption properties of 1-DPS are also investigated at considered LC orientations and different radii of NPs.

A unique kind of optically periodic medium, photonic crystal (PC) contains alternating dielectric layers in different dimensions with periodic variation of dielectric functions or refractive indices. Depending on the periodic variation of refractive indices, PCs are divided into categories; one-dimensional photonic crystal (1-DPC), two-dimensional photonic crystal (2-DPC), and three-dimensional photonic crystal (3-DPC). PCs are a fascinating optical medium and exhibit photonic band gap (PBG) regions in the transmission bands. The PBG regions are the range of finite frequencies or wavelengths which are not allowed to propagate in the PCs and hence periodic materials can control the transmission of EMW. PCs have various applications due to exhibiting unusual characteristics in many optical devices; omni-directional reflectors, mirrors, optical filters, switch, and so on [1-12]. Typically, reflector and filter applications depend on the omni-directional characteristics (reflection or transmission) of PCs. PCs containing metallic layers or metallic photonic crystals (MPCs) can be used in optical devices that rely on absorption characteristics as microwave absorbers or sensors, etc. [13-21]. The nonlinear characteristics of nanocomposite based on silver nanoparticles have been described experimentally and led to the conclusion that the controlled nonlinear optical responses were very useful in nonlinear optical applications [22].

To obtain the tunability of PBG in the photonic crystals (PCs), the dielectric material is used as a defect layer in the PCs which produces tunable defect mode in transmission spectra. The transmission of defect mode depends on the optical constant of the defect layer in the 1-DPS. As a defect layer of liquid crystal (LC) in 1-DPS, such defective 1-DPS is a very useful material that gives the tunable transmissions of defect modes in the PBG region with the orientation of LC molecules. The anisotropic organic material LC shows a transitional phase between pure liquid and crystalline solid; LC has both flow and crystalline properties. They also have external field-dependent ordinary and extraordinary dielectric indices; therefore, LCs based 1-DPS exhibit tunable transmissions with defect mode. The direction-dependent transmissions of LCs as well as other anisotropic materials are very applicable in various nonlinear devices [20-22]. Moreover, the dielectric indices of LC change with the variation of temperature and applied electric field, hence the optical responses of

LC-based PCs could be regulated by temperature as well as the applied electric field. The tunable behavior of PCs was theoretically explained by Busch et al. [23] using inverse opal LC coating and experimentally performed by Yoshino et al. [24]. LC-based PCs are very convenient in tunable optical applications depending on the orientation of LC molecules [25-38]. The optical properties on LC rely on its tensor dielectric function consists of extraordinary and ordinary indices $(\varepsilon_{\parallel}, \varepsilon_{\perp})$ and anisotropy (ε_a) of the material which can be expressed in matrix form as equation 5.1 [39-42];

$$\tilde{\varepsilon} = \begin{pmatrix} \varepsilon_{\perp} + \varepsilon_a \sin^2\phi & 0 & \varepsilon_a \sin\phi\cos\phi \\ 0 & \varepsilon_{\perp} & 0 \\ \varepsilon_a \sin\phi\cos\phi & 0 & \varepsilon_{\perp} + \varepsilon_a \cos^2\phi \end{pmatrix} \tag{5.1}$$

The tensor dielectric function of LC also depends on the orientation (ϕ) of molecules and has a 3x3 matrix form; such matrix obtains a diagonalized form only for 0^o or 90^o orientation (ϕ) of molecules. Considering 0^o or 90^o orientation of LC molecules, the transfer matrix method (TMM) [43] could be applied to investigate the optical characteristics of LCs.

As we know that the dielectric properties of LCs are affected by doping nanoparticle and temperature, therefore, the nanocomposite based on spherical silver nanoparticles with the host E7 LC has obtained tunable characteristics. As a defect layer in PCs is inserted, such nanocomposite (NC) layers produce tunable PBGs in the transmission spectra because of variation in the dielectric function of NC due to the orientation of LC molecules. Additionally, the optical transmissions of PC are also affected with varying radii and filling fractions of nanoparticles (NPs) which are arbitrarily doped in LC [44-48]. The modified dielectric permittivity of NC containing the dispersion of Ag-NPs in the host E7 LC has been calculated by the Maxwell-Garnett method [49-51]. The optical characteristics of 1-DPC with defect layer of nanocomposite (NC) investigated at different radii and filling fractions of NPs with different temperatures and orientations of the molecules [52].

In this chapter, the effective dielectric characteristics of NC based on silver nanoparticles (Ag-NPs) mixed in E7 LC are investigated at different temperatures. The transmission of 1-DPS of TiO_2 and SiO_2 with a defect layer of nanocomposite (NC) are also studied at different temperatures and filling fractions. To design a

nanocomposite, we have considered the inclusion of Ag-NPs in host E7 LC with dissimilar radii and filling fractions of NPs at 0^o and 90^o molecular orientations of LC. The used E7 LC is the mixture of different LCs: 8OCB ($C_{21}H_{25}NO$), 7CB ($C_{20}H_{23}N$), 5CB ($C_{18}H_{19}N$) and 5CT ($C_{24}H_{23}N$) [53]. The refractive indices of E7 LC depend on the temperature and the wavelength of incident waves [54]. The dielectric properties of NC (E7 LC+Ag-NPs) and optical characteristic of defective 1-DPS $(TiO_2|SiO_2)^m|NC|(TiO_2|SiO_2)^m$ with m=5,3 are investigated at different radii, filling fractions of Ag-NPs as well as orientations of LC molecules. Depending on the radii, filling fractions of Ag-NPs in NC, 1-DPS tunable transmission with defect modes are investigated which can be used in various tunable devices: filters, detectors, switches, sensors, wavelength selectors, etc.

5.2 Theoretical modeling

The schematic diagram of considered 1-DPS of TiO_2 and SiO_2 materials with NC of Ag-NPs in host E7 LC as defect layer, $(TiO_2|SiO_2)^m|NC|(TiO_2|SiO_2)^m$, with m=5, 3, is shown in figure 5.1.

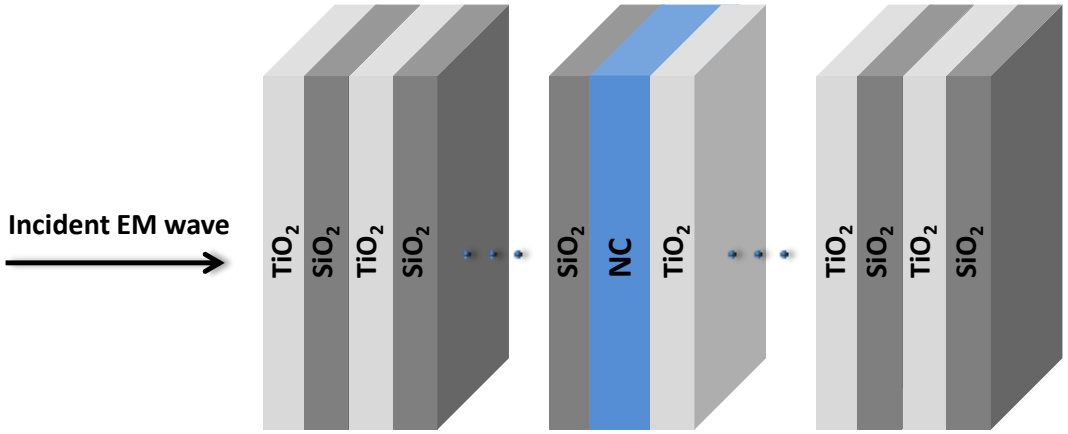

Figure 5.1: Schematic diagram of 1-DPS of TiO_2 and SiO_2 materials with NC as defect layer of Ag-NPs in E7 LC; $(TiO_2|SiO_2)^m|NC|(TiO_2|SiO_2)^m$ with m=5,3.

To explain the optical properties, the refractive indices, and thicknesses of TiO_2, SiO_2 materials are taken as 2.4, 1.5 and 91.6nm, 56.2nm, respectively in the 1-DPS. The transmission characteristics of the 1-DPS with the NC defect layer are calculated through the transfer matrix method (TMM) [43] as discussed in chapter 2. The temperature-dependent extraordinary (n_e) and ordinary (n_o) refractive indices of E7 LC are given as;

$$n_e(T) = A - BT + \frac{2(\Delta n)_o}{3}\left(1 - \frac{T}{T_C}\right)^{\beta} \tag{5.2}$$

$$n_o(T) = A - BT - \frac{(\Delta n)_o}{3}\left(1 - \frac{T}{T_C}\right)^{\beta} \tag{5.3}$$

The values of presented constant parameters A, B, β, $(\Delta n)_o$, T_C of LC are $1.7230, 5.24\times10^{-4}, 0.3485, 0.2542$, and 330K, respectively at the wavelength of 1500nm [53, 54]. Both dielectric indices ($\varepsilon_{\parallel}, \varepsilon_{\perp}$) of E7 LC are easily calculated by taking the square of refractive indices (n_e, n_o) represented by equations 5.2 and 5.3, respectively.

The dielectric function of NC consisting of silver nanoparticles in E7 LC is determined by Maxwell-Garnett formulation [49-51]. The silver nanoparticles of different radii with different filling fractions are arbitrarily mixed in the E7 LC. Thus, the effective dielectric function of NC is calculated using equation 5.4 as;

$$\varepsilon_{eff} = \frac{2\varepsilon_{LC} f(\varepsilon_m - \varepsilon_{LC}) + \varepsilon_{LC}(\varepsilon_m + 2\varepsilon_{LC})}{2\varepsilon_{LC} + \varepsilon_m + f(\varepsilon_{LC} - \varepsilon_m)} \tag{5.4}$$

where ε_{LC} = dielectric function of LC, ε_m = dielectric permittivity, and f=filling fraction of Ag-NPs in the host LC. The dielectric permittivity of the spherical Ag-NPs is calculated with Drude model as;

$$\varepsilon_m = \varepsilon_0 - \frac{{\omega_p}^2}{\omega^2 + i\omega\eta} \tag{5.5}$$

where ω_p = plasmon frequency, ε_0 = relative dielectric permittivity, and η = damping frequency of Ag-NPs. The damping frequency is dependent on the Ag-NP size and the electron velocity (ν_f) at Fermi-energy as equation 5.6.

$$\eta(r) = \eta_0 + \frac{\nu_f}{r} \tag{5.6}$$

where, η_0 = decay constant acquired by electrons through electron-phonons and electron-electron scatterings etc.

To study the effect of size and filling fraction of NPs, the transmission properties of 1-DPS of TiO_2 and SiO_2 materials with NC defect layer, $(TiO_2|SiO_2)^m|NC|(TiO_2|SiO_2)^m$

with m=5, 3 have been calculated by transfer matrix method (TMM) [43]. The considered 1-DPS also shows the absorption properties due to silver nanoparticles which supports the surface plasmon resonance (SPR) effect in the material.

5.3 Results and discussion

This segment is separated into three parts; the first part describes the dielectric properties of LC and NC at different radii, filling fraction of NPs, temperature, and orientation of LC. The second and third parts provide the optical properties of 1-DPS $(TiO_2|SiO_2)^m|NC|(TiO_2|SiO_2)^m$ with m=5 and 3 at different parameters of the NC layer, respectively.

5.3.1 Dielectric behavior of LC and NC with the variation of filling fractions, radii of NPs at different temperatures, orientations of LC

As explained earlier, refractive indices of LC depend on the temperature; the behavior of E7 LC refractive indices is shown in figure 5.2. The extraordinary and ordinary refractive indices of E7 LC increase and decrease, respectively and attain the value 1.55 at 330K temperature. At 330K temperature, LC is converted into isotropic phase and both indices follow the same behavior and their values constantly decrease with higher temperatures.

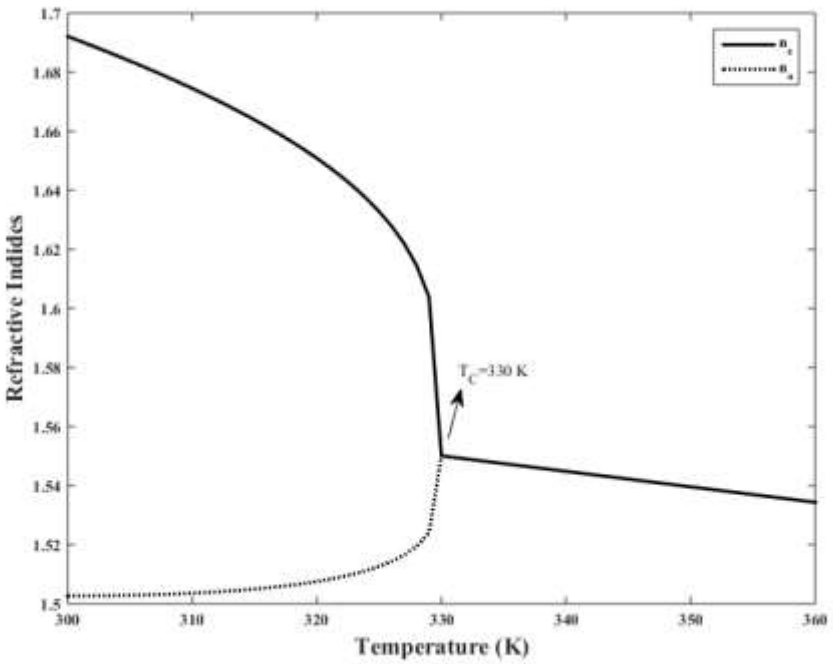

Figure 5.2: Variation of refractive indices (n_e, n_o) of E7 LC with temperature (K).

Further, we have studied the effective dielectric function of the NC designed of E7 LC with spherical NPs of 5nm radius with varying filling fractions (f) in NC. The dielectric permittivity of LC varies with temperature; therefore, the effective dielectric function of NC (LC+Ag-NPs) also changes with temperature. Hence, the dielectric function of NC has deliberated at different temperatures viz. 300K and 329K. The real values of effective dielectric function are positive and negative for 300K and 329K; however, the imaginary values have positive magnitude only. The deviation parallel and perpendicular components (ordinary and extraordinary) of NC are described at the considered temperature in figures 5.3 and 5.4. In designing of NC, the plasmon frequency ω_p and decay constant for spherical Ag-NPs are taken as $2\pi \times 2.17 \times 10^{15}$ Hz and $2\rho \acute{} 4.8 \acute{} 10^{12}$ Hz respectively with $\varepsilon_0 = 5$ [47-49]

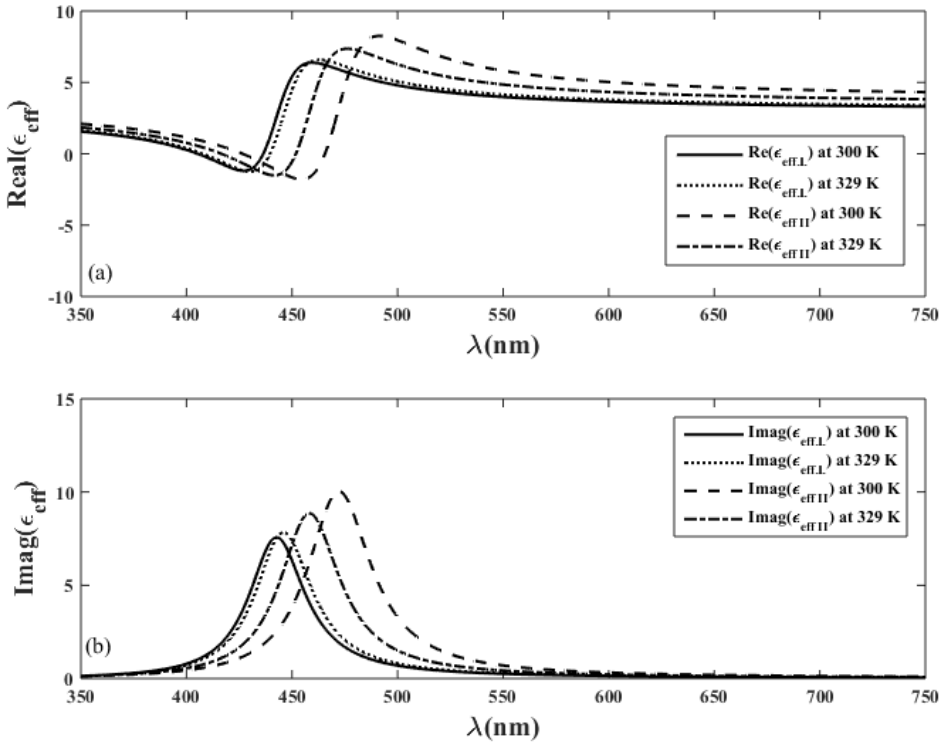

Figure 5.3: Variation of real and imaginary parts of perpendicular and parallel components of the effective dielectric function of NC at 300K, 329K temperature, and 0.1 filling fraction.

Essentially, the LC molecules maintain the 0^o director angle for the intensity lower than the threshold value, Freedericksz transition intensity, so, perpendicular component ($\varepsilon_\perp$) or ordinary dielectric constant of NC is responsible for optical

characteristics of NC embedded PCs. The LC molecules show switching for the intensity equal to or higher than the Freedericksz transition intensity and molecules attain the maximum orientation 90^o. At this transition in LCs, the optical properties are also affected by the extraordinary dielectric permittivity of LC. The effective dielectric responses of NC get moved to higher values at high temperatures as represented in figure 5.3.

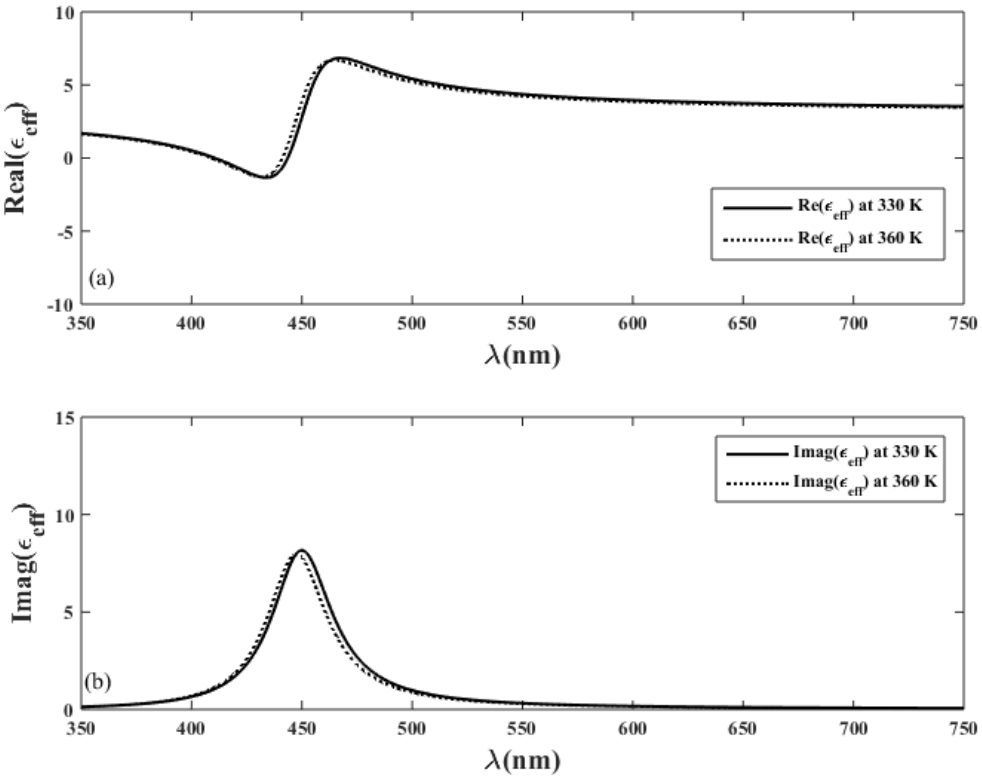

Figure 5.4: Variation of real and imaginary parts of the effective dielectric function of NC at 330K, 360K temperatures.

The anisotropic behavior of E7 LC changes into isotropic at phase transition temperature 330K. The ordinary and extraordinary dielectric indices of the NC attain the same value at phase transition temperature 330K. The behavior of the effective dielectric function of NC at 330K and 360K temperature are revealed in figure 5.4.

The variation of effective dielectric functions of NC is described at dissimilar filling fractions and molecular orientations of LC using Maxwell-Garnett model. The effective dielectric function of NC at 0.05, 0.10, 0.15 filling fractions (f) of Ag-NPs and 0^o, 90^o director angles of the LC is described as shown in figures 5.5 and 6.6. The

filling fraction (f) modifies the dielectric function of NC and attains higher values at a higher filling fraction as shown in both figures 5.5 and 5.6. A comparative study of both perpendicular and parallel components of the dielectric function of NC at 0^o and 90^o director angle of LC is given in figure 5.7.

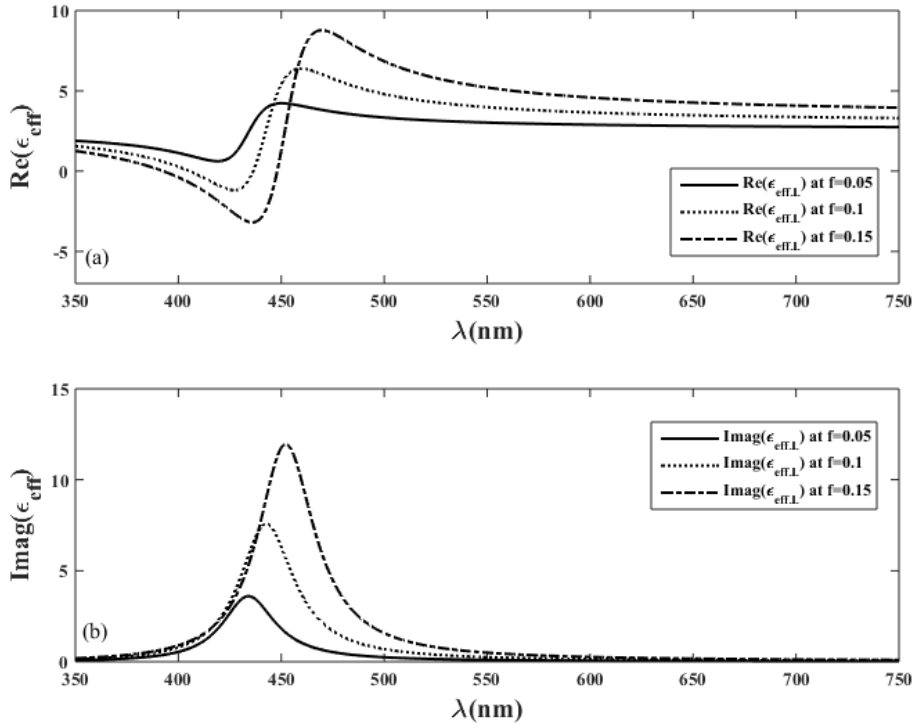

Figure 5.5: Variation of real and imaginary parts of the perpendicular component of effective dielectric functions of NC at the filling fraction: 0.05, 0.10, and 0.15.

The effective dielectric function of NC is designed on basis of the Maxwell-Garnett model given by equation 5.4. The different sizes of Ag-NPs result in the variation in surface plasmon resonance (SPR) through the scattering of waves and hence the effective dielectric function of NC also varies with SPR. Generally, the SPR band is the group of excitation of free electrons, and the size of NPs affects the position as well as the width of the SPR band. The SPR band becomes broader for the larger radii of the NPs because of the radiation damping effect. As the size of NPs decreases, the scattering rate increases for conduction electrons, and hence SPR exhibits a redshift that influenced the dielectric properties of NC. With the size variation, temperature also affects the SPR that produces extra shift and broadening in the band [55, 56].

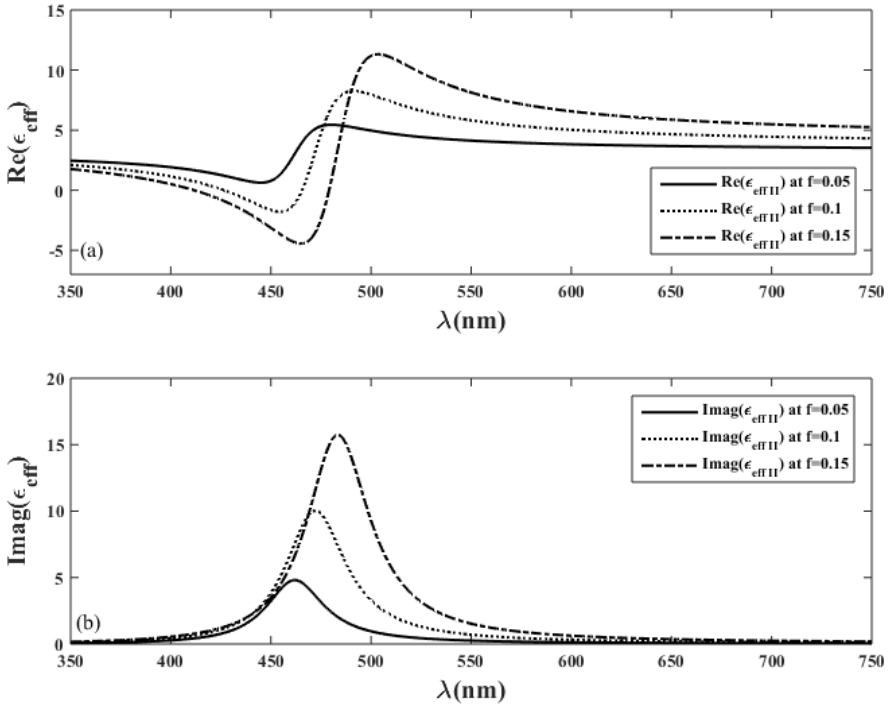

Figure 5.6: Variation of real and imaginary parts of the parallel component of effective dielectric functions of NC at the filling fraction: 0.05, 0.10, and 0.15.

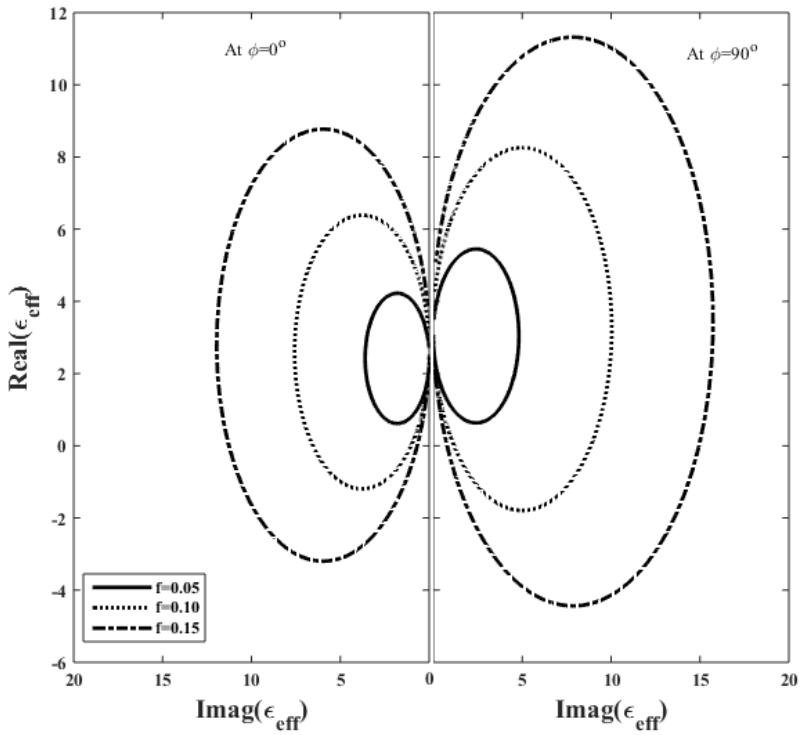

Figure 5.7: Comparative diagram of real values with imaginary values of the effective dielectric function of NC at considered filling fractions.

The real and imaginary parts of NC dielectric functions at 3nm, 5nm, 7nm, and 9nm radius of Ag-NPs for 0^o and 90^o orientations of molecules are shown in figures 5.8 and 5.9, respectively. The imaginary and real portions of effective dielectric functions show symmetric and asymmetric nature, respectively having positive values. The real part of the dielectric function first decreases with wavelength and then increases, while the imaginary part increases and then decreases. The values of both parts are increased with radii of nanoparticles in the NC considering 0^o and 90^o orientations of molecules.

A feasible variation in both parts of the effective dielectric functions of NC is found between 350nm to 550nm wavelengths. The obtained outcomes support the SPR modification through the radii variation of NPs in the NC layer. Still, the effective dielectric permittivity of NC has a higher value at 90^o orientation angle than at 0^o orientation angle of LC. The observed results suggest that the SPR is also related to the molecular orientation of E7 LC which adjusts the effective dielectric index of NC. By study the refractive indices with SPR, the interaction of Ag-NPs with LC also can be investigated fundamentally.

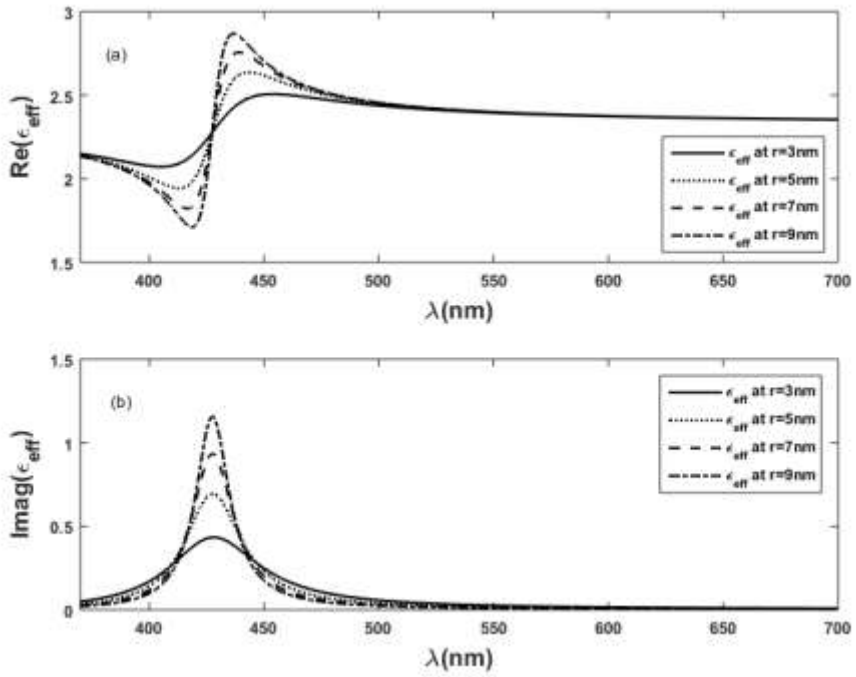

Figure 5.8: Variation of the effective dielectric function of NC with wavelength (a) real values (b) imaginary values at 0^o molecular orientation and radii of Ag-NPs: 3nm, 5nm, 7nm, and 9nm.

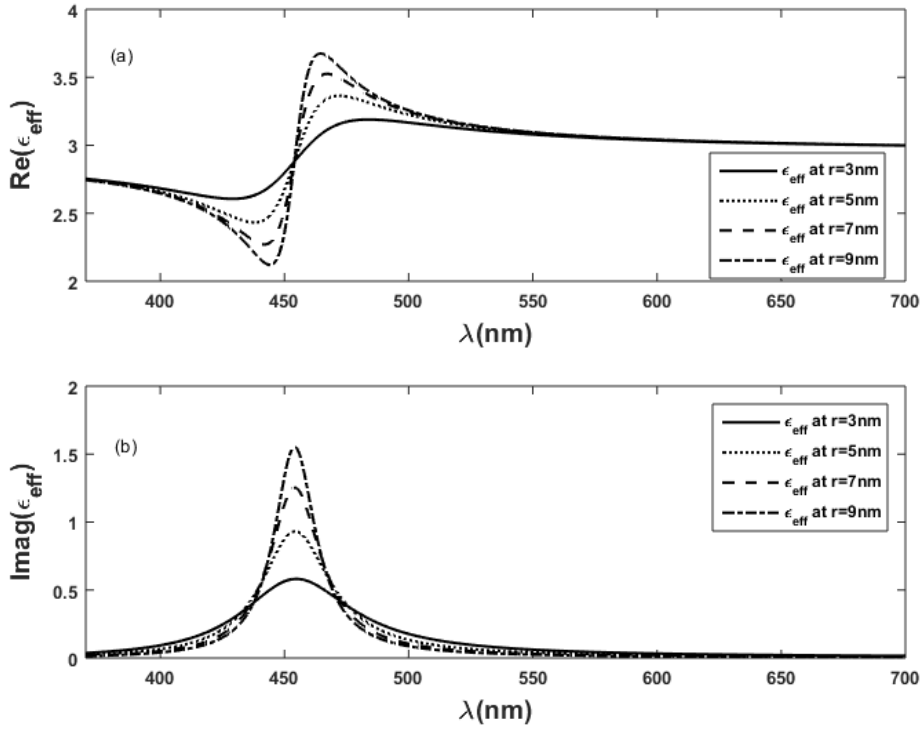

Figure 5.9: Variation of the effective dielectric function of NC with wavelength (a) real values (b) imaginary values at 90^o molecular orientation and radii of Ag-NPs: 3nm, 5nm, 7nm, and 9nm.

To study the interaction of Ag-NPs in an alternative way, a comparative investigation of imaginary and real values of effective dielectric functions has been made at different radii of NPs with 0^o and 90^o orientations of molecules as shown in figure 5.10 and 5.11. The zones among curves of real components of effective permittivity increase with radii of NPs considering both orientation angles but the differences between the curves decrease as shown in figure 5.10. After a 7nm radius of nanoparticles, the curves of real components also show additional loops which approach the symmetric nature of dielectric function at 7nm radii of NPs. Similarly, the imaginary parts also obtain comparatively higher values at a 90^o orientation angle than at 0^o orientation angle of molecules. The interaction of Ag-NPs with the orientation of molecules is improved with variable radii supporting the enhanced SPR and effective permittivity of the NC layer.

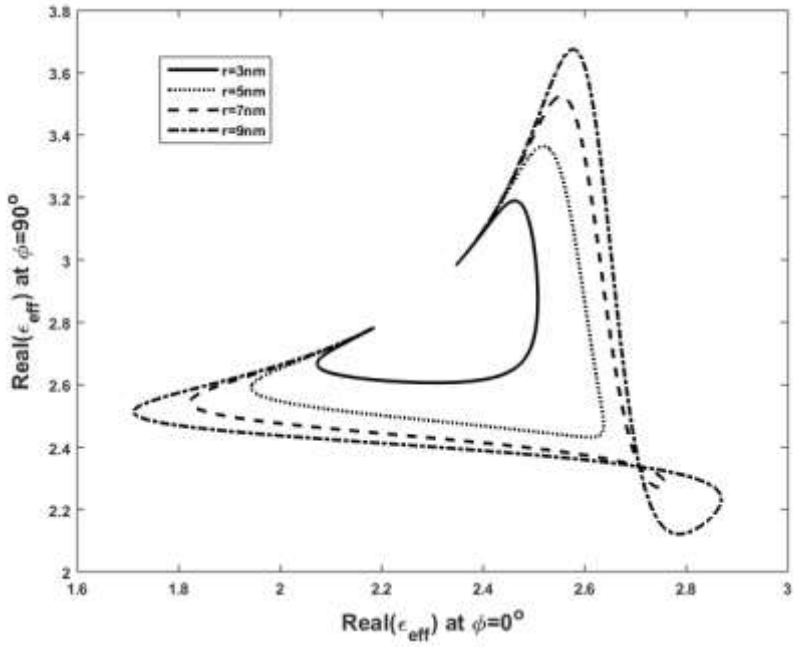

Figure 5.10: Comparative diagram of real values of the effective dielectric function at 90^o orientation angle with real values of the dielectric function at 0^o orientation angle of the NC molecules for considered radii of Ag-NPs.

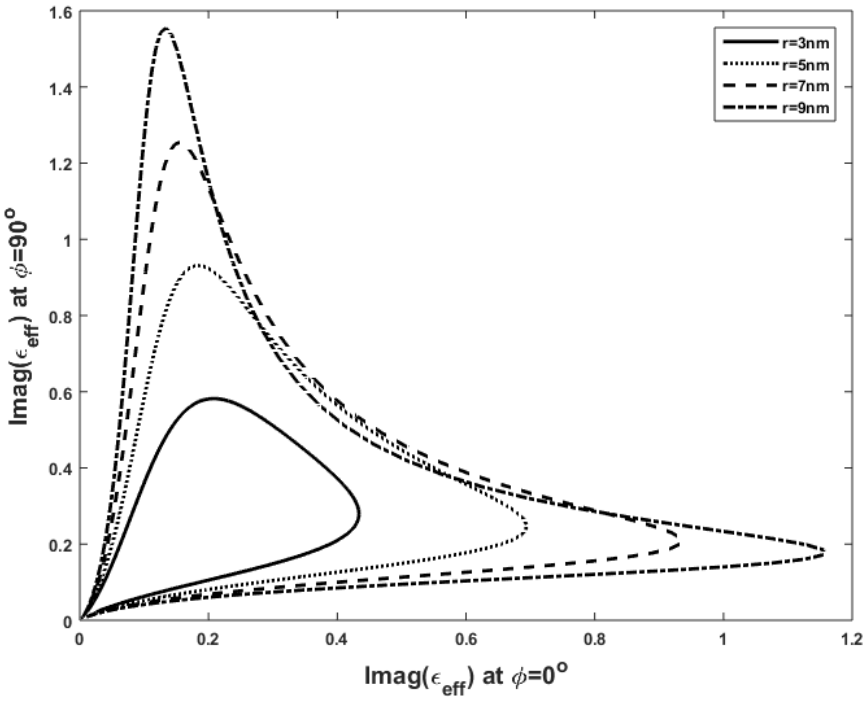

Figure 5.11: Comparative diagram of imaginary values of the effective dielectric function at 90^o orientation angle with imaginary values of the dielectric function at 0^o orientation angle of the NC molecules for considered radii of Ag-NPs.

5.3.2 Transmission and absorption characteristics of $(TiO_2|SiO_2)^5|NC|(TiO_2|SiO_2)^5$ periodic structure with the variation of radii, filling fractions of NPs, temperatures, and orientations of LCs

In this section, the optical characteristics of 1-DPS of TiO_2 and SiO_2 materials with NC (LC+Ag-NPs) defect layer are investigated using a simple transfer matrix method (TMM). To design and study the optical properties of the 1-DPS, the refractive indices, and thicknesses of TiO_2, SiO_2 materials are taken as 2.4, 1.5 and, 57.3 nm, 91.6 nm, respectively while the thickness of the NC layer is 100nm. For Ag-NPs, the values of ω_p and η_0 are equal to $2\pi\times 2.17\times 10^{15}$ Hz and $2\pi\times 4.8\times 10^{12}$ Hz, with $\varepsilon_0 = 5$ considered with varying radii and filling fractions of NPs [47-49].

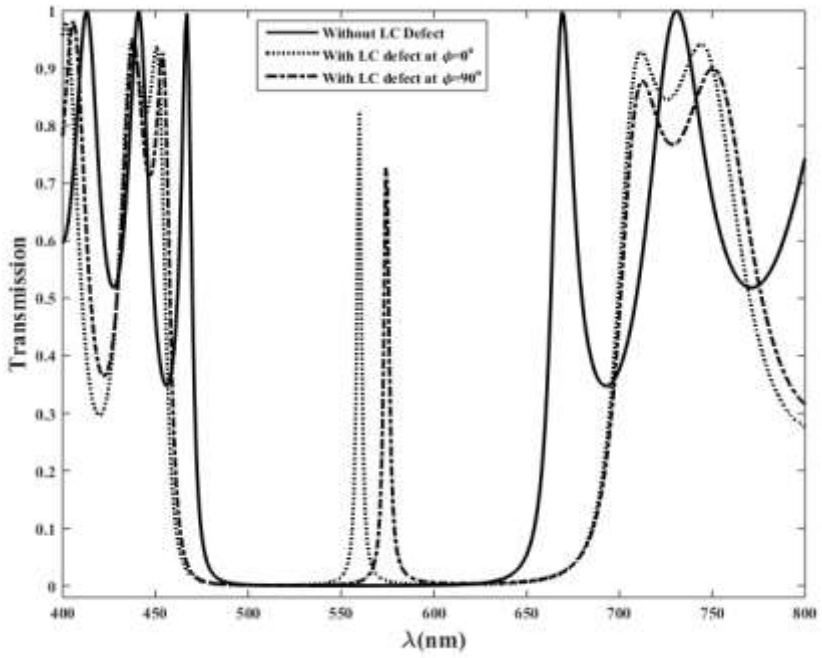

Figure 5.12: Transmission properties of 1-DPS without NLC layer (solid line) and with NLC defect layer at two molecular orientations (ϕ) of NLC (dashed line).

The transmission properties of 1-DPS consisting of TiO_2, SiO_2 materials without (solid line) and with (dashed line) defect of the LC layer are shown in figure 5.12. In absence of the LC layer as a defect in the 1-DPS, the transmission of 1-DPS exhibits a PBG region between 467nm to 669nm wavelength range. Using LC as a defect layer in 1-DPS, the obtained PBG has a defect mode at 560nm wavelength with 82.4% transmission at 0^o director angle, which is shifted towards 451nm-712nm wavelength

range. The defect mode in the PBG region is shifted to 574nm wavelength with 72% transmission at the 90^o director angle. By investigating the transmission of 1-DPS, it reveals that the obtained defect mode in PBG gets shifted to a higher wavelength considering the higher orientation (director) angle of LC. The proposed 1-DPS with the defect layer could may to design tunable optical filters, switches, and so on.

The transmissions of 1-DPS $(TiO_2|SiO_2)^5|NC|(TiO_2|SiO_2)^5$ are studied at 0.05 filling fraction of Ag-NPs considering 0^o, 90^o orientation angles, and 300K, 329K temperatures of LC as shown in figure 5.13. The silver nanoparticles (Ag-NPs) in the NC layer vary the position of defect modes as well as transmissions of 1-DPS. The observed defect mode in the PBG region exhibits a red shifting at 90^o orientation angle of LC. Due to the presence of Ag-NPs in the NC layer, 1-DPS also possesses absorption of defect mode for both molecular orientations of LC.

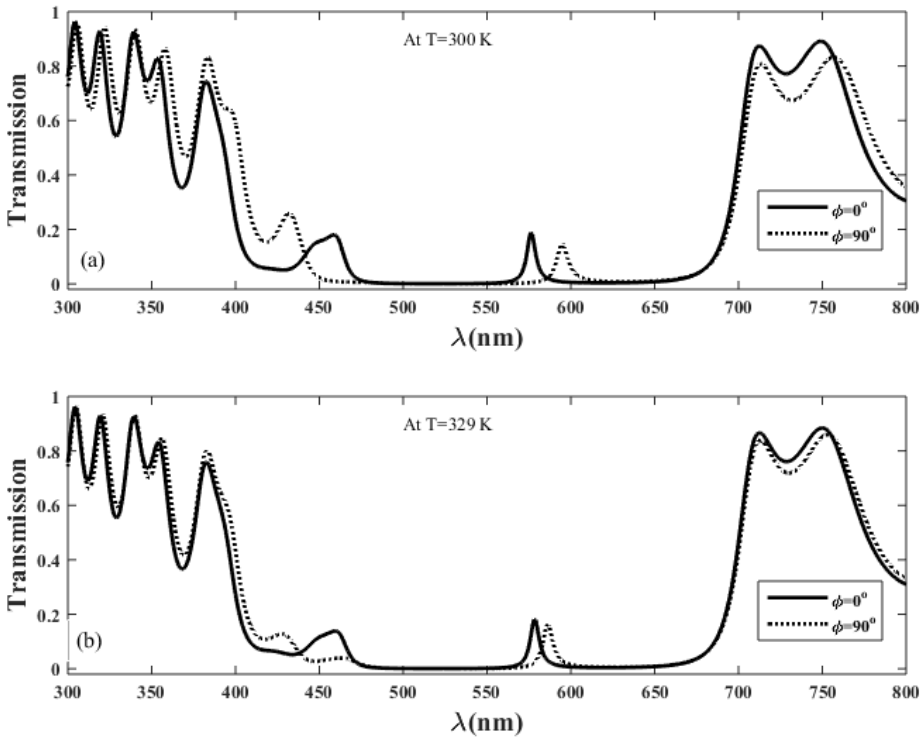

Figure 5.13: Transmission properties of 1-DPS with NC at 0^o, 90^o molecular orientations of LC for (a) T= 300K, and (b) T=329K.

The absorption properties of 1-DPS $(TiO_2|SiO_2)^5|NC|(TiO_2|SiO_2)^5$ at 0^o, 90^o orientations, and 300K, 329K temperatures are shown in figure 5.14. The maximum absorption 85.33% is found at 425nm wavelength while the defect mode absorption

wavelength has 26.74% 576nm for 0^o director angle and 300K temperature of LC. Similarly, maximum absorption at is 456nm wavelength is 80.53% and defect mode obtains 23.75% absorption at 595nm wavelenght for 90^o orientation angle and 300K temperature of LC as shown in figure 5.14(a). Same study has been made for 329K temperature and the absorption values of defect modes are slightly shifted for 329K temperature. Figure 5.14(b) reveals that the 426nm, 452nm wavelengths have 85.93%, 85.23% absorptions at 0^o, 90^o director angles of LC, respectively. Moreover, the defect mode absorptions for 579nm, 586nm wavelengths have found 25% and 24.93% at considered director angles respectively as described in figure 5.14 (b). By comparing the transmission and absorptions of defect modes for both temperatures and orientations, it has been observed that the separation of defect mode peaks at 300K temperature is greater than at 329K temperature considering 0^o and 90^o orientations of LC molecules.

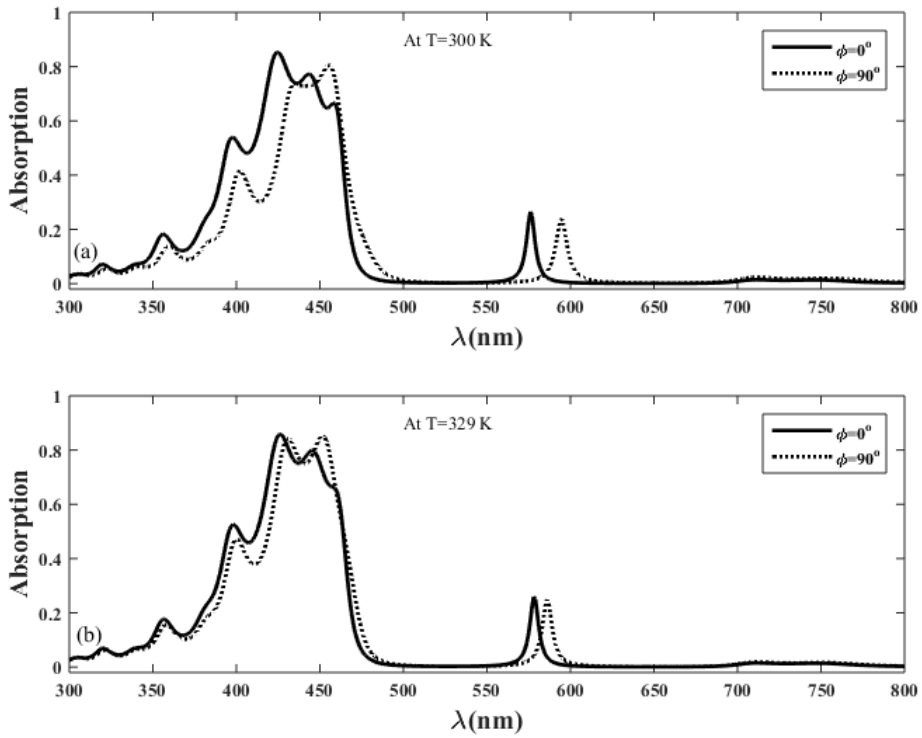

Figure 5.14: Absorption properties of 1-DPS with NC at 0^o, 90^o molecular orientations of LC for (a) T= 300K, and (b) T=329K.

Further, we have determined the optical characteristics of the 1-DPS at 330K and 360K temperatures for 0.05 filling fraction of Ag-NPs. At 330K clearing temperature,

the perpendicular and parallel components of effective dielectric function have identical values and hence the anisotropy nature of NC has vanished. As a consequence, the optical characteristics of the 1-DPS are not only varied with the orientation of the molecules but also affected the temperature. The transmission and absorption characteristics of 1-DPS $(TiO_2|SiO_2)^5|NC|(TiO_2|SiO_2)^5$ have studied at 330K and 360K temperatures as in figures 5.15 and 5.16. By analyzing figures 5.16(a) and 5.16(b), it has been found that the maximum values of absorptions for 427nm wavelength are 85.91% and 86.83% at 330K and 360K temperatures respectively. Along with maximum absorptions, defect mode absorptions for 581nm, 579nm wavelengths have found 25.71% and 25.77% at 330K, 360K temperatures of LC, respectively.

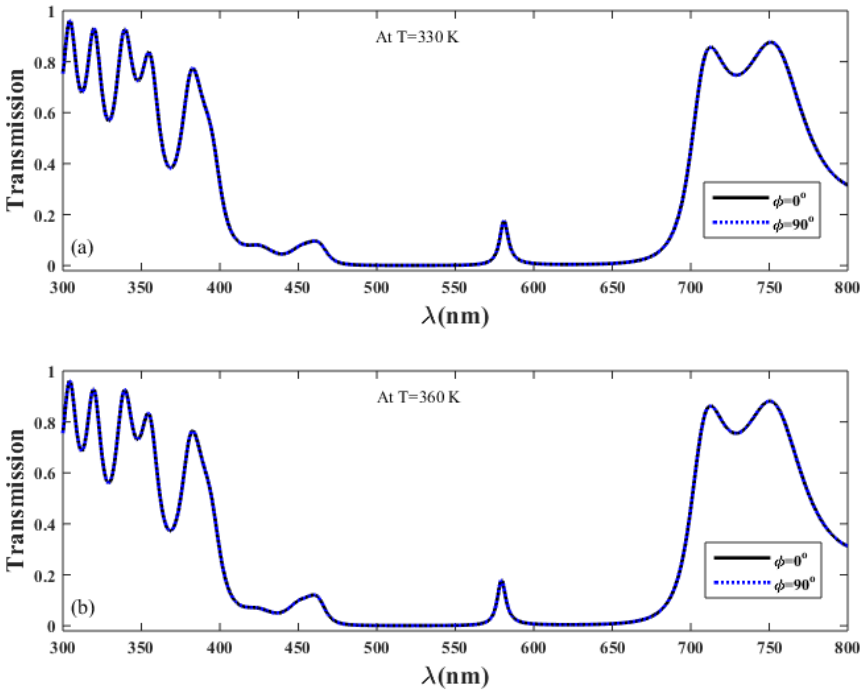

Figure 5.15: Transmission properties of 1-DPS with NC at 0^o, 90^o molecular orientation of LC for (a) T= 330K, and (b) T=360K.

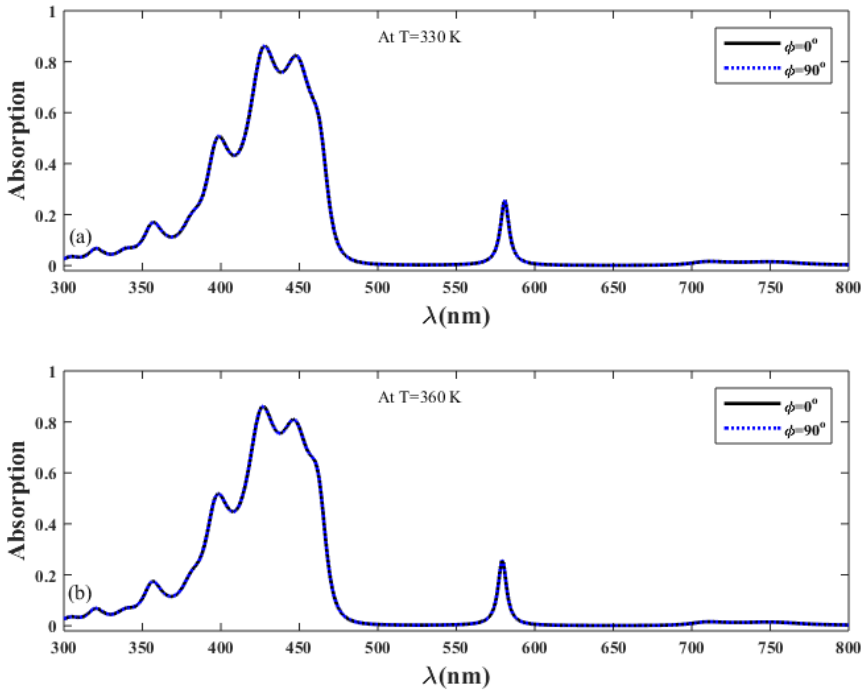

Figure 5.16: Absorption properties of 1-DPS with NC at 0^o, 90^omolecular orientation of LC for (a) T= 330K, and (b) T=360K.

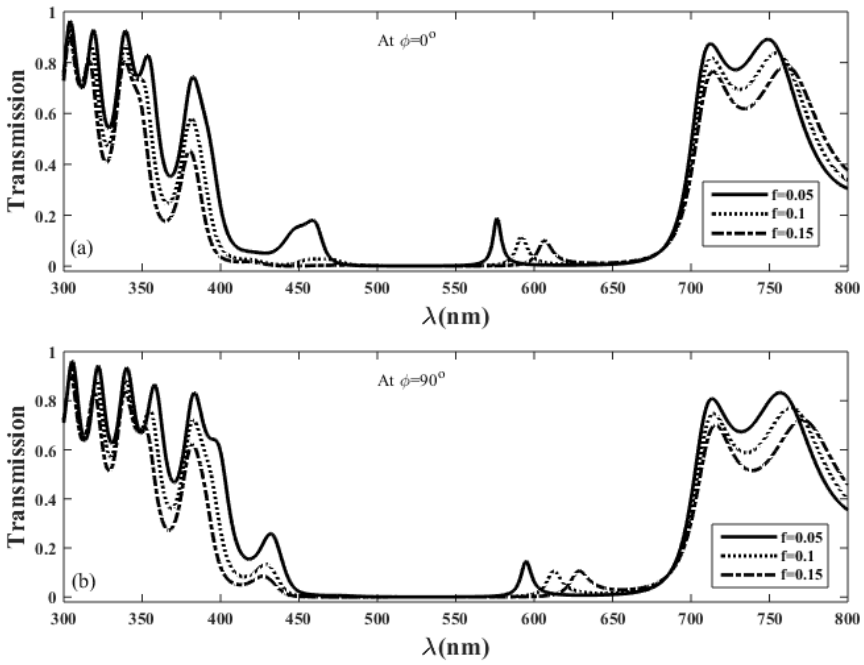

Figure 5.17: Transmission properties of 1-DPS with NC at 0.05, 0.10, and 0.15 filling fractions of Ag-NPs for (a) $\phi = 0^o$ and (b) $\phi = 90^o$.

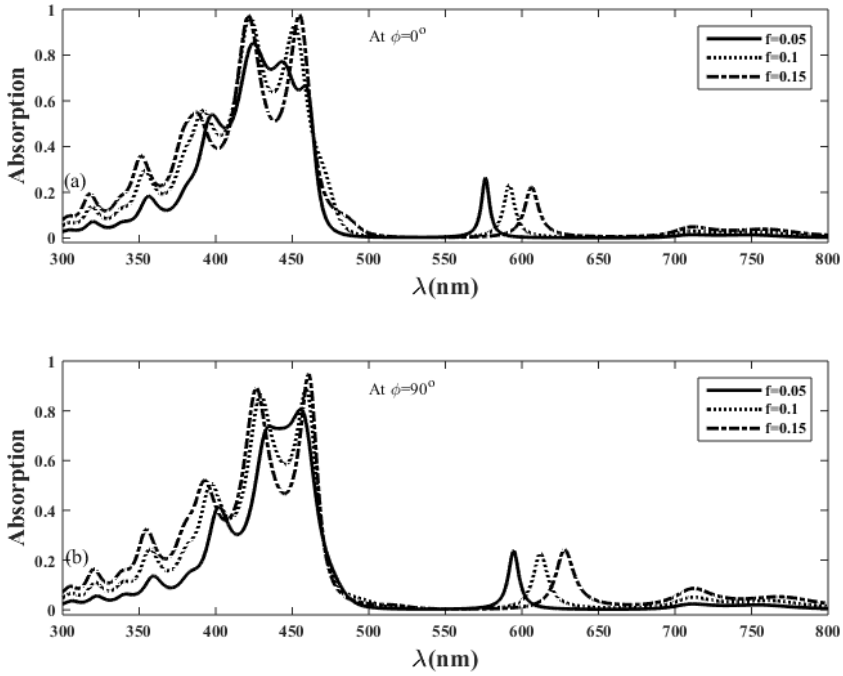

Figure 5.18: Absorption properties of 1-DPS with NC at 0.05, 0.10, and 0.15 filling fractions of Ag-NPs for (a) $\phi = 0^o$ and (b) $\phi = 90^o$.

As previously addressed, the temperature of the LC layer affects the optical characteristics of periodic structures, therefore, both transmission and absorption of 1-DPS $(TiO_2|SiO_2)^5|NC|(TiO_2|SiO_2)^5$ are studied with temperatures. The transmission properties of 1-DPS consisting of the NC layer have been described with the variation of filling fractions of NPs and director angles of LC molecules (0^o, 90^o) as shown in figure 5.17. Correspondingly, the absorption properties of the 1-DPS at different filling fractions of Ag-NPs have been shown in figure 5.18. A comparative investigation of absorptions of 1-DPS at different filling fractions is given in table 5.1.

Table 5.1: Absorption analysis of 1-DPS with NC at 0.05, 0.10, and 0.15 filling fractions of Ag-NPs.

Absorption							
Orientation angle		f=0.05		f=0.10		f=0.15	
		λ (nm)	Ab (%)	λ (nm)	Ab (%)	λ (nm)	Ab (%)
ϕ =0^o	Defect Peak	576	25.47	592	23.35	606	22.27
	First Max. Value	425	85.33	422	97.24	422	97.07

	Second Max. Value	425	85.33	451	92.78	455	97.73
ϕ =90^o	Defect Peak	595	23.35	612	22.67	628	24.22
	First Max. Value	456	84.74	430	86.22	427	89.10
	Second Max. Value	434	73.56	451	88.69	461	94.88

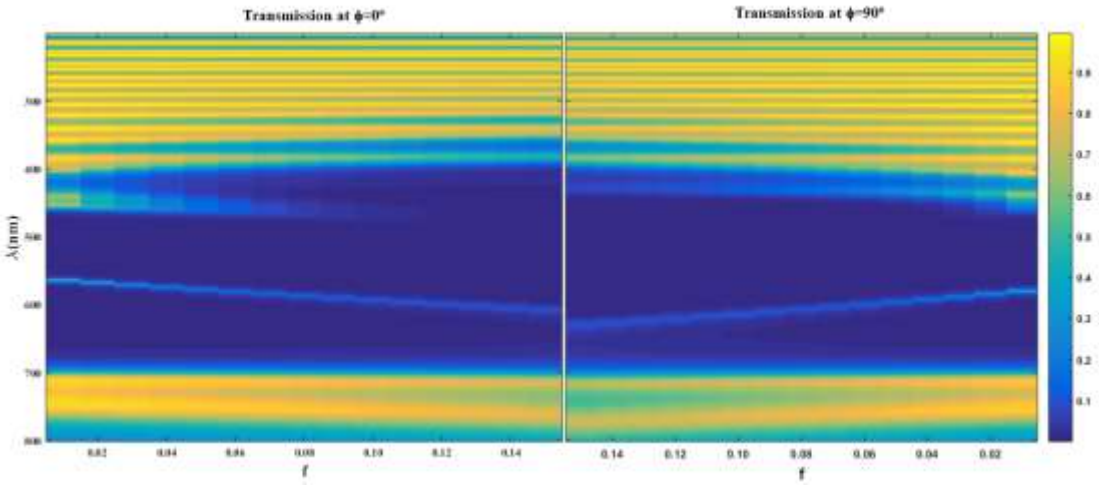

Figure 5.19: Comparative diagram of the transmission of 1-DPS consisting of NC defect layer with the variation of filling fractions at 0^o, 90^o orientations of LC molecules.

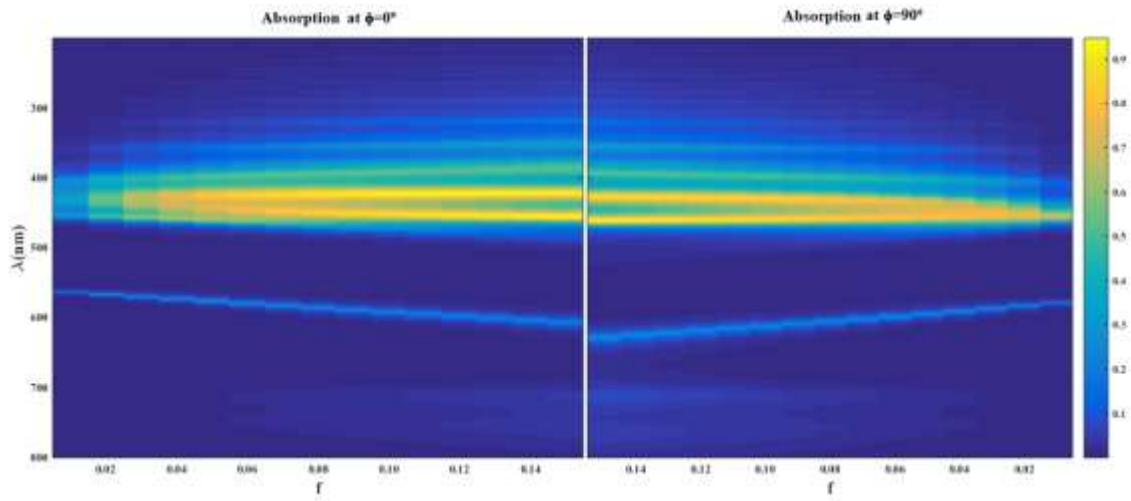

Figure 5.20: Comparative diagram of absorption of 1-DPS consisting of NC defect layer with the variation of filling fractions at 0^o, 90^o orientations of LC molecules.

The optical properties (transmission and absorption) of the considered 1-DPS are investigated at two different possible orientation angles (0^o and 90^o) of LC; before and after the Freedericksz transition intensity in the LC cell. The comparative diagram of transmissions and absorptions considering both possible orientations of LC with the variation of filling fractions have been given in figures 5.19 and 5.20. The diagrams reveal that the transmission and absorption are significantly affected by the orientations of molecules and filling fractions of NPs in the host E7 LC.

5.3.3 Transmission and absorption properties of $(TiO_2|SiO_2)^3|NC|(TiO_2|SiO_2)^3$ periodic structure with the variation of radii of Ag-NPs, temperatures, and orientations of LCs

The optical properties (transmission and absorption) of 1-DPS of the TiO_2/SiO_2 materials with nanocomposite (NC) defect layer; $(TiO_2|SiO_2)^3|NC|(TiO_2|SiO_2)^3$, have calculated by transfer matrix method (TMM). The nanocomposite layer is made of E7 LC doped with spherical silver nanoparticles (Ag-NPs) of different radii. The transmission properties along with defect modes in PBG are investigated at different radii of NPs and orientations of LC molecules as represented in figures 5.21 and 5.22.

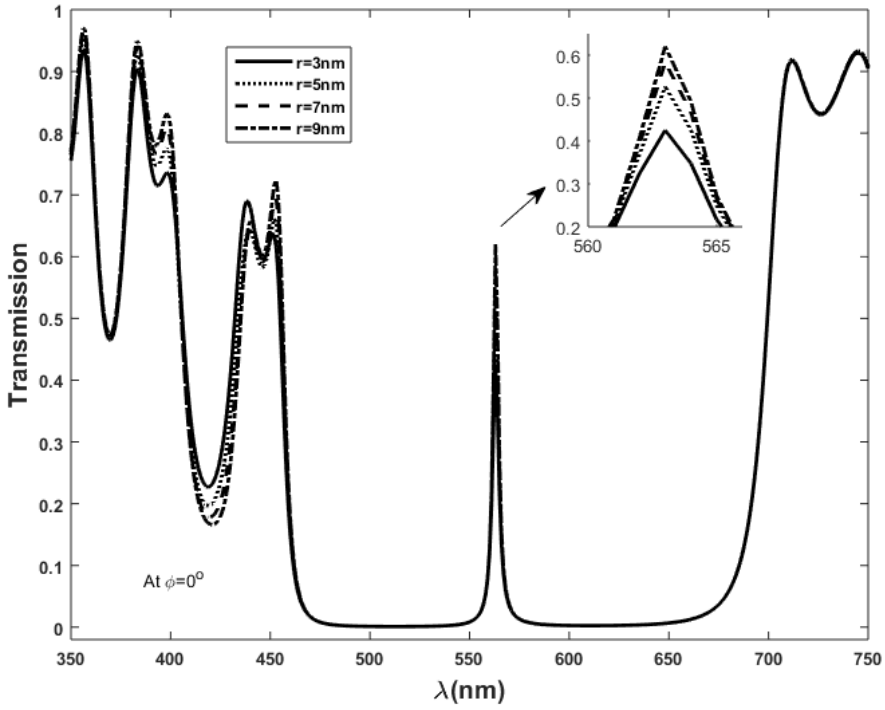

Figure 5.21: Transmission properties of 1-DPS $(TiO_2|SiO_2)^3|NC|(TiO_2|SiO_2)^3$ at 0^o orientation angle of LC molecules for varying radii of Ag-NPs.

The transmission characteristics of 1-DPS with NC defect layer are investigated at 3nm, 5nm, 7nm, and 9nm radii of Ag-NPs considering 0^o orientation angle of LC as presented in figure 5.21. The transmissions of defect mode 563nm wavelength are found 42.5%, 52.6%, 58.3%, and 62% for studied radii of NPs, respectively. Also, the transmission of wavelength at the lower edge of the band varies with the variation of radii of silver NPs. As the size of Ag-NPs increases, defect mode transmission also increased with the significant variation in the effective dielectric functions of NC through the varying size of Ag-NPs in the NC layer.

Likewise, the transmission properties of 1-DPS with NC layer at 90^o orientation angle for the same radii of NPs are given in figure 5.22. The defect modes transmission at 579nm wavelength has found 31.4 %, 41.5%, 47.6%, and 51.7% for the same radii of NPs i.e. 3nm, 5nm, 7nm, and 9nm and 90^o orientation angle of LC. The transmissions at the lower edge of the band show some fluctuations with the variation of radii of NPs and it also has found lower values at 90^o orientation angle in comparison to at 0^o molecular orientation of LC.

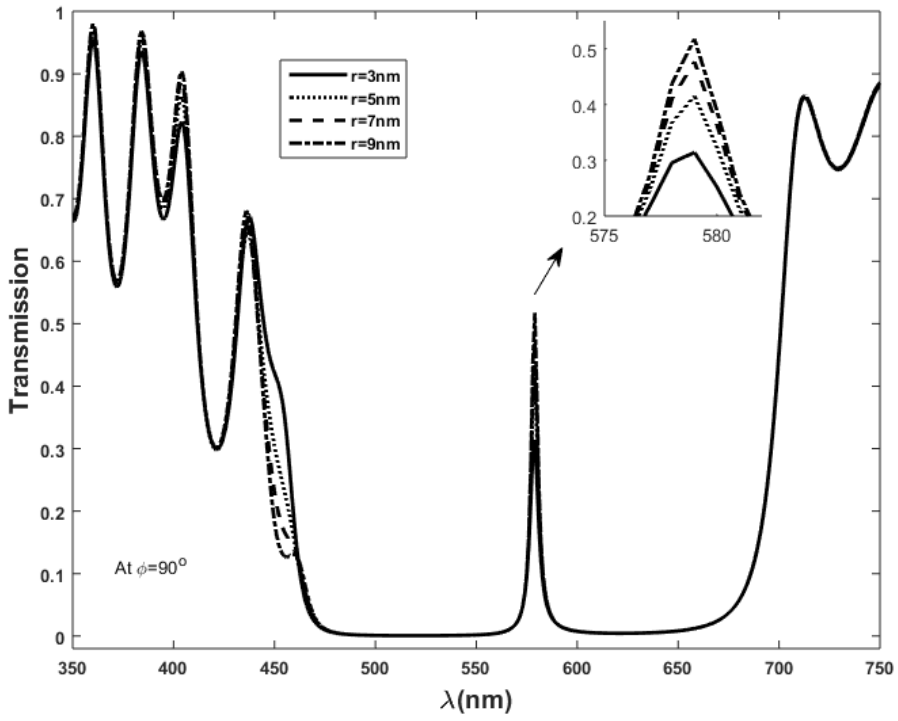

Figure 5.22: Transmission properties of 1-DPS $(TiO_2|SiO_2)^3|NC|(TiO_2|SiO_2)^3$ at 90^oorientation angle of LC molecules for varying radii of Ag-NPs.

The defect mode wavelength 563nm in the PBG region gets shifted to 579nm by the change in LC orientations from 0^o to 90^o. The obtained results suggest that the transmissions of defect modes are shifted to higher wavelength but the transmission with lower values are found due to SPR through the size variation of NPs. The defect mode transmissions have higher values at 0^o orientation of LC in comparison to at 90^o orientation of LC, because of effective dielectric responses of NC possesses lower losses in the SPR interaction with the molecular orientation of LC.

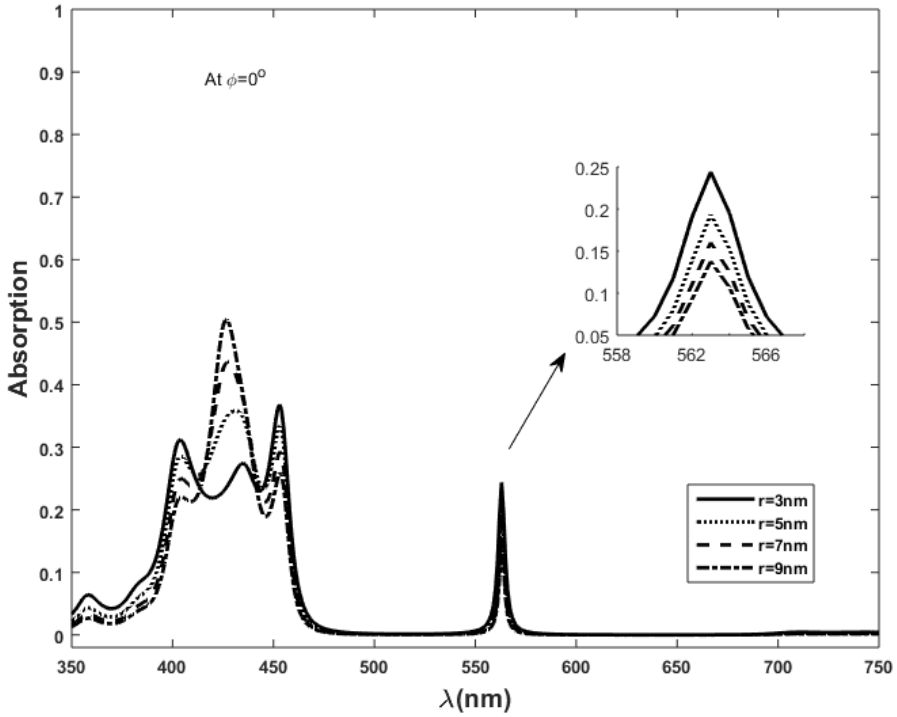

Figure 5.23: Absorption properties of 1-DPS $(TiO_2|SiO_2)^3|NC|(TiO_2|SiO_2)^3$ at 0^o molecular orientation of LC molecules for varying radii of Ag-NPs.

Along with the transmission, the absorption features of 1-DPS are also investigated at varying radii of Ag-NPs and orientations of LC molecules. Specifically, we have emphasized the absorption values at the lower end of the band because the absorption of 1-DPS has significantly changed with the NC layer in the periodic structure. The corresponding absorptions of defect mode for wavelength 563nm are 13.7%, 16%, 19.3%, and 24.3% for considered radii of Ag-NPs; 3nm, 5nm, 7nm, and 9nm, respectively and 0^o orientation of molecules as shown in figure 5.23. The lower end of the band has almost 38% absorption and its values decrease with increasing size of NPs. The analysis discloses that the improved absorption values of defect modes at 0^o

orientation angle are established with the variation of SPR effect of Ag-NPs as occurred in the NC around the 350-550nm wavelength region.

Also, the defect mode absorptions for 579nm wavelength at 90^o orientation are 15.7%, 17.2%, 20%, and 23.4% for 3nm, 5nm, 7nm, and 9nm, radii of NPs, respectively as exposed in figure 5.24. The maximum absorptions of 1-DPS with LC defect layer are found 69.6 %, 73%, and 75% for wavelengths 455nm, 454nm, and 453nm respectively at 90^o orientation of molecules. The lower end of the band has 61% absorption value which increases with the radius of Ag-NP. For 9nm radii of Ag-NP, the absorption is found about 75%, (approximate) and the absorption value gets enhanced at 90^o orientation angle around the identical wavelength because of the SPR effect of silver nanoparticles due to damping characteristics.

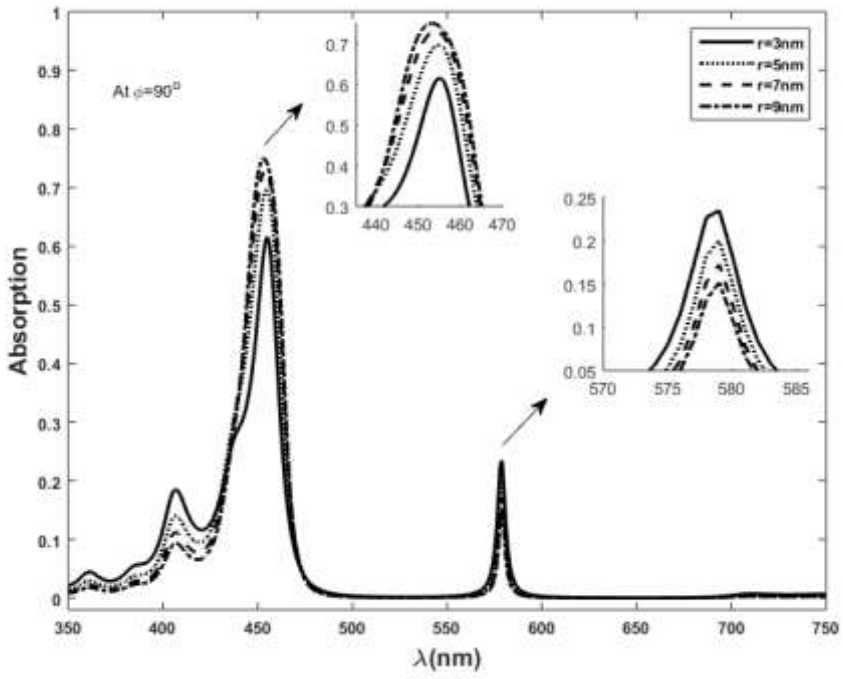

Figure 5.24: Absorption properties of 1-DPS $(TiO_2|SiO_2)^3|NC|(TiO_2|SiO_2)^3$at 90^o molecular orientation angle of LC for varying radii of Ag-NPs.

The transmission and absorption of the defective 1-DPS with NC are interconnected with the effective dielectric function through the size variation of NPs. The dielectric property of NC is related to surface plasmon resonance (SPR) by varying sizes of NPs and molecular orientations LC. As the radii of Ag-NPs increases, the effective dielectric permittivity of NC and corresponding SPR are increased due to the decreasing scattering rate of conduction electrons. The whole optical properties of 1-

DPS are tuned with size variation of NPs which considerably alters the dielectric response of the defect NC layer.

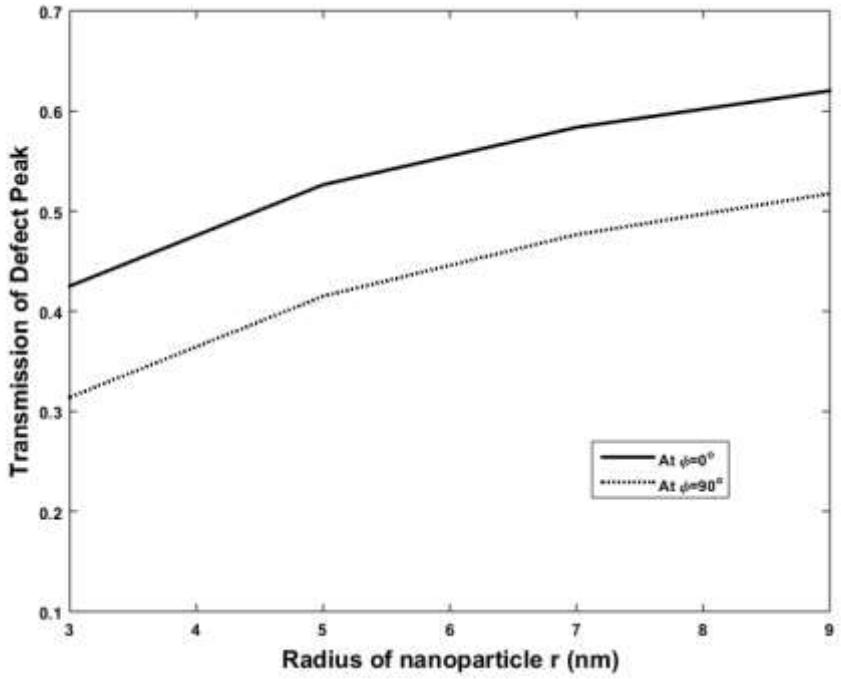

Figure 5.25: Variation of defect mode transmissions with radii of Ag-NPs in NC at 0^o (solid), 90^o (dash) orientations of LC molecules.

We have previously defined the transmission and absorption characteristics of 1-DPS with the variation of radii of NPs for both 0^o and 90^oorientation angles. Next, we have investigated the deviation in transmission and absorption values of defect mode wavelength obtained at 0^o and 90^o molecular orientations with the radius of Ag-NPs which are displayed as figures 5.25 and 5.26. An important conclusion from the figure 5.10 is that the transmission of defect mode peak is increased with radii of Ag-NPs in NC due to having a significant modified dielectric function with nanoparticles. The transmission continuously increases with Ag-NPs size but absorption decreases with increasing Ag-NPs size. The absorption values of defect peaks for both 0^o and 90^o orientations of molecules are identical at 4.2nm radius of nanoparticles as shown in figure 5.26. The orientation angle 0^o of the molecules shows comparatively lower value of absorption than the orientation angle 90^o for the larger size of the Ag-NPs in the NC layer.

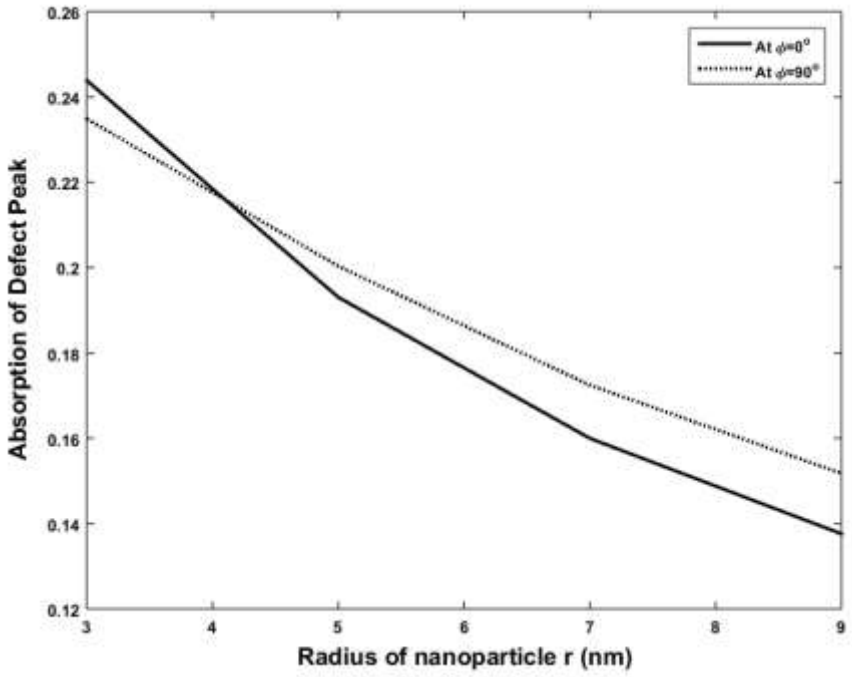

Figure 5.26: Variation of defect mode absorptions with the radii of Ag-NPs in NC at 0^o (solid), 90^o (solid) orientations of LC molecules.

5.4. Conclusion

In this chapter, we have explored the effective dielectric functions of the NC layer consists of silver nanoparticles (Ag-NPs) in the host E7 LC by the Maxwell-Garnett model at different radii, filling fractions (f) of Ag-NPs and molecular orientations of LCs. The study suggests that the surface plasmon resonance (SPR) of Ag-NPs is inter-connected with parallel/perpendicular constituents of the effective dielectric functions (ordinary/extraordinary dielectric constants) of the NC with the variation of NPs sizes at distinct temperatures and molecular orientations of LCs. The defect mode in the PBG region gets also shifted to a higher wavelength for the high value of the filling fraction of Ag-NPs in the NC defect layer. The variation in temperatures leads to modification in the dielectric functions which regulate the tunability of defect modes in PBG regions. By analyzing the transmissions and absorptions properties of considered 1-DPS with NC defect layer, $(TiO_2|SiO_2)^m|NC|(TiO_2|SiO_2)^m$ with m=5,3; this has suggested that defective NC in the periodic structures may be applicable to design tunable devices due to significant changes in the dielectric function of NC layer by variable radii and filling fractions of Ag-NPs with different orientations of LC molecules. Along with filling fractions and radii of Ag-NPs, the temperature of

LC is also varied the dielectric functions of NC and the defect mode transmission properties of 1-DPS are also varied. The transmission of defect mode wavelength in the PBG region is increased with increasing size of Ag-NPs which change the dielectric functions of NC at the constant filling fraction. Apart from the increasing transmission, absorption of defect mode is decreased with increasing Ag-NPs size. With the tunability in the absorptions at the lower edge of the band, and defect mode absorption for 90^o orientation show vice-versa nature at dissimilar radii of Ag-NPs. The absorption at the lower end of the band is found near about 75% for a 9nm radius of Ag-NPs at 90^o orientated molecules. The proposed 1-DPS $(TiO_2|SiO_2)^m|NC|(TiO_2|SiO_2)^m$ with m=5,3 may be used in the fabrication of absorption dependent tunable devices like optical switches, detectors, sensors, and filters.

References

[1] S. Obayya, M. F. O. Hameed, N. F. F. Areed, *Computational Liquid Crystal Photonics: Fundamentals, Modelling, and Applications,* John Wiley and Sons, United Kingdom, 2016.

[2] E. Yablonovitch, Inhibited Spontaneous Emission in Solid-State Physics and Electronics, *Phys. Rev. Lett.*,58, 2059-2062, 1987.

[3] S. John, Strong localization of photons in certain disordered dielectric superlattices, *Phys. Rev. Lett.,* 58, 2486-2489, 1987.

[4] J. D. Jonopoulos, P. Villeneuve and S. Fan, Photonic crystals: putting a new twist on light, *Nature*, 386, 143-149, 1997.

[5] Q. R. Zheng, Y. Q. Fu and N. C. Yuan,Characteristics of planar PBG structures with a cover layer, *Journal of Electromagnetic Waves and Applications*, 20, 1439–1453, 2006.

[6] Y. Fink, J. N. Winn, S. Fan, C. Chen, J. Michel, J. D. Joannopoulos and E. L. Thomas, A dielectric omnidirectional reflector, *Science*,282, 1679-1682, 1998.

[7] J. A. M. Rojas, J.Alpuente, J.Pineiro and R. Sanchez, Rigorous full vectorial analysis of electromagnetic wave propagation in 1D, *Progress In Electromagnetics Research*, 63, 89-105, 2006.

[8] J. D. Joannopoulos, R. D. Meade and J. N. Winn, *Photonic Crystals: Molding the Flow of Light* (Princeton Univ. Press, Princeton, NJ, 1995).

[9] R. Srivastava, K. B.Thapa, S. Pati and S. P. Ojha, Design of photonic band gap filter, *Progress In Electromagnetic Research,* 81, 225-235, 2008.

[10] K. B. Thapa, SK Singh and SP Ojha, Omnidirectional high reflector for infrared wavelength, *Int. J. Infrared Millimeter Waves* 27, 1257-1268, 2006.

[11] S. K. Singh, J. P.Pandey, K. B.Thapaand S. P.Ojha, Structural Parameters in the Formation of Omnidirectional High Reflectors, *Progress In Electromagnetics Research*, 70, 53-78, 2007.

[12] Y. Kalra and R. K.Sinha, Photonic Band gap Engineering in 2D Photonic Crystals, *Pramana – J. Phys.* 67, 1155-1164, 2006.

[13] K. B. Thapa, S. Srivastava, S. Tiwari, Enlarged photonic band gap in heterostructure of metallic photonic and superconducting photonic crystals, *J. Superconductivity and Novel Magne.* 23 517-525, 2015.

[14] K. B. Thapa, S. Srivastava, and S. Tiwari, Enlarged photonic band gap in heterostructure of metallic photonic and superconducting photonic crystals, *J. Supercond.*, 23, 517–525, 2010.

[15] S. K. Singh, K. B. Thapa and S. P.Ojha, Large Frequency Range of Omnidirectional Reflection in Si-based One-Dimensional Photonic Crystals, *Int. J. Micro. Opt. Technol.* 1, 686-690, 2006.

[16] G. N. Pandey, N. Kumar, K. B. Thapa, and S. P. Ojha, Reflectance properties of one-dimensional metal-dielectric ternary photonic crystals, *AIP Conference Proceedings*, 1728, 0203310(1-3), 2016.

[17] K. B. Thapa, N. K. Mishra, G. N.Pandeyand S. P.Ojha, Enhanced absorption in periodic one-dimensional metallic-organic periodic structure, *Progress In Electromagnetic Research*, 8, 221-233, 2009.

[18] I. El-Kady, M. M. Sigalas, R. Biswas, K. M. Ho and C. M. Soukoulis, Metallic photonic crystals at optical wavelengths, *Phy. Rev. B*, 62, 299-302, 2000.

[19] V. Rinnerbauer, A. Lenert, D. M. Bierman, Y. X. Yeng, W. R. Chan, R. D. Geil, J. J. Senkevich, J. D. Joannopoulos, E. N. Wang, M. Soljačić, and I. Celanovic, Metallic photonic crystal absorber-emitter for efficient spectral control in high-temperature solar thermophotovoltaics, *Adv. Energy Mater.*, 4, 1400334-10, 2014.

[20] G. Veronis, R. W. Dutton and S. Fan, Metallic photonic crystals with strong broadband absorption at optical frequencies over wide angular range, *J. Appl. Phys.*, 97, 093104-4, 2005.

[21] E. Özbay, B. Temelkuran, M. Sigalas, G. Tuttle, C. M. Soukoulis and K. M. Ho, Defect structures in metallic photonic crystals, *Appl. Phys. Lett.*,69, 3797-3799, 1996.

[22] A. Gharaati and Z. Zare, The effect of temperature on one-dimensional nanometallic photonic crystals with coupled defects, *Pramana – J. Phys.* 88, 75(1-6), 2017.

[23] B. Bhushan, S. S. Talwar, T. Kundu and B. P. Singh, Synthesis, characterization and third-order nonlinear optical properties of polydiacetylene nanostructures, silver nanoparticles and polydiacetylene–silver nanocomposites, *Pramana – J. Phys.*,87, 56(1-11), 2016.

[24] S. Chandrasekhar, *Liquid Crystals*, Cambridge Univ. Press, New York, 1992.

[25] I. C. Khoo, *Liquid Crystals*, John Wiley and Sons, New Jersey, 2007.

[26] L. M. Blinov, *Structure and Properties of Liquid Crystals*, Springer, New York, 2011.

[27] K. Busch and S. John, Liquid-Crystal Photonic-Band-Gap Materials: The Tunable Electromagnetic Vacuum, *Phys. Rev. Lett.*, 83, 967-970, 1999.

[28] K. Yoshino, Y.Shimoda, Y. Kawagishi, K. Nakayama and M. Ozaki, Temperature tuning of the stop band in transmission spectra of liquid crystal infiltrated synthetic opal as tunable photonic crystal, *Appl. Phys. Lett.*,75, 932-934, 1999.

[29] S. W. Leonard, J. P. Mondia, H. M. van Driel, O. Toader, S. John, K. Busch, A Birner, U.Gosele and V. Lehmann, Tunable two-dimensional photonic crystals using liquid-crystal infiltration, *Phys. Rev. B*, 61,R2389-R2392 (2000)

[30] Ch. Schuller, F.Klopf, J. P. Reithmaier, M. Kamp and A. Forchel, Tunable photonic crystals fabricated in III-V semiconductor slab waveguides using infiltrated liquid crystals, *Appl. Phys. Lett.*,82, 2767-2769, 2003.

[31] D. Kang, J. E .Maclennan, N. A. Clerk, A. A.Zakhidov and R. H. Baughman, Electro-optic Behavior of Liquid-Crystal-Filled Silica Opal Photonic Crystals: Effect of Liquid-Crystal Alignment, *Phys. Rev. Lett.*,86, 4052-4055, 2001.

[32] E. Graubard, J. S. King, S. Jain, C. J. Summers, Y. Z. Williams and I. C.Khoo, Electric-field tuning of the Bragg peak in large-pore TiO2 inverse shell opals, *Phys. Rev. B*,72, 233105(1-4), 2005.

[33] V. G. Arkhipkin, V. A. Gunyakov, S. A. Myslivsts, V.Ya. Zyryanov and V. F. Shabanov, Angular tuning of defect modes spectrum in the one-dimensional photonic crystal with liquid-crystal layer, *Eur. Phys. J. E*, 24, 297-302, 2007.

[34] Y. M. Strelniker, D. Stroud and A. O. Voznesenkaya, Control of extraordinary light transmission through perforated metal films using liquid crystals, *Eur. Phys. J. B,* 52, 1, 2006.

[35] S. F. Mingaleev, M. Schillinger, D. Hermann and K. Busch, Tunable photonic crystal circuits: concepts and designs based on single-pore infiltration, *Opt. Lett.* 29, 2858-2860, 2004.

[36] B. Y. Zel'dovich, N. V. Tabiryan and Y. S. Chilingaryan, Freedericksz transition under action of light fields, *Zh. Eksp. Teor. Fiz.,*81, 72, 1981.

[37] H. L. Ong, Optically induced Freedericksz transition and bistability in a nematic liquid crystal, *Phys. Rev. A,* 28, 2393-2407, 1983.

[38] M. S. Mohamed, M. F. O. Hameed, M. M. El-Okr and S. S. A. Obayya, Characterization of one dimensional liquid crystal photonic crystal structure, *Optik,*127, 8774-8781, 2016.

[39] R. Ozaki, H. Miyoshi, M. Ozaki and K. Yoshino, Tunable Defect Mode in One-Dimensional Photonic Crystal with Liquid Crystal Defect Layer, *Mol. Cryst. Liq. Cryst*., 433, 247-257, 2005.

[40] H. L. Ong, Optical-field-enhanced and static-field-induced first-order Fréedericksz transitions in a planar parallel nematic liquid crystal *Phys. Rev. A*, 33, 3550-3553, 1986.

[41] A. E. Miroshnichenko, I. Pinkevych and Y. S. Kivshar, Tunable all-optical switching in periodic structures with liquid-crystal defects *Opt. Exp.* 14 2839-2844, 2006.

[42] S. R. Entezar, A. Madani, M. K. Habil, A. Namdarand H. Tajalli, Temperature dependent transmission and optical bistability in a 1D photonic crystal with a liquid crystal defect layer,*J. Mod. Opt.*, 60 1883-1891, 2013.

[43] P. Yeh, *Optical Waves in Layered Media*, John Wiley & Sons, New York, 1988.

[44] H. A. Elsayed and A. H. Aly, Terahertz frequency superconductor-nanocomposite photonic band gap, *Int. J. Mod. Phys. B,* 32, 1850056(1-10), 2018.

[45] S. Y. Vetrov, R. G. Bikbaev and I. V.Timofeev, Optical Tamm states at the interface between a photonic crystal and a nanocomposite with resonance dispersion *J. Exp. Theor. Phys.* 117, 988-998, 2013.

[46] H. Aly, H. A. Elsayed, and C. Malek, Optical properties of one-dimensional defective photonic crystal containing nanocomposite material, *J. Nonlin. Opti. Phys. Mater.*,26, 1750007(1-10) 2017.

[47] N. R. Ramanujam, K. S. J. Wilson and V. Revathy, Effect of Temperature on Nanocomposite of Metal Nanoparticles in Photonic Crystals *Progress In Electromagnetic Research M,* 41,105-114, 2015.

[48] S. G. Moiseev, V. A. Ostatochnikov and D. I. Sementsov, Defect mode suppression in a photonic crystal structure with a resonance nanocomposite layer, *Quantum Electron.* 42, 557-560, 2012.

[49] S. G. Moiseev, Thin-film polarizer made of heterogeneous medium with uniformly oriented silver nanoparticles, *Appl. Phys. A,* 103, 775-777, 2011.

[50] S. G. Moiseev, Composite medium with silver nanoparticles as an anti-reflection optical coating, *Appl. Phys. A,* 103, 619-622, 2011.

[51] S. G.Moiseev and V. Ostatochnikov, Influence of the Size-Dependent Permittivity of Metal Inclusions on the Optical Characteristics of a One-Dimensional Photonic Crystal with a Nanocomposite Defect, *Opti. Quant. Electr.,* 47, 3193-3200 (2015)

[52] P. Singh, K. B. Thapa, N. Kumar, D. Singh and D. Kumar, Effective optical properties of one-dimensional periodic structure of TiO_2 and SiO_2 layers with a defect layer of nanocomposite consisting of silver nanoparticle and E7 liquid crystal *Pramana- J. Phys.*, 93, 50(1-14), 2019.

[53] A. Mouquinho, M.Saavedra, A. Maiau, K. Petrova, M. T. Barros, J. L. Figueirinhas and J. Sotomayor, Films Based on New Methacrylate Monomers: Synthesis, Characterisation and Electro-Optical Properties, *Mol. Cryst. Liq. Cryst.*, 542, 32/[654]-140/[662], 2011.

[54] J. Li, S. T. Wu, S Brugioni, R Meucci and S Faetti, Infrared refractive indices of liquid crystals, *J. Appl. Phys.*,97, 073501(1-5), 2005.

[55] O. A. Yeshchenko, I . M. Dmitruk, A. A. Alexeenko, A. V. Kotko, J. Verdal, A. O. Pinchuk, Size and Temperature Effects on the Surface Plasmon Resonance in Silver Nanoparticles, *Plasmonics,* 7, 685-694, 2012.

[56] V. Amendola, O. M. Bakr, F. Stellacci, A Study of the Surface Plasmon Resonance of Silver Nanoparticles by the Discrete Dipole Approximation Method: Effects of Shape, Size, Structure, and Assembly, *Plasmonics*, *5,* 85-97, 2010.

CHAPTER 6

Conclusions and future prospects

CHAPTER 6

Conclusions and future prospects

The molecules of anisotropic materials show dielectric constants in different directions, and using this direction dependency of anisotropic molecules, the tunable optical properties of the materials could be described. In nature, various anisotropic materials occur and many anisotropic materials also can be chemically synthesized in the laboratory. Generally, anisotropic materials have two different dielectric indices; extraordinary and ordinary dielectric index. The ordinary dielectric index follows Snell's law, while the extraordinary dielectric index does not follow Snell's law. The directional behavior of an extraordinary dielectric index can easily be studied by geometrical constructions. Along with various anisotropic materials, liquid crystals (LCs) are also organic anisotropic materials that can be synthesized by the various chemical routes. LC is a stage between pure liquid and perfect solid state and it can possess both flow and crystalline properties. The LCs have three main categories: lyotropic, polymeric, thermotropic. The phase transition of thermotropic LCs has temperature-dependent, and the optical properties of the thermotropic LCs are changed when the phase changes. Hence, the thermotropic LC occurs in three phases viz. nematic, cholesteric, and smectic phase. Among all phases, the nematic phase LCs are widely studied to use in many optical and photonic devices. The photonic devices are the periodic arrangement of dielectric layers in different directions and the optical properties of such photonic materials can be varied with material parameters, especially dielectric function. Such dielectric periodic structures have exhibited photonic bandgap (PBG) due to the periodicity of materials and PBGs are manipulated intensity of defect layers in such periodic structures. The tunability of defect mode peaks inside PBG is easily occurred due to the changing dielectric function of defect materials in the periodic structures. A tunable defect photonic device, defective one-dimensional photonic crystal (1-DPC), can be designed by using the defect layer of nematic LCs.

In this thesis, we have focused on the tunable optical properties of 1-DPC or one-dimensional periodic structure (1-DPS) of dielectric materials with defects of LC and other anisotropic materials like $LiNbO_3$ and graphene. In our work, a nonlinear differential equation for the distribution of molecules in the LC layer has been solved with the help of Dirichlet boundary conditions. The LC molecules show fluctuations in their orientation depending on the intensity of incident electromagnetic waves. For below the threshold intensity, the molecules do not show any fluctuations, however, the molecules show fluctuations for a threshold value of intensity due to change in the orientation. This threshold intensity is called the Freedericksz transition intensity where the molecules show orientation and attain the extreme value of orientation in the middle of the LC cell. The Freedericksz transition is a basic phenomenon that occurs in the LCs, which can be first-order or second-order and dependent on the Frank elastic constants of LCs. The threshold intensity, Freedericksz transition intensity, has different values for increasing and decreasing intensity of the electromagnetic waves; and the molecules follow the different paths for orientation and reorientation in the LC. In the orientation and reorientation of LC molecules, the hysteresis loop is formed. The hysteresis loop of the LCs and transmittance of defective photonic crystals (PCs) with LCs are different for different wavelengths because both properties depend upon the interaction of a particular wavelength of LC molecules.

A nematic liquid crystal (NLC) sandwiches with/without graphene layers is taken as a defect layer in the 1-DPS of glass and Si materials. The tunable optical characteristics of 1-DPS of dielectric materials of glass and Si with/without graphene layers of the NLC have been analyzed by considering the orientation/reorientation of LC molecules. Without graphene layers of the NLC, it means that 1-DPS of Si and glass with defect NLC only. The whole optical characteristics (absorption (A) transmission (T) and reflection (R)) of multilayered structures have been investigated through the transfer matrix method (TMM). The transmission 1-DPS of glass and Si materials with nematic liquid crystals (NLC) layer shows a defect mode in the PBG region and this transmission peak is tunable with the orientation of molecules. Such a periodic structure of glass and Si with the NLC defect layer does not show any absorption for defect mode peaks. But the proposed structure of 1-DPS with graphene of the NLC layers shows finite absorption of defect peaks because graphene layers have a metallic

nature. However, the absorption values are also tuned with the number of the periodicity of multilayers in 1-DPS. The nematic liquid crystal (NLC) sandwiches with graphene layers has tuned the optical properties of the 1-DPS of glass and Si materials containing a defect of graphene layers of the NLC. The studied periodic structures may have many applications in the various optical devices including all-optical switching device, optical filter, single or multichannel filter, sensor, omnidirectional mirror, absorption-based device, modulator, waveguide, etc. Such studies also open a way to investigate the transmission of the periodic structures consisting of LC sandwiches with other materials like carbon nanotube (CNT), modified graphene, fullerene, chiral, smectic, and blue phase liquid crystals.

Further, we have used a 4x4 matrix method for study the transmission characteristics of 1-DPS of TiO_2 and SiO_2 materials containing a defect layer of lithium niobate ($LiNbO_3$) sandwiches with E7 LC. As the LC, the $LiNbO_3$ (LNO) is also an electro-optic material and its refractive index varies with applied voltage and incident angle of EMW. Using the electro-optical characteristics of LNO, the transmission of 1-DPS of TiO_2 and SiO_2 materials containing a defect of lithium niobate ($LiNbO_3$) sandwiches with E7 liquid crystals (LC) are studied with the variation of voltage, temperature, incident angle, and molecular orientation for TE and TM modes. Due to variation in voltage, temperature, and incident angle, the transmission spectra of the defect modes are shifted towards lower and higher wavelengths, which may help to design tunable devices. The optical transmission of considered terminal wavelengths through the periodic structure shows the optical switching characteristics against temperature for the finite value of voltage and the incident angle. The minimum values of transmission at transition temperature are affected by the nature of applied voltage. The applied positive voltage has a transmission of terminal wavelength in comparison to the applied negative voltage at the transition temperature of LC. In the case of TE mode, the shifting of defect modes in transmission spectra is higher for applied voltage in comparison to the incident angle of EMWs. The calculated analysis is suggested that the proposed structure may be used in the optical switching devices including bistable devices, optoelectronic devices, etc. Besides of the LNO, other electro-optical materials like $BaTiO_3$, KH_2PO_4, etc. may also be used as a defect in 1–DPS to investigate the tunability optical characteristics of 1-DPS containing such defect layers with the LC. Instead of the uniaxial LCs, the biaxial LCs survive

numerous electro-optical responses and can modify the transmission of periodic structure which can be solved by the 4x4 matrix method. Mostly, the 4x4 Berreman matrix method can also be applied to study the transmission of waves through interfaces of uniaxial to uniaxial material and interfaces of uniaxial to isotropic materials, where these materials periodically assembled. The effective refractive index of such assembled materials is calculated by the effective medium theory. The dispersion relation of quasi-periodic PCs with anisotropic materials or chiral nematic LCs having nonlinear tunable characteristics can be studied which are very interesting to fulfill the demand of the tunable optical devices in the near future. Moreover, electro-optical and magneto-optical devices may also be prepared by a periodic structure consisting of uniaxial, biaxial anisotropic, or bi-anisotropic materials.

To study the optical properties of the anisotropic materials, various methods are available viz. plane wave method (PWE), finite difference time domain (FDTD) method, finite element method (FEM), and transfer matrix method (TMM). The blue phases of LCs with different inclusions are fascinating to examine by the above methods because these methods are the most prominent methods to study the optical behavior of the LCs. Additionally, these methods are interesting to investigate the possibility for obtaining the complete bandgap with dye-doped LCs through. Correspondingly, the optical properties of the two-dimensional (2-D) PCs are investigated by FDTD and FEM, however, the dispersion relations are calculated by PWE. In general, the 2-DPCs can be performed for the complex devices as multiplexers, switches, filters, etc.

In the whole thesis work, we have adopted TMM to study the optical properties of the one-dimensional periodic structure, i.e. 1-DPS. Similar to the TMM, the scattering matrix also could be helpful to study the PCs with anisotropic materials including LCs. The tuning of phases is also important for various devices; therefore the fast tuning ferroelectric LCs agree with various novel devices. The dielectric properties of the LCs are also affected by the doping of nanoparticles (NPs). Due to the tuning of the dielectric property of LC with nanoparticles, the optical characteristics of periodic structures can be tuned by the size and shape of nanoparticles. To study the dielectric behavior of LC with nanoparticles, the various theoretical methods are available but the Maxwell-Garnett model is adopted to study the dielectric function of

nanocomposite (NC) of E7 LC with silver nanoparticles (Ag-NPs). The dielectric function of the NC layer has been studied at different radii of NPs, orientations, and temperatures of the E7 LC. The real and imaginary parts of the dielectric function of NC for 90^o orientation of the molecules show the shifting towards the higher wavelength region. Due to plasmonic characteristics in the Ag-NPs, the imaginary dielectric function of the Ag-NPs is responsible for the absorption characteristics of NC. However, both extraordinary and ordinary indices of the NC are merged to a single value at the transition temperature of LC where the LC exists in the isotropic phase. The whole optical properties (A, T, R) of the 1-DPS of TiO_2 and SiO_2 layers containing NC are tuned with different sizes and shapes of Ag-NPs. The transmission properties of the defective NC in 1-DPS are also tuned with filling fraction of NPs and orientation of LC molecules. The 90^o orientation angle of molecules has been observed the lower value of transmittance of defect peaks in comparison to the 0^o orientation angle of molecules. As the filling fraction of NPs in NC increases, the transmission of the defect modes are found to low values and shifted towards the higher wavelength for both orientations. The low orientation angle of LC molecules has a higher value of absorption in comparison to the high orientation angles. For the temperature below than the transition temperature, the uniaxial behavior of NC has both the extraordinary and the ordinary indices but LC converted into isotropic phase at the transition temperature. The extraordinary and the ordinary indices are merged to maintain the linear behavior of the refractive index with the transition temperature and hence the shifting between the transmission defect modes has vanished. The study of the refractive index of NC with Ag-NPs has also shown some negative-index characteristics and hence the NC acts as a metamaterial for particular shape and size of NPs. The investigated 1-DPS with NC of LC and Ag-NPs may be useful in the fabrication of optical filters, switches, sensors, absorbers, etc. The size and shape of NPs modify the dielectric properties of NC and hence the optical properties of 1-DPS with a defect of the NC could be tuned by different shapes of NPs as spherical, cubic, cuboid, or ellipsoid and so on. The different shaped and sized plasmonic NPs in the NC layer supports the various surface waves at the interface of dielectric and anisotropic materials; hence LC can also be supported by the Dyakonov waves, Ghost waves, etc. at the material surfaces and such surface waves may also be useful to study the various effects in the materials. With the metallic NPs in different LCs,

Tamm-Plasmons can be studied in NPs embedded periodic structures. The dielectric properties of NC are also tuned with different types of LCs because such LCs have a different orientation and translational symmetry in their molecular arrangements.

All the phases of LCs (nematic, cholesteric, smectic, blue phase, and other phases) have different molecular patterns; therefore, the optical properties may be tuned with fluctuations in their molecular order. The optical characteristics of LC are varied with the electric field as well as the magnetic field. So, the magneto-optical devices may be feasible in the same LC by applying the magnetic field. The doping of dye and polymer in the chiral smectic-C phase may be used as photonic materials that offer potential applications in the electro-optical devices. The theoretical calculations of dye-doped chiral nematics and the related PCs containing such LCs are very complicated task in coming future. However, 3-DPCs with blue phase LCs may be employed to design low threshold lasers, which can have tunability and simultaneously operated in multiple directions. By stretching in LCs, the blue and redshift could be obtained in opposite directions with affecting the pitch of LCs. Absorption and gain medium of the 3-DPCs also are investigated by FDTD. Moreover, FDTD is also helpful to study the optical properties of the composite of nonlinear material with left-handed metamaterials, metals, and anisotropic materials. By solving the problem of coupling, the efficiency of 3-D waveguides could be modified. The FDTD is required to develop to study the nonlinear effects like Raman, effects, Kerr effects, etc. However, three-dimensional calculations by FDTD are complicated, but it gives accurate results for 3-DPCs consisting of anisotropic materials. The LCs have been used in various display applications like liquid crystal display (LCD), and the efficiency and property of the display process can be modified by doping of the various elements in the LCs. The quantum dots doped LCs are efficiently used in enhanced LCD applications. The different shape and size quantum dots doped LCs produce the quantum confinement effects and may be used to enhance the display applications of LCDs.

The optics of cholesteric liquid crystals (CLCs) is complicated but the CLC is a potential candidate for future application in various optical devices because CLC can easily control the material's parameters and fast tuning with applied fields without any alignment layer. The CLCs could be used in selective reflection based on index

matching between other material and CLCs. Moreover, the periodic structure with CLCs with the application of DC (direct current) and AC (alternating current) fields could be fruitful to investigate for photonic applications in the future. Along with the study of the periodic structure, the topological studies of LCs are also important because the interactions and knots in LCs can be studied topologically which helps to understand the behavior of LCs and precisely tuned with external fields on the LCs. Another type of LC is quantum liquid crystals which have novel properties. The three-dimensional quantum liquid crystals (3-DQLCs) is an important material in the field of spintronics and such 3-DQLC also may be played an important role to build quantum computers using topological quantum computing.

Eur. Phys. J. E (2018) **41**: 100
DOI 10.1140/epje/i2018-11710-0

THE EUROPEAN PHYSICAL JOURNAL E

Regular Article

Tunable transmission of a nematic liquid crystal as defect in a 1D periodic structure of dielectric materials by orientation and re-orientation of liquid crystal molecules

Pawan Singh, Khem B. Thapa[a], Narinder Kumar, and Devesh Kumar

Department of Physics, School for Physical and Decision Sciences Babasaheb Bhimrao Ambedkar University, Lucknow, India

Received 19 May 2018 and Received in final form 14 July 2018
Published online: 3 September 2018
© EDP Sciences / Società Italiana di Fisica / Springer-Verlag GmbH Germany, part of Springer Nature, 2018

Abstract. In this paper, we investigate tunable transmission characteristics of a one-dimensional periodic structure (1DPS), designed with periodic dielectric materials containing a nematic liquid crystal (NLC) as a defect layer, on the basis of orientation and re-orientation of LC molecules. The nonlinear differential equation for the director of the liquid crystal under the light field is solved numerically. The relation between the liquid crystal director and the intensity of the electromagnetic wave (EMW) is derived. Transmittances of the liquid crystal defect layer in the 1DPS are calculated with the variation of the intensity of the incident wave and liquid crystal director tilt angles. By varying the director tilt angle of the liquid crystal molecules as well as the incident angle of the EMW, the shifting of the transmitted defect mode wavelengths is studied. Such study is helpful to understand how orientation and reorientation of the molecules affect the transmittance of the considered periodic structure when the EMW interacts with an embedded liquid crystal as a defect layer in the 1DPS of dielectric materials. Such photonic structure of dielectric materials with the liquid crystal layer as a defect layer can be used to fabricate bistable switches, optical filters, feedback lasers, etc.

1 Introduction

Liquid crystals (LCs) were discovered by Reinitzer and Lehmann in the 19th century. LCs are wonderful materials having an intermediate phase between the liquid and the crystalline states [1]. The LC has flow property like a liquid and a solid-like crystalline property. There are different types of liquid crystals, *e.g.*, thermotropic, lyotropic and metallotropic, having different optical properties [2].

Today, photonic crystals have aroused a great deal of interest in research due to their uses in optical computing, communication, etc. The photonic crystals have the capacity to obstruct the propagation of an electromagnetic wave (EMW) over special frequency regions called photonic band gaps (PBGs) [3]. Such photonic band gap materials have a very special nature, so that they can be used in electronics, micro-photonic and integrated optics because these crystals are capable of guiding the electromagnetic wave (photons) propagation in dielectric layers as in photonics, which is analogous to the control of the electronic motion in electronics [4]. The transmission of the electromagnetic wave through photonic crystals depends on the refractive index contrast of the dielectric materials, geometry and topology, etc. The dynamical control of the electromagnetic wave can be achieved by the tunability of photonic band gaps in photonic crystals [5]. The photonic band gap can be continuously tuned by coating the inverse opal with the liquid crystal as explained by Bush *et al.* and later confirmed experimentally by Yoshino *et al.* [6,7]. The tuning of the photonic band gap of the periodic structure with the liquid crystal layer as defect depends upon the temperature, external field and refractive index of the liquid crystal [7–13]. Infiltration of individual pores in the photonic crystals is another method to achieve the tuning of the photonic crystal [14] and to find the effect of the liquid crystal layer as a defect layer in the periodic structure [15].

The liquid crystal has very high nonlinear optical properties that can be used in optical device applications [16, 17] like all-optical switching and control of the electromagnetic wave in the periodic structure. Mohamed *et al.* [18] reported the effect of the liquid crystal director tilt angle and temperature on the transmission of 1DPS containing a nematic liquid crystal as a defect layer. Similarly, nonlinear and linear responses of a 1DPS of dielectric materials with a liquid crystal as a defect layer have been studied by Entezar *et al.* [19]. They concluded that the bistable property, *i.e.* gained threshold intensity, is dependent upon the

[a] e-mail: khem.bhu@gmail.com (corresponding author)

operating temperature. They have discussed the effect of the operating temperature on the transmission property of the periodic structure. The transmittance of defect mode peak wavelengths in the PBG region is also dependent upon the director angle of the liquid crystal. The propagation and transmission of the electromagnetic wave in the 1DPS with the liquid crystal as a defect is dependent on the directions of the ordinary and extraordinary optical axes of the liquid crystal [20].

In the presence of an electromagnetic wave, a nonlinear differential equation for the director of the nematic liquid crystal (NLC) is solved and a relation between the maximum director angle and the intensity (I) of the electromagnetic wave for the liquid crystal is determined. This relation is used to study the propagation of the electromagnetic wave field, where the intensity of light depends upon the molecular orientation of the liquid crystal. The molecules of the liquid crystal orient when the intensity of the electromagnetic wave becomes equal or greater than threshold intensity commonly named as Freedericksz transition intensity ($I_{\rm fr}$). By calculating the transmittance of a one-dimensional periodic structure of glass/Si layers with the NLC as a defect layer, we analyze the effect of orientation/reorientation of the molecule by varying the intensity as well as the incidence angle of the electromagnetic wave. We also calculate the transmittance of the defect structure of the nematic liquid crystal for three different director tilt angles of the liquid crystal. The shifting of the transmitted defect mode peak wavelengths of the periodic structure depends upon the incident angle of the electromagnetic wave as well as the director tilt angle of the liquid crystal.

2 Theory and mathematical formulation

The liquid crystals are highly nonlinear anisotropic materials having dielectric permittivity in the tensor form [2]. The dielectric tensor ($\tilde{\varepsilon}$) of a liquid crystal layer can be represented in terms of parallel ($\varepsilon_{\rm II}$) and perpendicular ($\varepsilon_{\perp}$) components of the dielectric constant, and the dielectric anisotropy ($\varepsilon_{\rm a} = \varepsilon_{\rm II} - \varepsilon_{\perp}$), which is given as [5,17]:

$$\tilde{\varepsilon} = \begin{pmatrix} \varepsilon_{\perp} + \varepsilon_{\rm a}\sin^2\phi & 0 & \varepsilon_{\rm a}\sin\phi\cos\phi \\ 0 & \varepsilon_{\perp} & 0 \\ \varepsilon_{\rm a}\sin\phi\cos\phi & 0 & \varepsilon_{\perp} + \varepsilon_{\rm a}\cos^2\phi \end{pmatrix}. \quad (1)$$

The dielectric tensor of the liquid crystal is in the matrix form and depends upon the liquid crystal parameters, *i.e.* $\varepsilon_{\rm II}$, $\varepsilon_{\perp}$ and its director tilt angle (ϕ) with respect to the z-axis (fig. 1). The dielectric tensor matrix can be diagonalized for the angle $\phi = 0°$ and $\phi = 90°$, but the dielectric tensor matrix is represented by eq. (1) and is not diagonalized for any other director angles except the tilt angles 0° and 90°. To use the transfer matrix method (TMM), we diagonalize the tensor matrix for any other director orientation angles [19]. The liquid crystal dielectric tensor is dependent on the director tilt angle parameter

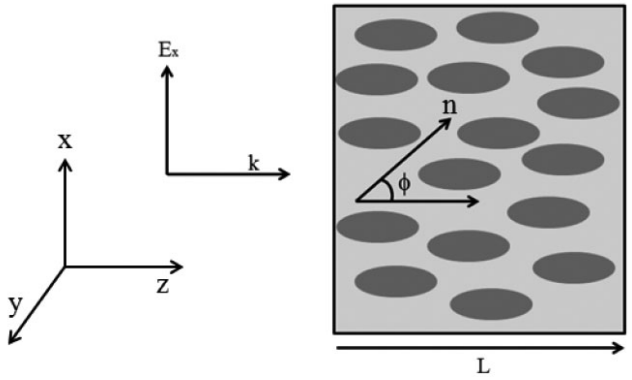

Fig. 1. Schematic diagram of a liquid crystal (LC) molecule director (ϕ) under an external electric field.

and the profile is similar to the effective dielectric constant of the liquid crystal [21,22]. The effective dielectric constant of the liquid crystal is given as

$$\varepsilon_{\rm eff} = \frac{\varepsilon^2 - (\frac{\varepsilon_{\rm a}}{2})^2}{\varepsilon - (\frac{\varepsilon_{\rm a}\cos 2\phi}{2})}, \quad \varepsilon = \frac{\varepsilon_{\rm II} + \varepsilon_{\perp}}{2}, \quad (2)$$

where ϕ is the tilt angle of the director with respect to the z-axis in the layer. On considering such effective dielectric constant, the light field propagates along the z-direction.

To investigate the effect of the director tilt angle, we have considered a liquid crystal cell having thickness L with a homeotropic arrangement of molecules. The distribution of the LC director is defined by $\phi(z)$. When the electromagnetic wave enters the cell, the molecules of the liquid crystals orient a director tilt angle $\phi(z)$ with respect to the normal to the cell as shown in fig. 1. When the value of intensity reaches the Freedericksz transition intensity, the molecules reorient inside the cell. This intensity of the field, electromagnetic wave (EMW), is called the threshold value for molecular orientation. The optical properties of the liquid crystal are tuned when the interaction between the intensity ratio ($I/I_{\rm fr}$) and the director field is considered. The liquid crystal director tilt angle $\phi(z)$ of the molecule under the interaction of the field can be analysed with the variation of the intensity ratio ($I/I_{\rm fr}$). The reorientation of the liquid crystal molecules due to the coupling with electric field of the EMW is given by the solution of the nonlinear differential eq. (3) [23]:

$$\phi_{zz} - \frac{k\sin(2\phi)}{2(1 - k\sin^2\phi)}{\phi_z}^2 + \frac{\pi^2 I\sin(2\phi)}{2L^2 I_{\rm fr}(1 - k\sin^2\phi)(1 - \beta\sin^2\phi)^{3/2}} = 0. \quad (3)$$

The solution of the nonlinear differential equation is dependent upon the liquid crystal parameters like the intensity ratio of the incident intensity to the Freedericksz threshold intensity ($I/I_{\rm fr}$) and the boundary condition. Here ϕ_z and ϕ_{zz} are the first- and second-order partial derivatives of ϕ with respect to z, respectively. The mentioned parameters k_{33} and k_{11} are bend and splay the elastic constants of the liquid crystal, and β is a constant

depending upon the ordinary ($n_{\rm o}$) and the extraordinary ($n_{\rm e}$) refractive indices of the liquid crystal. k and β are given by

$$k = \frac{k_{33} - k_{11}}{k_{33}}, \qquad \beta = 1 - \left(\frac{{n_{\rm o}}^2}{{n_{\rm e}}^2}\right). \tag{4}$$

The Freedericksz threshold intensity, *i.e.*, $I_{\rm fr}$ is given by

$$I_{\rm fr} = \frac{ck_{33}\pi^2}{n_{\rm o}\beta L^2}, \tag{5}$$

where c is the speed of light in the vacuum. We apply the Dirichlet-type boundary conditions (BCs) to solve eq. (3) to determine the director orientation of the liquid crystal which is given by

$$\phi(z=0) = 0, \qquad \phi(z=L) = 0. \tag{6}$$

Equation (6) is considered for the strong anchoring of liquid crystals which helps to get the solution of eq. (3). With above BCs, we first multiply eq. (3) by $2\phi_z$ and then integrate with respect to z; the integration constant is determined in terms of the maximum director angle $\phi^0_{\rm max}$ and we get the following deduced equation:

$$(1 - k\sin^2\phi)\left(\frac{{\rm d}\phi}{{\rm d}z}\right)^2 = \frac{4A}{\beta}\left[\frac{1}{(1-\beta\sin^2\phi^0_{\rm max})^{1/2}} - \frac{1}{(1-\beta\sin^2\phi)^{1/2}}\right]. \tag{7}$$

Now, with single elastic constant ($k_{11} = k_{22} = k_{33}$) approximation $k = 0$, we have obtained

$$\left(\frac{{\rm d}\phi}{{\rm d}z}\right)^2 = \frac{4A}{\beta}\left[\frac{1}{(1-\beta\sin^2\phi^0_{\rm max})^{1/2}} - \frac{1}{(1-\beta\sin^2\phi)^{1/2}}\right], \tag{8}$$

where $A = \frac{\pi^2 I}{2L^2 I_{\rm fr}}$, and the maximum director tilt angle $\phi^0_{\rm max}$ reaches the maximum in the middle of the cell at $z = L/2$. For such a condition, we have

$$\int_0^{\phi^0_{\rm max}} \frac{{\rm d}\phi}{\sin^2\phi^0_{\rm max} - \sin^2\phi} = \frac{L}{2}(2A)^{1/2}. \tag{9}$$

We get the solution for the maximum director angle of the molecules as

$$\phi^0_{\rm max} = \sin^{-1}\left[2\left(\frac{I}{I_{\rm fr}} - 1\right)^{1/2}\right]. \tag{10}$$

From eq. (10), we conclude that molecules have orientation in a certain direction when $I < I_{\rm fr}$, and molecules get reorientation when $I > I_{\rm fr}$. Between the orientation and reorientation of the molecules, a maximum value $\phi^0_{\rm max}$ is reached in the middle of the cell. To find the solution of eq. (3), we consider the second-order terms in calculations when the intensity ratio ($I/I_{\rm fr}$) increases. But for the ratio ($I/I_{\rm fr}$) decreasing, the high-order degree terms like the fourth order are considered in the calculation. The orientation and reorientation of the liquid crystal molecules are dependent on the intensity (I) of the electromagnetic wave, which can be equal or greater than the Freedericksz transition intensity ($I_{\rm fr}$) for the orientation and orientation of LC molecules in the layer.

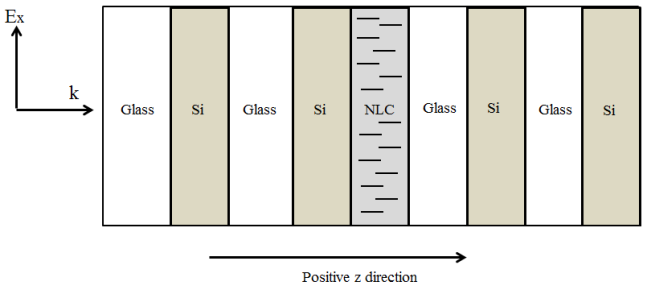

Fig. 2. Schematic diagram of the periodic structure of glass/Si materials with a liquid crystal layer as a defect layer.

The optical properties of the NLC as a defect layer in the 1DPS of glass/Si layers are calculated. In this case, we consider a plane EMW propagating along positive z-direction and normally incident on the considered periodic structure, as shown in fig. 2. The solution of eq. (3) can be obtained by solving eq. (9), where we get the following equation which depends upon the dielectric parameters ($\varepsilon_\perp, \varepsilon_{\rm II}, \varepsilon_{33}$) of liquid crystals:

$$E_z = -\frac{\varepsilon_{13}}{\varepsilon_{33}}E_x = -\left[\frac{\varepsilon_{\rm a}\sin\phi\cos\phi}{(\varepsilon_\perp + \varepsilon_{\rm a}\cos^2\phi)}\right]E_x. \tag{11}$$

From Maxwell's equations, we obtain the equation for an electric field given as

$$\frac{{\rm d}^2E_x}{{\rm d}z^2} + k^2E_x = 0, \tag{12}$$

where $k^2 = {k_0}^2\frac{\varepsilon_\perp\varepsilon_{\rm II}}{\varepsilon_{33}}$ with $k_0 = \frac{2\pi}{\lambda}$, λ is the wavelength of the electromagnetic wave incident on the considered structure.

For the light scattering in the layer, the z-component of the Poynting vector $I = S_z = (c/8\pi)E_xH_y^*$ remains constant and can be used to study the properties of the layer. The solution of eq. (10) may be in form of eq. (11) as given below,

$$E_x = \left\{\begin{array}{ll} A\exp(ikz) + B\exp(-ikz), & z \le 0 \\ C\exp(ikz) + D\exp(-ikz), & z \ge L \end{array}\right\}, \tag{13}$$

where A, B, C, D are the incident, reflection and transmission coefficients of the electromagnetic wave. Such coefficients give the transmittance and reflectance properties of the liquid crystal layer. The solution to eq. (11) is dependent on the liquid crystal dielectric parameters as well as the director tilt angle for the nonlinear transmission through the liquid crystal layer. Here, the polarization is in the x-z plane and parallel to the plane of incidence of the wave, assuming the variations of director and electromagnetic fields only along the z-direction as in fig. 1.

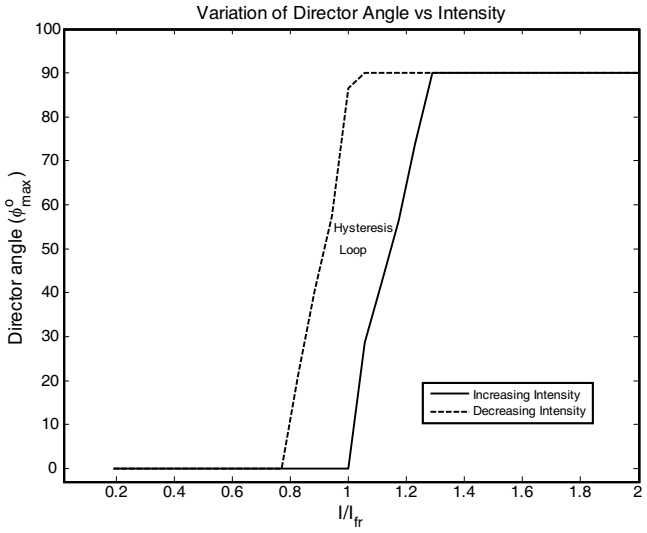

Fig. 3. Variation of the liquid crystal director ($\phi^0_{\max}$) *versus* intensity ratio ($I/I_{\rm fr}$) for increasing and decreasing intensities.

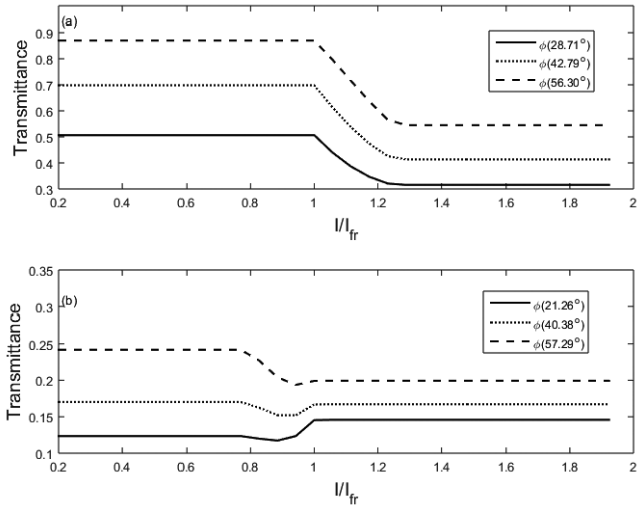

Fig. 4. Comparative diagram of transmission variation *versus* intensity ratio ($I/I_{\rm fr}$) for increasing and decreasing intensities at different liquid crystal directors.

3 Results and discussion

3.1 Orientation of the liquid crystal director with intensity ratio (I/I_{fr})

In this section, we discuss the director tilt angle of the nematic liquid crystal PAA (p-Azoxyanisole) and the transmittance of the liquid crystal at a fixed director tilt angle by varying $I/I_{\rm fr}$. The switching behavior of the LCs director can easily be analyzed by solving the differential eq. (3) and the solution of this equation is given in eq. (10). The derivative of the director tilt angle ϕ along the z-axis is dependent upon $\phi^0_{\max}$ as well as on ϕ itself. The maximum director tilt angle $\phi^0_{\max}$ value is solved in terms of the intensity of the wave, and we obtained $\phi^0_{\max}$ as in eq. (10). The behavior of the director tilt angle ($\phi^0_{\max}$) *versus* the intensity ratio ($I/I_{\rm fr}$) is shown in fig. 3, where $I_{\rm fr}$ is the Freedericksz transition intensity. For calculations, we have taken the elastic constants of the PAA molecules as $k_{11} = 4.5 \times 10^{-7}$ dyn, $k_{33} = 9.5 \times 10^{-7}$ dyn, $\varepsilon_{\rm a} = 0.896$, $\varepsilon_{\perp} = 2.45$ $\varepsilon_{\rm II} = 3.346$, where $\varepsilon_{\rm a}$ is dielectric anisotropy, $\varepsilon_{\perp}$, $\varepsilon_{\rm II}$ are the ordinary and extraordinary dielectric constants, respectively [24]. The value of the director tilt angle ($\phi^0_{\max}$) increases when the intensity of the electromagnetic wave increases and the director tilt angles are 0°, 28.71°, 42.79°, 56.3°. These angles are obtained when the intensity of the wave is equal or above the threshold intensity. Below the threshold value, however, the director angle ($\phi^0_{\max}$) decreases in reversed direction as the intensity of incident electromagnetic wave decreases. The different director tilt angles are obtained when the intensity decreases. These angles are 0°, 21.26°, 40.38°, 57.29°. There exists a hysteresis loop in the transmission process for director tilt angles with intensity ratio ($I/I_{\rm fr}$). The study of the hysteresis loop of the LC molecules shows that they do not follow the same path when varying the intensity ratio ($I/I_{\rm fr}$). As a result, hysteresis loops appear in the LC cell. Hysteresis loops show the first-order nature of their optical field-induced transition. In such a transition, the director orientation changes discontinuously at the threshold intensity ($I_{\rm fr}$) from $\phi^0_{\max} = 0$ to $\phi^0_{\max} = 90$. The free energy landscapes first and then attains local energy minima close to the Freedericksz transition, resulting in metastability and hysteresis in the cell. From the obtained results, we conclude that the molecules are oriented and reoriented in a particular direction when the intensity of the EMW increases and decreases, respectively. The hysteresis loop which appeared in the switching process shows the first-order nature of the optically induced transition in the LC cell.

3.2 Transmission characteristics with intensity ratio (I/I_{fr})

The transmission of the electromagnetic wave through the defect layer NLC in the 1DPS of glass/Si layers *versus* the intensity ratio ($I/I_{\rm fr}$) for increasing and decreasing intensities with the variation of director tilt angles is shown in fig. 4. The electromagnetic wave interacts with liquid crystal molecules and allows to transmit the electromagnetic wave with a constant transmission but when the intensity of the electromagnetic wave (I) reaches equal or higher threshold intensity (Freedericksz transition intensity $I_{\rm fr}$) the molecule switches in a particular direction. Hence the transmission of the electromagnetic wave gets affected and becomes lower in comparison to $I < I_{\rm fr}$. The transmittances of the 1DPS with liquid crystal as defect layer are found to be 51%, 69%, 86% for director tilt angles 28.71°, 42.79°, and 56.31°, respectively. On switching of the LC molecules, transmittances decrease up to 31%, 41%, and 54% for the same director tilt angles. As the molecules of liquid crystal orient for the increasing intensity case, similarly, molecules reorient in a particular direction for the decreasing intensity case, but follow a different path to reorient and produce different director tilt angles due to new

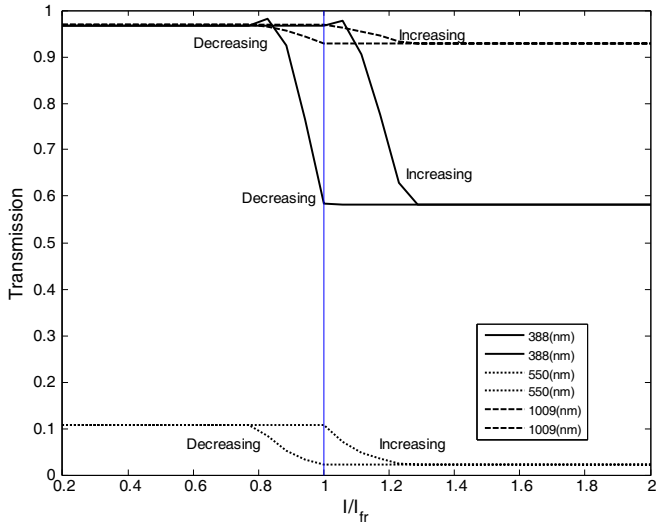

Fig. 5. Comparative diagram of transmission variation *versus* intensity ratio ($I/I_{\rm fr}$) for increasing and decreasing intensities at different wavelengths.

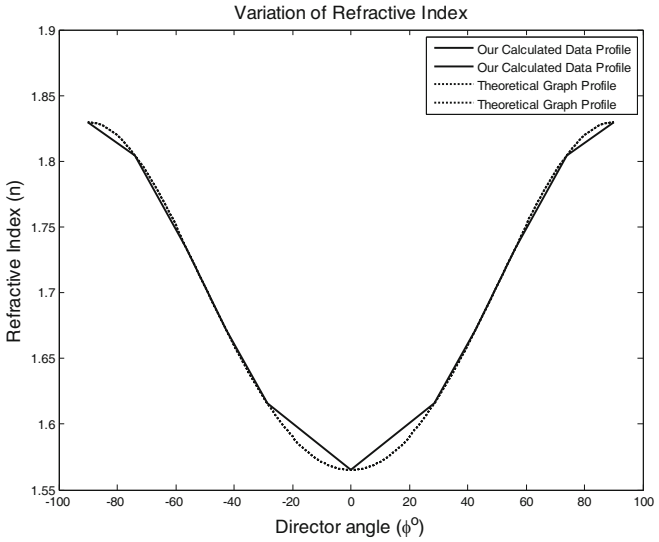

Fig. 6. Comparative diagram of the variation of the refractive index of the LC *versus* liquid crystal director.

threshold intensity $I'_{\rm fr}$, which is less than $I_{\rm fr}$. This suggests that the director tilt angles of the molecules are different for both increasing and decreasing intensity cases. New tilt angles of the LC director gave unusual transmission properties of 1DPS as shown in fig. 4(b). For the decreasing intensity process, the molecules follow different paths to reorientation, which leads to the loss in the transmission properties of the 1DPS with the liquid crystal as a defect layer. Hence the transmittance is set lower and is found to be 14%, 21%, 19% for the director tilt angles 21.26°, 40.38°, and 57.29°, respectively. This transmittance decreases for the director tilt angles 21.26°, 40.38° but increases for the angle 57.29°. This means that the transmittance of the LCs becomes low above the Freedericksz transition value ($I_{\rm fr}$) due to the scattering, polarization and order parameter of the LC molecules. Similarly, the same effect is obtained for the reverse case except for the director angle 57.29°. When the intensity of the wave (I) is equal or greater to $I_{\rm fr}$, the molecules start to orient and obtain a low transmittance as compared to the intensity below to $I_{\rm fr}$.

3.3 Transmission characteristics with ($I/I_{\rm fr}$) at different wavelengths

The orientation of the molecules affects the transmittance of the wave. So here we have calculated the transmission *versus* $I/I_{\rm fr}$ for the liquid crystal molecules for different wavelengths, *i.e.*, 388 nm, 1009 nm, and 550 nm, as shown in fig. 5. These wavelengths are laid in the band gap range of 1DPS with the liquid crystal as a defect layer. The hysteresis loops for different wavelengths are found for both increasing and decreasing intensity ratio $I/I_{\rm fr}$ as shown in fig. 5. The transmissions of 1DPS with the liquid crystal as a defect layer are reduced from 94% to 58% and 94% to 92%, for 388 nm and 1009 nm, respectively. The transmission is reduced from 10% to 2% only for, wavelength 550 nm at Freedericksz transition.

3.4 Liquid crystal dielectric profile

The liquid crystals (LCs) are anisotropic materials and their refractive index is dependent on the temperature, external field, etc. For the molecules of the liquid crystal, the refractive index (n) is variable up to a certain value and it depends upon the parameters: $n_{\rm o}$, $n_{\rm e}$ and ϕ, which is given as [21,22,25]

$$n^2 = \frac{{n_{\rm o}}^2 {n_{\rm e}}^2}{({n_{\rm e}}^2 \cos^2\phi + {n_{\rm o}}^2 \sin^2\phi)}, \qquad (14)$$

where $n_{\rm o}$, $n_{\rm e}$ and ϕ are the ordinary, extraordinary refractive indices and the director tilt angle, respectively. If the director tilt angle of LC varies from 0° to 90° then the director profile almost matches our calculated data as shown in fig. 6. The refractive index of the liquid crystal is low at the low director tilt (ϕ) angle, and the refractive index increases as the director angle (ϕ) increases. The refractive index of LC attains the maximum value for the maximum director tilt angle (ϕ). The obtained director angles are verified with the simulation data by the Gaussian 09 software package A02. We have only considered three director tilt angles for analyzing the effects of the molecular orientation on the optical characteristics of the 1DPS with the defect layer (NLC).

3.5 Transmission characteristic of (glass|Si)^2|NLC|(glass|Si)^2

Now, the periodic structure of glass and silica materials are considered without and with the defect layer PAA liquid crystal: without defect, 1DPS is represented as $(\text{glass}|\text{Si})^N$, with $N = 4$; and with the PAA liquid crystal defect 1DPS is $(\text{glass}|\text{Si})^N|\text{NLC}|(\text{glass}|\text{Si})^N$ with $N = 2$. The considered periodic structure $(\text{glass}|\text{Si})^N$ with the liquid crystal as a defect layer is shown in fig. 2. The refractive indices of the glass and Si materials are 1.5 and

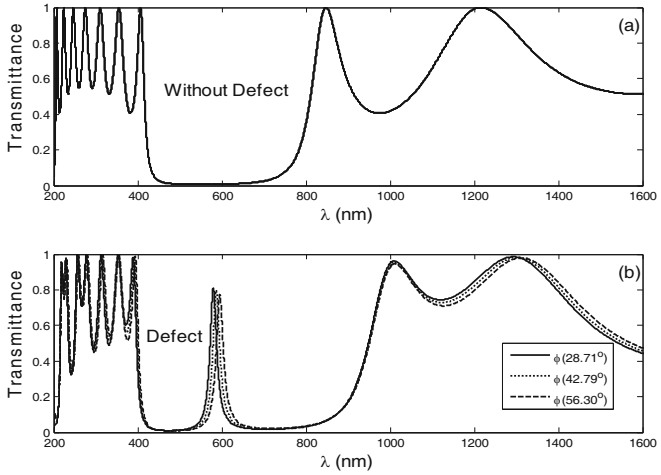

Fig. 7. Comparative diagram of transmission *versus* wavelength without and with the defect of the LC periodic structure at different liquid crystal directors.

3.4 having thicknesses $d_1 = 91\,\text{nm}$ and $d_2 = 40\,\text{nm}$, respectively with central wavelength $\lambda_0 = 550\,\text{nm}$. Using the above data, the transmissions of the considered structure without and with the defect layer NLC are calculated by using the transfer matrix method (TMM) [26]. The obtained results for both structures are compared. The transmittance of the considered structure *versus* wavelength is shown in fig. 7. The calculated transmission of the considered structure without defect layer, $(\text{glass}|\text{Si})^N$ with $N = 4$, shows a photonic band gap (PBG) region between 407 nm to 848 nm ($\Delta\lambda = 441\,\text{nm}$), which is shown in fig. 7(a). The transmittance of the considered structure with the NLC defect layer is calculated with the variation of the director tilt angle as 28.71°, 42.79° and 56.10° for the increasing case of I/I_{fr}, and these director angles are verified with the Gaussian09 software package A02 [27].

Now, we have studied the effect of the orientation of the liquid crystal molecules in the considered structure. The sharp defect mode peak wavelengths are produced in the photonic band gap region due to the defect layer in the periodic structure [28]. Figure 7(b) shows the transmittance of the considered periodic structure with the defect layer NLC at the director tilt angles 28.71°, 42.79° and 56.10°. From earlier discussions, we know that the incident wave in the NLC has a switching behavior due to the orientation of the NLC molecules and it is a very interesting optical switching behavior of the liquid crystal.

3.6 3D and 2D image of transmittance of $(\text{glass}|\text{Si})^2|\text{NLC}|(\text{glass}|\text{Si})^2$

To visualize the transmittance of such periodic structure with NLC as defect layer *versus* varying incident wavelength and director tilt angle, we plotted a 3D diagram, which clearly shows the shifting of the defect mode peak wavelengths at the director tilt angles 28.71°, 42.79° and 56.10° with the variation of the wavelength as shown in fig. 8. The optical tunability of defect mode periodic structure is dependent on the LC director tilt angles. LC has

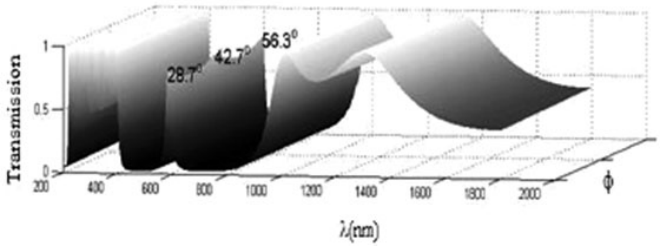

Fig. 8. 3D diagram of transmission *versus* wavelengths and director angles for the periodic structure with the defect layer of LC.

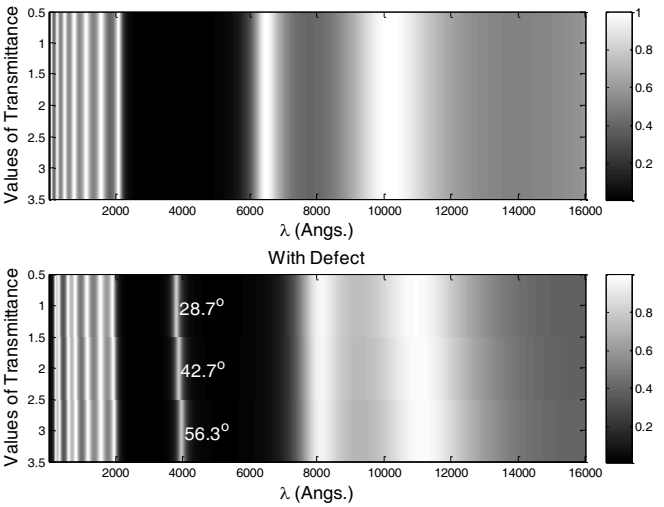

Fig. 9. Comparative image diagram of transmittance *versus* wavelength without and with a defect layer of NLC in the periodic structure.

three different director orientation angles which transmit the defect mode wavelength peaks in the PBG region. Such defect mode sharp peak wavelengths may be used in optical switching for photonic applications. The 2D image diagram of transmission *versus* wavelength (λ) without and with defect layer (NLC) are shown in fig. 9. The comparative image of transmittance without and with a defect layer (NLC) clearly shows the shifting of the transmitted defect mode peak wavelengths at different director tilt angles 28.71°, 42.79° and 56.30°. From fig. 9, it is clear that the liquid crystal as the defect in 1DPS leads to a small enhancement of PBG in the transmission spectra. Besides this, the transmittance of the considered periodic structure *versus* incidence angle (θ) at different director tilt angle (ϕ) is studied for both modes, *i.e.* the TE and TM mode. The transmission of peak wavelengths for a certain director tilt angle (ϕ) is shifted at the higher incidence angle. Figure 10 shows the comparative study of the transmitted peak wavelengths for TE and TM modes. From fig. 10, we concluded that the optical properties of 1DPS with the NLC as defect depend upon the incident angle of the electromagnetic wave. As the incident angle increases from a normal angle to a higher angle, *i.e.* from 0° up to 75°, the peak wavelengths are shifted to lower wavelengths in the PBG region. The values of the peak wavelengths are high at the normal incidence angle, *i.e.*,

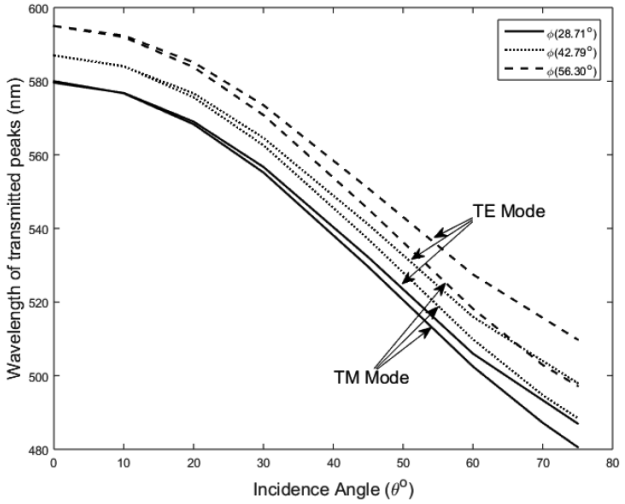

Fig. 10. Comparative diagram of the shifting of transmitted defect mode peaks *versus* incidence angles with different liquid crystal director ($\phi^0_{\max}$) for TE and TM modes.

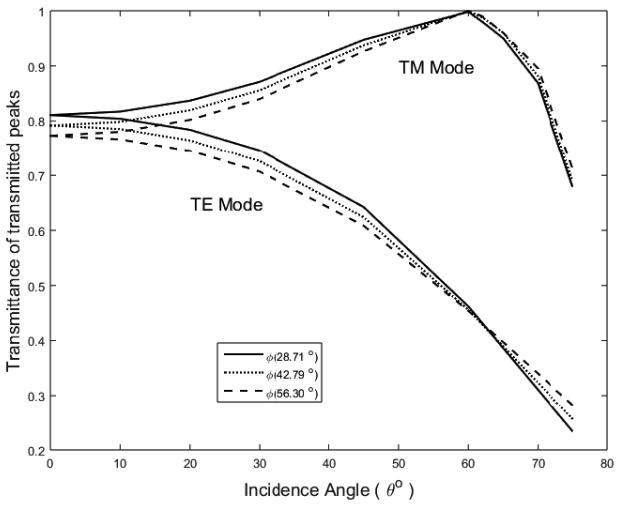

Fig. 11. Comparative study diagram of the transmittance of defect mode peaks *versus* incidence angles with different liquid crystal director ($\phi^0_{\max}$) for TE and TM modes.

0°, but these peaks are shifted towards lower values at a high incidence angle. It is found that there is an almost 8 nm difference between the values of the defect mode peak wavelength. But this difference is almost constant for a low incident angle and increases at a high incident angle. The comparative study confirmed that the shifting of the peak wavelength attains higher values in the TE mode than in the TM mode.

Again, we have studied the comparative transmittance of the shifted peak wavelength *versus* the incident angle for both TE and TM modes at different angles of the LC director as shown in fig. 11. Figure 11 depicts that the origin of the transmittance for TE and TM mode is the same, but the transmittance of the wavelength peaks shifts to different values as the incident angle increases. The transmittance for TE mode is continuously decreasing as the incident angle increases up to 63°. The transmittance of the wavelength peaks for the TM mode increases and reaches the maximum incident angle 60° and then it further decreases. The director tilt angle of the NLC molecules for the TM mode is more effective as compared to the director tilt angle of the NLC molecules for the TE mode when the wavelength peaks are studied. Such an effect is analogous to the effect of the Brewster angle at the interfaces of the dielectric materials.

4 Conclusions

In this paper, we have solved the nonlinear differential equation for the director of a NLC under the influence of an electromagnetic field and discussed the nonlinear behaviour of the director of a NLC under the applied electric field. At a threshold value called Freedericksz transition, a sharp switching behavior of the liquid crystal molecules is observed when the electromagnetic wave propagates inside the LC cell. The first-order phase nature of the optical-field–induced transition take places, hence hysteresis loops appear in the LC cell. Due to orientation/reorientation of the NLC molecules, the optical effect of the NLC molecules is studied by comparing the transmittance of the periodic structure of glass/Si layers (1DPS) containing a NLC defect layer and without the defect layer. A sharp defect mode peak wavelength in the transmittance periodic structure $(\text{glass}|\text{Si})^2|\text{NLC}|(\text{glass}|\text{Si})^2$ shows the optical switching behavior in the photonic band gap region. By applying an external field, the different molecular orientations of the molecules correspond to different transmission wavelength peaks in the PBG region. The different molecular orientations and reorientations of the LC molecules at a certain director are responsible for the optical switching. We have also studied the effect of the incident angles *versus* the shifting in wavelength peaks as well as the transmittance of the wavelength peaks for three different director tilt angles. The molecular orientation and reorientation behavior of the liquid crystal may be used to achieve optical switching in periodic photonic structures. Such periodic structures with NLC as a defect layer can be applicable in electronic as well as photonic devices, *e.g.* bistable switches, optical filters, feedback lasers, etc.

PS would like to acknowledge Babasaheb Bhimrao Ambedkar University, Lucknow, India, for financial support as UGC non-NET fellowship. Authors are also thankful to Dr. Devendra Singh, Assistant Professor, Dept. of Physics, Babasaheb Bhimrao Ambedkar University, Lucknow and Dr. Narendra Kumar, Assistant Professor, Mody University of Science and Technology, Laxmangarh, Rajasthan, India, for carefully reading the manuscript.

Author contribution statement

All authors have equally contributed to write and to present this manuscript.

References

1. S. Chandrasekhar, *Liquid Crystals* (Cambridge University Press, New York, 1992).
2. I.C. Khoo, *Liquid Crystals* (Wiley Interscience, NJ, 2007).
3. J.D. Joannopoulos, R.D. Meade, J.N. Winn, *Photonic Crystals: Molding the Flow of Electromagnetic Wave* (Princeton University Press, Princeton, 1995).
4. E. Yablonovitch, Phys. Rev. Lett. **58**, 2059 (1987).
5. E. Miroshnichenko, I. Pinkevych, Y.S. Kivshar, Opt. Express **14**, 2839 (2006).
6. K. Bush, S. John, Phys. Rev. Lett. **83**, 967 (1999).
7. K. Yoshino, Y. Shimoda, Y. Kawagishi, K. Nakayama, M. Ozaki, Appl. Phys. Lett. **75**, 932 (1999).
8. S.W. Leonard, J.P. Mondia, H.M. van Driel, O. Toader, S. John, K. Bush, A. Birner, U. Gosele, V. Lehmann, Phys. Rev. B **61**, R2389 (2000).
9. Ch. Schuller, F. Klopf, J.P. Reithmaier, M. Kamp, A. Forchel, Appl. Phys. Lett. **82**, 2767 (2003).
10. D. Kang, J.E. Maclennan, N.A. Clerk, A.A. Zakhidov, R.H. Baughman, Phys. Rev. Lett. **86**, 4052 (2001).
11. E. Graubard, J.S. King, S. Jain, C.J. Summers, Y. Zhang Williams, I.C. Khoo, Phys. Rev. B **72**, 233105 (2005).
12. V.G. Arkhipkin, V.A. Gunyakov, S.A. Myslivsts, V.Ya. Zyryanov, V.F. Shabanov, Eur. Phys. J. E **24**, 297 (2007).
13. Y.M. Strelniker, D. Stroud, A.O. Voznesenkaya, Eur. Phys. J. B **52**, 1 (2006).
14. S.F. Mingaleev, M. Schillinger, D. Hermann, K. Bush, Opt. Lett. **29**, 2858 (2004).
15. E.P. Kosmidou, E.E. Kriezis, T.D. Tsiboukis, IEEE J. Quantum Electron **41**, 657 (2005).
16. B.Ya. Zel'dovich, N.V. Tabiryan, Yu.S. Chilingaryan, Zh. Eksp. Teor. Fiz. **81**, 72 (1981) (Sov. Phys. JETP **81**, 7, (1981)).
17. H.L. Ong, Phys. Rev. A. **28**, 2393 (1983).
18. M.S. Mohamed, M.F.O. Hameed, M.M. El-Okr, Salah S.A. Obayya, Optik **127**, 8774 (2016).
19. S.R. Entezar, A. Madani, M.K. Habil, A. Namdar, H. Tajalli, J. Mod. Opt. **60**, 1883 (2013).
20. R. Ozaki, H. Miyoshi, M. Ozaki, K. Yoshino, Mol. Cryst. Liq. Cryst. **433**, 247 (2005).
21. P.D. Berezin, I.N. Kompanets, V.V. Nikitin, S.A. Pikin, Zh. Eksp. Teor. Fiz. **64**, 599 (1973).
22. I.C. Khoo, Phys. Rev. A **23**, 2077 (1981).
23. A.C. Polycarpou, M.A. Christou, N.C. Papanicolaou, IEEE Trans. Microwave Theory Tech. **60**, 2950 (2012).
24. M.J. Stephen, J.P. Straley, Rev. Mod. Phys. **46**, 617 (1974).
25. L.M. Blinov, *Structure and Properties of Liquid Crystals* (Springer, New York, 2011).
26. P. Yeh, *Optical Waves in Layered Media* (John Wiley & Sons, New York, 1988).
27. M.J. Frisch, G.W. Trucks, H.B. Schlegel, G.E. Scuseria, M.A. Robb, J.R. Cheeseman, G. Scalmani, V. Barone, G.A. Petersson, H. Nakatsuji, X. Li, M. Caricato, A. Marenich, J. Bloino, B.G. Janesko, R. Gomperts, B. Mennucci, H.P. Hratchian, J.V. Ortiz, A.F. Izmaylov, J.L. Sonnenberg, D. Williams-Young, F. Ding, F. Lipparini, F. Egidi, J. Goings, B. Peng, A. Petrone, T. Henderson, D. Ranasinghe, V.G. Zakrzewski, J. Gao, N. Rega, G. Zheng, W. Liang, M. Hada, M. Ehara, K. Toyota, R. Fukuda, J. Hasegawa, M. Ishida, T. Nakajima, Y. Honda, O. Kitao, H. Nakai, T. Vreven, K. Throssell, J.A. Montgomery jr., J.E. Peralta, F. Ogliaro, M. Bearpark, J.J. Heyd, E. Brothers, K.N. Kudin, V.N. Staroverov, T. Keith, R. Kobayashi, J. Normand, K. Raghavachari, A. Rendell, J.C. Burant, S.S. Iyengar, J. Tomasi, M. Cossi, J.M. Millam, M. Klene, C. Adamo, R. Cammi, J.W. Ochterski, R.L. Martin, K. Morokuma, O. Farkas, J.B. Foresman, D.J. Fox, *Gaussian09* (Gaussian, Inc., Wallingford CT, 2009).
28. T.C. King, C.J. Wu, Physica E **69**, 39 (2015).

Materials Research Express

RECEIVED
28 December 2018

REVISED
1 March 2019

ACCEPTED FOR PUBLICATION
15 March 2019

PUBLISHED
29 March 2019

PAPER

Graphene layers on semi-finite 1D asymmetric periodic structure of Si/Glass materials with defect of nematic liquid crystal for a sensor device

Pawan Singh, Khem B Thapa , Narinder Kumar, Krishan Pal and Devesh Kumar

Department of Physics, School of Physical and Decision Sciences, Babasaheb Bhimrao Ambedkar University, Lucknow, India

E-mail: khem.bhu@gmail.com

Keywords: nematic liquid crystal (NLC), graphene (G), absorption, semifinite 1D asymmetric periodic structure, sensor

Abstract

In this work, the effective absorption property of graphene layers on one-dimensional periodic structure (1DPS) of Si/Glass materials with nematic liquid crystal (NLC) as a defect has been studied theoretically. The graphene sheets are stuck on the one end of Si as well as Glass of the semifinite periodic structure of Si/Glass materials. Now the nematic liquid crystal (NLC) is embedded with the semifinite periodic structure of Si/Glass materials containing graphene layers. Using the transfer matrix method (TMM), the transmission and absorption behavior of graphene layers on semi-finite 1D asymmetric periodic structure of Si/Glass materials with a defect of nematic liquid crystal have been studied. Our results suggest that defect layer of nematic liquid crystal (NLC) in the semi-finite 1D asymmetric periodic structure with graphene layers (G),$(Si|Glass)^m|G|NLC|G|(Si|Glass)^n$ with $m = 3$ & $n = 5$, may be used as sensor device due to high absorption behavior for a specific director angle of molecules of the nematic liquid crystal (NLC). Besides this, the absorption behavior of the structure for TE mode, $(Si|Glass)^3|G|NLC|G|(Si|Glass)^5$, is more effective in comparison to the absorption behavior of the structure for TM mode at normal incidence wave.

1. Introduction

Photonic crystal (PC) belong to a unique class of periodic structure of dielectric materials that control the propagation of electromagnetic wave and exhibit photonic band gap (PBG) regions in the transmission of PC. Photonic Band Gap (PBG) are special regions which do not allow to propagate the electromagnetic wave in that region due to the contrast of refractive index and spatially periodicity of the dielectric materials. Therefore, PCs are divided into three categories depending on the periodic modulation of refractive index; one-dimensional photonic crystal (1DPC), two-dimensional photonic crystal (2DPC) and three-dimensional (3DPC). The behavior of PBG depends on the refractive indices of dielectric materials and geometrical parameters of PCs [1]. PC with a defect layer lead to a variety of applications in different ways due to their unique optical properties [2, 3]. The periodic structure of dielectric materials with tunable defect layer can be used in tunable optical devices. The transmission properties of PCs and the photonic band gap (PBG) can be enhanced by changing the geometrical parameters of dielectric materials [4].

Nonlinear optical properties of the liquid crystal (LC) can be used in electro-optics devices, widely [5–7]. The defect layer of nematic liquid crystal (NLC) in one-dimensional periodic structure shows all-optical switching behavior of PC [8]. To understand switching property of LC, nonlinear differential equation of director has been solved and obtained the relation between intensity ratio (I/I_{fr}) and maximum director angle of LCs [9]. InLC as defect layer in a periodic structure, when the intensity (I) of the electromagnetic wave reaches to threshold intensity, Freedericksz transition (I_{fr}), LC molecules switch according to intensity ratio (I/I_{fr}) and execute tunable transmission of one-dimensional periodic structure [10, 11]. It is well known that LC has nonlinear optical and electronic properties, graphene (G) also novel optical and electronic properties [12].

© 2019 IOP Publishing Ltd

The discovery of graphene leads the new way to development in the field of nanoscience and nanotechnology [13]. Graphene is a 2D nanomaterial with honeycomb lattice of carbon atoms and such lattice form the basic planer structure for graphite [14, 15]. Due to unique properties, graphene widely used in optical display and instead of transparent electrodes and window electrodes for solar cell applications [16–18]. Graphene also has semiconductor nature with the zero bandgap and massless electrons and holes, such electrons and holes can be characterized as Dirac-Fermions [19]. Graphene has two bands known as interband and intraband and because of these bands, graphene has remarkable optical and electrical properties. The optical conductivity of graphene sheet can be easily evaluated by consisting both interband and intraband contributions. By evaluating the optical conductivity, we can calculate the dielectric function of graphene which depends on the chemical potential [20]. The optical properties of graphene in visible region independent of frequency [21] which enhance the absorption property of PC [22]. The absorption property of graphene can be tuned by the incident angle of the electromagnetic wave as well as the position of the graphene layer in PCs [23].

On the basis of total reflection, Zhao *et al* [24] suggested that the absorption property of graphene layers can be amplified from visible to IR region. The optical property of graphene is dependent on the direction and magnitude of strain i.e. transmission properties are dependent on the incident polarization [25]. Graphene also applicable in photodetectors and the efficiency of graphene-based photodetectors can be enhanced by using the combination of graphene with plasmonic nanostructures and Fabri-Perot cavities [26, 27]. The optical properties of graphene are dependent on the polarization and enhanced coupling of electromagnetic wave with graphene which is very useful in optical device application [28]. The maximum absorption can be achieved with doped graphene nanodisks array attached to substrate under total internal reflection and it can be used in solar cell and many other novel device application [29].

Graphene is used in the plasmonic device due to the high density of states. Moreover, a graphene embedded photonic crystals are also used to modify the PBG by the effective parameter of the graphene layer like chemical potential [30]. The dispersion curves of graphene are obtained through effective medium theory and which is confirmed with the derived dispersion curves. The transmission and dispersion relations of graphene had enlightened by the variation of incident angle and effective permittivity of the graphene [31]. By studying the transmission of the graphene embedded PC, the defect mode has obtained with a variation of the incident angle and the gate voltage of graphene, and such graphene embedded PC is used as a tunable device, optical filters, sensors [32]. As a graphene defect in the PC, the graphene exhibits different frequencies for the localization of incident electromagnetic wave, and PBG is tuned by the localized mode of the electromagnetic wave in the PCs [33]. Graphene-based periodic structures of different materials have various novel applications in optics and photonics due to having the variable parameters chemical potential, incident angle etc.

In this work, we have used well-known transfer matrix method (TMM) [34] to study the transmission and absorption properties of defect nematic liquid crystal (NLC) in semi-finite 1D asymmetric periodic structure of Si/Glass materials with and without graphene (G) layers. The defect of NLC in 1D periodic structure (PS) with graphene layers is a semifinite periodic structure of Si/Glass material where graphene is stuck on Si and Glass surface, and NLC is embedded with stuck graphenes with one end of Si as well as Glass in an asymmetric manner. We have focused our calculations to study the absorption characteristics of defect NLC in 1D semifinite periodic structure of Si/Glass materials containing graphene layers with different orientation of NLC'smolecule for TE and TM modes.

2. Theory and structural model

We consider a nematic liquid crystal (NLC) cell of thickness L with the homeotropic arrangement of LC molecules defined by $\phi(z)$ which is called director angle. When an electromagnetic wave interacts with NLC cell, LC molecules orient and reorients that is dependent on the intensity ratio of the incident light wave (I) to Freederikcsz transition intensity (I_{fr}). The director angle ($\phi(z)$) of LC reaches a maximum value ϕ_{max} at the middle of the cell. To understand the switching property of molecules of LCs, we have solved the nonlinear differential equation of director given as:

$$\phi_{zz} - \frac{k \sin(2\phi)}{2(1 - k \sin^2 \phi)}\phi_z^2 + \frac{\pi^2 I \sin(2\phi)}{2L^2 I_{fr}(1 - k \sin^2 \phi)(1 - \beta \sin^2 \phi)^{3/2}} = 0 \quad (1)$$

where ϕ_{zz}, ϕ_z are double and single partial derivatives of ϕ with respect to z, k and β are given as:

$$k = \frac{(k_{33} - k_{11})}{k_{33}}, \quad \beta = 1 - \left(\frac{{n_o}^2}{{n_e}^2}\right) \quad (2)$$

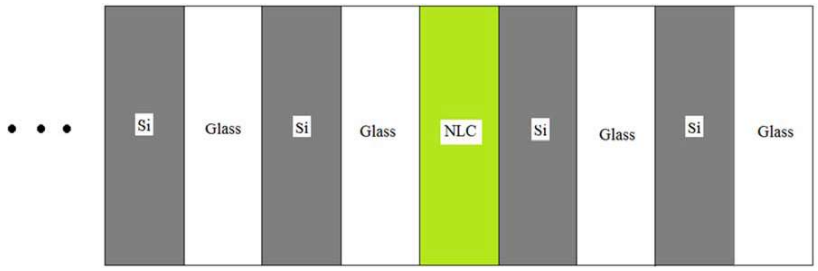

Figure 1. Schematic diagram of the one-dimensional periodic structure of Si/Glass materials with nematic liquid crystal (NLC) as a defect.

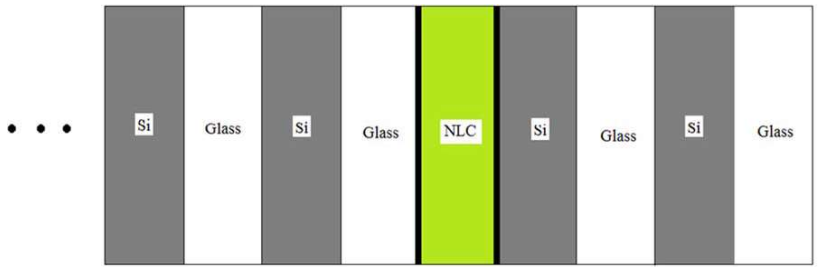

Figure 2. Schematic diagram of stuck graphene layers (dark black line) on Si and Glass material in one-dimensional periodic structure of Si/Glass materials with nematic liquid crystal (NLC) as a defect layer.

The solution of equation (1) can be obtained using Dirichlet type boundary conditions (BCs):

$$\phi(z = 0) = 0; \quad \phi(z = L) = 0 \tag{3}$$

The relation between maximum director angle ϕ_{max} and intensity ratio (I/I_{fr}) can be obtained by solving equation (1). When the intensity (I) of electromagnetic wave is less than Freedericksz transition intensity (I_{fr}) i.e. $I < I_{fr}$, there is no orientation of LC molecules, the intensity (I) becomes equal or higher to Freedericksz transition (I_{fr}), LC molecules switches in particular directions depending on the intensity ratio (I/I_{fr}) [35].

The complex dielectric function of graphene which depends on the chemical potential has also studied. To obtain the dielectric function of graphene, we have used the total conductivity of graphene which can be represented as:

$$\sigma_{total} = \sigma_{intra} + \sigma'_{inter} + i\sigma''_{inter} \tag{4}$$

where $\sigma_{int\ ra} = \frac{\sigma_0 4\mu}{\pi\hbar(\tau_1 - i\omega)}$, and $\sigma'_{inter} = \sigma_0\left(1 + \frac{1}{\pi}\arctan\left(\frac{\hbar\omega - 2\mu}{\hbar\tau_2}\right) - \frac{1}{\pi}\arctan\left(\frac{\hbar\omega + 2\mu}{\hbar\tau_2}\right)\right)$ and $\sigma''_{int\ er} = -\sigma_0\frac{1}{2\pi}\ln\frac{(2\mu + \hbar\omega)^2 + (\hbar\tau_2)^2}{(2\mu - \hbar\omega)^2 + (\hbar\tau_2)^2}$.where $\sigma_0 = e^2/(4\hbar)$ is universal optical conductance equal to 60.8 μS; the dielectric function of graphene sheet given as:

$$\varepsilon(\omega) = 1 + \left(\frac{i\sigma(\omega)}{\omega\varepsilon_0 d_g}\right) \tag{5}$$

where d_g is the thickness of the graphene layer and ε_0 is vacuum permittivity.

In our calculations, we have considered two periodic structures: (i) one-dimensional periodic structure of Si/Glass materials with nematic liquid crystal (NLC) as defect i.e. $(Si|Glass)^m|NLC|(Si|Glass)^n$ as shown in figure 1, (ii) Graphene layers (G) in one dimensional periodic structure of Si/Glass materials with nematic liquid crystal (NLC) as defect, $(Si|Glass)^m|G|NLC|G|(Si|Glass)^n$, where m, n are number of periodicity of Si/Glass, as shown in figure 2. The transmittance and absorption properties of the considered periodic structures have been calculated using the transfer matrix method (TMM) [34].

3. Results and discussion

In this section, the variation of maximum director angle (ϕ_{max}) of molecules of the LC versus I/I_{fr} and nature of the dielectric function of graphene versus wavelength (μm) have discussed. When the intensity (I) of the

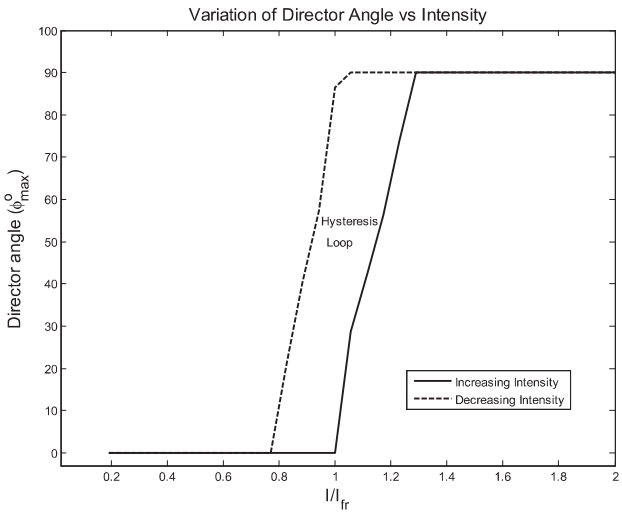

Figure 3. Variation of maximum director angle (ϕ_{max}) with I/I_{fr} for the increase and decrease intensities.

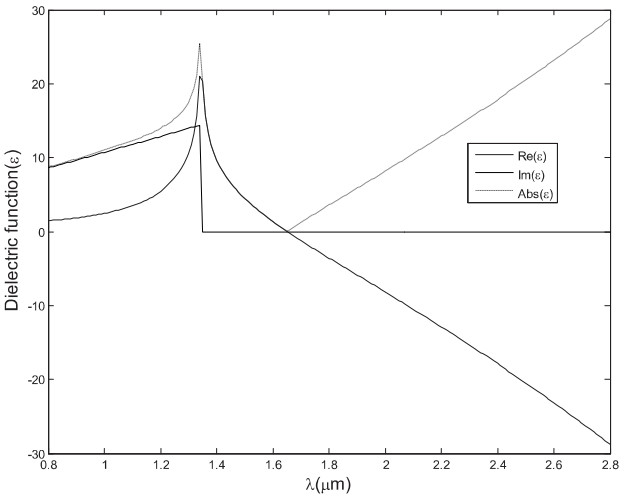

Figure 4. Variation of a dielectric function of graphene versus wavelength in the microwave region at $\mu = 0.4$ eV.

electromagnetic wave is reached to Freedericksz transition intensity (I_{fr}), LC molecules orient at different director angles 0°, 28.7°, 42.7°, 56.3°, 73° and 90° for increasing intensity [36, 37]. Similarly, LC molecules obey different path to reorient with different director angles for decrease the intensity as shown in figure 3. As a result, a hysteresis loop is found which shown the optical switching process of the LC cell. The reason for hysteresis is the landscape of free energy of LC which leads to the first order nature of optically induced transition in LC. For the study the optical properties of considered periodic structures, we have considered only three arbitrary directory angles, 28.7°, 42.7°, and 56.3°.

Now, we discuss the behavior of the dielectric function of graphene in 0.8 μm to 2.8 μm wavelength region. The complex conductivity of graphene depends on the angular frequency (ω), relaxation time (τ), the chemical potential (μ) and fixed temperature as in equations (4) and (5) [38, 39]. The dielectric function of graphene calculated as the function of chemical potential for $\lambda = 1550$ nm, temperature (T) = 296 K and $\tau_1 = 1.2$ ps, $\tau_2 = 10$ fs for interband and intraband conductivity, respectively. The dielectric function of graphene has real and imaginary values which are responsible for the 'metallic nature' of graphene. Figure 4 shows a variation of the dielectric function of single-layer graphene with wavelength at chemical potential $\mu = 0.4$ eV. Having the imaginary values of the dielectric function, the graphene shows metallic nature which is responsible for absorption property [40]. Figure 4 depicted that the real value of dielectric function first increases and becomes maximum at $\lambda = 1.3$ μm, then further decreases with wavelength. The imaginary part of the dielectric function

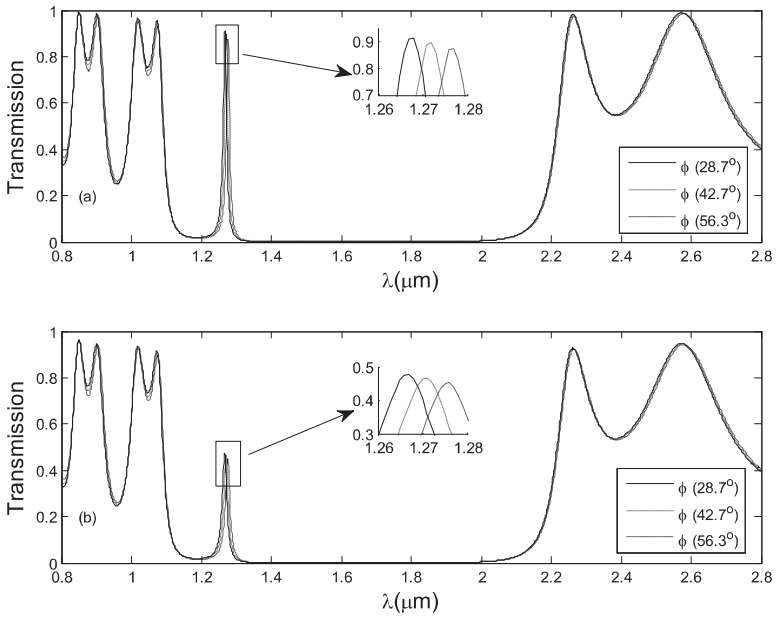

Figure 5. Transmission spectra of periodic structuresat three LC director angles with m = n = 3. (a) $(Si|Glass)^m|NLC|(Si|Glass)^n$ (b) $(Si|Glass)^m|G|NLC|G|(Si|Glass)^n$.

first increases and becomes maximum at $\lambda = 1.3\ \mu$m and then sharply decreases to zero and becomes constant for all further wavelength up to 2.8 μm.

To study the effect of graphene layers in 1D periodic structure of Glass and Si materials with NLC as a defect, the thicknesses of Glass, Si, NLC, and graphene (G)layers are considered as 110 nm, 250 nm, 100 nm, and 0.34 nm, respectively. We have considered the periodic structure $(Si|Glass)^m|NLC|(Si|Glass)^n$ and $(Si|Glass)^m|G|NLC|G|(Si|Glass)^n$ with m = n = 3, as shown in figures 1 and 2. The transmittance and absorption properties of $(Si|Glass)^m|NLC|(Si|Glass)^n$ and $(Si|Glass)^m|G|NLC|G|(Si|Glass)^n$ periodic structure with m = n = 3 has been shown in figures 5 and 6, respectively, where NLC is nematic liquid crystal, G is a single graphene layer. The transmittance and absorption properties of the considered periodic structures are analyzed using the transfer matrix method (TMM) [34]. The transmissions of $(Si|Glass)^m|NLC|(Si|Glass)^n$ and $(Si|Glass)^m|G|NLC|G|(Si|Glass)^n$ periodic structures at three LC director angles, 28.7°, 42.7°, and 56.3°, for m = n = 3, are shown in figure 5. Figure 5(a) shows the transmission of $(Si|Glass)^3|NLC|(Si|Glass)^3$ periodic structure with 90% 88% and 86% transmission of defect peaks, respectively. Now, we calculate the transmittance of $(Si|Glass)^3|G|NLC|G|(Si|Glass)^3$ periodic structure as shown in figure 5(b), where graphene layers are stuck on the surfaces of Si and Glass materials. The transmittance of the defect peaks obtains in transmission of $(Si|Glass)^3|NLC|(Si|Glass)^3$ at 28.7°, 42.7° and 56.3° director angles of LC, respectively and reduced to 48%, 46%, and 44% for $(Si|Glass)^3|G|NLC|G|(Si|Glass)^3$ periodic structure. The transmission properties of $(Si|Glass)^3|NLC|(Si|Glass)^3$ periodic structure show that the defect transmission peak is affected in the presence of graphene layers. Such defect mode peaks obtained in the transmission of the one-dimensional periodic structure of Si/Glass materials with NLC as defect without and with graphene layers are also shifted when director angle increases as shown in figure 5. We can conclude that the presence of graphene layers transmittance of defect peaks obtained in the transmission spectra of PC. The positions of obtained defects can be tuned by variation of LC director angle or intensity of the electromagnetic wave. Although the transmission properties of PC are affected, the PBG regions are not affected by the variation of LC director angle.

The effective absorption properties of both considered periodic structures $(Si|Glass)^m|NLC|(Si|Glass)^n$ and $(Si|Glass)^m|G|NLC|G|(Si|Glass)^n$, with m = n = 3, shown in figure 6. Figure 6(a) shows that no absorption of defect peaks are obtained in the transmission of $(Si|Glass)^3|NLC|(Si|Glass)^3$ periodic structure, either LC molecules are oriented or reoriented by the applied field. Again, we have studied the absorption spectra of $(Si|Glass)^3|G|NLC|G|(Si|Glass)^3$ structure as shown in figure 6(b). The absorption of defect mode peaks obtained for $(Si|Glass)^3|G|NLC|G|(Si|Glass)^3$ structure increases from 0% to 28%, 27% and 26% for three LC director angles. The absorption of defect peaks are found to be 28%, 27% and 26% for 28.7°, 42.7°, and 56.3° LC director angle, respectively. The absorption of the considered periodic structure with graphene layers is enhanced due to the metallic behavior of the graphene layer which is already discussed in figure 4. The

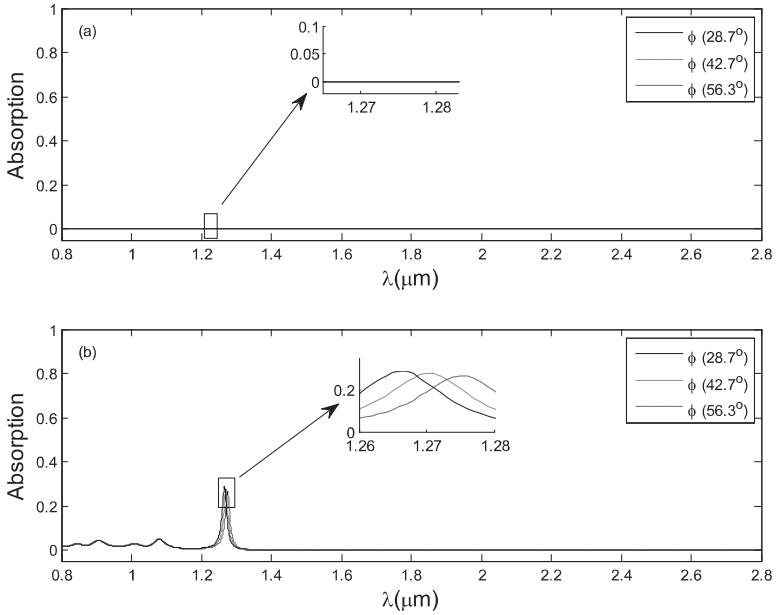

Figure 6. Absorption spectra of periodic structures three LC director angle with m = n = 3. (a) $(Si|Glass)^m|NLC|(Si|Glass)^n$ (b) $(Si|Glass)^m|G|NLC|G|(Si|Glass)^n$.

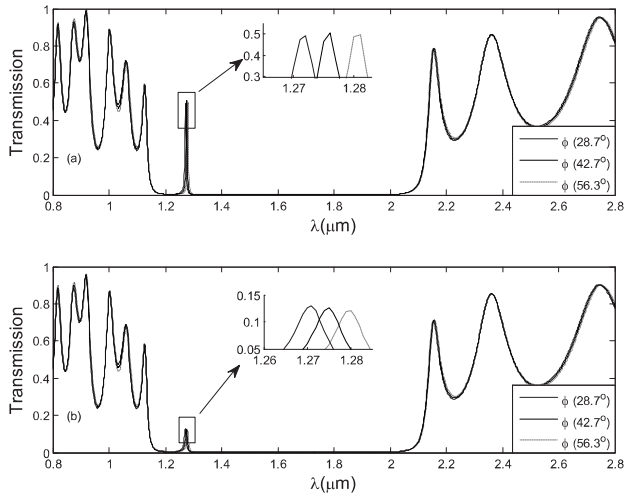

Figure 7. Transmission spectra of periodic structuresat three LC director angles with m = 3, n = 5. (a) $(Si|Glass)^m|NLC|(Si|Glass)^n$ (b) $(Si|Glass)^m|G|NLC|G|(Si|Glass)^n$.

absorption of periodic structure can be tuned by the variation of chemical potential (gate voltage) of the graphene layers and director angle of LC.

The transmission and absorption of $(Si|Glass)^m|NLC|(Si|Glass)^n$ and $(Si|Glass)^m|G|NLC|G|(Si|Glass)^n$ periodic structure at different LC director angle with m = 3, n = 5 are shown in figures 7 and 8. The transmission of defect peaks is reduced to 48%, 50%, 52% from 90%, 88%, 86% for 28.7°, 42.7°, and 56.3°LC director, respectively as shown in figure 7(a). Again, the transmittance of $(Si|Glass)^3|G|NLC|G|(Si|Glass)^5$ periodic structure is calculated as shown in figure 7(b). The transmittance of defect peaks is reduced to 13%, 12%, and 11% for 28.7°, 42.7°, and 56.3° LC director angles, respectively due to the imaginary refractive index of graphene.

However the transmission of defect peaks is reduced, no absorption found for any defect peaks in the considered wavelength region (μm), as shown in figure 8(a). Figure 8(b) shows the enhancement absorption of defect peaks up to 85%, 84% and 82% at three LC director angles 28.7°, 42.7°, and 56.3°, respectively. The absorption of defect peaks is obtained in the transmission of periodic structure $(Si|Glass)^3|G|NLC|G|(Si|Glass)^3$,

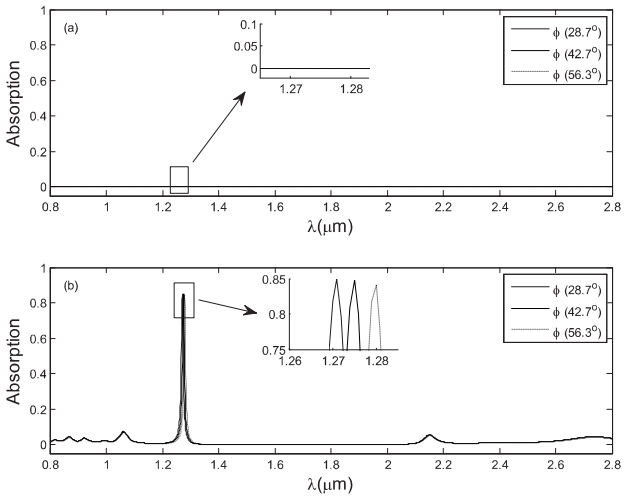

Figure 8. Absorption spectra of periodic structuresat three LC director angles with m = 3, n = 5. (a) $(Si|Glass)^m|NLC|(Si|Glass)^n$ (b) $(Si|Glass)^m|G|NLC|G|(Si|Glass)^n$.

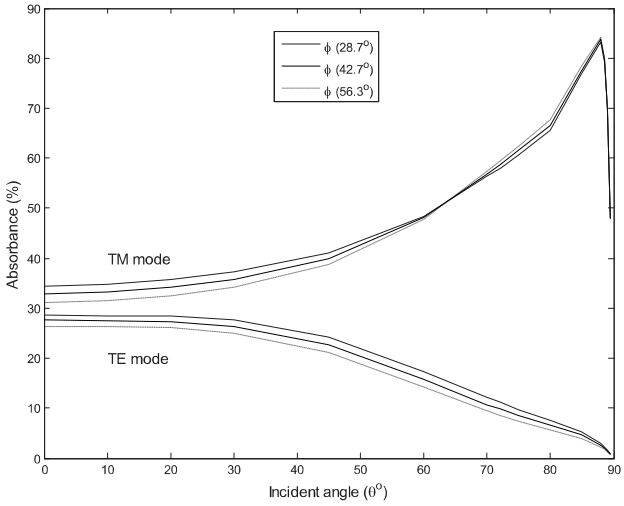

Figure 9. Variation of absorption of defect peaks obtained at three LC director angles in the transmission of $(Si|Glass)^3|G|NLC|G|(Si|Glass)^3$ with the incident angle for TE and TM modes.

is found to be 28%, 27%, and 26% but the absorption of defect peaks in case of periodic structure $(Si|Glass)^3|G|NLC|G|(Si|Glass)^5$, is found to be 85%, 84% and 82% for LC director angles 28.7°,42.7°, and 56.3°, respectively. The enhancement in the absorption of the periodic structure is found when the periodicity of dielectric layers is changed from n = 3 to 5.

Beside this, we have also studied the absorption of defect peaks which was obtained for transmission of $(Si|Glass)^3|G|NLC|G|(Si|Glass)^3$ periodic structure with the variation of incident angle at three LC director angles for TE and TM modes. Figure 9 shows the comparative absorption behavior of $(Si|Glass)^3|G|NLC|G|(Si|Glass)^3$ periodic structure for both modes. The absorption of defect peaks decreases as the incident angle of electromagnetic wave increases for TE mode. But in case of TM mode, absorption first increases up to incident angle 88° and then decreases sharply. The comparative study of the absorption of defect peaks for TE and TM modes shows that the absorption for TM mode is more effective than TE mode due to the changed refractive index of the graphene at chemical potential (μ) = 0.4 eV as shown in figure 4. The changed phase of the absorbance in TM mode shows that the refractive of graphene has metallic nature.

Similarly, we have studied the absorption behavior of defect peaks which was obtained for transmission of $(Si|Glass)^3|G|NLC|G|(Si|Glass)^5$ periodic structure at different LC director angles for TE and TM modes as shown in figure 10. The absorption of defect peaks decreases as the incident angle increases for TE mode. But the

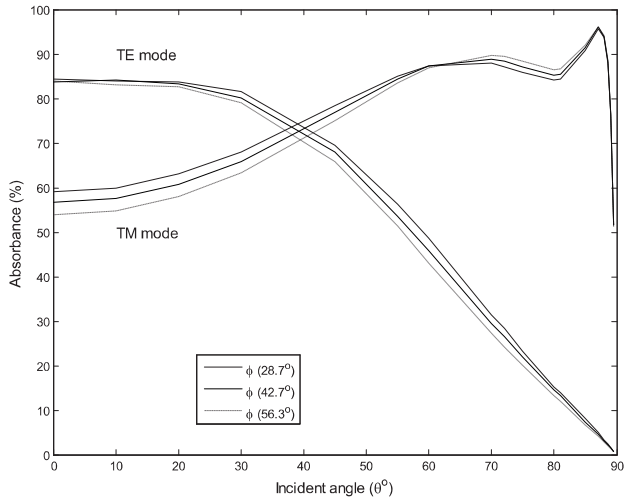

Figure 10. Variation of absorption of defect peaks obtained at three LC director angles in the transmission of $(Si|Glass)^3|G|NLC|G|(Si|Glass)^5$ with the incident angle for TE and TM modes.

absorption of defect peaks for TM mode increases with the incident angle up to 63° then decrease up to 80°, and again absorption increases up to 88° and sharply decreases with incident angle. Here, high absorption is obtained for TE mode in comparison to TM mode at normal incidence, but the absorption becomes high for TM modes at exiting Brewster's angle behavior in the considered periodic structures.

4. Conclusions

In this work, we have investigated the transmission and absorption spectra of $(Si|Glass)^m|G|NLC|G|(Si|Glass)^n$ periodic structure at three LC director angles i.e. 28.7°, 42.7°, and 56.3°, where m and n are the periodicities of layers. The absorption spectra of the $(Si|Glass)^3|G|NLC|G|(Si|Glass)^3$ and $(Si|Glass)^3|G|NLC|G|(Si|Glass)^5$ periodic structures have been compared. The high absorption has obtained for $(Si|Glass)^3|G|NLC|G|(Si|Glass)^5$ periodic structure for three LC director angles: 28.7°, 42.7°, 56.3°. The enhanced absorption of the periodic structure $(Si|Glass)^3|G|NLC|G|(Si|Glass)^5$ has been found for TE mode at three defect peaks obtained in the transmission spectra. Such absorption property of $(Si|Glass)^3|G|NLC|G|(Si|Glass)^5$ periodic structure may be used as sensor and detector devices for three particular wavelengths (1.26 μm, 1.273 μm, 1.278 μm) at normal incidence for LC director angles; 28.7°, 42.7°, 56.3°. The absorption of such periodic structure $(Si|Glass)^3|G|NLC|G|(Si|Glass)^5$ is more effective for TE mode in comparison to TM mode at normal incidence of the electromagnetic wave.

Acknowledgments

We are thankful to Babasaheb Bhimrao Ambedkar University, Lucknow, for providing Non-NET UGC fellowship. This research work did not receive any specific grant from funding agencies in the public, commercial, or not-for-profit sectors.

ORCID iDs

Khem B Thapa https://orcid.org/0000-0003-2639-0652

References

[1] Sukhoivanov I A and Guryev I V 2009 *Physics and Practical Modeling* (Berlin: Springer)
[2] Russell P 2003 Photonic crystal fibers *Science* **299** 358–62
[3] Akahane Y, Asano T, Shik B and Noda S 2003 High –Q photonic nanocavity in a two-dimensional crystal *Nature* **425** 944–7
[4] Fu J, Chen W and Lv B 2016 Tunable defect mode realized by graphene-based photonic crystal *Phys. Lett.* A **380** 1793–8
[5] Blinov L M 2011 *Structure and Properties of Liquid Crystals* (New York: Springer)
[6] Chandrasekhar S 1992 *Liquid Crystals* (New York: Cambridge University Press)
[7] Stephen M J and Straley J P 1974 Physics of liquid crystals *Rev. Mod. Phys.* **46** 617–704

[8] Miroshnichenko E, Pinkevych I and Kivshar Y S 2006 Tunable all-optical switching in periodic structure with liquid-crystal defects *Opt. Exp.* **14** 2839–44
[9] Polycarpou C, Christou M A and Papanicolaou N C 2012 A Mode-matching approach to electromagnetic wave propagation in nematic liquid crystals *IEEE Trans on Micro. Theo. and Tech.* **60** 2950–8
[10] Zel'dovich B Y, Tabiryan N V and Chilingaryan Y S 1981 Freedericksz transition induced by electromagnetic wave fields *Zh. Eksp. Teor. Fiz.* **81** 72–83
[11] Ong H L 1983 Optically induced Freedericksz transition and bistability in a nematic liquid crystal *Phys. Rev.* A **28** 2393–407
[12] Berman O L and Kezerashvili R Y 2012 Graphene-based one-dimensional photonic crystal *J. Phys: Condens Matter* **24** 015305
[13] Novoselov K S, Geim A K, Morozov S V, Jiang D, Zhang Y, Dubonos S V, Grigorieva I V and Firsov A A 2004 Electric field effect in atomically thin carbon films *Science* **306** 666–9
[14] Geim K and Novoselov K S 2007 The rise of graphene *Nat. Mat.* **6** 183–91
[15] Zhang Y, Small J P, Amori M E S and Kim P 2005 Electric field modulation of galvanomagnetic properties of mesoscopic graphite *Phys. Rev. Lett.* **94** 176803
[16] Al-sheqefi F U Y and Belhadj W 2015 Photonic band characteristics of one-dimensional graphene-dielectric periodic structures *Superlattice and Microstructures* **88** 127-38
[17] Wang X, Zhi L and Mullen K 2008 Transparent, conductive graphene electrodes for dye-sensitized solar cells *Nano Lett.* **8** 323–7
[18] Bae S *et al* 2010 Roll-to-roll production of 30-inch graphene films for transparent electrodes *Nat. Nanotechnol* **5** 574–8
[19] Sharma S D, Hwang E H and Tse W K 2007 Many-body interaction effects in doped and undoped graphene: fermi liquid versus non-fermi liquid *Phys. Rev.* B **75** 121406 (R)
[20] Gosciniak J and Tan D T H 2013 Theoretical investigation of graphene-based photonic modulators *Sci. Rep.* 1–6
[21] Falkovsky L A 2008 Optical properties of graphene *J. Phys. Conf. Ser.* **129** 012004–7
[22] Khaleque A and Hattori H T 2016 Absorption enhancement in graphene photonic crystal structures *Appl. Opt.* **55** 2936–42
[23] Liu J T, Liu N H, Li J, Li X J and Huang J H 2012 Enhanced absorption of graphene with one-dimensional photonic crystal *Appl. Phys. Lett.* **101** 052104
[24] Zhao W, Shi K and Lu Z 2013 Greatly enhanced ultrabroadband light absorption by monolayer graphene *Opt. Lett.* **38** 4352–4345
[25] Pereira V M, Ribeiro R M, Peres N M R and Neto A C 2010 Optical properties of strained graphene *Europhys. Lett.* **92** 67001
[26] Echtermeyer T J, Britnell L, Jasnos P K, Lombardo A, Gorbachev R V, Grigorenko A N, Geim A K, Ferrari A C and Novoselov K S 2011 Strong plasmonic enhancement of photovoltage in graphene *Nat. Commun.* **2** 458
[27] Ferreira A, Peres N M R, Ribeiro R M and Stauber T 2012 Graphene based photodetector with two cavities *Phys. Rev.* **85** 115438–9
[28] Ye Q, Wang J, Liu Z, Deng Z C, Kong X T, Xing F, Chen X D, Zhou W Y, Zheng C P and Tian J G 2013 Polarization-dependent optical absorption of graphene under total internal reflection *Appl. Phys. Lett.* **102** 021912–4
[29] Thongrattanasiri S, Koppens F H and de Abajo F J G 2012 Complete optical absorption in periodically patterned graphene *Phys. Rev. Lett.* **108** 047401–5
[30] Qiu G P, Qiu W, Lin Z, Chen H, Tang Y, Wang J-X, Kan Q and Pan J-Q 2016 Investigation of the band structure of graphene-based plasmonic photonic crystals *Nanomaterials* **6** 166
[31] Qui L and Liu C 2017 Complex band structures of 1D anisotropic graphene photonic crystal *Photonics Research* **5** 543–51
[32] Mahmoodzadeh H and Rezaei B 2018 Tunable Bragg defect mode in one-dimensional photonic crystal containing a graphene-embedded defect layer *Appl. Opt.* **57** 2172–6
[33] Berman O L, Boyko V S, Kezerashvili R Y, Kolesnikov A A and Lozovik Y E 2018 On transmittance and localization of the electromagnetic wave in two-dimensional graphene-based photonic crystals *Phys. Lett.* A **382** 2075–80
[34] Yeh P 1988 *Optical Waves in Layered Media* (New York: Wiley)
[35] Berezin P D, Kompanets I N, Nikitin V V and Pikin S A 1973 Orienting effect of an electric field on nematic liquid crystals *Zh. Eksp. Teor. Fiz.* **64** 599–607
[36] Frisken B J and Palffy M P 1989 Freedericksz transitions in nematic liquid crystals: the effects of an in-plane electric field *Phys. Rev.* A **40** 6099–102
[37] Ong H L 1986 First- and second-order Freedericksz transitions in nematic liquid crystals subjected to static and optical-electromagnetic fields *IEEE Transactions on Electron Devices* **33** 1195–200
[38] Gosciniak J and Tan D T H 2013 Graphene-based waveguide integrated dielectric-loaded plasmonic electro-absorption modulators *Nanotechnology* **24** 185202
[39] Chen P Y, Argyropoulos C, Farhat M and Diaz J S G 2017 Flatland plasmonics and nanophotonics based on graphene and beyond *Nanophotonics* **6** 1239–62
[40] Guo C, Zhang J, Xu W, Liu K, Yuan X, Qin S and Zhu Z 2018 Graphene-based perfect absorption structures in the visible to terahertz band and their optoelectronics applications *Nanomaterials* **8** 1033

Results in Physics 13 (2019) 102346

Contents lists available at ScienceDirect

Results in Physics

journal homepage: www.elsevier.com/locate/rinp

Study of transmission property of periodic layer consisting of SiO_2 and TiO_2 layers with anisotropic liquid crystal (LC) and $LiNbO_3$ as defect layers for optical switching

Pawan Singh, Khem B. Thapa*, Narinder Kumar, Devendra Singh, Devesh Kumar

Department of Physics, School of Physical and Decision Sciences, Babasaheb Bhimrao Ambedkar University (A Central University), Vidya Vihar, Raebareli Road, Lucknow 226025, UP, India

ARTICLE INFO

Keywords:
Anisotropic liquid crystal (LC)
$LiNbO_3$
4 × 4 transfer matrix method (TMM)
Blue shift

ABSTRACT

This paper reports the theoretical investigation of transmission properties of a one-dimensional periodic layer consisting of SiO_2 and TiO_2 layers with anisotropic liquid crystal (LC) and $LiNbO_3$as defect layers with the variation of incident angle, temperature and applied a voltage across the crystal. The optical transmission properties of the considered structure have been calculated by using a 4 × 4 transfer matrix method (TMM). The transmittance of the considered structure with LC and $LiNbO_3$as defects gives rise to defect mode wavelength peak inside the bandgap region. The transmittance peak of the defect mode shows the blue shift in the transmission of periodic structure for TE and TM polarizations with incident angle, applied voltage, and temperature. Further, the transmission behavior of defect modes and terminal wavelengths are analyzed with the variation of incident angle and temperature. The transmission of the considered structure has found the tunable characteristics due to the presence of anisotropic defect layer LC and $LiNbO_3$. The one-dimensional periodic layer consisting of SiO_2 and TiO_2 layers with the defect layers of anisotropic materials, liquid crystal (LC) and $LiNbO_3$, as may be used to design optical switching devices.

Introduction

Photonic crystal (PC) is a special kind of optical periodic media which consist of a periodic arrangement of a dielectric layer with periodic modulation of dielectric constants in different directions. PCs can be classified into three types: one-dimensional, two-dimensional, and three-dimensional photonic crystal. The optical properties of the periodic optical media depend upon the interaction of the electromagnetic wave with the dielectric materials and the periodicity of dielectric parameters. Due to the periodicity of dielectric constants, PCs have the ability to control the propagation of the electromagnetic wave in the periodic media and possess the photonic band gap (PBG) in the transmission spectra. PBGs are special region of certain frequency range, where no electromagnetic wave can transmit inside the PCs and such property of PCs can be utilized in many optical devices [1–11]. If we introduce a defect layer into pure PCs then a sharp defect mode peak of high transmission appears in the PBG regions due to the changed refractive index contrast of the structure [12–14]. The optical properties of PCs can be tuned by applying external parameters viz. electric field, voltage, temperature, etc. Hence, PCs can be used as active material in optical devices, microwave and optoelectronic applications [15–24]. The tunability of PCs can be achieved by introducing a defect layer into PCs with an externally controlled refractive index of the dielectric layer. A lot of work has been done to achieve the tunability of photonic crystal using external parameters e.g. electric and magnetic fields, Kerr effect, temperature, etc. [25–27]. By applying positive and negative bias on the defect mode layer in the PCs, blue and red shift was detected in the transmissions of PCs. The blue shift of transmission peak depends upon the incident angle of the electromagnetic wave for both TE and TM modes. The tunable optical filter application of PCs has been studied by 4 × 4 transfer matrix method (TMM) [28–29]. The $LiNbO_3$ is a uniaxial anisotropic material and the refractive index of such materials varies with applied voltage and incident angle. Such anisotropic material is used as a defect layer into PCs to achieve the tunability of PCs [30–32]. Liquid crystal (LC) is also an anisotropic material similar to $LiNbO_3$ material, and LC can be used for tunability of the PCs.

Generally, liquid crystals are organic materials which have both types of properties viz. solid like crystalline property and liquid-like flow properties. LCs are the birefringent materials and mainly classified into three categories: lyotropic, thermotropic and metallotropics. The

* Corresponding author.
E-mail address: khem.bhu@gmail.com (K.B. Thapa).

https://doi.org/10.1016/j.rinp.2019.102346
Received 25 February 2019; Received in revised form 10 May 2019; Accepted 10 May 2019
Available online 17 May 2019
2211-3797/ © 2019 Published by Elsevier B.V. This is an open access article under the CC BY-NC-ND license (http://creativecommons.org/licenses/BY-NC-ND/4.0/).

dielectric parameters of thermotropic LCs depend on the temperature and external field. They are found in mostly three phases i.e. nematic, cholesteric, and smectic. The nematic phase is a common phase and found in various LCs. LCs are nonlinear and anisotropic materials which converted into isotropic phase at clearing temperature (T_C) and hence, LCs can be used in nonlinear tunable optical devices [33–35]. LCs are birefringent materials, have electric field and temperature dependent dielectric tensor, hence the tunable optical transmission can be achieved by introducing LCs as a defect layer into PCs. Busch et al. [36] suggested that the tunable optical transmission can be produced by the varnish the inverse opal and Yoshino et al. confirmed it [37]. The optical characteristics of the LCs can be tuned by temperature and external field; hence the optical characteristics of PCs can be controlled by the electric field and temperature. In view of experiments, the infiltration of pores with LCs in PCs is another method of achieving tunable optical transmission [38–42]. LCs are extraordinary optical materials and used in tunable devices due to their novel optical properties, all-optical switching, and regulated transmissions. The transmission of one-dimensional periodic structure (1DPS) consisting LC defect layer with the influence of LC director and the temperature was investigated by Mohamed et al. [43] and the optical reactions of a 1DPS with LC as a defect layer was studied by Entezar et al. [44]. They concluded that the tunability of PCs can be achieved by regulating the dielectric parameters of LCs [45–47] and also suggested the dependence of bistability of PCs on the temperature and demonstrated the effects of temperature on the optical characteristics of the PCs due to the LC. LCs are anisotropic organic material and they have LC director distortion angle dependent dielectric tensor. Pankin et al. [48] studied the hybrid Tamm-microcavity modes in one-dimensional photonic crystal and proposed that hybrid modes could be tuned by the variation of temperature and applied an electric field. LC dielectric tensor ($\tilde{\varepsilon}$)can be expressed in terms of dielectric components ($\varepsilon_{||}$, $\varepsilon_{\perp}$)[46,49] and the dielectric anisotropy ($\varepsilon_a = \varepsilon_{||} - \varepsilon_{\perp}$) of the LC;

$$\tilde{\varepsilon} = \begin{pmatrix} \varepsilon_{\perp} + \varepsilon_a \sin^2\varphi & 0 & \varepsilon_a \sin\varphi\cos\varphi \\ 0 & \varepsilon_{\perp} & 0 \\ \varepsilon_a \sin\varphi\cos\varphi & 0 & \varepsilon_{\perp} + \varepsilon_a \cos^2\varphi \end{pmatrix} \tag{1}$$

The dielectric tensor of LC can be expressed by Eq. (1) which is a 3 × 3 matrix with non-diagonalized elements. The elements of the matrix have LC molecule orientation dependent parameters e.g.$\varepsilon_{||}$, $\varepsilon_{\perp}$and distortion tilt angle (φ) with respect to the z-axis. The dielectric tensor matrix can be reduced to simple diagonalized matrix for the distortion angles $\varphi = 0^{\circ}$ and $\varphi = 90^{\circ}$. In these conditions, we may apply the transfer matrix method (TMM) to study the optical properties [50].

In this paper, we have studied the refractive indices of E7 liquid crystal (LC) mixture with different temperatures, and $LiNbO_3$ material (LNO) with different voltages. Using 4 × 4 transfer matrix method, the optical transmission of a one-dimensional photonic crystal with a composite defect of the E7 LC mixture and LNO material, $(SiO_2|TiO_2)^5|LC|LNO|LC|(TiO_2|SiO_2)^5$, has been investigated with the variation of temperature and applied voltage.

Theory and methodology

The one-dimensional periodic structure of SiO_2 and TiO_2 layers with a defect of the composite materials viz. E7 liquid crystal (LC) and $LiNbO_3$ material (LNO) has been considered. The LNO is sandwiched with two LC layers, LC|LNO|LC; and constructed a defect periodic structure i.e. $(SiO_2|TiO_2)^5|LC|LNO|LC|(TiO_2|SiO_2)^5$ which is shown in Fig. 1. The one-dimensional PC is situated in the x-y plane which is perpendicular to z-axis where wave propagates.

The refractive indices and thicknesses of the dielectric layers, SiO_2 and TiO_2, are n_1, n_2, d_1, and d_2, respectively. The thicknesses of defect layers of the LC and LNO are d_3 and d_4 respectively. The optical properties of the one-dimensional periodic structure $(SiO_2|TiO_2)^5|LC|LNO|LC|(TiO_2|SiO_2)^5$ have been investigated using 4 × 4 transfer matrix method (TMM). By considering the interaction of electromagnetic wave (E and H field component) with layers, the transmission property of the periodic structure is studied at an incident angle $\theta$with respect to the z-axis. To calculate the characteristics matrix of the periodic structure, Maxwell'sequations are used;

$$\vec{\nabla} \times \vec{E} = i\omega\mu_o \vec{H} \tag{2}$$

$$\vec{\nabla} \times \vec{H} = -i\omega\varepsilon_o \varepsilon \vec{E} \tag{3}$$

The tangential components of the electric field and the magnetic field can be acquired by solving Eqs. (2) & (3);

$$\frac{\partial \psi}{\partial z} = ik_o \Delta\psi \tag{4}$$

where $k_o = \omega/c$, $\psi = (\sqrt{\varepsilon_o}E_x, \sqrt{\mu_o}H_y, \sqrt{\varepsilon_o}E_y, \sqrt{\mu_o}H_x)$, and Δis the coefficient matrix containing optical property dependent parameters.

As we know that $LiNbO_3$ is a uniaxial and anisotropic material, the relative permittivity tensor of such material is:

$$\varepsilon = \varepsilon_o \begin{bmatrix} n_o^2 & 0 & 0 \\ 0 & n_o^2 & 0 \\ 0 & 0 & n_e^2 \end{bmatrix} \tag{5}$$

The extraordinary (n_e) and ordinary (n_o) refractive indices of the $LiNbO_3$ are given as;

$$n_o(V) = n_o - \frac{1}{2} r_{13} n_o^3 \left(\frac{V}{d_4}\right) \tag{6}$$

$$n_e(V) = n_e(\theta) - \frac{1}{2} r_{33} n_e(\theta)^3 \left(\frac{V}{d_4}\right) \tag{7}$$

where r_{13} and r_{33} are electro-optical coefficients of LNO material and extraordinary refractive index of LNO is voltage (V) and incident angle (ɵ) dependent as;

$$n_e(\theta) = \frac{n_e n_o}{\sqrt{n_o^2\cos^2\theta + n_e^2\sin^2\theta}} \tag{8}$$

On solving Eqs. (2) and (3), the Δmatrix can be obtained as;

$$\Delta = \begin{bmatrix} 0 & 1 - n_0^2\sin^2\theta/\varepsilon_z & 0 & 0 \\ \varepsilon_x & 0 & 0 & 0 \\ 0 & 0 & 0 & 1 \\ 0 & 0 & \varepsilon_y - n_0^2\sin^2\theta & 0 \end{bmatrix} \tag{9}$$

where n_0 is refractive index of incident medium and θ is incident angle of electromagnetic wave, respectively. The transfer matrix for uniaxial anisotropic LNO material can be written as;

$$M = \begin{bmatrix} \cos(\gamma_{1z}k_o d_4) & \frac{ik_{z1}\sin(\gamma_{1z}k_o d_4)}{\Delta_{12}} & 0 & 0 \\ \frac{i\Delta_{12}\sin(\gamma_{1z}k_o d_4)}{\gamma_{1z}} & \cos(\gamma_{1z}k_o d_4) & 0 & 0 \\ 0 & 0 & \cos(\gamma_{2z}k_o d_4) & \frac{i\sin(\gamma_{2z}k_o d_4)}{\gamma_{1z}} \\ 0 & 0 & ik_{z1}\sin(\gamma_{2z}k_o d_4) & \cos(\gamma_{2z}k_o d_4) \end{bmatrix} \tag{10}$$

where $\gamma_{1z} = \sqrt{\varepsilon_x(1 - n_o^2\sin^2\theta/\varepsilon_z)}$and $\gamma_{2z} = \sqrt{\varepsilon_y - n_o^2\sin^2\theta}$. Similarly, we can obtain transfer matrix for different layers i.e. LC, SiO_2, and TiO_2. The total transfer matrix for the periodic structure $(SiO_2|TiO_2)^5|LC|LNO|LC|(TiO_2|SiO_2)^5$ can be written as;

$$M = (M_{SiO2}M_{TiO2})^5\, M_{LC}M_{LNO}M_{LC}\, (M_{TiO2}M_{SiO2})^5$$

$$\text{or, } M = \begin{bmatrix} M_{11} & M_{12} & M_{13} & M_{14} \\ M_{21} & M_{22} & M_{23} & M_{24} \\ M_{31} & M_{32} & M_{33} & M_{34} \\ M_{41} & M_{42} & M_{43} & M_{44} \end{bmatrix} \tag{11}$$

The transmission coefficientsof the considered one-dimensional

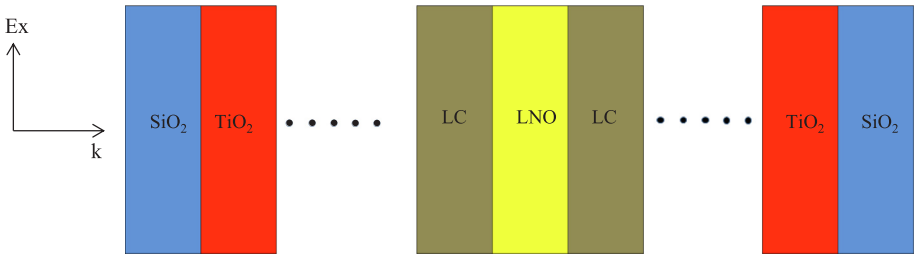

Fig. 1. Schematic arrangement of the one-dimensional periodic structure (1DPS) of SiO_2 and TiO_2 layers with a defect of liquid crystal and $LiNbO_3$ material i.e. $(SiO_2|TiO_2)^5|LC|LNO|LC|(TiO_2|SiO_2)^5$.

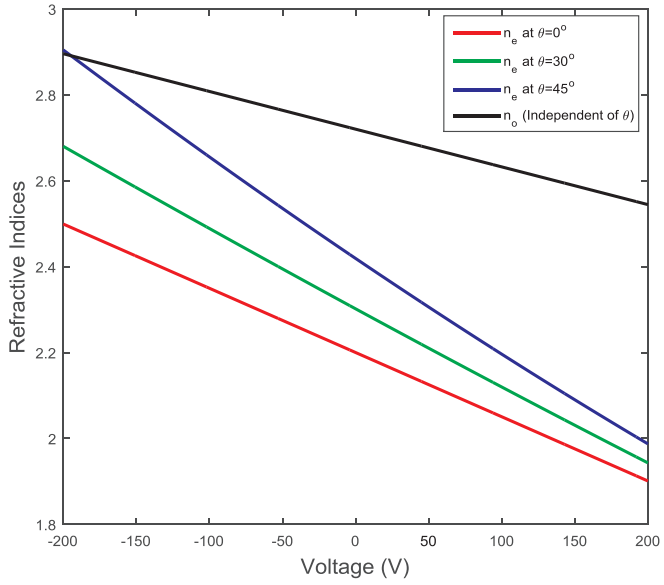

Fig. 2. Refractive indices (n_e, n_o) of LNO versus applied voltage at different incident angles.

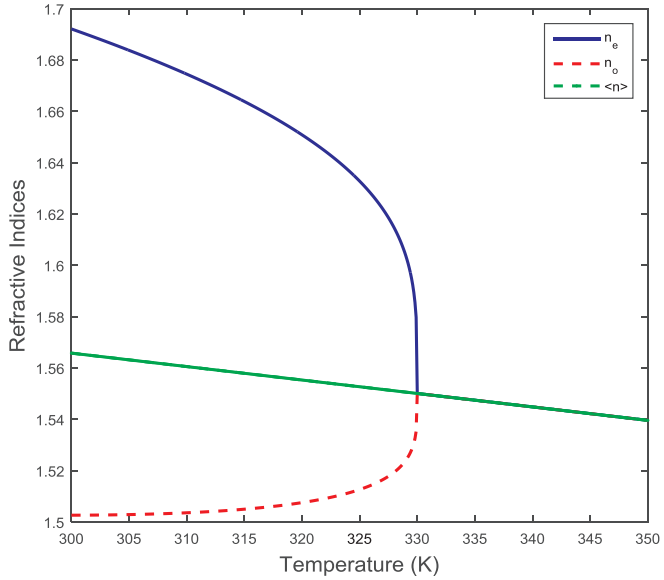

Fig. 3. Refractive indices n_e, n_o, ⟨n⟩ of E7 LC mixture versus Temperature (K).

periodic structure for both TE and TM polarization can be written as;

$$t_{TE} = \frac{M_{11}}{M_{11}M_{33} - M_{13}M_{31}} \tag{12}$$

$$t_{TM} = \frac{M_{33}}{M_{11}M_{33} - M_{13}M_{31}} \tag{13}$$

The final transmissions of the periodic structure are;

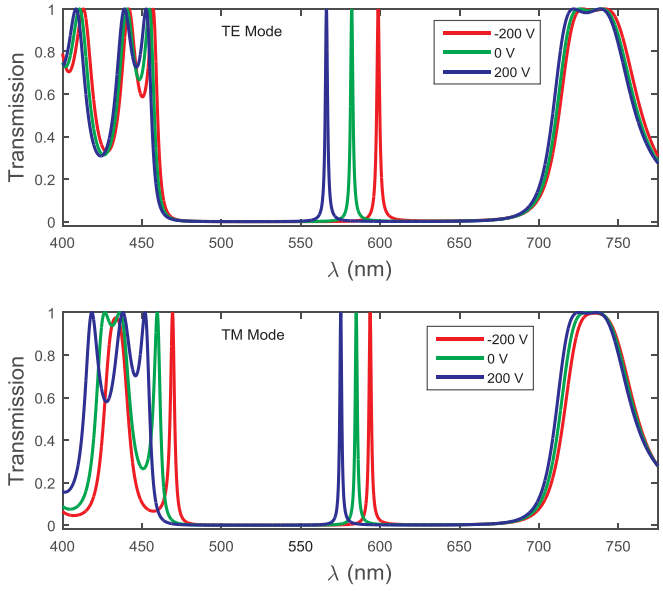

Fig. 4. Transmissions of $(SiO_2|TiO_2)^5|LC|LNO|LC|(TiO_2|SiO_2)^5$ periodic structure versus wavelength at voltages −200 V, 0 V, 200 V for both TE and TM polarizations.

$$T_{TE}=|t_{TE}|^2,\ T_{TM} = |t_{TM}|^2 \tag{14}$$

Results and discussion

From Eqs. (6) and (7), the refractive index of the $LiNbO_3$ (LNO) is dependent upon the voltage (V) and the incident angle (θ)of the electromagnetic wave. In absence of electric field, electro-optical constants r_{13}, r_{33}, extraordinary (n_e) and ordinary (n_o) refractive indices of the LNO are 9.6 pmV^{-1}, 30.9 pmV^{-1}, 2.20, and 2.70 respectively [31,32]. The variation of refractive indices of $LiNbO_3$ with the varying voltage at different incident angles is shown in Fig. 2. The maximum and minimum values of the extraordinary refractive index of $LiNbO_3$are found to be 2.499 and 1.902 respectively −200 V voltage applied to the LNO material at incident angle 0°. This extraordinary refractive index of LNO decreases linearly with voltage but increases with the incident angle. The maximum and minimum values of the extraordinary refractive index (n_e) of $LiNbO_3$ are 2.678 and 1.943 at incident angle 30°; and 2.904 and 1.987 at incident angle 45° under the voltage range −200 V to +200 V. The ordinary refractive index of $LiNbO_3$ is independent of incident angle but dependent upon the voltage V. The maximum and minimum values of the ordinary refractive index of $LiNbO_3$are 2.896 and 2.544, respectively under the voltage range −200 V to +200 V.

E7 liquid crystal consists of 5CB ($C_{18}H_{19}N$), 7CB ($C_{20}H_{23}N$), 8OCB ($C_{21}H_{25}NO$), and 5CT ($C_{24}H_{23}N$) molecules [51]. The extraordinary (n_e) and ordinary (n_o) refractive indices of the E7 liquid crystal mixture are temperature dependent which is given as [52];

Table 1
Shifting of defect mode transmissions of periodic structures at different voltages for TE and TM polarizations.

Polarization	Voltage					
	−200 V		0 V		+200 V	
	Wavelength Peak (nm)	Transmission (%)	Wavelength Peak (nm)	Transmission (%)	Wavelength Peak (nm)	Transmission (%)
TE	598.8	99.97	582.1	99.89	566.2	99.99
TM	593.7	99.94	585	99.86	575.2	99.95
	−100 V		0 V		+100 V	
TE	590.4	100	582.2	99.43	574.1	99.57
TM	589.5	99.77	585	99.86	580.3	99.20

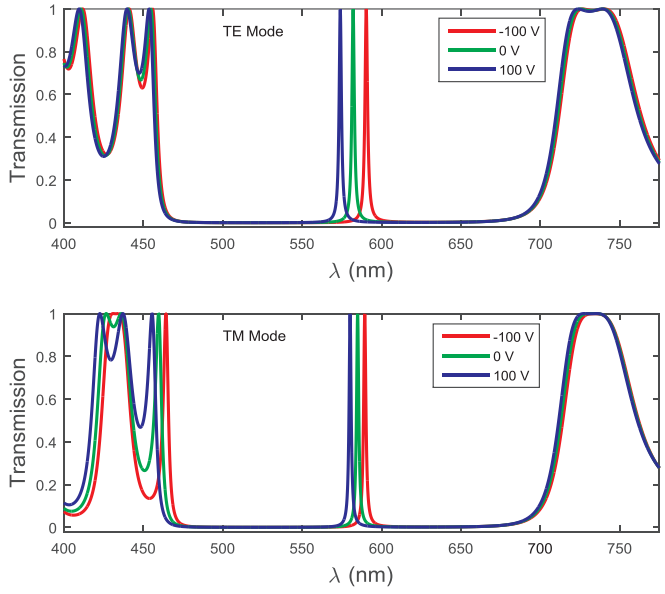

Fig. 5. Transmissions of $(SiO_2|TiO_2)^5|LC|LNO|LC|(TiO_2|SiO_2)^5$ periodic structure versus wavelength at voltages −100 V, 0 V, 100 V for both TE and TM polarizations.

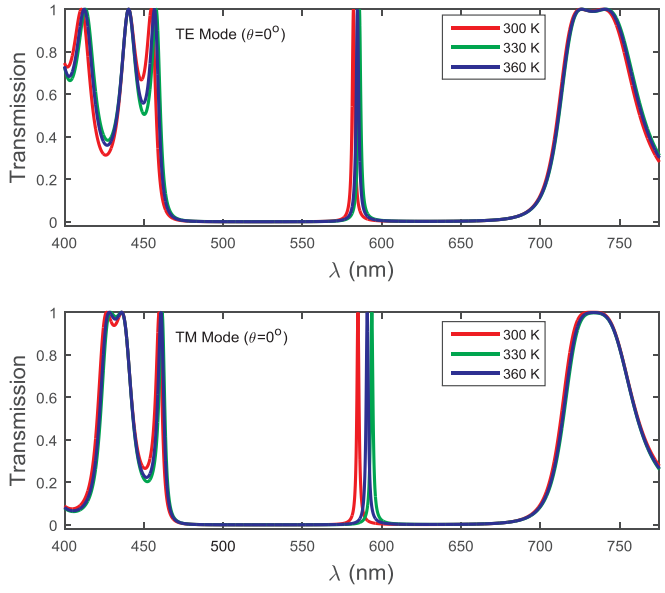

Fig. 6. Transmissions of $(SiO_2|TiO_2)^5|LC|LNO|LC|(TiO_2|SiO_2)^5$ periodic structure versus wavelength at temperatures 300 K, 330 K, 360 K for both TE and TM polarizations with 0 V.

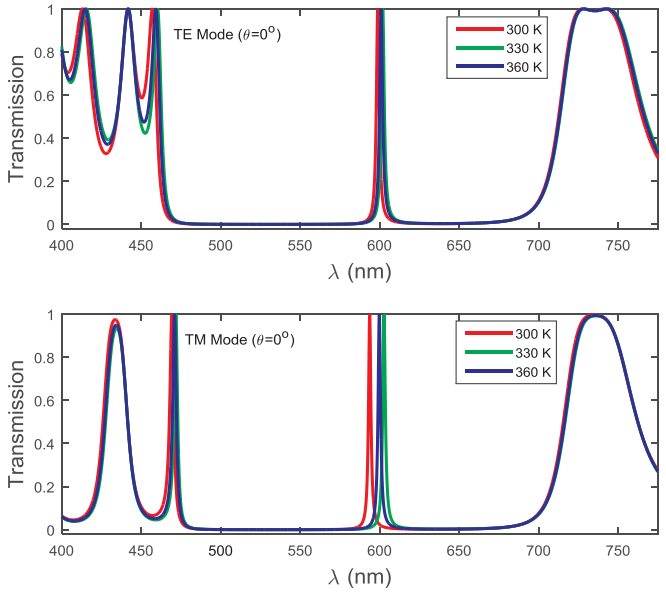

Fig. 7. Transmissions of $(SiO_2|TiO_2)^5|LC|LNO|LC|(TiO_2|SiO_2)^5$ periodic structure versus wavelength at temperatures 300 K, 330 K, 331 K for both TE and TM polarizations with −200 V.

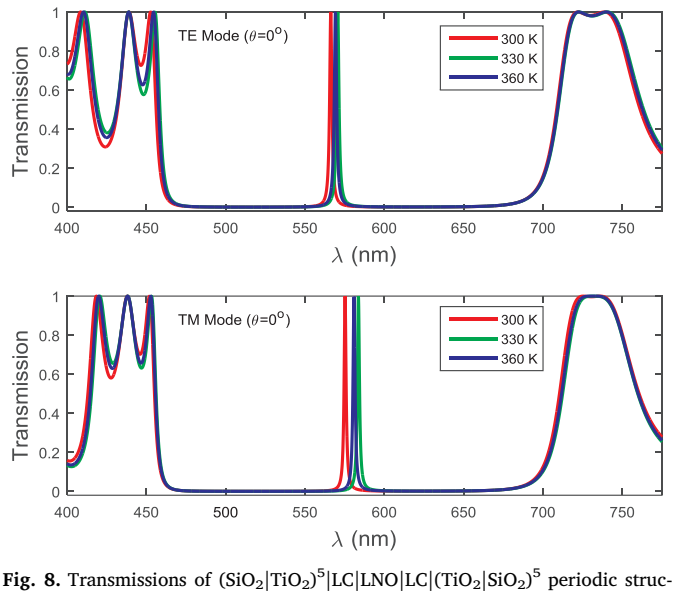

Fig. 8. Transmissions of $(SiO_2|TiO_2)^5|LC|LNO|LC|(TiO_2|SiO_2)^5$ periodic structure versus wavelength at temperatures 300 K, 330 K, 331 K for both TE and TM polarizations with 200 V.

Table 2
Transmission of defect peaks at different voltages and temperatures for both TE and TM modes.

Polarization	Temperature					
	300 K		330 K		360 K	
	Wavelength Peak (nm)	Transmission (%)	Wavelength Peak (nm)	Transmission (%)	Wavelength Peak (nm)	Transmission (%)
Temperature (K) with 0 V						
TE	582.1	99.89	585.9	99.97	584.7	99.84
TM	585	99.86	593.7	99.94	590.8	99.84
Temperature (K) with − 200 V						
TE	599	99.97	601.9	99.85	600.9	100
TM	593.7	99.94	602.7	99.85	599.8	99.87
Temperature (K) with 200 V						
TE	566.2	99.99	571	99.96	569	99.7
TM	575	99.95	583.6	99.93	580.8	99.66

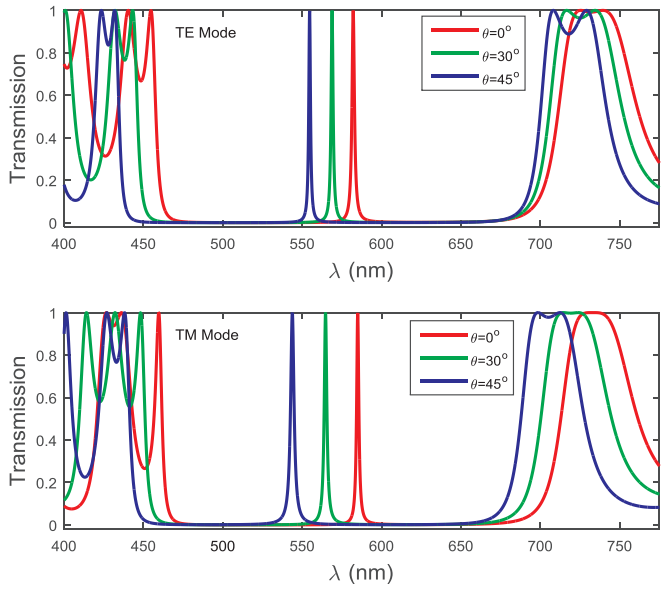

Fig. 9. Transmissions of $(SiO_2|TiO_2)^5|LC|LNO|LC|(TiO_2|SiO_2)^5$ periodic structure versus wavelength at incident angles 0°, 30°, and 45° for both TE and TM polarizations with 0 V.

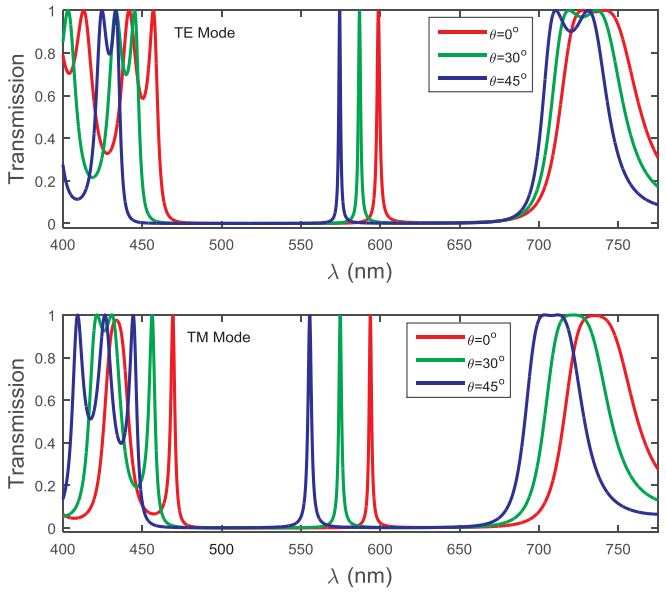

Fig. 10. Transmissions of $(SiO_2|TiO_2)^5|LC|LNO|LC|(TiO_2|SiO_2)^5$ periodic structure versus wavelength at incident angles 0°, 30°, and 45° for both TE and TM polarizations with −200 V.

$$n_e(T) = A - BT + \frac{2(\Delta n)_o}{3}\left(1 - \frac{T}{T_C}\right)^{\beta} \tag{15}$$

$$n_o(T) = A - BT - \frac{(\Delta n)_o}{3}\left(1 - \frac{T}{T_C}\right)^{\beta} \tag{16}$$

where A, B, $(\Delta n)_0$, $\beta$are wavelengths dependent parameters of LC and T_C is clearing temperature of LC. Using Eqs. (15) and (16), the extraordinary refractive index (n_e), ordinary refractive index (n_o) and birefringence ($dn = n_e - n_o$) of the E7 LC mixture are studied.

The constant parameters for E7 liquid crystal mixture are $A = 1.7230$, $B = 5.24 \times 10^{-4}$, $(\Delta n)_o = 0.3485$, $\beta = 0.2542$and $T_C = 330$ K [52]. All the constants of the E7 LC mixture, n_e and n_o are considered at 1.5 μmwavelength. The average refractive index of LC can be obtained as;

$$\langle n \rangle = \frac{2n_o + n_e}{3} \tag{17}$$

The behavior of extraordinary and ordinary refractive indices of E7 liquid crystal mixture with temperature is shown in Fig. 3. The maximum and minimum values of extraordinary and ordinary refractive indices are 1.692 and 1.55 for 300 K temperature and 1.55, 1.503 for 350 K temperature, respectively. The maximum value of the extraordinary refractive index is 1.55 which is equal to the minimum value of the ordinary refractive index at the phase transition temperature 330 K of LC mixture. As we know that the nematic phase LC mixture changes the phase and converts to the isotropic phase LC mixture at clearing temperature330 K.

On considering changed refractive indices of the LNO and LC with varying incident angle, applied voltage and temperature, we have calculated the optical properties of one-dimensional periodic structure with defects LC and LNO $(SiO_2|TiO_2)^5|LC|LNO|LC|(TiO_2|SiO_2)^5$ using 4×4 transfer matrix method (TMM). The refractive indices of dielectric layers SiO_2 and TiO_2 are 1.5 and 2.49, respectively. The thicknesses of layersSiO_2, TiO_2, LC, and LNO are takenas91.6 nm, 55.2 nm, 100 nm, and 110 nm respectively.

(i) Transmissions of the considered periodic structure at voltages −200 V, 0 V, and 200 V: As discussed above, the refractive indices of LNO are voltage dependent (Eqs. (6) and (7)), and hence voltage tunes the defect mode wavelength peak of the structure $(SiO_2|TiO_2)^5|LC|LNO|LC|(TiO_2|SiO_2)^5$. Therefore, we discuss the optical transmissions of the periodic structure at −200 V, 0 V, and 200 V for both TE and TM polarizations.

As discussed earlier that the refractive index of the LNO is voltage dependent and hence voltage affects the optical transmission spectra of the considered periodic structure. We have calculated the transmission

Table 3
Transmission of defect mode peaks at different voltages and incident angles for constant temperature 300 K.

Polarization	Incident angle (θ°)					
	0° with 0 V		30°		45°	
	Wavelength Peak (nm)	Transmission (%)	Wavelength Peak (nm)	Transmission (%)	Wavelength Peak (nm)	Transmission (%)
TE	582.2	99.89	568.8	99.89	554.7	99.7
TM	585	99.86	564	100	543	99.96
with −200 V						
TE	599	99.97	586.9	99.96	574	99.91
TM	593.7	99.94	574.4	98.46	555.6	99.65
with 200 V						
TE	566.2	99.99	552.6	99.98	536	99.95
TM	575.2	99.95	553.3	99.93	530.2	99.97

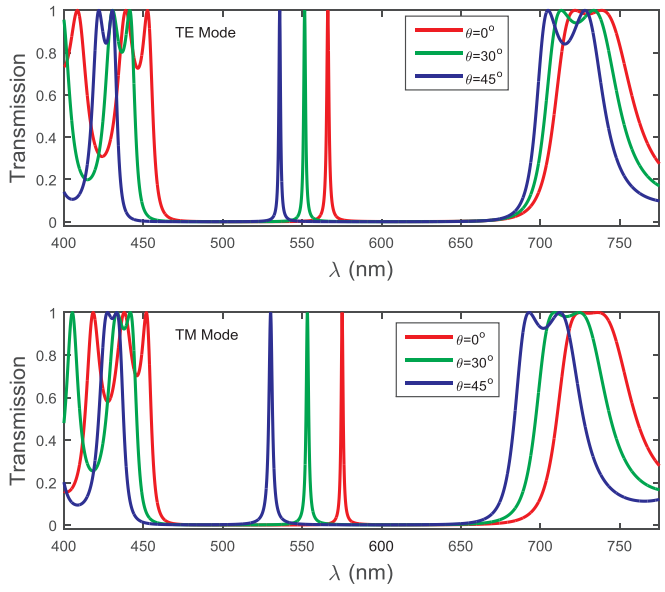

Fig. 11. Transmissions of $(SiO_2|TiO_2)^5|LC|LNO|LC|(TiO_2|SiO_2)^5$ periodic structure versus wavelength at incident angles 0°, 30°, and 45° for both TE and TM polarizations with 200 V.

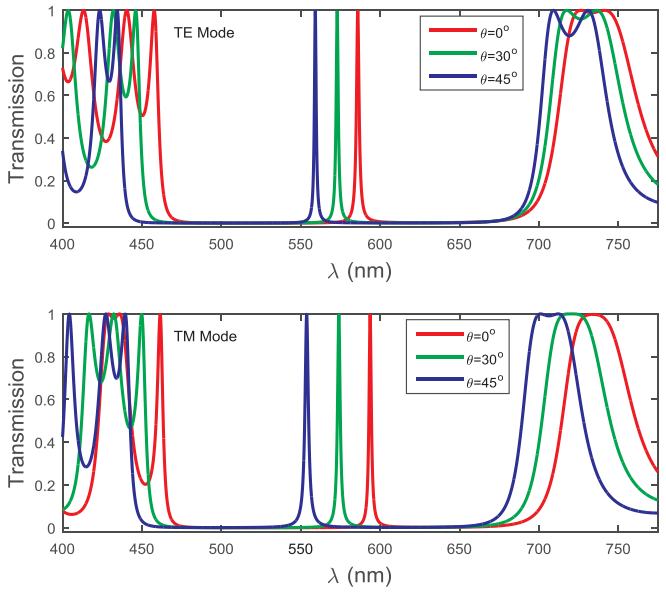

Fig. 12. Transmissions of $(SiO_2|TiO_2)^5|LC|LNO|LC|(TiO_2|SiO_2)^5$ periodic structure versus wavelength at incident angles 0°, 30°, and 45° and temperature 330 K for both TE and TM.

spectra at selected voltages −200 V, 0 V, and 200 V for both polarizations (Fig. 4). The defect mode peak wavelength is shifted toward the lower wavelength (blue shift) as the voltage applied of the LNO increases. The shifting of defect mode peak wavelength in TE polarization is larger than TM polarization. The shifting property can be used to designing the optical switch because as the voltage varies. The defect mode wavelength shifts their position depending on the applied voltage which can be negative or positive. The amount of shifting of wavelength depends on the applied voltage; higher the applied voltage, higher the shifting of defect wavelength in the transmission spectra and such shifting is more effective in TE mode. The detailed property of shifting of the defect mode transmission of the periodic structure at selected voltages is tabulated in Table 1.

Similarly, we have analyzed the transmissions of one-dimensional periodic structure for −100 V, 0 V, 100 V (Fig. 5). The corresponding transmittance of defect mode peak wavelengths is tabulated in Table 1. The broadening of defect mode transmittance peak for TE mode is low in comparison to the TM mode.

(ii) Transmission of the periodic structure at 300 K, 330 K, and 360 K temperatures for different voltages: Now, the shifted transmissions defect peak wavelength for both TE and TM polarizations are investigated with the influence of temperature. As we know that the refractive indices of E7 LC mixture are temperature dependent; the phase of nematicLC changes and converts into the isotropic phase at clearing temperature. The changing in the phase of the LC has also affected the refractive indices. Therefore, the optical transmission of the periodic structure may also is affected. The clearing temperature of the E7 LC mixture is 330 K and hence the transmission characteristic is calculated for three selected temperatures, 300 K, 330 K, and 360 K, with a fixed voltage, 0 V, −200 V and +200 V. Fig. 6 shows the transmission for 300 K, 330 K, and 360 K at 0 V applied voltage for both polarization TE and TM. From Fig. 6, we conclude that transmittance of the considered structure for TM mode polarization changes in the wavelength in comparison to TE polarization. The defect mode peak transmittance for TE mode is found at 582.1 nm, 585.9 nm and 584.7 nm for 300 K, 330 K, and 360 K temperature, respectively. Similarly, defect mode peak transmittance is found at 585 nm, 593.7 nm, and 590.8 nm for 300 K, 330 K and 330 K for TM polarization, respectively. In addition to this, we have calculated the optical transmission of the periodic structure at −200 V and +200 V as shown in Figs. 7 and 8. The detailed study of the defect mode peak transmission at the different voltages is shown in Table 2. The analyzed study shows that we can design the optical switch based on temperature and voltage. Basically, the temperature affects phase and refractive indices of the LC, therefore the temperature also affects optical properties of the periodic structure with a defect of the anisotropic layers. Hence, the temperature based

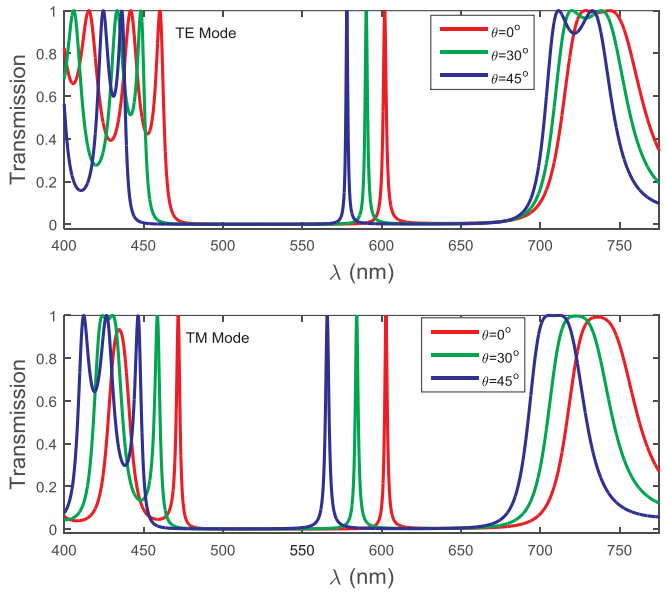

Fig. 13. Transmissions of $(SiO_2|TiO_2)^5|LC|LNO|LC|(TiO_2|SiO_2)^5$ periodic structure versus wavelength at incident angles 0°, 30°, and 45° and temperature 330 K for both TE and TM polarizations with −200 V.

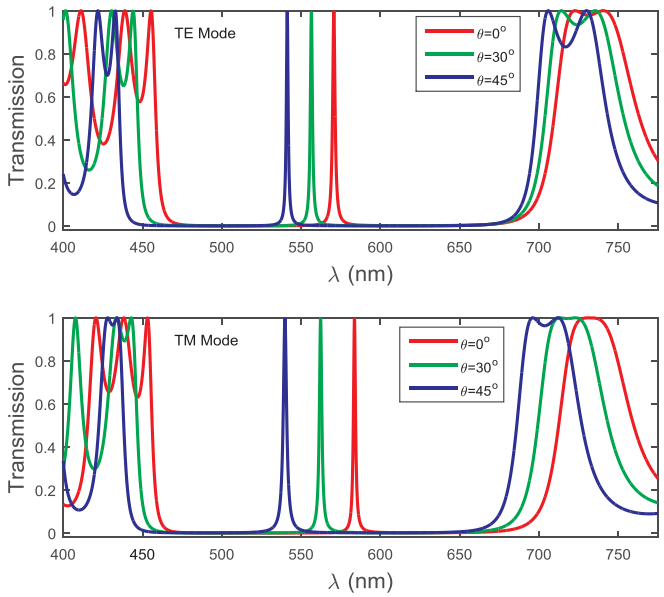

Fig. 14. Transmissions of $(SiO_2|TiO_2)^5|LC|LNO|LC|(TiO_2|SiO_2)^5$ periodic structure versus wavelength at incident angles 0°, 30°, and 45° and temperature 330 K for both TE and TM polarizations with +200 V.

optical devices can be designed by using such type periodic structure which can operate at different voltages.

(iii) Transmission of the periodic structure at 0°, 30°, and 45°incident angles for 300 K temperature: As we know that the extraordinary refractive index of LNO is dependent on voltage and incident angle, the transmission can be tuned by the variation of an incident angle as well as the applied voltage. So, we have calculated the optical transmission at three different incident angles, 0°, 30°, and 45°, with fixed voltages 0 V, −200 V and +200 V. Fig. 9 shows the optical transmission calculated at 0°, 30° and 45°for 0 V. The defect mode transmission peak for TE polarization is found at 582.2 nm, 568.8 nm, and 554.7 nm for incident angles 0°, 30°, and 45° respectively. Similarly, the defect mode transmission peak for TM polarization is found at 585 nm, 564 nm, and 543 nm for 0°, 30° and 45°, respectively as shown in Fig. 10. As the incident angle varies, the position of defect mode wavelength also varies. Hence, the tunable omnidirectional band gap of the considered periodic structure can be obtained through varying the angle of incidence which can operate in different at different voltages for different optical device applications.

The shifting of defect mode transmittance peak for TM mode is high in comparison to TE mode. We conclude that the defect mode transmission peaks shift to low wavelength (blue shift)as incident angle increases. We have also calculated the optical transmissions of one-dimensional periodic structure for −200 V and 200 V as represented in

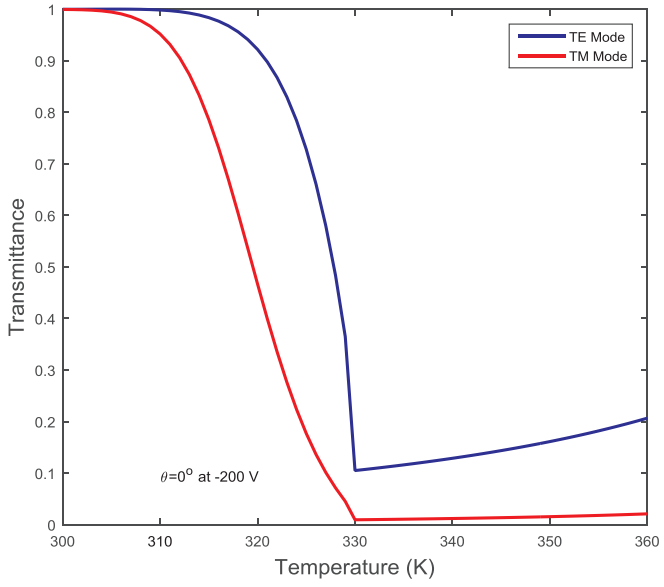

Fig. 15. Variation of transmittance of defect mode wavelength peak versus temperature at Incident angle (θ) 0° for −200 V.

Table 4
Transmission of defect mode peaks at different voltage and incident angles for 330 K Temperature.

Polarization	Incident angle (θ°)					
	0°		30°		45°	
	Wavelength Peak (nm)	Transmission (%)	Wavelength Peak (nm)	Transmission (%)	Wavelength Peak (nm)	Transmission (%)
TE	586	99.29	573	99.47	559	99.85
TM	593.8	99.20	574.1	98.96	553.8	99.84
with −200 V						
TE	602	99.75	590	99.96	578	99.99
TM	602.8	99.61	584.9	98.99	565.7	99.95
with 200 V						
TE	570.7	99.15	556.5	99.64	541.2	99.29
TM	584.6	99.93	562.3	99.84	539.9	99.23

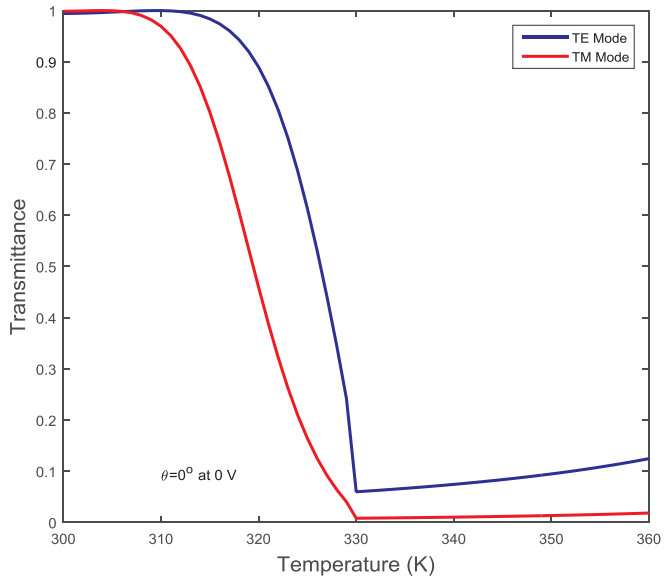

Fig. 16. Variation of transmittance of defect mode wavelength peak versus temperature at Incident angle (θ) 0° for 0 V.

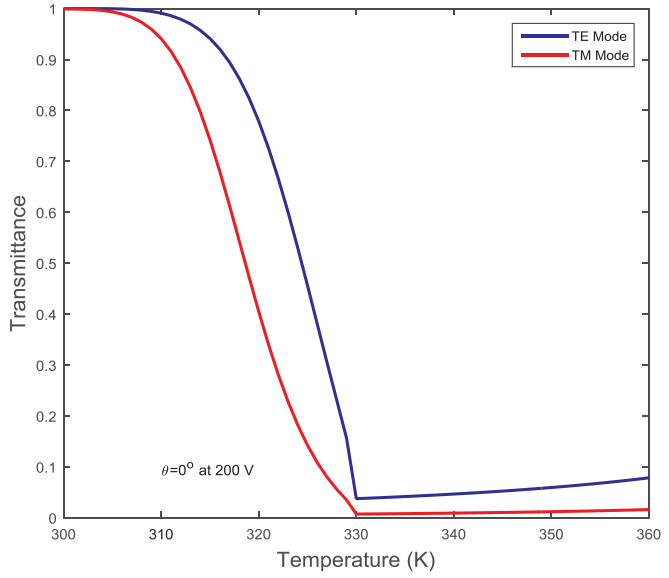

Fig. 17. Variation of transmittance of defect mode wavelength peak versus temperature at Incident angle (θ) 0° for 200 V.

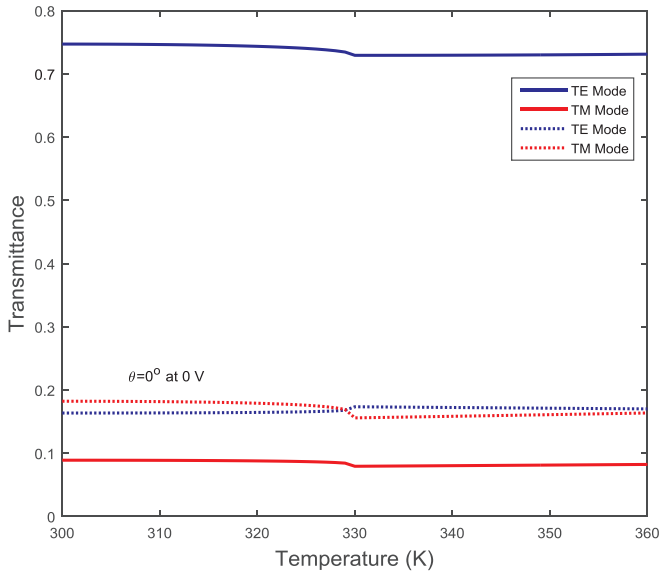

Fig. 18. Variation of transmittance of terminal wavelengths 400 nm (-Solid lines), 800 nm (Dotted lines) vs.Temperature at Incident angle (θ) 0° for 0 V.

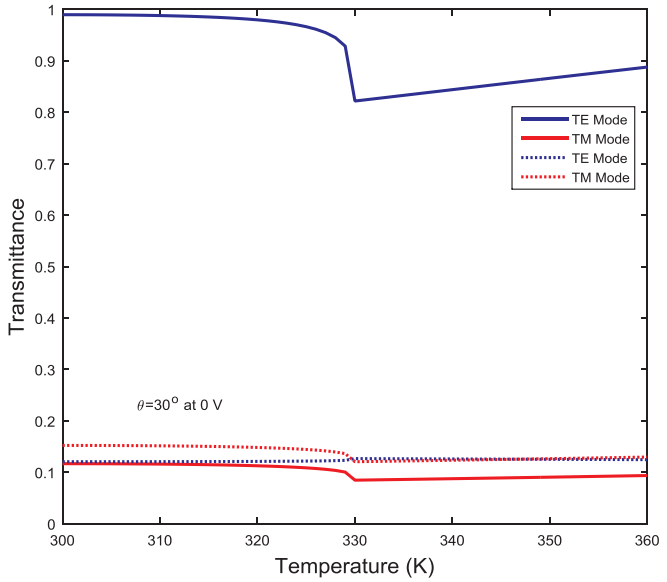

Fig. 19. Variation of transmittance of terminal wavelengths 400 nm (-Solid lines), 800 nm (Dotted lines) vs.Temperature at Incident angle (θ) 30° for 0 V.

Table 3.

(iv) Transmission of the periodic structure at incident angles 0°, 30°, and 45°for 330 K temperature: The transmission of the periodic structure at clearing temperature 330 K for different incident angles, 0°, 30°, and 45°are calculated for fixed voltages −200 V, 0 V, and 200 V. The clearing temperature of the E7 LC is $T_C = 330$ K. So the nematic phase of LC is converted to the isotropic phase, and the refractive index of the LC is continuously decreased when the temperature increases (Fig. 3). The transmissions of the periodic structure at different incident angles with fixed voltage are shown in Figs. 11, 12 and 13.

Fig. 11 shows that the defect mode transmission peaks for TE mode are at 586 nm, 573 nm, and 559 nm for incident angles 0°, 30°, and 45° in 0 V. Similarly, the defect mode transmission peaks for TM mode are at 593.8 nm, 574.1 nm, and 553.8 nm for the same incident angle. In this case, the shifting of defect mode transmission peak for TM polarization changed as more in comparison to TE polarization. Again we have also calculated the optical transmissions of the periodic structure for −200 V and 200 V as shown in Figs. 12 and 13. The details of optical transmission of the periodic structure are given in Table 4. We have drawn the important conclusion that the shifting of defect mode wavelength is more effective for TM mode than TE mode when the variation of incident angle is considered as shown in Fig. 14. But the shifting of defect mode wavelength is more effective for TE mode is more effective than TM mode when voltage variation is considered. It means that the optical properties of the considered periodic structure can be tuned by incident angles and voltages. The switching devices of such structure may be used to operate by variation of incident angles at a constant voltage.

We have drawn the important conclusions that the shifting of defect mode wavelength is more effective for TM mode than TE mode when the variation of incident angle is considered. But the shifting of defect mode wavelength is more effective for TE mode is more effective than TM mode when voltage variation is considered. Hence, the optical

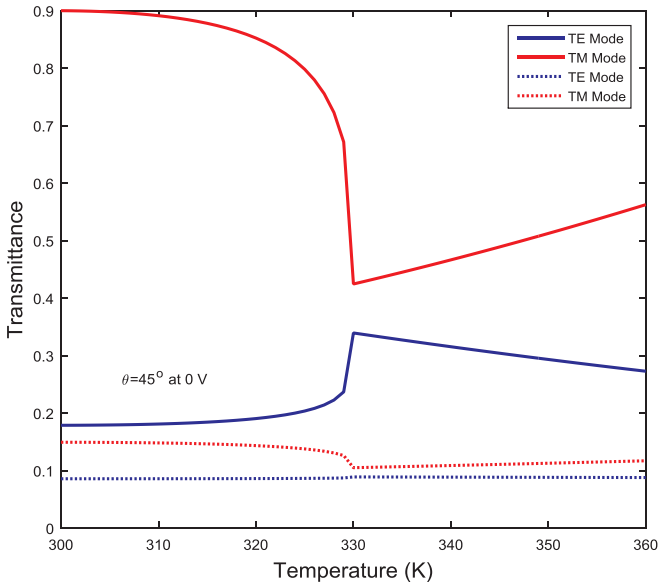

Fig. 20. Variation of transmittance of terminal wavelengths 400 nm (-Solid lines), 800 nm (Dotted lines) vs. Temperature at Incident angle (θ) 45° for 0 V.

properties of the considered periodic structure can be tuned by incident angles at a constant voltage. The switching devices of such structure may be used to operate by variation of incident angles at a constant voltage.

(v) Transmission of wavelength peak with the temperature at different voltages: Fig. 15 shows the transmission of defect mode peak for both TE and TM polarizations versus temperature for wavelength 598.8 nm and applied a voltage −200 V. The transmittance of defect mode peak for TE polarization remains maximum up to 310 K temperature and then decreases rapidly with temperature, and attains 10% transmission of maximum at clearing temperature 330 K. On further increasing the temperature, the transmission increases. Similarly, the transmittance of defect mode peak for TM polarization with wavelength 593.7 nm remains maximum up to 305 K, then the transmittance of defect mode peak decreases for TM polarization and attains the minimum value0.9%. On further increasing the temperature, the transmittance slowly increases.

Further, we have also calculated the transmittance of defect mode wavelength peaks for both TE and TM polarizations versus temperature at 0 V and 200 V, as shown in Figs. 16 and 17. The nature of transmittance of defect mode peaks for 0 V and 200 V are found almost the same transmittance as for −200 V, but the different minimum values are found for both TE and TM polarizations. At 0 V, the defect mode transmission peaks are found 5.4% and 0.8% at 582.1 nm and 585 nm, respectively at $T_C = 330$ K for both polarizations. The minimum transmittances are found 3.37% at 566.2 nm and 7% at 575.2 nm wavelength for TE and TM polarizations, respectively at 200 V. The transmittances of defect mode peak at clearing temperature are found in decrease order for −200 V, 0 V, and 200 V.

The calculated results of the transmission of defect peaks with the temperature at different voltages suggest that the considered periodic structure can be used as an optical switch because the transmittance of defect peak rapidly falls at a clearing temperature of LC. The optical transmission of defect peaks shows the better optical switching to TE mode in comparison to TM mode at different voltages. The phase of LC changes and converts to isotropic phase with order parameter (S) equal to 0 at clearing temperature (T_C), and hence, the transmission properties get affected. From the Figs. 15–17, we propose that transmission for TE and TM modes constants (ON state) for the initial state and then falls (OFF state) for a final state with temperature. On the basis of the transmission variation, the temperature based optical switch can be designed at a different voltage. The minimum values of transmission for both TE and TM modes are obtained at 330 K temperature for different voltages.

(v) Effect of incident angle on the transmission wavelength 400 nm and 800 nm at incident angles 0°, 30°, and 45°: In this section, we have discussed the transmittance of terminal wavelengths 400 nm and 800 nm at different incident angles 0°, 30°, and 45° for TE and TM polarization as shown in Figs. 18–20. At incident angle 0°, the transmittance of wavelength 400 nm remains almost constant at 74% and 9% below the clearing temperature 330 K, but transmissions reduce to 72.92% and 7.9% above the clearing temperature 330 K, for TE and TM mode polarizations, respectively. The transmissions are found 16% and 18%for800nm wavelengths, but corresponding transmittances got reduced to 17.39% and 15.59% at clearing temperature 330 K for TE and TM polarizations, respectively. The transmission for TE mode remains constant near about 74% or 72.92% (ON state) and the transmission for TM mode is found lower value 9% or 7.9% (OFF state) with variation temperature in case of polarization states at 400 nm wavelength at normal incidence with 0 V. Such obtained transmission for the structure may be used to design optical switch.

At incident angle 30°, the transmittances of wavelengths 400 nm and 800nmare found as 82.16% and 8.54%, 12.65%, and 12.05% at clearing temperature 330 K for TE and TM polarizations, respectively. Similarly, at incident angle 45°, the transmittance of 400 nm and 800 nm wavelengths found to be 42.45% and 33.93%, 8%and 10.5%, at clearing temperature 330 K, respectively. The study shows that the transmissions of the terminal are affected by wavelengths 400 nm and 800 nm by the variation of temperature and incident angle of the electromagnetic wave. The transmission of terminal wavelengths remains almost constant at 0° incident angle for TE and TM modes with a very small change in the transmission at clearing temperature 330 K. Such transmission can be used as an optical filter. The transmissions of terminal wavelengths are affected due to the variation of temperatures and refractive indices of LC and LNO materials through the incident angle. The periodic structure shows the unusual transmission characteristics of defect peaks at 45° incident angle because the refractive indices of LNO material depend on the incident angle and applied voltage.

Conclusion

The optical transmission of the periodic structure of SiO_2 and TiO_2 with a composite defect of LC with LNO has been investigated by using a 4×4 transfer matrix method (TMM). The study shows that the transmission defect peaks of the considered structure affect sufficiently by the temperature and the incident angle of the electromagnetic wave. The transmission of defect mode peak is found the blue shift by the variation of incident angle, temperature, and voltage. The blue shifts of the transmission of defect mode peak are found due to the change of refractive index of liquid crystal and LNO material with the effective parameters. Further, the LC has obtained zero (0) of the order parameter at the clearing temperature due to the isotropic phase of LC. Hence the transmission of defect modes and terminal wavelengths are affected by the temperature at different incident angles. The switching behevior is dependent on the the variation and shifting of defect mode transmission peaks. The shifting of defect mode transmission peaks has more effective with the variation of voltage for TE mode. But the shifting of defect mode transmission peaks has effective with the incident angle for TM mode. Such a periodic structure consisting of anisotropic materials, LNO and LC, as defect layer may be used as tunable optical filters, switches for optoelectronic devices.

Acknowledgments

PS acknowledges the BabasahebBhimraoAmbedkar University Lucknow, for providing the NON-NET UGC fellowship and NK thanks to

UGC New Delhi for providing the NFSC fellowship.

References

[1] Yablonovitch E. Inhibited spontaneous emission in solid state physics and electronics. Phys Rev Lett 1987;58:2059–62.
[2] John S. Strong localization of photons in certain disordered dielectric superlattices. Phys Rev Lett 1987;58:2486–9.
[3] Jonopoulos JD, Villeneuve P, Fan S. Photonic crystals: putting a new twist on light. Nature 1997;386:143–9.
[4] Zheng QR, Fu YQ, Yuan NC. Characteristics of planer PBG structures with a cover layer. J Electromagn Waves Appl 2006;20:1439–53.
[5] Fink Y, Winn JN, Fan S, Chen C, Michel J, Joannopoulos JD, et al. A dielectric omnidirectional reflector. Science 1998;282:1679–82.
[6] Rojas JAM, Alpuente J, Pineiro J, Sanchez R. Rigorous full vectorial analysis of electromagnetic wave propagation in 1D. PIER 2006;63:89–105.
[7] Joannopoulos JD, Meade RD, Winn JN. Photonic crystals: molding the flow of light. Princeton, NJ: Princeton Univ. Press; 1995.
[8] Srivastava R, Thapa KB, Pati S, Ojha SP. Omni-direction reflection in one dimensional photonic crystal. Prog Chem Org Nat ProdIn Electromagn Res B 2008;7:133–43.
[9] Thapa KB, Srivastava S, Tiwari S. Enlarged photonic band gap in heterostructure of metallic photonic and superconducting photonic crystals. J Supercond Novel Magn 2010;23:517–25.
[10] Thapa KB, Singh SK, Pojha S. Omnidirectional high reflector for infrared frequency. Int J Infrared Milli Waves 2006;27:1257–68.
[11] Pandey GN, Thapa Khem B, Ojha SP. Omni-directional reflection bands in one-dimensional plasma dielectric photonic crystals. Optik 2013;124:3396–401.
[12] Smith DR, McCall SL, Platzman PM, Dalichaouch R, Kroll N, Schultz S. Photonic band structure and defects in one and two dimensions. J Opt Soc Am B 1993;10:314–21.
[13] Yuan-Jiang X, Xiao-Yu D, Shuang-Chun W. Effects of negative index medium defect layers on the transmission properties of onedimensional photonic crystal. Optoelectron Lett 2007;3:144–7.
[14] Hideyuki A, Mariko YJ, Yong T, Hattori N Hiroki, Kazuyuki H. Optical properties of a total-reflection-type one dimensional photonic crystal. IEEE J Quantum Electron 2002;38:867–71.
[15] Schuller C, Klopf F, Reithmaier JP, Kamp M, Forchel A. Tunable photonic crystals fabricated in III-V semiconductor slab waveguides using infiltrated liquid crystals. Appl Phys Lett 2003;82:2767–9.
[16] Leonard SW, Mondia JP, van Driel HM, Toader O, John S, Busch K, et al. Tunabletwodimensional photonic crystals using liquid crystal infiltration. Phys Rev B 2000;61:R2389–92.
[17] Jia W, Li Y, Xi Y, Jiang P, Xu X, Liu X, et al. Tunability of photonic crystals based on the Faraday effect. J Phys Condens Matter 2003;15:6731–7.
[18] Liu CC, Wu CJ. Analysis of defect mode in a dielectric photonic crystal containing ITO defect. Optik 2014;125:7140–2.
[19] Wu M-R, Wu C-J, Chang S-J. Investigation of defect modes in a defective photonic crystal with a semiconductor metamaterial defect. Physica E 2014;64:146–51.
[20] Ha Y-K, Yang Y-C, Kim J-E, Park HY, Kee C-S, Lim H, et al. Tunable omnidirectional reflection bands and defect modes of a one-dimensional photonic band gap structure with liquid crystals. Appl Phys Lett 2001;79:15–7.
[21] Panoiu NC, Bahl M, Osgood RM. All-optical tunability of a nonlinear photonic crystal channel drop filters. Opt Express 2004;12:1605–10.
[22] Dadoenkova NN, Zabolotin AE, Lyubchanskii IL, Lee YP, Rasing T. One-dimensional photonic crystal with a complex defect containing an ultrathin superconducting sublayer. J Appl Phys 2010;108:093117.
[23] Park D, Kim S, Park I, Lim H. Higher order optical resonant filters based on coupled defect resonators in photonic crystals. J Lightwave Technol 2005;23:1923–8.
[24] Lin PT, Wessele BW. Ferroelectric thin film photonic crystal waveguide and its electro-optic properties. J Opt A 2009;11:075005.
[25] Zhu Q, Zhang Y. Defect modes and wavelength tuning of one dimensional photonic crystal with lithium niobate. Optik 2009;120:195–8.
[26] Ozaki R, Matsui T, Ozaki M, Yashino K. Electrically colortunable defect mode lasing in one-dimensional photonic-band-gap system containing liquid crystal. Appl Phys Lett 2003;82:3593–5.
[27] Nemec H, Kuzel P, Duvillaret L, Pashkin A, Dressel M, Sebastian MT. Highly tunable photonic crystal filter for the terahertz range. Opt Lett 2005;30:549–51.
[28] Abdulhalim I. Analytic propagation matrix method for linear optics of arbitrary biaxial layered media. J Opt A 1999;1:646–53.
[29] Yeh P. Electromagnetic propagation in birefringent layered media. J Opt Soc Am 1979;69:742–56.
[30] Yariv A, Yeh P. Optical waves in crystals propagation and control of laser radiation. Wiley; 1983.
[31] Jamshidi-Ghaleh K, Kazempour B. Effect of incident angle and polarization on electrically-tunable defect mode in anisotropic photonic crystals. App Opt 2016;55:4350–6.
[32] Deng Jun, Hussain Sajid, Kumar Vanga Sudheer, Jia Wei, Png Ching Eng, Thor Lim Soon, et al. Modeling and experimental investigations of Fano resonances in free-standing LiNbO3 photonic crystal slabs. Opt Express 2013;21:3243–52.
[33] Chandrasekhar S. Liquid crystals. New York: Cambridge Univ. Press; 1992.
[34] Khoo IC. Liquid crystals. New Jersey: WileyInterscience; 2007.
[35] Blinov LM. Structure and properties of liquid crystals. New York: Springer; 2011.
[36] Bush K, John S. Liquid-crystal photonic-band-gap materials: the tunable electromagnetic vacuum. Phys Rev Lett 1999;83:967–70.
[37] Yoshino K, Shimoda Y, Kawagishi Y, Nakayama K, Ozaki M. Temperature tuning of the stop band in transmission spectra of liquid-crystal infiltrated synthetic opal as tunable photonic crystal. Appl Phys Lett 1999;75:932–4.
[38] Kang D, Maclennan JE, Clerk NA, Zakhidov AA, Baughman RH. Electro-optic behavior of liquid-crystal-filled silica opal photonic crystals: effect of liquid-crystal alignment. Phys Rev Lett 2001;86:4052–5.
[39] Graubard E, King JS, Jain S, Summers CJ, Zhang Williams Y, Khoo IC. Electric-field tuning of the Bragg peak in large-pore TiO2 inverse shell opals. Phys Rev B 2005;72:233105–14.
[40] Arkhipkin VG, Gunyakov VA, Myslivsts SA, Zyryanov VYa, Shabanov VF. Angular tuning of defect modes spectrum in the one-dimensional photonic crystal with liquid-crystal layer. Eur Phys J E 2007;24:297–302.
[41] Strelniker YM, Stroud D, Voznesenkaya AO. Control of extraordinary light transmission through perforated metal films using liquid crystals. Eur Phys J B 2006;52:1–7.
[42] Mingaleev SF, Schillinger M, Hermann D, Bush K. Tunable photonic crystal circuits: concepts and designs based on single-pore infiltration. Opt Lett 2004;29:2858–60.
[43] Mohamed MS, Hameed MFO, El-Okr MM, Obayya Salah SA. Characterization of one dimensional liquid crystal photonic crystal structure. Optik 2016;127:8774–81.
[44] Ozaki R, Miyoshi H, Ozaki M, Yoshino K. Tunable defect mode in one-dimensional photonic crystal with liquid crystal defect layer. Mol Cryst Liq Cryst 2005;433:247–57.
[45] Polycarpou AC, Christou MA, Papanicolaou NC. A mode-matching approach to electromagnetic wave propagation in nematic liquid crystals. IEEE Trans On Micro Theo Tech 2012;60:2950–8.
[46] Miroshnichenko E, Pinkevych I, Kivshar YS. Tunable all-optical switching in periodic structures with liquid-crystal defects. Opt Express 2006;14:2839–44.
[47] Entezar SR, Madani A, Habil MK, Namdar A, Tajalli H. Temperature dependent transmission and optical bistability in a 1D photonic crystal with a liquid crystal defect layer. J Mod Opt 2013;60:1883–91.
[48] Pankin PS, Vetrov SYa, Timofeev IV. Tunable hybrid Tamm-microcavity states. J Opt Soc Am B 2017;34:2633–9.
[49] Ong HL. Optical-field-enhanced and static-field-induced first-order Fréedericksz transitions in a planar parallel nematic liquid crystal. Phys Rev A 1986;33:3550–3.
[50] Yeh P. Optical waves in layered media. New York: John Wiley & Sons; 1988.
[51] Mouquinho, Saavedra M, Maiau A, Petrova K, Barros MT, Figueirinhas JL, et al. Films based on new methacrylate monomers: synthesis, characterisation, and electro-optical properties. Mol Cryst Liq Cryst 2011;542:132–40.
[52] Li J, Wu ST, Brugioni S, Meucci R, Faetti S. Infrared refractive indices of liquid crystals. J Appl Phys 2005;97:073501–73505.

Pramana – J. Phys. (2019) 93:50
https://doi.org/10.1007/s12043-019-1812-5

© Indian Academy of Sciences

Effective optical properties of the one-dimensional periodic structure of TiO_2 and SiO_2 layers with a defect layer of nanocomposite consisting of silver nanoparticle and E7 liquid crystal

PAWAN SINGH, KHEM B THAPA*, NARINDER KUMAR, DEVENDRA SINGH and DEVESH KUMAR

Department of Physics, School of Physical and Decision Sciences, Babasaheb Bhimrao Ambedkar University, Vidya Vihar, Rae Bareli Road, Lucknow 226 025, India
*Corresponding author. E-mail: khem.bhu@gmail.com

MS received 1 December 2018; revised 5 March 2019; accepted 25 March 2019; published online 10 July 2019

Abstract. In this work, the dielectric property of a nanocomposite (NC) consisting of silver nanoparticle and E7 liquid crystal (LC) has been investigated theoretically at different temperatures. The study shows that the surface plasmon resonance (SPR) and filling fraction of the silver nanoparticle significantly change the dielectric property of the NC. To study the optical property of the defective periodic structure, the NC was considered as a defect layer in a semifinite one-dimensional periodic structure (1DPS) of TiO_2 and SiO_2 layers, i.e. $(TiO_2|SiO_2)^5|NC|(TiO_2|SiO_2)^5$. The optical properties of the 1DPS with the NC as the defect layer have been studied by the simple transfer matrix method (TMM). Moreover, the transmission and absorption characteristics of the 1DPS in the presence of silver nanoparticle in the NC have been studied with different orientations of the LC molecule.

Keywords. Liquid crystal; silver nanoparticle; transfer matrix method; filling fraction; orientation.

PACS Nos **42.70.Df; 42.70.Qs; 61.46.+w**

1. Introduction

A special class of optical periodic medium, commonly known as photonic crystals (PCs), has been developed. A PC consists of alternating stacks of dielectric materials in different directions. Therefore, PCs are classified into three types: one-dimensional PCs (1DPC), two-dimensional PCs (2DPC) and three-dimensional PCs (3DPC). PCs are very interesting due to the existence of a photonic band gap (PBG) in the transmission spectra of the optical periodic medium. PBGs are special regions in the transmission spectra of the PCs which prohibit the propagation of an electromagnetic wave in that region. PCs are capable of controlling the flow of electromagnetic wave due to the periodicity of dielectric materials. Due to their unusual properties, PCs find application in many optical devices, viz. optical filters, reflectors, switches, etc. [1–12]. Mostly, optical filter and reflector applications of PCs are based on the omnidirectional reflection and transmission properties of PCs. The metallic photonic crystal is used as absorption-based optical devices such as sensors, microwave absorbers, etc. [13–21]. The third-order nonlinear optical properties of the silver nanocomposite (NC) have been studied experimentally and it was concluded that the control of optical nonlinearity may lead to novel device applications [22]. Certain optical anisotropic materials, known as liquid crystals (LCs), exhibit a transitional stage between liquids and solids. LC has both properties: flows like liquids while being crystalline as solid. LC has extraordinary and ordinary components of electric permittivity. Hence, electric permittivity of the LC can be expressed in tensor form which is dependent upon the molecular orientation of the LC. Such birefringent materials are used as tunable nonlinear optical devices [23–25]. The dielectric properties of the LC are tuned by the external electric field and temperature which affect the electric permittivity of the LC. The optical transmission of a photonic crystal with the LC as the defect layer can be regulated by varying the applied electric field and temperature. By coating the inverse opal with the LC, the

tunability of PBG in PCs can be controlled as suggested by Bush and John [26] and confirmed experimentally by Yoshino *et al* [27]. PCs with LC as the defect layer are used as tunable optical devices based on the external application of an electric field or magnetic field and temperature [28–41]. It is known that the LCs are anisotropic materials and the optical properties of the LC are dependent upon the orientation of the molecules. The dielectric tensor of the LCs, consisting of ordinary and extraordinary components of the electric permittivity and anisotropy (ε_a) [42] is expressed in the matrix form as

$$\tilde{\varepsilon} = \begin{pmatrix} \varepsilon_\perp + \varepsilon_a \sin^2\phi & 0 & \varepsilon_a \sin\phi\cos\phi \\ 0 & \varepsilon_\perp & 0 \\ \varepsilon_a \sin\phi\cos\phi & 0 & \varepsilon_\perp + \varepsilon_a \cos^2\phi \end{pmatrix}. \quad (1)$$

This dielectric tensor of the LC is a non-diagonal matrix containing an orientation-dependent matrix element which shows the anisotropic behaviour of the LC. The dielectric tensor of the LC is reduced to a diagonal matrix if we consider the orientation angle of the LC director (ϕ) to be either 0 or 90°. Hence, the transfer matrix method (TMM) [43] can be used to study the optical properties of the LC's director angle, $\phi = 0°$ or 90°.

The dielectric permittivity of the E7 LC is temperature-dependent and it is also affected by external doping materials in the LC. NC material can be synthesised by the dispersion of nanoparticles into a host material (e.g. LC). Such NC material helps to produce new PBG regions in the transmission of the PC due to the change in dielectric constant. In addition to this, the optical characteristics of the PC are also observed to be affected by the filling fraction and the radii of the doped nanoparticles [44–48]. The effective dielectric function of the NC consisting of a doped nanoparticle (silver) in the LC host can be written by using the well-known Maxwell-Garnett model [49–51].

In the present work, we have investigated the effect of the inclusion of silver nanoparticle in the E7 LC mixture at different temperatures. The optical properties of the one-dimensional periodic structure (1DPS) with the NC as the defect layer, i.e. $(TiO_2|SiO_2)^5|NC|(TiO_2|SiO_2)^5$, are discussed at different temperatures and filling fractions. In our study, we have theoretically proposed to design a NC consisting of a silver nanoparticle of radius 5 nm and an E7 LC mixture. Here, the E7 LC is the mixture of four different LCs: 5CB ($C_{18}H_{19}N$), 7CB ($C_{20}H_{23}N$), 8OCB ($C_{21}H_{25}NO$) and 5CT ($C_{24}H_{23}N$) [52]. The ordinary and the extraordinary dielectric constants of the E7 LC are dependent upon the wavelength and the clearing temperature (T_C) of the LC [53]. For inclusions of the nanoparticle in the LC host, a spherical silver nanoparticle of radius 5 nm is considered and the optical properties of the NC (LC + AgNPs) as well as the defect periodic structure with such a NC defect ($(TiO_2|SiO_2)^5|NC|(TiO_2|SiO_2)^5$) have been studied.

2. Theoretical modelling

The periodic arrangement of the TiO_2 and SiO_2 layers in one direction has been considered for designing 1DPC with NC of silver nanoparticle with E7 LC as the defect layer, $(TiO_2|SiO_2)^5|NC|(TiO_2|SiO_2)^5$, as shown in figure 1.

In our study, we have taken the refractive indices of SiO_2 and TiO_2 layers as 1.5 and 2.4, respectively, and the thicknesses of the SiO_2 and TiO_2 layers as 56.2 and 91.6 nm, respectively. The optical properties of the photonic crystal with NC as the defect layer are studied using the TMM. The extraordinary (n_e) and the ordinary (n_o) refractive indices of the E7 LC mixture are dependent on the temperature, and are represented as

$$n_e(T) = A - BT + \frac{2(\Delta n)_o}{3}\left(1 - \frac{T}{T_C}\right)^\beta, \quad (2)$$

$$n_o(T) = A - BT - \frac{(\Delta n)_o}{3}\left(1 - \frac{T}{T_C}\right)^\beta, \quad (3)$$

where $A, B, (\Delta n), \beta$ are the wavelength-dependent parameters of LC and T_C is the clearing temperature

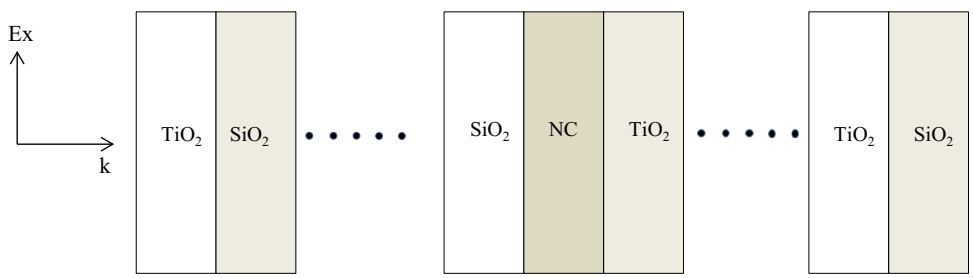

Figure 1. Schematic representation of the 1DPCs of the TiO_2 and SiO_2 dielectric layers with a defect layer of NC layer consisting of nanoparticle and E7 LC.

of the LC mixture. All constants are used to determine the refractive indices of the E7 LC mixture at 1.5 μm wavelength. The extraordinary dielectric permittivity ($\varepsilon_{||}$) and ordinary dielectric permittivity ($\varepsilon_{\perp}$) of LC can be obtained by squaring the value of n_e and n_o using eqs (2) and (3), respectively.

The Maxwell–Garnett model is used to determine the refractive index of the NC consisting of silver nanoparticles and E7 LC. The silver nanoparticles are arbitrarily dispersed in the host LC. Consequently, the effective electric permittivity of NC can be written as

$$\varepsilon_{\text{eff}} = \frac{2\varepsilon_{\text{LC}} f(\varepsilon_m - \varepsilon_{\text{LC}}) + \varepsilon_{\text{LC}}(\varepsilon_m + 2\varepsilon_{\text{LC}})}{2\varepsilon_{\text{LC}} + \varepsilon_m + f(\varepsilon_{\text{LC}} - \varepsilon_m)}, \tag{4}$$

where ε_{LC}, ε_m and f are the dielectric permittivities of the LC, silver nanoparticle and the volume fraction of nanoparticles inclusion in the LC, respectively. The dielectric permittivity of the silver nanoparticle can be considered using the Drude model:

$$\varepsilon_m = \varepsilon_0 - \frac{\omega_{\text{p}}^2}{\omega^2 + \text{i}\omega\eta}, \tag{5}$$

where ω_{p}, ε_0 and η are plasmon frequency, relative permittivity of the metal nanoparticles and damping frequency, respectively. The damping frequency is dependent upon the radius (r) of the nanoparticle and the velocity (v_{f}) of the electron at Fermi energy, which is described as

$$\eta(r) = \eta_0 + \frac{v_{\text{f}}}{r}, \tag{6}$$

where η_0 is the decay constant obtained by the scattering of free electron with phonons, electrons, etc.

3. Results and discussion

This section is divided into five subsections. In the first subsection, we have studied the refractive indices of the LC and the effective permittivity of the NC at different temperatures. The effective dielectric permittivities of the NC at different filling fractions are studied in §2. In §3, we have studied the optical property of the considered periodic structure without and with the defect layer LC. The transmission and absorption properties of the 1DPS with NC as the defect layer at different temperatures for filling fraction $f = 0.05$ are studied in §4. Lastly, the transmission and absorption characteristics of the 1DPS with NC as the defect at different filling fractions (f) for $T = 300$ K are studied in §5.

3.1 *Refractive indices of LC and the effective refractive index of NC at different temperatures*

First, the variation of refractive indices of the E7 LC mixture with temperature is investigated (figure 2). The extraordinary refractive index attains a minimum value of 1.55 when $T_{\text{C}} = 330$ K. Similarly, the ordinary refractive index increases with temperature and attains the maximum value 1.55 which is equal to the minimum value of extraordinary refractive index at $T_{\text{C}} = 330$ K. A further increase in temperature leads to a constant

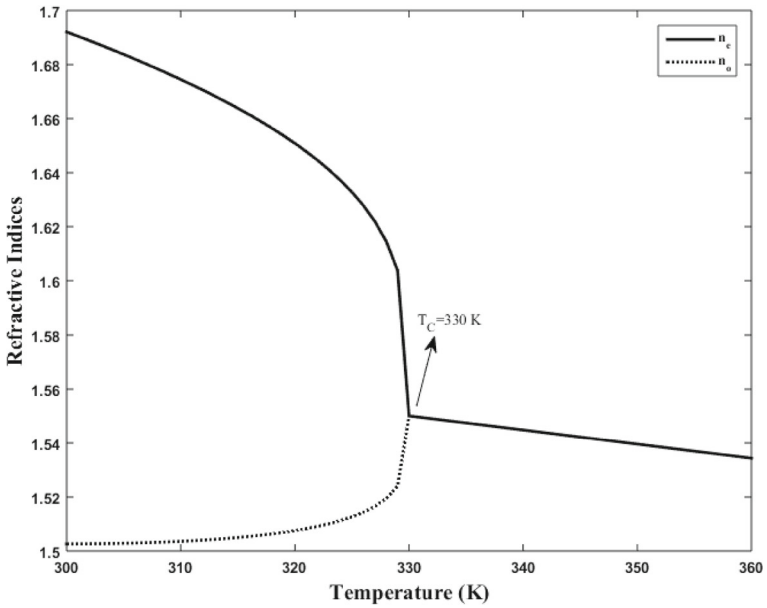

Figure 2. Variation of refractive indices of E7 LC mixture with temperature (K).

decrease in both refractive indices having the same nature. At $T_C = 330$ K, the phase of the E7 LC mixture changes and converts into an isotropic phase. Hence, both refractive indices vary with temperature in the same manner.

The optical properties of the 1DPS containing alternating layers of TiO_2 and SiO_2 with NC material (LC + AgNPs) as the defect layer were studied using the TMM. In our calculation, the refractive indices and the thicknesses of TiO_2 and SiO_2 layers are taken as discussed earlier in theoretical modelling. The thickness of the LC composite is 100 nm. The plasmon frequency ω_p and the decay constant of the silver particle are $2\pi \times 2.17 \times 10^{15}$ and $2\pi \times 4.8 \times 10^{12}$ Hz, respectively. The radius (r) of the spherical silver nanoparticle inclusion in the LC host is taken as 5 nm with $\varepsilon_0 = 5$.

Next, the effective dielectric permittivity of the NC of the silver nanoparticle with the E7 LC mixture has been studied. For the composite structure, the spherical silver nanoparticle of 5 nm radius is dispersed in the E7 LC mixture with different filling fractions (f). The dielectric constants of the E7 LC mixture are temperature-dependent, and the effective permittivity of the NC structure (LC + AgNPs) changes with temperature also. So we have calculated the dielectric permittivity of the NC at 300 and 329 K (figure 3). The real part of the effective dielectric permittivity has both positive and negative values, but the imaginary part has only positive values. The variations of ordinary and extraordinary dielectric permittivities of the NC at different temperatures are shown in figures 3 and 4.

Basically, the molecules retain the director distortion angle 0° below the Fréedericksz transition of the LC. It means that the ordinary or perpendicular component ($\varepsilon_\perp$) of dielectric permittivity of the NC dominates for all optical properties of the PCs. But, the molecules get switched above the Fréedericksz transition of the LC and finally attain the orientation angle 90°. At this transition, the extraordinary or parallel component of the dielectric permittivity ($\varepsilon_{||}$) is responsible for changing the optical properties of the defective PC. At higher temperatures, the effective dielectric permittivity of the NC is shifted towards higher values as shown in figure 3.

The E7 LC mixture is known to be anisotropic. It changes its phase and converts into the isotropic phase at 330 K. The ordinary and extraordinary dielectric permittivities of the NC become equal at 330 K. The effective dielectric permittivity of the NC structure at 330 and 360 K are shown in figure 4. The anisotropy of the NC vanishes at clearing temperature T_C and it gets converted into the isotropic phase. In the isotropic phase, the effective permittivity of the NC shifts to lower values at higher temperatures.

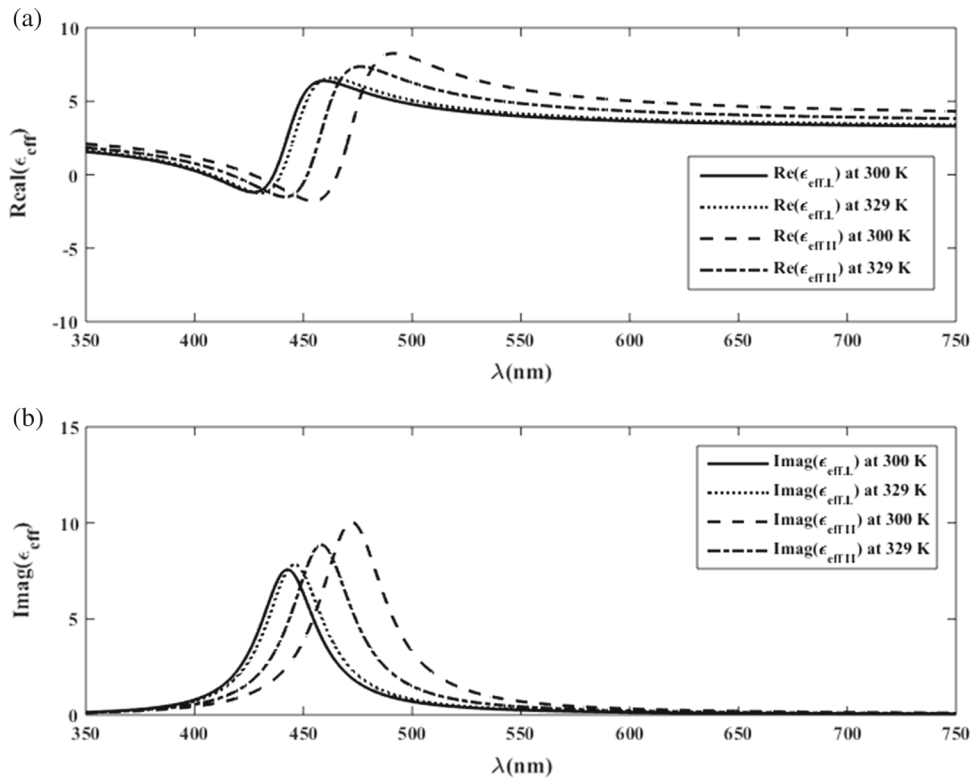

Figure 3. Real and imaginary parts of ordinary and extraordinary components of effective permittivity of the NC at different temperatures with $f = 0.1$.

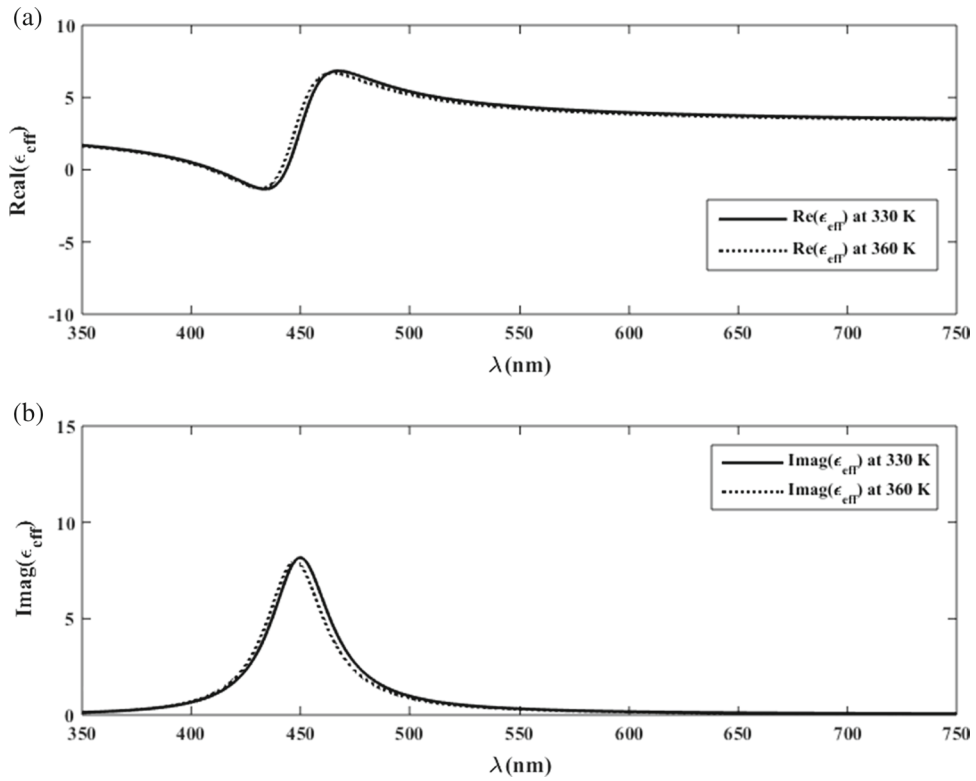

Figure 4. Real and imaginary parts of the effective permittivity of the NCs at different temperatures.

3.2 *Effective dielectric permittivity of NC at different filling fractions f*

In this subsection, the effective dielectric permittivity of the NC is calculated at different filling fractions and different director distortion angles (0°, 90°) of the LC. Figure 5 shows the effective dielectric permittivity of the NC at different filling fractions $f = 0.05$, 0.10 and 0.15 of silver nanoparticle inclusion in the host E7 LC with different orientations of LC. The filling fraction (f) affects the effective permittivity of the NCs as shown in figure 5. The effective permittivity shifts towards higher values for a high filling fraction as shown in figure 6. A comparison of the parallel and perpendicular components of the effective permittivity of the NC at the LC director distortion angles 0° and 90° is shown in figure 7.

3.3 *Transmission and optical properties of the* 1*DPS without and with a defect of NC*

The optical properties of the 1DPC of the TiO_2 and SiO_2 layers with a defect layer of the NC of silver nanoparticle in E7 LCs have been studied using the TMM. Figure 8 shows the optical transmission characteristics of the 1DPS of the TiO_2 and SiO_2 layers. Such a pure periodic structure of the TiO_2 and SiO_2 layers shows a PBG region between the 467 and 669 nm region of the transmission spectra. Now, the same structure is symmetrically sandwiched by a defect layer NC that possesses a PBG region between the 451 and 712 nm wavelength range. A defect mode transmission peak of about 82.4% is obtained at 560 nm wavelength when the director distortion angle is 0°. When the distortion angle is 90°, the defect mode peak transmission is shifted at 574 nm wavelength with 72% transmission. The PBG region is also slightly changed towards the lower frequency range and the band region is found to be 454–712 nm. The transmission spectra of the 1DPS study show that the transmission of the defect mode peak is shifted towards a higher wavelength when the LC director distortion angle changes from 0° to 90°. Such a 1DPS with the NC as the defect layer can be used to design optical filters, switching devices, etc.

3.4 *Transmission and absorption properties of the* 1*DPS with an NC at different temperatures when* $f = 0.05$

Now, the optical properties of the periodic structure $(TiO_2|SiO_2)^5|NC|(TiO_2|SiO_2)^5$ with the NC defect layer at $f = 0.05$ have been studied for different temperatures for both 0° and 90° orientation angles. The

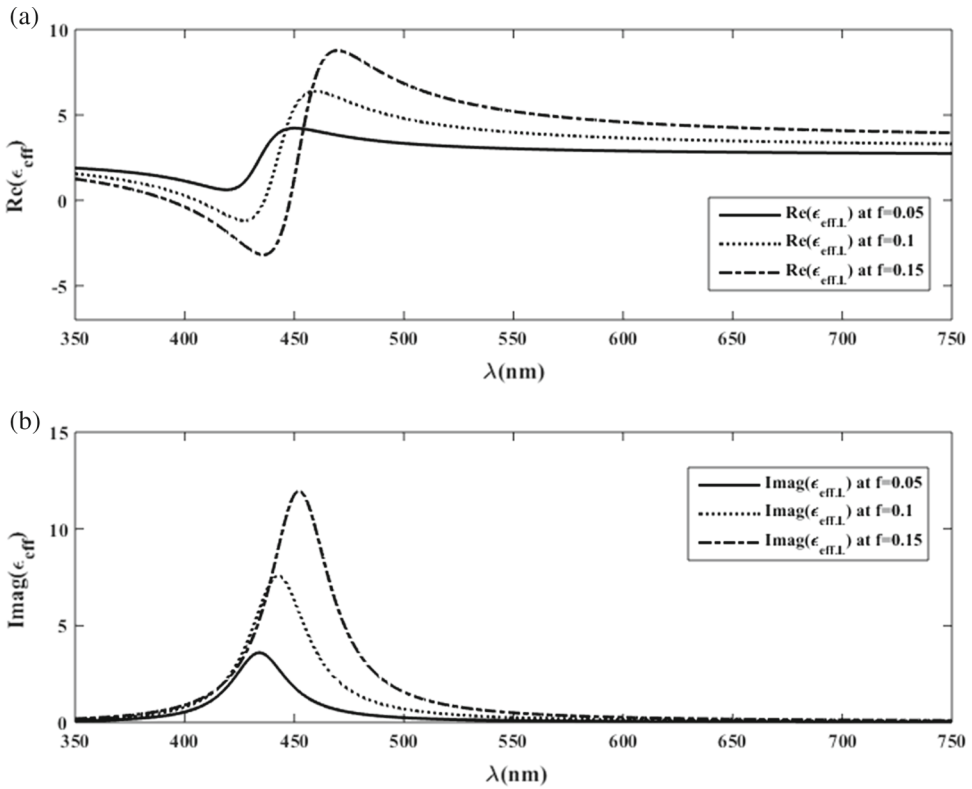

Figure 5. Real and imaginary parts of the ordinary effective permittivity of the NCs at different filling fractions.

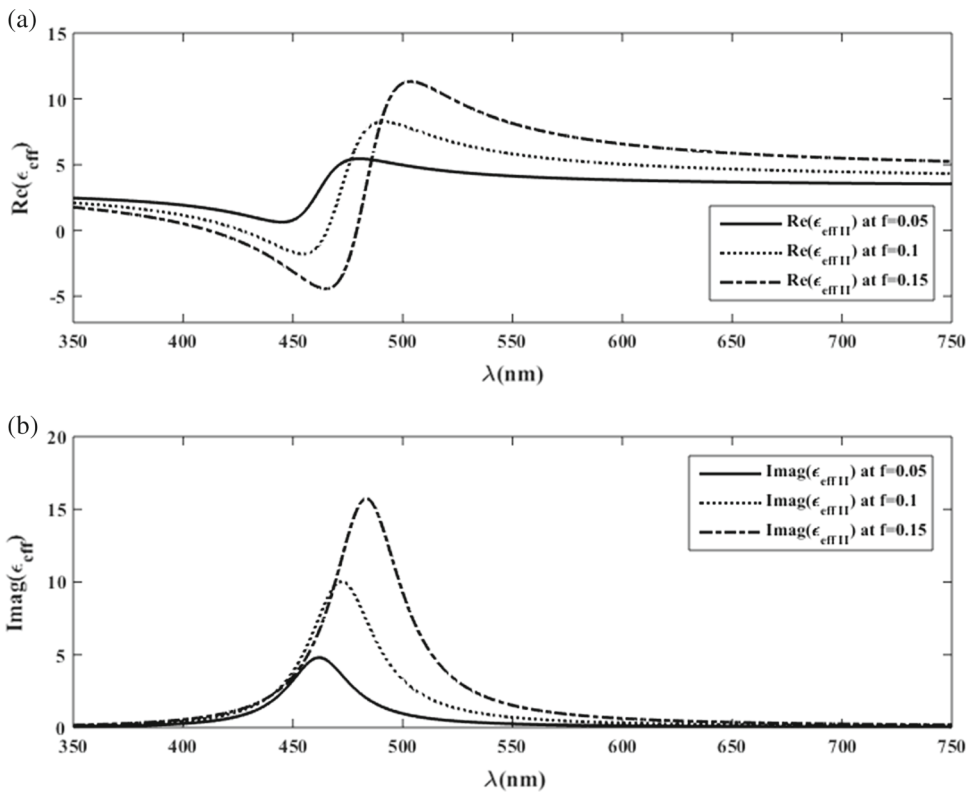

Figure 6. Real and imaginary parts of the extraordinary effective permittivity of the NCs at different filling fractions.

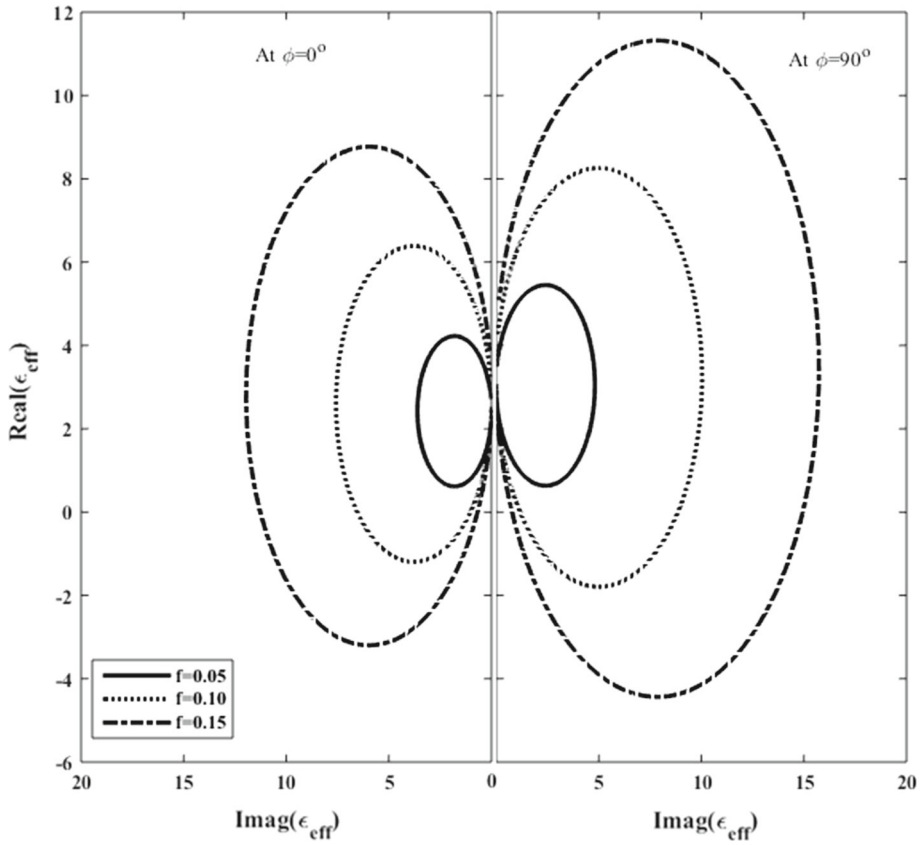

Figure 7. Real part vs. imaginary part of the effective permittivity of the NC at different filling fractions.

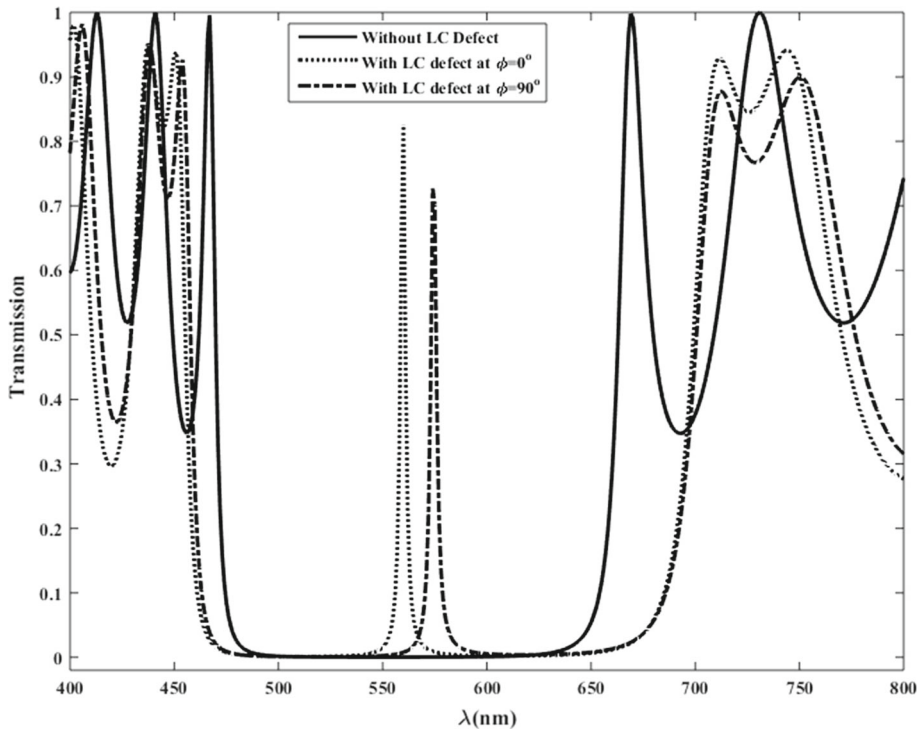

Figure 8. Transmission of the 1DPS without and with LC defect at different orientations (ϕ) of LC molecules.

transmission properties of the 1DPS $(TiO_2|SiO_2)^5|NC|(TiO_2|SiO_2)^5$ with a defect of the NC for 300 and 329 K at different orientation angles (0° and 90°) are shown in figure 9. The presence of silver nanoparticles in the NC affects the transmission of defect mode wavelengths. The obtained defect transmission peak lowers slightly and shows a redshift for an orientation angle of 90°. Such a periodic structure also shows absorption characteristics of the defect mode wavelengths at different orientation angles.

The absorption spectra of the periodic structure $(TiO_2|SiO_2)^5|NC|(TiO_2|SiO_2)^5$ are shown in figure 10 for both 0° and 90° orientations of the LC molecules at 300 and 329 K. Figure 10a shows the maximum value of absorption as 85.33% for 425 nm and the absorption of the defect mode peak is 26.74% for 576 nm at a director angle of 0° and temperature of 300 K. For 90° orientation angle, the maximum absorption is found to be 80.53 and 23.75%, at 456 and 595 nm wavelengths, respectively. Furthermore, we have also calculated absorption spectra at 329 K. The absorption value gets shifted by a small value. Figure 10b shows that the maximum absorptions are 85.93 and 85.23% at 426 and 452 nm for 0° and 90° director angles, respectively. The absorption of the defect peak is found to be 25 and 24.93% at 579 and 586 nm for both director angles, respectively, as shown in figure 10b. The separation between defect transmissions or absorptions peaks obtained at 300 K for both director angles is greater than the separation between peaks obtained at 329 K.

Now, we have calculated the optical properties of the considered periodic structure at 330 and 360 K for $f = 0.05$. The anisotropy property of the NC vanishes because parallel and perpendicular components of the effective dielectric permittivity become equal at $T_C = 330$ K. As a result, transmission and absorption properties of the 1DPS are not affected by the orientation of the LC molecules but it is affected only by temperature. The transmission and absorption of the considered periodic structure $(TiO_2|SiO_2)^5|NC|(TiO_2|SiO_2)^5$ at 330 and 360 K are shown in figures 11 and 12, respectively. Figures 11a and 12a represent the transmission and absorption spectra of PC at 330 K. The transmission and absorption spectra observed at 360 K are shown in figures 11b and 12b. The maximum absorption is found to be 85.91 and 86.83% at 427 nm at 330 and 360 K, respectively. The absorption of the defect mode peaks is 25.71 and 25.77% at 581 and 579 nm at 330 and 360 K, respectively.

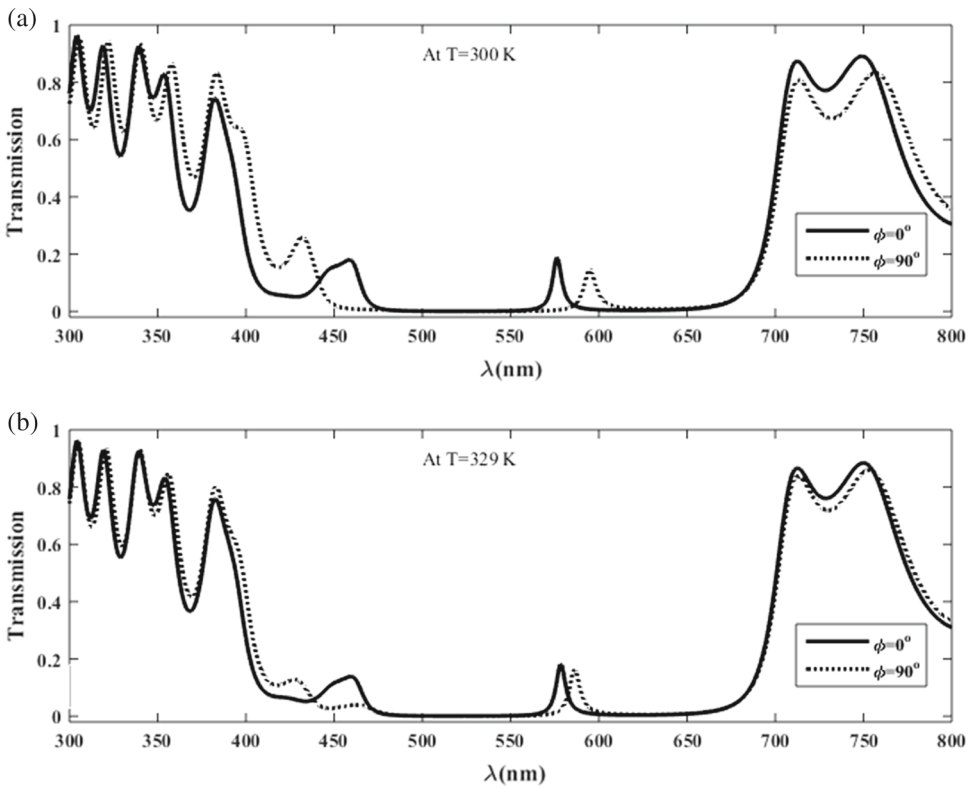

Figure 9. Transmission of the 1DPS with the NC at different orientations of molecules: (**a**) at $T = 300$ K and (**b**) at $T = 329$ K.

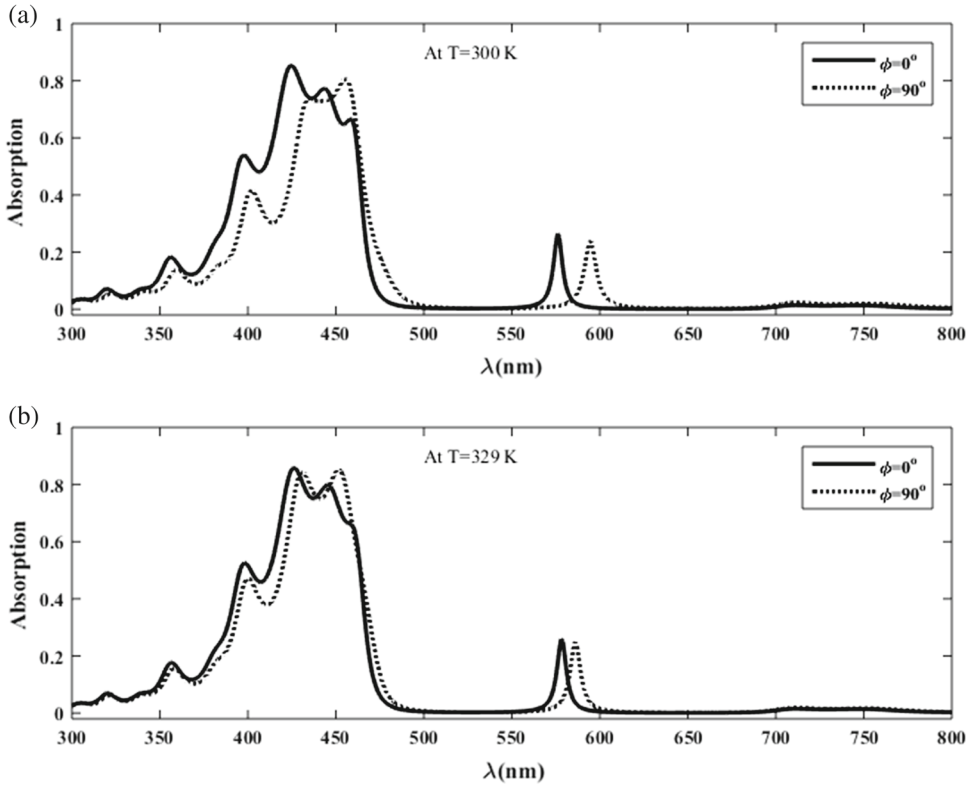

Figure 10. Absorption of the 1DPS with the NC at different orientations of LC: (**a**) at $T = 300$ K and (**b**) at $T = 329$ K.

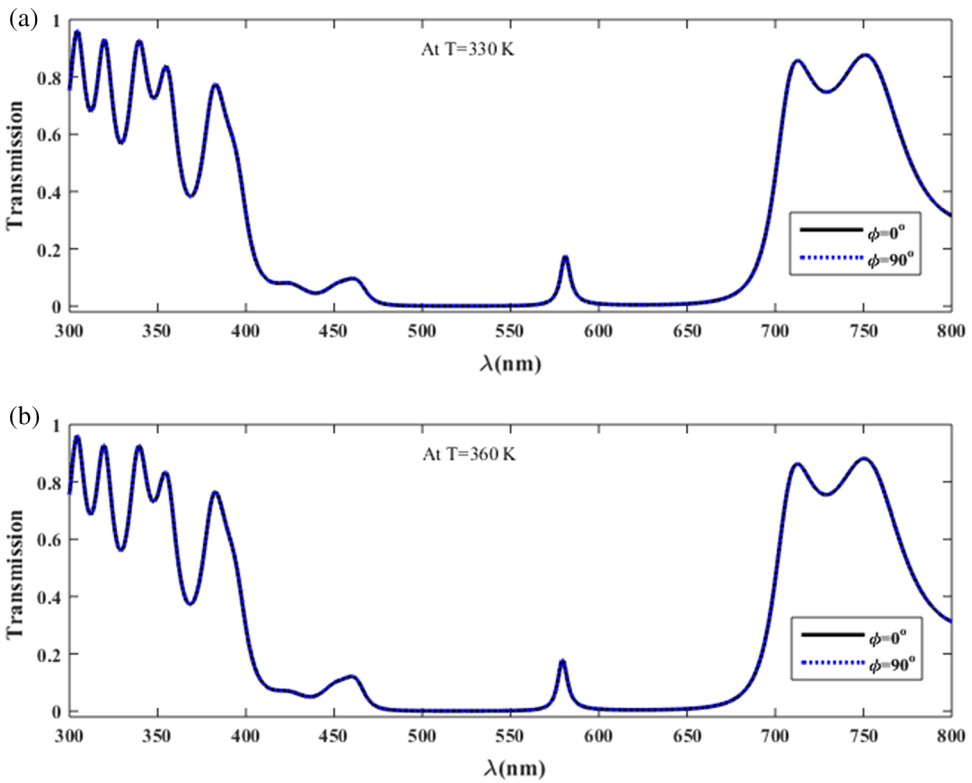

Figure 11. Transmission of the 1DPS with the NC defect: (**a**) at $T = 330$ K and (**b**) at $T = 360$ K.

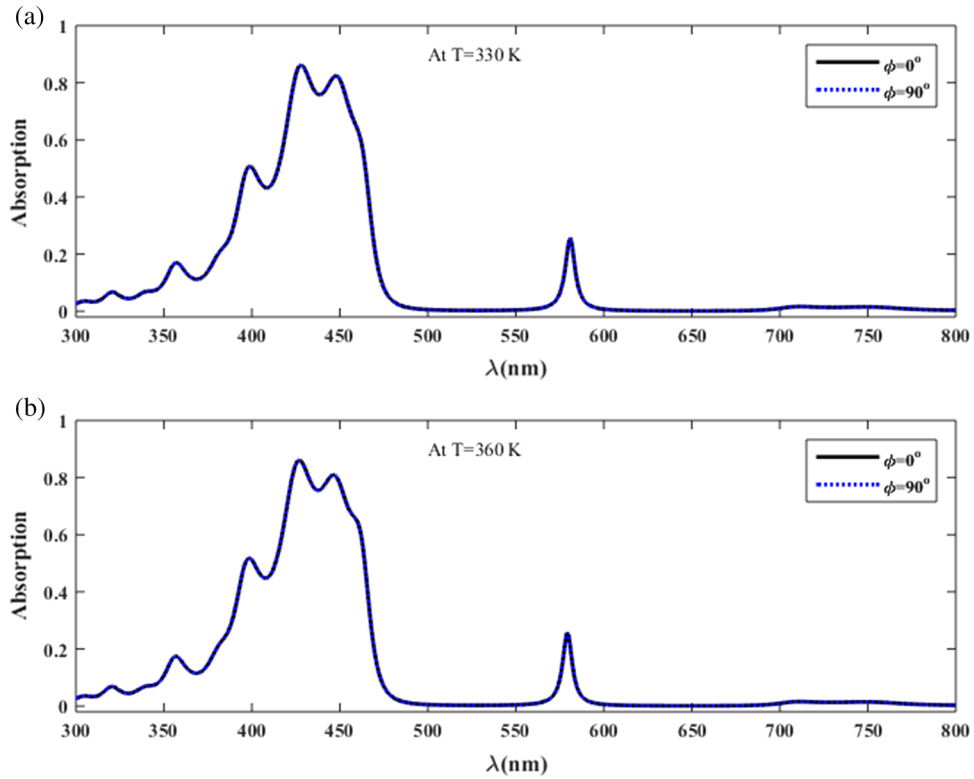

Figure 12. Absorption of the 1DPS with the NC defect: (**a**) at $T = 330$ K and (**b**) at $T = 360$ K.

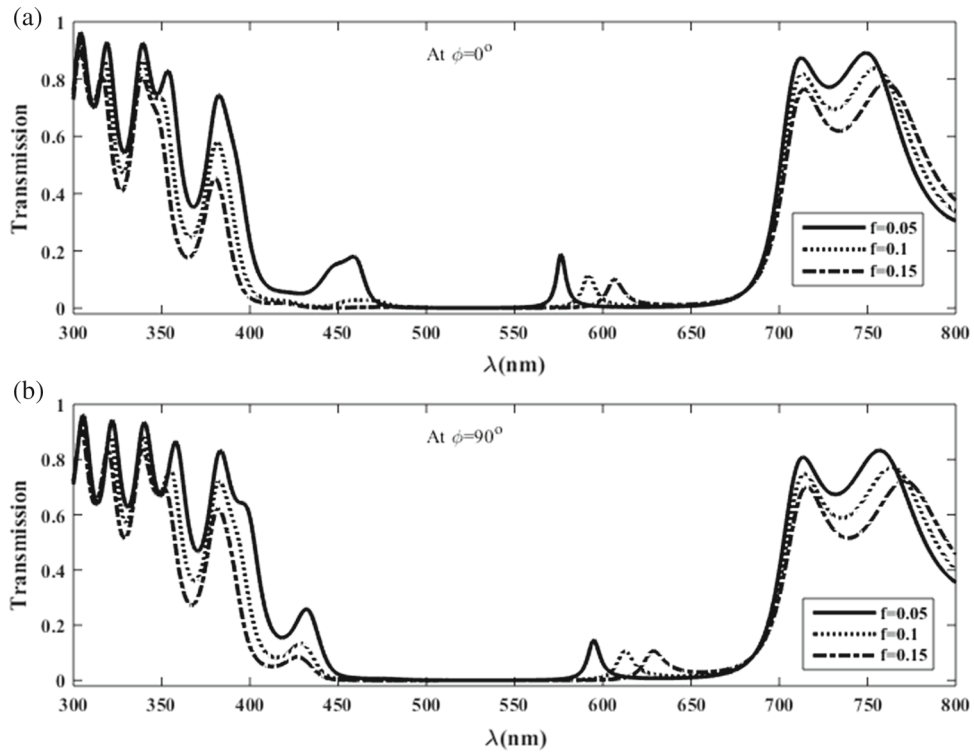

Figure 13. Transmission of the 1DPS with the NC at different filling fractions for the director angle: (**a**) at $\phi = 0°$ and (**b**) at $\phi = 90°$.

3.5 *Transmission and absorption properties of the 1DPS with NC at different filling fractions (f) when $T = 300\ K$*

As discussed earlier, transmission and absorption of the considered periodic structure $(TiO_2|SiO_2)^5|NC|(TiO_2|SiO_2)^5$ are affected by temperature. The transmission of the periodic structure with a defect of NC with different filling fractions at 0° and 90° director angles are shown in figure 13. Similarly, the absorption of the periodic structure $(TiO_2|SiO_2)^5|NC|(TiO_2|SiO_2)^5$ with different filling fractions is shown in figure 14. At different filling fractions (f), the absorption of PCs with NC can be seen in table 1.

The transmission and absorption properties of the 1DPS $(TiO_2|SiO_2)^5|NC|(TiO_2|SiO_2)^5$ are studied with 0° and 90° director angles of the LC, for tranistions above and below the Fréedericksz transitions. A comparative study of the optical properties at both LC director angles is shown in figures 15 and 16. It shows that optical transmission and absorption are affected by the filling fractions of the silver nanoparticle on the NC of E7 LC.

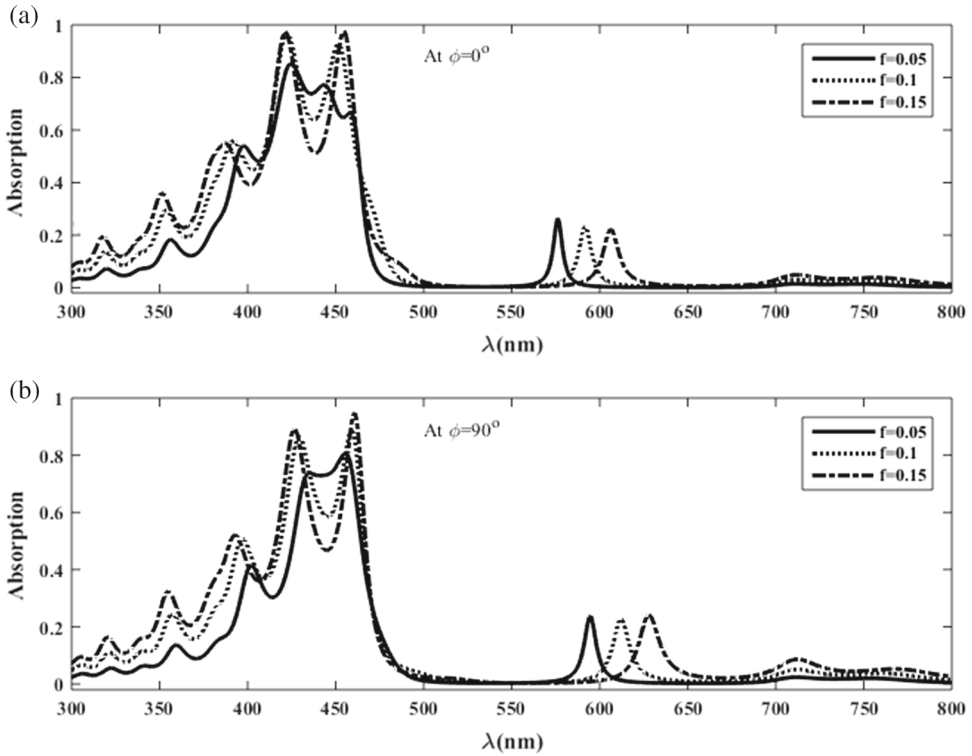

Figure 14. Absorption of the 1DPS with the NC at different filling fractions for the director angle: (**a**) at $\phi = 0°$ and (**b**) at $\phi = 90°$.

Table 1. Absorption detail of the 1DPS with NC defect layer at different filling fractions.

		Absorption					
		$f = 0.05$		$f = 0.10$		$f = 0.15$	
		Wavelength (nm)	Absorption (%)	Wavelength (nm)	Absorption (%)	Wavelength (nm)	Absorption (%)
$\phi = 0°$	Defect peak	576	26.47	592	23.35	606	22.27
	Maximum value	1425	85.33	422	97.24	422	97.07
	Maximum value	2425	85.33	451	92.78	455	97.73
$\phi = 90°$	Defect peak	595	23.35	612	22.67	628	24.22
	Maximum value	1456	84.74	430	86.22	427	89.10
	Maximum value	2434	73.56	451	88.69	461	94.88

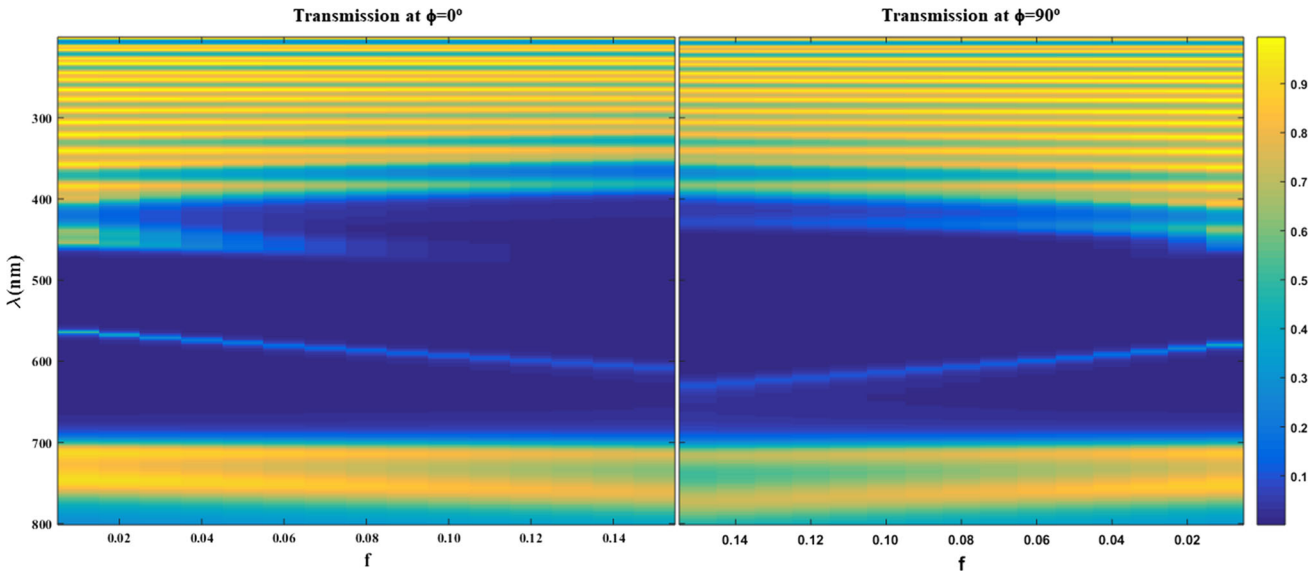

Figure 15. Transmission of the 1DPS with the NC as a defect layer vs. filling fractions at orientation angles of LC: (**a**) at $\phi = 0°$ and (**b**) at $\phi = 90°$.

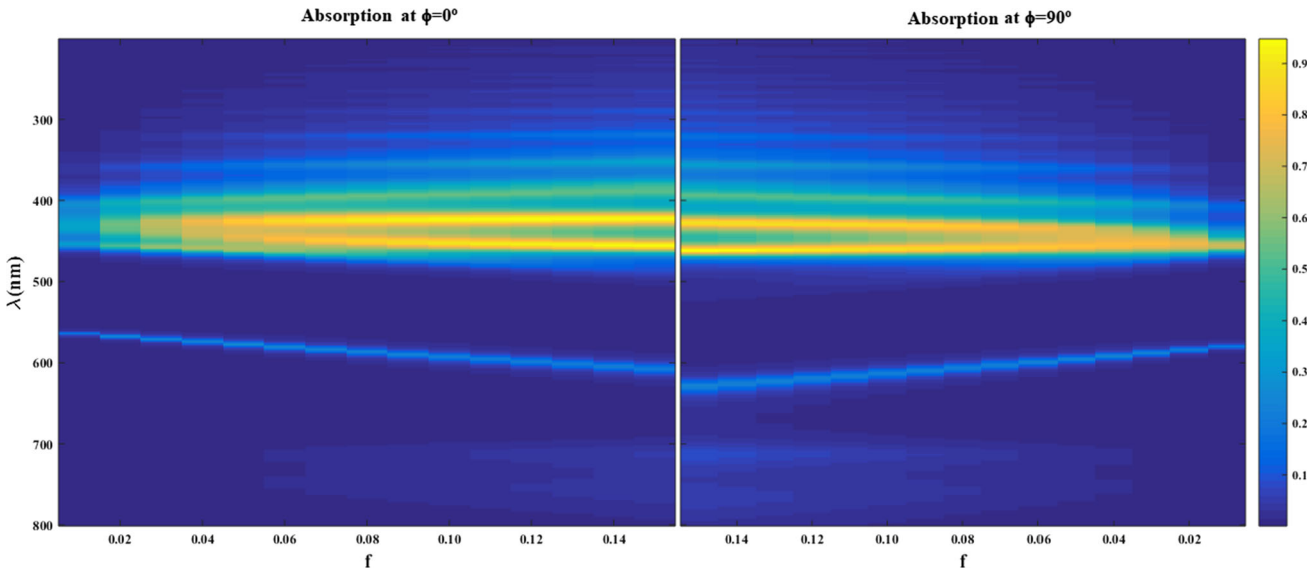

Figure 16. Absorption of the 1DPS with the NC as a defect layer vs. filling fractions at orientation angles of LC: (**a**) at $\phi = 0°$ and (**b**) at $\phi = 90°$.

4. Conclusion

In this paper, we have investigated the effective permittivity of the NC consisting of a silver nanoparticle and a E7 LC, i.e. the inclusion of a silver nanoparticle in E7 LC as the host material. The effective permittivity of the silver nanoparticle has been calculated using the Maxwell–Garnett model. Our study shows that the surface plasmon resonance of the nanosilver particle is affected by the ordinary and extraordinary components of the effective dielectric permittivity of the NC at different temperatures. The study of transmittance and absorption of the 1DPS with the defect layer NC reveals that an NC with a defect layer in the 1DPS may be used to design optical devices because the effective permittivity of the NC is significantly changed at different filling fractions. The study also reveals that the optical properties of the 1DPS are affected significantly

at different filling fractions as well as at different orientations of the LC. Such periodic structure containing NC defect, $(TiO_2|SiO_2)^5|NC|(TiO_2|SiO_2)^5$, may be used to fabricate filters, switches, tunable devices, absorbers, sensors, etc.

Acknowledgements

PS acknowledges Babasaheb Bhimrao Ambedkar University for providing NON-NET UGC fellowship and NK thanks UGC New Delhi for financial support through the NFSC fellowship.

References

[1] E Yablonovitch, *Phys. Rev. Lett.* **58**, 2059 (1987)
[2] S John, *Phys. Rev. Lett.* **58**, 2486 (1987)
[3] J D Jonopoulos, P Villeneuve and S Fan, *Nature* **386**, 143 (1997)
[4] Q R Zheng, Y Q Fu and N C Yuan, *J. Electromagn. Waves Appl.* **20**, 1439 (2006)
[5] Y Fink, J N Winn, S Fan, C Chen, J Michel, J D Joannopoulos and E L Thomas, *Science* **282**, 1679 (1998)
[6] J A M Rojas, J Alpuente, J Pineiro and R Sanchez, *Prog. Electromagn. Res.* **63**, 89 (2006)
[7] J D Joannopoulos, R D Meade and J N Winn, *Photonic crystals: Molding the flow of light* (Princeton University Press, Princeton, NJ, 1995)
[8] R Srivastava, K B Thapa, S Pati and S P Ojha, *Prog. Electromagn. Res.* **7**, 133 (2008)
[9] R Srivastava, K B Thapa, S Pati and S P Ojha, *Prog. Electromagn. Res.* **81**, 225 (2008)
[10] K B Thapa, S K Singh and S P Ojha, *Int. J. Infrared Millimeter Waves* **27**, 1257 (2006)
[11] S K Singh, J P Pandey, K B Thapa and S P Ojha, *Prog. Electromagn. Res.* **70**, 53 (2007)
[12] Y Kalra and R K Singha, *Pramana – J. Phys.* **67**, 1155 (2006)
[13] K B Thapa, S Srivastava and S Tiwari, *J. Supercond. Novel Magn.* **23**, 517 (2015)
[14] S K Singh, K B Thapa and S P Ojha, *Int. J. Micro. Opt. Technol.* **1**, 686 (2006)
[15] G N Pandey, N Kumar, K B Thapa and S P Ojha, *AIP Conf. Proc.* **1728**, 020310 (2016)
[16] K B Thapa, N K Mishra, G N Pandey and S P Ojha, *Prog. Electromagn. Res.* **8**, 221 (2009)
[17] I El-Kady, M M Sigalas, R Biswas, K M Ho and C M Soukoulis, *Phys. Rev. B* **62**, 299 (2000)
[18] V Rinnerbauer, A Lenert, D M Bierman, Y X Yeng, W R Chan, R D Geil, J J Senkevich, J D Joannopoulos, E N Wang, M Soljacic and I Celanovic, *Adv. Energy Mater.* **4**, 1 (2014)
[19] G Veronis, R W Dutton and S Fan, *J. Appl. Phys.* **97**, 093104 (2005)
[20] E Özbay, B Temelkuran, M Sigalas, G Tuttle, C M Soukoulis and K M Ho, *Appl. Phys. Lett.* **69**, 3797 (1996)
[21] A Gharaati and Z Zare, *Pramana – J. Phys.* **88**: 75 (2017)
[22] B Bhushan, S S Talwar, T Kundu and B P Singh, *Pramana – J. Phys.* **87**: 56 (2016)
[23] S Chandrasekhar, *Liquid crystals* (Cambridge University Press, New York, 1992)
[24] I C Khoo, *Liquid crystals* (Wiley Interscience, New Jersey, 2007)
[25] L M Blinov, *Structure and properties of liquid crystals* (Springer, New York, 2011)
[26] K Bush and S John, *Phys. Rev. Lett.* **83**, 967 (1999)
[27] K Yoshino, Y Shimoda, Y Kawagishi, K Nakayama and M Ozaki, *Appl. Phys. Lett.* **75**, 932 (1999)
[28] S W Leonard, J P Mondia, H M van Driel, O Toader, S John, K Bush, A Birner, U Gosele and V Lehmann, *Phys. Rev. B* **61**, R2389 (2000)
[29] Ch Schuller, F Klopf, J P Reithmaier, M Kamp and A Forchel, *Appl. Phys. Lett.* **82**, 2767 (2003)
[30] D Kang, J E Maclennan, N A Clerk, A A Zakhidov and R H Baughman, *Phys. Rev. Lett.* **86**, 4052 (2001)
[31] E Graubard, J S King, S Jain, C J Summers, Y Z Williams and I C Khoo, *Phys. Rev. B* **72**, 233105 (2005)
[32] V G Arkhipkin, V A Gunyakov, S A Myslivsts, V Ya Zyryanov and V F Shabanov, *Eur. Phys. J.* **E24**, 297 (2007)
[33] Y M Strelniker, D Stroud and A O Voznesenkaya, *Eur. Phys. J. B* **52**, 1 (2006)
[34] S F Mingaleev, M Schillinger, D Hermann and K Bush, *Opt. Lett.* **29**, 2858 (2004)
[35] B Ya Zel'dovich, N V Tabiryan and Y S Chilingaryan, *Zh. Eksp. Teor. Fiz.* **81**, 72 (1981), [*Sov. Phys. JETP* **81**, 7 (1981)]
[36] H L Ong, *Phys. Rev. A* **28**, 2393 (1983)
[37] M S Mohamed, M F O Hameed, M M El-Okr and S S A Obayya, *Optik* **127**, 8774 (2016)
[38] R Ozaki, H Miyoshi, M Ozaki and K Yoshino, *Mol. Cryst. Liq. Cryst.* **433**, 247 (2005)
[39] A C Polycarpou, M A Christou and N C Papanicolaou, *IEEE Trans. Microw. Theory Tech.* **60**, 2950 (2012)
[40] E Miroshnichenko, I Pinkevych and Y S Kivshar, *Opt. Express* **14**, 2839 (2006)
[41] S R Entezar, A Madani, M K Habil, A Namdar and H Tajalli, *J. Mod. Opt.* **60**, 1883 (2013)
[42] H L Ong, *Phys. Rev. A* **33**, 3550 (1986)
[43] P Yeh, *Optical waves in layered media* (John Wiley & Sons, New York, 1988)
[44] H A Elsayed and A H Aly, *Int. J. Mod. Phys. B* **32**, 1850056 (2018)
[45] S Y Vetrov, R G Bikbaev and I V Timofeev, *J. Exp. Theor. Phys.* **117**, 988 (2013)
[46] A H Aly, H A Elsayed and C Malek, *J. Nonlin. Opt. Phys. Mater.* **26**, 1750007 (2017)
[47] N R Ramanujam, K S J Wilson and V Revathy, *Prog. Electromagn. Res. M* **41**, 105 (2015)

[48] S G Moiseev, V A Ostatochnikov and D I Sementsov, *Quantum Electron.* **42**, 557 (2012)
[49] S G Moiseev, *Appl. Phys. A* **103**, 775 (2011)
[50] S G Moiseev, *Appl. Phys. A* **103**, 619 (2011)
[51] S G Moiseev and V Ostatochnikov, *Opt. Quantum Electron.* **47**, 3193 (2015)
[52] A Mouquinho, M Saavedra, A Maiau, K Petrova, M T Barros, J L Figueirinhas and J Sotomayor, *Mol. Cryst. Liq. Cryst.* **542**, 132/[654] (2011)
[53] J Li, S T Wu, S Brugioni, R Meucci and S Faetti, *J. Appl. Phys.* **97**, 073501 (2005)

Physica Scripta

PAPER

Theoretical investigation of enhanced sensing property in 1D TiO_2/SiO_2 periodic layers containing a defect layer of the nanocomposite with different radii of silver nanoparticles in the host liquid crystal

To cite this article: Pawan Singh *et al* 2020 *Phys. Scr.* **95** 065507

View the article online for updates and enhancements.

This content was downloaded from IP address 148.253.213.132 on 28/09/2020 at 11:58

IOP Publishing Physica Scripta
Phys. Scr. 95 (2020) 065507 (11pp) https://doi.org/10.1088/1402-4896/ab82c5

Theoretical investigation of enhanced sensing property in 1D TiO_2/SiO_2 periodic layers containing a defect layer of the nanocomposite with different radii of silver nanoparticles in the host liquid crystal

Pawan Singh[1], Vivek Kumar Nautiyal[1], Ram Janma[2] and Khem B Thapa[1]

[1] Department of Physics, School of Physical and Decision Sciences, Babasaheb Bhimrao Ambedkar University, Lucknow-226025 (UP), India
[2] Department of Physics, University of Engineering & Technology, CSJM University, Kanpur-208024 (UP), India

E-mail: khem.bhu@gmail.com

Received 24 December 2019, revised 20 March 2020
Accepted for publication 24 March 2020
Published 18 May 2020

Abstract

In this paper, we have theoretically investigated the effective dielectric permittivity of the nanocomposite (NC) layer of liquid crystal (LC) with silver nanoparticles at different radii using the Maxwell-Garnett model. The optical properties of a one-dimensional periodic structure (1DPS) of TiO_2/SiO_2 dielectric materials containing defect NC layer, $(TiO_2|SiO_2)^3|NC|(TiO_2|SiO_2)^3$, with different radii of silver nanoparticles studied theoretically using the well-known transfer matrix method (TMM). The effective permittivity of NC for $\phi = 0^\circ$ and 90° orientation angles of LC is calculated with varying sizes of the nanoparticles because the size of the silver nanoparticles affects the surface plasmon resonance (SPR). The transmission of defect mode wavelength peaks for 0° and 90° orientation angle of the LC is studied for different radii of nanoparticles. Besides this, we have also studied the absorption characteristics of the considered NC defect structure for different orientation of the LC with varying radii of the nanoparticles.

Keywords: liquid crystal, silver nanoparticle, SPR, transfer matrix method (TMM), transmission, absorption

(Some figures may appear in colour only in the online journal)

1. Introduction

Optical media consisting of alternating dielectric materials with periodic modulation of refractive indices in different dimensions is known as Photonic Crystals (PCs). Regular repetition of the refractive indices in three directions gives three types of PC: one-dimensional photonic crystal (1DPC), two-dimensional photonic crystal (2DPC), and three-dimensional photonic crystal (3DPC). The transmission spectra of periodic optical media of different materials are fascinating the PCs due to exhibiting photonic bandgap (PBG) regions for certain frequency ranges. PBGs are particular regions in the transmission spectra of PCs, where no frequency or electromagnetic wave can circulate. Due to exhibiting the unusual properties, PCs have been used in various optical devices viz. optical filters, optical switches, and reflectors, etc [1–11]. Many researchers have performed numerous works to fabricate the optical filters and reflectors based on the omni-directional properties of PCs. Moreover, metallic photonic crystal (MPC) has been used to design absorption-based

 © 2020 IOP Publishing Ltd Printed in the UK

optical devices such as microwave absorbers and sensors, etc [12–19].

For the tunability of PC, in general, a dielectric layer is infiltrated as a defect inside the periodic structures which gives tunable defect mode transmission. The tunable defect mode transmission is dependent on the optical parameters of the defect layer. By considering liquid crystal (LC) as a defect layer in 1DPC, the optical properties of defect mode are tuned by the orientation of molecules in LC. As we know that liquid crystal (LC) is an anisotropic material that has extraordinary and ordinary dielectric permittivities, hence LC is useful material as a tunable defect layer in 1DPC. The dielectric permittivity of LC is a tensor quantity and can be represented in matrix form. The directional dependent optical properties of anisotropic materials (LC) are used in nonlinear optical devices [20–22]. Besides this, the extraordinary and ordinary dielectric permittivities of LC are dependent on the temperature and electric field. It means the optical properties of LC can be controlled by applying the electric field as well as temperature. With LC as a defect layer in a PC, the transmission characteristics of PCs can be regulated by applied electric field or temperature. The tunability of PBG regions of the inverse opal coated with LC theoretically suggested by Busch *et al* and experimentally established by Yoshino *et al* [23, 24]. PCs with LC as a defect layer have been used as various novel tunable devices [25–38].

The optical property of LCs is dependent on the orientation of molecules which is given by the orientation angle (ϕ) of LC director. The dielectric tensor of LC consists of ordinary ($\varepsilon_\perp$), extraordinary dielectric permittivity ($\varepsilon_\parallel$) and dielectric anisotropy (ε_a) with orientation angle (ϕ) that is given as [37, 39]:

$$\tilde{\varepsilon}_{LC} = \begin{pmatrix} \varepsilon_\perp + \varepsilon_a \sin^2\phi & 0 & \varepsilon_a \sin\phi\cos\phi \\ 0 & \varepsilon_\perp & 0 \\ \varepsilon_a \sin\phi\cos\phi & 0 & \varepsilon_\perp + \varepsilon_a \cos^2\phi \end{pmatrix}, \tag{1}$$

The dielectric tensor of LC is simplified to a diagonal matrix when the orientation angle (ϕ) of the LC director is 0° and 90°. Hence, the transfer matrix method (TMM) [40] may now apply to study the optical properties of LC for the orientation angle $\phi = 0°$ and 90°. The transmission spectra of defective PC are found with defect mode wavelength peaks due to a defect layer.

The liquid crystal (LC) can be used as a nanocomposite (NC) layer when spherical nanoparticles are randomly mixed with LC. Such a nanocomposite (NC) layer of liquid crystal (LC) with nanoparticles has tunable effective dielectric permittivity, therefore NC can be used as a defect layer in 1DPC. The transmission properties of defective PC with NC are tunable with the filling fraction and radii of doped nanoparticles [41–44]. The effective dielectric permittivities of NC consist of doped silver nanoparticles in the E7 LC mixture that can be obtained through Maxwell-Garnett model [45–47]. The transmission and absorption properties of one-dimensional photonic crystal with NC defect layer have been studied with filling fraction of nanoparticles in liquid crystal nanocomposite, orientation of LC molecules and temperatures [48].

In this work, we study optical properties of the periodic structure of TiO_2/SiO_2 with defect nanocomposite (NC) where NC is a liquid crystal with the inclusion of silver nanoparticles (Ag-NPs). We have considered the composition of four different LC, E7 liquid crystal, as a host material for the inclusion of silver nanoparticles [49, 50]. The effective dielectric permittivity of NC has been studied for different radii of Ag-NPs. The transmission characteristics of the defect NC periodic structure, $(TiO_2|SiO_2)^3|NC|(TiO_2|SiO_2)^3$, for two different orientation angles of LC, are studied for different radii of silver nanoparticles. Based on the radius of nanoparticles and the orientation of LC molecules, we study the defect transmission peaks for designing tunable optical filters, detectors, and sensors.

2. Theoretical model

We theoretically study a nanocomposite of LC with different radii of silver nanoparticles. The effective dielectric permittivity of nanocomposite is calculated using the Maxwell-Garnett Model [45, 46]. We consider that the spherical silver nanoparticles are randomly distributed in the host material E7 LC, where E7 LC is the composition of four different LC viz. 5CB, 7CB, 8OCB, 5CT. Thus, the effective dielectric permittivity of the nanocomposite (NC) layer is given as [47];

$$\varepsilon_{eff} = \frac{2\varepsilon_{LC} f(\varepsilon_m - \varepsilon_{LC}) + \varepsilon_{LC}(\varepsilon_m + 2\varepsilon_{LC})}{2\varepsilon_{LC} + \varepsilon_m + f(\varepsilon_{LC} - \varepsilon_m)}, \tag{2}$$

where ε_{LC}, ε_m and f are the dielectric permittivity of LC, silver (Ag) nanoparticle and the filling fraction of silver nanoparticles, respectively. The dielectric permittivity of the spherical silver nanoparticle is obtained with the Drude model [49]:

$$\varepsilon_m = \varepsilon_0 - \frac{{\omega_p}^2}{\omega^2 + i\omega\eta}, \tag{3}$$

where $\omega_p\varepsilon_0$ and η are plasmon frequency, the relative dielectric permittivity of silver nanoparticle, and damping frequency, respectively. The damping frequency of silver nanoparticles depends on the radius (r) of nanoparticle and velocity (ν_f) of the electron at Fermi-energy, given as [47];

$$\eta(r) = \eta_0 + \frac{\nu_f}{r}, \tag{4}$$

where η_0 is the decay constant obtained by scattering of the free electron with phonons, electrons, etc.

The extraordinary (n_e) and ordinary (n_o) refractive indices of E7 LC mixture depends on temperature as [50, 51]:

$$n_e(T) = A - BT + \frac{2(\Delta n)_o}{3}\left(1 - \frac{T}{T_C}\right)^\beta, \tag{5}$$

$$n_o(T) = A - BT - \frac{(\Delta n)_o}{3}\left(1 - \frac{T}{T_C}\right)^\beta, \tag{6}$$

where A, B, Δn, β are material parameters of LC and T_C is

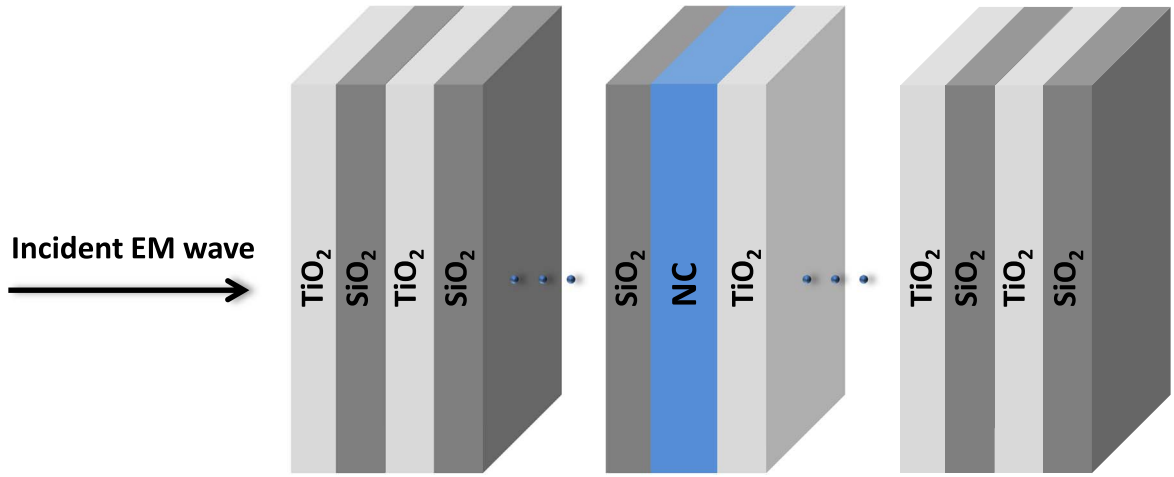

Figure 1. Schematic representation of the one-dimensional periodic structure of TiO_2/SiO_2 with the defect of nanocomposite (NC) layer i.e. $(TiO_2|SiO_2)^3|NC|(TiO_2|SiO_2)^3$.

clearing temperature of LC mixture. All the constants existing in the calculation of refractive indices of LC are assumed at 1.5 μm wavelength [50]. The extraordinary ($\varepsilon_{||}$) and ordinary permittivity ($\varepsilon_{\perp}$) of LC can be obtained by squaring the values of extraordinary (n_e) and ordinary (n_o) refractive indices, respectively.

To investigate the effect of different radii silver nanoparticles, we have calculated the transmission spectra of the one-dimensional periodic structure of TiO_2 and SiO_2 layers, $(TiO_2|SiO_2)^3|NC|(TiO_2|SiO_2)^3$, with the defect of NC using simple transfer matrix method (TMM) [40]. The schematic representation of the considered periodic structure of TiO_2 and SiO_2 layers with NC as a defect layer is shown in figure 1. The thicknesses and refractive indices of TiO_2 and SiO_2 layers are d_1, d_2, and, n_1, n_2, respectively.

3. Results and discussion

The nanocomposite (NC) of liquid crystal (LC) with spherical silver nanoparticles (Ag-NPs) has been theoretically considered to design a defect layer. The effective permittivity of the nanocomposite (NC) is calculated using Maxwell-Garnett model that is represented by equation (2). The size of silver nanoparticles affects the surface plasmon resonance (SPR) due to scattering the waves. So, the effective permittivity of nanocomposite is also affected through SPR. The SPR band is the collection of excitation of free electrons. Such a band is influenced by the width and the position of free electrons. Hence, the surface plasmon resonance (SPR) changes as the radius of the nanoparticle changes. The SPR band is enlarged with the large radii of the nanoparticles. The scattering rate of conduction electrons increases as the radius of the nanoparticle decreases. Hence, a redshift appears in the SPR, which affects the effective dielectric permittivity of the NC [51, 52].

The imaginary and real components of the effective permittivity of nanocomposite for both orientation angle 0° and 90° are inspected for radii 3 nm, 5 nm, 7 nm, and 9 nm of the silver nanoparticles in figures 2 and 3, respectively. The real and imaginary parts of effective permittivity have positive values in an asymmetric and symmetric manner, respectively. We observed that real and imaginary parts of the effective permittivity increases for both orientation angle 0° and 90° as the radii of the silver nanoparticle in composite increases. The real and imaginary values of effective permittivity of NC, are laid from 350 nm to 550 nm range. The observed results reveal that the SPR gets affected as the effective permittivity of nanocomposite changes. However, the effective permittivity of NC at orientation angle 90° is larger than the effective permittivity of NC at orientation angle 0°. It means that the orientation of LC molecules interacts with SPR, and the effective permittivity of nanocomposite is enhanced.

To better understand this interaction, we compare the comparison of real and imaginary parts of effective permittivity of NC at different orientation angles (ϕ) of the LC, 0° and 90°, with different radii of nanoparticles are shown in figures 4 and 5 respectively. From figure 4, we can easily see that the area between the curves of real parts of effective permittivities for both orientations is increased as the radius of nanoparticle increases but the difference between theses curves is decreased. After the radius of 7 nm, the curves for real effective permittivities also show extra areas. Similarly, imaginary effective permittivities also attain the higher values (figure 5) for orientation angle 90° in comparison to orientation angle 0°. It shows that the interaction of the orientation of LC molecules with SPR is enhanced the effective permittivity of the nanocomposite.

Now, the interaction of the orientation of LC molecules with SPR can also be better understand, if the optical properties of the defective NC periodic structure of TiO_2/SiO_2 for the orientation angle of LC molecules viz. 0° and 90° have studied with different radii of the silver nanoparticles. The refractive indices and thicknesses of TiO_2 and SiO_2 layers are taken 2.4, 1.5 and, 57.3 nm, 91.6 nm, respectively. The width of the NC (LC & Ag-NPs composite) is taken as 100 nm. The plasmon frequency ω_p and the decay constant η_0 of the silver

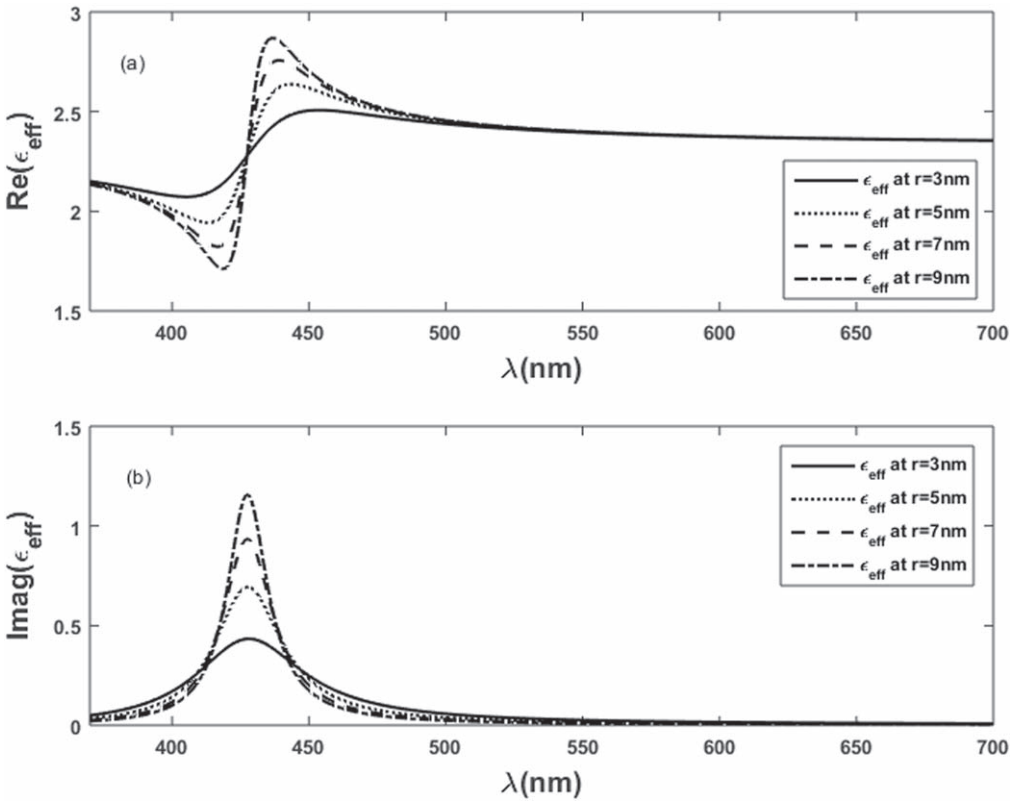

Figure 2. Effective permittivity of nanocomposite (NC) versus wavelength (a) Real part (b) Imaginary part at orientation angle (ϕ) = 0° and for different radii of nanoparticles.

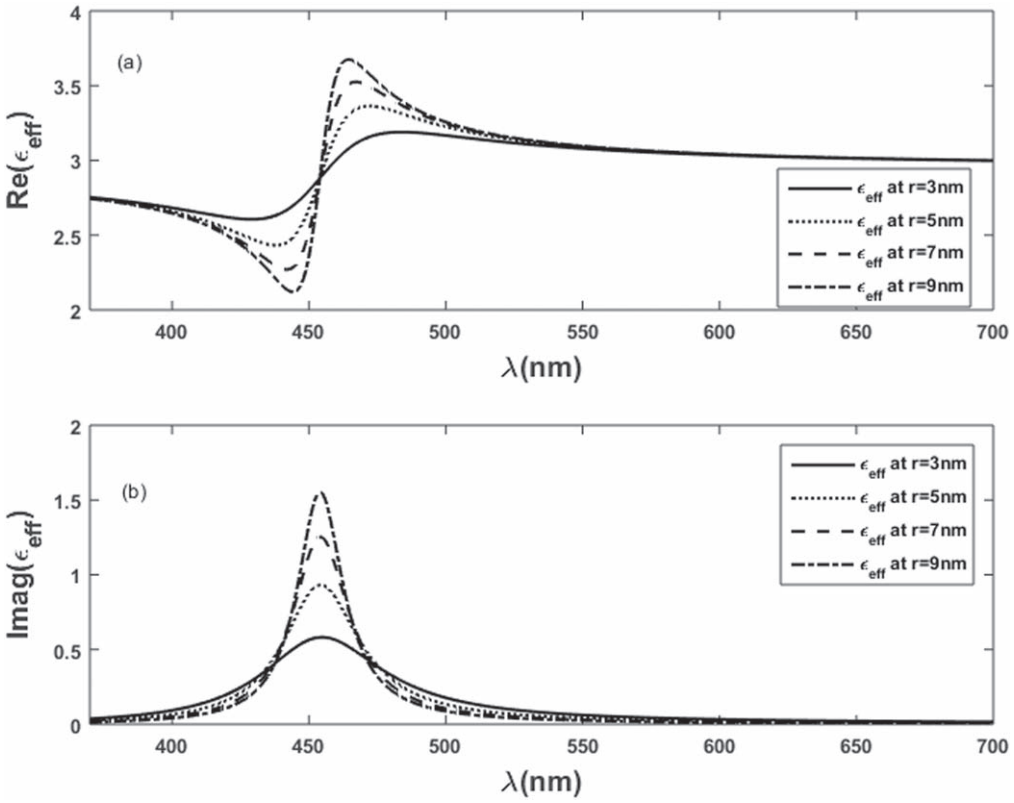

Figure 3. Effective permittivity of nanocomposite (NC) versus wavelength (a) Real part (b) Imaginary part at orientation angle (ϕ) = 90° and for different radii of nanoparticles.

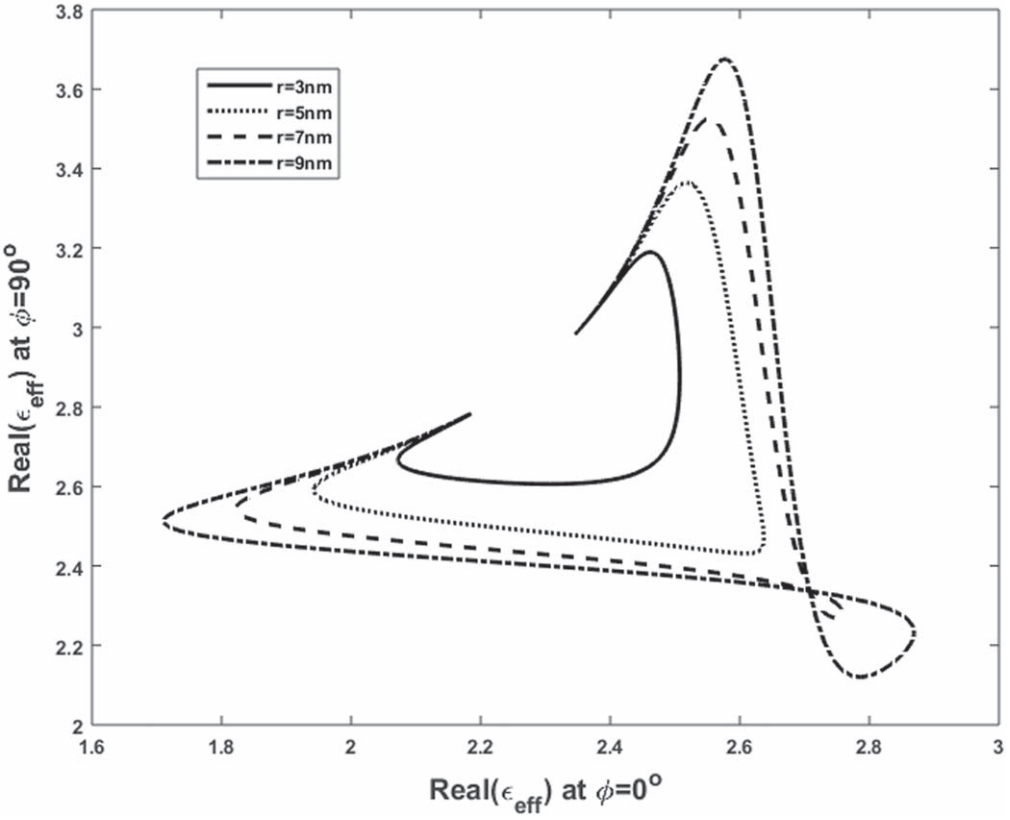

Figure 4. Real part of effective permittivity at $\phi = 90^{\circ}$ versus Real part of effective permittivity at $\phi = 0^{\circ}$ for different radii of nanoparticles.

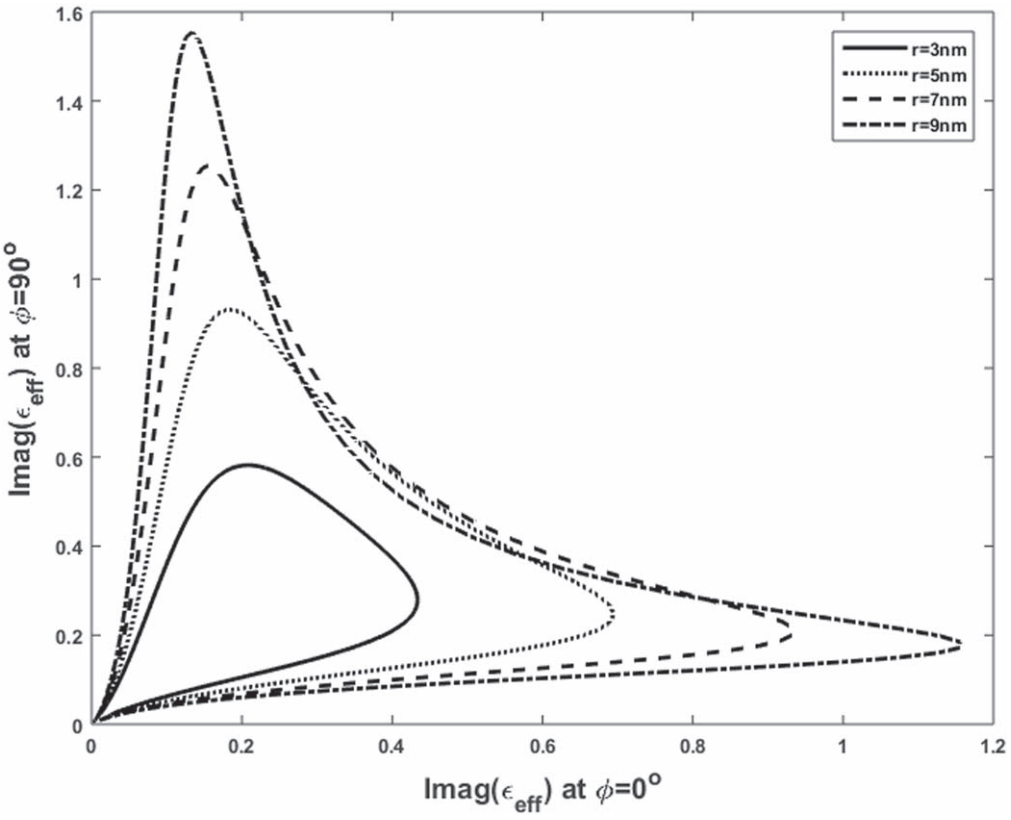

Figure 5. Imaginary part of effective permittivity at $\phi = 90^{\circ}$ versus Imaginary part of effective permittivity at $\phi = 0^{\circ}$ for different radii of nanoparticles.

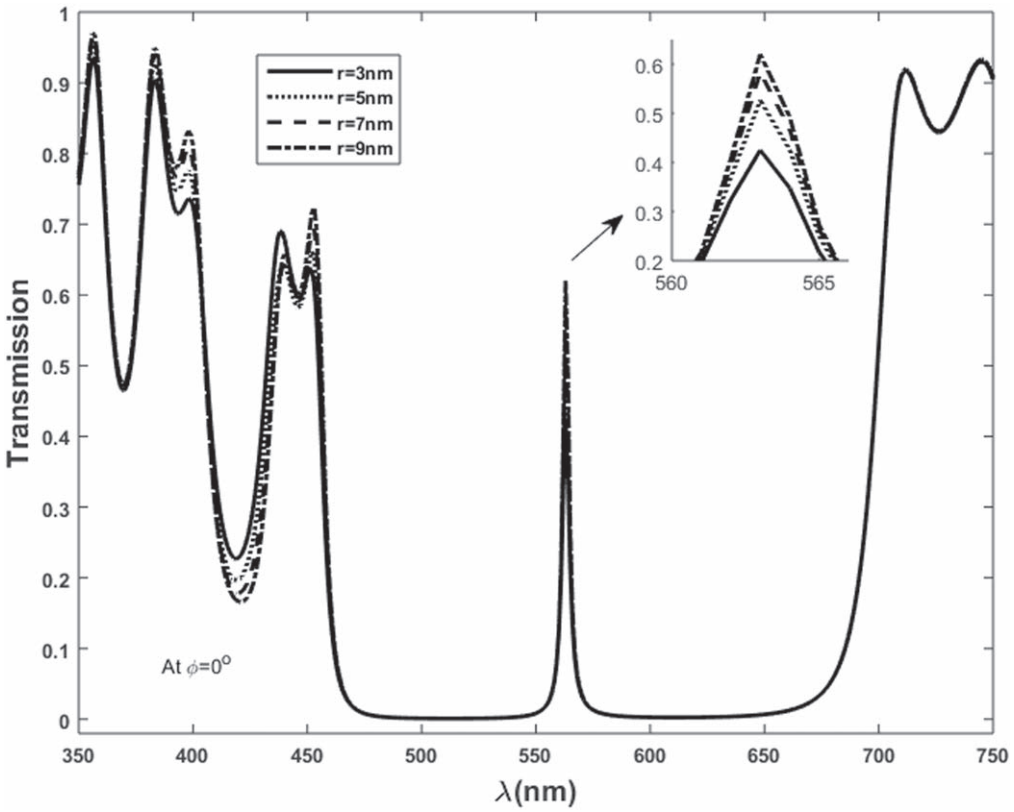

Figure 6. Transmission spectra of $(TiO_2|SiO_2)^3|NC|(TiO_2|SiO_2)^3$ versus wavelength at orientation angle $(\phi) = 0°$ for different radii of nanoparticles.

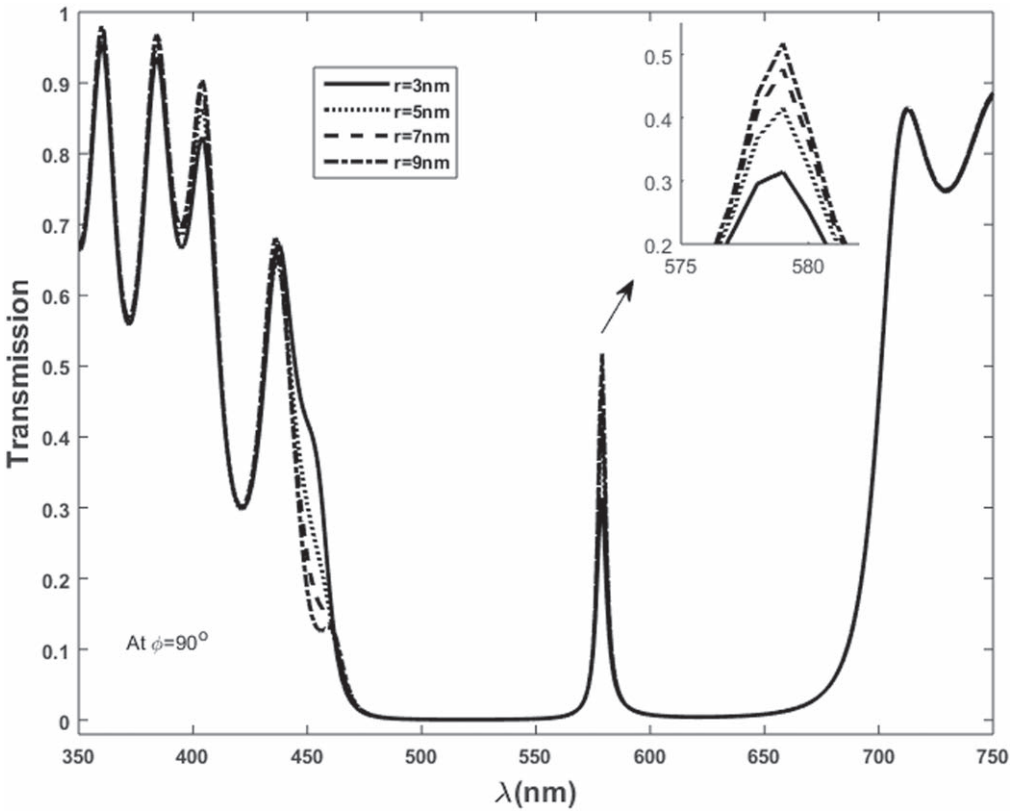

Figure 7. Transmission spectra of $(TiO_2|SiO_2)^3|NC|(TiO_2|SiO_2)^3$ versus wavelength at orientation angle $(\phi) = 90°$ for different radii of nanoparticles.

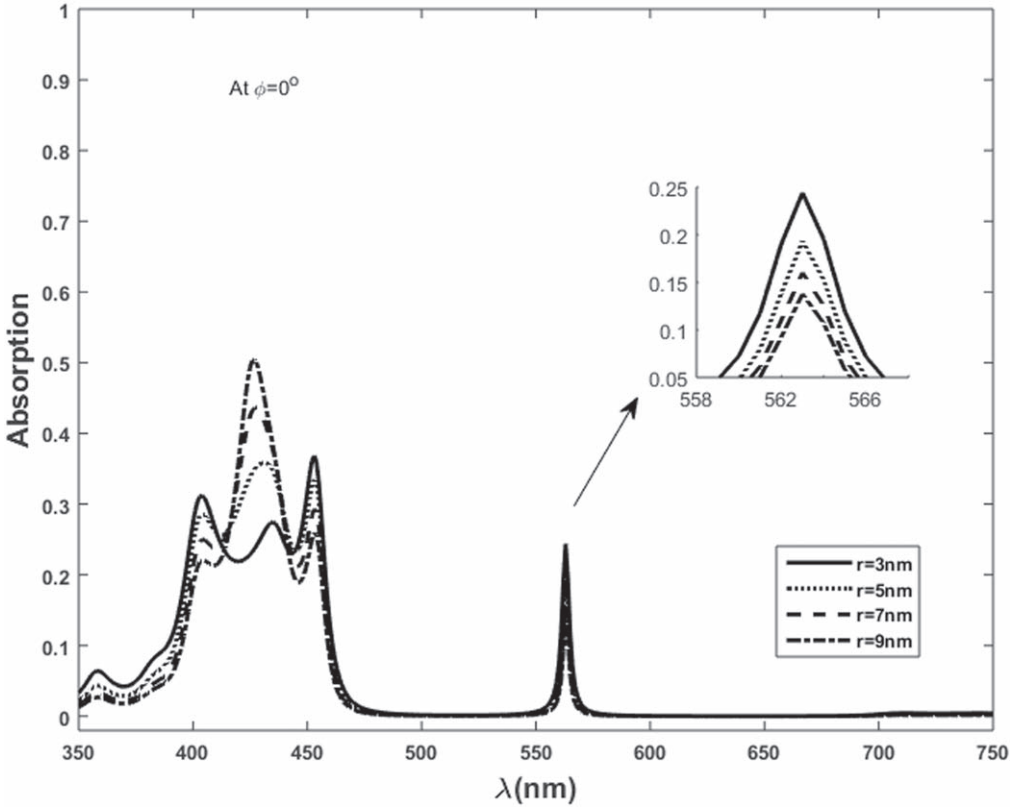

Figure 8. Absorption spectra of $(TiO_2|SiO_2)^3|NC|(TiO_2|SiO_2)^3$ versus wavelength at orientation angle $(\phi) = 0°$ for different radii of nanoparticles.

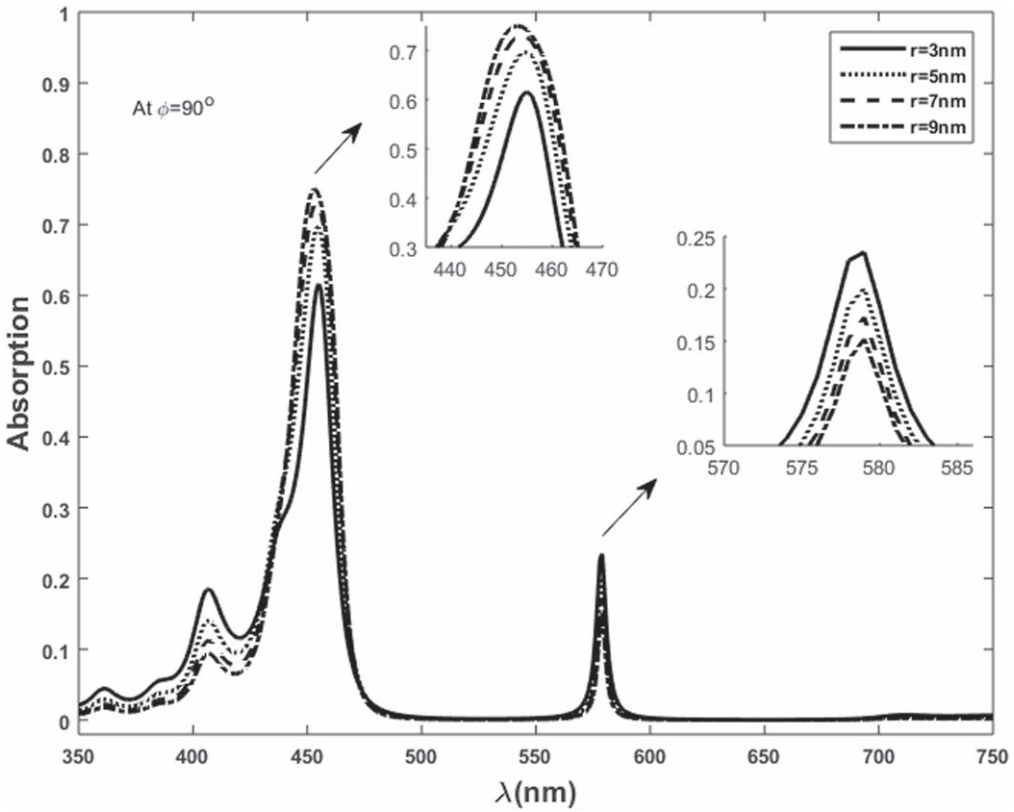

Figure 9. Absorption spectra of $(TiO_2|SiO_2)^3|NC|(TiO_2|SiO_2)^3$ versus.wavelength at orientation angle $(\phi) = 90°$ for different radii of nanoparticles.

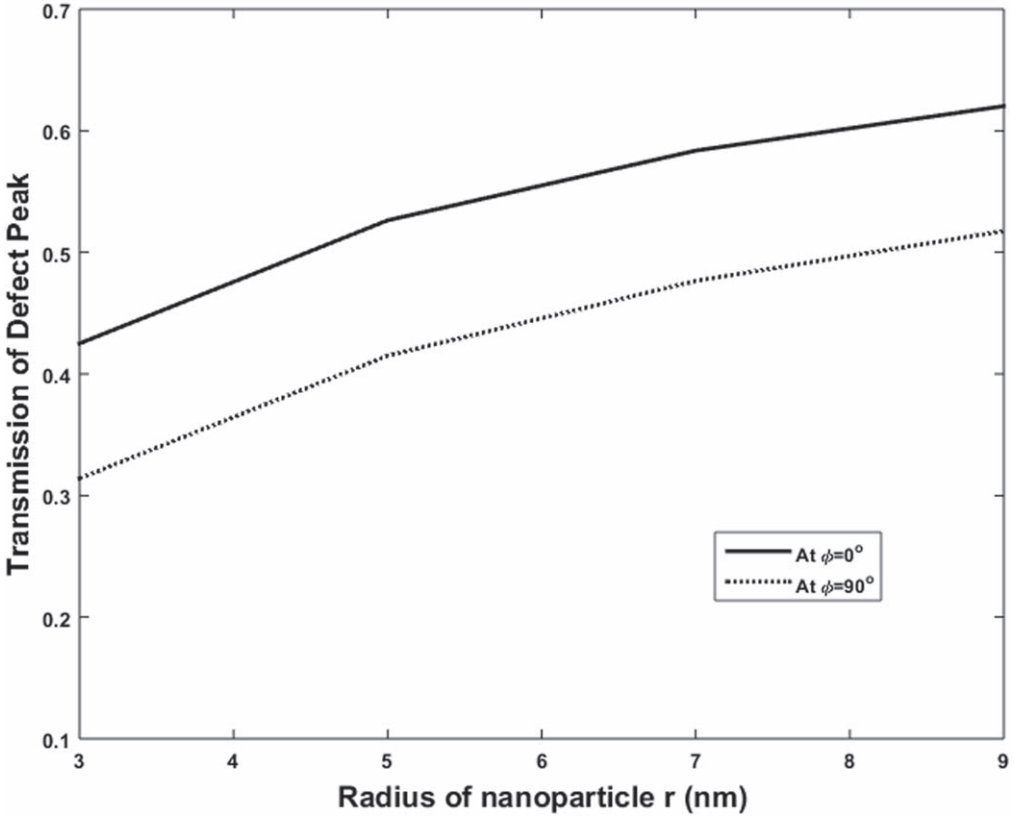

Figure 10. Transmission behavior of defect mode wavelength peaks with the radii of nanoparticles presented in nanocomposite (NC) at orientation angles $\phi = 0^{\circ}, 90^{\circ}$.

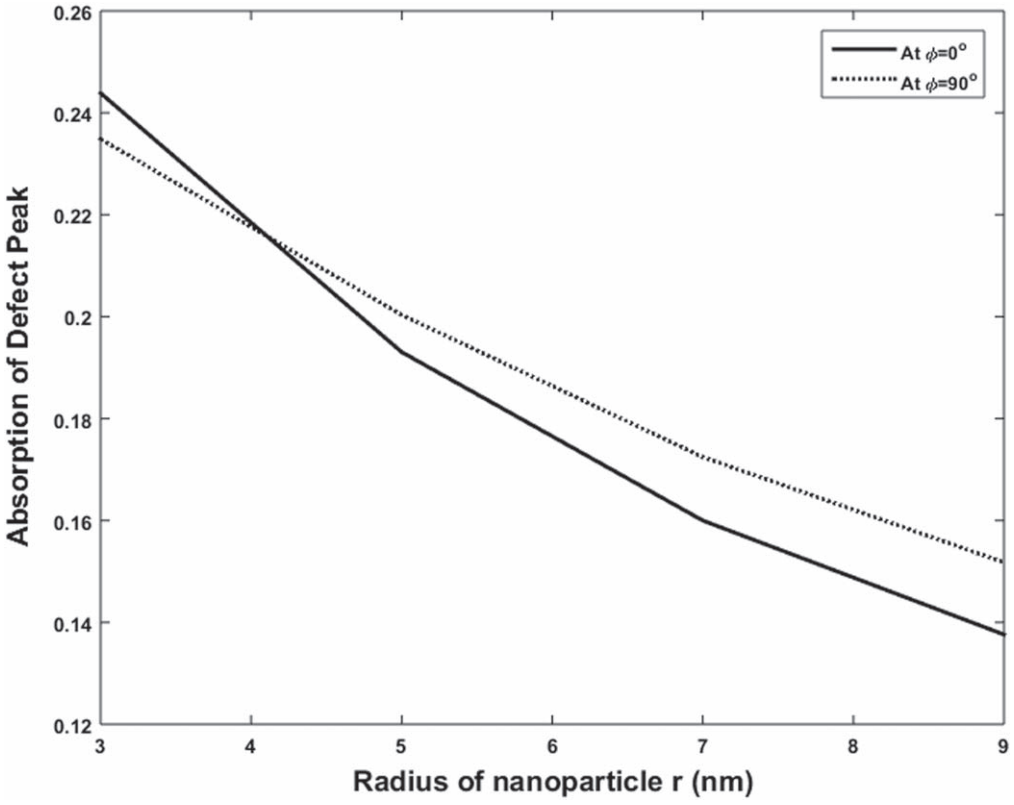

Figure 11. Absorption behavior of defect mode wavelength peaks with the radii of nanoparticles presented in nanocomposite (NC) at orientation angles $\phi = 0^{\circ}, 90^{\circ}$.

nanoparticles are considered as $2\pi \times 2.17 \times 10^{15}$Hz and $2\pi \times 4.8 \times 10^{12}$Hz, respectively and the radii (r) of the spherical silver nanoparticle are taken as 3 nm, 5 nm, 7 nm, and 9 nm with $\varepsilon_0 = 5$ [45–47].

The transmission properties of the one-dimensional periodic structure of the TiO_2/SiO_2 layer with the defect of nanocomposite (NC), $(TiO_2|SiO_2)^3|NC|(TiO_2|SiO_2)^3$, are studied using transfer matrix method (TMM). The transmittance of defect mode peaks for the director angles of the LC is investigated with different radii of silver nanoparticles as shown in figures 6 and 7. Figure 6 shows the transmission of the considered periodic structure with NC defect layer at 0° orientation angle of the LC for different radii (r) of the nanoparticles i.e. 3 nm, 5 nm, 7 nm, and 9 nm. For 0° orientation angle of LC molecules, the transmittance of defect mode peaks at 563 nm wavelength is 42.5%, 52.6%, 58.3% and 62% for the radii of nanoparticles 3 nm, 5 nm, 7 nm, and 9 nm, respectively. Besides this, the transmission at lower wavelength band edge also observed maximum due to the effective refractive index of the NC. The transmission of defect peak is increased as the radii of silver nanoparticles increases due to significant modification in the effective permittivity of the nanocomposite material by changing the radii of the silver nanoparticles.

Similarly, we also study the transmission of the considered defect NC periodic structure at 90° orientation angle of the LC for different radii (r) of the nanoparticles as shown in figure 7. The transmittances of defect mode wavelength peaks at 579 nm wavelength with 90° orientation angle are 31.4%, 41.5%, 47.6%, and 51.7% for 3 nm, 5 nm, 7 nm, and 9 nm radii of nanoparticles, respectively. The transmission at lower wavelength band edge has also observed maximum due to the optical density of the NC. The transmissions at 90° orientation angle of LC molecules are found lower in comparison to the transmissions at 0° orientation angle of LC molecules. The defect mode transmission peak is shifted toward higher wavelength i.e. 563 nm wavelength to 579 nm wavelength due to change of orientation angle 0° to 90°. These observations indicate that defect mode transmission peak is increased as well as shifted to higher wavelength due to the presence of the SPR. But the defect mode transmission peak for 0° orientation angle of LC molecules has obtained large transmission because the effective permittivity is low loss during the interaction of SPR and orientation angle of LC molecules.

In addition to this, we also study the absorption of the considered defect NC periodic structure for different orientation angles of the LC with different radii of the nanoparticles. Specially, we focus on the absorption at lower band edge because the absorption of the defective periodic structure is more effectively changed due to the presence of defect NC layer. Figure 8 shows that the absorptions of defect mode peak at 563 nm wavelength for orientation angle 0° are found 13.7%, 16%, 19.3%, and 24.3% for radii 3 nm, 5 nm, 7 nm, and 9 nm, respectively. The absorption at lower wavelength band edge has found about 38%, and it decreases as the size of nanoparticles increases. The study reveals that the enhanced absorption for orientation angle 0° is confirmed due to SPR property of Ag-NP which is already observed in permittivity of NC around the same wavelength range, 350–550 nm.

Similarly, 15.7%, 17.2%, 20%, and 23.4% absorptions of defect mode peak at wavelength 579 nm for orientation angle 90° are obtained for 3 nm, 5 nm, 7 nm, and 9 nm, respectively as shown in figure 9. The absorptions of defect mode peaks for orientation angle 90° are obtained 69.6%, 73%, and 75% at 455 nm, 454 nm, and 453 nm wavelengths, respectively. The maximum absorption at lower wavelength band edge has also found about 61% and the absorption is increased with increasing the radius of Ag-NP. The maximum transmission is found 75% for the 9 nm radius of Ag-NP. The enhanced absorption for orientation angle 90° is found around the same wavelength range due to the SPR property of Ag-NP. The enhanced absorption of the band edge is found for the 90° orientation angle because the SPR interaction with LC molecules shows high damping nature.

These results can be correlated with the effective permittivity which is changed with varying the radius of nanoparticles as discussed earlier in figures 2 and 3. Hence, the transmission and the absorption properties of the defect NC periodic structure are interrelated with the effective permittivity of the nanocomposite. The effective permittivity of nanocomposite is associated with SPR through the size of nanoparticles and orientation angle of LC molecules, because of the scattering rate of conduction electrons is decreased where the SPR and the effective permittivity of NC are increased as increasing the radii of the nanoparticles. The variation of the nanoparticle radius significantly modifies the optical properties of the whole periodic structure.

We have described the behavior of the transmittance of defect peak with the different radius of nanoparticles for orientation angles 0° and 90°. Now, we study the transmission and the absorption defect peaks for 0° and 90° orientation of LCs molecules versus the radius of the Ag-NPs which are shown in figures 10 and 11, respectively. From figure 10, we conclude that transmission of defect mode peak is increased as the radius of the nanoparticles in NC increases due to significant enhancement of the effective permittivity of nanocomposite material. The transmission of defect peak increases continuously as the size of the nanoparticle increases but the absorption of defect peak decreases as the size of the nanoparticle increases. The absorption line matches at the radius of 4.2 nm for both orientation angles and the low absorption show for the larger radius of the nanoparticles.

4. Conclusion

In this paper, we have calculated the effective permittivity of nanocomposite with different radius of silver nanoparticles for orientation angles of LC $\phi = 0°$, 90°. The effective permittivity of the NC is dependent upon the size of silver nanoparticles where the radius of the nanoparticle affects the surface plasmon resonance (SPR). Besides this, we found that the effective permittivity of nanocomposite for different radii of nanoparticles is also dependent upon the molecular

orientation of LC. The transmittance and absorption of one-dimensional periodic structure with NC defect layer with different radius of silver nanoparticles were studied for 0° and 90° molecular orientation of LC. The transmission defect mode peak of the periodic structure became high when the radius of nanoparticles is increased because the size of the nanoparticle affects the effective permittivity NC. On increasing the size of the nanoparticle for both orientation angles, the transmission of the defect peak was increased; while the absorption was decreased. However, the absorption of the band edge for the 90° orientation angle of LC was found about 75% for the 9 nm radius of Ag-NP. By studying the effect of different radius nanoparticles and orientation of LC's molecules on the dielectric permittivity of the NC, the considered periodic structure with the defect layer of the NC may be used as the absorption-based optical devices viz. sensors, detectors, optical switches, etc.

Acknowledgments

Author PS would like to thank Babasaheb Bhimrao Ambedkar University Lucknow for the non-NET UGC fellowship.

ORCID iDs

Khem B Thapa https://orcid.org/0000-0003-2639-0652

References

[1] Yablonovitch E 1987 Inhibited spontaneous emission in solid-state physics and electronics *Phys. Rev. Lett.* **58** 2059–62
[2] John S 1987 Strong localization of photons in certain disordered dielectric superlattices *Phys. Rev. Lett.* **58** 2486–9
[3] Jonopoulos J D, Villeneuve P and Fan S 1997 Photonic crystals: putting a new twist on light *Nature* **386** 143–9
[4] Zheng Q R, Fu Y Q and Yuan N C 2006 Characteristics of planer PBG structures with a cover layer *J. Electromagn. Waves Appl.* **20** 1439–53
[5] Fink Y, Winn J N, Fan S, Chen C, Michel J, Joannopoulos J D and Thomas E L 1998 A dielectric omnidirectional reflector *Science* **282** 1679–82
[6] Rojas J A M, Alpuente J, Pineiro J and Sanchez R 2006 Rigorous full vectorial analysis of electromagnetic wave propagation in 1D *Progress In Electromagnetics Research* **63** 89–105
[7] Joannopoulos J D, Meade R D and Winn J N 1995 *Photonic Crystals: Molding the Flow of Light* (Princeton, NJ: Princeton Univ. Press)
[8] Srivastava R, Thapa K B, Pati S and Ojha S P 2008 Omni-direction reflection in one dimensional photonic crystal *Progress In Electromagnetics Research* **7** 133–43
[9] Srivastava R, Thapa K B, Pati S and Ojha S P 2008 Design of photonic band gap filter *Progress In Electromagnetics Research* **81** 225–35
[10] Thapa K B, Singh S K and Ojha S P 2006 Omnidirectional high reflector for infrared wavelength *Int. J. Infrared Millimeter Waves* **27** 1257–68
[11] Singh S K, Pandey J P, Thapa K B and Ojha S P 2007 Structural parameters in the formation of omnidirectional high reflectors *Progress In Electromagnetics Research* **70** 53–78
[12] Thapa K B, Srivastava S and Tiwari S 2015 Enlarged photonic band gap in heterostructure of metallic photonic and superconducting photonic crystals *J. Supercond. Novel Magn.* **23** 517–25
[13] Singh S K, Thapa K B and Ojha S P 2006 Large frequency range of omnidirectional reflection in Si-based one dimensional photonic crystals *Int. J. Micro. Opt. Technol.* **1** 686–90
[14] Pandey G N, Kumar N, Thapa K B and Ojha S P 2016 Reflectance properties of one-dimensional metal-dielectric ternary photonic crystal *AIP Conf. Proc.* **1728** 020310
[15] Thapa K B, Mishra N K, Pandey G N and Ojha S P 2009 Enhanced absorption in periodic one-dimensional metallic-organic periodic structure *Progress In Electromagnetics Research* **8** 221–33
[16] Kady I E, Sigalas M M, Biswas R, Ho K M and Soukoulis C M 2000 Metallic photonic crystals at optical wavelengths *Phys. Rev.* B **62** 299–302
[17] Rinnerbauer V *et al* 2014 Metallic photonic crystal absorber-emitter for efficient spectral control in high-temperature solar thermophotovoltaics *Adv. Energy Mater.* **4** 1–10
[18] Veronis G, Dutton R W and Fan S 2005 Metallic photonic crystals with strong broadband absorption at optical frequencies over wide angular range *J. Appl. Phys.* **97** 093104–093104
[19] Özbay E, Temelkuran, Sigalas B M, Tuttle G, Soukoulis C M and Ho K M 1996 Defect structures in metallic photonic crystals *Appl. Phys. Lett.* **69** 3797–9
[20] Chandrasekhar S 1992 *Liq. Cryst.* (New York: Cambridge Univ Press) 1992
[21] Khoo I C 2007 *Liq. Cryst.* (New Jersey: Wiley Interscience) 2007
[22] Blinov L M 2011 *Structure and Properties of Liquid Crystals* (New York: Springer) 2011
[23] Bush K and John S 1999 Liquid-crystal photonic-band-gap materials: the tunable electromagnetic vacuum *Phys. Rev. Lett.* **83** 967–70
[24] Yoshino K, Shimoda Y, Kawagishi Y, Nakayama K and Ozaki M 1999 Temperature tuning of the stop band in transmission spectra of liquid-crystal infiltrated synthetic opal as tunable photonic crystal *Appl. Phys. Lett.* **75** 932–4
[25] Leonard S W, Mondia J P, Driel H M V, Toader O, John S, Bush K, Birner A, Gosele U and Lehmann V 2000 Tunable two-dimensional photonic crystals using liquid crystal infiltration *Phys. Rev.* B **61** R2389–92
[26] Schuller C, Klopf F, Reithmaier J P, Kamp M and Forchel A 2003 Tunable photonic crystals fabricated in III-V semiconductor slab waveguides using infiltrated liquid crystals *Appl. Phys. Lett.* **82** 2767–9
[27] Kang D, Maclennan J E, Clerk N A, Zakhidov A A and Baughman R H 2001 Electro-optic behavior of liquid-crystal-filled silica opal photonic crystals: effect of liquid-crystal alignment *Phys. Rev. Lett.* **86** 4052–5
[28] Graubard E, King J S, Jain S, Summers C J, Williams Y Z and Khoo I C 2005 Electric-field tuning of the Bragg peak in large-pore TiO_2 inverse shell opals *Phys. Rev.* B **72** 233105–4
[29] Arkhipkin V G, Gunyakov V A, Myslivsts S A, Zyryanov V Y and Shabanov V F 2007 Angular tuning of defect modes spectrum in the one-dimensional photonic crystal with liquid-crystal layer *Eur. Phys. J.* E **24** 297–302
[30] Strelniker Y M, Stroud D and Voznesenkaya A O 2006 Control of extraordinary light transmission through perforated metal films using liquid crystals *Eur. Phys. J.* B **52** 1–7
[31] Mingaleev S F, Schillinger M, Hermann D and Bush K 2004 Tunable photonic crystal circuits: concepts and designs based on single-pore infiltration *Opt. Lett.* **29** 2858–60

[32] Zel'dovich B Y, Tabiryan N V and Chilingaryan Y S 1981 Fredericks transitions induced by light fields *Zh. Eksp. Teor. Fiz.* **81** 72–83
[33] Ong H L 1983 Optically induced Freedericksz transition and bistability in a nematic liquid crystal *Phys. Rev.* A **28** 2393–407
[34] Mohamed M S, Hameed M F O, El-Okr M M and Obayya S S A 2016 Characterization of one dimensional liquid crystal photonic crystal structure *Optik* **127** 8774–81
[35] Ozaki R, Miyoshi H, Ozaki M and Yoshino K 2005 Tunable defect mode in one-dimensional photonic crystal with liquid crystal defect layer *Mol. Cryst. Liq. Cryst.* **433** 247–57
[36] Polycarpou A C, Christou M A and Papanicolaou N C 2012 A mode-matching approach to electromagnetic wave propagation in nematic liquid crystals *IEEE Trans. On Micro. Theo. and Tech.* **60** 2950–8
[37] Miroshnichenko E, Pinkevych I and Kivshar Y S 2006 Tunable all-optical switching in periodic structures with liquid-crystal defects *Opt. Exp.* **14** 2839–44
[38] Entezar S R, Madani A, Habil M K, Namdar A and Tajalli H 2013 Temperature dependent transmission and optical bistability in a 1D photonic crystal with a liquid crystal defect layer *J. Mod. Opt.* **60** 1883–91
[39] Ong H L 1986 Optical-field-enhanced and static-field-induced first-order Fréedericksz transitions in a planar parallel nematic liquid crystal *Phys. Rev.* A **33** 3550–3
[40] Yeh P 1988 *Optical Waves in Layered Media* (New York: Wiley)
[41] Elsayed H A and Aly A H 2018 Terahertz frequency superconductor-nanocomposite photonic band gap *Int. J. Mod. Phys.* B **32** 1850056
[42] Vetrov S Y, Bikbaev R G and Timofeev I V 2013 Optical Tamm states at the interface between a photonic crystal and a nanocomposite with resonance dispersion *J. Exp. Theor. Phys.* **117** 988 - 998
[43] Aly A H, Elsayed H A and Malek C 2017 Optical properties of one-dimensional defective photonic crystal containing nanocomposite material *J. Nonlin. Opti. Phys. Mater.* **26** 1750007
[44] Ramanujam N R, Wilson K S J and Revathy V 2015 Effect of temperature on nanocomposite of metal nanoparticles in photonic crystals *Progress In Electromagnetics Research* M **41** 105–14
[45] Moiseev S G 2011 Thin-film polarizer made of heterogeneous medium with uniformly oriented silver nanoparticles *Appl. Phys.* A **103** 775 - 777
[46] Moiseev S G 2011 Composite medium with silver nanoparticles as an anti-reflection optical coating *Appl. Phys.* A **103** 619 - 622
[47] Moiseev S and Ostatochnikov V 2015 Influence of the size-dependent permittivity of metal inclusions on the optical characteristics of a one-dimensional photonic crystal with a nanocomposite defect *Opti Quanum. Electron* **47** 3193 - 3200
[48] Singh P, Thapa K B, Kumar N, Singh D and Kumar D 2019 Effective optical properties of one-dimensional periodic structure of TiO_2 and SiO_2 layers with a defect layer of nanocomposite consisting of silver nanoparticle and E7 liquid crystal *Pramana- J. Phys.* **93** 50
[49] Mouquinho A, Saavedra M, Maiau A, Petrova K, Barros M T, Figueirinhas J L and Sotomayor J 2011 Films based on new methacrylate monomers: synthesis, characterisation, and electro-optical properties *Mol. Cryst. Liq. Cryst.* **542** 132–40
[50] Li J, Wu S T, Brugioni S, Meucci R and Faetti S 2005 Infrared refractive indices of liquid crystals *J. Appl. Phys.* **97** 073501–5
[51] Yeshchenko O A, Dmitruk I M, Alexeenko A A, Kotko A V, Verdal J and Pinchuk A O 2012 Size and temperature effects on the surface plasmon resonance in silver nanoparticles *Plasmonics* **7** 685–94
[52] Amendola V, Bakr O M and Stellacci F 2010 A study of the surface plasmon resonance of silver nanoparticles by the discrete dipole approximation method: effects of shape, size, structure, and assembly *Plasmonics* **5** 85–97

International Journal of Modern Physics B
Vol. 33, No. 18 (2019) 1950194 (19 pages)
© World Scientific Publishing Company
DOI: 10.1142/S0217979219501947

World Scientific
www.worldscientific.com

Int. J. Mod. Phys. B 2019.33. Downloaded from www.worldscientific.com
by RUTGERS UNIVERSITY on 08/09/19. Re-use and distribution is strictly not permitted, except for Open Access articles.

Tunable optical filter based on one-dimensional periodic structure composed of SiO_2 and anisotropic metamaterial (AMM) with a liquid crystal defect layer sandwiched by two SiO_2

Pawan Singh, Khem B. Thapa*, Narinder Kumar,
Anil K. Yadav and Devesh Kumar

Department of Physics, School of Physical and Decision Sciences,
Babasaheb Bhimrao Ambedkar University (A Central University),
Vidya Vihar, Raebareli Road, Lucknow 226025, UP, India
khem.bhu@gmail.com

Received 14 November 2018
Revised 19 May 2019
Accepted 22 May 2019
Published 23 July 2019

This paper reports the tunable transmission properties of asymmetric one-dimensional periodic structure (1DPS) composed of SiO_2 and anisotropic metamaterial (AMM) layers with defect of liquid crystal (LC) sandwiched by two SiO_2 layers, i.e., $(SiO_2|AMM)^3|SiO_2|LC|SiO_2|(SiO_2|AMM)^3$ using the transfer matrix method (TMM). We have studied the optical properties of the periodic structure $(SiO_2|AMM)^3|SiO_2|LC|SiO_2|(SiO_2|AMM)^3$ with a different incident angle of the electromagnetic wave for particular director angle of LC molecules. The tunability of the transmission property of the considered 1DPS shows that the transmittance depends upon the orientation of LC molecules. Such an asymmetric periodic structure (1DPS) composed of SiO_2 and AMM with a defect of LC sandwiched by two SiO_2 layers, $(SiO_2|AMM)^3|SiO_2|LC|SiO_2|(SiO_2|AMM)^3$, may be used as a tunable optical filter and bistable device.

Keywords: Liquid crystal; anisotropic metamaterial; TMM.

PACS numbers: 42.70.Df, 42.79.Kr, 42.70.Qs, 78.67.Pt

1. Introduction

An optical medium of alternating dielectric materials in different dimensions with periodic regulation refractive indices is called photonic crystal (PC). PCs exhibit interesting properties to regulate the propagation of the electromagnetic wave inside the crystal. PCs are classified into three categories: one-dimensional photonic

*Corresponding author.

Temperature sensor and monochromatic filter based on one-dimensional photonic crystal containing Si and SiO_2 with a defect layer of liquid crystal

PAWAN SINGH[a], KHEM B. THAPA[a,*], GIRIJESH N. PANDEY[b]
[a]*Department of Physics, School of Physical and Decision Sciences, Babasaheb Bhimrao Ambedkar University (A Central University), Vidya Vihar, Raebareli Road, Lucknow-226025 (UP), India*
[b]*Department of Applied Physics, Amity Institute of Applied Sciences, Amity University, Sector- 125, Express Highway, Noida (UP), India*

In this article, we have proposed a temperature sensor and monochromatic filter based on one-dimensional photonic crystal (1DPC) containing Si and SiO_2 layers with liquid crystal (LC) as a defect layer i.e. $(Si|SiO_2)^3|LC|(Si|SiO_2)^3$ structure. By applying the transfer matrix method (TMM), we have studied transmission properties of the $(Si|SiO_2)^3|LC|(Si|SiO_2)^3$ structure. The tunable transmission characteristics of the periodic structure $(Si|SiO_2)^3|LC|(Si|SiO_2)^3$ are investigated with the variation of temperature of the LC layer as well as the incident angle of the electromagnetic wave. The calculated transmission peak of defect mode lies in photonic band gap (PBG) region of the 1DPC, and the transmission peak of the defect mode shifts with the temperature variation of the LC. The transmittance of defect mode peak in PBG region of the 1DPC has analyzed with the variation of temperature, and suggested a temperature sensor as well as a monochromatic filter based on the $(Si|SiO_2)^3|LC|(Si|SiO_2)^3$structure.

(Received August 28, 2018; accepted August 20, 2019)

Keywords: Temperature sensor, Liquid crystal, Photonic crystal and transfer matrix method

1. Introduction

Photonic Crystals (PCs) are periodically composition of dielectric materials in one dimension (1D), two dimension (2D) and three dimensions (3D). Such PCs are very interesting to investigate because such periodic layered optical media have special characteristics, which can be used in the optical devices [1-4]. PCs control the electromagnetic wave propagation inside the periodic dielectric materials and due to having a regular arrangement of dielectrics, such PCs yields a special domain of frequencies called photonic band gap (PBG) [5-7]. In such PCs, the electromagnetic wave can't propagate inside PBG region of the PCs, which is a novel property of the PCs. Hence, such periodic materials or PCs can be used in optical devices to control the propagation of electromagnetic wave [8-10].

Liquid crystals (LCs) are novel organic materials, which have a transitional segment between liquids and solids. LC has the flow characteristics like liquid and crystalline characteristics like solid. LC is extraordinary and highly birefringent material, and applicable in tunable optical devices [11-13]. The refractive indices of LC have extraordinary (n_e) and ordinary refractive indices (n_o) and these refractive indices are electric fields and temperature dependent. Hence, the tunable transmission of one-dimensional photonic crystal (1DPC) with liquid crystal as a defect layer can be achieved by varying temperature dependent optical parameters of LC like refractive index, director angle and incident angle etc. Such tunable transmission properties of the 1DPC with LC defect layer can be used in many tunable optical devices like optical filters, bistable switches, multichannel filters etc. Busch et al. proposed that the optical tunability of PBG regions can be achieved by coating the inverse opal with LC, and verified it experimentally by Yoshino et al. [14,15]. As discussed above, LC has electric field and temperature dependent optical parameter and these optical properties of LC can be tuned by the variation of electric field and the temperature. The optical transmissions of PCs can be tuned by controlling the optical parameters of LC as a defect layer in PCs [16-21]. The photonic crystals with infiltrated holes with LC are also a method to attain the tunable optical transmissions characteristics of PCs [22]. LCs are birefringent and nonlinear optical materials and they have remarkable optical characteristics which can be used in the novel optical devices [23, 24] like all-optical switching in PC, and moderated transmissions of the electromagnetic wave in the PC. Mohamed et al. investigated the effect of LC director orientation angle and temperature on the transmissions of 1DPC with LC as a defect layer. Similarly, the optical properties of 1DPC with LC as a defect layer was investigated by Entezar et al. and they have demonstrated that the tunability of PCs could be achieved by regulating the optical parameter of LC [25-29]. Authors had also discussed the bi-stable characteristics of PC, which was dependent upon the functioning temperature and examined the influence of temperature on the optical transmission properties of the PC.

Journal of Physical Science, Vol. 30(3), 117–129, 2019

Omnidirectional Reflection Band of One-dimensional Periodic Structure (1DPS) of Si/SiO_2 with Defect Mode of Nematic Liquid Crystal (5CB)

Pawan Singh, Khem B Thapa,* Narinder Kumar and Devesh Kumar

Department of Physics, School of Physical and Decision Sciences,
Babasaheb Bhimrao Ambedkar University (A Central University),
VidyaVihar, Rae Bareli Road, Lucknow-226025 (UP), India

*Corresponding author: khem.bhu@gmail.com

Published online: 25 November 2019

To cite this article: Singh, P. et al. (2019). Omnidirectional reflection band of one-dimensional periodic structure (1DPS) of Si/SiO_2 with defect mode of nematic liquid crystal (5CB). *J. Phys. Sci.*, 30(3), 117–129, https://doi.org/10.21315/jps2019.30.3.8

To link to this article: https://doi.org/10.21315/jps2019.30.3.8

ABSTRACT: *In this paper, an omnidirectional reflection band of a one-dimensional periodic structure (1DPS) of Si and SiO_2 with a nematic liquid crystal (5CB) as a defect layer, i.e., $(Si|SiO_2)^3|NLC|(Si|SiO_2)^3$, is investigated. The geometry of the 5CB molecules NLC is optimised with the help of density functional theory (DFT) using Gaussian 09 Software packageA02 and the order parameter (S) of the 5CB molecules is calculated. The S value for the 5CB molecules is found to be 0.53 for the range of the applied electric field and confirms the nematic phase of the liquid crystal at the microwave region. By taking average of the ordinary and extraordinary refractive indices of the 5CB molecules NLC, the refractive index has been calculated. The optical properties of the 1DPS of Si and SiO_2 with a 5CB molecules NLC defect layer are calculated to study the optical defect mode as well as the bi-channelled omnidirectional reflection behaviour of the 1DPS $(Si|SiO_2)^3|NLC|(Si|SiO_2)^3$ and tuned by the electro-optic property of 5CB NLC. Such omnidirectional reflecting behaviour of the considered structure may be used to design b-channelled omnidirectional reflector and defect mode filter and others.*

Keywords: Nematic liquid crystal, 5CB, 1DPS, omnidirectional reflection band, DFT

© Penerbit Universiti Sains Malaysia, 2019. This work is licensed under the terms of the Creative Commons Attribution (CC BY) (http://creativecommons.org/licenses/by/4.0/).

Advances in Photonic Crystals and Devices

Edited by
Narendra Kumar
Bhuvneshwer Suthar

CRC Press
Taylor & Francis Group
Boca Raton London New York

CRC Press is an imprint of the
Taylor & Francis Group, an **informa** business

K39656_C000.indd 3 07/18/19 7:08:56 PM

8

Embedded Liquid Crystal Defect with Graphene Layers in Asymmetric One-Dimensional Photonic Crystal as Sensor Application

Pawan Singh, Krishan Pal, Khem B. Thapa, Narinder Kumar, and Devesh Kumar

CONTENTS

8.1 Introduction

Photonic crystals (PCs) have been of great interest in the past decades to investigate, which is due to photonic bandgaps (PBGs) that have special property to obstruct the transmission of electromagnetic wave. Reyleigh (1887) investigated that the control of electromagnetic wave is inside the periodic structure. Bykov (1972) suggested that the periodic structure can be used to control the spontaneous emission. John (1987) and Yablonovitch (1987) successfully suggested that the possibility of spontaneous emission management and propagation of radiation can be controlled using a periodic structure of the dielectric materials. Many research papers have published in the field of PCs and its technology in addition to the above-mentioned articles. Basically, PCs are the media in which dielectric materials are arranged periodically with regulation or modulation of the refractive indices in periodic structures. Such periodic arrangements of the dielectric materials have some special properties that can be used in different areas such as photonics, optoelectronic, nanoscience, and nanotechnology.

K39656_C008.indd 121 06/12/19 6:10:48 PM

Copyright © 2019 American Scientific Publishers
All rights reserved
Printed in the United States of America

SENSOR LETTERS
Vol. 17, 1–4, 2019

Tunable Sensing Property of 1D Periodic Structure with Defect of Liquid Crystal Sandwiched by Metallic Layers

Pawan Singh[1], Krishan Pal[1], Narinder Kumar[1], Sudesh K. Singh[2], Khem B. Thapa[1,*], and Devesh Kumar[1]

[1] *Department of Physics, School of Physical and Decision Sciences, Babasaheb Bhimrao Ambedkar University, Lucknow 226025, India*
[2] *Department of Physics, TDPG College, Jaunpur 222001 (U.P.), India*

(Received: 22 July 2019. Accepted: xx Xxxx xxxx)

In this paper, we have investigated the optical properties of one-dimensional periodic structure of dielectric materials with defect of liquid crystal (LC) sandwiched with two silver (Ag) layers. The transmission, reflection and absorption properties of considered periodic structure have calculated theoretically using transfer matrix method (TMM). Our study reports that the tunability of absorption defect peak of the defect periodic structure is achieved by the variation in the incident angle of electromagnetic wave. The obtained result suggests that such defect periodic structure may be used as tunable sensor and filter devices.

Keywords: Liquid Crystal, Silver, Absorption, Transfer Matrix Method (TMM), Temperature, Incident Angle.

RESEARCH ARTICLE

1. INTRODUCTION

The periodic layered structures of dielectric materials with periodic modulation of dielectric constants in different dimension are known as photonic crystal (PC). PCs are classified into mainly three categories; one-dimensional photonic crystal (1DPC), two-dimensional photonic crystal (2DPC), and three-dimensional photonic crystal (3DPC). With the interaction of electromagnetic wave, PC exhibits photonic band gap (PBG) region which have special property to obstruct the electromagnetic wave propagation in the PCs. Therefore, PCs are used in many tunable optical devices i.e., omnidirectional reflector, sensor, filter, etc. [1–5]. Another way to gain the tunablity of PC is the use of liquid crystal (LC) as a defect layer in PC. Liquid crystals are highly birefringent organic material which has temperature dependent extraordinary and ordinary refractive indices [6, 7]. Hence, PC with LC as defect can be used in many nonlinear novel devices. The optical characteristics of LC are dependent on the temperature, electric field, molecular orientation etc. Hence the tenability of PC can be obtained through controlling the applied field and optical parameters of LC as defect layer [8–15]. PC with LC as a defect layer shows various applications in optical devices i.e., all optical switching, multichannel optical filter, bistable switch, sensor etc.

*Corresponding author; E-mail: khem.bhu@gmail.com

In this paper, we have theoretically studied the optical properties of considered periodic structure with the variation of incident angle of electromagnetic wave using transfer matrix method (TMM) [15]. For study, we have taken the E7 liquid crystal which is composition of four different liquid crystals 5CB, 7CB, 8OCB, and 5CT [16, 17]. Our results suggest that defect periodic structure may be used as tunable optical sensor and filter.

2. THEORY AND METHODOLOGY

To study the optical properties, we have considered the periodic structure of dielectric layers with refractive indices n_1 and n_2. The LC layer sandwiched with two silver layers is used as defect in one-dimensional periodic structure as shown in Figure 1. We have consider the E7 liquid crystal of thickness 100 nm and the dielectric parameters (n_e, n_o) of LC which depends on the temperature are given as;

$$n_e(T) = A - BT + \frac{2(\Delta n)_o}{3}\left(1 - \frac{T}{T_C}\right)^{\beta} \quad (1)$$

$$n_o(T) = A - BT - \frac{(\Delta n)_o}{3}\left(1 - \frac{T}{T_C}\right)^{\beta} \quad (2)$$

where A, B, $(\Delta n)_o$, β, and T_C are the constants parameter and clearing temperature of LC layer. In our calculation,

Plasmonics
https://doi.org/10.1007/s11468-020-01210-x

Study of Design Tunable Optical Sensor and Monochromatic Filter of the One-Dimensional Periodic Structure of TiO /MgF with Defect Layer of Liquid Crystal (LC) Sandwiched with Two Silver Layers

Pawan Singh[1] · Khem B. Thapa[1] · Sudesh K. Singh[2] · Alok K. Gupta[3]

Received: 19 December 2019 / Accepted: 1 June 2020
© Springer Science+Business Media, LLC, part of Springer Nature 2020

Abstract
In this paper, we have inspected the optical characteristics of one-dimensional periodic structure (1DPS) of TiO_2 and MgF_2 dielectric materials with defect layer of liquid crystal (LC) sandwiched with two silver layers, i.e., $(TiO_2|MgF_2)^3|Ag|LC|Ag|(TiO_2/MgF_2)^3$ using transfer matrix method (TMM). The optical tunable properties of considered periodic structures investigated at different incident angles and temperatures for TE and TM modes. Our study shows that absorption peak of 1DPS varies with incident angle and temperature. The defect layer (Ag-LC-Ag), sandwiched LC within two metallic (Ag) layers, exhibits the surface plasmon waves at the metal LC interfaces. The effect of surface plasmon waves can be better understand through the optical sensing property of such defect periodic structure. The detailed study concludes that such a type of one-dimensional periodic structure (1DPS) may be useful to design a tunable sensor and monochromatic filter.

Keywords Optical properties · Transfer matrix method (TMM) · Silver (Ag) · Liquid crystal · Surface plasmon resonance

Introduction

In inference to control the electromagnetic wave, photonic crystals are the interesting optical medium, which controls the propagation of electromagnetic wave inside periodic dielectric layers. Photonic crystals (PCs) are the regular arrangement of dielectric slabs in different dimensions with periodical repetition of dielectric functions. Such periodic structures show novel properties on the interaction of the electromagnetic field with the matter. Including controlled transmission, PCs exhibit photonic band gap (PBG) regions, which block the flow of the electromagnetic wave. In point of view of the dielectric function, PCs are divided into three classes: one-dimensional photonic crystal (1DPC), two-dimensional photonic crystal (2DPC), and three-dimensional photonic crystal (3DPC). PCs have various applications based on the desired application, e.g., optical filters, switches, and omnidirectional reflectors [1–11]. Based on omnidirectional characteristics, PCs show different applications in optical devices. Optical devices such as microwave absorbers and sensors can be fabricated based on absorption characteristics of photonic crystals with the metallic interface or metallic photonic crystal (MPC) [12–19]. PCs with a tunable defect layer control the tunable transmission of defect mode in the optical characteristics. PCs with a defect layer in the structure give defect mode in the transmission spectra, which can be regulated through the voltage or electric field [12–14]. PCs with a tunable defect layer can be varied by electric field and voltage, and therefore, PCs used have many applications in optical devices. [15–24].

To obtain tunability of PCs, the magnetic and electric field, temperature, Kerr effect, etc., are the external parameters of liquid crystal and these parameters can be changed the optical property of a photonic crystal with liquid crystal as a defect layer [25–27]. Liquid crystals have extraordinary and ordinary dielectric constants dependent on the orientation of molecules; therefore, liquid crystal can be used as a tunable defect layer to achieve voltage-controlled tunability. The non-rubbed and rubbed metallic films can control the orientation of liquid crystal molecules. The rubbed and non-rubbed metallic films align the liquid crystal homogeneously in planer arrangement

✉ Khem B. Thapa
khem.bhu@gmail.com

[1] Department of Physics, School of Physical and Decision Sciences, Babasaheb Bhimrao Ambedkar University, Vidya Vihar, Raebareli Road, Lucknow, U.P 226025, India

[2] Department of Physics, T.D.P.G. College, Jaunpur, U.P. 222002, India

[3] Ministry of Human Resource Development, Government of India, National Institute of Open Schooling, Regional Centre, Kochi 682036, India

Published online: 08 June 2020

Solar Energy Materials and Solar Cells 196 (2019) 138–156

Contents lists available at ScienceDirect

Solar Energy Materials and Solar Cells

journal homepage: www.elsevier.com/locate/solmat

Current challenges and future prospects for a highly efficient (> 20%) kesterite CZTS solar cell: A review

Krishan Pal, Pawan Singh, Abhishikta Bhaduri, Khem B. Thapa*

Department of Physics, School of Physical and Decision Sciences, Babasaheb Bhimrao Ambedkar University (A Central University), Lucknow-226025 (UP), India

ARTICLE INFO

Keywords:
Kesterite
Recombination
Band offset
Defect
Interface layer
CZTS solar cell

ABSTRACT

CZTS has kesterite structure and the composition's formula is $Cu_2ZnSn(S/Se)_4$. The efficiency of CZTS-Se (Copper—Zinc—Tin-Sulphur-Selenium) solar cell, ~12.6%, is much lower than the efficiency of CIGS (Copper—Indium—Gallium—Selenium) solar cell, ~22.6%. But the CZTS-Se may be the counterpart of the CIGS and the efficiency may be increased up to 32.2% as theoretically predicted by the Shockley-Queisser (SQ) limit. In solar cell technology, it has been depicted that the efficiency of the solar are affected by the two parameters: (i) variation of the solar insolation and (ii) quality of the materials. Besides this, the narrow phase stability of quaternary phases, unfavorable band alignments, mid-gap states and band tails are main reasons of deficit in the efficiency of kesterite due to the coexistence of the secondary and ternary phases, carrier recombination at the interfaces, defects and series resistances. As a result, the kesterite solar cell has the fluctuated open circuit voltage and the loss of energy. In addition to this, the champion CZTS-Se solar cell is not so environmental friendly because Se is the toxic and the rare earth element. This review provides the vital approaches by discussing the proper materials processing and the appropriate solution to enhance the efficiency of kesterite (CZTS, CZTSe and CZTS/Se) solar cells. Due to the large area quality, high absorption and low-cost materials of the kesterite, it may be used directly in harvesting the solar energy. We have also discussed how to reduce the recombination of the electron-hole pairs by using the interfacial layer so that the efficiency of the kesterite solar cells can be improved.

1. Introduction

The energy crisis is a fascinating problem in this world for twenty-first century. The current energy consumption of the world is 16 TW (16×10^{12} Watt) and it will become 30 TW in 2050 [1]. The 80% energy is generated from the sustainable energy sources e.g. oil, gas, coal etc. and remaining 20% energy from renewable energy sources e.g. water, solar, wind etc. [2]. The solar, wind and water energy sources are abundant on the earth and are to be free of cost if we are able to develop low cost devices, that is, solar cell that converts solar energy to electric energy. The sustainable energy is used at mankind's demand and may affect the climate change for the long-term by producing outcome harmful products. On the other hand, the renewable energy is an alternative source of energy, which is environment friendly for the earth and the best for health security purpose.

The solar energy is easily available, directly accessible and free source of energy on the earth and it is free of cost. The solar insolation on the earth is incident directly about 1.2×10^5 TW ($1\ TW = 10^{12}$ Watt) on the earth surface in which 3.6×10^4 TW on land only [1]. The change in the amount of radiation emitted by the Sun at a particular location increases dramatically due to local effects such as clouds and seasonal variations, as well as other effects such as “the length of the sunny day” at the particular latitude. But the solar radiation in desert regions tends to have lower variations due to local atmospheric phenomena such as clouds [3]. The solar radiant energy spectrum with percentage distribution intensity versus wavelength of the incident photons is shown in Fig. 1.1 [4]. This figure predicts that the maximum intensity of the radiation is to have in the visible wavelength range.

The high-energy conversion devices like solar cells are dependent upon the material's property. The materials quality modifies the photovoltaic property and enhances efficiency of the solar cells. So, researchers are working to enhance the materials quality by manipulating the “material compositions”. The efficiency of the solar cell can be enhanced up to Shockley-Queisser limit by manipulating the material with the help of the material processing. The solar cell is the best source to fulfill the large energy requirements globally without any harmful effect to the atmosphere and environment.

The development of the solar cell is categorized into three

* Corresponding author.
E-mail address: khem.bhu@gmail.com (K.B. Thapa).

https://doi.org/10.1016/j.solmat.2019.03.001
Received 2 July 2018; Received in revised form 23 February 2019; Accepted 2 March 2019
0927-0248/ © 2019 Published by Elsevier B.V.

Eur. Phys. J. Plus (2020) 135:388
https://doi.org/10.1140/epjp/s13360-020-00386-9

THE EUROPEAN PHYSICAL JOURNAL PLUS

Regular Article

Odd–even effect of 7O.m liquid crystal compound series studied under the effect of the electric field by density functional theory (DFT) methods

Narinder Kumar[1], **Pawan Singh**[1], **Pranav Upadhyay**[2], **Shivani Chaudhary**[1], **Khem B. Thapa**[1], **A. K. Dwivedi**[3], **Devesh Kumar**[1,a]

[1] Department of Physics, School for Physical and Decision Sciences, Babasaheb Bhimrao Ambedkar University, VidyaVihar, Raebareli Road, Lucknow, UP 226025, India
[2] Department of Physics, Sri J. N. P. G College (KKC), Charbag, Lucknow 226001, India
[3] Department of Physics, M. L. K. P. G. College, Balrampur, UP 271201, India

Received: 5 June 2019 / Accepted: 6 April 2020
© Società Italiana di Fisica and Springer-Verlag GmbH Germany, part of Springer Nature 2020

Abstract The homologous series of the organic compound *N*(*p*-*n*-heptyloxy-benzylidene) *p*-toluidine (7O.m) expresses the odd–even effect under the influence of an external applied electric field by density functional theory (DFT) methods. The dipole moment, order parameter, and birefringence express an odd–even effect. At the same time, the Homo–Lumo gap and isotropic polarizability do not exhibit any odd–even effect under the influence of an external applied electric field. The Homo–Lumo gap remains constant for the homologous series of 7O.m ($m = 1$–10). The isotropic polarizability and refractive index continuously increase with an extension of alkyl chain length. The DFT methods (B3LYP and M062X) exhibit the same nature of optical characteristics for all the series but with different values.

1 Introduction

The electronegative oxygen atom plays a crucial role in the compound series of *N*(*p*-*n*-heptyloxy-benzylidene) *p*-toluidine nO.m ($n = 7$, $m = 1$–10); the presence of an oxygen atom in the series of 7O.m is responsible for the nematic phase. By increasing the length of alkyl or alkoxy chain, the dipole moment increases with the liquid crystalline range of molecules [1, 2]. The nematic to smectic-A (N-A) phase transition has observed if the alkyl chain length increased. The nO.m compound series exhibits the odd–even effect under the applied temperature [3]. The order parameter (S) is studying with the help of optical birefringence and molecular polarizability [4]. The removal of an oxygen atom from one or both sides of the NO.Om compound series is responsible for the reduction in dipole moment and transition temperature. The presence of oxygen atom on both sides of the compounds NO.Om causes the growth of the clearing temperature and liquid crystalline range [5–8]. The Schiff bases compound (NO.O.m, nO.m, and n.m) are very sensitive to the atmosphere [9]. The nO.m compounds exhibit the orthogonal phase for the $n \leq 6$, and $m \geq 7$ exhibit the smectic-F and smectic-G phases. The 7O.1 liquid crystals molecules exhibit the nematic as well as monotropic smectic-A and smectic-B phase under the effect of temperature. The

[a] e-mail: dkclcre@yahoo.com (corresponding author)

Published online: 01 May 2020

Absorption and Bandwidth Properties of Graphene Based 1D-Photonic Crystal for THz Devices

Roshni Maurya[1], Pawan Singh[1], Prabal P. Singh[2], Krishan Pal[1], Girijesh N Pandey[3] and Khem B. Thapa[1, a)]

[1]*Department of Physics, School of Physical and Decision Sciences, Babasaheb Bhimrao Ambedkar University, Vidya Vihar, Rae Bareli Road, Lucknow-226025 India*
[2]*Department of Physics, University Institute of Engineering & Technology, CSJM University, Kanpur-208024 India*
[3]*Department of Physics, Amity Institute of Applied Sciences, Amity University, Uttar Pradesh, India*

[a)]Corresponding author: khem.bhu@gmail.com

Abstract. In this paper, we study effect of chemical potential, temperature and the number of graphene on the tunable optical characteristics and photonic band gap (PBG) of one-dimensional graphene based photonic crystal (1D-GPC). For this, we use the transfer matrix method (TMM) which is based on the solution of Maxwell's equation and Bloch's function. As the inherent property of graphene like chemical potential or gate voltage and temperature, the tunable absorption and photonic band gap (PBG) are affected in the terahertz (THz) frequency region. Our investigation reports that the PBG of 1D-GPC is varied with number of the graphene layers at different temperatures and different chemical potentials. The proposed graphene based periodic structure with large number of graphene layers at high chemical potential and low temperature may be used in THz devices.

Keywords: Graphene, 1D-GPC, PBG, Chemical potential and Temperature, THz device

INTRODUCTION

Graphene is a novel material of a basic unit cell of graphite that has 2D lattice in honeycomb structure with closed packed carbon atoms [1, 2]. Due to high value of electron mobility and doping characteristics, the Graphene deals with various applications of graphene in optoelectronic devices [3, 4]. Moreover, graphene has unusual dielectric function depends on the chemical potential, temperature and relaxation time. Therefore, the optical properties of graphene based photonic crystals (GPCs), especially one-dimensional, are studied to have ability to tune on the basis of chemical potential or gate voltage. Absorption property of one-dimensional photonic crystal is enhanced with graphene layer when such 2D materials attaches to the surface of photonic crystal [5]. Dispersion relation and complex band structure of graphene based photonic crystals were studied using the effective medium theory. The existence of omnidirectional behavior of the graphene based photonic crystals was reported at incident angle 80^{o} [6]. The periodically arrangement of graphene and dielectric materials, called graphene photonic crystal, is used in THz device applications. The tunable transmission characteristics of graphene based photonic crystal were studied to different applications [7-11]. Recently, Graphene is an excellent material to design the hyperbolic metamaterial. The graphene hyperbolic metamaterials are used in the various applications like modulator, sensor, super absorber etc. The tunable properties of dual gated grapehene based photonic crystal was studied by Ning et al. [12], and the multiband absorption characteristics was achieved by interchanging the thickness of dielectric materials and chemical potential in the near infrared frequency regions. Fibonacci quasi periodic structure with graphene layer at different chemical potential are also observed the tunable omnidirectional PBG property. The omnidirectional band gap of graphene photonic crystals are usually found independent on the polarization mode [13].

3rd International Conference on Condensed Matter and Applied Physics (ICC-2019)
AIP Conf. Proc. 2220, 020084-1–020084-4; https://doi.org/10.1063/5.0001755
Published by AIP Publishing. 978-0-7354-1976-6/$30.00

Broadband Reflector of 1D Photonic Crystal Containing TiO_2/SiO_2 Material at Visible Region

Asish Kumar[1], Pawan Singh[1], Krishan Pal[1], Narendra Kumar[2] and Khem B. Thapa[1*]

[1]*Department of Physics, School of Physical and Decision Sciences, Babasaheb Bhimrao Ambedkar University, Lucknow 226025, India*
[2]*Department of Physics, School of Sciences, Mody University of Science and Technology, Lakshmangarh 332311, Sikar, India*

[*]Email: khem.bhu@gmail.com

Abstract. Using the transfer matrix method (TMM) and Bloch function, the optical property of 1D photonic crystal of titanium dioxide (TiO2) and silicon dioxide (SiO2) material was theoretically analyzed. The dispersion curve versus wavelength (nm) study shows that lower band edge varies with increase in angle of incidence, and the structure offers a huge bandwidth. On comparing the dispersion curves and the reflection spectra for the considered structure, they are found to be in the same wavelength band. From the study of the reflection spectra with increase in incident angle, we find a blue shift at visible range with a huge bandwidth, and hence the structure may be used as a broadband reflector. Due to advanced development in the thin film technology, the obtained results may be useful to design the photonic devices of titanium dioxide (TiO2) and silicon dioxide (SiO2) material at visible region of electromagnetic spectrum.

Keywords: Photonic crystal, TiO_2 and SiO_2 material, broadband reflector, photonic devices, thin film technology

INTRODUCTION

The periodic structure of nanostructures and microstructure of two or more than two optical constant medium in the space has the interference of the wave at each surface is called Photonic Crystal (PC). Such PC has one of the unique properties called photonic band gap (PBG) and PBG can use to control the electromagnetic wave (photons) propagation in the materials. The origin of PBGs was first time experimentally and theoretically analyzed by Yablonovitch and John in the year 1987 [1, 2]. The PBG material has the great application in research and technology because PBG control and manipulate the flow of electromagnetic wave through the medium. The PBG of the periodic structure depends on refractive index, unit cell, filling fraction of the material, frequency and dimensionality etc. [3]. One-dimensional photonic crystal (1D-PC) is most popular in the thin film technology due to ease fabrication and have a lots of applications in optical engineering, photonic device, optical filter; resonance cavity, laser application, high-reflecting omnidirectional mirror, and optoelectronic circuit etc. [4–8]. The periodic structure of the different refractive index materials affects the photon propagation due to different PBG, and such PBG plays a crucial role in optical applications [9-12].

THEORETICAL METHODOLOGY

The dispersion curve and the reflection spectra are theoretically calculated by well known TMM and Bloch's function [13]. In this paper we have considered one-dimensional periodic crystal which is composed with titanium dioxide (TiO_2) and silicon dioxide (SiO_2) material. The photonic crystal containing TiO_2 and SiO_2 is in the periodic

3rd International Conference on Condensed Matter and Applied Physics (ICC-2019)
AIP Conf. Proc. 2220, 020068-1–020068-4; https://doi.org/10.1063/5.0002138
Published by AIP Publishing. 978-0-7354-1976-6/$30.00

IOP SciNotes

OPEN ACCESS

RECEIVED
20 January 2020

REVISED
6 March 2020

ACCEPTED FOR PUBLICATION
12 March 2020

PUBLISHED
29 May 2020

Original content from this work may be used under the terms of the Creative Commons Attribution 4.0 licence.

Any further distribution of this work must maintain attribution to the author(s) and the title of the work, journal citation and DOI.

ARTICLE

Molecular spectroscopy and adverse optical properties of *N-(p-hexyloxy-benzylidene)–p-toluidine* (HBT) liquid crystal molecule studied by DFT methodology

Narinder Kumar , Pawan Singh, Khem B Thapa and Devesh Kumar[1]

Department of Physics, School of Physical & Decision Sciences, Babasaheb Bhimrao Ambedkar University, Vidya Vihar, Raebareli Road, Lucknow (U.P.) 226025, India

[1] Author to whom any correspondence should be addressed.

E-mail: dkclcre@yahoo.com

Keywords: HBT liquid crystal, Molecular spectroscopy, electro-optical effect, DFT(B3LYP)

Abstract

In present work, we report the *N-(p-hexyloxy-benzylidene)–p-toluidine* (HBT) liquid crystal (LC) molecule having maximum absorbance due to the O–C stretching (carbon atom of benzene ring) during the intermolecular interaction. Under the expansion of an external electric field, the HBT LC having nematic to smectic phase stability with adverse (negative values) order parameter and birefringence. The refractive index expresses stability in the nematic, smectic, and isotropic phases. The director angle maintains stability for the nematic phase in the adverse order and smectic phase stable in positive order.

1. Introduction

The Liquid crystal (LC) phase represents a different state of matter characterized by the mobility and order of the molecule. All the particles in the crystalline state possess an orientational and three-dimensional positional order. Liquid crystal phases possess both orientational order and, in some cases, positional order in one or two dimensions [1]. The liquid crystal behavior of molecules is responsible for the different types of intermolecular interaction acting between sides, planes, and ends of a pair of the molecule [2]. Liquid crystal (LC) phases are formed by anisotropic molecule, having one molecular axis very different from the other two [3]. The rod-like molecule is the most common type of LC molecular shape. The nematic phase exhibits long-range orientational order but no positional order of the molecule [4]. The impact of the external electric field on liquid crystal can be studied by analyzing the polarizability of the molecule [5, 6]. In liquid crystals, the molecular polarizability and its anisotropy are important inherent molecular properties because the intermolecular interaction energies depend on them [7]. LC materials may consist of polar and non-polar molecules that depend upon the physical structure of LC [8]. The LC molecules can possess permanent dipole along the long molecular axis, which enhances the dielectric anisotropy of LC. The dipole moment parallels to the long molecular axis, then $\Delta\varepsilon > 0$, and the molecules tend to orient along the electric field direction because LC posses more significant dielectric anisotropy along the molecular axis (*x*-axis). If the molecule carries fewer dipole moments long molecular axis, then $\Delta\varepsilon < 0$ and fragment tend to orient perpendicular to the electric field direction because of the polarity of the molecule is negligible [9]. The orientational order of the LC molecule does not change in the applied external electric field. The applied external electric field to the LC molecule causes the reorientation of the director angle. The LC molecule responds to the applied external electric field E collectively that causes the director angle to fluctuate [10].

Luckhurst *et al* [11] reported the Schiff base compound increases the polarity of the molecule, which enhances the dielectric anisotropy. The dielectric anisotropy is suitable for the electro-optical effect in display applications. Alkyl chain also increased the liquid crystal properties, such as the nematic-isotropic or nematic, to a smectic phase transition temperature [12, 13]. The molecular polarizabilities and the anisotropy of liquid crystal molecules are considered as an essential characteristic inherent molecular properties because the intermolecular interaction energies, according to different theoretical models, are dependent on them. The refractive index of HBT LC is 1.58.

© 2020 The Author(s). Published by IOP Publishing Ltd

Spectroscopy Existing behind the Electro-Optical Properties with an Even-Odd Effect of nCB Liquid Crystal Molecules: A Theoretical Approach

N. Kumar[a], P. Singh[a], S. Chaudhary[a], K.B. Thapa[a], P. Upadhyay[b], A.K. Dwivedi[c] and D. Kumar[a,*]

[a]Department of Physics, School of Physical and Decision Sciences, Babasaheb Bhimrao Ambedkar University, Vidya Vihar, Raebareli Road, Lucknow (U.P.) 226025, India

[b]Department of Physics, Sri J.N.P.G. College (KKC), Charbagh, Lucknow-226001, India

[c]Department of Physics, M.L.K.P.G. College, Balrampur (U.P.) 271201, India

(Received November 27, 2019; in final form February 4, 2020)

In this work, we have studied the effect of the external electric field on the nCB series with an extension of the alkyl chain length of liquid crystal molecules. The stretching of C–C and C–H atom contributes to the anisotropy of polarizability for the new compound of the nCB series. The molecular polarizability is responsible for an even-odd effect of the optical parameters. The electric field is another method (alternative of temperature) to find out the optical parameters of the liquid crystal series. Under the impact of an external electric field, the order parameter and birefringence are expression of an even-odd effect. The transition temperature and birefringence enhance for the odd member and reduce for even members of the alkyl chain. The birefringence decreases with an even-odd effect while the order parameter increases with minor deviation.

DOI: 10.12693/APhysPolA.137.1135

PACS/topics: nCB liquid crystal, electric field, order parameter, birefringence, spectroscopy

1. Introduction

The electro-optical response depends on the physical property and molecular structure of the liquid crystal (LC) molecules. The cyanobiphenyl (nCB) LCs are highly polar, so it has very high thermal and electrochemical stability. The external electric field sufficiently affects the optical properties of rod shape LCs through the polarization of both ends of molecules. Under the effect of an external electric field, the one end of the nCB molecule has favorable charges. In contrast, the other end is negatively charged and formed an electric dipole. The director of the LC molecules will reorient along the direction of the applied external electric field [1–3]. The molecular polarizability increases with an increment of carbon atom number of the alkyl chain of the tail of the nCB LC molecules [4]. The family of the nCB LC first times synthesized by Gray et al. [5, 6] for the electro-optical application of the display technology. The nCB LC is colorless and stable to the moisture that is the best feature of these molecules. When the nCB LC having a unique property for the alkyl chain length is changed, then the molecular properties of the mesophase change [5, 6]. The nCB LC molecules indicate on an even-odd effect under the extension of the alkyl chain. The optical polarizability of the nCB LC molecule follows the even-odd effect and gives the interchange polarizability. The order parameter also exhibits the even-odd effects for the even-odd number of the carbon atom of the alkyl chain in the tail of the nCB LC [7, 8].

The birefringence is an electro-optical phenomenon used to find out the Kerr effect under the impact of the electric field. The birefringence is a fundamental property of the LC, which gives valuable information of LCs to use in various optical device applications. The electric field to the LC molecules has a rapid method to calculate birefringence and polarizability for the electro-optical application in the display technology. The electro-optical effect is used to study the pretransitional behavior (related to the order parameter) of the nCB LC. The nCB LC has a positive Kerr constant because of the intense, permanent dipole moment and highly conjugated π-electrons [9–11]. The polarization of LC molecules induced by an applied electric field to the molecule depends on the direction of the applied field. The electric field corresponds to an essential parameter to find out the electro-optic property of the LC molecules [12, 13]. Rod shape LC molecules are less tilted with a comparison to the bent-core type LC molecules. The electrically induced tilt affects observed in several types of bent-core and hockey-stick type LC molecules [14].

The polarization and bending plane of the molecules are parallel in the absence of an electric field, and these will be perpendicular to the plane in the presence of an electric field. The smectic phase of the LC molecule tilted continuously with the increased electric field [15–18]. The switching behavior of the even-odd numbered carbon atom in the tail of the LC is different [19]. The notation

*corresponding author; e-mail: dkclcre@yahoo.com

Journal of Molecular Liquids 318 (2020) 114254

Contents lists available at ScienceDirect

Journal of Molecular Liquids

journal homepage: www.elsevier.com/locate/molliq

Electro-optical odd-even effect of APAPA liquid crystal molecules studied under the influence of an extraneous electric field (THz): A theoretical approach

Narinder Kumar *, Shivani Chaudhary, Pawan Singh, Khem B. Thapa, Devesh Kumar *

Department of Physics, School of Physical & Decision Sciences, Babasaheb Bhimrao Ambedkar University, Vidya Vihar, Raebareli Road, Lucknow (U.P.) 226025, India

ARTICLE INFO

Article history:
Received 2 June 2020
Received in revised form 2 September 2020
Accepted 5 September 2020
Available online 8 September 2020

Keywords:
APAPAm LC
Electric field
Density functional theory (DFT)
Odd-even effect
Electro-optical effect

ABSTRACT

The homologous series of APAPA (*anisylidene-para-amino-phenyl-acetate*) liquid crystal (LC) express the odd-even effect under the influence of an electric field in THz frequency region. The homologous series revealed an odd-even effect under the impact of temperature. The electron affinity and ionization potential have exhibited an odd-even effect with the extension of the alkyl chain length. The birefringence has expressed an odd-even effect under the influence of an extraneous electric field. The homologous series has positive as well as the negative orientation of the birefringence, which is suitable for electro-optical application devices. The order parameter and refractive index have continually increased with an expansion of alkyl chain length. The director angle remains constant at $\theta = 90°$ for the whole series of LC. The extraneous influence of the electric field has correlated with the impact of temperature variation.

© 2020 Elsevier B.V. All rights reserved.

1. Introduction

The liquid crystal (LC) is organic substance that flows like a liquid; however, it has some degree of order to arrange the molecules. The LC phase is the intermediate phase exists between the crystalline and liquid phases. The lowest symmetry-based nematic LC is mostly uniaxial and does not show any translational correlation of the molecular center. Rod-like nematic LC is easy to rotate along the long molecular axis under the impact of the electric field. Rod-like LC has strong electron conjugation, which is better for the display and other applications. The dielectric behavior of LC contributes to the dielectric anisotropy, which is responsible for the reorientation of the LC molecules under the influence of an electric field. The reorientation of the LC plays a crucial role in the electro-optical device applications. An imine based liquid crystal does made from a double bond between N and C presented in the molecular structure which contributes to the molecular polarizability and resulting intermolecular interactions in the nematic liquid crystals. The different terminal location has different dipole moment; therefore, the suitable place of the polar group can enhances the molecular polarizability; thus, molecular polarizability contributes to the stability of LC phase. The APAPA LC contains two benzene rings connected with the Schiff base linkage group and the terminal of the benzene ring combined with the alkoxy and ester group [1,2]. Mandal et al. [3] have reported that APAPA LC expresses the dynamic scattering effect, which helps to liquid crystal display (LCD) application. The APAPA LC has a nematic phase between 83 °C to 108 °C temperature. The Schiff base LC compound is susceptible to the atmosphere moisture; therefore, during the fabrication of the optical devices using such liquid crystals, the protection from the moisture is necessary. The order parameter of APAPA LC has value between 0.61 and 0.40. APAPA LC is also known as MBA LC which maintains the nematic phase under the impact of temperature and pressure. Leenhouts et al. [4] have reported that the homologous series of APAPA LC can also be denoted as the APAPAm LC, where m stands for the number of the carbon atom in the alkyl chain length of the ester group $OCOC_m\ H_{2m+1}$. The elastic constant of the homologous series of APAPA LC decreases with an extension of alkyl chain length due to short-range correlation in the plane perpendicular to the director (Y-axis). Somashekar et al. [5] have reported that the order parameter of 1MBA LC exists between 0.5 and 0.6, while the order parameter of 3MBA LC exists between 0.5 and 0.65. Onnagawa et al. [6] have reported that APAPA LC maintain alignment in the nematic phase under the influence of electric and magnetic field. Meulen et al. [7] have investigated that the elastic properties of nematic LC easy to calculate by dynamic light scattering. Moreover, Deutsch et al. [8] have reported the laser light scattering by APAPA LC in the dynamic scattering mode; therefore, it may be used as a scattering material. In the present work, we have applied electric field to the homologous series of APAPA LC. Under the influence of an extraneous electric field,

* Corresponding authors.
E-mail addresses: knarinder7@gmail.com (N. Kumar), dkclcre@yahoo.com (D. Kumar).

https://doi.org/10.1016/j.molliq.2020.114254
0167-7322/© 2020 Elsevier B.V. All rights reserved.

Optical and Quantum Electronics (2020) 52:423
https://doi.org/10.1007/s11082-020-02548-6

Study of super absorption properties of 1D graphene and dielectric photonic crystal for novel applications

Asish Kumar[1] · Pawan Singh[1] · Khem B. Thapa[1]

Received: 20 December 2019 / Accepted: 12 September 2020
© Springer Science+Business Media, LLC, part of Springer Nature 2020

Abstract
In this article, we have theoretically analyzed the variation of real and imaginary components of electric permittivity and also the variation of refractive index of the graphene material in the Terahertz frequency range. The optical characteristics of One-Dimensional Periodic Structure (1-DPS) of graphene and dielectric materials have analyzed using Transfer Matrix Method. The transfer matrix method is very eminent method to analyze the optical characteristics of 1-DPS like dispersion relation, phase velocity, group velocity, reflection, transmission and absorption characteristics, etc. The absorption characteristics of considered graphene-based multilayered periodic structure have been analyzed with the variation of chemical potential (μ_c) of the graphene layer. The calculated absorption spectra of considered 1-DPS at the certain threshold frequency have found high and threshold value for the high chemical potential (gate voltage) of the graphene having the large thickness of the dielectric layer. Such the high and threshold absorption property of graphene-based 1-DPS, which acts as super absorber at terahertz region of the electromagnetic spectrum, may be used for the novel super absorber applications.

Keywords Graphene · Dielectric · Multilayer structure · Chemical potential · Super-absorption · TMM

1 Introduction

Photonic Crystals (PCs) are periodic structures of dielectric materials with the periodic modulation of dielectric constant of two or more media varied in the space. Yablonovitch and John studied the origin of Photonic Band Gap (PBG) of the PCs in the year 1987 (Yablonovitch 1987; John 1987). PCs are the more attractive optical media due to their abnormal properties of the PBG in respective to control the electromagnetic radiations (photons). Photonic crystal has unique feature of the photonic band gap where a specific domain of frequencies cannot be allowed to propagate from periodically structured materials. Therefore, PBG has the great applications in science and technology in controlling the flow of

✉ Khem B. Thapa
khem.bhu@gmail.com

[1] Department of Physics, School of Physical and Decision Sciences, Babasaheb Bhimrao Ambedkar University, Lucknow, U.P. 226025, India

Published online: 17 September 2020